Investigating the Endogenous Role of Human *N*-Acetyltransferase 1, as potential Breast Cancer Biomarker, using Chemical Biology

Nicola Laurieri

St. John's College

Department of Pharmacology

University of Oxford

A thesis submitted for the degree of Doctor of Philosophy

in Pharmacology

Hilary Term 2012

Supervisors: Prof. Edith Sim and Dr Angela Russell

"Teach us (o Lord) to number our days

that we may gain a heart of wisdom"

(Psalm 90,12)

Investigating the Endogenous Role of Human *N*-Acetyltransferase 1, as potential Breast Cancer Biomarker, Using Chemical Biology

Nicola Laurieri, St. John's College, Department of Pharmacology, University of Oxford.

A thesis submitted for the degree of Doctor of Philosophy, Hilary Term 2012.

Human *N-acetyltransferase 1* (*hNAT1*) is one of the ten most highly overexpressed genes in oestrogen-receptor-positive (ER+ve) breast cancers and its overexpression is strongly related to tumour grade. *N*-acetyltransferases from prokaryotic and eukaryotic kingdoms catalyse the transfer of an acetyl group from acetyl coenzyme A (CoA) to a variety of arylamines and arylhydrazines. While the other human isoenzyme hNAT2 has widely been assessed as a phase-II xenobiotic metabolising enzyme, the exact endogenous role of hNAT1 is still unknown. The association of hNAT1 with ER levels in breast tumours may imply a role in cancer progression, making it an attractive potential biomarker for ER+ve breast cancers and/or a novel therapeutic target.

Mice offer a good animal model for investigations on human NATs: *hNAT1* and mouse *NAT2* (*mNat2*) are orthologous genes and the corresponding proteins, hNAT1 and mNat2, are homologous on the basis of sequence identity (82%), substrate specificity and expression profile.

Investigating selective inhibitors for hNAT1 and mNat2 is described in this thesis with the aim of using these inhibitors to aid in determining the *in vivo* function of hNAT1 and its mouse homologue.

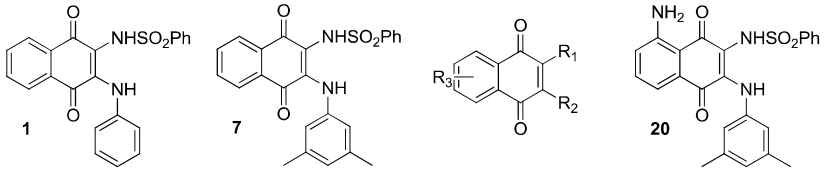
Naphthoquinone **1** was identified as a selective competitive inhibitor for hNAT1 and mNat2 ($IC_{50,hNAT1}$=1.65 μM and $IC_{50,mNat2}$=1.86μM) from a high-throughput screening of 5000 drug-like compounds against five distinct pure recombinant NATs. This compound also displays a distinctive colour change from red (λ_{max} = 484nm) to blue (λ_{max} = 610nm) in the presence of both hNAT1 and mNat2, but not the other human and murine isoenzymes. The colourimetric change was also observed by titration of compound **1** with an alkali.

Physicochemical, biochemical and computational studies were conducted on naphthoquinone **7**, an analogue of **1** with improved pharmacological properties ($IC_{50,mNat2}$=0.99μM) and colour intensity, to support the hypothesis that the colour change event is related to deprotonation of the sulfonamide-N*H* of the ligand by the side-chain guanidine of Arg127 within the active site of both enzymes, hNAT1 and mNat2.

Furthermore, the comparison of the arylamine substrate profiles of eight different mammalian NATs, alongside their preferences for inhibitor **7**, provided substantial elements on the key role of Phe125, Arg127 and Tyr129 on isoenzyme selectivity for both substrate and inhibitor. This supports the development of this family of naphthoquinones as highly selective inhibitors of hNAT1 and mNat2 to elucidate the endogenous role of these proteins *via* Chemical Genetics, and as colourimetric biosensors to detect and quantify hNAT1 in breast cancer tissues.

Selective recognition of hNAT1 by antibody allowed a preliminary estimation of the enzyme overexpressed in the breast cancer cell line ZR-75-1: 1pg per cell, for which the binding affinity and the colourimetric properties of compound **7** were found to need further improvement.

With the goal of improving both inhibitory potency and colourimetric properties of compound **7**, a set of analogues varying at R_1, R_2 and R_3 positions was chemically synthesised. The resulting substitutions altered inhibitory activity, range of colour change, molar extinction coefficient and acidity of the naphtoquinone derivatives, with compound **20** offering a tenfold increase in inhibitory potency towards both hNAT1 and mNat2 over **7**, but less suitable colourimetric properties.



Besides investigating the ability of different eukaryotic and prokaryotic NATs to use also *n*-propionylCoA as substrate, hNAT1 and mNat2 were exclusively identified to act as folate-dependent acetylCoA hydrolases compared to a panel of diverse eukaryotic and prokaryotic NATs, from which new hypotheses are proposed in the endogenous role of these enzymes in relation to folate, fat catabolism and cancer. (Number of words: ~48,000)

Acknowledgements

None of this work would have been possible without the constant assistance and the warm support of a large number of people during my DPhil, in particular in very difficult moments.

First and foremost, I would like to express my wholehearted thankfulness to my supervisors Professor Edith Sim and Doctor Angela Russell, for their lovely support, enthusiastic encouragements, and, when necessary, the forthrightness to guide me in the correct direction. They took me as a MedChem DPhil student and heartened me in the fascinating world of science. Without their endless mentorship and their stupendous cooperation, this thesis would not have been achievable. I cannont forget to thank Cancer Research UK for its financial support for my DPhil.

I am also immensely grateful to all members of Sim's and Russell's groups, as outstanding collaborators for all their technical advices and constant friendly support in and out the laboratories, and who made the labs such enjoyable environments to work in.

Firstly, I wish to thank all excellent Part II students who have greatly contributed to develop this fascinating project on both aspects, Biochemistry and Chemistry: Amy and Siu Lee for their help in expressing and purifying enzymes, James and Cyrille for their keen contribution in advancing the chemical synthesis of hit-compound derivatives, and Matthew for initiating this project on the right track before my Msc.

Then, I would also like to give special thanks to Dr Ali Ryan, for his unwavering help throughout the thesis, in particular in crystallography, protein modelling, and fluorimetry studies in collaboration with Dr Oleg Fedorov at the Structural Genomic Consortium, Oxford, Dr Camilo Quevedo for introducing me in docking softwares, Dr Julien Dairou (University of Paris VII) for kindly providing and developing studies on pure recombinant human enzymes, Dr Bob Sim for his critical reading of this thesis and technical advices, Dr Tim Claridge for his assistance in NMR experiments, Hilary for her help in cellular researches, and Souhad Kaleef for her temporary technical aid in molecular biology.

I am also really appreciative to all past and present colleagues and friends from both laboratories, who have generously supported me on this work under different aspects, including but limited to: Areej, Munirah, Helen, Dr. Peter Seden, Anna, Ornella, Lindsay.

I would also like to thank European colleagues who have kindly contributed to the development of this work through productive discussions and collaborative experiments: Prof. Jean Marie Dupret and Dr Fernando Rodriguez-Lima from the University of Paris VII, France, and Dr Sotiria Boukouvala, Dr Giannoulis Fakis and Heleni Karagianni from the University of Alexandroupoli, Greece.

I am also immensely thankful to all members from the Equality, Diversity, and Disability Offices of the University, St John's College and the Department of Pharmacology, which have all constituted a boon in allowing me to complete my thesis in a comfortable manner.

I am very grateful to my family for their unconditional love, support and advice. They have installed in me an intellectual curiosity which has led me into science, and a determination which kept me there. I would also like to thank all my lovely and caring friends in Oxford who made the whole duration of my DPhil an enjoyable time, and all my friends in Italy and in France for their amazing friendship.

Thanks to God, and with the cooperation of all of them, family, friends, supervisors and colleagues, I have been able to finish this work. To all I dedicate this thesis.

Publications

Laurieri, N., Crawford, M. H. J., Kawamura, A., Westwood, I. M., Robinson, J., Fletcher, A. M., Davies, S. G., Sim, E. & Russell, A. J. (2010). Small Molecule Colourimetric Probes for Specific Detection of Human Arylamine *N*-Acetyltransferase 1, a Potential Breast Cancer Biomarker. *Journal of the American Chemical Society* **132**, 3238-9.
***Highlighted in** Anslyn, E. Supramolecular and Chemical Cascade Approaches to Molecular Sensing, *J. Am. Chem. Soc.* **2010**, *132*, 15833-15835; *JACS Select #10* "Supramolecular and Chemical Cascade Approaches to Molecular Sensing".

Ryan, A., **Laurieri, N.**, Westwood, I., Wang, C. J., Lowe, E. & Simi, E. (2010). A Novel Mechanism for Azoreduction. *Journal of Molecular Biology* **400**, 24-37.

Lack, N. A., Kawamura, A., Fullam, E., **Laurieri, N.**, Beard, S., Russell, A. J., Evangelopoulos, D., Westwood, I. & Sim, E. (2009). Temperature stability of proteins essential for the intracellular survival of Mycobacterium tuberculosis. *Biochemical Journal* **418**, 369-378.

Russell, A. J., Westwood, I. M., Crawford, M. H. J., Robinson, J., Kawamura, A., Redfield, C., **Laurieri, N.**, Lowe, E. D., Davies, S. G. & Sim, E. (2009). Selective small molecule inhibitors of the potential breast cancer marker, human arylamine *N*-acetyltransferase 1, and its murine homologue, mouse arylamine *N*-acetyltransferase 2. *Bioorganic & Medicinal Chemistry* **17**, 905-918.

Ballester, P. J., Westwood, I., **Laurieri, N.**, Sim, E. & Richards, W. G. (2010). Prospective virtual screening with Ultrafast Shape Recognition: the identification of novel inhibitors of arylamine *N*-acetyltransferases. *Journal of the Royal Society Interface* **7**, 335-342.

Wang, C. J., **Laurieri, N.**, Abuhammad, A., Lowe, E., Westwood, I., Ryan, A. & Sim, E. (2010). Role of tyrosine 131 in the active site of paAzoR1, an azoreductase with specificity for the inflammatory bowel disease prodrug balsalazide. *Acta Crystallographica Section F-Structural Biology and Crystallization Communications* **66**, 2-7.

Ryan, A., Wang, C. J., **Laurieri, N.**, Westwood, I. & Sim, E. (2010). Reaction mechanism of azoreductases suggests convergent evolution with quinone oxidoreductases. *Protein Cell* **1**, 780-90.

Ryan, A., Kaplan, E., Laurieri, N., Lowe, E. & Sim, E. (2011). Activation of nitrofurazone by azoreductases: multiple activities in one enzyme. *Sci. Rep.* **1**.

Rodrigues-Lima, F., Dairou, J., Laurieri, N., Busi, F. & Dupret, J. M. (2011). Fifth International Workshop on Arylamine *N*-Acetyltransferases. University Paris Diderot, Paris, France, 1-3 September 2010. *Pharmacogenomics* **12**, 1091-3.

Sim, E., Fakis, G., Laurieri, N. & Boukouvala, S. (2012). Arylamine N-Acetyltransferases - from drug metabolism and pharmacogenetics to identification of novel targets for pharmacological intervention. *Advances in Pharmacology*. (Review accepted).

Patent

"Ligands for arylamine *N*-acetyltransferases (NATs)", PCT Patent Application Number: PCT/GB2010/051840. Inventors: A. J. Russell, E. Sim, S. G. Davies, I. M. Westwood, A. Kawamura, **N. Laurieri**, M. J. C. Crawford.

Conference proceedings

RSC-SGC Chemical Biology for Drug Discovery, December 2009, Medical Sciences Teaching Centre, Oxford, (UK)

Poster: Small Molecule Colourimetric Probes for Specific Detection of Human Arylamine *N*-Acetyltransferase 1, a Potential Breast Cancer Biomarker

5th International Workshop on Arylamine *N*-acetyltransferases, September 2010, Paris, Université Paris Diderot, (France)

Talk: Optimisation of isoenzyme-specific reagents: organic synthesis and biological characterisation of naphthoquinones as selective inhibitors of human *N*-acetyltransferase 1 (hNAT1) and mouse Nat2 (mNat2)

Poster: Novel reduction mechanism of azo pro-drugs into anti-inflammatory arylamines by azoreductases from Pseudomonas aeruginosa.

Medical Science Division DPhil Day 2011, 12th July 2011

Talk: Colourimetric detection of human *N*-acetyltransferase 1, as a potential breast cancer biomarker

Scientific Symposium for Prof. Edith Sim Retirement, 16th-17th July 2011

Department of Pharmacology, University of Oxford, Oxford.

Talk: Detection of human *N*-acetyltransferase 1 - a potential breast cancer marker.

Abbreviations

4APY	4-aminopyridine
4AS	4-aminosalicylic acid
4AV	4-aminoveratrole
4BA	4-bromoaniline
4CA	4-chloroaniline
4IA	4-iodoaniline
5AS	5-aminosalicylic acid
AcCoA	acetyl coenzyme A
AcOH	Acetic acid
ANL	aniline
ANS	4-methoxyaniline
aq.	aqueous
BANAT	*Bacillus anthracis* NAT
BC	breast cancer
BLAST	Basic Local Alignment Search Tool
BOA	4-butoxyanline
CAPS	*N*-cyclohexyl-3-aminopropanesulfonic acid
CHES	*N*-cyclohexyl-2-aminoethanesulfonic acid
CoA	coenzyme A
D or *d*	deuterated
DBU	1,8-Diazabiciclo[5.4.0]undec-7-ene
DCIS	ductal carcinoma *in situ*
ddH_2O	double distilled water
DMAB	dimethylaminobenzaldehyde
DMSO	Dimethylsulfoxide
DNA	deoxyribonucleic acid
dNTP	Deoxyribonucleotidetriphosphate
DSF	differential scanning fluorimetry
DTNB	5,5'-dithio-bis(2-nitrobenzoic acid)
DTT	dithiothreitol
EBI	European Bioinformatics Institute
EDTA	Ethylenediaminetetraacetic acid
EGFR	Epidermal growth factor receptor
EOA	4-ethoxyaniline
ER	Oestrogen receptor
ER+ve/-ve	ER positive/negative
EtOH	Ethanol
E-value	expected value
FISH	fluorescent *in situ* hybridasation
GOLD	Genetic Optimization for Ligand Docking
HDZ	hydralazine
HEPES	4-(2-hydroxyethyl)-1-piperazineethane sulfonic acid
HER-2/neu	human epidermal growth factor receptor 2 from gene ERBB2
His-	hexahistidine-
HMO	Hückel molecular orbital
hNAT1	human NAT 1
hNAT2	human NAT 2
HOA	hexyloxyaniline
HOMO	highest occupied molecular orbital
HPLC	High-performance liquid chromatography
HTP	high throughput
IHC	immunohistochemistry
IMAC	immobilised metal affinity chromatography
INH	isoniazid or isonicotinylhydrazine
IPTG	isopropyl β-D-thiogalactopyranoside
LB	Luria-Bertani
LCIS	lobuar carcinoma *in situ*
LUMO	lowest unoccupied molecular orbital
MEC	molar extinction coefficient
MES	2-(*N*-morpholino)ethanesulfonic acid
miRNA	micro interfering RNA
MMNAT	*Mycobacterium marinum* NAT
mNat1	mouse NAT 1
mNat2	mouse NAT 2
MRI	magnetic resonance imaging
mRNA	messenger RNA
MSNAT	*Mycobacterium smegmatis* NAT
NADH	reduced nicotinamide adenine dinucleotide
NADPH	reduced nicotinamide adenine dinucleotide phosphate
NAT	*N*-aceyltransferase
nbs	number of binding sites
NCBI	National Center for Biotechnology Information
Ni-NTA	nickel-nitrilotriacetic acid
NMR	nuclear magnetic resonance
OD	optical density
pABA	para-aminobenzoic acid
pABAglu	para-aminobenzoyl glutamic acid
PANAT	*Pseudomonas aeruginosa* NAT
PBS	phosphate-buffered saline
PCR	polymerase chain reaction
PDB	Protein Data Bank
PEG	polyethylene glycol
PHZ	phenylhydrazine
PNPA	4-nitrophenyl acetate
POA	4-phenoxyaniline
PR	progesterone receptor
PR+ve	progesterone receptor
PRO	procainamide
qRT-PCR	quantitative real time PCR
RNA	ribonucleic acid
RNAi	interfering RNA
rpm	revolution per minute
RPMI	Roswell Park Memorial Institute
SAR	structure-activity relationship
SBTI	soybean trypsin inhibitor
SDS-PAGE	Sodium Dodecyl Sulfate-PolyAcrylamide Gel Electrophoresis
SERM	selective oestrogen receptor modulators
shNat	Syrian hamster NAT
siRNA	short interfering RNA
SMZ	sulfamethazine
SNP	single nucleotide polymorphism
SOC	Super Optimal broth with Catabolite repression
STNAT	*Salmonella typhimurium* NAT
TBNAT	*Mycobacterium tuberculosis* NAT
TBST	Tris-Buffered Saline and Tween 20
TCA	trichloroacetic acid
TEMED	Tetramethylethylenediamine
TNB	5-thio-2-nitrobenzoic acid
U	enzyme unit
USR	Ultrafast shape recognition
v/v	volume/volume
wt or WT	wild type
w/v	weight/volume
ε	molar extinction coefficient
ε_{CB}	ε of the conjugate base of the dye
ε_{N}	ε of the neutral dye

A crib sheet with the chemical structure of the NAT substrates and the NAT inhibitors used throughout this study is offered in a separate sheet for the examiners (**Appendix 3**).

Each chapter is introduced by paintings, prints and sculptures representing subjects with likely symptoms of breast cancer. All figures are in the public domain according to their respective owners (Wikipedia.org, Wikigallery.org, Wikimedia.org. Wikipaintings.com, nlm.nih.gov). Other internet sources of images are appropriately stated in the figure legend after validating copyright permission.

Table of Contents

CHAPTER I: INTRODUCTION 1

I.1 BREAST CANCER 2

I.1.1 Epidemiology 3

I.1.2 Molecular biology and genetics 6

I.1.3 Risk factors 8

I.1.4 Preventive screening and symptoms 9

I.1.5 Diagnosis 10

I.1.6 Treatments 11

I.1.6.1 Surgery 11

I.1.6.2 Radiation 11

I.1.6.3 Adjuvant therapy 12

I.1.6.3.1 Chemotherapy 13

I.1.6.3.2 Endocrine therapies 15

I.1.6.3.3 Biological therapies 21

I.1.7 Prognosis 24

I.1.8 Conclusion 26

I.2 ARYLAMINE *N*-ACETYLTRANSFERASES 27

I.2.1 Historical background 28

I.2.2 Human NATs 29

I.2.3 Eukaryotic NATs 32

I.2.4 Prokaryotic NATs 33

I.2.5 X-ray crystal structures 34

I.2.6 Catalytic mechanism 37

I.3 HUMAN NATS AND DISEASE 39

I.3.1 NAT polymorphism and its consequences 40

I.3.2 Relationship between hNAT1 and breast cancer 43

I.4 DRUG DISCOVERY 45

I.4.1 Known inhibitors of hNAT1 and mNat2 47

I.4.2 Discovery of novel inhibitors of hNAT1 by HTP screen 50

I.4.3 Lead inhibitors 51

I.4.3.1 Rhodanine 5 51
I.4.3.2 Naphthoquinone 1 53
I.4.3.2.1 Improvement via medicinal chemistry studies 56
I.4.3.2.2 Improvement via virtual shape recognition 58
I.5 CONCLUSIONS 61
I.6 AIMS 62
CHAPTER II: MATERIALS AND METHODS 63
II.1 MATERIALS 64
II.1.1 Chemicals and reagents 64
II.1.2 Growth media 64
II.1.3 Plasmids and bacterial strains 64
II.1.4 Antibodies 65
II.2 METHODS 67
II.2.1 Bioinformatic analyses 67
II.2.2 Molecular Biology 67
II.2.2.1 DNA purification 67
II.2.2.2 Determination of nucleotide quantity and quality 67
II.2.2.3 Polymerase chain reaction (PCR) 68
II.2.2.4 Site-directed mutagenesis 69
II.2.2.5 Plasmid transformation into *E. coli* strains 69
II.2.2.6 Selection of positively transformed colonies 70
II.2.2.7 DNA sequence analysis 70
II.2.2.8 Storage of nucleic acids and transformed *E. coli* cells 71
II.2.3 Gene expression and protein purification 71
II.2.3.1 Expression of wild-type and mutated *mNat2* genes 71
II.2.3.2 Cell lysis 72
II.2.3.3 Protein purification 72
II.2.3.4 Buffer exchange and protein concentration 73
II.2.4 Recombinant protein characterisation 73
II.2.4.1 Determination of protein concentrations 73
II.2.4.2 Determination of protein molecular weight 74
II.2.4.3 Determination of protein melting temperature 75
II.2.5 Enzymatic assays 76

II.2.5.1 Estimation of NAT activity 76
II.2.5.1.1 Determination of NAT activity following arylamine acetylation 77
II.2.5.1.2 Determination of NAT activity following AcCoA hydrolysis 78
II.2.5.1.3 Determination of NAT activity via NMR 79
II.2.5.2 NAT Substrate profile 79
II.2.5.2.1 Arylamine substrates 79
II.2.5.2.2 AcylCoA substrates 80
II.2.5.1 Estimation of folate-dependent AcylCoA hydrolysis activity by NAT 81
II.2.5.1.1 Determination of folate-dependent AcylCoA hydrolysis activity by NATs using DTNB 81
II.2.5.1.2 Determination of folate-dependent AcCoA hydrolysis activity by mNat2 via NMR 82
II.2.6 Inhibitor study 82
II.2.6.1 Enzymatic assays with inhibitors 82
II.2.6.1.1 Determination of NAT activity following arylamine acetylation 83
II.2.6.1.2 Determination of NAT activity following AcCoA hydrolysis 83
II.2.6.2 Determination of the mode of inhibition 83
II.2.6.3 Colourimetric properties of the inhibitors 83
II.2.6.3.1 Visual Colourimetric Observations 83
II.2.6.3.2 Spectrophotometry 84
II.2.6.3.3 Determination of pK_a values 84
II.2.6.3.4 Determination of molar extinction coefficients (ε) 85
II.2.6.3.5 Determination of the most acidic proton of compound 7 via NMR 86
II.2.6.3.6 Determination of the dissociation constant (K_d) and the number of binding sites of 7 to mNat2 86
II.2.7 Structural studies 87
II.2.7.1 Crystallisation of protein solution 87
II.2.7.1.1 Purification of mNa2 protein via size-exclusion gel filtration 87
II.2.7.1.2 Crystallisation trial of mNat2 with ligand 87
II.2.7.2 Structural study 88
II.2.7.2.1 Structural modelling 89
II.2.7.2.2 Structural docking 89
II.2.8 Eukaryotic and prokaryotic cell growth 90
II.2.8.1 Cell cultures 90
II.2.8.1.1 The human breast cancer ER+ve cell line ZR-75-1 90
II.2.8.1.2 The lymphoblastoid Raji cell line 91
II.2.8.1.3 The mouse leukaemic monocyte/macrophage Raw 264.7 cell line 91

II.2.8.1.4 Prokaryotic cells: E. coli JM 109 91
II.2.8.2 Estimation of native hNAT1 in ZR-75-1 cell lysates 92
II.2.8.2.1 Western blot 92
II.2.8.2.2 Dot blot 92
II.2.8.3 Effect of naphthoquinone 7 on cells 93
II.2.8.3.1 Cell penetration 93
II.2.8.3.2 Cytotoxicity 94

CHAPTER III: ISOENZYME SELECTIVITY OF NAPHTHOQUINONE 7 95

III.1 INTRODUCTION 96
III.2 RESULTS 98
III.2.1 Heterologous over-expression and purification of mNat2 98
III.2.2 Isoenzyme selectivity of naphthoquinone 7 102
III.2.3 Biochemical characterisation of mNat2-7 complex 106
III.2.3.1 Binding reversibility of compound 7 towards mNat2 106
III.2.3.2 Colourimetric properties of naphthoquinone 7 *versus* mNat2 protein folding 107
III.2.3.3 Mode of inhibition of compound 7 against mNat2 109
III.2.3.4 Determination of the dissociation constant (K_d) of the complex mNat2-7 111
III.3 DISCUSSION 119

CHAPTER IV: MOLECULAR MECHANISM OF THE COLOUR CHANGE EVENT 124

IV.1 INTRODUCTION 125
IV.2 RESULTS 130
IV.2.1 Colourimetric properties of naphthoquinones 1 and 7 130
IV.2.1.1 Spectrophotometric properties of 1 and 7 at different pHs 130
IV.2.1.2 Effect of a non-nucleophilic alkali on compound 7 133
IV.2.1.3 Oxidoreduction of naphthoquinones 1 and 7 135
IV.2.1.4 Weak acidity of sulfonamide-N*H* of naphthoquinone 7 139
IV.2.2 Colour change event of compound 7 upon binding to mNat2, as a model for hNAT1 146
IV.2.2.1 Investigating the possible role of Cys68 in the colour change event 150
IV.2.2.2 Investigating the possible role of Arg127 in the colour change event 153
IV.2.2.3 The importance of Phe125 and Tyr129 in inhibitor selectivity 163
IV.2.2.4 Screening mammalian NATs with inhibitor 7 169
IV.2.3 structural studies 170
IV.2.3.1 Crystal trials 170

IV.2.3.1 *In silico* docking of compound 7 within the active site of hNAT1 and mNat2 174

IV.3 DISCUSSION 182

CHAPTER V: SUBSTRATE SPECIFICITY OF MAMMALIAN NAT ISOENZYMES 189

V.1 INTRODUCTION 190

V.2 RESULTS 194

V.2.1 Arylamine substrate profiles of mNat2 mutants R127G and R127L 194

V.2.2 Modelling mNat1 based on the structure of hNAT2 195

V.2.3 AcylCoA substrate profiles of murine NATs 197

V.3 DISCUSSION 200

V.3.1 Arylamine substrate specificity of NAT isoenzymes 200

V.3.2 The use of different AcylCoAs by NATs 214

CHAPTER VI: APPLYING COMPOUND 7 FOR DETECTION AND TARGETING OF HNAT1 IN BREAST CANCER CELLS 218

VI.1 INTRODUCTION 219

VI.2 RESULTS 221

VI.2.1 Estimation of hNAT1 in ZR-75-1 cell line 221

VI.2.2 Inhibitor study on ZR-75-1 breast cancer cell line 226

VI.2.3 Effect of compound 7 on growing cell cultures 231

VI.2.3.1 Cellular intake of compound 7 231

VI.2.3.2 Effects of compound 7 on cell cultures 234

VI.3 DISCUSSION 239

CHAPTER VII: COLOUR CHEMISTRY AND STRUCTURE-ACTIVITY RELATIONSHIP OF HNAT1 INHIBITORS 242

VII.1 INTRODUCTION 243

VII.1.1 Glossary 243

VII.1.2 Colour chemistry 243

VII.1.1 Solvatochromism of naphthoquinone 7 250

VII.1.2 Ideal characteristics of selective hNAT1 biosensors 252

VII.1.3 Parallel chemical syntheses 253

VII.2 RESULTS 258

VII.2.1 Characterisation of analogues of 7 258
VII.2.2 Docking studies of compound 20 with hNAT1 266
VII.3 DISCUSSION 268
CHAPTER VIII: INVESTIGATING AROUND THE ENDOGENOUS ROLE OF HNAT1 274
VIII.1 INTRODUCTION 275
VIII.2 RESULTS 279
VIII.2.1 Single-time point activity assays 279
VIII.2.2 NMR real-time activity assay 284
VIII.2.3 Inhibitor study of mNat2 as folate-dependent AcCoA hydrolase 295
VIII.3 DISCUSSION 297
VIII.3.1 Selectivity of hNAT1 and mNat2 as AcCoA hydrolases in the presence of folate 297
VIII.3.2 Possible physiological significance of the AcCoA depletion by hNAT1 305
VIII.3.3 Potential association between hNAT1 and folate in treating cancer 306
CHAPTER IX: CONCLUSIONS AND FURTHER WORK 309
IX.1 FINAL CONCLUSIONS 310
IX.2 FURTHER WORK 314
IX.2.1 Biosensor development 314
IX.2.2 Drug development 316
IX.2.3 Investigation about hNAT1 endogenous role 317
REFERENCES 318
APPENDICES 360

List of Figures

Figure I.1: Breast morphology. 2

Figure I.2: Cancer incidence worldwide. 4

Figure I.3: Most commonly diagnosed cancers worldwide and their consequences. 5

Figure I.4: BC mortaliy and incidence in women worldwide. 6

Figure I.5: Chemical structures of steroid hormones. 15

Figure I.6: Mechanisms of action of different endocrine therapies used in BC treatment. 17

Figure I.7: ER-ligand interaction. 18

Figure I.8: Chemical structure of Fulvestrant. 21

Figure I.9: Scoring immmunochemistry for HER-2/neu. 23

Figure I.10: Chemical structure of Lapatinib. 23

Figure I.11: Examples of reactions catalysed by NAT enzymes. 27

Figure I.12: Genetic control of human NAT genes. 30

Figure I.13: Probe arylamine substrates for hNAT1 and hNAT2. 30

Figure I.14: Potential role of hNAT1 in folate degradation. 31

Figure I.15: Overall structure of hNAT1 and MMNAT. 35

Figure I.16: Multiple sequence alignment of selected NAT proteins. 36

Figure I.17: Structures of hNAT2, MMNAT and BANAT1, each with a molecule of CoA bound. 37

Figure I.18: Proposed catalytic mechanism of NAT reaction. 38

Figure I.19: Acetyl donors used in enzymatic investigations on NATs. 39

Figure I.20: Location of SNPs on human NATs. 41

Figure I.21: Metabolic pathway of aromatic and heterocyclic amine carcinogens. 42

Figure I.22: Overexpression of hNAT1 in BC. 44

Figure I.23: Drug discovery process. 47

Figure I.24: Mechanism of inhibition of human NAT enzymes by *N*-arylhydroxamic acids and nitrosoarenes. 48

Figure I.25: Small molecules identified as inhibitors of hNAT1. 48

Figure I.26: Lead compounds selected from HTP screenings. 50

Figure I.27: Chemical synthesis pathway of rhodanine 5. 51

Figure I.28: Biochemical evaluation of rhodanine 5 as inhibitor of mNat2 and hNAT1. 52

Figure I.29: inhibition of tumorigenic properties of MDA-MB-231 cells by Rhod-o-hp. 53

Figure I.30: Determination of the inhibition mode of naphthoquinone 1 to mNat2. 54

Figure I.31: Colourimetric properties of naphthoquinone 1. 55

Figure I.32: Colourimetric properties of compounds 1, 5-8. 57

Figure I.33: Ultrafast Shape Recognition (USR) algorithm. 59

Figure I.34: Comparison of USR query molecule 1 and the best three USR results. 60

Figure II.1: pET28b(+) vector map and key features. 66

Figure III.1: Spectral properties of 1 and 7 in the visible range. 96

Figure III.2: Growth curve of *E. coli* RosettaBlue(DE3)pLysS with pET28b(+) plasmid containing *mNat2*. 98

Figure III.3: Purification of recombinant mNat2. 99

Figure III.4: Enzymological characterisation of pure recombinant mNat2. 101

Figure III.5: Screening of different NATs with 1 and 7. 103

Figure III.6: Spectrometric screening of different NATs with 7. 104

Figure III.7: Spectrometric properties of 7 in the presence of hNAT1. 105

Figure III.8: Colourimetric properties of compounds 1 and 7 in the presence of pure recombinant mNat2. 105

Figure III.9: Reversible non-covalent binding of compound 7 to mNat2. 107

Figure III.10: Melting curve of mNat2 estimated using DSF. 108

Figure III.11: Interaction between 7 and both folded and unfolded mNat2. 109

Figure III.12: Kinetic analysis of mNat2 inhibition by compound 7. 110

Figure III.13: Standard curves of 7 as both red species and blue species at different concentrations. 113

Figure III.14: Spectral properties of 7 in the visible range. 114

Figure III.15: Preliminary assessment of K_d and nbs sites of 7 to mNat2. 116

Figure III.16: Standard curves of 7 as red species, blue species and as ligand to mNat2. 117

Figure III.17: Refined ssessment of K_d and nbs of compound 7 to mNat2 using corrected values of θ. 118

Figure III.18: Hypothesis about the colour change event involving compound 7 interacting with hNAT1. 120

Figure IV.1: Multiple sequence alignment of selected NAT proteins. 126

Figure IV.2: Active site of hNAT1. 126

Figure IV.3: Optical properties of compounds 1 and 7 at different pHs. 131

Figure IV.4: Weak acidity of compounds 1 and 7. 132

Figure IV.5: pH titration curves of naphthoquinones 1 and 7. 133

Figure IV.6: Chemical interaction between 7 and DBU, as non-nucleophilic base. 134

Figure IV.7: Optical properties of compounds 1 and 7 in the presence of different reducing agents. 136

Figure IV.8: Oxidoreduction mechanism of compounds 1 and 7 in the presence of DTT, as reducing agent, and O_2 as oxidising agent. 137

Figure IV.9: UV spectra of naphthoquinones 1 and 7 in the presence of DTT as reducing agent. 138

Figure IV.10: NMR analysis of 7 analogue with ^{15}N-labelled sulfonamide. 142

Figure IV.11: Comparison of chemical and optical properties of 7 *versus* *N*-methyl-7. 144

Figure IV.12: Optical properties of 7 and *N*-methyl-7. 145

Figure IV.13: Effect of compounds 7 and *N*-methyl-7 on mNat2 activity. 146

Figure IV.14: Active site of hNAT1. 148

Figure IV.15: Optical properties of 7 in the presence of different amino acids. 149
Figure IV.16: Colourimetric properties of 7 in the presence of NaSEt. 150
Figure IV.17: Optical properties of compound 7 with inactive mNat2 after treatment with iodoacetamide. 152
Figure IV.18: Multiple sequence alignment of wild-type *mNat2* gene and mutated *mNat2* genes. 154
Figure IV.19: Growth curves of *E. coli* cultures expressing mNat2 variants. 155
Figure IV.20: SDS-PAGE gels following purification of mNat2 variants *via* Ni-NTA affinity chromatography. 158
Figure IV.21: Thrombin cleavage of His-tag from recombinant mNat2 variants. 160
Figure IV.22: End-point NAT activity assays conducted with three mNat2 mutants over time. 161
Figure IV.23: IC_{50} curves of compound 7 as inhibitor of different mNat2 variants. 162
Figure IV.24: Visible spectra of compound 7 in the presence of different mNat2 variants. 163
Figure IV.25: Multiple sequence alignment of hNAT1, mNat2 and shNAT2 proteins. 165
Figure IV.26: IC_{50} curves of compound 7 as inhibitor of different mammalian NATs. 167
Figure IV.27: Visible spectra of compound 7 in the presence of different mammalian Nat variants. 168
Figure IV.28: Screening of different wt mammalian NATs and mNat2 mutants with compound 7. 169
Figure IV.29: SDS-PAGE gel of fractions obtained after purification of mNat2 *via* size-exclusion chromatography. 170
Figure IV.30: Purification of recombinant mNat2 *via* size-exclusion chromatography. 171
Figure IV.31: Size-exclusion chromatograms of impure recombinant mNat2 and two protein standards. 172
Figure IV.32: Illustrative pictures of interesting crystallization trials. 174
Figure IV.33: Overlay of hNAT1 template structure and corresponding structural mNat2 model. 176
Figure IV.34: Overall structures of hNAT1 and mNat2 with compound 7 docked. 177
Figure IV.35: Substrate binding pockets of hNAT1 and mNat2 with compound 7 docked. 179
Figure IV.36: Overall structures of mNat2 and shNat2 models overlaid. 181
Figure IV.37: Overall structures of two different models of shNat2. 181
Figure IV.38: Acid-base proton exchange between compound 7 and a base (B) at the origin of the colour change event. 182
Figure IV.39: Possible acid-base proton exchange between compound 7 and Arg127 of mNat2, generating the colour change 184
Figure IV.40: Possible acid-base proton exchange between compound 7 and hNAT1, generating the colour change event. 184
Figure IV.41: Substrate binding pockets of hNAT1 and mNat2 with compound 7 docked. 186
Figure IV.42: Schematic representation of compound 7 modelled in hNAT1 and mNat2 active sites. 187
Figure IV.43: Relationship between NAT key residues in substrate specificity and NAT inhibition by 7. 188
Figure V.1: Proposed pathway of cholesterol metabolism. 192
Figure V.2: Comparison of arylamine substrate specificities of mNat2, R127G, and R127L. 194

Figure V.3: Overlay of hNAT2 template structure and corresponding structural mNat1 models. 196
Figure V.4: Overlay of hNAT2 structure and mNat1 model. 197
Figure V.5: AcylCoA substrate profile of murine NATs. 198
Figure V.6: Specific activity of different NATs with two different AcylCoA as substrates. 199
Figure V.7: Multiple sequence alignment of human and murine NAT proteins. 200
Figure V.8: Comparison of the substrate specific activity profiles of hNAT1, mNat2, hNAT2, and mNat1. 201
Figure V.9: Zoomed view of the active sites of human NAT structures and murine NAT models. 203
Figure V.10: Overlay of mNat2 and mNat1 structural models. 203
Figure V.11: Comparison of the substrate profiles of mNat2, R127G, R127L and mNat1. 206
Figure V.12: Comparison of the substrate profiles of mNat2, shNat2, mNat2_F125S and mNat1. 207
Figure V.13: Zoomed view of the active sites of mammalian NAT models: mNat2 and shNat2. 208
Figure V.14: Comparison of specific activity profiles of NATs investigated in this study. 209
Figure V.16: Variation of NAT activity against arylamine substrate AlogP. 214
Figure V.17: Zoomed view of the active site pocket of four bacterial NAT structures. 216
Figure VI.1: Detection and quantification of hNAT1 in ZR-75-1 cell lysate. 222
Figure VI.2: Enzymological characterisation of native hNAT1 from BC cell lysate. 225
Figure VI.3: Enzymatic assays with hNAT1 in the presence of naphthoquinones 1 and 7. 227
Figure VI.4: Spectrophotometric study of compound 7 in ZR-75-1 cell lysates. 228
Figure VI.5: Cell pellet and colourless supernatant observed after centrifugation of Raji cells incubated with 7. 232
Figure VI.6: Schematic representation of the technique used to extract extracellular compound 7. 233
Figure VI.7: Experimental results on cellular intake of compound 7. 234
Figure VI.8: Effect of compound 7 on the breast cancer cell line ZR-75-11 235
Figure VI.9: Effect of compound 7 on other mammalian cell lines. 236
Figure VI.10: Overview of the results obtained from cell proliferation studies conducted with inhibitor 7. 237
Figure VI.11: Effect of compound 7 on the growth of *E. coli* JM109. 238
Figure VII.1: chemical structures of some common chromophores and auxochromes. 246
Figure VII.2: chemical synthesis of compound 7 as inhibitor of hNAT1 and mNat2. 249
Figure VII.3: Explanation of the colour change event of 7 according to the molecular orbitals theory. 249
Figure VII.4: Positive and negative solvatochromisms of a dye. 251
Figure VII.5: λ_{max} of compound 7 in the presence of organic, inorganic or biological reagents. 252
Figure VII.6: Hit compound 7 and substitution pattern of variation. 254
Figure VII.7: Representative examples of naphthoquinone analogue series. 256
Figure VII.8: Molecular structure of compounds 7, 10-12. 258
Figure VII.9: effect of compounds 7, 10-12 on mNat2, hNAT1 and hNAT2 activity. 259
Figure VII.10: Optical properties of 7, 10-12. 260

Figure VII.11: effect of compounds 7, 13, 16, 17 and 20 on mNat2, hNAT1 and hNAT2 activity. 262
Figure VII.12: Optical properties of 7, 13, 19, and 20. 265
Figure VII.13: Substrate binding pockets of hNAT1 with compounds 7 and 20 docked. 266
Figure VII.14: Inductive and mesomeric effects at the basis of the different weak acidity of some analogues of compound 7. 269
Figure VII.15: Delocalisation of the negative charge generated after deprotonating sulfonamide and amide analogues. 270
Figure VIII.1: Scheme of the methylation cycle of folate and homocysteine metabolism proposing an endogenous role for hNAT1 and mNat2..... 276
Figure VIII.2: AcCoA hydrolysis activity of hNAT1 in the presence of folic acid in the assay. 277
Figure VIII.3: Standard curves of detectable reagents in assays with NATs. 280
Figure VIII.4: AcCoA hydrolysis by mNat2 in the presence of folic acid alone in the assay. 282
Figure VIII.5: Screen of mammalian and bacterial NATs as AcCoA hydrolases in the presence of folate. 283
Figure VIII.6: Initial linear activities of mNat2, as AcCoA hydrolase in the presence of varying concentrations of folate. 284
Figure VIII.7: Two hypotheses for the catalytic AcCoA hydrolysis reaction by mNat2 in the presence of folate. 285
Figure VIII.8: Structures and proton NMR spectra of AcCoA and CoA..... 287
Figure VIII.9: NMR spectra of reagents and possible products present in an AcCoA hydrolysis assay with mNat2. 288
Figure VIII.10: Real-time ^{1}H-NMR analysis of mNat2 activity with pABA as arylamine substrate in PBS-D_2O..... 289
Figure VIII.11: Real-time ^{1}H-NMR analysis of mNat2 activity as folate-dependent AcCoA hydrolase performed in PBS-D_2O. 290
Figure VIII.12: Enzymatic reaction progress curves of folate-dependent AcCoA hydrolytic activity by mNat2. 292
Figure VIII.13: Comparison of the integration of characteristic peaks of both substrate and products *versus* 6*d*-DMSO, as internal standard..... 293
Figure VIII.14: Reaction progress curves of mNat2 activity as AcCoA hydrolase in the presence of folate, estimated using ^{1}H-NMR after correction. 294
Figure VIII.15: Screening of different enzymatic assays with mNat2 in the presence of inhibitors 1 and 7. 295
Figure VIII.16: IC_{50} curve of compound 7 as inhibitor of folate-dependent AcCoA hydrolytic activity by mNat2... 296
Figure VIII.17: Comparison of pK_a values of folate and aniline. 298
Figure VIII.18: Structures of folic acid and amethopterin..... 301
Figure VIII.19: Overall structure of hNAT2 and MMNAT, both with CoA bound. 303
Figure VIII.20: Third domain of two human NAT enzymes. 304
Figure VIII.21: The Krebs cycle. 305
Figure IX.1: Possible compounds to be synthesised in order to improve colour intensity. 315
Figure IX.2: Chemical structure of *β*-carotene. 316

List of Tables

Table I.1: Genes associated with BC susceptibility. 7

Table I.2: Reproductive factors influencing BC risk. 8

Table I.3: Non-reproductive lifestyle factors increasing BC risk. 9

Table I.4: Main tumour stages in BC. 10

Table I.5: Biomarkers used in BC diagnosis and treatment. 11

Table I.7: Most common chemotherapeutic drugs used in BC treatment. 14

Table I.6: Combinations of chemotherapeutics. 15

Table I.8: Quick (Allred) scoring for IHC assessment of ERs and PRs. 16

Table I.9: Front-line SERM therapies used in BC treatment. 19

Table I.10: Chemical drugs used to inhibit the aromatase enzyme. 20

Table I.11: HER-2/neu testing techniques 22

Table I.12: HER-2/neu grading system. 23

Table I.13: Review of major molecular prognostic factors studied in BC. 25

Table I.14: Summary of key findings supporting the functional homology between mNat2 and hNAT1. 33

Table I.15: Summary of known crystal structures of NATs by X-ray. 34

Table I.16: IC_{50} values of both steroidogenic compounds and xenobiotic oestrogens against mNat2. 49

Table I.17: Comparison of inhibitory activity of comound 1 towards human and mouse NATs. 54

Table I.18: Preparation and pharmacological characterisation of a set of analogues of 1. 56

Table I.19: Colour change of 1, 5-8 with aq. NaOH or mNat2 (2 eq.). 57

Table I.20: Properties of compound 9 as biosensor to detect mNat2. 58

Table II.1: Growth media used throughout this study. 64

Table II.2: *E. coli* strains used throughout the study presented in this thesis. 65

Table II.3: DNA primers used for PCR amplification. 68

Table II.4: Typical PCR amplification mixture. 68

Table II.5: Primers used for site-directed mutagenesis study. 69

Table II.6: Sample requirements for DNA sequence analysis. 71

Table II.7: Concentration of pure recombinant mNat2 protein stocks. 73

Table II.8: ε_{280} and theoretical molecular masses of recombinant mNat2 mutants 74

Table II.9: Buffered solutions used for titrating the inhibitors. 85

Table II.10: Conditions screened in the crystallisation trials. 88

Table III.1: Activity and recovery of recombinant mNat2 expressed in *E. coli*. 100

Table III.2: Apparent kinetic constants determined for mNat2. 102

Table III.3: Percentage activity inhibition of different NAT enzymes in the presence of 1 and 7. 104

Table III.4: Biochemical parameters from titration of mNat2 with increasing amounts of 7. 115

Table III.5: Effect of compounds 1 and 7 on different NAT enzymes. 120

Table III.6: Comparison of amino acid sequences and substrate specificities of human and mouse NAT isoenzymes. 121

Table IV.1: UV-vis properties of compounds 1 and 7 in the presence of different chemical reagents. 139

Table IV.2: pK_a values of non-proteogenic amino acids. 148

Table IV.3: Primers used for site-directed mutagenesis PCR reaction. 153

Table IV.4: Purification of mNat2 variants using Ni-NTA affinity chromatography. 158

Table IV.5: Conditions screened in crystallisation trials. 173

Table IV.6: Parameters estimating the general quality of mNat2 model. 175

Table IV.7: Residues from unreliable regions in murine NAT models. 176

Table IV.8: Parameters estimating general quality of shNat2 model 180

Table IV.9: Summary of the effects of 7 on different mammalian NATs. 186

Table V.1: Parameters estimating general quality of mNat1 model. 195

Table V.2: Residues of the unreliable regions in murine NAT models. 196

Table V.3: Comparison of arylamine substrate profiles of different mammalian NATs in relation to the physicochemical properties of the substrates tested. 211

Table V.4: Comparison of acetyl transfer and *n*-propionyl transfer activities by NATs. 215

Table VI.1: Different estimations of the amount of hNAT1 in ZR-75-1 cell lysates. 223

Table VI.2: Prediction for optimal affinity and colour intensity of the ligand. 230

Table VII.1: Colourimetric characterisation of compounds 7, 10-12. 258

Table VII.2: Structural substitution around the naphthoquinone core. 261

Table VII.3: IC_{50} values for 7, 13-20 against mNat2 and hNAT1. 261

Table VII.4: Colourimetric data for compounds 7, 13-20. 264

Table VII.5: Colourimetric data for compounds 7, 13-20, interacting with mNat2. 272

Table VIII.1: Detection of reagents involved in NAT assays. 280

Table VIII.2: Estimates of folate-dependet AcCoA hydrolysis by mNat2. 294

Table VIII.3: Apparent kinetic constants determined for mNat2 and hNAT1. 300

Table VIII.4: Summary of inhibition studies conducted on NATs with folate analogues. 302

List of Equations

Equation II.1: Estimation of [$7_{unbound}$] from OD at 514nm. 87

Equation III.1: Equation for the Bi-Bi Ping-Pong mechanism. 102

Equation III.2: Dissociation reaction of the complex mNat2-7. 111

Equation III.3: Definition of K_d constant. 111

Equation III.4: Definition of θ and K_d in the dissociation equilibrium of the complex mNat2-7. 111

Equation III.5: Mathematical relationship between [$7_{unbound}$] and OD red at 514nm, ... 112

Equation III.6: Estimation of [$7_{unbound}$] following reading the OD of the assay at 514nm. 112

Equation III.7: Michaelis-Menten equation. 115

Equation III.8: Hughes-Klotz equation. 115

Equation III.9: Scatchard equation. 115

Equation VI.2: Definition of K_d constant. 229

List of Schemes

Scheme II.1: NAT activity determined by detection of arylamine acetylation using DMAB. 77

Scheme II.2: NAT activity determined by detection of CoA formation using DTNB. 78

Scheme IV.1: Hypothesised mechanisms for colour change of 7 within the hNAT1 active site. 127

Scheme IV.2: Chemical synthesis of compound 7 analogue with an ^{15}N-labelled sulfonamide. 140

Scheme IV.3: Chemical synthesis of *N*-methyl-7. 143

Chapter I:

Introduction



THEODORIC DE LUCEA (ITALY, 1205-1248) PERFORMING SURGICAL DRAINING OF AN ABSCESS (MIDDLE AGES).

His surgical technique advocated scrupulous cleanliness and the healing of most surgical wounds by granulation without sutures.
(www.imageofsurgery.com/surgery_history_art.htm).

I.1 Breast cancer

Breast cancer (BC), also called malignant breast neoplasm, is a disease characterised by the growth of malignant cells in the mammary glands, mainly lining the milk ducts or in the lobules which provide the ducts with milk (**Figure I.1**).

The process of breast tumorigenesis seems to result from 'benign to malignant' progression wherein the accumulation of multiple genetic mutations allows evolution from normal breast epithelium to different subtypes of abnormal conditions: benign proliferative lesions, atypical proliferative lesions, carcinoma *in situ* or invasive tumours.

If the cancer is diagnosed along milk ducts is called ductal carcinoma, whereas it is named lobular carcinoma if it is discovered in the lobules.

Moreover, the lesions associated with the greatest risk of invasive BC are hyperplasia of usual type, atypical ductal hyperplasia, ductal carcinoma *in situ* (DCIS) and lobular carcinoma *in situ* (LCIS) (Allred et al, 2001).

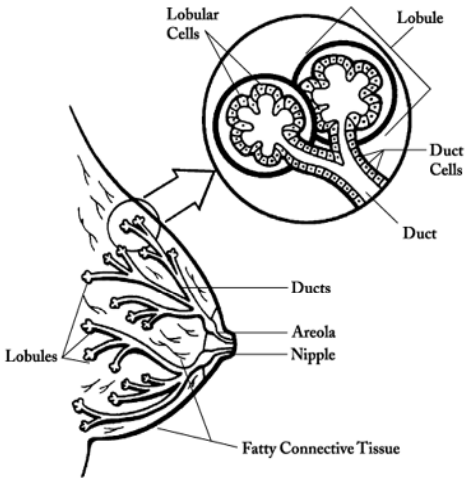


Figure I.1: Breast morphology.

Breast tissue is broadly divided into two regions: a glandular region and a fatty region. The glandular region is composed of structures called 'lobules' and these lobules connect to the nipple *via* tube like structures called 'ducts'. The figure is adapted from the website http://www.cancer.org/Healthy/FindCancerEarly/WomensHealth/Non-CancerousBreastConditions/non-cancerous-breast-conditions.

I.1.1 Epidemiology

The international Agency for Research on Cancer and the World Health Organisation have recently described the variation in cancer incidence and mortality in the world (Ferlay et al, 2010) (**Figure I.2**). According to this report, out of an estimated world population of 6.75 billion people in 2008, approximately 12.66 million people have been diagnosed with malignant tumours, excluding non-melanoma skin cancer (Ferlay et al, 2010). Cancer is estimated to account for about 14% of all deaths worldwide in 2008 (Curado M. P. et al, 2008; Ferlay et al, 2010), with different distributions across the regions of the world, from 5% in Africa to 21 % in the Western Pacific region.

BC is certainly the most widespread cancer diagnosed in women worldwide and, considering both sexes, ranks second overall (10.9%) after lung cancer (Curado M. P. et al, 2008) (**Figure I.3**).

An increasing number of BC cases has been observed in most countries worldwide over the last decades, mainly in economically developed countries (Glass et al, 2007; Hery et al, 2008): this has been partly attributed to a modern lifestyle, environmental and socio-economic factors (Jemal et al, 2011) (**Figure I.4**). Also in the UK, BC is the most common cancer in women (31% in 2008) ahead of lung cancer (19% in 2008) (Cancer-Reserch-UK, 2011).

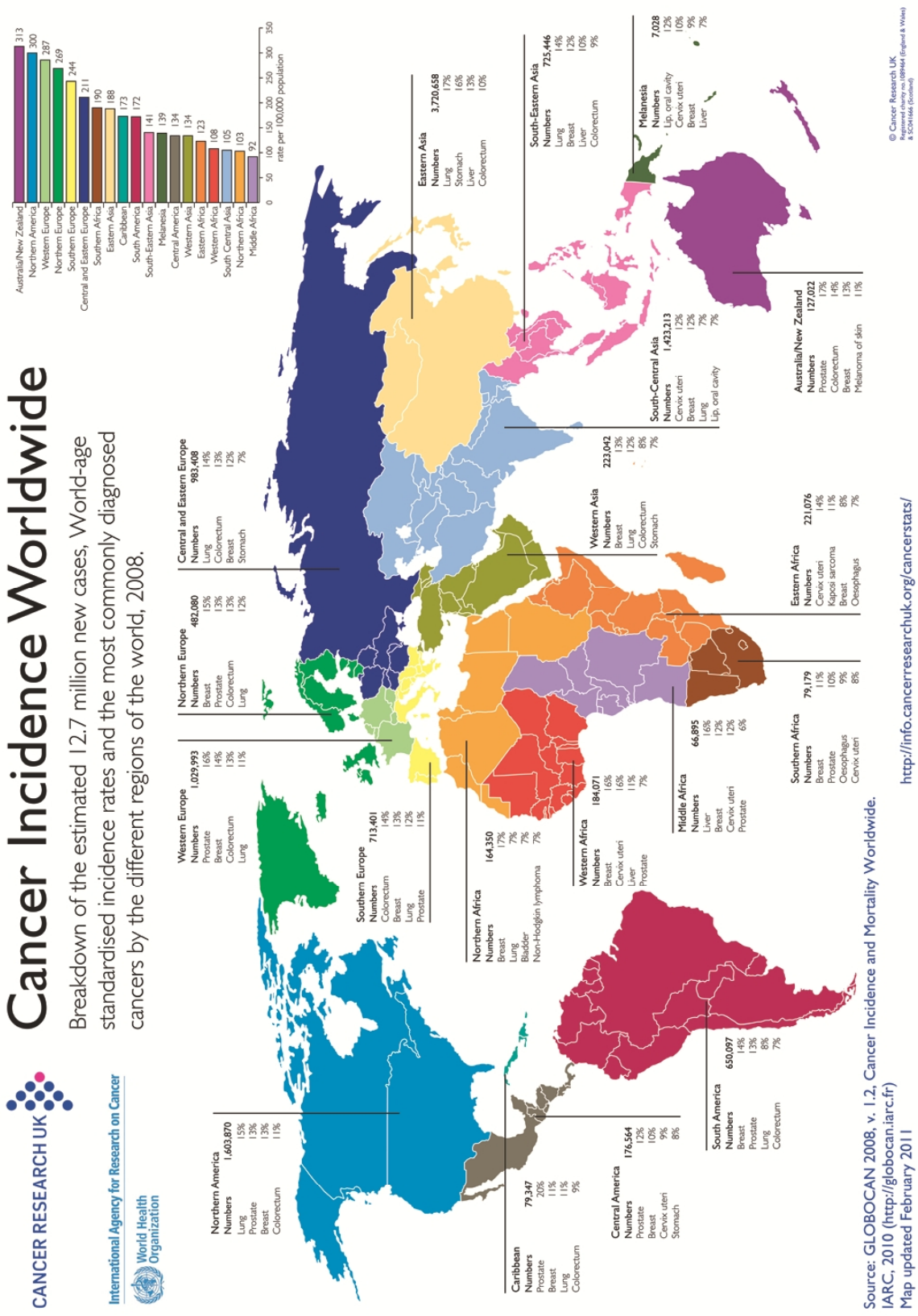


Figure I.2: Cancer incidence worldwide.

From info.cancerresearchuk.org/cancerstats/world/the-global-picture/ after (Ferlay et al, 2010).

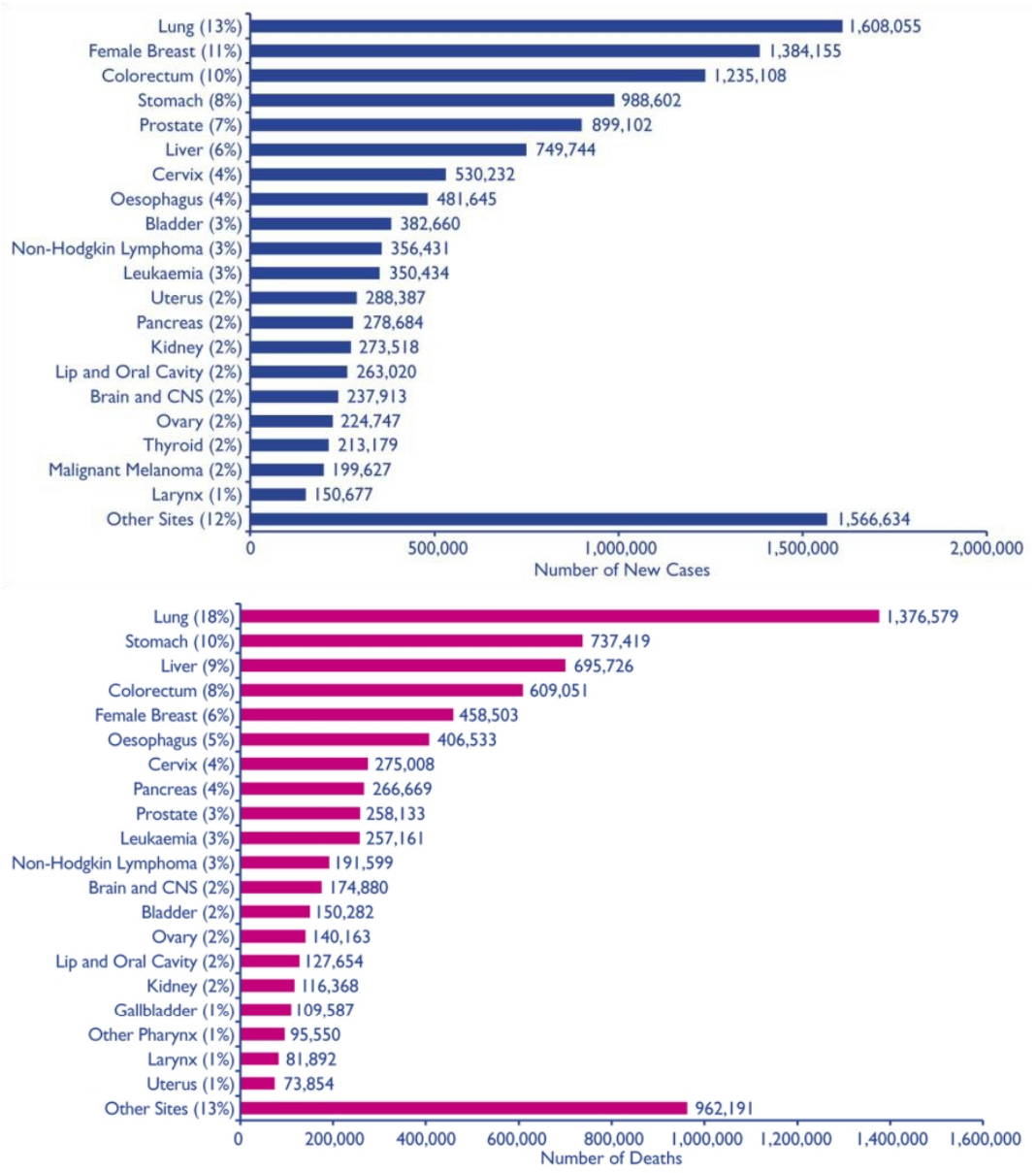


Figure I.3: Most commonly diagnosed cancers worldwide and their consequences.

(top) the 20 Most Commonly Diagnosed Cancers Worldwide, 2008 Estimates. **(bottom)** the 20 Most Common Causes of Death from Cancer Worldwide, 2008 Estimates. The figure is adapted from http://info.cancerresearchuk.org/cancerstats/world/the-global-picture/ after (Ferlay et al, 2010).

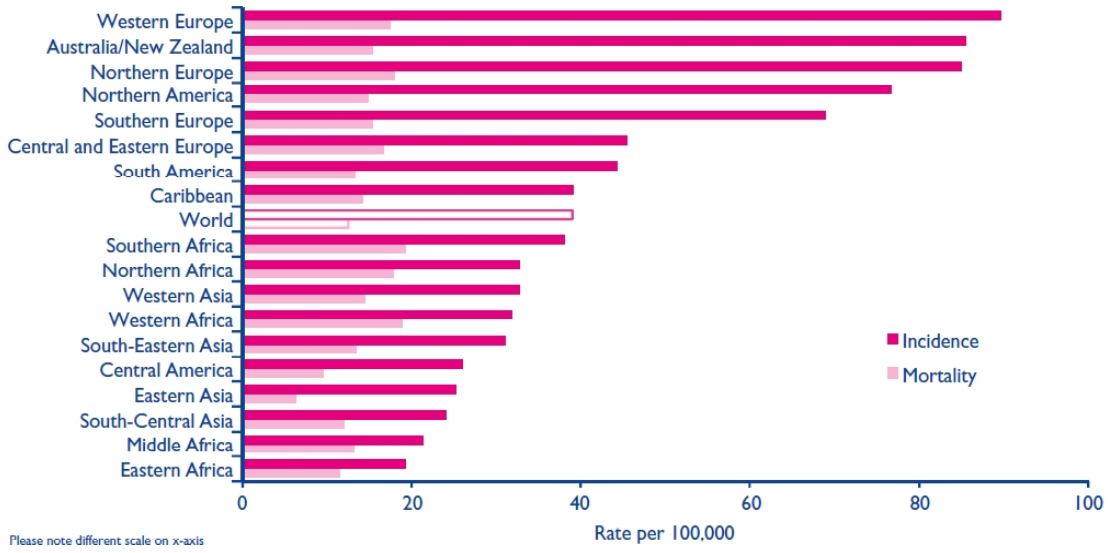


Figure I.4: BC mortaliy and incidence in women worldwide.

World Age-Standardised Incidence and Mortality Rates, Regions of the World, 2008 Estimates. The figure is adapted from http://info.cancerresearchuk.org/cancerstats/world/the-global-picture/ after (Ferlay et al, 2010)

I.1.2 Molecular biology and genetics

As for other cancers, BC results from an interaction between the environment and defective genes. BC is fundamentally caused by the accumulation of multiple genetic abnormalities in breast epithelial cells. These mutations can be inherited or somatic, which means that they are accumulated during a woman's lifetime.

In order to identify some 'high-risk' genes contributing to BC susceptibility, an intense research into the genetic basis of familial BC led to the discovery of *BRCA1* (17q) and *BRCA2* (13q) genes in the 1990s (Miki et al, 1994; Wooster et al, 1995), which are tumour suppressor genes. The protein products are involved in a multitude of pivotal cellular processes: in particular, they contribute to DNA repair and transcriptional regulation in response to DNA damage (Yoshida & Miki, 2004).

Women with deleterious mutations in the *BRCA* genes have a 45-65% risk of developing BC by the age of 70 (Antoniou, 2003), and these abnormalities appear to account for

approximately 90-95% of familial BC cases (Ross et al, 2003). However, these mutations constitute only 2-3% of all BCs, and represent less than 20% of the inherited genetic component of the risk (Antoniou & Easton, 2006).

Other genes have been associated with susceptibility to BC, together with other common cancers (Ross et al, 2003) (**Table I.1**).

Table I.1: Genes associated with BC susceptibility.

The table is adapted from (Ross et al, 2003).

Gene	Location	Familial breast cancer association	Sporadic breast cancer association	Other cancers
BRCA1	17q	High (40%)	High	Ovary (colon, prostate)
BRCA2	13q	High (40%)	High	No ovary, male breast (prostate)
p53	17p	Low	High	Carcinomas, sarcomas, leukemias
RAS (HRAS)	11p	Low in young, higher in old	High in old	Carcinomas, sarcomas, leukemias
Ataxia telangectasia	11q	Low	Low	Lymphomas, leukemias
hMSH2 *hMLH1* (lynch II)	2p 3p	Low	Low	Colon, skin, stomach
Neurofibromatosis 1	17q	Very low	Low	Nerve, brain
Androgen receptor	Xq	Only males, low	Only males	Male breast

As regards acquired somatic mutations, they are responsible for approximately 90% of BCs (Teschendorff & Caldas, 2009). However, only one somatic abnormality and incorrect amplification of the gene human epidermal growth factor receptor 2 (*HER2/neu*) is currently used to define a clinical subtype, accounting for approximately 18-20% of BC cases (Slamon et al, 1987).

In recent years, a number of mutational profiling studies have further identified clinically relevant mutations in genes encoding for growth factors and receptors, intracellular signalling molecules, cell cycle regulators, apoptosis regulators and adhesion molecules (Bieche & Lidereau, 2011).

Generally, the mutational genetic landscape of BC is largely complex because of the surprising richness of low-frequency mutants in contrast with the relative rarity of high-frequency cases leading to a tumour (Teschendorff & Caldas, 2009).

I.1.3 Risk factors

Different risk factors have widely been investigated in relation to BC development.

After gender, BC risk is strongly related to age with 81% of cases occurring in women aged 50 years and over.

Whilst few cases of BC occur in women aged less than 20 years, almost half of cases are diagnosed in women aged between 50 and 69 years (Cancer-Reserch-UK, 2011; Sasieni et al, 2011).

Another important factor is the personal life style of a woman which highly influences the risk of BC with many aspects relating to her reproductive history (**Table I.2**).

Table I.2: Reproductive factors influencing BC risk.

+ stands for increased risk, whilst - stands for diminished risk to develop BC.

Factor	Risk	References
early age of menarche	+	(Garcia-Closas et al, 2006)
childbearing	-	(Beral et al, 2002; Ewertz et al, 1990; Ma et al, 2006)
breastfeeding	-	(Beral et al, 2002)
late menopause	+	(Beral & al., 1997)

Higher levels of endogenous and exogenous oestrogen hormones are also associated with increased BC risk (Yager & Davidson, 2006). In particular, the intake of oral contraceptives (Collaborative-Group-on-Hormonal-Factors-in-Breast-Cancer, 1996) and drugs from hormone replacement therapy during menopause (Million-Women-Study-Collaborators, 2003) moderately increase the risk of BC.

An additional risk factor is the presence of close relatives affected by BC in the family (Beral et al, 2001; Pharoah et al, 1997).

As in many other forms of cancers, lifestyle factors may influence the incidence of BC, as summarised in **Table I.3**: most of these factors indirectly have an effect on the endogenous metabolic levels of hormones.

Table I.3: Non-reproductive lifestyle factors increasing BC risk.

+ stands for positive association, ND = not determined.

Factor	References	Association to hormone levels
high body weight	(Reeves et al, 2007)	+ (Deapen et al, 2002)
high-fat diet	(Bingham et al, 2003; Blackburn & Wang, 2007; Boyd et al, 2003)	+ (Velentzis et al, 2009)
low physical activity	(Monninkhof et al, 2007)	+ (Chan et al, 2007)
high alcohol consumption	(Baan et al, 2007)	+ (Rinaldi et al, 2006)
shift work	(Megdal et al, 2005)	+ (Schernhammer & Hankinson, 2005)
radiation exposure	(Feig & Hendrick, 1997; John et al, 2007)	ND
high tobacco smoking	(Xue et al, 2011)	ND

I.1.4 Preventive screening and symptoms

An early diagnosis of BC is assumed to improve clinical outcome. Therefore, a number of screening tests are used to examine healthy women for BC in an attempt to achieve an earlier diagnosis: clinical and self breast palpation, mammography, magnetic resonance imaging and ultrasound (Beers & Merck Research Laboratories., 2006).

Different symptoms of BC have been reported, including a lump feeling different from the rest of the breast tissue, change in breast size or shape, altered skin texture, nipple inversion and breast pain, called mastodynia (Beers & Merck Research Laboratories., 2006). **Table I.4** summarises the criteria relating to each stage of BC.

Table I.4: Main tumour stages in BC.

Adapted from: http://info.cancerresearchuk.org/cancerstats/types/breast/symptomsandtreatment.

Stage	Criteria
I	tumour size up to 2cm no lymph nodes affected no evidence of spread beyond the breast
II	tumour size between 2cm and 5 cm lymph nodes in armpit affected no evidence of spread beyond armpit
III	tumour size more than 5cm lymph nodes in armpit affected no evidence of spread beyond armpit
IV	tumour of any size lymph nodes in armpit often affected cancer has spread to other parts of the body

I.1.5 Diagnosis

The results of non-invasive examinations, such as mammography, ultrasound or magnetic resonance imgaging (MRI), are frequently adequate to detect BC.

However, only a biopsy of the suspected tissue can give a definitive diagnostic and define the more suitable curative therapies (Assersohn et al, 2002; Dunmire et al, 2002; King et al, 1983).

The analysis of the biopsy sample usually allows the identification of tumour-specific biomarkers. These results, combined with information about tumour size, differentiation grade, lympho-vascular invasion and nodal stage subsequently help predict response to therapy, guide treatment planning and categorise patients into different prognostic groups.

The most common biomarkers used to classify the diagnosed BC are listed in **Table I.5**. They also play the role of drug targets in clinical therapies. The description of these biomarkers is detailed in **Section I.1.6.3**.

Table I.5: Biomarkers used in BC diagnosis and treatment.

Abbreviation	Full-length name
ER	oestrogen receptor
PR	progesterone receptor
HER-2/neu or ErbB-2	human epidermal growth factor receptor 2

I.1.6 Treatments

BC is a heterogeneous disease and different treatments including surgery, radiation and pharmacological therapy are administrated with increasing aggressiveness according to prognostic and predictive factors.

I.1.6.1 Surgery

Surgery involves the physical removal of the cancerous tissue, sometimes together with the surrounding normal tissue. The region to be excised is mainly evaluated following mammograms, MRI and ultrasounds. Standard surgeries can remove the whole breast (mastectomy) or a part of it (quadrantectomy or lumpectomy).

I.1.6.2 Radiation

Radiotherapy to the breast is a routine adjuvant treatment after breast surgery and is administered to the region of the tumour bed and local lymph nodes in order to destroy other possible minor remaining cancer cells. Radiotherapy works by damaging the DNA of exposed tissue in order to control cell growth using high-energy particles, charged molecules or photons.

This energy can also damage healthy cells, which does not help the therapeutic purpose of the treatment and can increase side effects, together with the probability of secondary

cancer induction (Curtis, 2006). However, intraoperative radiotherapy can help impair BC cell proliferation and motility caused by surgical wounding (Belletti et al, 2008; Vaidya et al, 2006). In general, radiation can reduce the risk of recurrence by 50% up to 70%.

I.1.6.3 Adjuvant therapy

Chemotherapeutic drugs are also used after surgery or in addition to radiation as adjuvant therapies in order to reduce the risk of cancer recurrences or the spread of the cancer throughout the body.

The risk of subsequent recurrences or death is increased in association to certain factors, such as the growing size of the primary cancer, the high histological grade and the presence of tumour in the axillary nodes.

Historically, the frontline chemotherapy has related to the use of cytotoxic drugs to destroy cancer cells by interrupting cancer cell growth *via* different mechanism of actions. The rationale of these therapies lies in the fact that cancerous cells replicate indefinitely and faster than normal cells (Franks & Teich, 1997).

The systemic administration of these therapies allows the treatment of cancers located in different organs, but also the disruption of the growth of normal cells, in particular fast growing cells, which constitutes the main cause of most common side effects (Airley, 2009).

Afterwards, the development of targeted therapies against specific BC biomarkers, such as ER, PR, and HER-2/neu, has helped treat BC invasiveness and aggressiveness more selectively according to the results obtained after biopsy analyses.

I.1.6.3.1 Chemotherapy

A summary of the major chemotherapeutic drugs used nowadays to treat BC, together with their mechanism of action and the side effects, is shown in **Table I.6**.

The antimitotic and cytotoxic activity of most of the chemotherapeutic drugs is the result of the inhibition of DNA synthesis, cellular replication and protein biosynthesis *via* different mechanisms.

The alkylating agents act by modifying DNA bases, thereby preventing DNA biosynthesis and RNA transcription from the affected DNA, or by forming cross-links within the DNA or by inducing mispairing of the nucleotides leading to mutations.

The inhibitors of topoisomerase II, DNA helicase and thymidylate synthetase enzymes disrupt the correct DNA biosynthesis, which leads to cell death.

Chemotherapeutics also affect the non-cancerous fast-dividing cells of the body, thereby causing side effects on different tissues, mainly blood cells and epithelial cells from skin, mouth, stomach, and intestines.

Chemotherapeutic treatments can be given to patients before surgery to diminish tumour size (neoadjuvant therapy), after surgery to limit the possibilities of the cancer spreading or recurrences (adjuvant therapy), or as treatment after recurrence.

The use of chemotherapy is predominant in diseases at stages 2-4, being particularly beneficial in BCs which do not present abnormal overexpression of ER, PR or HER-2/neu, commonly called triple negative cancers (Vaklavas & Forero-Torres, 2011).

Chemotherapies are usually administrated in combinations of 2 or 3 drugs for a period of 3-6 months and can also be associated with radiotherapy (**Table I.7**).

Table I.6: Most common chemotherapeutic drugs used in BC treatment.

The pharmacological information about the following drugs are taken from DrugBank (Wishart et al, 2008).

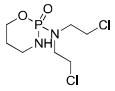
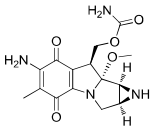
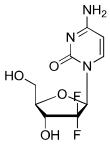
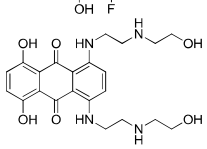
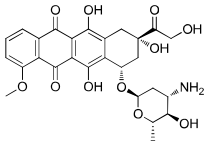
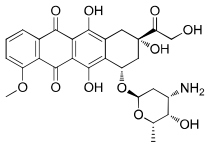
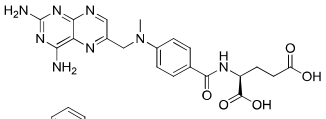
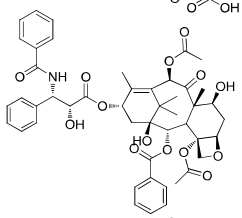
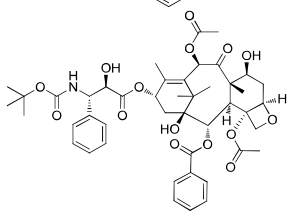
Drug	Chemical structure	Origin	Mechanism of action
Cyclophosphamide		organic	Alkylating agent to DNA.
Mitomycin		from *Streptomyces caespitosus*	Alkylating agent.
Fluorouracil		organic	Inhibitor of thymidylate synthase and interfering agent in RNA processing.
Gemcitabine		organic	Inhibitor of thymidylate synthetase, and inhibitor of ribonucleotide reductase *via* its metabolite Gemcitabine diphosphate.
Mitoxantrone		organic	Intercalating agent to DNA and inhibitor of topoisomerase II.
Doxorubicin		from *Streptomyces peucetius*	Intercalating agent to DNA and inhibitor of toposiomerase II.
Epirubicin		organic	Intercalating agent to DNA and inhibitor of topoisomerase II activity.
Methotrexate		organic	Inhibitor of folic acid reductase.
Paclitaxel		from *Taxus brevifolia*	Interfering agent to microtubule growth.
Docetaxel		semi-synthetic	Interfering agent to microtubule growth.

Table I.7: Combinations of chemotherapeutics.

Multiple chemotherapeutic agents may be used in combination to treat patients with BC.

Acronym	Drugs
CMF	cyclophosphamide, methotrexate and fluorouracil
FEC	epirubicin, cyclophosphamide and fluorouracil
FECT	epirubicin, cyclophosphamide, fluorouracil and taxotere (docetaxel)
ECMF	epirubicin followed by CMF
AC	doxorubicin (adriamycin) and cyclophosphamide
EC	epirubicin and cyclophosphamide
MMM	methotrexate, mitoxantrone and mitomycin
MM	methotrexate and mitoxantrone

I.1.6.3.2 Endocrine therapies

Steroid hormones, such as oestrogens and progesterone (**Figure I.5**), have long been established to play a role in human mammary gland development (Laron et al, 1989) (Humphreys et al, 1997).

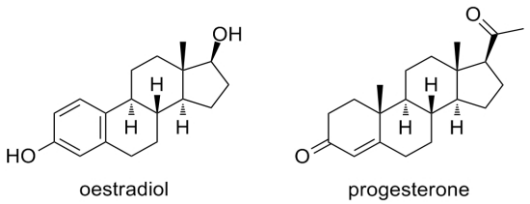


Figure I.5: Chemical structures of steroid hormones.

There are two receptors for oestradiol, ERα and ERβ (Nilsson et al, 2001), and also progesterone has two candidate receptors, PRA and PRB (Anderson, 2002). They are all members of the steroid-thyroid hormone nuclear receptor superfamily, and they work as ligand-dependent nuclear transcription factors.

The relationship between ERs, PRs and proliferation in tumorigenesis has long been investigated (Key & Pike, 1988), in particular, increased expression and the deregulation of ERs (Allred et al, 2001; Anderson, 2002; Lawson et al, 1999) and/or PRs (Mote et al, 2002) contribute significantly to BC formation and development, with PR expression

being thought to indicate a functioning ER pathway (Horwitz et al, 1978).

Whilst up to two-thirds of women aged less than 50 years will have ER positive (ER+ve) BC and around 80% of all cancer tumours in women over 50 years are ER+ve (Payne et al, 2008), around 60% of invasive breast carcinomas overexpress PRA and/or PRB.

The standard methodology used for assessment of hormone receptors status is based on immunohistochemistry (IHC) and can be applied to both core biopsy and surgical excision (Harvey et al, 1999) (**Table I.8**).

The levels of ER and PR immunoreactivity of each individual tumour allow an adequate endocrine therapy to be estalished. Nevertheless, the IHC assay, being a semiquantitative test, is highly sensitive to technical problems and sometimes may lead to false-negative tests in borderline cases (Payne et al, 2008).

Table I.8: Quick (Allred) scoring for IHC assessment of ERs and PRs.

The quick (Allred) score is conventionally used to associate the intensity of immunoreactivity to ER and PR status and also ensures standardisation between laboratories (Harvey et al, 1999).

Proportion reactive	Score
No reactivity	0
<1% nuclei reactive	1
1-10% nuclei reactive	2
11-33% nuclei reactive	3
34-66% nuclei reactive	4
67-100% nuclei reactive	5

The inhibition of the activity of ER receptors has long constituted the basis of endocrine therapy and forms the mainstay of the adjuvant BC therapy (Beers & Merck Research Laboratories., 2006).

Endocrine therapies act according to different mechanisms of action: the therapy can modulate ER activity using selective oestrogen receptor modulators (SERMs), lower the systemic levels of oestrogens *via* aromatase inhibitors, or modulate both ER activity and

protein expression levels (Fulvestrant) (**Figure I.6**).

A reduction of the systemic levels of oestrogens could also be achieved with an oophorectomy.

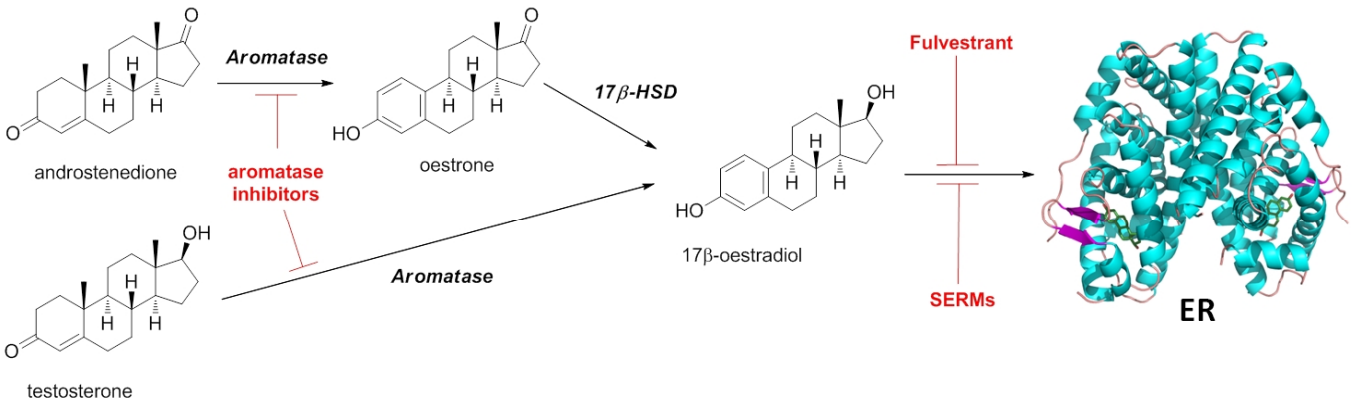


Figure I.6: Mechanisms of action of different endocrine therapies used in BC treatment.

In order to prevent the activation of ER by 17β-oestradiol, current endocrine therapies either interrupt oestrogen production or inhibit oestrogen binding to the receptor. The structure of a dimer of ERα (pdb: 1ERE) presents the ligand 17β-oestradiol bound (green) (Brzozowski et al, 1997). Abbreaviation: 17β-HSD (17β-hydroxysteroid dehydrogenase).

Within the panel of SERMs available, tamoxifen has been classified as the gold standard of SERM therapies in patients with ER+ve BCs for more than 20 years (Riggs & Hartmann, 2003) and acts as an antagonist of the ER in BC tissue *via* its active metabolite, 4-hydroxytamoxifen (Shiau et al, 1998) (**Figure I.**7, **Table I.9**).

However, Tamoxifen modulates ER activity as agonist in other tissues expressing considerable amounts of ER proteins, such as endometrium (Mylonas et al, 2005), bones (Turken et al, 1989) and hypothalamus (Skynner et al, 1999; Skynner et al, 2001), thereby increasing the risk for or causing uterine cancers amongst other side effects.

Therefore, Toremifene, a derivative of Tamoxifen, has been synthesised and tested in different clinical trial studies, but no significant differences have been found between treatments with either tamoxifen or toremifene (Lewis et al, 2010) (**Table I.9**).

Moreover, the benzothiophene Raloxifene has been established to act as selective ER antagonist in both breast and uterus, which seems to reduce the incidence of endometrial cancers after the SERM therapy when compared to Tamoxifen (Vogel et al, 2006) (**Table I.9**).

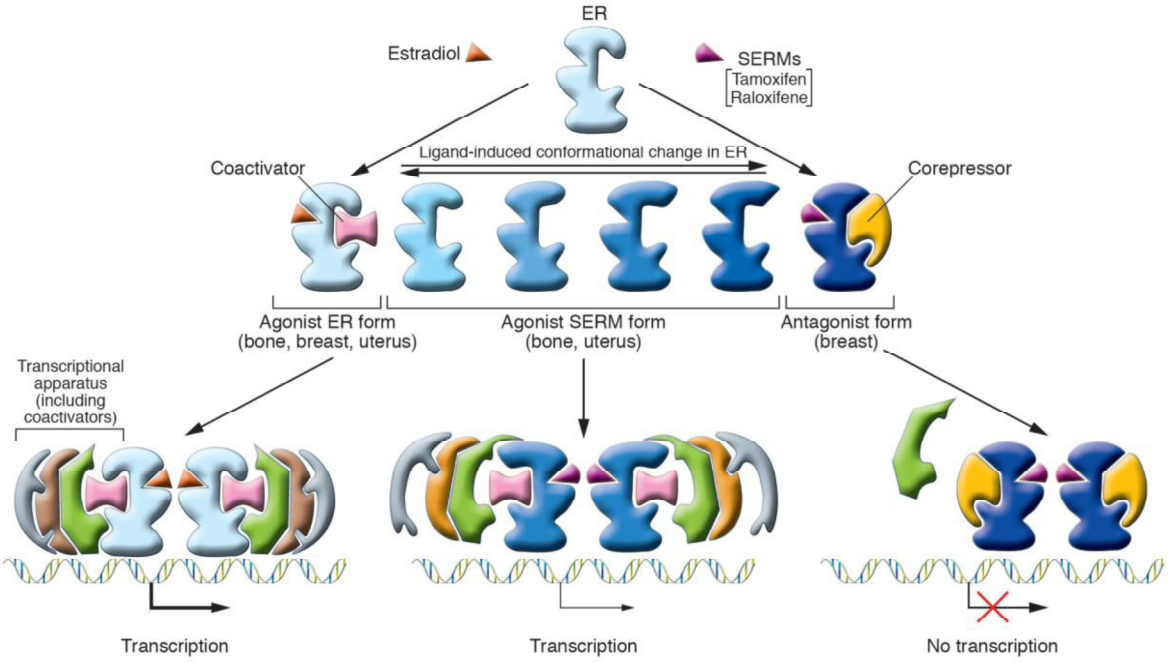
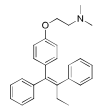
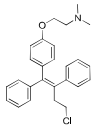
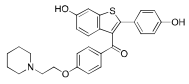


Figure I.7: ER-ligand interaction.

The figure is adapted from (Deroo & Korach, 2006). When an oestrogen analogue, anti-oestrogen, or SERM bind to an ER, the ER undergoes a conformational change which allows its spontaneous dimerization and facilitates the subsequent interaction of the dimer with oestrogen response elements located within target genes. The ER-ligand complex can also bind to various coregulator proteins which can lead to different activity of the ER as transcriptional factor. The binding of different SERMs to the ER allows the receptor to adopt diverse conformational states and SERM activity can be influenced by the relative levels of expression of the coregulator proteins (corepressors and coactivators) in different target cells.

Table I.9: Front-line SERM therapies used in BC treatment.

SERM	Chemical structure
tamoxifen	
toremifene	
raloxifene	

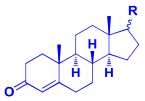
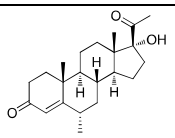
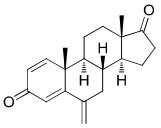
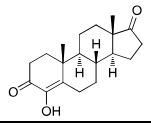
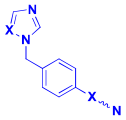
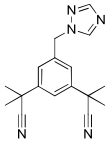
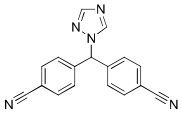
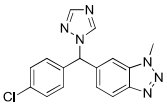
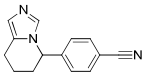
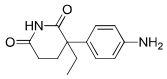
As regards the systemic production of oestrogens in women, in premenopausal women the ovaries are the principal source of oestradiol. In postmenopausal women when the ovaries cease the production of oestrogens, oestradiol is synthesised in a number of extragonadal sites, such as liver, adrenal glands, breast and adipose tissues, where the conversion of androstenedione and testosterone into oestrone and oestradiol respectively occurs. The enzyme responsible for this conversion is aromatase (Simpson, 2003) (**Figure I.6**).

The inhibition of aromate inhibitor has long constituted the base of therapies widely used to reduce the systemic levels of oestrogen in BC patients (Lake & Hudis, 2002).

The aromatase inhibitors are divided into two groups: steroidal or type-1 inhibitors, which can be purely competitive inhibitors or irreversible 'suicide' substrates, and non-steroidal or type-2 inhibitors, which bind to the haem group of the aromatase enzyme by co-ordination through an alkaline nitrogen atom.

Currently, the last generation of highly selective aromatase inhibitors includes anastrozole, letrozole and exemestane (**Table I.10**). The aromatase inhibitors are better tolerated than tamoxifen in terms of vaginal bleeding and discharge, as well as venous thromboembolic events and endometrial cancer (Janni & Hepp, 2010).

Table I.10: Chemical drugs used to inhibit the aromatase enzyme.

Group (Common chemical pattern)	Name	Chemical structure	Mechanism of action
steroidal inhibitors (R=O or acetyl) 	**Progestin**		competitive inhibitor
	Exemestane		irreversibile competitive inhibitor
	Formestane		competitive inhibitor
non-steroidal inhibitors (X= C or N and ∿∿= double or triple bond) 	**Anastrozole**		competitive inhibitor
	Letrozole		competitive inhibitor
	Vorozole		competitive inhibitor
	Fadrozole		competitive inhibitor (only in Japan)
other non-steroidal inhibitor	**Aminoglutethimide**		competitive inhibitor

Another drug, Fulvestrant, forms part of the endocrine therapy group for BC, with a unique structure and mode of action (**Figure I.8**). It possesses a steroidal core like oestrogen with an additional fluorinated alkyl chain, and competitively binds to ER with high affinity. It also down-regulates ER expression by functional blockade and increased turnover (Howell et al, 2004).

Fulvestrant has shown equivalent or improved clinical efficacy compared to established endocrine agents in pre-clinical and clinical studies (Howell et al, 2004). As a pure oestrogen antagonist, fulvestrant avoids the risk of detrimental side effects characteristic to SERMs, such as the partial agonist cross reactivity of tamoxifen in endometrium, and is well tolerated (Johnston & Cheung, 2010). Fulvestrant is the subject of further investigation which tries to exploit the unique mechanism of action and to optimise clinical efficacy in different stages of BC (Johnston & Cheung, 2010).

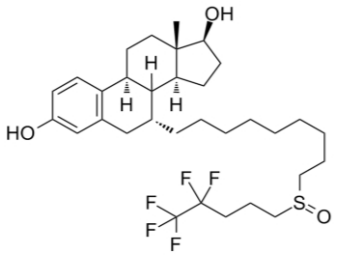


Figure I.8: Chemical structure of Fulvestrant.

I.1.6.3.3 Biological therapies

The human epidermal growth factor receptor 2 gene *HER-2/neu* (also known as *ERBB2*) encodes a tyrosine kinase, a member of the epidermal growth factor receptor (EGFR) family and plays a crucial role in cell differentiation, adhesion and motility (Hanna et al, 1999).

Amplification and overexpression of the gene are seen in approximately 18-20% of BCs

(Slamon et al, 1987), and up to 34% of invasive BCs (Ross & Fletcher, 1999). The ligand for the corresponding protein has not yet been identified and its activation may occur through homo- or heterodimerisation with other EGFRs (Michell, 2010).

HER-2/neu status is a predictive factor of response to a specific systemic therapy using a humanised monoclonal antibody, Trastuzumab, commercially known as Herceptin™. Histology-based and molecular techniques have been used to measure HER-2/neu status in BC clinical samples and a good correlation between gene copy status and protein expression levels has usually been reported (**Table I.11**) (Hayes & Thor, 2002; Masood & Bui, 2002; Ross & Fletcher, 1999; Schnitt & Jacobs, 2001).

Nevertheless, problems with standardisation in slide scoring have recently been highlighted in relation to the conventional IHC method, most commonly used to determine the HER-2/neu status to predict response to Trastuzumab (**Table I.12, Figure I.6**) (Paik et al, 2002).

Table I.11: HER-2/neu testing techniques.

The table is adapted from (Ross et al, 2003).

Method	Target	FDA-approved	Slide-based
IHC	Protein	Yes§	Yes
FISH	Gene	Yes§	Yes
Southern blot	Gene	No	No
PCR	Gene	No	No
RT-PCR	mRNA	No	No
Tumor ELISA	Protein	No	No
Serum ELISA	Protein	Yes	No

§Approved for trastuzumab selection.
ELISA: Enzyme-linked immunosorbent assay; FDA: US Food and Drug Administration; FISH: Fluorescence *in situ* hybridization; IHC: Immunohistochemistry.

Table I.12: HER-2/neu grading system.

The table is adapted from (Ellis et al, 2004).

Description	Score	Interpretation	Figure
No reactivity or membraneous reactivity in <10% of tumour cells	0	Negative	A
Faint/barely perceptible partial reactivity detected in >10% of tumour cells	1	Negative	B
Weak or moderate complete reactivity is seen in >10% of tumour cells	2	Borderline reactivity	C
strong complete reactivity in seen in >10% of tumour cells	3	Positive	D

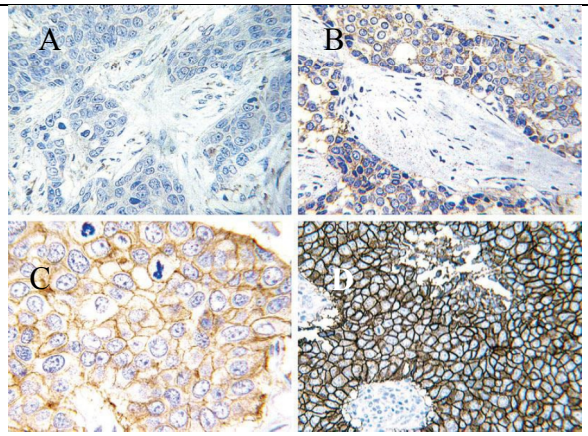


Figure I.9: Scoring immmunochemistry for HER-2/neu.

The figure is adapted from (Payne et al, 2008).

More recently, a new orally active chemical drug for BC has been developed to interfere with HER-2/neu pathway. Its name is Lapatinib (**Figure I.10**) and it has been approved as front-line therapy in triple positive BCs, which are simultaneously ER+ve, PR+ve, and HER-2/neu-positive, and in advanced tumours overexpressing HER-2/neu after previous treatment with Trastuzumab.

apatinib is a tyrosine kinase inhibitor which interrupts the HER-2/neu growth receptor pathway (Burris, 2004; Higa & Abraham, 2007) and also inhibits the oncogene EGFR involved in the same cellular pathway as HER-2/neu (Wood et al, 2004).

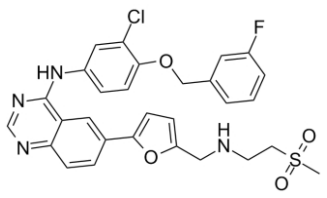


Figure I.10: Chemical structure of Lapatinib.

I.1.7 Prognosis

In patients diagnosed with BC, prognostic factors are designed to forecast the most probable clinical outcome of the disease, whereas predictive factors envisage either the probability that BC will occur in a healthy woman or the possible responsiveness of a patient to a specific single or multiple therapy (Ross et al, 2004).

The well-established prognostic tests, also known as ancillary tests, include hormone receptor status and HER-2/neu status. ER and PR are the most powerful individual prognostic and predictive factors examined in BC in relation to the response to anti-oestrogen therapy (Locker, 1998; Osborne, 1998).

Generally, patients with ER+ve BC tend to respond to hormonal therapy in proportion to receptor protein content (Ciocca & Elledge, 2000; Lemieux & Fuqua, 1996). However, ER and PR status are less useful as general predicitve factor for the disease (Osborne, 1998; Ross et al, 2004).

On the other hand, HER-2/neu overexpression has been consistently associated with the more aggressive and extensive forms of BC (Moreno et al, 1997; Simon et al, 2001), including also a lymph node involvement (Burstein, 2005), a higher rate of disease recurrence and mortality, and thus a poorer prognosis (Stark et al, 2000; Yamauchi et al, 2001).

A wide variety of other prognostic and predictive biomarkers are currently under investigation on the basis of preliminary results and are exhaustively reviewed by Ross et al. (Ross et al, 2003; Ross et al, 2004) (**Table I.13**).

Furthermore, whole-genome transcriptional profiling has also been used to define individual and specific BC (Huang et al, 2003; Sotiriou et al, 2003; West et al, 2001) and determine prognosis in BC (Sorlie et al, 2001; van 't Veer et al, 2002; van de Vijver et al, 2002).

Table I.13: Review of major molecular prognostic factors studied in BC.

The table is adapted from (Ross et al, 2004). Both hormone receptor status and NER-2/neu status constitute the keystones of ancillary prognostic tests. Other biomarkers allow the following of BC evolution taking into account other cellular aspects: cytogenetics, DNA ploidy and S phase analysis, cell cycle associated markers (cyclins D and E), growth factors (EGFR, VEGF), oncogenes, tumour suppressor genes (p53), cell adhesion molecules (E-cadherin, CD44 v6), invasion-associated proteases and proteins (Cathepsin D, uPA/PAI-1,mMPs 2, 9, 11), markers of drug resistance (MDR), apoptosis and apoptosis regulators (Bcl-2), transcription factors (NF-κB), telomerase, DNA repair and microsatellite instability, DNA methylation status.

Biomarker	Assay	Target of therapy	Therapy	Current Status	Future prospectes
ER/PR	IHC Binding assay	yes	Tamoxifen, SERMS, Aromatase inhibitors	Standard of care	Improved IHC with anibodies that are negative when Erα in truncated to reduce false positives
HER-2/neu	IHC - FISH	yes	Trastuzumab, other antibodies, gene therapy	Standard of care	CISH assay may replace both IHC and FISH
DNA ploidy	Cyrometry	no		Common use	Decreased use
S-phase	Cyrometry	no		Common use	Maintained use
Cell proliferaion index	IHC	no		Common use	Increased use of Ki-67 IHC
Cyclin D	IHC	possible	flavopyridol - translocation targets	Clinical trials	May select new drug use, such as proteasome inhibitors
Cyclin E	IHC - Western	no		RUO	Prognostic significance much be validated
EGFR	IHC - FISH	yes	Geftinib - Erlotinib - Cetuximab	Increasing use - Clinical trials	Targeting the anti-EGFR drugs likely combined with pharmacogenomics
VEGF	IHC	yes	Bevacizumab - small molecules	Increasing use - Clinical trials	Increasing use for prognosis. Initial targeted therapy disappointing
p52	IHC - SSPC sequencing	yes	Gene therapy	Increasing use - Clinical trials	Tageted therapies disappointing todate
E-cadherin	IHC - Methylation-PCR	yes	5-azacytidine - Demethylation	Increasing use - Clinical trials	Diagnosis of pleomorphic lobular carcinoma
CD44 v6	IHC	no		RUO	Predictive significance of v6 splice variant requires validation
Cathespin D	Immunoassay	no		Common use in Europe	IHC sudies disappointing; will continue to fade from view
uPA/PAI-1	Immunoassay	yes	small molecules	Common use in Europe	Targeted therapies in eraly stages. I?HC assays not validated to date restricting use in the USA
MMPs 2, 9, 11	IHC	yes	Marimistat	Clinical trials - RUO	Early results of targeted therapy disappointing
MDR	IHC	yes	small molecules	Clinical trials - RUO	Continued use
Bcl-2	IHC	yes	Genesense - Proteasome inhibitors	Increasing use - Clinical trials	Initial results of targeted therapies disappointing
Telomerase	TRAP - IHC - ISH	yes	small molecules	RUO	Increased use if slide-based assays are successful prognostic factors
NF-κB	IHC - Western	yes	Proteasome inhibitors	RUO	Will be use if targetd therapies are successful alone or in combinaion with cytotoxic drugs
Transcriptional profiling	cDNA assay - Oligonucleotide assay	no		RUO	Continued major expansion of use. Predictive marker sets will require multiple cross validation. Could become standard if initial results are confirmed

CISH: chromogenic *in situ* hybridization; EGFR: Epidermal growth factor receptor; ER: Oestrogen receptor; FISH fluorescence *in situ* hydridization; IHC: Immunohistochemistry; ISH: *In situ* hydribization; MDR: multidrug resistance; MMP: Matrix metalloprotease; NF: Nuclear factor; PAI Plasminogen activator inhibitor; PR: Progesterone receptor; RUO: research use only; SSCP: Single-strand conformation polymorphism; SERM: Selective oestrogen receptor modulator; TRAP: Telomere repeat amplification protocol; uPA: Urokinase plasminogen activator; VEGF: Vascular

I.1.8 Conclusion

Survival rates for BC have considerably been improved over the last 30 years (Rachet et al, 2009; Richards, 2008), although they strongly depend on age (Berrino et al, 2007; Rachet et al, 2009) and cancer stage at diagnosis (Woods et al, 2006), with older women at advanced stage having the worst survival rate values.

On the other hand, the clinical effect of SERM therapies is reduced by drug resistance (Berstein & Santen, 2008; Katoh, 2010) and the use of IHC staining to detect ERs and PRs for diagnostic purposes suffers from standardisation problems (Harvey et al, 1999). Similarly, the detection of HER-2/neu receptor needs a combination of different expensive techniques of detection (IHC, FISH) which still need to be refined to detect more subtle differences amongst cancer grades (Wolff et al, 2007).

In general, an earlier and more specific diagnosis and more accurate methods of predicting response to therapy will continue challenging the molecular diagnostic laboratories and industry at different levels in order to identify subgroups of BC patients and customise the treatments: biopsy techniques, proteomic methods, pharmacogenomics, and breast imaging (Ross et al, 2003).

As a result of this methodology, a recent proteomic analysis has detected upregulation of *human N-acetyltransferase 1 (hNAT1)* in ER+ve ductal and lobular breast carcinomas (Adam et al, 2003) and proteomic and transcriptomic data have identified *hNAT1* as one of the ten most highly overexpressed genes in ER+ve BCs (Tozlu et al, 2006). Its overexpression seems to be closely related to ER and PR overexpression and tumour grade (Sim et al, 2008b). These first observations have led to subsequent biochemical studies which have assessed hNAT1 as a novel potential biomarker in BC (Wakefield et al, 2008c) to be developed as a new diagnostic and therapeutic target for BC treatment.

I.2 Arylamine *N*-acetyltransferases

Arylamine *N*-acetyltransferases (NATs, EC. 2.3.1.5) constitute a unique family of phase-II drug metabolising enzymes which conjugate an acetyl group from acetyl coenzyme A (AcCoA) to the terminal nitrogen of aromatic and heterocyclic amines and arylhydrazines and the terminal oxygen of *N*-hydroxyarylamines (**Figure I.11**). They are involved in the detoxification and metabolic activation of xenobiotics.

NATs are distributed in a wide panel of species belonging to both prokaryotic and eukaryotic kindoms, and their molecular sizes are all in the range of 30 to 35 kDa.

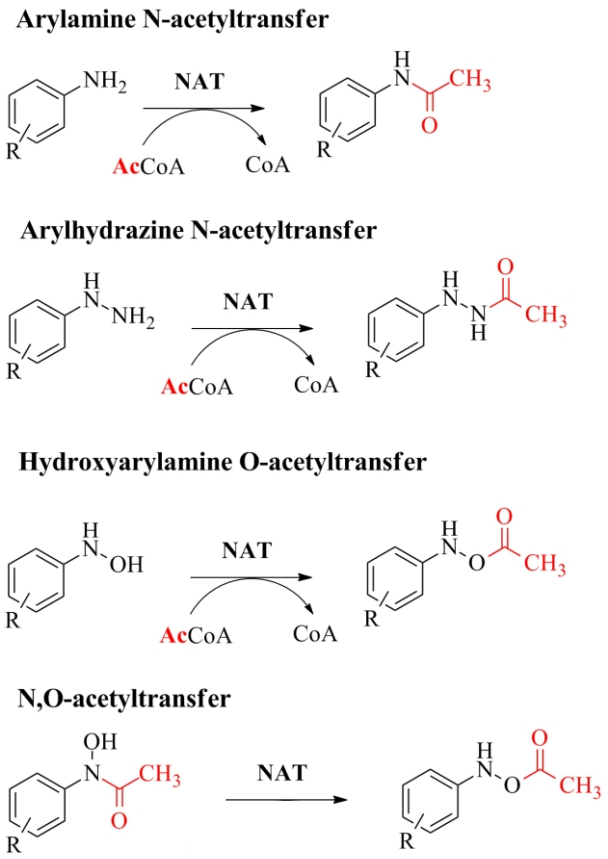


Figure I.11: Examples of reactions catalysed by NAT enzymes.

NAT enzymes acetylate a variety of aromatic and heterocyclic amines, arylhydrazines and hydrozyarylamines using AcCoA. NAT can also catalyse the intramolecular *N,O*-acetyltransferase without the need of an acetyl-donor. CoA= coenzyme A.

I.2.1 Historical background

In the 1950s, the widespread use of isoniazid (isonicotinic acid hydrazine, INH) as anti-tubercular drug (Bernstein et al, 1952) prompted investigations into its metabolism. Inter-individual variations in the amount of the acetylated metabolite excreted in the urine were found among patients treated with isoniazid (Hughes, 1953; Hughes et al, 1954). The difference in acetylating INH, as well as other drugs (the anti-microbial sulfamethazine (SMZ) and the anti-hypertensive hydralazine (HDZ)) within human populations subsequently generated two main groups of individuals: "rapid" and "slow" acetylators, with the slow acetylation phenotype inherited as a somatic recessive trait (Ellard & Gammon, 1976; Evans et al, 1960; Evans & White, 1964).

However, the acetylation of other arylamine xenobiotics, for instance *para*-aminobenzoate (pABA) and 4-aminosalicylate (4AS), was not polymorphic amongst humans (Evans & White, 1964). This discrepancy together with the first attempts at protein purification from human tissues suggested that two independent enzymes were likely to catalyse the *N*-acetylation of arylamines and arylhydrazines (Jenne, 1965; Mitchell & Bell, 1957): one displaying polymorphic activity, and the other acetylating substrates monomorphically.

Nowadays, both monomorphic and polymorphic enzymes are well known as human NAT1 (hNAT1) and human NAT2 (hNAT2), respectively (Louisville-University; Vatsis et al, 1995).

I.2.2 Human NATs

Three *NAT* loci were identified on human chromosome 8 at 8p22: *PNAT*, *hNAT1*, and *hNAT2* (Blum et al, 1990; Hickman et al, 1994). *PNAT* contained premature stop codons and was classified as a pseudogene (Blum et al, 1990), whilst the *hNAT1* and *hNAT2* genes were discovered to consist of an intronless open reading frame each with 870 base pairs (Ohsako & Deguchi, 1990).

Subsequent studies demonstrated that the structure and control of both hNAT1 and hNAT2 genes vary markedly (Sim et al, 2008a), with *hNAT1* being controlled by two promoters, the constitutive promoter P1 and the distal tissue-specific promoter P3 (Minchin et al, 2007).

The corresponding protein products, hNAT1 and hNAT2, were found to be functionally active and to have a molecular weight of ~34kDa each (Blum et al, 1990; Hein et al, 2008; Ohsako & Deguchi, 1990).

Subsequent investigations highlighted that proteins hNAT1 and hNAT2 possess distinct functional roles, based on their substrate profiles, their tissue distribution and the expression of the genes during development. The two human isoenzymes are differently expressed during development in the placenta and in the foetus, with their genes being subject to independent control of expression (Butcher et al, 2003; Minchin et al, 2007; Sim et al, 2008b) (**Figure I.12**).

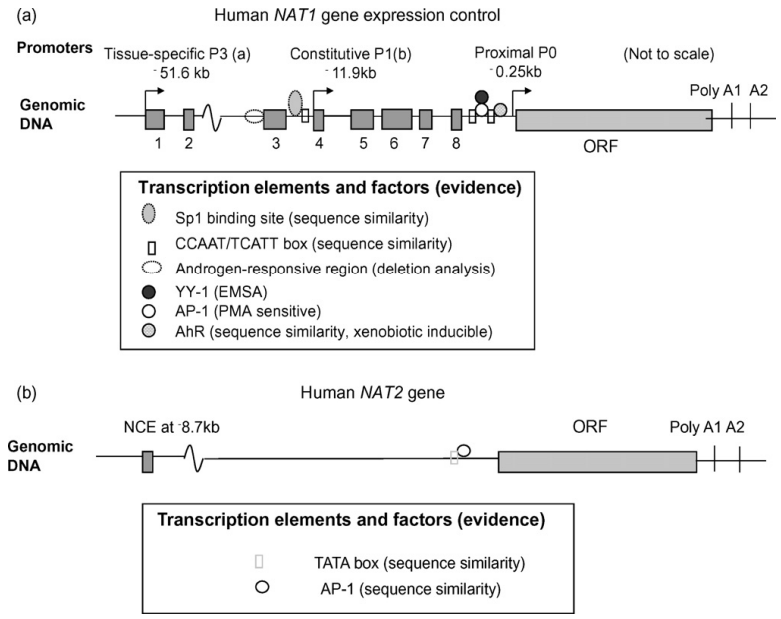


Figure I.12: Genetic control of human NAT genes.

The figure is adapted from (Sim et al, 2008a). (a) hNAT1 and (b) hNAT2.

As regards their functional roles, both pure recombinant hNAT1 and hNAT2 are able to acetylate xenobiotics; nevertheless they possess distinct substrate profiles, with some specific substrates used as "probe" substrates for that specific isoenzyme: pABA, para-aminobenzoyl glutamate (pABAglu) and 4AS for hNAT1, and INH and SMZ for hNAT2 (Kawamura et al, 2005) (**Figure I.13**).

Moreover, successive structural studies on both isoenzymes, together with a mutated form of hNAT1 (hNAT1_F125S), gave the first insight into the interactions within the active site pockets conferring substrate selectivity to the enzyme (Wu et al, 2007).

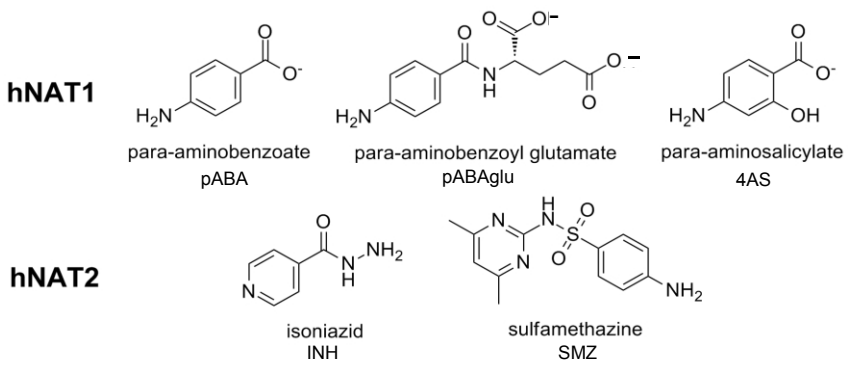


Figure I.13: Probe arylamine substrates for hNAT1 and hNAT2.

With regard to the functional role of hNAT1 and hNAT2, an endogenous role for hNAT1 has been hypothesised in relation to the breakdown of folate through acetylation of the folate catabolite pABAglu (**Figure I.14**) (Minchin, 1995; Minchin et al, 2007; Ward et al, 1995), whilst hNAT2 appears to be a drug metabolising enzyme (Boukouvala & Fakis, 2005).

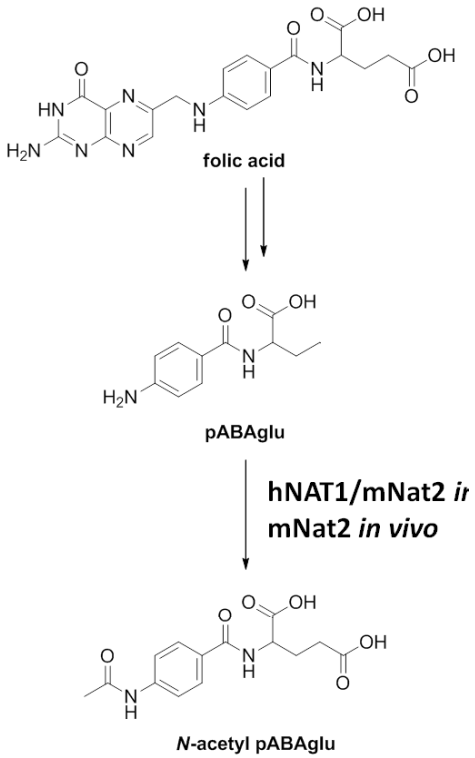


Figure I.14: Potential role of hNAT1 in folate degradation.

I.2.3 Eukaryotic NATs

NAT loci have also been identified in other mammalian species: there are three loci in rodents (Boukouvala et al, 2002; Kelly & Sim, 1994; Martell et al, 1992; Martell et al, 1991; Walraven et al, 2006), whilst in cats there appears to be only one locus (Trepanier et al, 1998); in rabbits there are two loci (Blum et al, 1989; Sasaki et al, 1991), as well as in hamsters (Jones et al, 1996), namely shNat1 and shNat2. However, in dogs (Trepanier et al, 1997) and musk shrews (Nakura et al, 1995), no *NAT* genes have been identified.

Rodent NATs have been investigated as good animal models for human NATs. Substrate specificities (Kawamura et al, 2008; Walraven et al, 2006), tissue distribution (Fakis et al, 2000; Stanley et al, 1998; Windmill et al, 2000), gene structure (Boukouvala et al, 2003) and developmental expression of rodent NAT genes have widely been compared to those of human NATs (Mitchell et al, 1999).

In particular, on the basis of the expression profile and tissue distribution, *hNAT1* is considered orthologous gene to mouse *Nat2* (*mNat2*) (Kawamura et al, 2008). Both enzymes hNAT1 and mNat2, share 80% identical primary sequence and have also been established to be functionally similar (Kawamura et al, 2005; Kawamura et al, 2008) (**Table I.14**). This also allowed the assessment of mNat2 as good murine model for hNAT1 (Kawamura et al, 2008).

NAT loci have also been found in other eukaryotic genomes, such as pigeon (Riddle & Jencks, 1971), chicken (Ohsako et al, 1988) and zebrafish (Sim et al, 2008a).

Table I.14: Summary of key findings supporting the functional homology between mNat2 and hNAT1.

	mNat2	hNAT1
Specificity for isoniazid	- *(Kawamura et al, 2008)*	- *(Kawamura et al, 2005)*
Specificity for 4AS	+ *(Kawamura et al, 2008)*	+ *(Kawamura et al, 2005)*
Specificity for pABA	++ *(Kawamura et al, 2008)*	+++ *(Kawamura et al, 2005)*
Expression in the placenta	✓ *(Mitchell et al, 1999)*	✓ *(Upton et al, 2000)*
Early expression in foetal development	✓ *(Mitchell et al, 1999)*	✓ *(Smelt et al, 2000)*
Folate metabolism	✓ *(Payton et al, 1999b; Wakefield et al, 2007)*	✓ *(Minchin, 1995; Ward et al, 1995)*
Expression in breast epithelial cells	✓ *(Stanley et al, 1997)*	✓ *(Williams et al, 2001)*
Expression in the gut	✓ *(Stanley et al, 1998)*	✓ *(Hickman et al, 1998; Windmill et al, 2000)*

Information was obtained from a range of different sources, as stated in the table.
Key: +++ very high; ++ high; + not very high; - very low; ✓ found.

I.2.4 Prokaryotic NATs

NATs have also been identified and characterised in other microorganisms, such as *Salmonella typhimurium* (*STNAT*) (Mushtaq et al, 2002; Sinclair et al, 2000; Watanabe et al, 1992), *Pseudomonas aeruginosa* (*PANAT*) (Westwood et al, 2005), *Mesorhizobium loti* which contains two *NAT* genes (Dairou et al, 2006; Holton et al, 2005; Rodrigues-Lima et al, 2006), *Bacillus anthracis* with three *NAT* genes (*BANAT*) (Pluvinage et al, 2007a; Pluvinage et al, 2007b) and *Streptomyces griseus* (Suzuki et al, 2007).

NAT has also been found in different strains of mycobacteria (*Microbacterium smegmatis* (*MSNAT*) (Sandy et al, 2002), *M. bovis BCG* (Anderton et al, 2006)*, M. Marinum* (*MMNAT*) (Fullam et al, 2008) and *M. Tuberculosis* (*TBNAT*) (Sikora et al, 2008)) and appears to play an essential role in endogenous metabolism for cell wall synthesis (Bhakta et al, 2004) in isoniazid metabolism (Payton et al, 1999a; Payton et al, 2001a; Payton et al, 2001b; Upton et al, 2001) and in cholesterol catabolism (Lack et al, 2009).

I.2.5 X-ray crystal structures

The first NAT structure for which the three dimensional structure was determined is STNAT (Sinclair et al, 2000), followed by other structures of prokaryotic enzymes, sometimes co-crystallised with a substrate ligand (**Table I.15**). This structure also helped identify the catalytic cysteine acetylated during the acetylation reaction: Cys69 in STNAT (Sinclair et al, 2000).

Table I.15: Summary of known crystal structures of NATs by X-ray.

Species	NAT Acronym	Observation	Reference
Salmonella typhimurium	STNAT	three-domain fold and catalytic Cys69	(Sinclair et al, 2000)
Mycobacterium smegmatis	MSNAT	isoniazid bound	(Sandy et al, 2005b; Sandy et al, 2002)
Mycobacterium smegmatis	MSNAT	acetylcysteine model	(Sandy et al, 2005a)
Pseudomonas aeruginosa	PANAT	distinct active site cleft	(Westwood et al, 2005)
Mycobacterium loti	-	model for M. Loti NAT2	(Holton et al, 2005)
Bacillus anthracis	BANAT3	mutant studies linked to drug resistance	(Pluvinage et al, 2007b)
Mycobacterium marinum	MMNAT	CoA binding site	(Fullam et al, 2008)
Homo sapiens	hNAT1	ligand bound	(Wu et al, 2007)
Homo sapiens	hNAT2	CoA binding site	(Wu et al, 2007)
Mycobacterium marinum	MMNAT	hydralazine bound	(Abuhammad et al, 2010)
Bacillus anthracis	BANAT1	endogenous CoA bound	(Pluvinage et al, 2011)

In general the structures of the prokaryotic NAT enzymes which have been solved so far are similarly shaped and the overall fold consists of a three-domain structure with each of the domains being roughly equal in length.

Structures of both human NAT isoenzymes, hNAT1 and hNAT2, have been solved and the fold of hNAT1 and hNAT2 largely resembles the overall structure of their prokaryotic counterparts (Wu et al, 2007) (**Figure I.15**). Moreover, the C-terminus from the third domain seems to control substrate specificity and enzymatic activity (Dupret et al, 1994; Sim et al, 2008b).

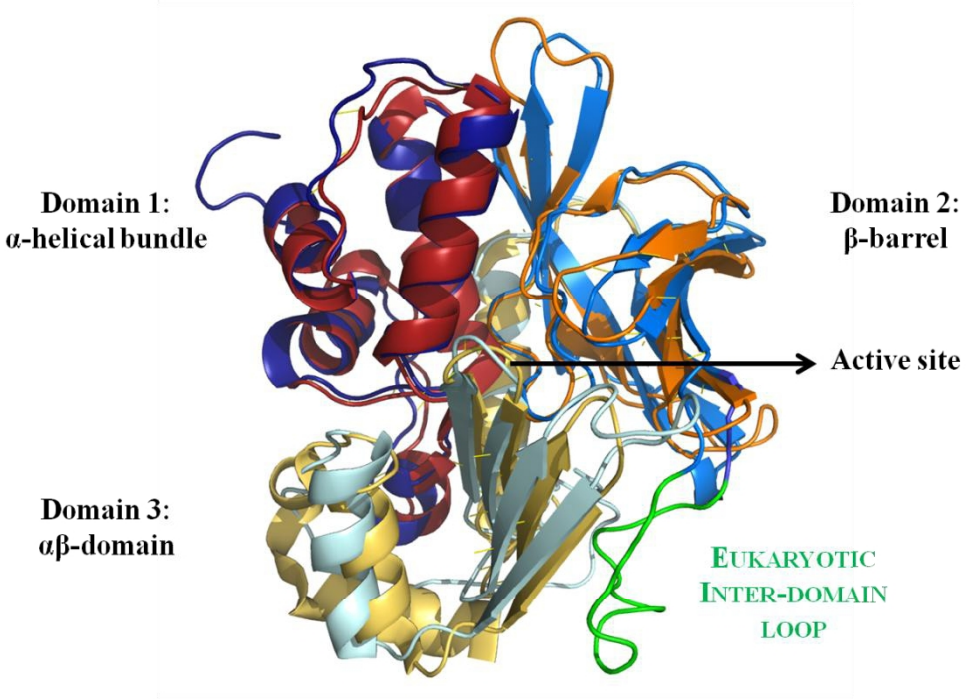


Figure I.15: Overall structure of hNAT1 and MMNAT.

Structure of hNAT1 (pdb code: 2PQT) (Wu et al, 2007) and MMNAT (pdb code: 2VFC) (Fullam et al, 2008) are superimposed. The structure is shown in ribbon format with the three domains labelled. The three domains of hNAT1 structure are coloured in different shades of blue, whilst the domains of MMNAT structure in different shades of orange. The domains are numbered from the amino terminus with domain 3 corresponding to the carboxy terminus of the protein. The active site region is indicated by an arrow. The characteristic eukaryotic loop is coloured in green.

Comparing the sequences and the structures of prokaryotic NATs with these of their eukaryotic counterparts highlights the presence of a loop of 17 residues between domains two and three in mammalian NATs (Payton et al, 2001b; Sandy et al, 2005b) (**Figures I.16**).

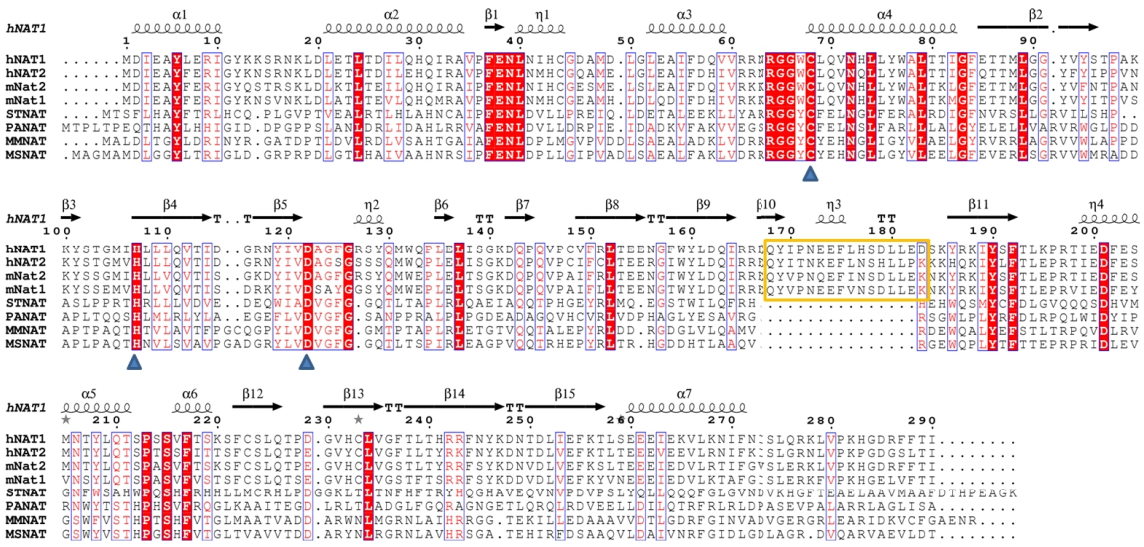


Figure I.16: Multiple sequence alignment of selected NAT proteins.

NAT proteins from *STNAT*, *PANAT*, *MMNAT* and *MSNAT* are aligned with murine and human NAT isoenzymes. Similar amino acids are highlighted in blue boxes; completely conserved residues are indicated by white lettering on a red background. The residues from the catalytic triad are indicated by a blue triangle and the residues constituting the additional loop in eukaryotic NATs are highlighted by an orange box. The secondary structure adapted is from hNAT1 crystal structure (pdb code: 2PQT) (Wu et al, 2007). Alignment was generated using Clustal W (Thompson et al, 1994). Figure was prepared using ESPript 2.2 (Gouet et al, 1999).

This loop has been hypothesised to be responsible for the diverse biding site of CoA in NATs. A recent structure of *M. Marinum* with CoA bound has provided useful information on the binding mode of the AcCoA in the prokaryotic NAT molecule (Fullam et al, 2008), which is different from the binding mode of CoA in hNAT2 (Wu et al, 2007) (**Figure I.17**).

The latest NAT structure solved to date is from *Bacillus anthracis* (BANAT1) and shows a novel biding mode of CoA to the enzyme compared to previous CoA-NAT structures (**Figure I.17**). Moreover, the CoA co-crystallised in the BANAT1 structure seemed to have an endogenous origin, despite the multiple steps in the process of producing and purifying the enzyme (Pluvinage et al, 2011) .

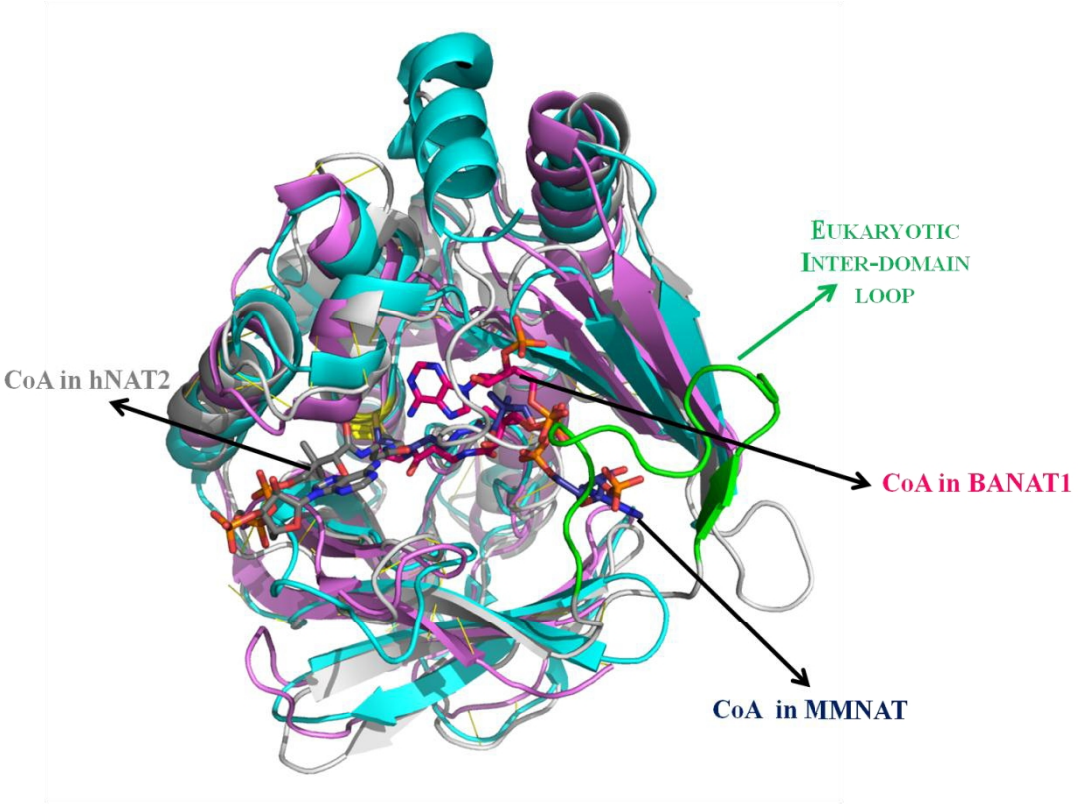


Figure I.17: Structures of hNAT2, MMNAT and BANAT1, each with a molecule of CoA bound.

Ribbon diagram showing the overlaid structures of hNAT2 (grey - pdb: 2PFR), MMNAT (blue - pdb: 2VFC) and BANAT1 (violet - pdb:3LNB). The structures were generated and aligned using the program PyMOL (W. L. DeLano (2002) PyMOL, DeLano Scientific, San Carlos, CA). The CoA which was co-crystallised with the appropriate enzyme is shown in sticks and labelled with carbon atoms in grey for hNAT2, in blue for MMNAT and in magenta for BANAT1, nitrogen in blue, oxygen in red, and sulfur in orange. The catalytic cysteine residue is shown in stick representation and coloured in yellow. The sulfydryl group of the active site Cys is suitably positioned for the transfer of the acetyl group from acetyl CoA. The characteristic eukaryotic loop is coloured in green.

I.2.6 Catalytic mechanism

The identification of the possible reactions catalysed by NAT enzymes has required many experiments leading to the conclusion that *N*-acetylation of arylamines (Weber & Hein, 1985), *O*-acetylation of arylhydroxylamines (King, 1974) and intramolecular *N,O* acetyl transfer in *N*-acetylhydroxamates (Flammang et al, 1987; Jones et al, 1996) can be catalysed by the NATs (Watanabe et al, 1992).

The transfer reaction occurs in two steps following a Bi-bi Ping-pong mechanism (Cleland, 1963; Jenne & Boyer, 1962): the enzyme is firstly acetylated to form an acetyl-enzyme intermediate, and then the acetyl group is transferred from the enzyme to the substrate (Andres et al, 1988; Andres et al, 1983a; Sinclair & Sim, 1997).

Moreover, the pioneering STNAT structure also allowed the discovery of a catalytic triad of cysteine, histidine and aspartate within the active site cleft which leads to the activation of the cysteine and is common to all NAT enzymes (Sinclair et al, 2000; Westwood et al, 2006).

Therefore, a catalytic mechanism of the NAT enzyme reaction has been proposed (Westwood et al, 2006) (**Figure I.18**).

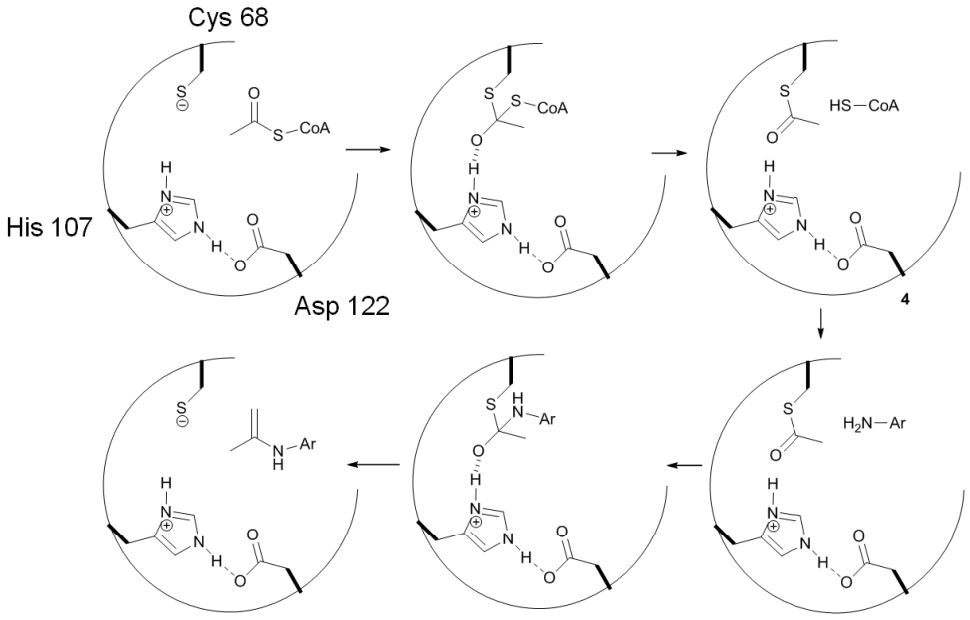


Figure I.18: Proposed catalytic mechanism of NAT reaction.

The mechanism is shown with AcCoA as acetyl donor. The residue numbering is referred to mammalian NAT sequences. The formation of the acetyl-enzyme intermediate requires the stabilisation of the charges across a Cys-His-Asp triad. The acetyl transfer occurs following nucleophilic attack of the acetylated intermediate by the arylamine substrate. The lifetime of an acetylated NAT intermediate differs among NAT species (Wang et al, 2005a). Figure is modified from (Westwood et al, 2006).

The measurement of NAT activity relies on either the acetylation of the arylamine substrate (Andres et al, 1985) or the hydrolysis of AcCoA (Brooke et al, 2003b).

A range of other acetyl donors has been used in enzymatic experiments, as shown in **Figure I.19**. Other AcylCoA derivatives, mainly *n*-propionylCoA, have also been used experimentally with NAT enzymes (Kawamura & Sim, 2005; Lack et al, 2009), although whether this has relevance *in vivo* has yet to be established.

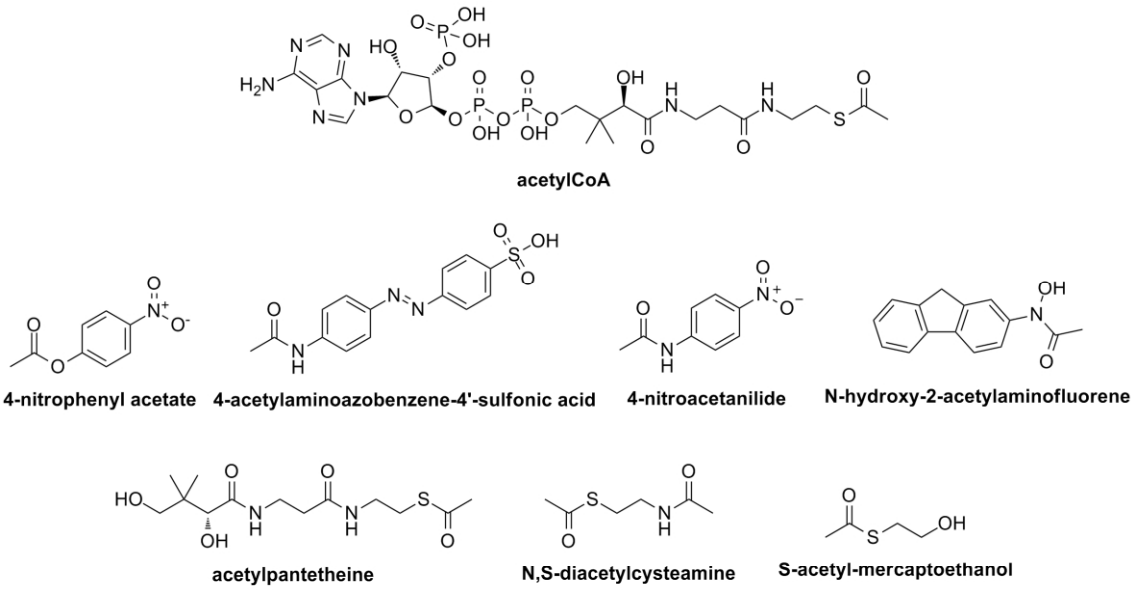


Figure I.19: Acetyl donors used in enzymatic investigations on NATs.

These different acetyl donors have been used in NAT enzymatic assays (Andres et al, 1983a; Lipmann, 1945; Mushtaq et al, 2002; Riddle & Jencks, 1971; Wang et al, 2005a; Wang et al, 2004b).

I.3 Human NATs and disease

There have been extensive studies of human *NAT* genotype and phenotype in relation to disease. Interindividual differences in isoniazid metabolism by NAT constitutes one of the first examples of polymorphism in human pharmacogenetics (Evans, 1989; Weber & Hein, 1985). Investigating the phenotypic consequences of the polymorphism led to studies relating NATs to pathological conditions, such as cancer.

I.3.1 NAT polymorphism and its consequences

The intense development of genetic techniques resulted in the identification of 29 variant alleles of *hNAT1*, associated with 11 residue alterations, whilst 32 variant alleles of *hNAT2* associated with 12 amino acid variations have been identified to date (Louisville-University) (**Figure I.20**).

Contrary to the initial belief that hNAT1 was monomorphic, hNAT1 was subsequently found to be indeed polymorphic (Payton & Sim, 1998; Vatsis & Weber, 1993) with SNPs found within and outside the coding region. Conversely, hNAT2 polymorphisms were identified much earlier than the hNAT1 polymorphisms, with a genotype-phenotype correlation well investigated (Hein et al, 2000b; Hickman et al, 1995; Kawamura & Sim, 2005; Wu et al, 2007) (**Figure I.20**).

NAT polymorphism can predispose humans to harmful drug-induced side effects (Sim et al, 1984a; Weber & Hein, 1985). Numerous studies have highlighted possible relationships amongst exposure to exogenous aryl and heterocyclic amines, NAT polymorphisms and cancer (Hein et al, 2000a).

In particular, the metabolism of heterocyclic amines generates products which can be unstable and mostly reactive with macromolecules in cells, like DNA and proteins (Beland & Kadlubar, 1985; Grant et al, 1997; Turesky et al, 1991) (**Figure I.21**).

This can lead to genome mutations and the development of malignant phenotypes (Lutgerink et al, 1989). Hence, the NAT phenotypes (rapid or slow acetylators) can affect the velocity of detoxification and activation of arylamines by *N*-acetylation and oxidation respectively in cells.

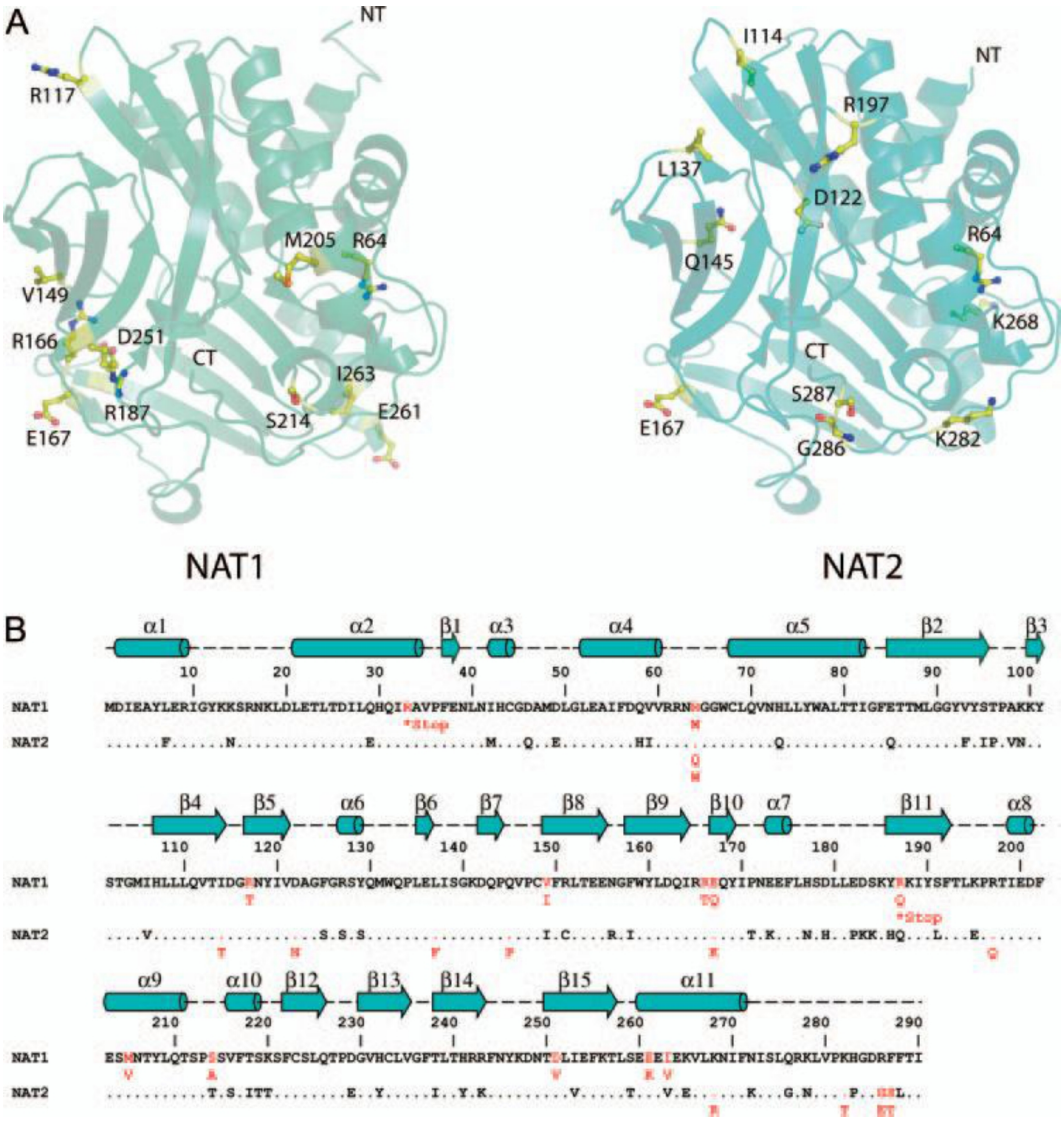


Figure I.20: Location of SNPs on human NATs.

The figure is adapted from (Wu et al, 2007). **(top)** The overall fold of hNAT1 **(left)** and hNAT2 **(right)** are shown in ribbon diagrams. The positions of unique amino acid substitutions in human NATs are shown in stick-and-ball representation with carbon atoms coloured yellow. The amino and carboxyl termini of both proteins are labelled NT and CT, respectively. **(bottom)** secondary structure and sequences of human NATs. The identical residues are shown as dots in hNAT2. The SNPs relative to the proteins generated based on *hNAT1*4* and *hNAT2*4* genes are highlighted in red. The residue numbers are shown above the sequence, and the amino acid substitutions are shown below the sequence.

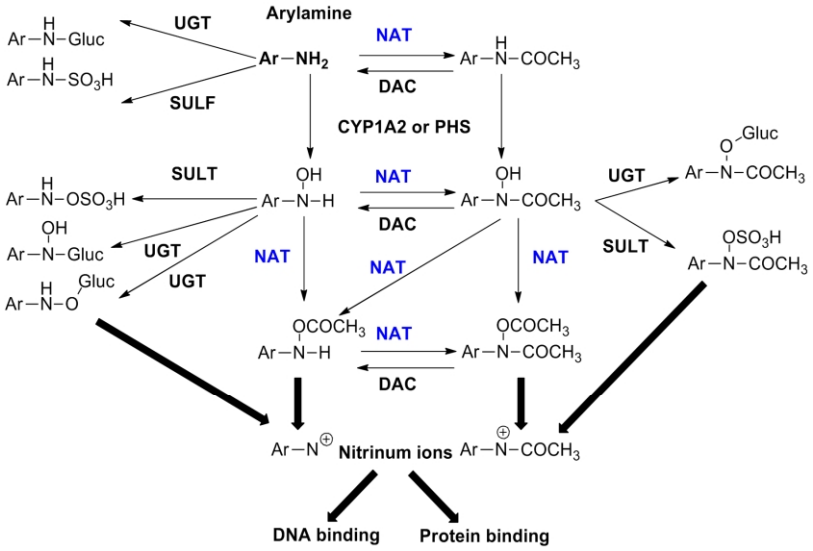


Figure I.21: Metabolic pathway of aromatic and heterocyclic amine carcinogens.

Abbreviations: SULT: sulfotransferase, UGT: UDP-glucuronosyltransferase, CYP: Cytochrome P450, PHS: prostaglandin H synthase, DAC:deacetylase. The figure is adapted from (Grant et al, 1997)

Moreover, studies conducted on polymorphism in *hNAT2* led to the association of the gene with a wide range of diseases, in particular bladder cancer (Cartwright et al, 1982; Risch et al, 1995; Rothman et al, 2007), BC (Ambrosone et al, 2008), colon cancer (Minchin et al, 1993), lung cancer (Bouchardy etal, 1998), head and neck cancers (Gonzalez *et al*, 1998), prostate cancers (Fukutome et al, 1999), drug-induced lupus erythematosus (Sim et al, 1984b), and diverse neurotoxicities induced by isoniazid (Duke & Mai, 1999; Rey et al, 1998; Yamamoto et al, 1996). Most of these pathological conditions appear to be related to the slow acetylator phenotype of hNAT2, although the clear link to NAT polymorphism remains somewhat controversial.

As regards hNAT1, genetic polymorphism can generate either a less efficient enzyme or a truncated version of the protein (Minchin et al, 2007). Interestingly, mutations outside the open reading frame, in particular at the 3' end of the gene, can affect the level of the transcript and the extent of the translation of that transcript, with a subsequent increased level of hNAT1 activity in the cell, although this aspect has been highly controversial (Minchin et al, 2007).

I.3.2 Relationship between hNAT1 and breast cancer

As previously mentioned, a proteomic analysis has detected upregulation of *hNAT1* in ER+ve ductal and lobular breast carcinomas (Adam et al, 2003).

Moreover, additional microarray-based studies have compared the expression profiles of a number of human genes from malignant and normal breast tissues, or between ER+ve and ER-negative (ER-ve) BCs (Wakefield et al, 2008b), as reported through the Oncomine database (www.oncomine.org). A very strong correlation between *hNAT1* overexpression and the ER+ve grade has been reported, alongside evident correlation between *hNAT1* levels and PR+ve status in BCs (Sim et al, 2008b).

Proteomic and transcriptomic data have identified *hNAT1* as one of the 10 most highly overexpressed genes only in ER+ve BC (Tozlu et al, 2006).

hNAT1 has also been found to be one of the five most highly overexpressed genes in ER+ve and PR+ve tumours, with late-stage tumours expressing lower levels of *hNAT1* than early-stage ones (Sim et al, 2008b) (**Figure I.22-left**).

Moreover, the upregulation of *hNAT1* was also related to high levels of NAT activity of BC cell lines (Wakefield et al, 2008b), such as the cell line ZR-75-1 (**Figure I.22-right**).

The increase in *hNAT1* expression in some BC lines has been found to be related to the control of gene expression rather than a duplication of the gene (Wakefield et al, 2008b).

The role of the secondary promoter of hNAT1 has been proposed to drive expression of additional hNAT1 mRNAs in cells (Barker et al, 2006) and has therefore been suggested to be critical in inducing further expression of additional transcripts in certain disease conditions (Sim et al, 2008b).

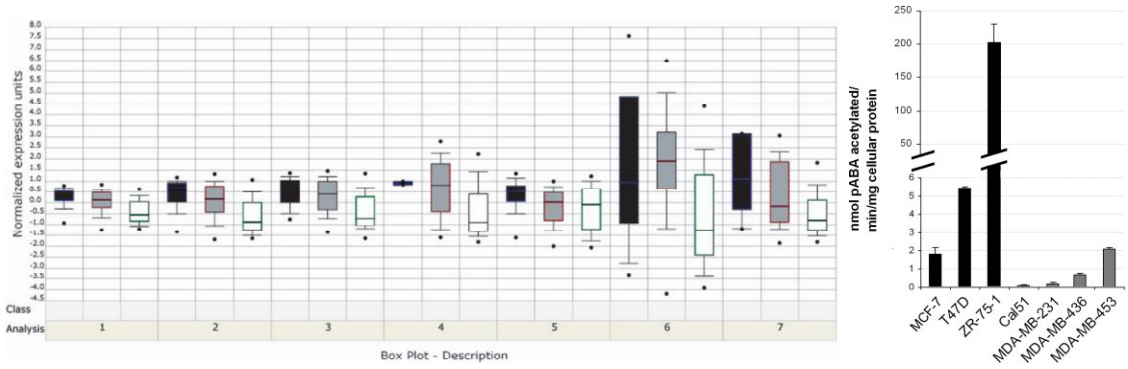


Figure I.22: Overexpression of hNAT1 in BC.

(left) Figure adapted from (Sim et al, 2008b). Oncomine hNAT1 expression profiles in BCs. Comparison of NAT1 expression at different stages of BC progression. The differential expression diagram was generated by the Oncomine database (Rhodes et al, 2004), using data from seven independent studies accessible on www.oncomine.org. (1) (Miller et al, 2005); (2) (Ivshina et al, 2006); (3) (Desmedt et al, 2007); (4) (Hess et al, 2006); (5) (Sotiriou et al, 2006); (6) (van 't Veer et al, 2002); (7) (Sorlie et al, 2001). **(right)** Figure adapted from (Wakefield et al, 2008b). NAT1-dependent acetylation rates in cell lysates. Cell lysates prepared from a range of ER+ve (black columns) and ER-ve (grey columns) cell lines were assayed for their ability to *N*-acetylate the hNAT1-specific substrate pABA.

The functional significance of the overexpression of *hNAT1* remains to be established; nevertheless, a number of parallel studies have shown an important association between hNAT1 activity and cancers. For instance, an indirect interference with hNAT1 activity by the SERM tamoxifen has been reported (Lee et al, 1997), and a subsequent study showed a correlation between response to tamoxifen and levels of hNAT1 expression (Bieche et al, 2004). Moreover, resistance to anti-oestrogen drugs used for BC treatment, like tamoxifen, has been reported and explained by alterations in drug metabolism and bioavailability (Bieche et al, 2004). This could be included in the intratumoral dysregulation of the expression of xenobiotic-metabolising enzymes, widely described in cancer. Interestingly, mNat2, the animal model of hNAT1, is inhibited by tamoxifen and oestrogen analogues, and these inhibitors bind near the active site of the enzyme (Kawamura et al, 2008).

The active overexpression of *hNAT1* in a normal luminal epithelial-derived cell line

demonstrated enhanced growth properties relative to control cells and increased resistance to arylamine cytotoxic agents (Adam et al, 2003). Recently, the results of a study conducted using RNAi against hNAT1_mRNA demonstrate that knocking-down the *hNAT1* gene considerably diminished BC growth and invasiveness (Tiang et al, 2010)

Additional studies conducted on other families of tumours have reported that *hNAT1* expression is induced by androgens in prostate cancer cells (Butcher et al, 2007), whereas knock-down of *hNAT1* gene in colon cancer cells inhibited cell contact at confluence and promoted apoptosis (Sim et al, 2008b).

There is therefore a need to unravel the regulatory networks underlying the abnormal expression of *hNAT1* in BC, as well as developing its therapeutic, diagnostic, and prognostic potentials as biomarker.

I.4 Drug discovery

In order to determine the *in vivo* function of a protein in physiological and pathological conditions, such as that of hNAT1 in this study, methods have been developed to alter the function and look for changes in the phenotype.

Genetic approaches, such as deletion or mutation of the gene, are limited in mammals by the slow rate of reproduction, large physical sizes, large genomes, complexity of genome expression, irreversibility of the effects and the high cost of such experiments (Stockwell, 2004).

Conversely, synthetic RNA molecules interfering with the mRNA produced following the expression of a gene (RNAi), such as micro interfering RNAs (miRNA) or small interfering RNAs (siRNA), have been used to decrease the production of a target protein in order to validate the target without deleting the original gene. This discovery has led to a surge in interest in harnessing RNAi for biomedical research and drug develop-

ment. Nevertheless, disrupting the biosynthesis of a target protein does not allow the study of the physiological function of the protein within the cell (Hannon & Rossi, 2004).

Finally, chemical genetics is a complementary pharmacological approach to investigate the function of a protein: it uses selective small-molecule ligands, which can selectively modulate the function of the target protein upon binding. The advantages of chemical genetics are that the entire expression of the target gene is not disrupted, the ligand-protein bonds are usually reversible and most of the ligands possess many of the required physicochemical properties of a lead compound for drug development (Westwood, 2004).

The current paradigm of drug discovery is based on this second approach: the modification of a target protein, mainly an enzyme, using small-molecule inhibitors can provide a rational basis for the discovery of new medicines (**Figure I.23**).

Empirical testing of a large number of chemical compounds from chemical libraries against the target biomolecule (High Throughput (HTP) screening) has been widely and successfully employed as a source of new potential selective ligands, called drug leads, following *in vitro* and *in silico* tests.

Structure-based tools, such as X-ray crystallography and computational modelling and screening, also called virtual screening, could also be used to aid lead identification and optimisation for some targets.

Since hNAT1 is characterised as a prominent biomarker in ER+ve BC (Wakefield et al, 2008b), the use of isoenzyme-specific inhibitors would greatly benefit enzymological and pharmacological characterisation of the enzyme.

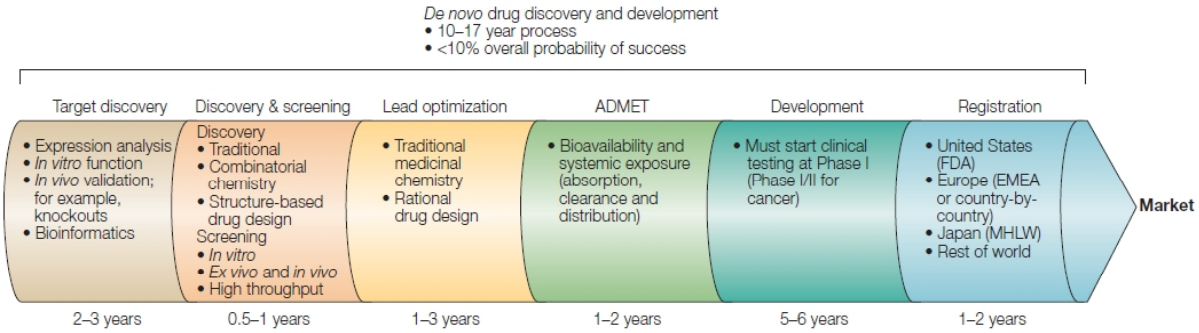


Figure I.23: Drug discovery process.

De novo drug discovery and development is a multistep and long-time process from idea to marketed drug. ADMET, absorption, distribution, metabolism, excretion and toxicity; EMEA, European Medicines Agency; FDA, Food and Drug Administration; MHLW, Ministry of Health, Labour and Welfare. The figure is adapted from (Ashburn & Thor, 2004).

Two types of inhibitors of NATs have emerged: mechanism-based inhibitors which have found applications in the elucidation of the catalytic mechanism of NATs (Cheon et al, 1992; Cheon & Hanna, 1992; Dairou et al, 2003; Dairou et al, 2004; Guo et al, 2004; Sticha et al, 1998; Voice et al, 1993; Wang et al, 2005a; Wang et al, 2004b) and structure-based inhibitors of prokaryotic NATs (Brooke et al, 2003a; Westwood et al, 2006). However, the specificity of inhibitors for hNAT1 has not yet been met and therefore needs to be addressed.

I.4.1 Known inhibitors of hNAT1 and mNat2

There have been limited examples of hNAT1 inhibitors. *N-A*rylhydroxamic acids and nitrosoarenes have been found to interact with the Cys68 thiolate of both human NATs to form a sulfinamide drug-adduct *via* covalent modification of the residue (Liu et al, 2009) (**Figure I.24**).

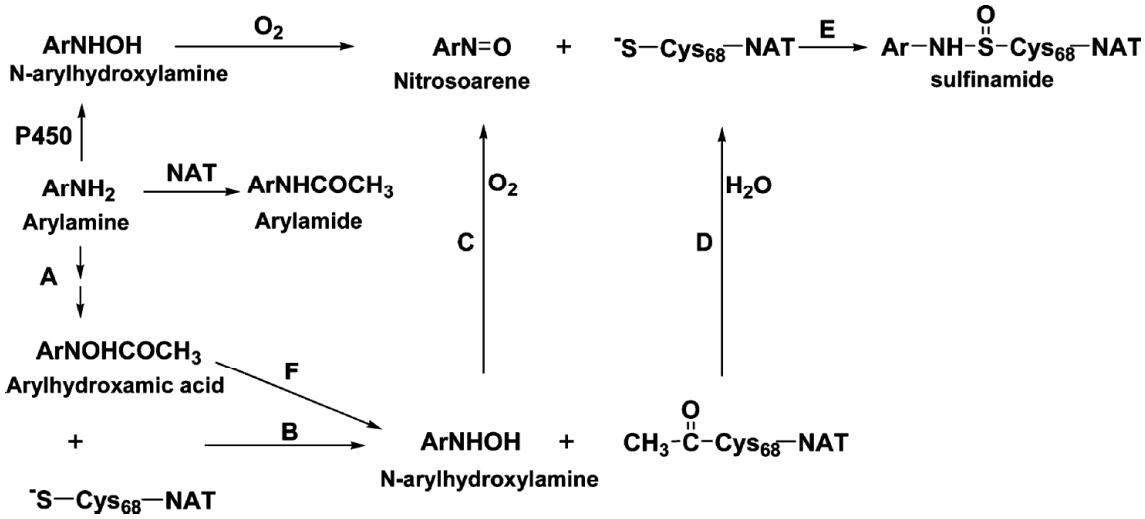


Figure I.24: Mechanism of inhibition of human NAT enzymes by *N*-arylhydroxamic acids and nitrosoarenes.

A: P450, NAT; B: NAT; C: nonenzymatic oxidation; D: non-enzymatic hydrolysis; E: non-enzymatic sulfinamide formation; F: esterases. The figure is adapted from (Liu et al, 2009).

Aside from the SERM tamoxifen which non-covalently inhibits hNAT1 *in vitro* (Lee et al, 1997; Lee et al, 2004; Lu et al, 2001), the chemotherapeutic agent cisplatin also inhibits hNAT1 by forming an irreversible bond with Cys68 (Ragunathan et al, 2009) (**Figure I.25**).

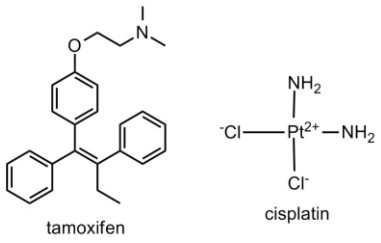


Figure I.25: Small molecules identified as inhibitors of hNAT1.

Alongside this, different types of polyphenolic compounds have been screened as inhibitors of hNAT1, but none of them showed high selectivity to hNAT1 against its isoform hNAT2 (Kukongviriyapan et al, 2006).

The effects of steroidogenic compounds and xenobiotic oestrogenic compounds, including the SERM tamoxifen, have been investigated on the activity of mNat2, which has

been validated as a good functional animal model of hNAT1 (Kawamura et al, 2008).

Oestrogenic compounds have been shown to inhibit mNat2, with 17-hydroxy-β-estradiol identified as the most potent inhibitor. Also, xenobiotic oestrogens, such as tamoxifen, inhibited mNat2 activity (**Table I.16**).

On the other hand, bisphenol A, which has been reported to activate the oestrogen receptor (Takeshita et al, 2001), constituted an inhibitor of mNat2 acetylation activity to a lower extent and showed interaction with mNat2 close to the active site region (**Table I.16**).

Generally, the few inhibitors investigated so far have not shown evident selectivity towards hNAT1 in comparison to other NATs.

Table I.16: IC_{50} values of both steroidogenic compounds and xenobiotic oestrogens against mNat2.

The values are adapted from (Kawamura et al, 2008).

Group	Name	IC_{50} mNat2 (µM)
steroidogenic compounds	Pregnenolone	>100
	17-Hydroxy-progesterone	>500
	Androstenedione	>500
	Testosterone	>500
	Estrone	370 ± 10
	17-Hydroxy-β-estradiol	55 ± 5
xenobiotic oestrogens	Tamoxifen	57 ± 3
	4-OH tamoxifen	65 ± 15
	Diethylstilbestrol (E)-3,4-Bis(4-hydroxyphenyl)-3-hexene	<50
	Zearalenone	220 ± 10
	Alpha-Zearalenol	70 ± 10
	Beta-Zearalenol	450 ± 10
	Bisphenol A	290 ± 10
	Genistein	45 ± 5

I.4.2 Discovery of novel inhibitors of hNAT1 by HTP screen

In order to identify selective potent inhibitors of hNAT1 for investigating its physiological role and the link between the enzyme and BC, a two-stage screening process has been carried out.

A library of 5016 compounds has been screened at 30 µM against 5 different eukaryotic and prokaryotic enzymes (hNAT1, shNat2, PANAT, MSNAT and STNAT) and (Russell et al, 2009; Westwood et al, 2011). Fifty compounds were identified as selective inhibitors of the eukaryotic NAT proteins.

Afterwards, those molecules were subjected to a secondary screen to confirm their unique selectivity towards hNAT1 *versus* a panel of mammalian NAT isoenzymes sharing more than 70% sequence identity with hNAT1: hNAT2, mNat2, and mNat1(Russell et al, 2009).

Six compounds showed selectivity for hNAT1 and mNat2, the murine homologue of hNAT1, over the other isoenzymes and were further investigated for their effects on the inhibition of hNAT1 activity in cell lysates from a BC cell line overexpressing hNAT1, ZR-75-1 (Wakefield et al, 2008b): only two compounds, namely **naphthoquinone 1** and **rhodanine 5** inhibited hNAT1 activity in the ZR-75-1 cell lysate (Russell et al, 2009) (**Figure I.26**).

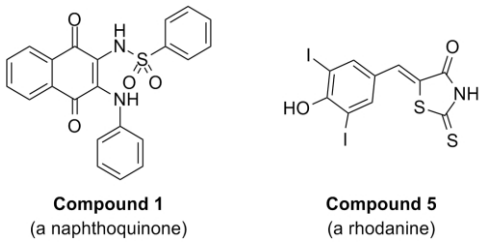


Figure I.26: Lead compounds selected from HTP screenings.

I.4.3 Lead inhibitors

The compounds **naphthoquinone 1** and **rhodanine 5** selected from the secondary screening were subsequently subjected to further studies and developed from the perspective of chemical genetics. *Ex novo* chemical synthesis and *in vitro* pharmacological evaluation of these two candidates against hNAT1 were subsequently undertaken in order to confirm initial findings. Afterwards, the synthesis of a range of structural analogues was carried out in order to attempt the optimisation of the pharmacological activity of the lead compound.

I.4.3.1 Rhodanine 5

Rhodanine **5** was initially selected for further studies. The synthesis and the evaluation of **rhodanine 5** and a series of derivatives as selective inhibitors of hNAT1 and mNat2 were successfully achieved (**Figure I.27**).

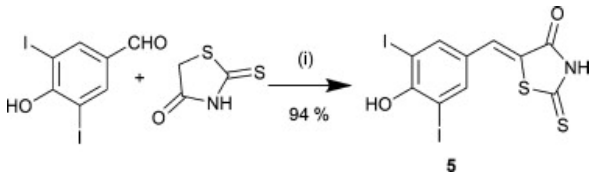


Figure I.27: Chemical synthesis pathway of rhodanine 5.

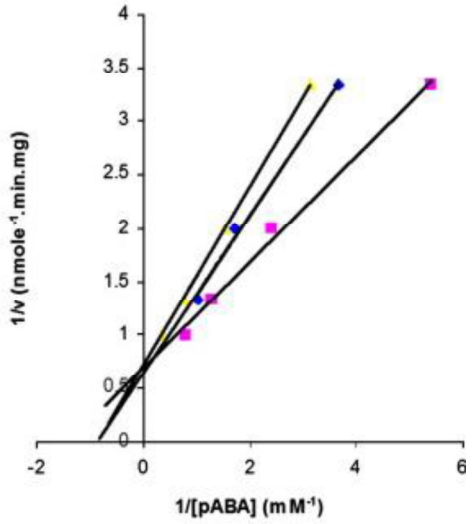
Reagents and condition: (i) NH_4OAc, Toluene, Δ, 24h.

The lead compound was shown to inhibit mNat2 in a competitive manner, binding within the putative active site of the enzyme according to both enzymology (**Figure I.28-left**) and ^{1}H-NMR studies.

The most potent inhibitors identified in that study showed submicromolar activity and inhibited hNAT1 as both pure recombinant protein and native protein in ZR-75-1 cell

lysate (Russell et al, 2009).

Unfortunately, the original hit compound **rhodanine 5** and other analogues showed >80% mouse macrophage cytotoxicity relative to the control (Russell et al, 2009) (**Figure I.28-right**).



	Toxicity[a]
DMSO	–
5	++

[a] ++, >80%; –, <80% cell death.

Figure I.28: Biochemical evaluation of rhodanine 5 as inhibitor of mNat2 and hNAT1.

(left) Kinetic analysis of **rhodanine 5**: double reciprocal plot shows inverse rates at inhibitor concentrations of 0 µM (square); 0.05 µM (diamond) and 0.1 µM (triangle). The inhibition seems to be competitive against mNat2. **(right)** Toxicity data for **rhodanine 5** at 10µg.ml^{-1} on mouse macrophages. The figure and the table are adapted from (Russell et al, 2009).

Recently, an optimisation study on **rhodanine 5** generated an ortho-hydroxy rhodanine analogue, namely **Rhod-o-hp**, with improved stability and cytotoxic properties (Tiang et al, 2010) (**Figure I.29**).

In these studies, Rhod-o-hp was demonstrated to inhibit tumorigenic properties (growth, proliferation and invasive ability) of the BC cell line MDA-MB-231 in a concentration-dependent manner, although the concentrations of the inhibitor used in that cellular study were higher than the inhibitory activity against recombinant hNAT1 and off-target effects could not be ruled out (Tiang et al, 2010).

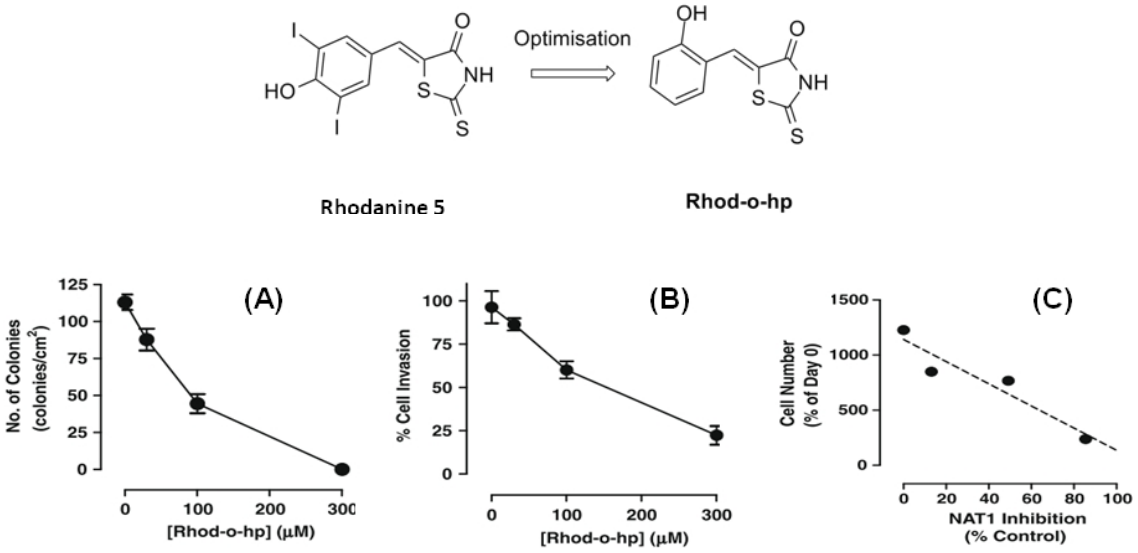


Figure I.29: inhibition of tumorigenic properties of MDA-MB-231 cells by Rhod-o-hp.

(top) chemical structures of **rhodanine 5** and **rhod-o-hp**. **(bottom)** (A) concentration-dependent reduction of colony formation in soft agar. (B) concentration-dependent reduction in cell invasiveness. (C) an increased hNAT1 inhibition decreases cell number. The plots are adpted from (Tiang et al, 2010)**.**

I.4.3.2 Naphthoquinone 1

Naphthoquinone 1 was discovered as a selective inhibitor of hNAT1 and mNat2, with IC_{50} = 1.65 and 1.86 μM respectively, with no inhibition of the other human and mouse NAT enzymes, hNAT2 and mNat1 (**Table I.17**). Compound **1** was also shown to be a competitive inhibitor of mNat2 (K_I = 520nm) from kinetic studies (Robinson, 2007) (**Figure I.30**). Furthermore, a solution of compound **1** was observed to undergo a distinctive colour change, observable by eye, from red to blue in the presence of either hNAT1 or mNat2 but not the other isoenzymes (**Table I.17**).

Table I.17: Comparison of inhibitory activity of comound 1 towards human and mouse NATs.

Percentage inhibition at 30 µM and colour change of **1** *versus* NAT isoenzymes. + indicates a colour change from red to blue, whilst - indicates no colour change.

Enzyme	% inhibition by compound 1 (Russell et al, 2009)	Colour change
hNAT1	> 95	+
mNat2	≥ 95	+
hNAT2	0	-
mNat1	0	-

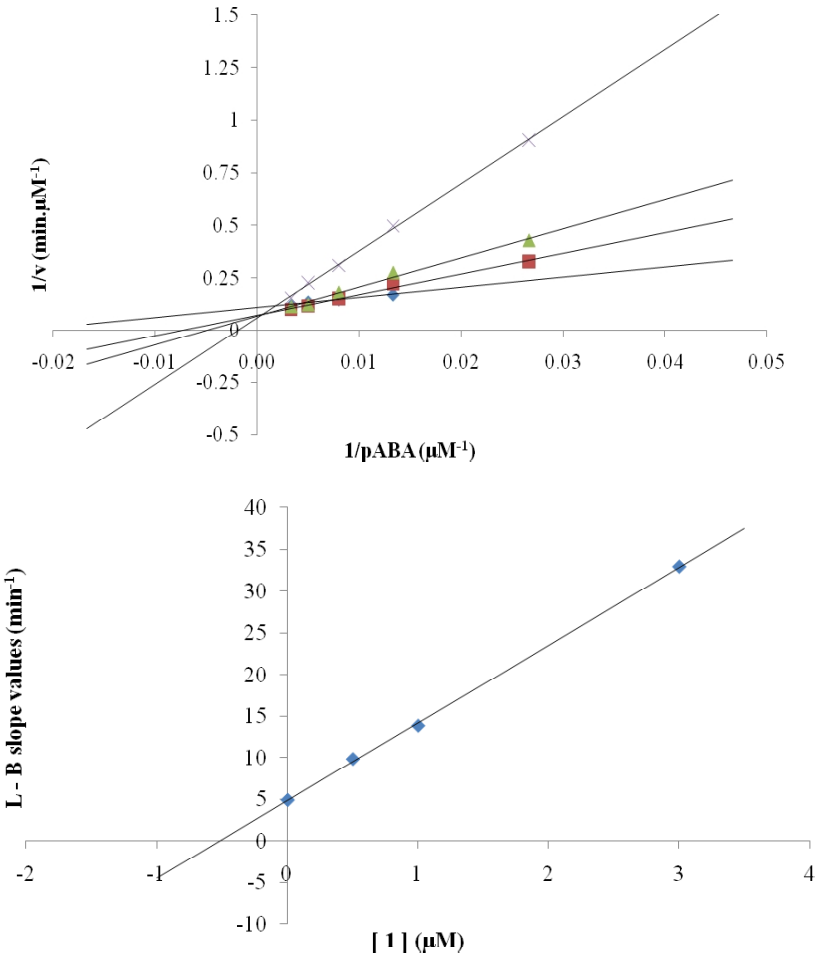


Figure I.30: Determination of the inhibition mode of naphthoquinone 1 to mNat2.

(left) Lineweaver-Burk plot shows mNat2 rates of hydrolysis with pABA as arylamine substrate, at inhibitor concentrations of 3µM (pink crosses), 1µM (green triangles), 0.5µM (red squares) and 0µM (blue diamonds). **(right)** Slope values from L-B graphs plotted against concentration of **naphthoquinone 1**. The figure is adapted from (Laurieri et al, 2010)

When an acid-base titration was carried out, the colour change of compound **1** was shown to be a pH-dependent event and a pK_a of ~9.5 was estimated for compound **1** using its colourimetric properties (**Figure I.31**).

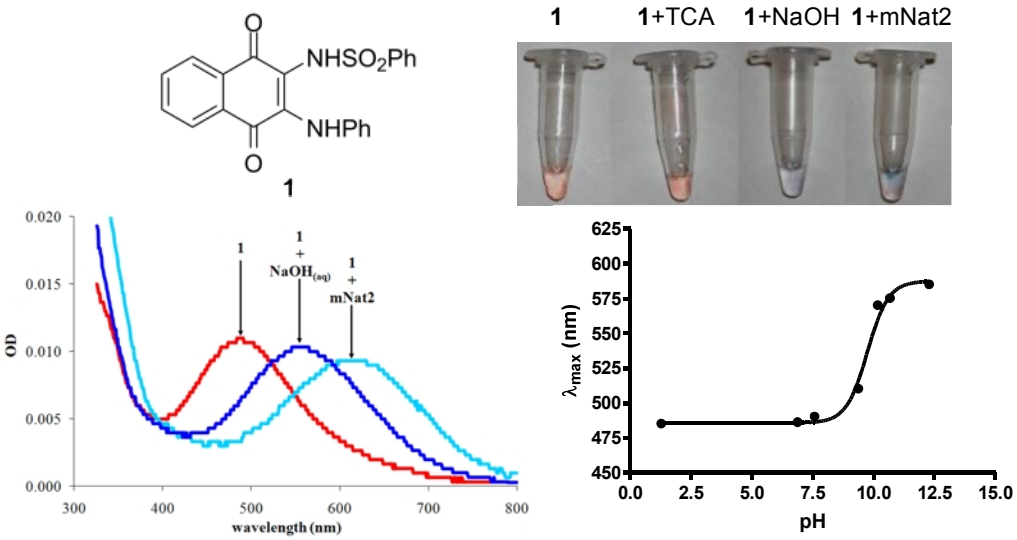


Figure I.31: Colourimetric properties of naphthoquinone 1.

(top left) chemical structure of **naphthoquinone 1**. **(top right) 1** (400µM) in aq. Tris.HCl (pH 8.0); 20 % trichloroacetic acid (TCA); 4 M aq. NaOH; or mNat2 in aq. Tris.HCl (pH 8.0). **(bottom left)** Visible spectra of **1** (10µM) in aq. Tris.HCl (pH 8.0, red line, λ_{max} = 489nm,), **1** in aq. NaOH solution (dark blue line, λ_{max} = 561nm), and **1** with 2 eq. of mNat2 in aq. Tris.HCl (pH 8.0, light blue line, λ_{max} = 610nm); **(bottom right)** pH titration curve for 1 (pK_a ~9.5) (Crawford, 2007). The figure is adapted from (Laurieri et al, 2010).

Early efforts were therefore directed towards the *de novo* synthesis of **naphthoquinone 1** (Crawford, 2007) and *in vitro* evaluation of **1** to validate its inhibitory activity against both hNAT1 and mNat2.

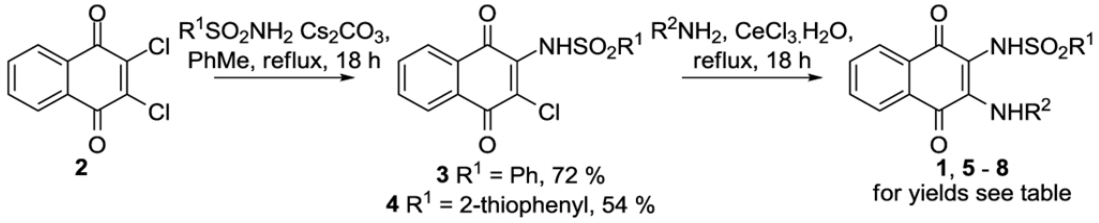
Afterwards, the optimisation of the lead compound **1** was sought by synthesising a range of derivative analogues (Laurieri, 2008) and screening a library of existing drug-like compounds to find analogues based on virtual-shape similarity (Ballester et al, 2010).

I.4.3.2.1 Improvement via medicinal chemistry studies

In order to probe the scope of the colour change event between **1** and hNAT1 and mNat2 and to improve the ligand potency, a series of analogues of **1** were prepared in a classical medicinal chemistry study (Laurieri, 2008; Laurieri et al, 2010) (**Table I.18**).

Table I.18: Preparation and pharmacological characterisation of a set of analogues of 1.

A set of analogues of **1** was synthesised. Compounds **1**, **5-8** were subsequently assessed as inhibitors of hNAT1 and mNat2. The activity of hNAT1 was determined as a decrease of the non-acetylated arylamine, with pABA as arylamine substrate and AcCoA as acetyl donor, in the presence of the appropriate inhibitor at a concentration of 5μM. The activity of mNat2 enzyme was determined as hydrolysis of AcCoA in the presence of pABA as arylamine substrate (Laurieri, 2008).



entry	substrate	R^1	R^2	product	yield (%)	% inhibition of hNAT1	IC_{50} (μM) *versus* mNat2	Colour change with mNat2	Colour change at pH 13
1	**3**	Ph	Ph	**1**	63	78.5 ± 8.7	1.86	+	+
2	**3**	Ph	4-BrC_6H_4-	**5**	10	91.0 ± 0.8	0.88	+	+
3	**3**	Ph	4-^{t}BuC_6H_4-	**6**	60	81.9 ± 0.9	5.86	-	-
4	**3**	Ph	3,5-$Me_2C_6H_3$-	**7**	53	77.0 ± 4.0	0.99	+	+
5	**4**	2-thienyl	Ph	**8**	54	75.0 ± 5.6	3.12	+	+

Analysis of the inhibitor activities of **1** and the analogues **5** - **8** against hNAT1 and mNat2 showed that all compounds inhibited both enzymes, to varying degrees.

The analysis of their colourimetric properties showed a distinctive colour change of most of the compounds upon basification or in the presence of mNat2 (Laurieri, 2008; Laurieri et al, 2010) (**Tables I.18, I.19, Figure I.32**).

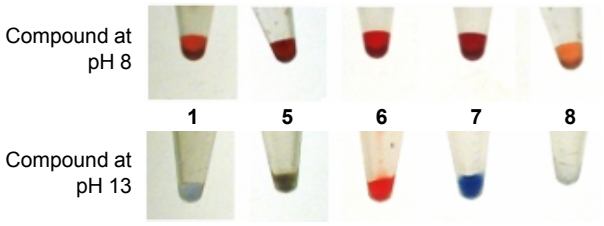


Figure I.32: Colourimetric properties of compounds 1, 5-8.

The compounds (2mM) were dissolved in Tris.HCl buffer (pH 8.0, top) or aq. NaOH (bottom) with 10% DMSO. The figure is adapted from (Laurieri et al, 2010).

Comparing the λ_{max} of the absorbance spectra of compounds **1**, **5**, **7** and **8** obtained at different conditions (**Table I.19**) showed to different extents a shift of the λ_{max} towards higher wavelengths upon basification and in the presence of mNat2.

This shift is formally named as **bathochromic shift** and it is opposite to **hypsochromic shift**.

Table I.19: Colour change of 1, 5-8 with aq. NaOH or mNat2 (2 eq.).

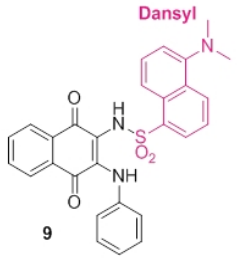
Compound (10 µM)	1	5	6	7	8
λ_{max} (nm) in 20mM Tris.HCl (pH 8)	489	487	484	498	490
$\Delta\lambda_{max}$ with NaOH (nm)	+72	+49	0	+74	+69
$\Delta\lambda_{max}$ with mNat2 (nm)	+121	+123	0	+127	+125

A derivative of compound **1, naphthoquinone 7**, was synthesised and showed moderately improved inhibitory potency *versus* mNat2 compared to the hit compound **1** (IC_{50}=0.99 µM *versus* IC_{50}=1.86µM), similar inhibition of recombinant hNAT1 in *E.coli* cell lysates, and a remarkably increased absorbance as both red (498nm) and blue (610nm) species related to **1** (Laurieri, 2008). Therefore, compound **7** became the new lead compound of this family. Besides this, an additional analogue of **naphthoquinone 1** with a fluorescent sulfonamide moiety (Dansyl) was also synthesised (compound **9**) (Laurieri, 2008) (**Table I.20**).

When compound **9** was excited at 361 nm in DMSO and tested with an aqueous solu-

tion containing mNat2 (2 equivalents) no difference was observed in the fluorescence spectrum in the presence of pure recombinant protein (Laurieri, 2008) (**Table I.20**). Moreover, as regards the colourimetric properties of compound **9**, it showed similar behaviour to **1** and **7**, but its lower inhibitor potency did not suggest further investigation.

Table I.20: Properties of compound 9 as biosensor to detect mNat2.



9

IC_{50} (μM) with mNat2	4.12
λ_{max} (nm) at pH 8.0	496
$\Delta\lambda_{max}$ at pH 13.8 (nm)	+ 68
$\Delta\lambda_{max}$ with mNat2 (nm)	+ 74
$\lambda_{max\text{-excitation}}$ (nm)	361
$\lambda_{max\text{-fluorescence}}$ (nm)	520
$\Delta\lambda_{max\text{-fluorescence}}$ with mNat2 (nm)	+ 0

In the end, the uniqueness of **naphthoquinone 1** to bind selectively to hNAT1 and mNat2 and change colour from red to blue upon binding to these pure recombinant proteins showed promising potential to be developed in detecting specifically hNAT1 as a biomarker in BC (Wakefield et al, 2008b).

I.4.3.2.2 Improvement via virtual shape recognition

One inexpensive way to address the current shortage of chemical molecules as bioactive probes for macromolecular targets is to use computational methods to screen databases of small molecules. This might help discover novel or better bioactive probes. Despite the applicability of virtual screening technology being well established, the results have

been somewhat mixed (Schneider, 2010).

A series of twenty-three potential inhibitors of hNAT1 was selected based on the structure of compound **1** using a recent method of virtual-comparison research, Ultrafast Shape Recognition (USR) (Ballester & Richards, 2007) (**Figure I.33**) amongst almost 700 million molecular conformers.

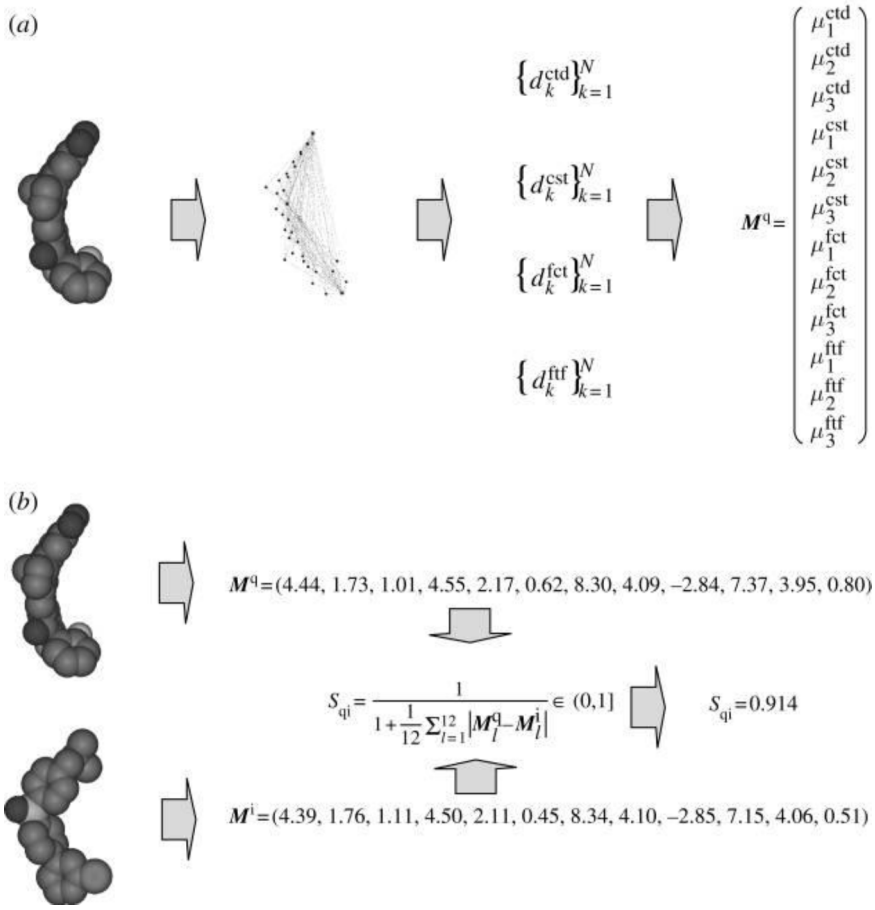


Figure I.33: Ultrafast Shape Recognition (USR) algorithm.

The figure is adapted from (Ballester et al, 2010). **(top)** USR encoding. The shape of the molecule is characterized by the distributions of atomic distances to four strategic reference locations. In turn, each of these distributions is described through its first three statistical moments. In this way, each molecule has associated a vector of 12 shape descriptors. **(bottom)** USR comparison. In order to establish the degree of similarity between the shape of two molecules, the Manhattan distance between the corresponding vectors of shape descriptors is calculated. Thereafter, this dissimilarity is monotonically inverted so as to define a normalized similarity score, where greater shape similarity is represented by scores nearer to 1. USR uses this score to determine which are the most similarly shaped molecules in a database to a given query molecule.

Although none of the these new bioactive mNat2 inhibitors were more potent than **naphthoquinone 1**, the most potent inhibitors (**Figure I.34**), were potentially considered as alternative starting points for a lead optimization process (Ballester et al, 2010).

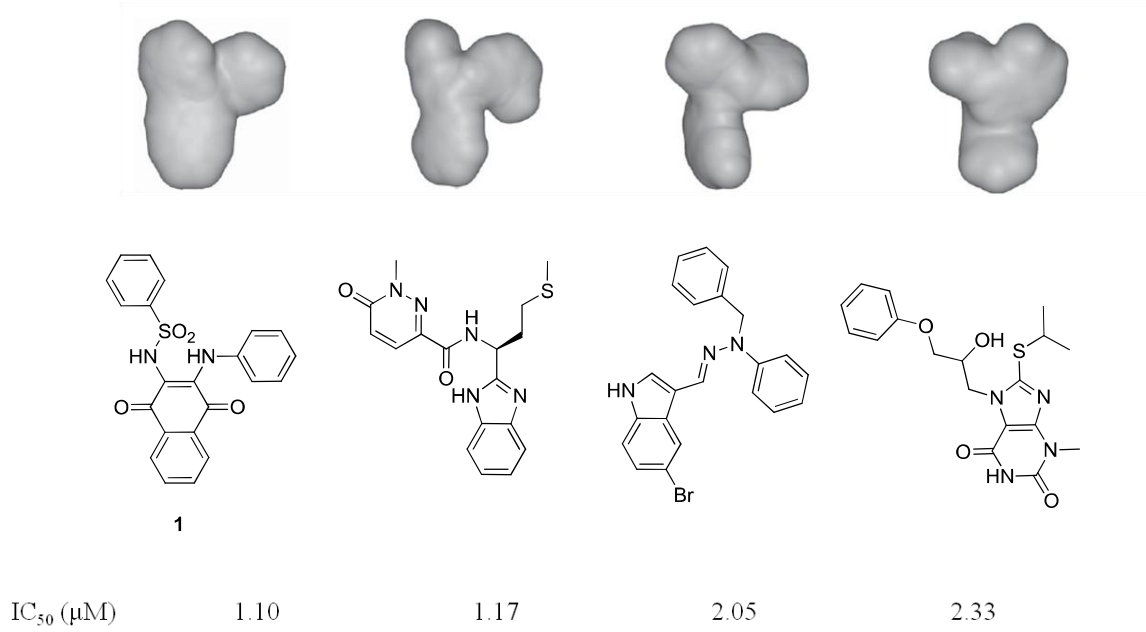


Figure I.34: Comparison of USR query molecule 1 and the best three USR results.

Shapes, chemical structure and IC_{50} values against pure recombinant mNat2 for the query molecule and the three most potent active molecules found by USR are shown (from left to right: S_0^{USR}=1.000, S_1^{USR}=0.969, S_3^{USR}=0.966 and S_{17}^{USR}=0.950). The figure is adapted from (Ballester et al, 2010) with minor modifications.

I.5 Conclusions

BC is the most common cancer in the United Kingdom and worldwide, with more than a million women diagnosed with BC every year. BC is a heterogeneous disease and different BC subtypes can be identified based on gene expression profiling. Current ER+ve BC therapies based on SERMs, such as tamoxifen, can be unsuccessful due to intrinsic or acquired resistance to these therapies. Comparing gene expression profiles of tumours, either responsive or resistant to current therapies, has been well established in identifying new markers of increased risk or of therapy failure.

In reality, after profiling gene expression in BC samples, hNAT1 was found to be a gene overexpressed in BC cells, constituting a new diagnostic marker or drug target for BCs.

The identification of a family of naphthoquinone reagents which could bind selectively to hNAT1 and its murine homologue mNat2 with a concomitant colour change constitute an interesting property to be investigated and subsequently exploited for diagnosis.

I.6 Aims

Previous studies about hNAT1 and BC together with preliminary work conducted on hNAT1 and naphthoquinones **1-8** suggested a potential application of these compounds as colourimetric biosensors and/or drug-like inhibitors of hNAT1 in BC cells. However, many questions remained unanswered about this enzyme, its role in both cell and disease, and the possible use of these napthoquinones as colourimetric biosensors or selective inhibitors. Therefore, the overall aims of this work are:

- To characterise the inhibitory properties of the new hit compound **7** towards pure recombinant hNAT1 and its murine homologue, mNat2, *versus* other NAT isoenzymes (**Chapter III**);

- To elucidate the molecular mechanism of interaction between compound **7** and mNat2, as a model for hNAT1 (**Chapter IV**);

- To study substrate specificity of human and murine native proteins *versus* mutant murine NAT enzymes (**Chapter V**)

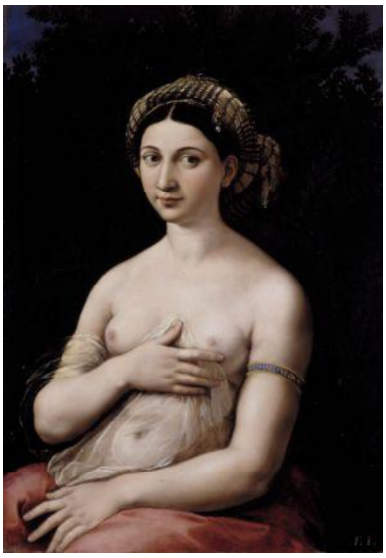
- To apply the lead compound **7** for detection of hNAT1 in the BC cell line ZR-75-1 and to investigate its effect on cells (**Chapter VI**);

- To optimise the affinity potency of compound **7** towards hNAT1 and mNat2 (**Chapter VII**);

- To investigate the endogenous role of hNAT1 and mNat2 as folate-dependent-AcCoA hydrolases (**Chapter VIII**).

Chapter II:

Materials and methods



LA FORNARINA (~1520), BY RAFFAELLO SANZIO (1483-1520).

The intricate interplay of colours, contrasts, and shadows visible at close range on the left breast, depicts La Fornarina's breast deformation. The medical analysis has suggested a diagnosis of a cancerous mass with possible morphological details of invasion (Espinel, 2002). (from Barberini collection, Rome)

II.1 Materials

II.1.1 Chemicals and reagents

All chemicals were purchased from Sigma-Aldrich unless otherwise stated. Molecular biology reagents were obtained from Promega (Southampton, UK). Competent *E. coli* cells were purchased from Promega and Invitrogen (Carlsbad, USA). The pH of buffer solutions was adjusted at the appropriate temperature.

II.1.2 Growth media

All bacterial cultures were grown in Luria-Bertani (LB) liquid medium or LB agar plate, as shown in **Table II.1**.

Table II.1: Growth media used throughout this study.

All media were sterilised by autoclaving for 30 min at 120°C.

Medium	Ingredients
Luria-Bertani (LB) liquid medium	10 $g.l^{-1}$ Bacto®-Tryptone (Difco Labs), 5 $g.l^{-1}$ Bacto®-Yeast Extract (Difco Labs), 10 $g.l^{-1}$ NaCl, pH 7.0
LB Agar	15 $g.l^{-1}$ agar (Difco Labs) in LB medium, molten at 60 ˚C and casted in Petri-dish
SOC medium	10mM NaCl, 2.5mM KCl, 20mM $MgSO_4$ and 20mM glucose in LB medium

II.1.3 Plasmids and bacterial strains

The Rosetta(DE3)pLysS *E.coli* strain containing the pET28b(+) plasmid (Novagen) with the *mNat2* gene appropriately cloned was kindly provided by Prof. Edith Sim (Kawamura et al, 2008).

pET28b(+) plasmid (**Figure II.1**) was also used as a vector for the mutated *mNat2* genes. pET28b**(+)** is 5,369 bp plasmid used for protein production in *E. coli* strains. *E. coli* JM109 was used for plasmid maintenance and site-directed mutagenesis studies. *E. coli* Rosetta(DE3)pLysS was used for gene expression and production of recombinant protein. Antibiotics were added to the overnight cultures for selection of positive clones, as stated in **Table II.2**.

Table II.2: *E. coli* strains used throughout the study presented in this thesis.

***E. coli* Strains**	**Genotype**	**Antibiotic used**
JM109 (Promega)	*endA*1, *recA*1, *gyrA*96, *thi*, *hsd*17 (r_K^-, j_k^+), *relA*1, *supE44,* Δ(*lac-proAB)*, [F', *traD*36, *proAB, lacI*^{q}ZΔM15]	Kanamycin (30μg.ml^{-1}) (when containing pET28b(+) vector)
Rosetta(DE3)pLysS (Novagen)	F$^-$ *ompT hsdS*$_B$(r_B^- m_B^-) *gal dcm* (DE3) pLysSRARE (Cam^R)	Chloramphenicol (34μg.ml^{-1}) (Kanamycin (30μg.ml^{-1}) when containing pET28b(+) vector)

All bacterial cultures were grown in LB liquid medium or LB agar plate with additional antibiotic supplement as stated.

II.1.4 Antibodies

A polyclonal antipeptide antiserum previously raised against the C-terminal decapeptide of mNat2 was kindly provided by Prof. Edith Sim (Stanley et al, 1998).

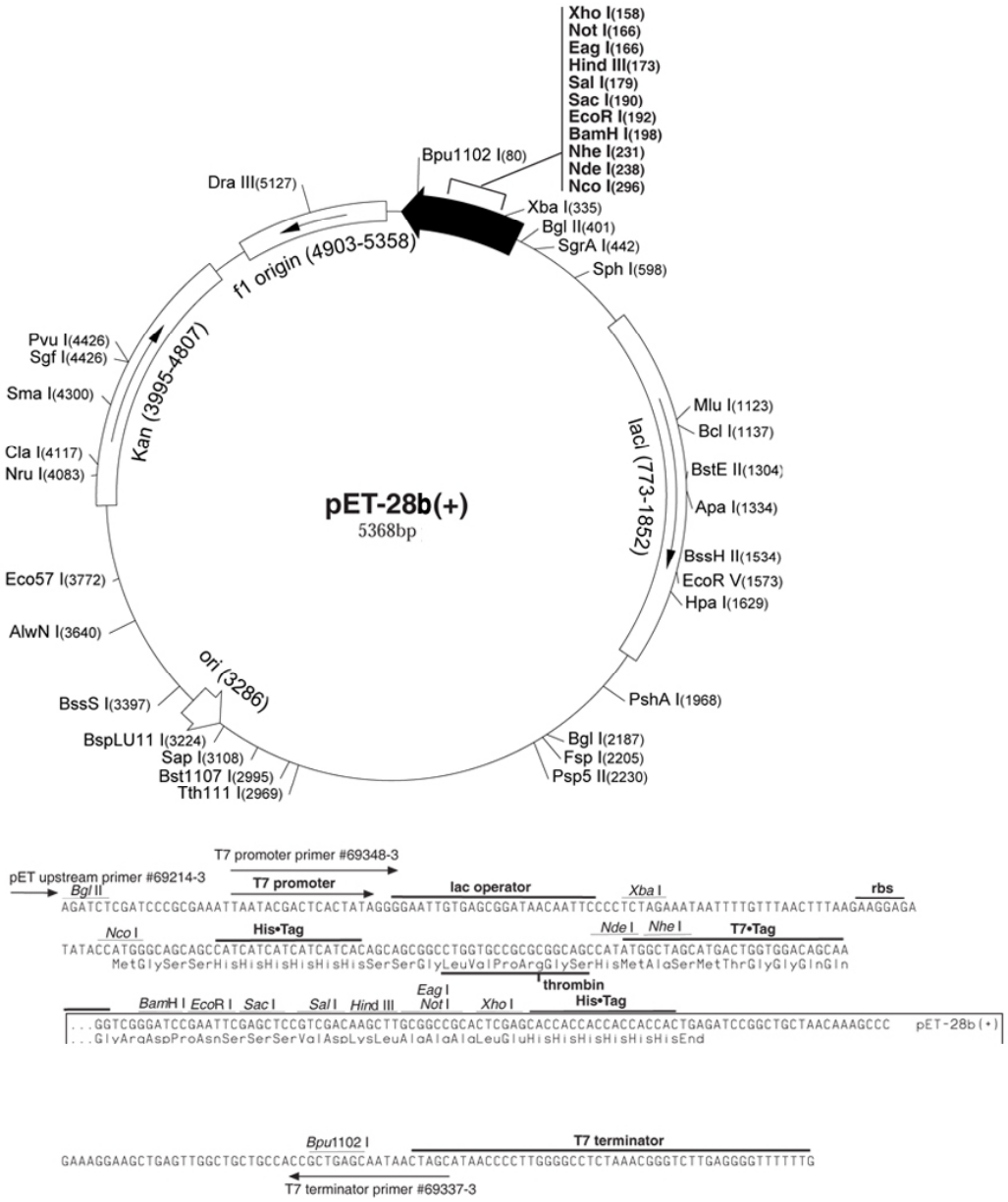


Figure II.1: pET28b(+) vector map and key features.

The figure is adapted from the Novagen website. In this expression system, the addition of isopropyl β-D-thiogalactopyranoside (IPTG) to a λ(DE3) E. coli lysogen induces the translation of the T7 bacteriophage RNA polymerase: this allows the insert cloned downstream of the plasmid-encoded T7 promoter to be transcribed. The multiple cloning sites offered by the pET28b(+) sequence lets commonly available restriction endonucleases be used and facilitates the production of *N*-terminal hexa-histidine tagged proteins. The vector also codes for a thrombin cleavage site (LVPRGS) for ease of removing the *N*-terminal hexa-histidine tag from a heterologously expressed protein. The T7 promoter and T7 terminator are located ~380 bp apart in the native plasmid sequence and the distance is increased after DNA-vector ligation. This could be a useful tool to screen DNA insertions. The vector contains a kanamycin resistance cassette which facilitates the selection of the bacterial strains containing the plasmid.

II.2 Methods

II.2.1 Bioinformatic analyses

Basic Local Alignment Search Tool (BLAST) analysis was performed using the National Center for Biotechnology Information (NCBI) BLAST tools (http://blast.ncbi.nlm.nih.gov/Blast.cgi). The nucleotide and protein sequences were downloaded from the NCBI Nucleotide and Protein databases. Nucleotide and protein sequence alignments were performed by using ClustalW2 (Thompson et al, 1994) from the European Bioinformatics Institute (EBI) at http://www.ebi.ac.uk/Tools/clustalw2/ with OUTPUT ORDER parameter set to 'input'. Alignment files (.txt) were converted to the 'PDF' format or 'TIFF' image format with ESPript 2.2 (Gouet et al, 1999) at http://espript.ibcp.fr/ESPript/, with the secondary structure input downloaded from RCSB Protein Data Bank (PDB) (http://www.rcsb.org/pdb/).

II.2.2 Molecular Biology

II.2.2.1 DNA purification

Plasmid DNA was extracted from 5 ml overnight bacterial cultures using a QIAprep spin miniprep kit (Qiagen) *via* standard protocols indicated by the manifacturer.

II.2.2.2 Determination of nucleotide quantity and quality

DNA samples were diluted to appropriate concentrations using sterile double distilled water in a UVette (Eppendorf): an accurate optical density (OD) at 260 nm was estimated to be between the values of 0.2 to 1.0.

The concentrations of DNA were measured spectrophotometrically with a BioPhotometer (Eppendorf): an absorbance of 1 unit at 260 nm corresponded to 50 μg ml^{-1}. A ratio of 1.6 to 1.9 of the absorbance values at 260 and 280 nm indicated the purity of the DNA.

II.2.2.3 Polymerase chain reaction (PCR)

For T7-primed screening, the specific primers used to amplify DNA for sequencing are shown in **Table II.3**.

The following thermo-cycling protocol was applied to all amplification mixtures (**Table II.4**): one cycle for denaturation (2 min at 95 ºC), 30 cycles for elongation (1 min for melting at 95 ºC, 30 s for annealing at 60 ºC, and 1 min for extension at 72 ºC), an extra cycle for an extension at 72 ºC for 10 min, and a final cooling cycle at 4 ºC for 5 min.

Table II.3: DNA primers used for PCR amplification.

Primer name	Sequence (5'→ 3')
T7 promoter	taatacgactcactataggg
T7 terminator	gctagttattgctcagcgg

Table II.4: Typical PCR amplification mixture.

Reagent	Comments	Volume (μL)
10 X *Pfu* DNA polymerase buffer	Mg^{2+} at 20mM	5
dNTPs	Mixture, 10mM of each	1
DMSO	6% final concentration	3
5' Primer	100μM final concentration	0.5
3' Primer	100μM final concentration	0.5
DNA template	0.1 $\mu g.\mu l^{-1}$	1
Pfu + *Taq* DNA polymerase	1:1 (unit) ratio	0.4
ddH_2O		38.6
Total volume		**50**

II.2.2.4 Site-directed mutagenesis

Site-directed mutagenesis was achieved by using QuikChange II kit (Stratagene) according to the manufacturer's instructions. The pET28b(+) plasmid containing the *mNat2* insertion was used as template. The oligonucleotides designed to set up the site-directed mutagenesis PCR reactions are listed in **Table II.5**.

The un-mutated parental DNA template present in the PCR product was digested by 10U of *Dpn* I (New England Biolabs) for 1 hour at 37°C. Mutant plasmids were verified by sequencing analysis to ensure the correct change before being transformed into the expression vector.

Table II.5: Primers used for site-directed mutagenesis study.

The imbedded mutations for each generation of each mutant of mNat2 are shown in bold.

Primer name	Sequence (5'→ 3')
R127G forward	gctgggtttgga**ggt**tcctaccagatgtgggagcc
R127G reverse	ggctcccacatctggtagga**acc**tccaaacccagc
R127L forward	gctgggtttgga**ctt**tcctaccagatgtgggagcc
R127L reverse	ggctcccacatctggtagga**aag**tccaaacccagc

II.2.2.5 Plasmid transformation into *E. coli* strains

The heat shock method (Sambrook et al, 1989) was used to transform vector plasmid into *E. coli* cells. Samples (50 µl) of thawed competent *E. coli* cells (Promega) were mixed with 2 µl of pure DNA plasmid in sterile 1.5 ml microcentrifuge tubes (Eppendorf) on ice for 5 min.

The transformation mixtures were then heat shocked at 42 ºC for 45 s and then cooled on ice for 2 min prior to dilution with 950 µl of pre-heated 37 ºC SOC medium.

II.2.2.6 Selection of positively transformed colonies

SOC medium containing transformed *E. coli* strains was recovered in a shaking incubator (180 rpm) at 37 ºC for 1 h, before being spread onto LB agar plates containing kanamycin. Plates were incubated at 37 ºC for 16 h.

The viability of the transformed cells was verified by a positive control, wherein no antibiotic was added to the LB agar plate. Also, the possibility of undesired contaminations was ruled out by a negative control, wherein non-transformed *E. coli* cells were spread on a plate containing kanamycin.

Positively transformed bacterial colonies were picked and used as templates in the gene specific-primed PCR analysis in order to confirm the presence of the correct DNA insertion within the plasmid.

Bacterial colonies with the correct DNA insertions were picked from the appropriate LB agar plate and grown overnight in 10 ml LB medium with the apposite antibiotic for further plasmid extraction and subsequent analyses.

II.2.2.7 DNA sequence analysis

Samples containing DNA were purified and adjusted to an appropriate concentration for DNA sequencing analyses (**Table II.6**), with the use of T7 primers. DNA sequencing was performed by GeneService at Department of Biochemistry, University of Oxford, UK.

Template plasmid, 15 µl, was supplied at a minimum concentration of 100ng.μl^{-1} for each sequencing reaction. Sequencing chromatograms were analysed with FinchTV (http://www.geospiza.com/finchtv.html).

Table II.6: Sample requirements for DNA sequence analysis.

The volumes are expressed as minimum requirement per reaction as requested by GeneService and the concentrations indicate the DNA concentrations in the mixture.

	PCR product	Plasmid	Primer (if required)
Volume (µl)	10	15	10
Concentration	20ng.µl^{-1}	100ng.µl^{-1}	3 pmol.µl^{-1}

II.2.2.8 Storage of nucleic acids and transformed *E. coli* cells

E. coli cells containing the correct plasmid insert were picked from the appropriate LB agar plates to inoculate 10 ml LB medium with the appropriate antibiotics. The culture was grown in a shaking incubator (37 ºC, 180 rpm) until the OD at 600 nm reached 0.4 - 0.6. Glycerol was added to the culture medium to a final concentration of 10% (v/v); the culture was then aliquoted into 1 ml fractions in 2 ml cryovials (Nalgene), snap-frozen in liquid nitrogen and stored at -80 ºC.

II.2.3 Gene expression and protein purification

II.2.3.1 Expression of wild-type and mutated *mNat2* genes

Thawed glycerol stocks of the appropriate *E.coli* Rosetta(DE3)pLysS strain (Novagen) (100µl), previously stored at -80°C with 10% (v/v) glycerol, were used to inoculate fresh LB media (10 ml) supplemented with kanamycin (30µg.ml^{-1}) and chloramphenicol (34µg.ml^{-1}) and the culture was incubated at 37°C for 16 h with shaking (180 rpm).

The starter culture was then diluted 100-fold into fresh LB media (1 l) supplemented with kanamycin (30µg.ml^{-1}), and chloramphenicol (34µg.ml^{-1}) which was then incubated at 37°C with shaking (180 rpm).

When the absorbance at 600 nm reached 0.4-0.6, the expression of mouse Nat2 was induced by addition of IPTG to a final concentration of 0.1mM. The culture was grown for a further 4 h.

A similar procedure was used to express the two *mNat2* genes mutated at residue 127.

II.2.3.2 Cell lysis

After incubation, the cells were harvested by centrifugation (6,000×*g*, 4°C, 20 min). Cell pellet was resuspended in 20 ml lysis buffer (300mM NaCl, 20mM Tris-HCl (pH 8.0) containing 1× EDTA-free Complete Protease Inhibitor (Roche) and then stored at −80°C.

The resuspended frozen cells were thawed at 37°C and sonicated on ice (30 cycles of 30 s on, 45 s off at 10MHz) using Soniprep 150 (MSE). The soluble lysate was isolated from the cell debris by centrifugation (12,000×*g*, 4°C, 20 min).

II.2.3.3 Protein purification

The immobilised metal-ion affinity chromatography (IMAC) method was chosen for the purification of the hexahistidine-tagged recombinant proteins. The soluble lysate collected from centrifugation was incubated with 5 ml of Ni-NTA resin (Qiagen) at 4°C for 5 min.

The resin was sequentially washed with buffer (20mM Tris.HCl, pH 8.0) containing increasing imidazole concentrations in a step-gradient manner at 4°C (1 or 2 washes each of 5 ml of 0, 1, 10, 50, 200, and 500mM imidazole). Fractions containing hexa-histidine tagged mNat2 (His-Nat2), were pooled and thrombin (5 $U.mg^{-1}$ of NAT) was added to remove the His-tag.

II.2.3.4 Buffer exchange and protein concentration

After 16 h incubation with thrombin at 4°C, the protein sample was dialysed against 4 L 20mM Tris.HCl (pH 8.0), 1mM dithiothreitol (DTT), 1mM EDTA buffer, using 20 kDa molecular weight cut-off dialysis tubing (Medicell).

Afterwards, recombinant protein solutions were concentrated by centrifugation in a 15 ml concentrator (Amicon). Buffer exchange was achieved by supplying a different buffer (20mM Tris.HCl, pH 8.0, 5% glycerol (v/v)) and repeating the same centrifugation where necessary.

Purified recombinant proteins were fractioned into 25µl aliquots, frozen in liquid nitrogen and stored at -80°C (**Table II.7**).

Table II.7: Concentration of pure recombinant mNat2 protein stocks.

Protein	Concentration
mNat2 (**Section III.2.1**)	20.5mg.ml^{-1}
mNat2 (**Section IV.2.2.2**)	1.8mg.ml^{-1}
mNat2_R127G	4.1mg.ml^{-1}
mNat2_R127L	4.0mg.ml^{-1}

II.2.4 Recombinant protein characterisation

II.2.4.1 Determination of protein concentrations

The concentration of purified protein in the solution was determined using the Beer-Lambert law: $\mathbf{A}_\lambda = \varepsilon_\lambda \cdot \mathbf{c} \cdot \mathbf{l}$, where the $\mathbf{A}_\lambda$ is the absorption and ε_λ is the molar extinction coefficient (MEC) at wavelength λ, **c** is the concentration of protein, and **l** is the length of the light path in cm.

The molar extinction coefficients at 280 nm (ε_{280}) and the molecular weights of recom-

binant mNat2 proteins were calculated by ExPASy ProtParam (Gasteiger et al, 2003; Gasteiger et al, 2005) on the website http://www.expasy.ch/tools/protparam.html (**Table II.8**).

Table II.8: ε_{280} and theoretical molecular masses of recombinant mNat2 mutants

Protein	ε_{280} ($M^{-1}.cm^{-1}$)	Molecular weight (Da) of thrombin-digested proteins
mNat2	42,860	33,701.4
mNat2_R127G	42,860	33,602.2
mNat2_R127L	42,860	33,658.3

The concentrations of protein in all imidazole-wash samples from the purification procedures were determined by the Bradford assay (Sigma Aldrich) using bovine serum albu min (BSA) as protein standard. Mean values of protein concentrations were calculated from triplicate determinations.

II.2.4.2 Determination of protein molecular weight

Sodium dodecylsulfate polyacrylamide gel electrophoresis (SDS-PAGE) was used to separate and visualise protein samples as previously described (Sambrook et al, 1989) and performed by the method of Laemmli (Laemmli, 1970).

The gel contained a 12% acrylamide separating gel (12.0 ml ProtoGel®, 7.8 ml ProtoGel® resolving buffer, 3.0 ml 1% ammonium persulfate, 7.15 ml deionised water, 0.05 ml tetramethylethylenediamine (TEMED)) and a 4% acrylamide stacking gel (3 ml ProtoGel®, 4ml ProtoGel® stacking buffer, 1.6 ml 1% ammonium persulfate, 8.5 ml deionised water, 0.05 ml TEMED).

Gels were cast in a vertical mini-gel apparatus Miniprotean III (Biorad**)**. 5µl of the appropriate sample was added to 15µl of reduced gel loading buffer (10mM pH 6.8

Tris.HCl, 8 M urea, 2% (w/v) SDS, 5mg.ml^{-1} DTT, 2% (v/v) glycerol containing 10µg.ml^{-1} bromophenol blue) and then heated to 95°C for 5 min to denature the protein. 10µl of the cooled solution was then loaded into one of the wells on the gel over air.

A reference ladder was loaded in a well, as indicated in each figure legend, and electrophoresis was carried out using a 25 mA current in a pre-cooled running buffer (50mM Tris.HCl (pH 8.3), 50mM glycine, 1% (w/v) SDS).

The gel was visualised by shaking for 15 min in a Coomassie Blue staining solution (0.375 % (w/v) Coomassie Brilliant Blue R-250, 18.75 % (v/v) acetic acid, 45 % (v/v) methanol, room temperature) and de-stained for 2 h in a de-staining solution (10% (v/v) ethanol, 10% (v/v) acetic acid, room temperature).

II.2.4.3 Determination of protein melting temperature

A modified Differential Scanning Fluorimetry (DSF) procedure was followed (Niesen et al, 2007). Pure recombinant mNat2 was diluted to 0.067mg.ml^{-1} in an appropriate buffer (500mM NaCl, 10mM HEPES pH 7.5) and 0.5 µl of 5,000× SYPRO Orange fluorescent dye (Invitrogen) was added per 1 ml of protein solution (1:2,000 dilution). 19.5 µl of this solution was added to wells of a white qRT-PCR low-profile plate (Abgene-Thermo) followed by addition of 0.5 µl buffer.

Plates were placed in a Stratagene Mx3005p real-time PCR machine (Agilent Technologies) and fluorescence measured as a function of temperature between 25 ^{o}C and 95 ^{o}C (increase of 3 ^{o}C per min). Results were processed with GraphPad Prism software and a sigmoidal dose-response curve was used as model to determine the melting temperature (T_m) by the method of least squares.

II.2.5 Enzymatic assays

The rates of all enzymatic assays are initial rates determined from the linear initial section of graphs of absorbance *versus* time. Assays were conducted in triplicate, and the rates and kinetic parameters quoted in this study are mean values of the three independent measurements±standard deviation, unless otherwise stated.

Since different sources of enzymes were used for activity assays, different protein concentrations and incubation times were selected to give a linear initial rate.

Recombinant mNat2 mutant proteins were obtained in this study as described in **Section II.2.3**, whereas the preparation of the cytosols from the ZR-75-1 cell lines containing significant amount of hNAT1 was performed as described in **Section II.2.8.1.1**.

All the other NAT enzymes used throughout this study were kindly provided as pure recombinant proteins by Prof. Sim.

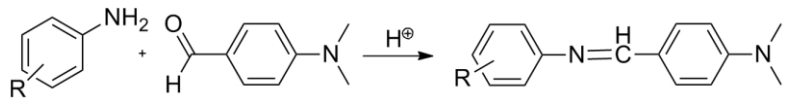
The NATs used were as follows, each previously prepared according to the procedures described in the past: hNAT1 (Kawamura et al, 2005; Wang et al, 2005b), STNAT (Sinclair et al, 2000), PANAT (Westwood et al, 2005), MMNAT (Fullam et al, 2008), MSNAT (Sandy et al, 2005a; Sandy et al, 2002), TBNAT (Abuhammad et al, 2011; Fullam et al, 2009).

II.2.5.1 Estimation of NAT activity

Two methods were used to determine NAT activity both of which have previously been demonstrated to give equivalent results (Brooke et al, 2003b): one quantified the direct disappearance of the arylamine over time, the other estimated the formation of the Coenzyme A (CoA) product, assuming that one molecule of CoA was formed per molecule of arylamine acetylated.

II.2.5.1.1 Determination of NAT activity following arylamine acetylation

Where specified, the rates of enzymatic reactions with arylamine substrates were determined using the colourimetric agent 4-dimethylaminobenzaldehyde (DMAB), using a modified literature method (Andres et al, 1985) (**Scheme II.1**). This procedure has the inconvenience of being applicable only for aniline derivatives, as substrates (Andres et al, 1985).



Scheme II.1: NAT activity determined by detection of arylamine acetylation using DMAB.

The enzymatic activity is measured by quantifying the disappearance of the arylamine substrate as reflected by decreasing Schiff's base formation with DMAB.

Samples of enzyme (as stated in each figure legend) and the appropriate arylamine (150μM) were pre-incubated at 37°C in assay buffer (20mM Tris.HCl, pH 8.0, 1mM DTT) for 5 min in a 96-well plate (Corning).

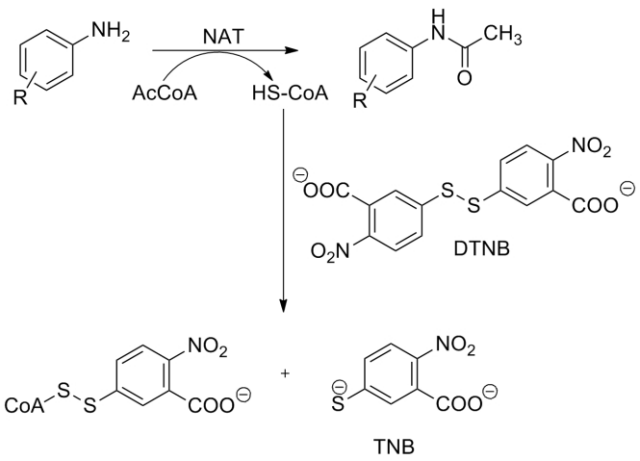
Pre-warmed AcCoA (400 μM final concentration, 37°C, in assay buffer) was added to start the reaction (final volume of 45μl), which was allowed to proceed at 37°C. The reaction was quenched with 45μl of 20 % (w/v) aqueous trichloroacetic acid (TCA) solution at 0°C. 150μl of DMAB (5% (w/v) in 90% aqueous CH_3CN solution) was added and the mixture was incubated at room temperature for 15 min.

The absorbance was measured at 450 nm in the 96-well micro plate using a plate reader (Tecan Sunrise), and the concentration of arylamine was calculated by reference to a standard curve. Controls with buffer alone were carried out and all reactions were performed under linear initial conditions.

II.2.5.1.2 Determination of NAT activity following AcCoA hydrolysis

The rate of formation of CoA was determined spectrophotometrically using the colourimetric agent 5,5'-dithio-bis(2-nitrobenzoic acid) (Ellman's reagent, DTNB) as previously described, with some minor modifications (Brooke et al, 2003b).

The extent of reaction is measured by detecting the coloured 5-thio-2-nitrobenzoic acid (TNB), which is produced by the reaction of DTNB with free thiol CoA formed during the NAT reaction and has a maximum absorbance at 412 nm (Brooke et al, 2003b; Riddles et al, 1983) (**Scheme II.2**).



Scheme II.2: NAT activity determined by detection of CoA formation using DTNB.

NAT activity reaction releases free CoA (HS-CoA) in the assay, and the amount of CoA produced is proportional to the amount of arylamine acetylated and was therefore quantified by spontaneous reaction with DTNB, which is added to the assay in a guanidine solution (pH 7.3).

This method has the benefit of being usable not only for arylamines, but also for a large variety of arylhydrazines, alkoxyanilines and arylhydroxylamines, as substrates for NATs (Brooke et al, 2003b). This assay was used mainly with pure recombinant NATs and the appropriate arylamine substrate was chosen according to Westwood *et al* (Westwood et al, 2006).

The appropriate NAT enzyme (as stated in each figure legend) was preincubated with the apposite arylamine substrate (150 - 500μM) in assay buffer (20mM Tris.HCl, pH 8.0) for 5 min at 37°C in a 96-well plate (Corning). Pre-warmed (37°C) AcCoA (400μM) in assay buffer was added to start the reaction (final volume of 100μl), which was allowed to proceed at 37°C. Simultaneous quenching and colour development was achieved by addition of the stop reagent: 25μl DTNB solution (5mM DTNB in 100mM Tris.HCl, 6.4 M guanidine.HCl, pH 7.3).

The absorbance was read immediately after the addition of the stop reagent at 405 nm using a plate reader (Tecan Sunrise). The rate of reaction was determined by reference to a standard curve. Controls with buffer alone were carried out and all reactions were performed under linear initial conditions.

II.2.5.1.3 Determination of NAT activity via NMR

Purified recombinant mNat2 (10μg) was preincubated with pABA (500μM) at 37°C in phosphate-buffered saline (PBS) solution in D_2O (pD 7.4). AcCoA (400μM) was added to start the reaction. Enzymatic activities were measured during real-time NMR at 37°C. NMR spectra were recorded on Bruker Avance spectrometer spectra AVII 500 in the deuterated solvent stated. The field was locked by external referencing to the relevant deuteron resonance (D_2O). NMR data were collected before and after adding AcCoA.

II.2.5.2 NAT Substrate profile

II.2.5.2.1 Arylamine substrates

The arylamine specific activity profiles for mNat2, mNat2_R127G and mNat2_R127L

were determined by measuring the rate of CoA production, as described in **Section II.2.5.1.2**. Purified enzyme (1.4μg of mNat2, 0.8μg of mNat2_R127G, and 5.5μg of mNat2_R127L) was incubated with the appropriate arylamine substrate (500μM) and AcCoA (400μM) in assay buffer (20mM Tris.HCl, pH 8.0) containing 0.5% DMSO (v/v) at 25°C. The specific activities were determined from the linear initial rates of reaction. All measurements were performed in triplicate.

Substrate abbreviations used for the substrate selectivity assays are as follows: 4-aminobenzoic acid (pABA), 4-aminobenzoyl-l-glutamate (pABAGlu), 4-aminosalicylic acid (4AS), 5-aminosalicylic acid (5AS), 4-chloroaniline (4CA), 4-bromoaniline (4BA), 4-iodoaniline (4IA), 4-methoxyaniline (ANS), 4-hexyloxyaniline (HOA), 4-phenoxyaniline (POA), 4-aminoveratrole (4AV), procainamide (PRO), sulfamethazine (SMZ), 4-aminopyridine (4APY), isoniazid (INH), hydralazine (HDZ). A 100mM stock solution for each substrate was prepared in DMSO, such that the final concentration of DMSO was less than 5% in the assay. Enzymatic assays containing DMSO-only were carried out as negative controls.

II.2.5.2.2 AcylCoA substrates

AcylCoA specific activity profiles for NAT enzymes were determined by measuring the AcylCoA hydrolysis rate and/or the arylamine acylation rate.

In AcylCoA hydrolysis assays, the appropriate arylamine substrate (500μM), as stated in the figure legend, was incubated with the NAT enzyme, as defined in the figure legend, at 37˚C for 5 minutes in a 96-well plate (Corning). Pre-warmed AcylCoA (400μM) was added to start the reaction (final volume 100μl).

In arylamine acetylation assays, samples of the appropriate NAT enzyme and the arylamine substrate (150μM), as detailed in the figure legend, were pre-incubated at

37°C in assay buffer (20mM Tris.HCl, pH 8.0, 1mM DTT) for 5 min in a 96-well plate (Corning). Pre-warmed AcCoA or *n*-propionylCoA (400μM, 37°C) was added to start the reaction (final volume of 45μl), which was allowed to proceed at 37°C.

II.2.5.1 Estimation of folate-dependent AcylCoA hydrolysis activity by NAT

II.2.5.1.1 Determination of folate-dependent AcylCoA hydrolysis activity by NATs using DTNB

The rate of formation of CoA by NAT in the presence of folate without any arylamine substrate, was spectrophotometrically determined using the colourimetric agent DTNB, based on the AcCoA hydrolysis assay described in **Section II.2.5.1.2** (Brooke et al, 2003b).

The appropriate NAT enzyme (as stated in each figure legend) was preincubated with folate (150μM) in assay buffer (20mM Tris.HCl, pH 8.0, 5% DMSO (v/v)) for 5 min at 37°C in a 96-well plate (Corning). Pre-warmed (37°C) AcylCoA (400μM) in assay buffer was added to start the reaction (final volume of 100μl), which was allowed to proceed at 37°C. Simultaneous quenching and colour development was achieved by addition of the stop reagent: 25μl DTNB solution (5mM DTNB in 100mM Tris.HCl, 6.4M guanidine.HCl, pH 7.3).

The absorbance was read immediately after addition of the stop reagent at 405 nm using a plate reader (Tecan Sunrise). The rate of reaction was determined by reference to a standard curve. Controls with buffer alone were carried out and all reactions were performed under linear initial conditions. Only two AcylCoA were tested for this purpose: AcCoA and *n*-propionylCoA.

II.2.5.1.2 Determination of folate-dependent AcCoA hydrolysis activity by mNat2 via NMR

Purified recombinant mNat2 (25µg) was mixed with folate (150µM), and AcCoA (400µM) in buffer PBS-D_2O (pD 7.4). The enzyme activity during real time NMR was carried out at 37°C. NMR data were collected before and after adding AcCoA, and NMR spectra were recorded on Bruker Avance spectrometer AVII 500 in the deuterated solvent stated.

The field was locked by external referencing to the relevant deuteron resonance. The NMR spectra of all possible reagents and products of the enzymatic assay were recorded on Bruker Avance spectrometer AVIII 700 in the deuterated solvent stated.

II.2.6 Inhibitor study

II.2.6.1 Enzymatic assays with inhibitors

Percentage inhibition was determined as the ratio of specific activity with the inhibitor related to specific activity without inhibitor (100%). IC_{50} values ere estimated graphically from plots of specific activities *versus* inhibitor concentration by using Kyplot® software.

A dose-response function was used as a model of regression for the data and the curves were estimated by the method of the least squares analysis. All the statistical tests were performed with Kyplot® software. 95% was chosen as confidence limit for these tests.

II.2.6.1.1 Determination of NAT activity following arylamine acetylation

For detection of inhibition, minor modifications were introduced to arylamine acetylation assays (**Section II.2.5.1.1**) containing the appropriate inhibitor. All inhibitors tested were dissolved in DMSO and the final percentage of DMSO in the assay was 5 % (v/v).

II.2.6.1.2 Determination of NAT activity following AcCoA hydrolysis

For detection of inhibition, minor modifications were introduced to AcCoA hydrolysis assays (**Section II.2.5.1.2**) containing the appropriate inhibitor. The inhibitors tested were dissolved in DMSO and the final percentage of DMSO in the assay was 5 % (v/v).

II.2.6.2 Determination of the mode of inhibition

Determination of the mechanism of inhibition of mNat2 by **7** was performed testing a range of concentrations of **7** from 0.16 to 5 μM and pABA as arylamine substrate from 25 to 250μM. mNat2 activities were determined by the AcCoA hydrolysis assay and 9ng of pure recombinant mNat2 were used in each assay.

II.2.6.3 Colourimetric properties of the inhibitors

II.2.6.3.1 Visual Colourimetric Observations

In order to create the pictures of each compound after addition of solutions at pH 8 and pH 13.75, 50μl of a 2mM stock solution of the requisite compound in DMSO were mixed with 10μl of the appropriate buffered solution, either 20mM Tris.HCl (pH 8) or 4

M NaOH (pH 13.75), in a 500µl Eppendorf tube.

II.2.6.3.2 Spectrophotometry

The requisite inhibitor was dissolved in DMSO before being added (final concentration of 10-15µM) to an aqueous solution with the appropriate chemical (as stated in each figure legend), provided that DMSO percentage in the final sample was 5%.

Visible spectra of each compound were recorded with a U-2001 spectrophotometer (Hitachi) using 1-ml plastic cells of 1cm path-length (FisherBrand) or '50µl' UVettes® (Eppendorf).

The wavelength scan was performed from λ=800 to 326 nm and the final volume of the sample was 300 - 500 µl in the plastic cells or 60 µl in the Uvettes®. All spectra were blank-corrected.

II.2.6.3.3 Determination of pK_a values

10µl of the inhibitor in DMSO (final concentration 0.1mM) was mixed to 90µl of a panel of solutions buffered at diverse pHs (**Table II.9**) in a flat-bottomed 384-well PS-microplate (Greiner).

A full absorbance spectrum was recorded on the FLUOstar Omega plate reader (BMG Labtech) for each sample. Recorded spectra were blank-corrected and λ_{max} was determined. In order to determine the pK_a of each inhibitor, λ_{max} values were plotted against pH values using GraphPad® software.

A sigmoidal dose-response (variable slope) curve was used as model to determine the pK_a by the method of least squares.

Table II.9: Buffered solutions used for titrating the inhibitors.

pH	Buffer
1.3 - 3.4	4 M Glycine.HCl
4.0 - 5.5	20mM AcO^-.AcOH, 20mM NaCl
6.0 - 6.5	20mM MES.AcOH, 20mM NaCl
7.0	20mM HEPES.AcOH, 20mM NaCl
7.5 - 7.7	20mM Tris.HCl
8.0	20mM Tris.HCl, 20mM NaCl
8.5	20mM Tris.HCl, 20mM NaCl
9.0 - 10.0	20mM CHES.NaOH, 20mM NaCl
10.5 - 11.0	20mM CAPS.NaOH, 20mM NaCl
12.0 - 12.5	70mM Na2HPO4.NaOH
13.0	35mM Na2HPO4.NaOH
13.8	4 M NaOH

II.2.6.3.4 Determination of molar extinction coefficients (ε)

In order to determine the molar extinction coefficient (ε) of the requisite inhibitor in both protonated (ε_N=neutral) and deprotonated (ε_{CB}=conjugated base) form, 10µl of the requisite inhibitor at different concentrations in DMSO (2, 1, 0.5, 0.25mM) were added in a flat-bottomed 384-well PS-microplate (Greiner) and firstly buffered at pH 8.0, adding 90µl of 20mM Tris.HCl (pH 8.0) buffer. Experiments were performed in duplicate. Full visible spectra were recorded on the FLUOstar Omega plate reader for all samples. Spectra were blank-corrected and the OD value at requisite λ_{max} was recorded for each final concentration of the inhibitor (200, 100, 50, 25µM).

In order to determine the ε_N of the neutral compound, the absorbance values were plotted against the final concentration values using Microsoft Excel®. A linear regression model was used to estimate the linear gradient, which was subsequently divided by the well path length (0.294 cm).

Afterwards, 10µl of 4 M NaOH was then added to all wells to deprotonate the inhibitor and the same procedure was used to assess the ε_{CB}, provided that a correction factor of 11/10 was applied to all final inhibitor concentration values and the path-length measure.

II.2.6.3.5 Determination of the most acidic proton of compound 7 via NMR

An analogue of compound **7** with a ^{15}N-labelled sulfonamide was synthesised in collaboration with C. Thinnes in the Department of Chemistry, University of Oxford (Thinnes, 2010) and NMR spectra were recorded of both protonated and deprotonated forms.

10 mg of the ^{15}N-labelled **7** analogue were dissolved in 600µl of a 95% DMSO-d_6 / 5% H_2O solution, and the spectrum was acquired using the Bruker DRX500 spectrometer in the deuterated solvent stated. In parallel, 10 mg of the ^{15}N-labelled **7** were dissolved in 600µl of a 95% DMSO-d_6 / 5% aq. NaOD solution and the spectrum was acquired using the same spectrometer in the deuterated solvent stated. In both cases, the field was locked by external referencing to the relevant deuteron resonance.

II.2.6.3.6 Determination of the dissociation constant (K_d) and the number of binding sites of 7 to mNat2

After determining the ε of both protonated and deprotonated forms of compound **7** at 514 nm and estimating the ε for the mNat2-**7** complex, visible spectra of samples containing 20 µM of pure recombinant mNat2 and different concentrations of **7** (10 - 20 - 40 - 60µM) were recorded in duplicate with a U-2001 spectrophotometer (Hitachi) across the wavelength of 750 to 326nm.

OD values at 514 nm were used to estimate the concentration of the unbound **7** in the mixture according to **Equation II.1**. The parameter θ was estimated as the concentration of **7** bound to mNat2 over the total concentration of mNat2 in the sample.

Michaelis-Menten, Hughes-Klotz and Scatchard plots were drawn according to the appropriate equations. K_d values were then determined from all graphs according to the

apposite regression model estimated with the least-squares method using the software Kyplot®.

$$[7_{unbound}] = \frac{OD_{514nm} - \varepsilon_{blue species} \times [7_{initial}]}{\varepsilon_{red\ species} - \varepsilon_{blue species}}$$

Equation II.1: Estimation of [$7_{unbound}$] from OD at 514nm.

II.2.7 Structural studies

II.2.7.1 Crystallisation of protein solution

II.2.7.1.1 Purification of mNa2 protein via size-exclusion gel filtration

Size-exclusion chromatography was carried out on a Superdex 200 column (GE Healthcare) connected to an ÄKTA Purifier system (GE Healthcare). The column was equilibrated with 20mM Tris.HCl pH 8.0 and 100mM NaCl, then mNat2 was loaded onto the column in the buffer described above at a flow rate of 0.5 $ml.min^{-1}$ at room temperature. The eluate was monitored at wavelengths of 280 and 460 nm with Unicorn software (GE Healthcare). Molecular weight standards loaded to the column were: ovalbu min (45 kDa) and Soybean Trypsin Inhibitor (SBTI) (21.5 kDa), all at $5mg.ml^{-1}$ in a total volume of 200 µl in 20mM TrisHCl pH 8.0 containing 0.3 M NaCl.

II.2.7.1.2 Crystallisation trial of mNat2 with ligand

Pure recombinant proteins were suitably concentrated with an Amicon ultracentrifugation concentrator (Millipore), and further incubated for 1 hour with the ligand desired (**Table II.1**).

After removing the possible traces of DMSO in the samples using several washes of the appropriate buffer (20mM Tris.HCl, pH 8), crystallisation trials were set up employing the sitting drop vapour-diffusion technique and a TECAN Genesis ProTeam150 machine was used to set up reservoir solutions in Innovaplate 2-well plates (Innovadyne Technologies). A mosquito® liquid-handling device (TTP LabTech) was used to mix 100 nl of protein with 100 nl of reservoir solution and plates were sealed and incubated at 25°C or 4°C.

Table II.10: Conditions screened in the crystallisation trials.

Protein	Concentration ($mg.ml^{-1}$)	Ligand	Screen	Temperature
mNat2	20	**1** (500µM)	JCSG*plus*™	4°C 25°C
mNat2	4.1	**7** (500µM)	Morpheus™	4°C 25°C
			Wizard™I/II	4°C 25°C
mNat2	6.3	CoA (2mM)	Morpheus™	4°C 25°C
			JCSG*plus*™	4°C 25°C
mNat2_R127G	10	CoA (2mM)	Morpheus™	4°C 25°C
			JCSG*plus*™	4°C 25°C
			Index™	4°C 25°C
			PACT™	25°C
mNat2_R127G	10	folate (2mM)	Morpheus™	4°C 25°C
			PEG/Ion™ 1/2	4°C 25°C
			Index™	25°C
mNat2	10	**7** (500µM)	Structure™	4°C 25°C
			Morpheus™	4°C 25°C
			Wizard™I/II	25°C

II.2.7.2 Structural study

All pictorial images showing protein structures were generated using the software PYMOL (W. L. DeLano (2002) PyMOL, DeLano Scientific, San Carlos, CA) .

II.2.7.2.1 Structural modelling

Structural models of some mammalian NAT proteins were generated based on existing structures of homologuous NAT enzyme with more than 70% primary sequence identity, using the on-line software SwissModel, Automated mode (http://swissmodel.expasy.org/) (Arnold et al, 2006; Kiefer et al, 2009; Peitsch, 1995a). The primary sequence of the protein to be modelled was given to the programme together with the PDB code or the pdb file of the template protein.

II.2.7.2.2 Structural docking

In order to dock a particular inhibitor into a selected pocket of the enzymes hNAT1 and mNat2, the ligand was first drawn as a 3D structure using the software ChemBio3D Ultra 12.0.

The molecular editor Avogadro was used to predict the ground state conformation of the ligand to be docked, which was subsequently saved as a .mol2 file. Both docking partners being defined, the analysis of the possible interactions between the protein and the ligand was performed using the licensed software GOLD (Verdonk et al, 2003) (Genetic Optimization for Ligand Docking), one of the leading virtual ligand docking algorithms available (Jones et al, 1997; Onodera et al, 2007).

A docking site was defined as a region of 10 Å around a key residue and the ligand was then loaded into the programme. The software ranked the generated solutions using the GOLD Score Fitness function (Verdonk et al, 2003). The docking results were presented in a three-dimensional diagram using the software PyMOL.

II.2.8 Eukaryotic and prokaryotic cell growth

II.2.8.1 Cell cultures

II.2.8.1.1 The human breast cancer ER+ve cell line ZR-75-1

The human breast cancer ER+ve ZR-75-1 cell line, containing elevated levels of hNAT1 (Wakefield et al, 2008b), were kindly provided by Prof. Edith Sim.

The cells were maintained in a RPMI-1640 medium (Gibco) supplemented with 10% (v/v) foetal bovine serum, 1% penicillin and 1% streptomycin, 2mM L-glutamine (Engel et al, 1978).

According to previous protocols (Wakefield et al, 2008b), flasks of ~10^7 cells were harvested 5 days after seeding and briefly rinsed in PBS pH 7.4 (Oxoid Ltd.). The cells were then detached from the flask by incubating with 3 ml trypsin/EDTA 0.25% for 15 min. Detached cells were resuspended in 8ml culture medium, and pelleted by centrifugation (200g, 20ºC, 5min). The supernatant was poured out and the cell pellet resuspended for splitting or preparing cell lysates.

In order to split the cells to create new fresh cell cultures, 4ml of culture medium was added to the cell pellets and cells aspirated by gentle pipetting. 1 ml aliquots of this cell suspension were added to new culture flasks with 12 ml of fresh medium. The culture flasks were incubated at 37ºC and 5% CO_2 in air.

To generate cell lysates, cell pellets were resuspended in a known amount of PBS and pelleted, and cells were counted using a haemocytometer. The cells were then resuspended in lysis buffer (20mM Tris.HCl (pH 8.0), 20mM NaCl, 1mM DTT, 0.5% Igepal and 1x complete protease inhibitor (Roche)) at ~5x10^7 cells per ml. The cells were lysed by gentle pipetting and afterwards centrifuged (14,000×g, 4ºC, 10 min) to remove de-

bris. 5% glycerol was added to the supernatant before ~100 µl aliquots were frozen in liquid nitrogen and stored at -80ºC.

II.2.8.1.2 The lymphoblastoid Raji cell line

Lymphoblastoid Raji cells derived from a Burkitt lymphoma were kindly donated by Dr R. Sim and seeded in 100 ml RPMI-1640 medium containing 10% (v/v) foetal bovine serum, 20 $U.ml^{-1}$ penicillin, 0.1$mg.ml^{-1}$ streptomycin and 2mM L-glutamine. Cultures were grown in 175 cm^2 flasks (Greiner) at 37^oC, 5% (v/v) CO_2 for 48 h. Cells were harvested by centrifugation at 200×g for 5 min and pellets were resuspended in 2-4 ml PBS buffer (Oxoid Ltd.).

II.2.8.1.3 The mouse leukaemic monocyte/macrophage Raw 264.7 cell line

The mouse leukaemic monocyte/macrophage Raw 264.7 cell line was kindly provided by Dr Robert Sim, University of Oxford. The cells were seeded in 500 ml RPMI-1640 medium containing 10% (v/v) foetal bovine serum, 20 $U.ml^{-1}$ penicillin, 0.1$mg.ml^{-1}$ streptomycin and 2mM L-glutamine. Cultures were grown in 175 cm^2 flasks (Greiner) at 37^oC, 5% (v/v) CO_2 for 48 h. Cells were harvested by centrifugation at 200×g for 5 min and pellets were resuspended in 2-4 ml PBS buffer (Oxoid Ltd.).

II.2.8.1.4 Prokaryotic cells: E. coli JM 109

Colonies of competent cells *E. coli* JM 109 (Promega) were grown on a LB agar solid medium for 24 h at 37°C in a 6-well culture plate (Corning).

II.2.8.2 Estimation of native hNAT1 in ZR-75-1 cell lysates

II.2.8.2.1 Western blot

Samples of ZR-75-1 cell lysates were run on a 12% SDS-PAGE gel as described in **Section II.2.4.2**. Proteins were then transferred to a polyvinylidene fluoride micro-porous membrane in a suitable buffer (48mM Tris.HCl, 39mM glycine, 20% methanol, pH 8.3) for 4 h using a semi-dry blotter. Membranes were blocked with 10% milk in Tris-Buffered Saline Tween-20 (TBST) (9g.l^{-1} NaCl, 6g.l^{-1} Tris.HCl, 0.05% v/v Tween-20), washed thrice with 3% milk and incubated with the polyclonal antibody 195 (Stanley et al, 1998) at a dilution of 1:2,000 for 1 hour. Following the wash, membranes were incubated with horse-radish peroxidise-conjugated mouse anti-rabbit IgG (at dilution 1:10,000) for 1 hour. Membranes were washed as before and the bound proteins were detected using a chemiluminescent kit (ECL Reagent Kit, Amersham).

II.2.8.2.2 Dot blot

Samples (200µl/well) were directly transferred onto a polyvinylidene fluoride membrane using the Bio-Dot® Microfiltration Apparatus. As for western blotting, membranes were blocked with 10% milk in TBST, washed thrice with 3% (w/v) milk and incubated with the polyclonal antibody 195 (Stanley et al, 1998) at a dilution of 1:2000 for 1 hour. Afterwards, membranes were incubated with horse-radish peroxidise-conjugated mouse anti-rabbit IgG (at dilution 1:10000) for 1 hour. Membranes were washed as before and the bound proteins were detected using a chemiluminescent kit (ECL Reagent Kit, Amersham).

II.2.8.3 Effect of naphthoquinone 7 on cells

II.2.8.3.1 Cell penetration

In order to evaluate the cellular uptake of the inhibitor **7** through the cell membrane, 150µl of the re-suspended Raji cell pellets were incubated for 15 min at 37°C with 4µl of 20mM compound **7** (~2.5% DMSO (v/v)). The aim of the experiment was to estimate by spectrophotometry the amount of **7** in all separable cellular fractions in order to assess the extent of the cellular permeability of the inhibitor.

After separation, absorbance spectra of each fraction were recorded with a U-2001 spectrophotometer using '50µl' UVettes®. The wavelength scan was performed from λ = 800 to 326nm. All spectra were blank-corrected. Two different protocols were tested to assess the cellular permeability of the napthoquinone **7**:

1. Incubated cells were centrifuged at 14,000×g for 1 min. The supernatant was poured out and the cell pellet was lysed with 150µl of distilled water and 4µl DMSO (~2.5% (v/v)). Lysed cells were subsequently centrifuged at 14,000×g for 10 min and the resulting supernatant and pellet were separated. The final pellet was resuspended in 150µl of distilled water with 4µl DMSO (~2.5% (v/v)).
2. Incubated cells were layered on top of with 150µl mineral oil and centrifuged at 14,000×g for 1 min. The aqueous supernatant and the oil layer were separated, and the cell pellet was lysed with 150µl of distilled water and 4µl DMSO (~2.5% (v/v)). Lysed cells were subsequently centrifuged at 14,000×g for 10 min and the resulting supernatant and pellet were separated. The final pellet was resuspended in 150µl of distilled water with 4µl DMSO (~2.5% (v/v)).

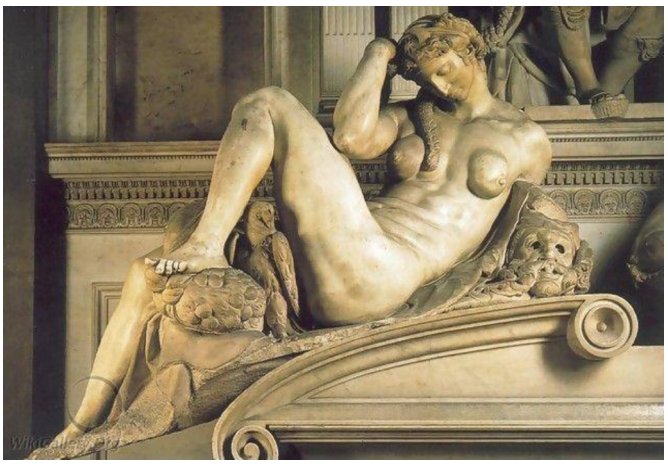
II.2.8.3.2 Cytotoxicity

In order to estimate the effect of compound **7** on the growth of mammalian cell lines, the appropriate cultures were grown in 175 cm^2 flasks (Greiner) at 37°C, 5% CO_2 (v/v) for 48 h and the inhibitor was added to final concentrations of 5 to 100µg.ml^{-1}, ensuring that the percentage of DMSO was 0.5% (v/v). Cells were harvested by centrifugation (200 *g*, 5 min) and pellets re-suspended in 2-4 ml PBS buffer (Oxoid Ltd.). Viability counts were performed using a glass haemocytometer slide (AbCam): 20µl cell suspension was mixed with 20µl of 0.4% Trypan Blue dye (v/v) (in 0.81% NaCl (v/v), 0.06% K_2HPO_4 (v/v)). Cells were loaded, counted and scaled according to manufacturer's instructions.

With the purpose of estimating whether the naphthoquinone **7** could also affect the growth of prokaryotic cells, colonies of competent *E. coli* JM 109 cells (Promega) were grown for 24 h at 37°C on LB agar solid medium with increasing concentrations of compound **7** (0-100µg.ml^{-1}) in a 6-well culture plate (Corning). The percentage of DMSO in each well was 0.5% and the appropriate controls were performed.

Chapter III:

Isoenzyme selectivity of naphthoquinone 7



NIGHT (1526-1531), BY MICHELANGELO BUONARROTI (1475-1564).

Abnormalities associated with locally advanced cancer are observed in the left breast of the sculpture (Stark & Nelson, 2000) (Michelangelo's Medici Chapel, Church of San Lorenzo, Florence, Italy).

III.1 Introduction

After screening a library of more than 5000 drug-like compounds by HTP screening against five different eukaryotic and prokaryotic NATs (Russell et al, 2009; Westwood et al, 2011), naphthoquinone **1** was identified as a selective inhibitor of hNAT1 and mNat2 (Crawford, 2007; Russell et al, 2009), and was also found to undergo a colour change from red to blue upon binding to both enzymes (Crawford, 2007) (**Figure III.1**). An analogue of the original hit compound **1,** naphthoquinone **7**, showed slightly improved inhibitory efficiency against both enzymes and remarkably higher optical density values as both unbound (red) and bound (blue) species (Laurieri, 2008) (**Figure III.1**).

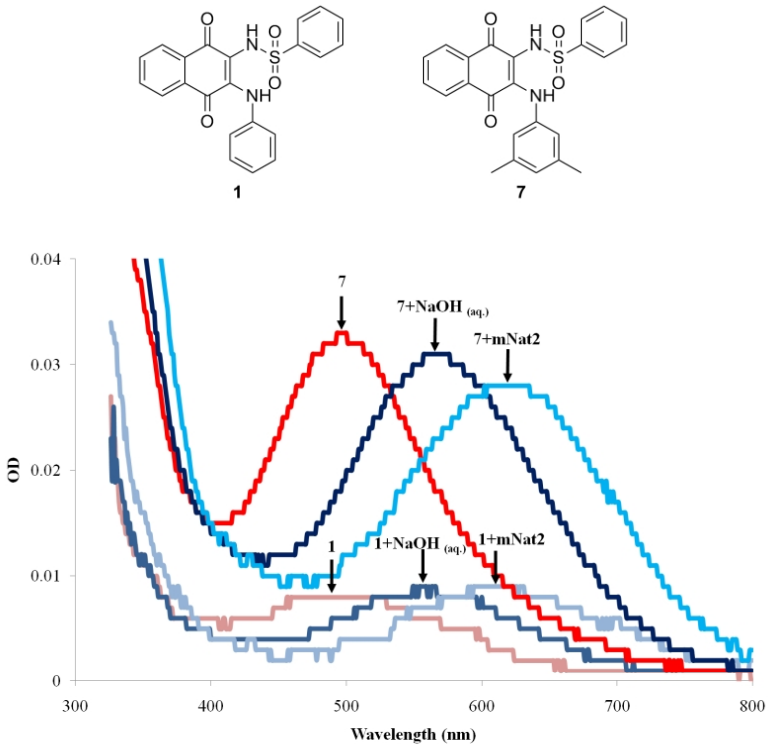


Figure III.1: Spectral properties of 1 and 7 in the visible range.

(top) Chemical structures of compounds **1** and **7**. **(bottom)** Wavelength scans of compounds **1** and **7** (10µM) in buffer (20mM Tris.HCl, pH 8, 5% DMSO (v/v)) (red lines), **1** and **7** (10µM) in alkaline solution (80mM NaOH, 5% DMSO (v/v)) (dark blue lines), **1** and **7** (10µM) with pure recombinant mNat2 (20µM) in buffer (as above) (light blue lines). All values of optical density were measured against an appropriate blank.

Therefore, in order to use these colourimetric probes to visually detect hNAT1 in breast cancer cell lysates, most of the investigations conducted in this study focused on compound **7** for its enhanced spectrophotometric characteristics.

Moreover, the murine homologue of hNAT1, mNat2, was previously used as an animal model for hNAT1 both *in vivo* (Cornish et al, 2003; Wakefield et al, 2007; Wakefield et al, 2008a) and *in vitro* (Kawamura et al, 2008) and was also produced as pure recombinant protein in a very good yield (~50 mg per litre of culture) (Kawamura et al, 2008).

These considerable yields of pure recombinant mNat2 protein (Kawamura et al, 2008) compared with the small amounts of hNAT1 obtained from similar biochemical techniques (Wang et al, 2005b), together with the higher stability over time of mNat2 than hNAT1, supported the idea of using mNat2 in our inhibitor studies in order to assist first screening of the inhibitors.

AIMS

In this chapter, further studies on the biochemical selectivity of the colourimetric and inhibitory interaction between ligands **1** or **7** and NAT proteins are presented, including the following:

- determination of NAT isoenzyme selectivity of **1** and **7**, as inhibitors and colourimetric probes of hNAT1 and mNat2
- biochemical characterisation of the interaction between **7** and mNat2.

In order to carry out these studies, production of pure recombinant mNat2 needed to be optimised: these studies are also presented in this section.

III.2 Results

III.2.1 Heterologous over-expression and purification of mNat2

mNat2 was expressed in RosettaBlue (DE3)pLysS *E. coli* with an *N*-terminal hexa-histidine tag (His-tag) using the plasmid pET28b(+), as previously described with minor modifications (Kawamura et al, 2008). pET28(+) was the vector of choice since the plasmid utilises the strong T7 promoter, and the expressed recombinant protein co-expresses an *N*-terminal His-tag for ease of downstream purification *via* immobilised metal affinity chromatography (IMAC), in particular an Ni-NTA column.

When the absorbance of the incubated bacterial culture reached 0.4 at 600nm, the expression of mNat2 was induced by addition of IPTG and the overexpression of the recombinant mNat2 protein in the *E. coli* host strain seemed to slow down the bacterial growth compared to a non-induced culture taken as control (**Figure III.2**).

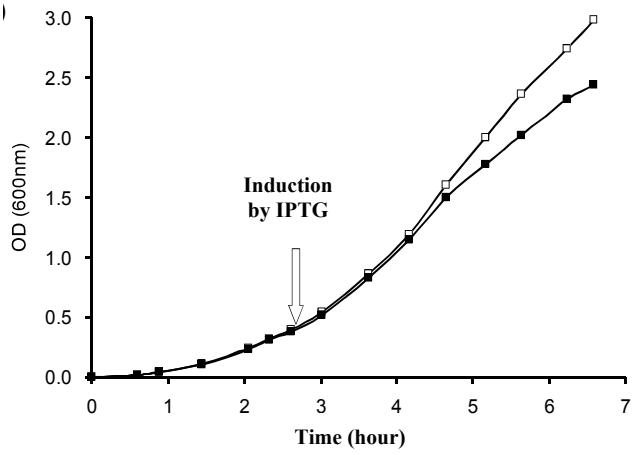


Figure III.2: Growth curve of *E. coli* RosettaBlue(DE3)pLysS with pET28b(+) plasmid containing *mNat2*.

OD_{600} of samples taken from the growing cultures was monitored over time. Expression of recombinant mNat2 was induced by adding IPTG to a final concentration of 0.1mM (solid squares); control without IPTG (open squares). *mNat2* was expressed with an *N*-terminal His-tag and then was purified by ion-metal affinity chromatography.

After lysing cells and separating both the soluble and insoluble fractions obtained, only the soluble lysate was incubated with an appropriate volume of Ni-NTA resin to start the purification of the recombinant protein (**Figure III.3**). The eluted fractions containing pure hexa-histidine tagged mNat2 were pooled together and incubated with thrombin to remove the His-tag, prior to dialysis (**Figure III.3**). The final sample with pure recombinant mNat2 was accurately aliquoted. Highly pure recombinant mNat2 was obtained in a very good yield (59.5 mg per litre of culture), which was slightly greater than the previous results (47.5mg.l^{-1}) (Kawamura et al, 2008) (**Table III.1**). The high yield and purity of recombinant mNat2 were ideal for enzymological studies and protein crystallography.

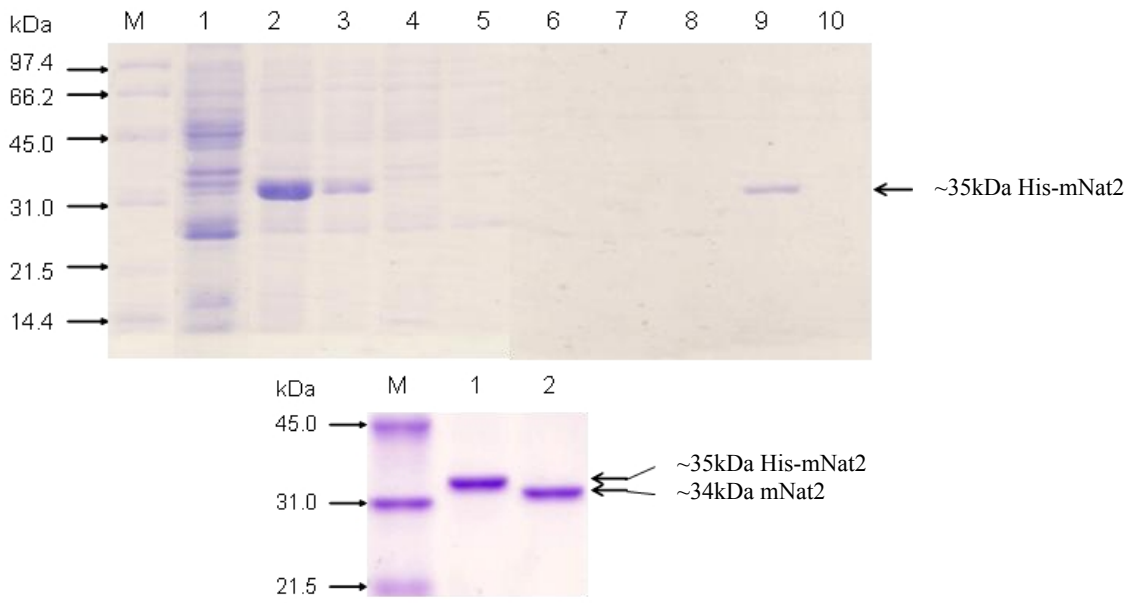


Figure III.3: Purification of recombinant mNat2.

(top) Coomassie blue-stained 12% SDS-PAGE analysing the fractions collected from each purification step. Samples were loaded onto the column for affinity binding and eluted with increasing concentrations of imidazole at 4ºC. Low range molecular weight markers (BioRad) were used throughout (lane M). Lanes: **1**, 2µl non-induced lysate; **2**, 1µl induced lysate; **3**, 1µl soluble fraction; **4**, 2µl unbound wash; **5**, 2µl 0mM imidazole wash; **6**, 2µl 1mM imidazole wash; **7**, 2µl 10mM imidazole wash; **8**, 2µl 50mM imidazole wash; **9**, 1µl 200mM imidazole wash; **10**, 2µl 500mM imidazole wash. **(bottom)** Thrombin cleavage of His-mNat2. Purified His-mNat2 was incubated with thrombin (5U.mg^{-1} mNat2) at 4ºC for 16 h for complete His-tag cleavage. Lanes: **1**, 1µl His-mNat2 only; **2**, 1µl thrombin-treated mNat2.

Table III.1: Activity and recovery of recombinant mNat2 expressed in *E. coli*.

Fraction	Volume (ml)	Total Protein[a] (mg)	Total Activity[b] ($mM.min^{-1}$)	Specific Activity ($mM.min^{-1}.mg^{-1}$)	Fold purification	Yield[c] (%)
Soluble lysate	15.0	195.0	1950.0	10.0	1.0	100
Unbound lysate	14.0	57.4	51.8	0.9		
0mM imidazole wash	15.0	27.0	13.5	0.5	0.05	0.7
1mM imidazole wash	7.0	2.8	0.56	0.2	0.02	0.03
10mM imidazole wash	11.0	3.3	0.11	0.03	0.003	0.01
50mM imidazole wash	5.5	2.8	2.2	0.8	0.08	0.1
200mM imidazole wash	19.0	57.0	1549.0	27.2	2.7	79.4
500mM imidazole wash	24.5	2.45	68.6	28.0	2.8	3.5

Soluble lysate from 1l of *E. coli* culture was incubated with Ni-NTA resin (4ºC for 5 min) and washed with buffer (20mM Tris.HCl (pH 8.0), 300mM NaCl) containing increasing concentrations of imidazole.
[a] Protein concentrations were measured by the Bradford assay.
[b] mNat2 activities were measured using the AcCoA hydrolysis assay at 37ºC, with 500µM 5-amino salycilate (5AS) as substrate in a total volume of 100µl. Imidazole did not affect the activity assay.
[c] The total activity of the soluble lysate was used as a reference of 100%.

Pure recombinant mNat2 was tested with pABA as arylamine substrate using both methods for detecting NAT activity: the AcCoA hydrolysis method and the arylamine acetylation method, which were found to be equivalent (**Figure III.4-left**). The linearity of the initial velocities over time in both types of assay suggested the correct folding of the enzyme.

Afterwards, the AcCoA hydrolysis method was chosen to determine the apparent kinetic constants with pABA as substrate. NAT initial activity has long been established to follow a Ping-Pong Bi-Bi equation (Wang et al, 2004b; Westwood et al, 2006) (**Equation III.1**).

Since the concentration of AcCoA is kept constant in all enzymatic assays, the V_{max} and the K_m values estimated in this study are considered apparent. The initial velocities were measured at different pABA concentrations up to 500µM, and fitted into a Michaelis-Menten curve (**Figure III.4-middle**). A Lineweaver-Burk plot was therefore drawn in order to assess the apparent kinetic constants (**Figure III.4-right**).

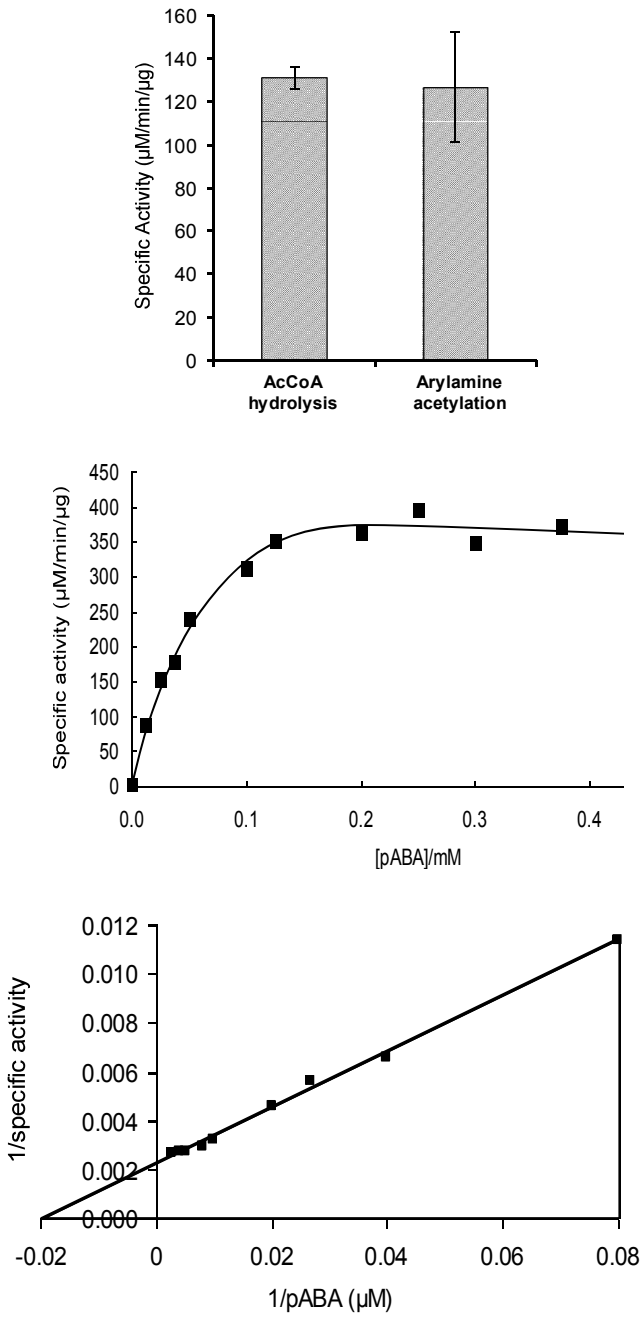


Figure III.4: Enzymological characterisation of pure recombinant mNat2.

(top) Comparison of AcCoA hydrolysis and arylamine acetylation methods in determination of NAT activity. Results were expressed as mean ± standard deviation from triplicates. 50ng of mNat2 and 150 µM pABA were mixed in the assay and subsequently incubated for 5 min at 37 C. 400 µM AcCoA was added in order to start the reaction. Appropriate quenching reagents were added in each assay (materials and methods). **(middle)** Michaelis-Menten curve drawn after measuring initial velocities of assays containing 50ng mNat2, 400 µM AcCoA, and different concentrations of pABA (0, 12.5, 25, 37.5, 50, 100, 125, 200, 250 and 375µM) in 20mM Tris.HCl buffer. **(bottom)** Lineweaver-Burk plot drawn using values from Michaelis-Menten curve.

$$v_i = \frac{V_{\max} \cdot [AcCoA][pABA]}{K_{m-AcCoA}[pABA] + K_{m-pABA}[AcCoA] + [AcCoA][pABA]}$$

Equation III.1: Equation for the Bi-Bi Ping-Pong mechanism.

The original reference is (Cleland, 1963).

The enzymatic data obtained, allowed an estimation of the kinetic constants, with V_{max}=449µM.min^{-1}.µg^{-1} of mNat2 and K_m=51µM. Twenty-five moles of pABA are acetylated per second by a mole of mNat2 in the presence of saturating concentrations of AcCoA in the assay.

Table III.2: Apparent kinetic constants determined for mNat2.

V_{max} (µM.min^{-1}.µg^{-1})	449
K_m (µM)	51
k_{cat} (s^{-1})	25
k_{cat}/K_m (min^{-1}.µM^{-1})	30

III.2.2 Isoenzyme selectivity of naphthoquinone 7

In order to confirm selectivity of **1** and evaluate selectivity of **7** more broadly, **1** and **7** were tested for inhibitory activity with a range of other mammalian and bacterial NAT enzymes previously produced as pure recombinant proteins (**Figure III.5**).

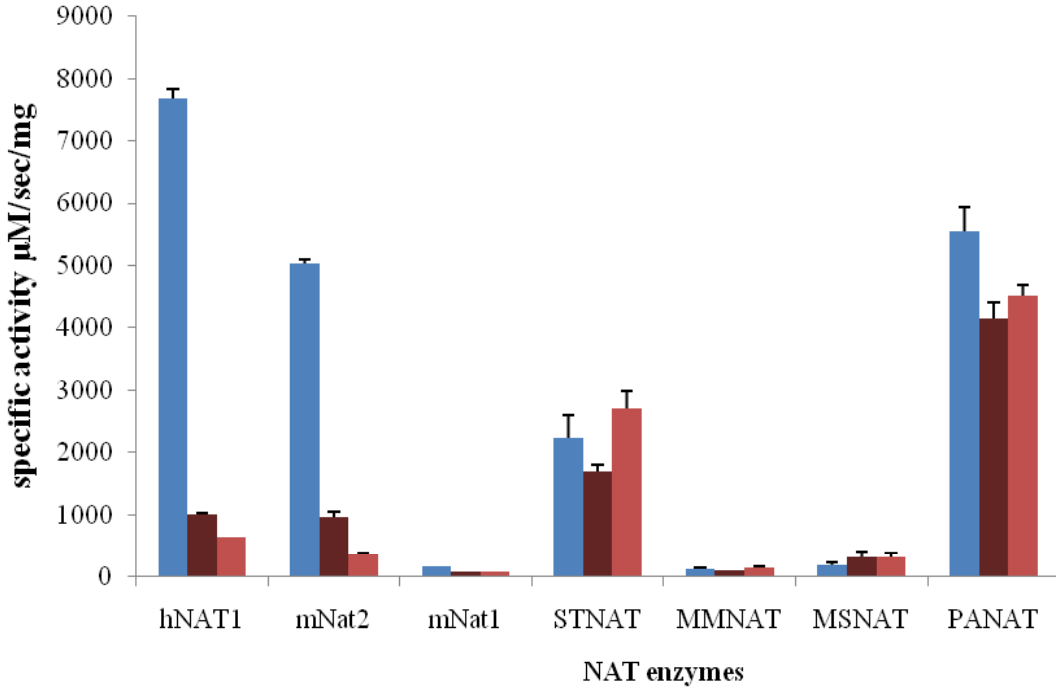


Figure III.5: Screening of different NATs with 1 and 7.

Screening of different NAT enzymes' activity in the presence of naphthoquinones **1** or **7** compared to standard enzymatic assays without inhibitor. The activity was determined by AcCoA hydrolysis assay. The substrate 5AS (500µM) was incubated with the appropriate NAT enzyme (100ng), at 37˚C for 5 minutes, with or without the inhibitor (10µM). Pre-warmed AcCoA (400µM) was added to start the reaction (final volume 100µl). Simultaneous quenching and colour development was achieved by addition of the stop reagent: 25µl DTNB solution (5mM DTNB in 100mM Tris.HCl, 6.4 M guanidine.HCl, pH 7.3). The absorbance was then read at 405nm. Assays were conducted in triplicate, and the linear activity rates are mean values ± standard deviation.

Drastic reduction of NAT activity was observed specifically with hNAT1 and mNat2 in the presence of either **1** or **7**. No significant changes in NAT activity were noticed with the other isoenzymes screened (**Figure III.5**). Inhibition values higher than 80% were only observed with hNAT1 and mNat2. However, partial cross reactivity occured with mNat1 (52.9% inhibition with **1**, 55.9% inhibition with **7** at 5µM). The prokaryotic NATs investigated were inhibited by both compounds **1** and **7** at most by 25% (**Table III.3**).

Table III.3: Percentage activity inhibition of different NAT enzymes in the presence of 1 and 7.

The activity of 100ng of the appropriate NAT was determined as hydrolysis of AcCoA (400µM) in the presence of 5-aminosalicylate (500µM), as arylamine substrate, and the requisite inhibitor (10µM).

Enzyme	hNAT1	mNat2	mNat1	STNAT	MMNAT	MSNAT	PANAT
Inhibition with 1 (%)	86.7 ± 0.3	81.1 ± 1.9	52.9 ± 5.3	23.5 ± 4.6	18.5 ± 3.6	< 5.0	25.1 ± 4.8
Inhibition with 7 (%)	91.7 ± 1.8	92.8 ± 0.4	55.9 ± 6.4	< 5.0	< 5.0	< 5.0	19.6 ± 3.0

When pure recombinant NAT proteins were subsequently tested with compound **7** in a concentration ratio 2:1 in order to detect the colour change event, a remarkable blue colour was observed only with mNat2 (**Figure III.6**) and hNAT1 (**Figure III.7**).

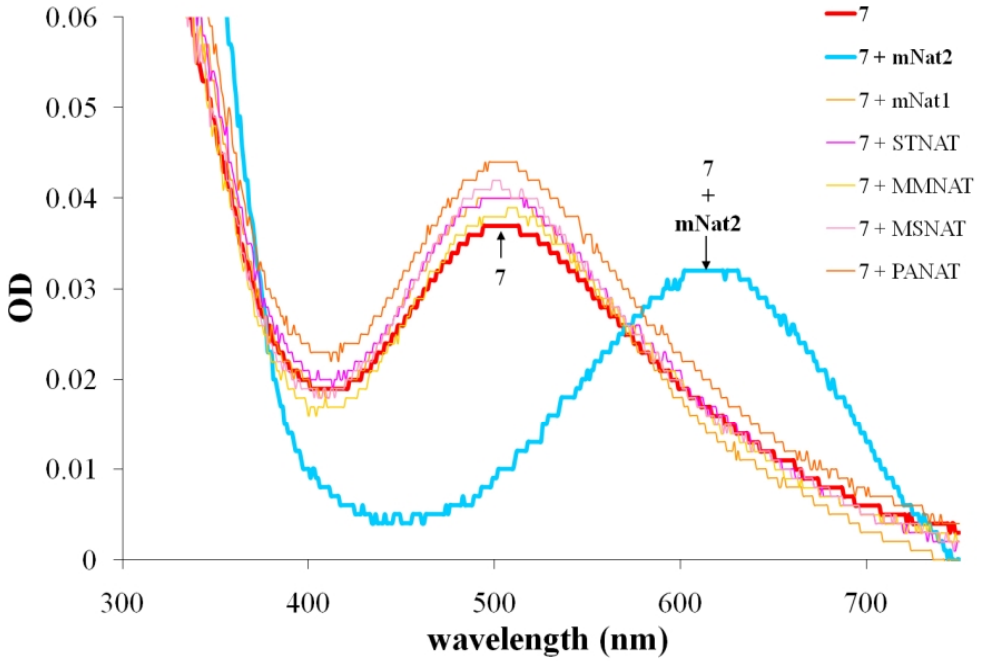


Figure III.6: Spectrometric screening of different NATs with 7.

Visible spectra of compound **7** (10µM) were recorded in the presence of different NAT enzymes (20µM) with U-2001 spectrophotometer (Hitachi) from 750 to 326nm.

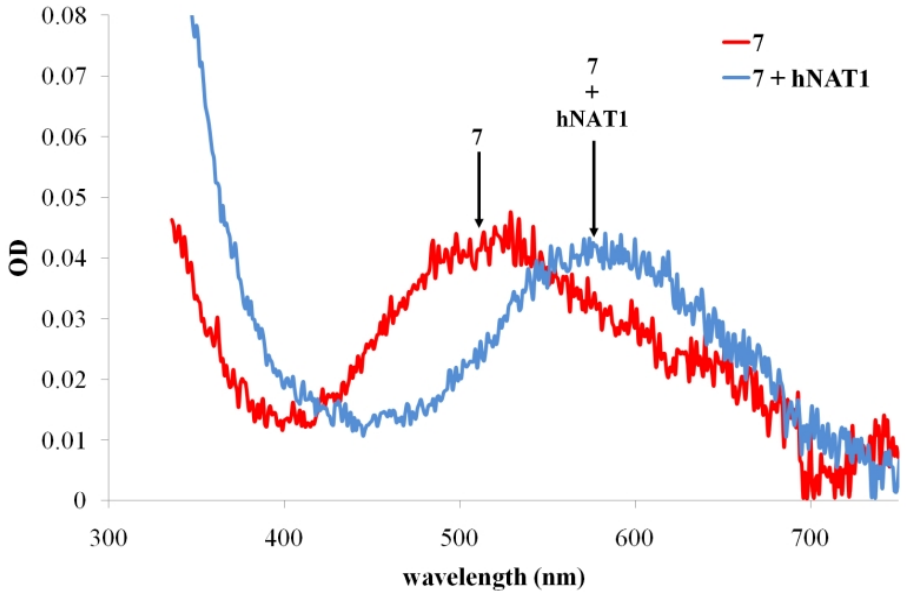


Figure III.7: Spectrometric properties of 7 in the presence of hNAT1.

Visible spectra of compound **7** (10µM) recorded in the presence of hNAT1 enzyme (20µM) using Spectrostar Omega (BMG LABTECH) from 750 to 326nm.

Moreover, the colour change event of compound **7** from red to blue was also observable by eye in the presence of pure recombinant mNat2 similar to previous results with compound **1** (Crawford, 2007) (**Figure III.8**).

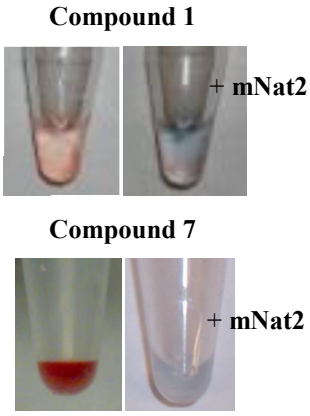


Figure III.8: Colourimetric properties of compounds 1 and 7 in the presence of pure recombinant mNat2.

(top) (left) 1 (400µM) in aqueous Tris.HCl, pH 8.0, or **(right)** in the presence of mNat2 (800µM) in aqueous Tris.HCl, pH 8.0 (Crawford, 2007). **(bottom) (left) 7** (1mM) in DMSO, or **(right) 7** (0.25mM) in the presence of mNat2 (500µM) in aqueous Tris.HCl, pH 8.0.

III.2.3 Biochemical characterisation of mNat2-7 complex

III.2.3.1 Binding reversibility of compound 7 towards mNat2

In order to assess the nature of the interaction between mNat2 and **7**, it was decided to exploit the characteristic colourimetric properties of compound **7** upon interacting with mNat2.

Initially, compound **7** was firstly incubated with mNat2 and a wavelength scan was recorded. The characteristic blue colour was observed. Comparing the spectrum of untreated **7** with that of the mixture containing **7** and mNat2, it was assumed that all molecules of **7** were appropriately bound to mNat2 (**Figure III.9**). Afterwards, the solution was filtered using a Vivaspin 500 eppendorf tube with a filter of 10kDa cut-off (Sartorius Stedim), to facilitate the separation of unbound **7** and mNat2 enzyme.

Two distinct solutions were obtained. The filtered solution had a red colour, whilst the original retentate remained clearly blue. Moreover, after having adequately adjusted both the filtered solution and the retentate to 400µl as the original mixture, the photometric spectra of the two solutions obtained were recorded (**Figure III.9**).

Comparing the height of the spectrophotometric peaks at the appropriate wavelengths allowed an approximate estimation of the amount of the compound **7** filtered (~24%) and the compound **7** still bound to the enzyme (~65%) (**Figure III.9**). The remaining 11% might be an error either due to the inaccuracies of detecting very small amounts of compound **7** by spectrophotometry or due to the fact that part of the unbound compound **7** might have stuck to the filter.

Finally, since compound **7** was observed to regain the characteristic red colour after being released from the enzyme, it was hypothesised that the formation of the complex mNat2-**7** is reversible, which seemed consistent with the hypothesis that compound **7** is a non-covalent ligand of mNat2.

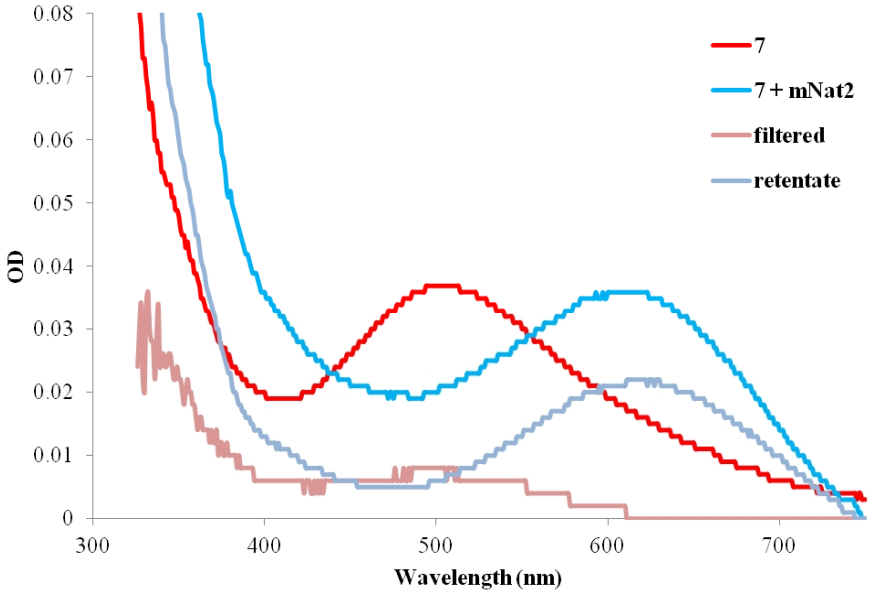


Figure III.9: Reversible non-covalent binding of compound 7 to mNat2.

Wavelength scans of **7** (10µM) in buffer (20mM Tris.HCl, pH 8, 5% DMSO (v/v)) (bright red line), **7** (10µM) with pure recombinant mNat2 (20µM) in buffer (as above) (bright blue line). The solution containing **7** and mNat2 was partially filtered using a Vivaspin 500 eppendorf tube with a filter of 10kDa cut-off (Sartorius Stedim). Wavelength scans of the filtered solution (faint red line), and the filtrate solution were recorded (faint blue line) All values of optical density were measured against an appropriate blank.

III.2.3.2 Colourimetric properties of naphthoquinone 7 *versus* mNat2 protein folding

It was questioned whether the correct folding of the protein mNat2 was required for the inhibitor **7** to bind to the enzyme and provide a colour change from red to blue.

Previous studies outlined that mammalian and bacterial NATs were thermally unstable and became unfolded at temperatures of 50°C or more (Kawamura et al, 2005; Kawamura et al, 2003; Lack et al, 2009; Sinclair et al, 2000). These temperatures were determined using both circular dichroism and enzymatic assays at different temperatures, both giving equivalent results. Therefore, a differential scanning fluorimetry (DSF) study was conducted on mNat2 and revealed a melting temperature (T_m) of 53.7 ± 0.1°C in 20mM Tris.HCl pH 8 buffer (**Figure III.10**).

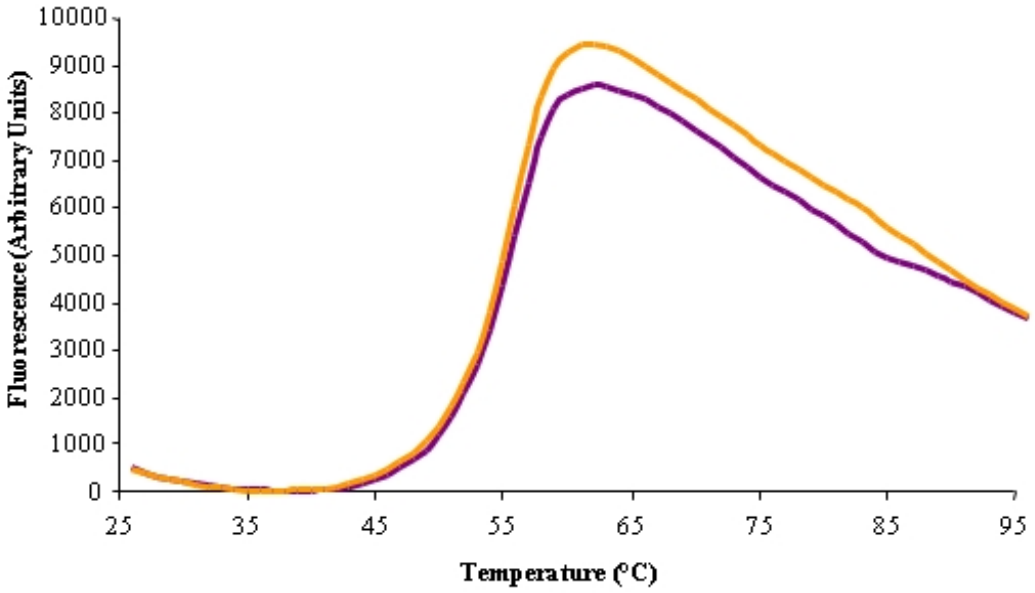


Figure III.10: Melting curve of mNat2 estimated using DSF.

A duplicate experiment was performed and each result is shown by a separate line (yellow or violet). 19.5µl of mNat2 (0.06µg.µl^{-1}) were incubated with Sypro Orange fluorescent dye (0.5µl.ml^{-1} protein) and added to each well. 0.5µl of buffer were added and plates were briefly centrifuged before reading fluorescence as a function of temperature between 25°C and 95°C at an increase of 3°C.min^{-1}, using an RT-PCR machine. GraphPad Prism software was used to process results and output T_m values.

Therefore, in order to ensure that the mNat2 protein was denatured in the spectrophotometric assay, a sample of 62µg of pure recombinant mNat2 was heated for 5 min at 95°C and allowed to cool to 37°C. After incubation with compound **7** (10µM), a visible wavelength scan of the mixture was recorded against a blank containing only denatured mNat2 (**Figure III.11**).

The spectrum obtained is superimposable to the spectrum of compound **7** (**Figure III.11**), thereby suggesting that compound **7** required a correctly folded mNat2 to bind to and to change colour.

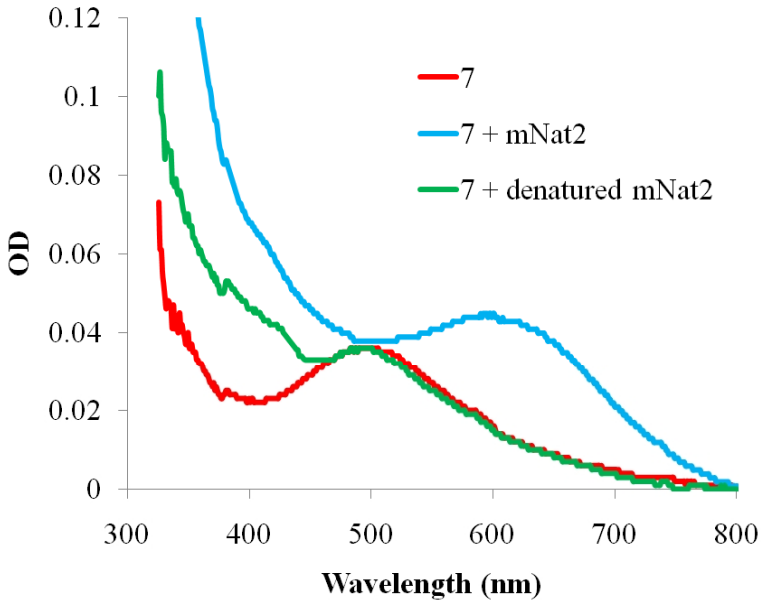


Figure III.11: Interaction between 7 and both folded and unfolded mNat2.

Wavelength scans of **7** (15µM) in buffer (20mM Tris.HCl, pH 8, 5% DMSO (v/v)) (red line), **7** (15µM) with pure recombinant mNat2 (30µM) in buffer (as above) (blue line), **7** (15µM) with pure recombinant mNat2 (30µM), unfolded by heating at 95°C for 5 minutes prior to addiction to **7** in buffer (as above) (green line).

III.2.3.3 Mode of inhibition of compound 7 against mNat2

In order to determine the mode of inhibition of **7** against mNat2 and compare it with the mode of inhibition of compound **1**, different concentrations of **7** were tested with different concentrations of pABA in enzymatic assays containing mNat2.

A Lineweaver-Burk plot was drawn and revealed a competitive mode of inhibition, since all the trend-lines intercept on the y-axis (**Figure III.12-top**).

Moreover, a Dixon plot confirmed that **7** is a competitive inhibitor of mNat2, as all trend-lines intercept above the x-axis, and the interception gives an estimation of the apparent K_I value: 420nM (**Figure III.12-bottom**).

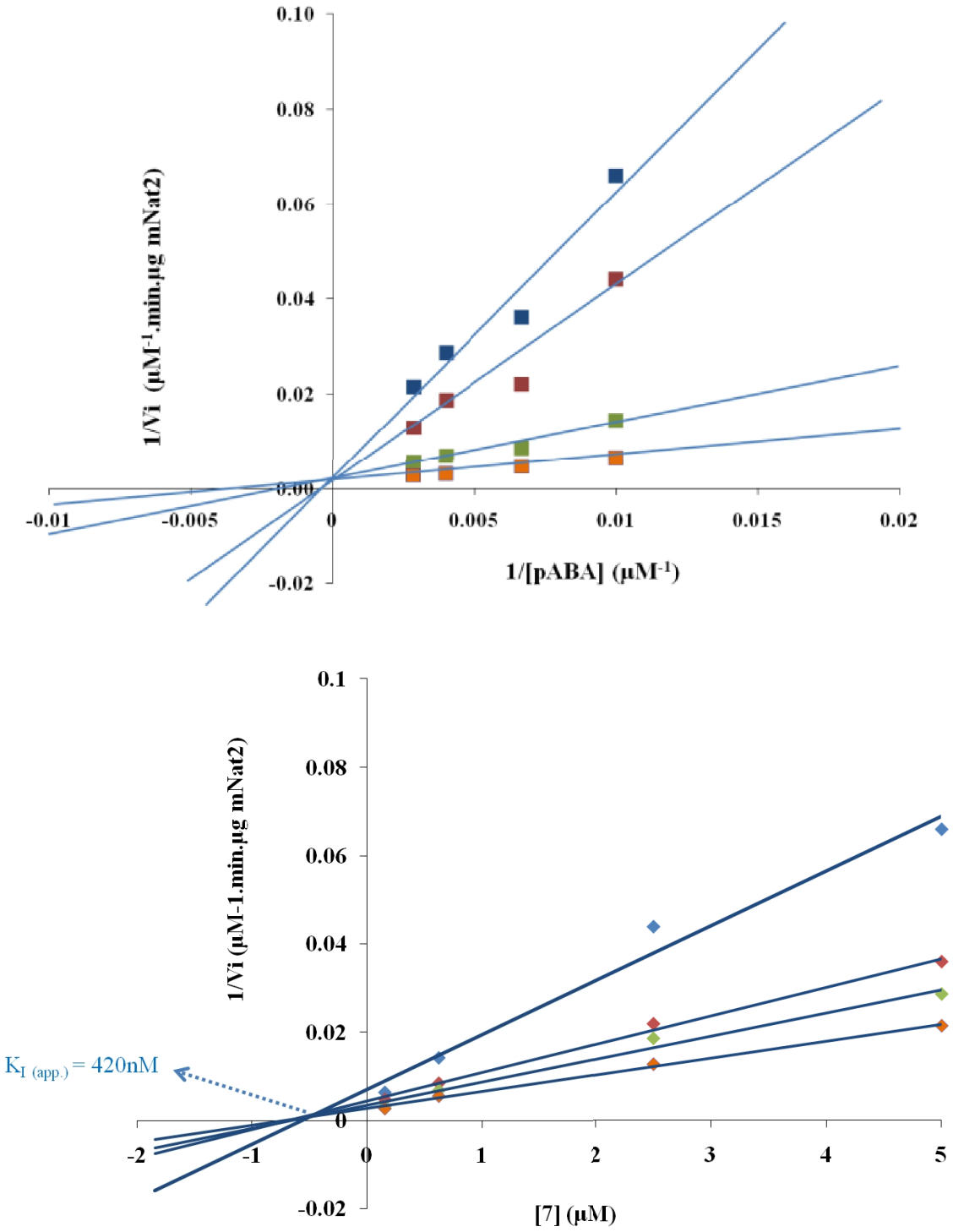


Figure III.12: Kinetic analysis of mNat2 inhibition by compound 7.

(top) Lineweaver-Burk shows rates at inhibitor concentrations of 5µM (blue squares), 2.5µM (red squares), 0.625µM (green squares) and 0.15625µM (orange squares). **(bottom)** Dixon plot shows rates at pABA concentrations of 25µM (orange diamonds), 50µM (green diamonds), 100µM (red diamonds), and 250µM (blue diamonds). mNat2 activities were determined by AcCoA hydrolysis assayusing 9ng of pure recombinant mNat2.

III.2.3.4 Determination of the dissociation constant (K_d) of the complex mNat2-7

Compound **7** acting as a colourimetric ligand probe for mNat2 and hNAT1 needed to be further characterised in terms of number of binding sites (nbs) and affinity constant (K_d) with mNat2, as a model for the interaction with hNAT1.

According to the dissociation equilibrium of the complex mNat2-**7** (**Equation III.2**), the K_d value (**Equation III.3**) would help define the affinity of **7** towards mNat2, and provide an indication of the concentrations of hNAT1 required to give an observable colour change in breast cancer cells.

$$\text{mNat2-}\mathbf{7}_{\text{bound}}\ (\text{P:}\mathbf{7}) \overset{K_d}{\rightleftharpoons} \text{mNat2 (P)} + \mathbf{7}_{\text{unbound}}$$

Equation III.2: Dissociation reaction of the complex mNat2-7.

$$K_d = \frac{[\text{P}] \cdot [7_{unbound}]}{[\text{P} : 7]}$$

Equation III.3: Definition of K_d constant.

For this purpose, a titration study using a fixed amount of mNat2 (20μM) was carried out with increasing concentrations of **7** (10, 20, 40 and 60μM).

An important parameter to be determined in each step of the titration experiment was θ, as defined in **Equation III.4**, which would help estimate the K_d value.

$$\theta = \frac{[\text{mNat2-}7_{bound}]}{[\text{mNat2}]_{total}} = \frac{[\text{P} : 7]}{[\text{P}] + [\text{P} : 7]} = \frac{\frac{[\text{P}][7_{unbound}]}{K_d}}{[\text{P}] + \frac{[\text{P}][7_{unbnoud}]}{K_d}} = \frac{[7_{unbound}]}{K_d + [7_{unbound}]}$$

Equation III.4: Definition of θ and K_d in the dissociation equilibrium of the complex mNat2-7.

To do so it was necessary to determine the concentration of the unbound **7** in each mix-

ture of mNat2 and ligand **7**. Applying **Equation III.5** allowed an estimate of the concentration of the unbound red species of **7** in each mixture from reading the optical density (OD) of each sample (**Equation III.6**).

$$OD_{(at\ X\ nm)} = \left[\varepsilon_{red\ species} \times [7_{unbound}] + \varepsilon_{blue\ species} \times ([7_{bound}])\right]$$
$$OD_{(at\ X\ nm)} = \left[\varepsilon_{red\ species} \times [7_{unbound}] + \varepsilon_{blue\ species} \times ([7_{initial}] - [7_{unbound}])\right]$$

Equation III.5: Mathematical relationship between [$7_{unbound}$] and OD red at 514nm,

$$[7_{unbound}] = \frac{OD_{(at\ X\ nm)} - \varepsilon_{blue\ species} \times [7_{initial}]}{\varepsilon_{red\ species} - \varepsilon_{blue\ species}}$$

Equation III.6: Estimation of [$7_{unbound}$] following reading the OD of the assay at 514nm.

Therefore, the striking colourimetric properties of **7** as both the bound (red) and unbound (blue) species needed to be exploited at a suitable wavelength in order to accurately estimate the concentrations of both the protein-ligand complex and the unbound ligand **7** in each mixture.

The estimation of these concentrations in each assay needed to rely on separate standard curves: one of **7** alone, the other of the complex mNat2-**7**.

Establishing a standard curve for the red species **7** was performed in a straightforward manner (**Figure III.13**), whereas carrying out standard curves of the complex mNat2-**7** would have demanded a considerable amount of highly concentrated pure recombinant mNat2, and would have yielded less accurate results due to a considerable background noise as a result of the width of the A_{280} peak related to the protein present in the sample.

Instead, in order to generate a standard curve of the blue form of **7**, different concentrations of **7** were incubated with 5mM NaOH (**Figure III.13**), since the solutions containing the alkali NaOH were observed to have a similar visible colour, consistent with an OD and a λ_{max} close to those generated by a mixture of mNat2 and **7** (**Figure III.14**).

A particular wavelength at which the estimation of both the red species of **7** and the blue complex mNat2-**7** could be suitably performed following previous assumptions, was identified between the λ_{max} of the red species of **7** and the λ_{max} of the blue species of **7**: 514nm.

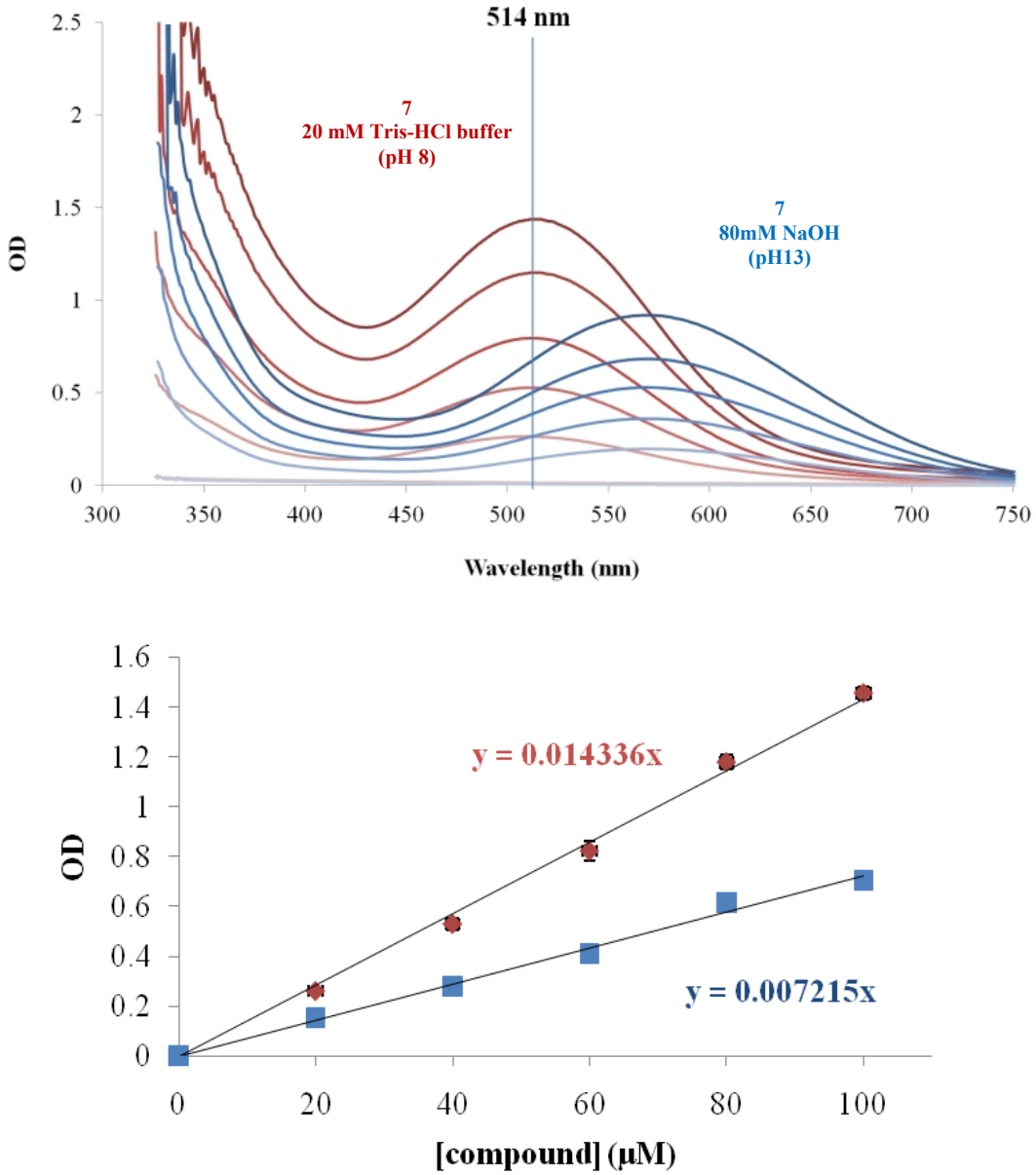


Figure III.13: Standard curves of 7 as both red species and blue species at different concentrations. **(top)** Wavelength scans of **7** in buffer (20mM Tris.HCl, pH 8, 5% DMSO (v/v)) at different concentrations (0, 20, 40, 60, 80, and 100µM) (light to dark red lines), **7** (0, 20, 40, 60, 80, and 100µM) in alkaline solution (80mM NaOH, 5% DMSO (v/v)) (light to dark blue lines). **(bottom)** standard curves of **7,** as both red species (red squares) and blue species (blue squares), obtained using the OD values of different concentrations of the appropriate form of **7** at 514nm.

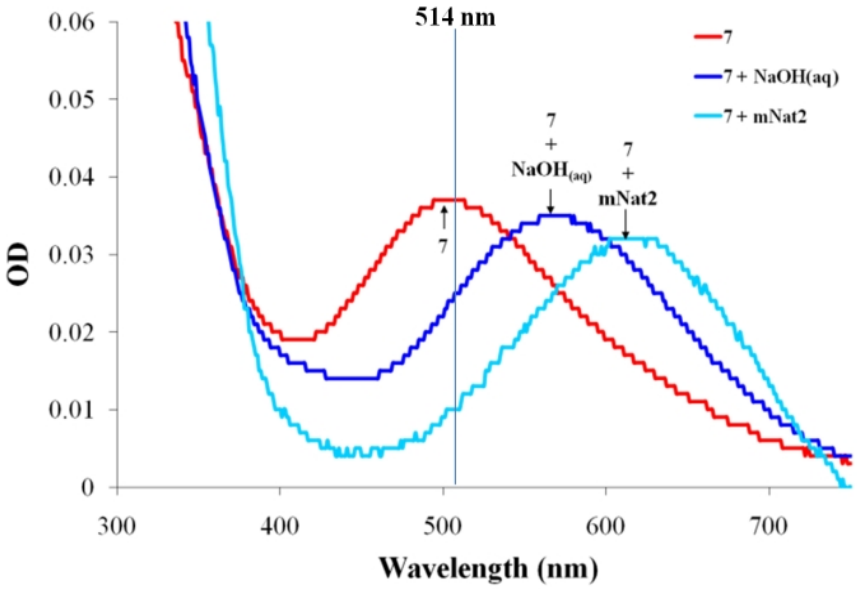


Figure III.14: Spectral properties of 7 in the visible range.

Wavelength scans of **7** (10µM) in buffer (20mM Tris.HCl, pH 8, 5% DMSO (v/v)) (red line), **7** (10µM) in alkaline solution (80mM NaOH, 5% DMSO (v/v)) (dark blue line), **7** (10µM) with pure recombinant mNat2 (20µM) in buffer (as above) (light blue line). All OD values were measured against an appropriate blank. 514 nm is the wavelength choosen to perform colourimetric assessment of the K_d value of the complex mNat2-**7**.

After determining the molar extinction coefficient of both the red species (14,336 $M^{-1}cm^{-1}$) and the blue species (7,215$M^{-1}cm^{-1}$) of compound **7** at 514nm, different concentrations of **7** (named as $[\mathbf{7}]_{initial}$ in **Table III.4**) were tested in the presence of 20 µM of mNat2, and the OD values of each sample was measured at 514nm.

After estimating the concentration of the two different forms of **7** (bound and unbound, **Equation III.6**) and the subsequent θ value (**Equation III.4**) for each titration assay (**Table III.4**), Michaelis-Menten (**Equation III.7**), Hughes-Klotz (**Equation III.8**) and Scatchard (**Equation III.9**) plots were drawn according to the appropriate equations (**Figure III.15**).

K_d values were then determined from all graphs according to the appropriate regression model estimated with the least-squares method.

Table III.4: Biochemical parameters from titration of mNat2 with increasing amounts of 7.

$[7]_{initial}$ (µM)	OD (514nm)	$[7_{unbound}]$ (µM)	$[7\text{-mNat2}]_{estimated}$ (µM)	θ	$1/[7_{unbound}]$	$1/\theta$	$\theta/[7_{unbound}]$
0	0.000	0	0	0.000	-	-	-
10	0.090	2.49	7.51	0.376	0.402	2.662	0.151
20	0.204	8.31	11.69	0.584	0.120	1.711	0.070
40	0.456	23.31	16.69	0.834	0.043	1.198	0.036
60	0.724	40.54	19.46	0.973	0.025	1.028	0.024

$$\theta = \frac{[7_{free}]}{K_d + [7_{free}]}$$

Equation III.7: Michaelis-Menten equation.

$$\frac{1}{\theta} = \frac{K_d}{[7_{free}]} + 1$$

Equation III.8: Hughes-Klotz equation.

$$\frac{\theta}{[7_{free}]} = \frac{1}{K_d} - \frac{\theta}{K_d}$$

Equation III.9: Scatchard equation.

All three plots gave a consistent value of one biding site per molecule of **7**, and the Scatchard and Hughes-Klotz plots, which are usually considered more accurate than the Michaelis-Menten curve (Atkins & Nimmo, 1975; Woosley & Muldoon, 1977), proposed a value for K_d of 4.45 µM on average.

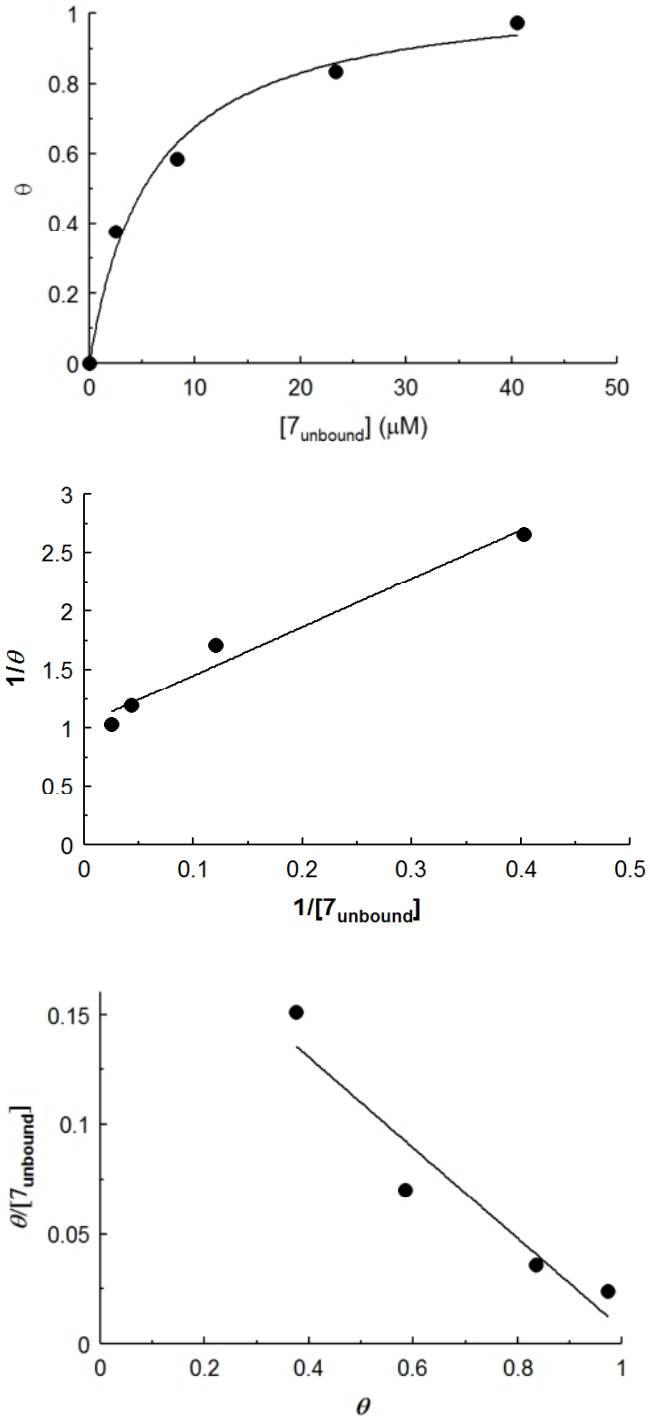


Figure III.15: Preliminary assessment of K_d and nbs sites of 7 to mNat2.

(top) Michaelis-Menten curve. K_d= 5.81μM, nbs = 1.07. **(middle)** Hughes-Klotz plot. Estimated linear equation y = 4.14x + 1.04. K_d= 4.14μM, nbs = 1.04 **(bottom)** Scatchard plot. Estimated linear equation y = -0.21x + 0.21. K_d= 4.76μM, nbs = 1.

However, since the real OD value of the complex mNat2-7 at 514 nm is lower than that generated by compound **7** treated with an alkali at the same (**Figure III.14**), the K_d

value estimated was considered to be approximate.

Therefore, the ratio $\frac{OD_{[7+mNat2]}}{OD_{[7+NaOH]}}$ =0.565 at 514 nm (**Figure III.14**) was used to help extrapolate a standard curve for the blue complex mNat2-**7** (**Figure III.16**) from the standard curve of the blue species of **7** (**Figure III.3-right**) in order to refine previous K_d estimate**.** Indeed, after correcting θ values, the dose-response regression model for the new Michaelis-Menten curve and the linear regression models for both the new Scatchard and Hughes-Klotz plots (**Figure III.17**) gave a higher estimate of the K_d value, on average 11.45µM, and confirmed the single binding site (nbs=0.98).

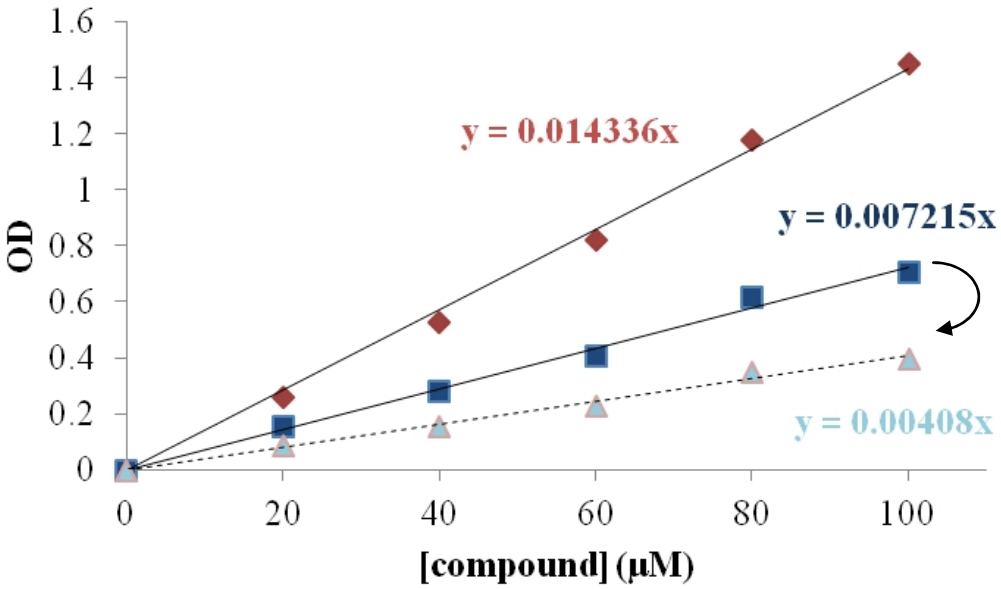


Figure III.16: Standard curves of 7 as red species, blue species and as ligand to mNat2.

Standard curves of **7** at different conditions, pH 8 (red diamonds), pH 13(dark blue squares) and in the presence of mNat2 (light blue triangles). The lines are generated using the OD values of different concentrations of the appropriate form of **7** at 514 nm and the OD values for the mNat2-**7** complex as approximated based on the ratio $\frac{OD_{[7+mNat2]}}{OD_{[7+NaOH]}}$ = 0.565 at 514nm.

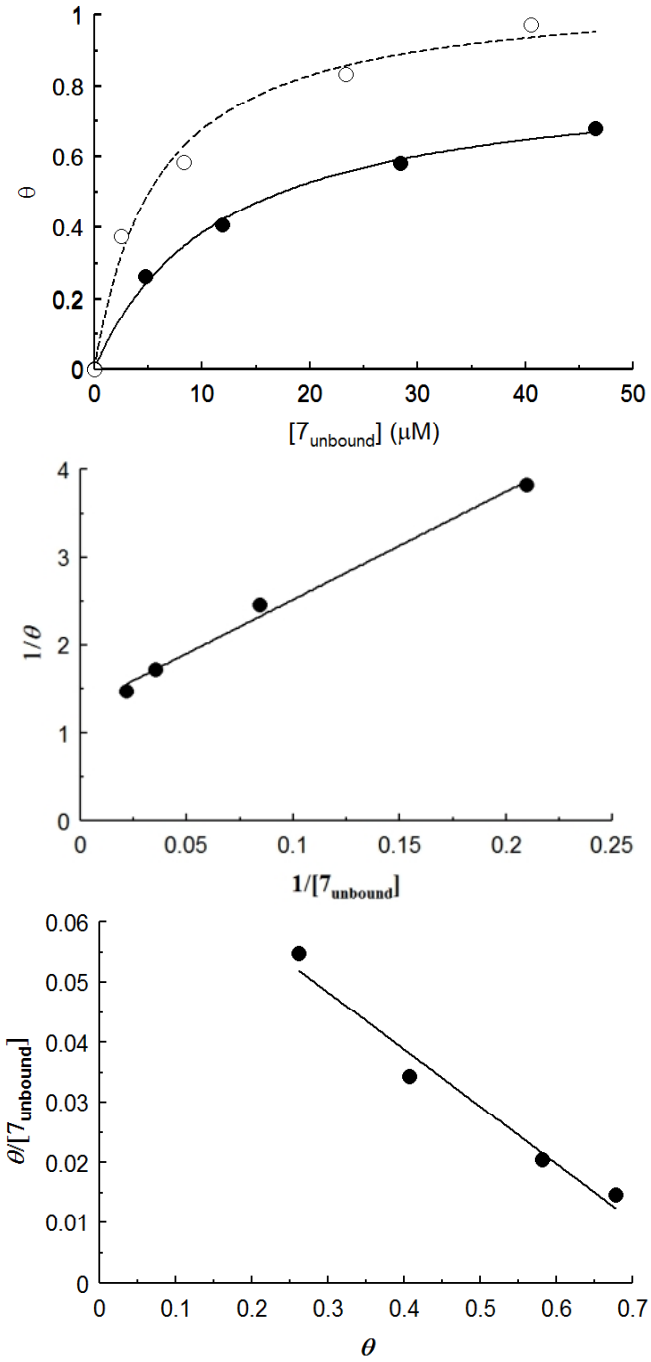


Figure III.17: Refined ssessment of K_d and nbs of compound 7 to mNat2 using corrected values of θ. (top) Michaelis-Menten regression curve. K_d= 11.59μM, nbs = 0.83. The white circles and the dashed dose-response regression curve refer to previous K_d estimate as presented in **Figure III.15 (middle)** Hughes-Klotz plot. Estimated linear equation y = 12.27x + 1.29. K_d= 12.27μM, nbs = 1.29 (**bottom)** Scatchard plot. Estimated linear equation y = -0.095x + 0.077. K_d= 10.49μM, nbs = 0.81.

III.3 Discussion

The opportunity to use hNAT1 as a new biomarker and possible drug target in ER+ve breast cancers was found to be really interesting for improving the classification of different breast tumours and customising therapies.

Moreover, the discovery of naphthoquinone **1**, as potent selective inhibitor against hNAT1 and mNat2 (Russell et al, 2009) and also potential biosensor for these enzymes, triggered a cascade of questions about the selectivity of the colourimetric properties of its derivative **7** towards the same enzymes.

Initially, in order to have considerable amounts of pure recombinant protein available for biochemical characterisation studies, the production and the purification of mNat2, as the murine homologue of hNAT1, yielded ~60 mg from one litre of culture.

Following initial investigations (Russell et al, 2009), in this study compound **1** was confirmed to selectively inhibit hNAT1 and mNat2 compared to other mammalian and bacterial NAT enzymes.

The derivative **7** was found to follow similar biochemical trend (**Table III.6**).

In addition, investigating around the colourimetric properties of compound **7** with a broad panel of prokaryotic and eukaryotic NATs demonstrated that the colour change event of **7** from red to blue occurred uniquely in the presence of both hNAT1 and mNat2 (**Table III.6**).

The distinctive selectivity of compounds **1** and **7** to inhibit hNAT1 and mNat2 and to change colour only upon binding to these enzymes underlined a close correlation between inhibition and colour change event for this family of compounds (**Table III.6**).

Table III.5: Effect of compounds 1 and 7 on different NAT enzymes.

10 µM is the concentration of the requisite inhibitor in enzymatic assays.

Enzyme	hNAT1	mNat2	mNat1	STNAT	MMNAT	MSNAT	PANAT
Primary sequence identity (%) *versus* hNAT1	100	82	74	18	25	29	21
Inhibition with 1 (%)	86.7 ± 0.3	81.1 ± 1.9	52.9 ± 5.3	23.5 ± 4.6	18.5 ± 3.6	< 5	25.1 ± 4.8
Inhibition with 7 (%)	91.7 ± 1.8	92.8 ± 0.4	55.9 ± 6.4	< 5	< 5	< 5	19.6 ± 3.0
λ_{max} of 7 (nm)	585	625	498	498	498	498	498

Moreover, the colourimetric shift of these inhibitors also occurred in the presence of sodium hydroxide. This suggested that a possible deprotonation of the compounds by the base is at the origin of the colour change event.

Therefore, compound **1**, as representative lead compound of this class of inhibitors, was hypothesised to undergo a deprotonation upon selective binding to both hNAT1 and mNat2, but no colour change occurred with other NAT isoforms. Similar assumptions were made in parallel for the analogue **7** (**Figure III.18**).

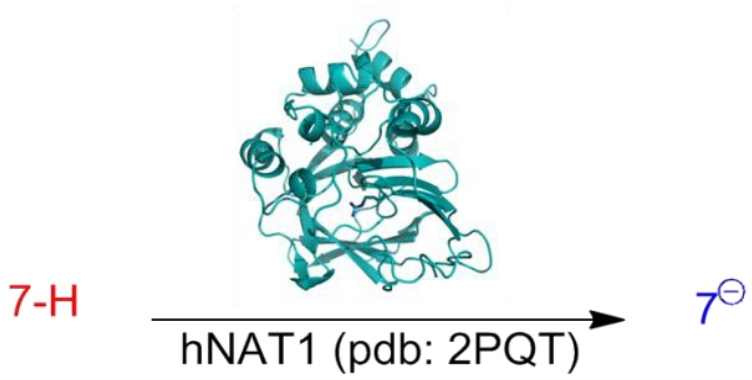


Figure III.18: Hypothesis about the colour change event involving compound 7 interacting with hNAT1.

hNAT1 is adapted from (Wu et al, 2007).

Considering functional murine and human NATs, the comparison of the probe substrate specificity with the inhibitor selectivity of naphthoquinone **1** suggested a possible parallelism between substrate and inhibitor specificity (**Table III.5**). Indeed, the observed differences between substrate and inhibitor specificity profiles in this family of isoen-

zyme exist even though all the isozymes share over 70% identity in amino acid sequence (Kawamura et al, 2008; Martell et al, 1992; Wu et al, 2007) (**Table III.5**).

Table III.6: Comparison of amino acid sequences and substrate specificities of human and mouse NAT isoenzymes.

Percentage inhibition at 30 μM and colour change of **1** *versus* NAT isoenzymes .

	% identity				Probe substrate (Kawamura et al, 2008; Martell et al, 1992)		% inhibition by compound 1 (Russell et al, 2009)	Colour change
Enzyme	**hNAT1**	**mNat2**	**hNAT2**	**mNat1**	**pABAglu**	**Isoniazid**		
hNAT1	100	-	-	-	+	-	> 95	+
mNat2	82	100	-	-	+	-	≥ 95	+
hNAT2	81	74	100	-	-	+	0	-
mNat1	74	81	72	100	-	+	0	-

Following enzymatic studies with the inhibitor **7** and mNat2, the mode of inhibition was determined to be competitive towards the arylamine substrate pABA, with a K_I value of 420nM. This confirmed former results about compound **1**, which was classified as competitive inhibitor of pABA-binding to mNat2 with a K_I of 520nM (Robinson, 2007), and showed that **7** is a slightly more potent inhibitor than **1.** The literature usually associates inhibitor competitiveness with the hypothesis that the ligand binds within the active site of the enzyme (Yon-Kahn et al, 2010).

Moreover, the ligand-protein interaction between compound **7** and pure recombinant mNat2 was further characterised using the colourimetric properties of the naphthoquinone. Filtration experiments supported the hypothesis of a non-covalent binding between **7** and mNat2 and the reversibility of this interaction. Enzymatic activity-recovery studies on compound **7** as enzyme inhibitor could further corroborate this hypothesis under an enzymological perspective.

Furthermore, when a sample of denatured mNat2 was incubated with compound **7**, no colour change of the compound occurred, suggesting that correct protein folding was essential for the ligand to bind to the enzyme and to turn blue.

Finally, the colourimetric properties of compound **7** were used to estimate the dissociation constant K_d between the ligand and mNat2. With appropriate technical refinements, K_d was estimated using two different mathematical approaches, giving 4.45 μM and 11.45 μM respectively. The difference could be due to the approximations introduced in each evaluation. Indeed, in the first instance the OD values estimated for the complex mNat2-**7** were overestimated using the standard curve of the blue form of **7** in an alkaline solution (**Figure III.13**) and this allowed an underestimation of the K_d values.

In the second instance, the standard curve for the enzyme-ligand complex at 514 nm was mathematically extrapolated from the standard curve of the blue species of **7**. However, considering that the absorption of complex mNat2-**7** was relatively low and kept close to the OD values of the background noise (**Figure III.16**), this extrapolation allowed an overestimation of the K_d values.

However, despite their difference, the two K_d values obtained in this study could give an estimate of the range wherein the real K_d value is situated: 4.45 - 11.45μM.

The use of compound **7** as titrating agent of pure recombinant mNat2 to estimate the K_d, anticipated the significance of these naphthoquinone ligands as colourimetric probes to detect hNAT1 in breast cancer.

At present, probes to enable the specific detection of biomacromolecules have been widely used in cellular biology and pathology. In particular, selective detection of native proteins using antibodies and specific recognition of recombinant proteins using affinity tags are now well established (Giepmans et al, 2006).

Moreover, recent reports have shown examples of small molecule probes (Cravatt et al, 2008; Soh, 2008) designed to label selectively native (Richard et al, 2009; Tsukiji et al, 2009; Verdoes et al, 2009; Wright et al, 2009; Zou & Yin, 2009) or engineered (Gallagher et al, 2009; Halo et al, 2009; Hasegawa et al, 2009; Kamoto et al, 2009) proteins, but the majority involve covalent tagging of the target.

These naphthoquinone compounds which have been identified as selective probes of hNAT1 and mNat2 constitute the first example of specific, non-covalent sensors to detect a potential protein biomarker in its native form without the need of a tag or an antibody (Anslyn, 2010; Laurieri et al, 2010).

Chapter IV:

Molecular mechanism of the colour change event



THE THREE GRACES (1635), BY SIR PETER PAUL RUBENS (1577-1640).

The grace on the right shows nipple retraction, reduction of volume and reddening on the skin of the left breast, as well as axillary lymph nodes. This was considered as a visual aspect of a locally advanced breast cancer (Grau et al, 2001a) (Museo del Prado, Madrid).

IV.1 Introduction

In the previous chapter it was hypothesised that compounds **1** and **7** undergo a deprotonation within the active site of hNAT1 or mNat2 upon selective binding, but no deprotonation occurs with other NAT isoforms.

This observation would be consistent with the requirement for both molecular recognition and the presence of a suitably located residue within the enzyme active site in order for the inhibitor to bind and the colour change to occur.

In 2007, crystal structures of both human NAT enzymes were solved (Wu et al, 2007). Docking studies with the appropriate substrate confirmed the importance of the active site residues 125-129 to explain human NAT substrate selectivity despite the high level of protein sequence identity (Goodfellow et al, 2000; Wu et al, 2007).

Primary sequences of all NATs tested in **Chapter III** together with hNAT2 were aligned and compared (**Figure IV.1**).

An additional residue was observed only in mammalian NATs: the residue 127 (numbering according to hNAT1 sequence). This residue is an arginine exclusively in both hNAT1 and mNat2 enzymes, whilst a serine and a glycine occupy the same position in hNAT2 and mNat1 respectively.

Moreover, considering the chemical properties of the residues within hNAT1 active site (Wu et al, 2007), in particular the thiolate group of Cys68 and the guanidine functionality of Arg127 (**Figure IV.2**), along with the known reactivity of the naphthoquinone system of compounds **1** and **7**, three possible mechanisms of enzyme-inhibitor interaction were postulated that could affect the colourimetric properties of the chromophore of **1** and **7**: deprotonation of the acidic sulfonamide-N*H*, conjugate addition or reduction (**Scheme IV.1**).

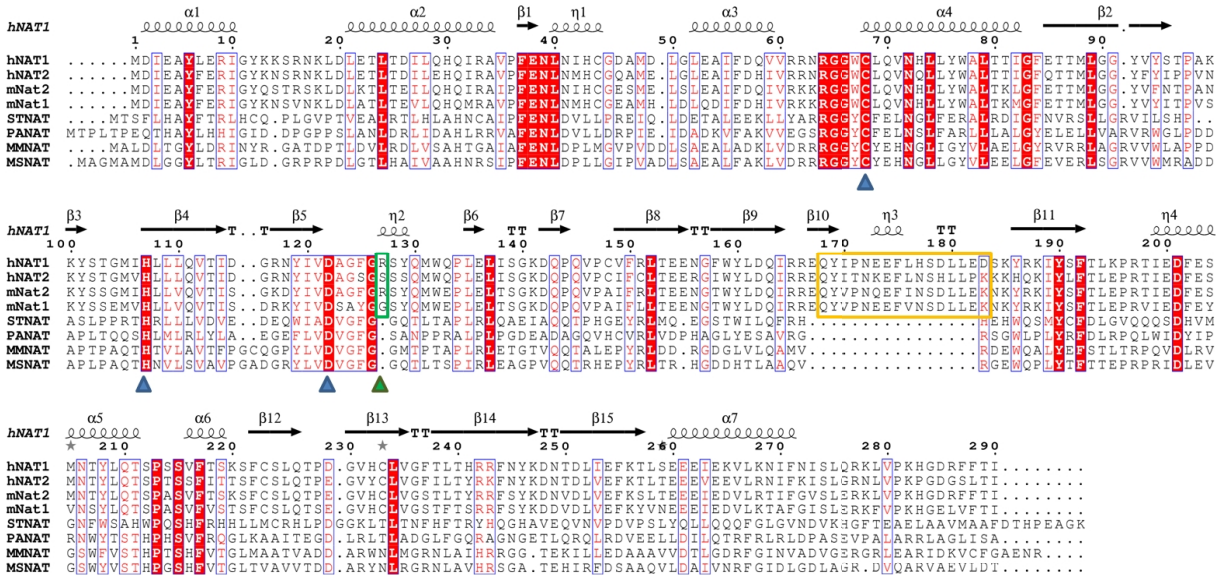


Figure IV.1: Multiple sequence alignment of selected NAT proteins.

NAT proteins from *S. typhimurium*, *P. aeruginosa*, *M. marinum* and *M. smegmatis* are aligned with murine and human NAT isoenzymes. Similar amino acids are highlighted in blue boxes; completely conserved residues are indicated by white lettering on a red background. The residues from the catalytic triad are indicated by a blue triangle, the putative residue involved in inhibitor selectivity is indicated by a green triangle, and the residues constituting the additional loop in eukaryotic NATs are highlighted in an orange box. The secondary structure is adapted from hNAT1 crystal structure (pdb code: 2PQT)(Wu et al, 2007). Alignment was generated using Clustal W (Thompson et al, 1994). Figure was prepared using ESPript 2.2 (Gouet et al, 1999)

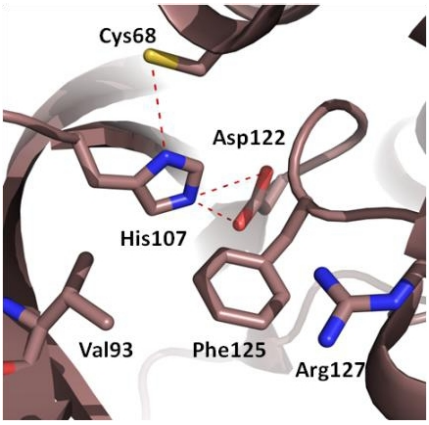
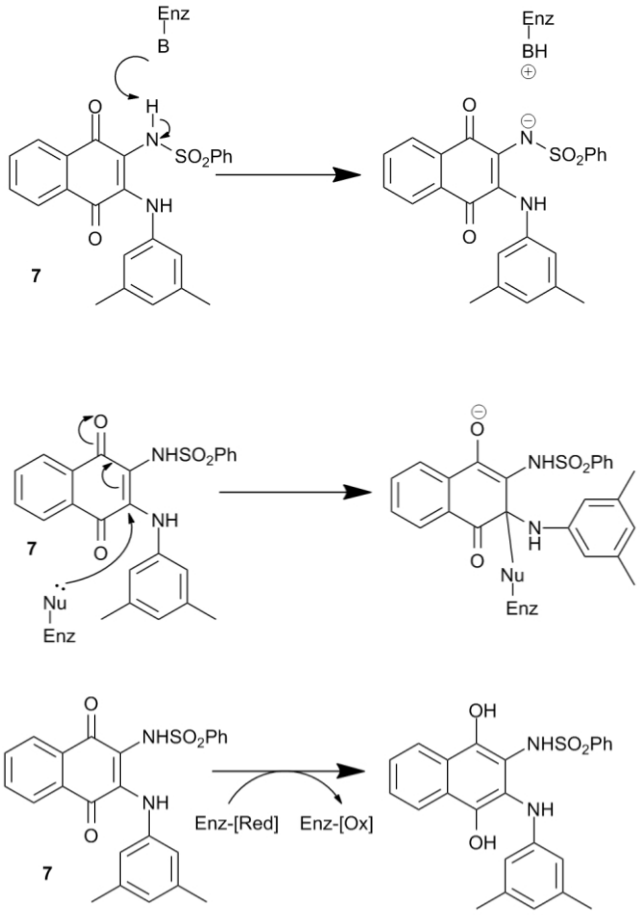


Figure IV.2: Active site of hNAT1.

Insight view of hNAT1 active site (pdb: 2PQT) (Wu et al, 2007) with side chains of key residues drawn in stick representation and labelled with carbon atoms in grey, nitrogen in blue, oxygen in red, and sulfur in orange. The catalytic triad Cys68-His107-Asp122 is shown.



Scheme IV.1: Hypothesised mechanisms for colour change of 7 within the hNAT1 active site.

(top) Possible deprotonation of compound **7** by an alkaline moiety (**B**) within the active site region of the enzyme. **(middle)** Possible conjugate addition of compound **7** by a nucleophilic group (**Nu**) from the enzyme. Either C_2 or C_3 in the naphthaquinone core are likely to react. **(bottom)** Possible oxido-reduction of compound **7** in interaction with hNAT1.

Notably, according to a literature precedent in support of the proton-exchange mechanism, other naphthoquinone analogues had previously been shown to possess similar colourimetric properties upon basification (Wu et al, 2009). Nevertheless, all three possibilities were investigated through structural and mechanistic studies.

The best approach would be to obtain and describe a crystal structure of an enzyme-inhibitor complex to establish the binding mode of the ligand. Moreover, the structure-based drug design process is greatly aided by the characterisation of the binding mode of the inhibitor (Gane & Dean, 2000; Noble et al, 2004).

A source of pure recombinant hNAT1 would be required to generate suitable crystals. However, previous studies highlighted that hNAT1 could be overexpressed with only moderate yield, but with considerable instability (Dairou et al, 2004; Wang et al, 2005b). This would affect the success of crystallographic trials. Indeed, in order to stabilise hNAT1 for crystallisation trials, the F125S mutant was generated and its crystallisation was successful prior to obtaining the crystal of the wild-type protein with a covalently modified Cys68 (Wu et al, 2007). Nevertheless, the substrate specificity of the F125S mutant of hNAT1 was shown to be altered compared to the wild-type enzyme (Wu et al, 2007).

On the other hand, mNat2, was identified to be a very good model for hNAT1 (Kawamura et al, 2008), and could be produced in a high yield and with much greater stability. It was therefore thought to be suitable for crystallisation trials.

Moreover, the gene *mNat2* could be used for mutagenetic studies to generate suitable mutants, in order to test previous hypotheses concerning the residue involved in the proton exchange with compound **1** or **7**.

In the end, in support of crystallisation trials of the appropriate NAT with the naphoquinone ligand bound, docking the ligand into a suitable site within the enzyme could be used to assist in determining which protein residues are involved in inhibitor binding. The data from such experiments would then help to design new inhibitors to target specific protein residues or pockets.

AIMS

The aim of the work presented in this chapter is to advance understanding of the colour change event observed when compounds **1** or **7** bind to hNAT1 and mNat2 active sites. The following series of approaches are described:

- physicochemical characterisation of **1** and **7**
- physicochemical characterisation of analogues of compound **7** with either a *N*-methylated sulfonamide or a ^{15}N-labelled sulfonamide
- spectrophotometric and kinetic studies of **7** in the presence of an inactive species of mNat2 for treatment with alkylating iodoacetamide
- generation and characterisation of two species of mNat2 mutated at position 127
- optimisation of purification of mNat2 for structural studies
- spectrophotometric characterisation of **7** with other mammalian NAT isoforms: mNat2_F125S, shNat2, and mNat1
- modelling mNat2 using the known hNAT1 structure
- *in silico* docking of **7** into hNAT1 and mNat2 active sites

This chapter is subdivided into two sections: the first section will focus on the physico-chemical properties of naphthoquinones **1** and **7** and the second section will elucidate the molecular mechanism of the colourimetric recognition of both hNAT1 and mNat2 by naphthoquinone **7** using two mNat2 mutants.

IV.2 Results

IV.2.1 Colourimetric properties of naphthoquinones 1 and 7

IV.2.1.1 Spectrophotometric properties of 1 and 7 at different pHs

Previous studies suggested that the colour change of **1** and **7** in the presence of either hNAT1 or mNat2 is due to deprotonation of the sulfonamide moiety within the enzyme active site.

Compounds **1** and **7** needed to be fully characterised in terms of relative acidity (pK_a) and colourimetric properties (λ_{max}, ε) following these preliminary observations.

1 and **7** showed a similar trend in differently buffered solutions (**Figure IV.3**). In particular, in buffer 20mM Tris.HCl, pH 8, **1** had a λ_{max} value of 489nm, likewise **7** had a λ_{max} value of 498nm; when the pH of the solution was adjusted to pH 13 using a strong alkali, NaOH, a bathochromic shift was observed in the visible spectra of both compounds with a concomitant colour change from red to blue, visible by eye, (+72 nm for **1**, and + 74 nm for **7**).

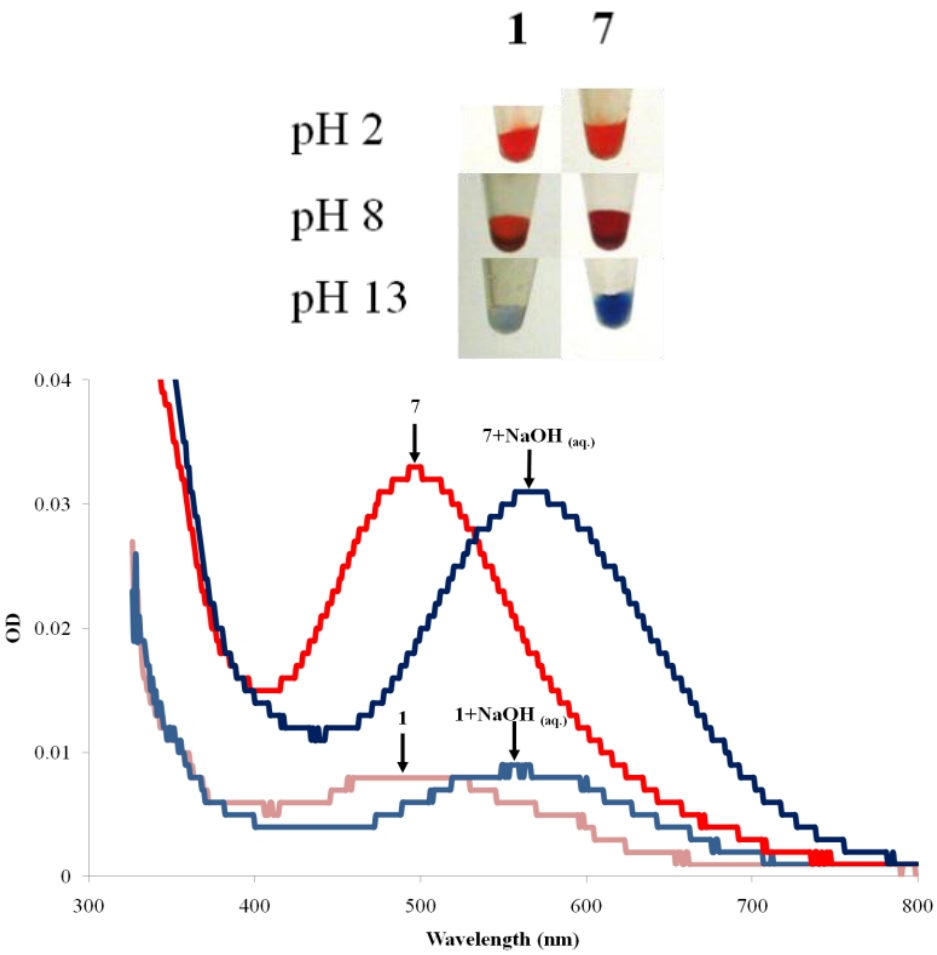


Figure IV.3: Optical properties of compounds 1 and 7 at different pHs.

(top) To 50µl of solution of compounds **1** and **7** (2mM) in DMSO, 10µl of different buffering solutions were added: Gly.HCl (4 M, pH 2.0), Tris.HCl buffer (20mM, pH 8.0) or aq. NaOH (pH 13.0). **(bottom)** Wavelength scans of **1** and **7** (10µM) in buffer (20mM Tris.HCl, pH 8, 5% DMSO (v/v)) (red lines), **1** and **7** (10µM) in alkaline solution (80mM NaOH, 5% DMSO (v/v)) (dark blue lines). All values of optical density were measured against an appropriate blank.

Two possible acidic protons are present in compounds **1** and **7**: the sulfonamide-N*H* or the secondary amine-N*H*. It is known that aromatic sulfonamides and anilines have significantly different pK_a values. For instance, 4-(trifluoromethyl)benzenesulfonamide possesses a pK_a=9.7 measured in DMSO, whilst the corresponding value for 4-(trifluoromethyl)aniline is pK_a=27 in DMSO (Bordwell & Algrim, 1976; Bordwell & Algrim, 1988).

Although the colourimetric assays were performed in an aqueous environment, the literature strongly supported that phenylsulfonamide-N*H* is a stronger acid than the aniline-N*H* (**Figure IV.4**). Indeed, when the sulfonamide-N*H* of compound **1** or **7** undergoes proton exchange in the presence of NaOH, the subsequent negative charge on sulfonamide-*N* could be stabilized by multiple delocalisations (**Figure IV.4**).

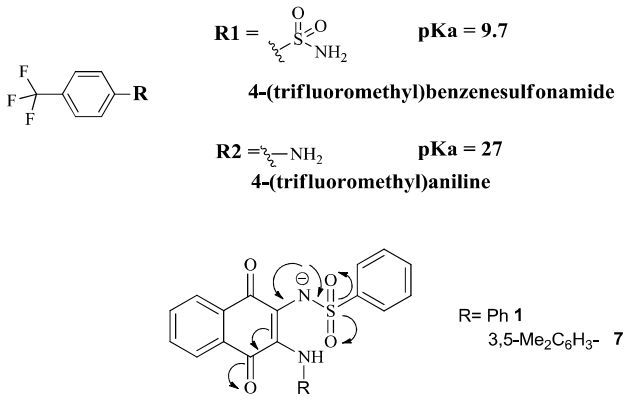


Figure IV.4: Weak acidity of compounds 1 and 7.

(top) Comparison of the pK_a values of examples of aniline and benzenesulfonamide in DMSO (Bordwell & Algrim, 1976; Bordwell & Algrim, 1988). **(bottom)** Multiple delocalisation of the negative charge generated on sulfonamide-*N* after deprotonation of compound **1** or **7**.

Again, the colourimetric properties of **1** and **7** at different pHs were used in order to titrate both species over a wide range of different pHs to estimate their respective pK_as (**Figure IV.5**). Sigmoidal titration curves gave a pK_a=9.50 for **1**, as previously shown (Crawford, 2007), and a pK_a=9.16 for **7** and reinforced the hypothesis that the colour change event is pH-dependent.

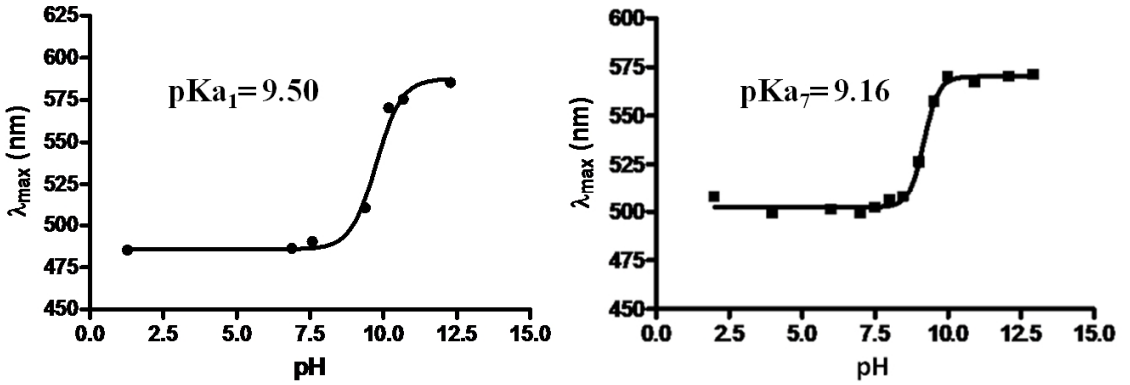


Figure IV.5: pH titration curves of naphthoquinones 1 and 7.

Wavelength scans of the appropriate compound (100μM) were recorded from 800 to 350 nm at different pHs, then the λ_{max} was determined for each spectrum. λ_{max} values were plotted on the y-axis against a pH scale on the x-axis and a sigmoidal titration curve was fitted using GraphPad. **(left)** pH titration curve for **1** (pH used = 1.3, 6.9, 7.6, 9.4, 10.2, 10.7, 12.3) (Crawford, 2007). **(right)** pH titration curve for 7 (pH used = 2, 4, 6, 7, 7.5, 8, 8.5, 9, 9.5, 10, 11, 12, 13)

IV.2.1.2 Effect of a non-nucleophilic alkali on compound 7

However, taking into account that the hydroxide ion could interact with quinone as a nucleophile (Pedersen, 1973), the chemical interaction between **7** and a non-nucleophilic amidine base seemed interesting to be investigated. 1,8-Diazabicyclo[5.4.0]undec-7-ene (DBU) was chosen for this purpose, since its pK_a value (12.0) (Granitza et al, 1995) was suitable to deprotonate compound **7** (9.16). If the colour change from red to blue were still observed when **7** was treated with DBU, this would strongly support that the deprotonation of **7** is at the origin of the colour change from red to blue rather than a nucleophilic addition/elimination reaction.

The λ_{max} of **7** shifts from 498 nm in 20mM Tris.HCl buffer (pH 8) to 580 nm in 80mM NaOH (pH 13.75); λ_{max} of **7** is 600 nm in the presence of 80mM DBU in DMSO (**Figure IV.6**), which is highly consistent with the value observed in aqueous NaOH. However, the discrepancy of 20 nm could be due to solvation effects as a result of the differ-

ent environments in the assays. Solvation effects are known to influence absorption properties (*vide infra*, **VII.1.3**).Therefore, the colour change is more likely to be attributed to a deprotonation mechanism, rather than the alternative addition pathway.

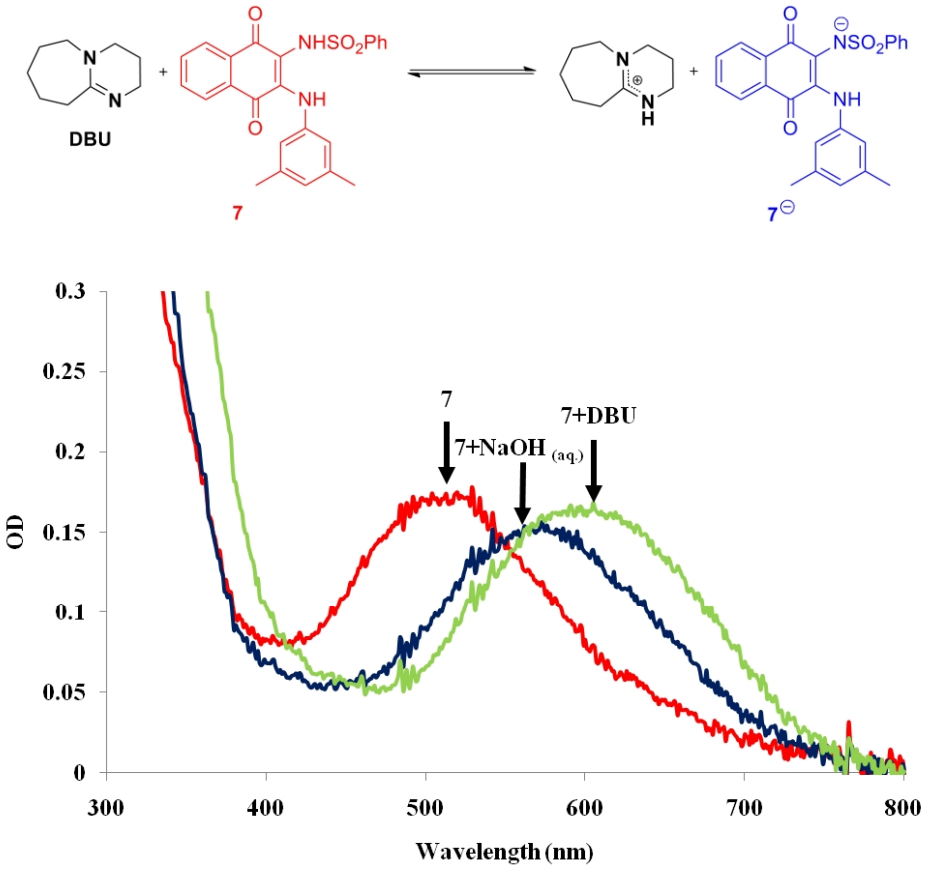


Figure IV.6: Chemical interaction between 7 and DBU, as non-nucleophilic base.

(top) Acid-base proton exchange between **7** and DBU. **(bottom)** Wavelength scans of **7** (10µM) in buffer (20mM Tris.HCl, pH 8, 5% DMSO (v/v)) (red line), **7** (10µM) in alkaline solution (80mM NaOH, 5% DMSO (v/v)) (blue line), **7** (10µM) in alkaline solution (80mM DBU, 5% DMSO (v/v)) (green line). All values of optical density were measured against an appropriate blank.

IV.2.1.3 Oxidoreduction of naphthoquinones 1 and 7

As an alternative explanation for the colour change of **1** and **7**, the susceptibility of the naphthoquinone functional groups towards reduction to the corresponding naphthoquinols led us to investigate whether any reducing agent may give rise to the bathochromic shift in the visible absorption spectrum of both compounds, especially DTT which is present in the recombinant protein solution at a final concentration of 34 μM in the spectrometric assay.

Treatment of both compounds **1** and **7** with DTT at 34 μM did not affect their colour (**Figure IV.7**), but using a higher concentration of DTT (100mM) under an atmosphere of argon led to the decolourisation of both **1** and **7**, which were reversed to red upon exposure to air (**Figure IV.8**).

Previous studies reported a similar observation: following treatment of naphthoquinones with reducing agents, an aerobic oxidation of the generated napthoquinols occurs (Hoover & Day, 1954).

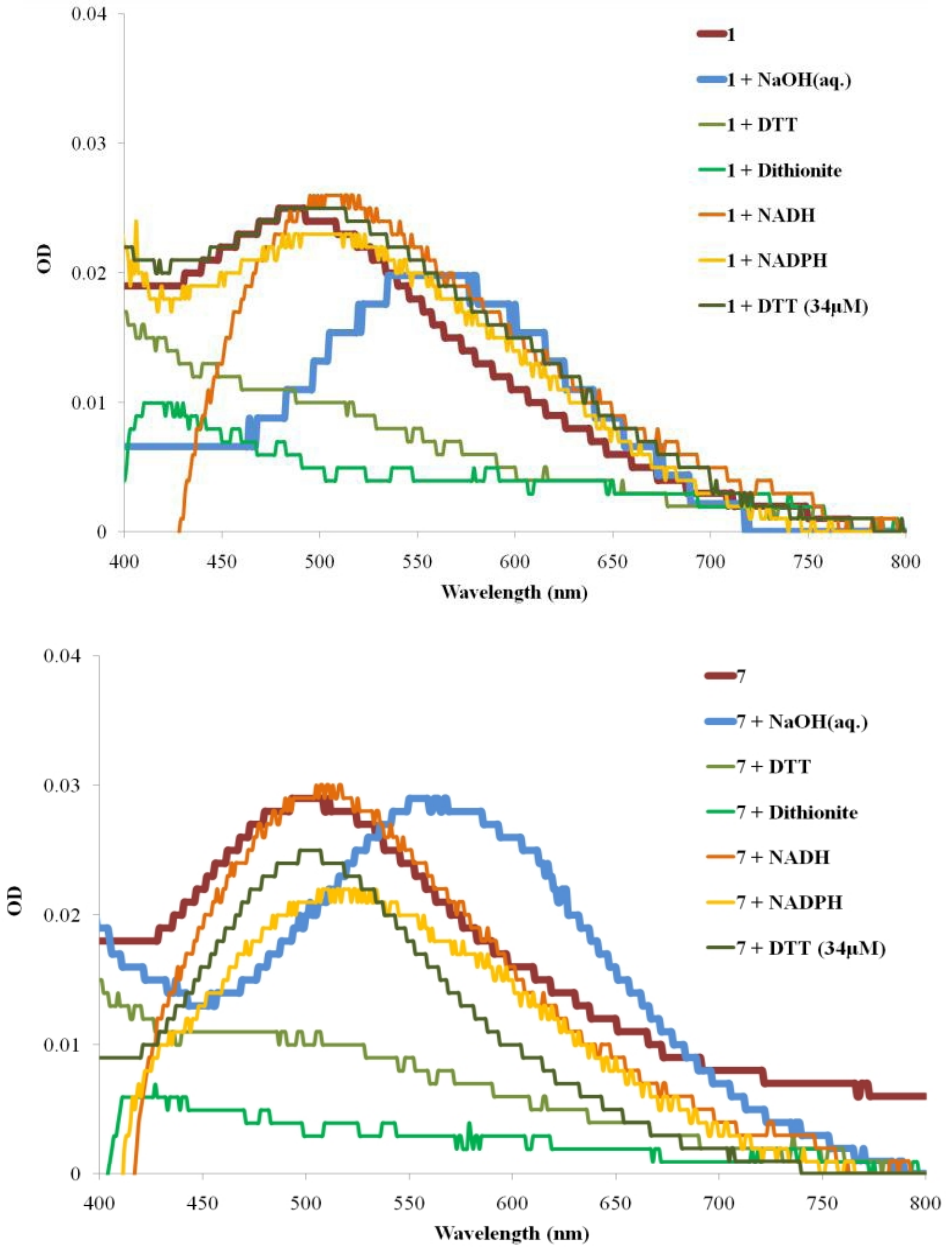


Figure IV.7: Optical properties of compounds 1 and 7 in the presence of different reducing agents. **(top)** Wavelength scans of **1** (20µM) recorded from 800 to 400 nm in the presence of different reducing agents (100mM). Appropriate wavelength scan of **1** (20µM) was recorded in the presence of aqueous NaOH (80mM), as a positive control for the colour change event. A wavelength scan of **1** (20µM) in the presence of DTT at 34 µM was recorded. Wavelength scans with DTT were recorded under an atmosphere of argon. **(bottom)** Wavelength scans of **7** (10µM) recorded from 800 to 400 nm in the presence of different reducing agents (100mM), as of **1**.

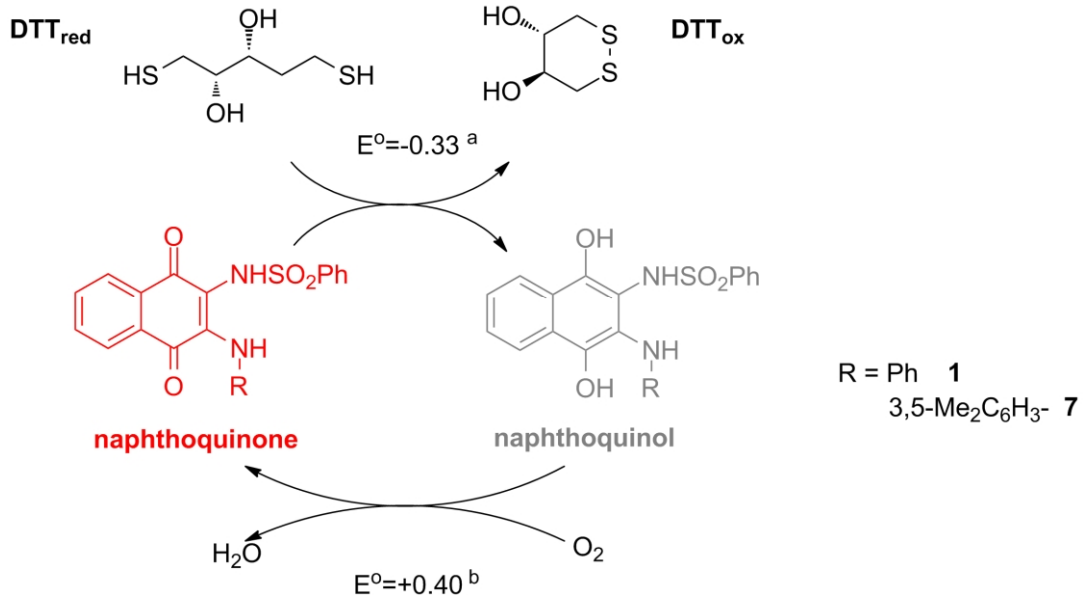


Figure IV.8: Oxidoreduction mechanism of compounds 1 and 7 in the presence of DTT, as reducing agent, and O_2 as oxidising agent.

[a] = (Nauser et al, 2006); [b] =(Atkins, 1998)

Also, analogous decolourisation of naphthoquinones **1** and **7** was observed in the presence of 100mM dithionite (**Figure IV.7**), a very strong reducing agent, but no reversibility to a red colour was detected after exposure to the atmosphere.

The difference in colour reversibility of naphthoquinones **1** and **7** in the presence of either DTT or dithionite could be due to a difference in their corresponding redox potentials. Indeed, DTT has a standard reduction potential of -0.33 V at pH 7.0 (Nauser et al, 2006). Conversely, sodium dithionite has a lower standard reduction potential, around -0.66 V at pH 7 (Mayhew, 1978), which makes dithionite a more potent reductant than DTT. This difference in standard reduction potentials might affect the thermodynamic oxido-reduction equilibria in the mixtures.

Other possible naturally occurring reducing agents, such as NADH and NADPH, were tested with compounds **1** and **7**, and gave neither visible colour change nor reduction, but only treatment with an alkali gave the characteristic bathochromic shift in the visible spectrum of both compounds.

Moreover, the UV properties of both **1** and **7** were also investigated by spectrophotometry in order to compare the spectrophotometric potential of these compounds in both the UV and visible ranges (**Figure IV.9**).

100mM DTT drastically changed the spectra of both compounds with a hypsochromic shift (~ -10 or -15nm) of around 10-15 nm in the UV region, whereas the smaller amount of DTT in the protein sample (34µM) did not alter the UV spectra, consistent with previous observations in their visible spectra (**Figure IV.9**). Conversely, when both compounds were treated with sodium hydroxide, the UV spectra showed a bathochromic shift (~ +10nm) which was smaller than the bathochromic shift observed in the visible spectra of both compounds **1** and **7** (~ +70nm) (**Table IV.1**).

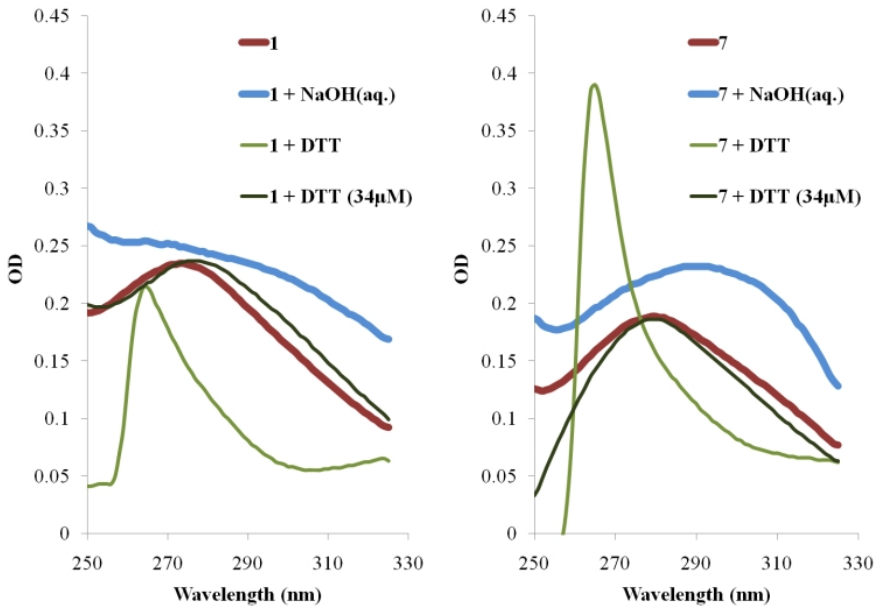


Figure IV.9: UV spectra of naphthoquinones 1 and 7 in the presence of DTT as reducing agent.

(left) Wavelength scans of **1** (20µM) were recorded from 325 to 250 nm in the presence of 20mM Tris.HCl (red line), 80mM aqueous NaOH (blue line), 100mM DTT under an atmosphere of argon (light green line), 34 µM DTT under an atmosphere of argon (dark green line). **(right)** Wavelength scans of **7** (10µM) were recorded from 325 to 250 nm in the presence of 20mM Tris.HCl (red line), 80mM aqueous NaOH (blue line), 100mM DTT under an atmosphere of argon (light green line), 34 µM DTT under an atmosphere of argon (dark green line).

Table IV.1: UV-vis properties of compounds 1 and 7 in the presence of different chemical reagents.

	1 (20µM)		7 (20µM)	
	UV λ_{max} (nm)	Vis λ_{max} (nm)	UV λ_{max} (nm)	Vis λ_{max} (nm)
Tris.HCl buffer (pH8)	274	489	280	498
NaOH (aq., 80mM)	~ +10	+72	+10	+74
DTT (34µM)	+2	+0	+0	+0
DTT (100mM)	-10	-	-15	-

IV.2.1.4 Weak acidity of sulfonamide-N*H* of naphthoquinone 7

After excluding conjugate addition or reduction as potential mechanisms for colour change of **1** and **7**, deprotonation of these naphthoquinones appeared to be the most plausible explanation for the bathochromic shift observed in their visible spectra.

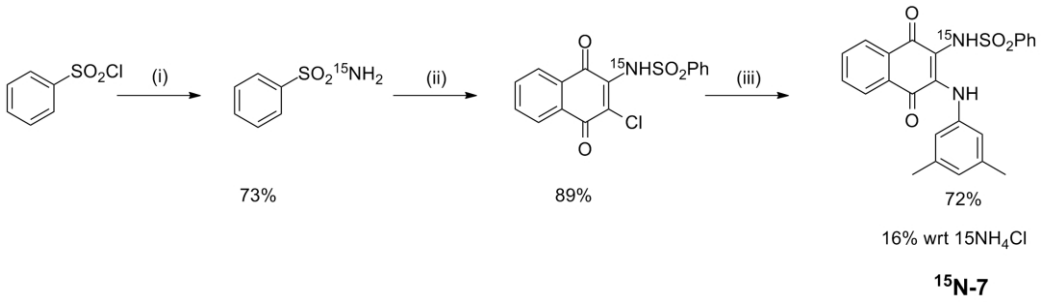
In order to verify that sulfonamide-N*H* is the acid proton source for the deprotonation of **7** in an alkaline environment, it was decided to investigate the use of proton nuclear magnetic resonance (^{1}H-NMR) to follow the resonance of the sulfonamide proton in both neutral and alkaline solutions.

The sulfonamide-N*H* can be easily identified in a ^{1}H-NMR spectrum of **7** in 100% DMSO-d_6 solution, δ_H (400MHz, DMSO-d_6) = 9.05 ppm.

In an attempt to simulate the enzymatic assay conditions (95% aqueous solution/5% DMSO), D_2O was added up to reach the ratio 5% DMSO/95% D_2O. However, as little as 5% D_2O present in the DMSO-d_6 solvent resulted in a broader signal arising from the sulfonamide-N*H* due to rapid proton-deuteron exchange with D_2O. Direct observation of sulfonamide-N*H* by ^{1}H-NMR spectroscopy was therefore not possible in the presence of D_2O, and its disappearance as a means to monitor proton transfer under alkaline conditions or in the presence of enzyme would not have been viable.

In order to circumvent this problem, it was decided to synthesise the corresponding ^{15}N-labelled sulfonamide analogue of **7** (**Scheme IV.2**), which should show a distinct shift in the ^{15}N-NMR spectrum under neutral and alkaline conditions. The chemical synthesis

was carried out by C. Thinnes, Department of Chemistry, Oxford (Thinnes, 2010), and ^{15}N-NMR experiments were performed in collaboration with Dr Tim Claridge, Chemistry Research Laboratories, University of Oxford.



Scheme IV.2: Chemical synthesis of compound 7 analogue with an ^{15}N-labelled sulfonamide.

Reagents and conditions: (i) $^{15}NH_4Cl$, 3 M aq. NaOH, 90°C, 30 min; (ii) 2,3-dichloronaphtalene-1,4-dione, Cs_2CO_3, PhMe, 170°C, µw, 40 min; (iii) $CeCl_3.7H_2O$ then 3,5-dimethylaniline, PhMe, 170°C, µw, 2 h. µw = microwave, wrt = with respect to. The scheme is adapted from (Thinnes, 2010).

Moreover, if the ^{15}N-labelled compound **7** was sufficiently soluble in the solvent system 5% DMSO/95% D_2O at the concentration required to generate a ^{15}N-NMR spectrum with sufficient resolution, it would be suitable for observing a distinctive shift in its ^{15}N-NMR spectrum upon deprotonation by pure recombinant mNat2 as in the spectrophotometric assays previously performed.

Unfortunately, the ^{15}N-labelled compound **7** showed limiting solubility in a 5% DMSO-d_6/95% D_2O solvent mixture and no signal for the ^{15}N could be observed. Nevertheless, the ^{15}N-NMR spectrum of **7** was successfully recorded in a 95% DMSO-d_6/5% D_2O solvent mixture. Thus, it was impossible to prove deprotonation of ^{15}N-labelled compound **7** by mNat2 *via* NMR, since protein folding was drastically affected by increasing the percentage of DMSO in the solution higher than 5% (Russell et al, 2009).

Conversely, the ^{15}N-NMR spectrum of ^{15}N-labelled **7** under alkaline conditions (95% DMSO-d_6/5% aq. NaOD) was acquired and compared to the spectrum obtained under

neutral conditions (**Figure IV.10**).

Whilst the ^{15}N-NMR spectrum of ^{15}N-labelled **7** under neutral conditions displayed a sharp peak at 104.7 ppm, the spectrum of ^{15}N-labelled **7** under alkaline conditions showed a broader peak at 166.3 ppm (**Figure IV.10**).

Moreover, acquisition times changed as well: the spectrum obtained under neutral conditions was well resolved after 15 min, whereas the spectrum obtained under alkaline conditions required accumulation of scans overnight to give a well-defined signal. These changes were consistent with the electron-density changing around the sulfonamide ^{15}N.

The broader signal observed in alkaline conditions was thought to be due to fast proton-exchange of the sulfonamide ^{15}N-*H* with bulk solvent (**Figure IV.10**).

Parallel pictures of the ^{15}N-labelled **7** species in both neutral and alkaline conditions showed a conserved red colour of the protonated ^{15}N-labelled **7** and an intense blue colour for the deprotonated ^{15}N-labelled **7** species (**Figure IV.10**).

The ^{15}N-NMR experiment thus supported sulfonamide-N*H* deprotonation as the origin of the colour change from red to blue of compound **7**.

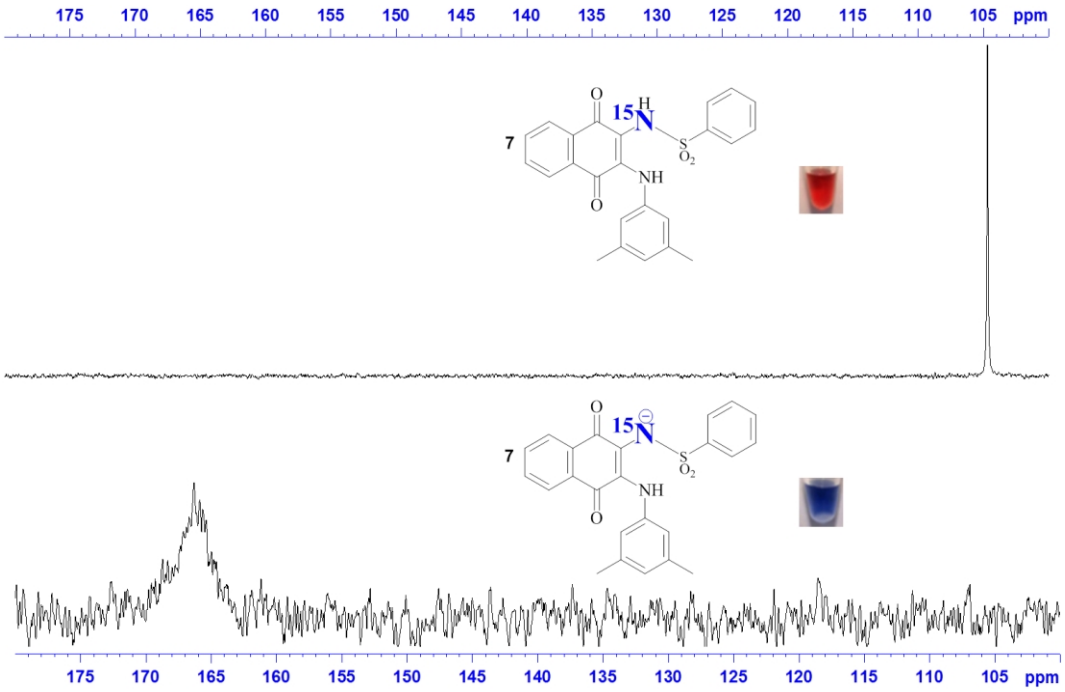
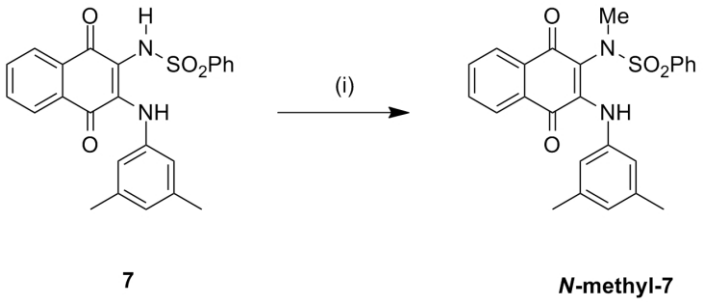


Figure IV.10: NMR analysis of 7 analogue with *[15]N*-labelled sulfonamide.

10 mg of *[15]N*-labelled **7** was used in 600µl of the appropriate buffer, which corresponds to a concentration of 38.2mM. Spectra were acquired on a Bruker DRX500 spectrometer. **(top)** ^{15}N-NMR spectrum of *[15]N*-labelled **7** in 95% DMSO-d_6 / 5% H_2O, δ_N 104.7 ppm. Picture of 50µl of *[15]N*-labelled **7** (2mM) in DMSO with 10µl of 20mM Tris.HCl, pH 8. **(bottom)** ^{15}N-NMR spectrum of *[15]N*-labelled **7** in 95% DMSO-d_6 / 5% aq. NaOD, to a final NaOD concentration of 75.8mM. δ_N 166.4 ppm. Picture of 50µl of *[15]N*-labelled **7** (2mM) in DMSO with 10µl of 4mM NaOH, pH 13.

In order to confirm whether the sulfonamide-N*H* is the source of the acid proton involved in the acid-base proton exchange between **7** and the enzymes hNAT1 and mNat2, an *N*-methyl sulfonamide analogue of compound **7** was successfully synthesised by C. Thinnes, Department of Chemistry, Oxford (Thinnes, 2010) (**Scheme IV.3**). This new compound, which is named *N*-methyl-**7** in this thesis, was stable and possessed a red colour. It was not anticipated to change colour in an alkaline solution, nor in the presence of mNat2.



7 ***N*-methyl-7**

Scheme IV.3: Chemical synthesis of *N*-methyl-7.

Reagents and conditions: $TMSCHN_2$ (17 eq.), MeOH, DCM, RT, 76 h. The scheme is adapted from (Thinnes, 2010).

Parallel pictorial images of compounds **7** and *N*-methyl-**7** revealed that the *N*-methylated species does not change colour at pH 13 compared to **7**, but keeps an orange colour in acid, neutral and alkaline buffered solutions (**Figure IV.11**).

When the λ_{max} was measured for *N*-methyl-**7** in a wide range of different pHs, no λ_{max} shift was observed throughout the pH scale, supporting the hypothesis that the colour change of **7** was due to the deprotonation of sulfonamide-N*H* (**Figure IV.11**).

The λ_{max} of *N*-methyl-**7** was not found to differ in the presence of mNat2 compared to aqueous NaOH or neutral conditions.

Moreover, when the visible spectra of *N*-methyl-**7** were recorded at pH 8 and 13.75 and also in the presence of mNat2, no bathochromic shift was observed also in the presence of the enzyme, compared to similar spectra recorded with compound **7**. However, it still remained to be proved that the compound binds to the enzyme.

N-methyl-**7** slightly inhibits mNat2 activity at 30 μM (20% inhibition), thereby suggesting that the compound binds to the enzyme (**Figure IV.12**). Provided that the binding mode of *N*-methyl-**7** to mNat2 is conserved relative to that assumed by compound **7** within the active site of the enzyme, this could provide supportive elements in the explanation of the mechanism of the colour change and enzyme inhibition by naphthoquinone **7** towards both hNAT1 and mNat2. In particular, the sulfonamide-N*H* is likely

to be the source of the acid proton involved in the acid-base proton exchange between **7** and the enzymes hNAT1 and mNat2.

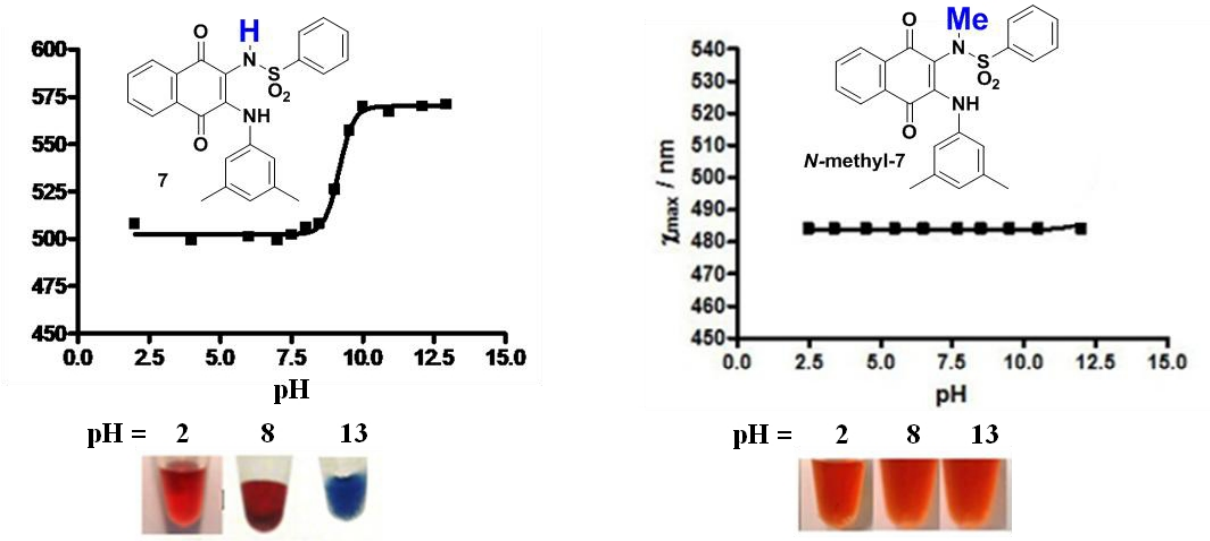


Figure IV.11: Comparison of chemical and optical properties of 7 *versus* *N*-methyl-7.

(top - left) pH titration curve for **7** (pH used = 2, 4, 6, 7, 7.5, 8, 8.5, 9, 9.5, 10, 11, 12, 13) pK_a=9.16. **(top - right)** pH titration curve for *N*-methyl-**7** (pH used = 2.5, 3.4, 4.5, 5.5, 6.5, 7.7, 8.5, 9.5, 10.5, 12.5) pK_a>12.5. **(bottom)** Optical characteristics of the appropriate compound at three different pHs **(bottom - left)** 50µl of solution of compound **7** (2mM) in DMSO were mixed with 10µl of different buffering solutions: Gly.HCl (4 M, pH 2.0), Tris.HCl buffer (20mM, pH 8.0) or aq. NaOH (pH 13.0). **(bottom - right)** 100µl of a solution of *N*-methyl-**7** (2mM) in DMSO were mixed with 20µl of the same buffers used for compound **7**.

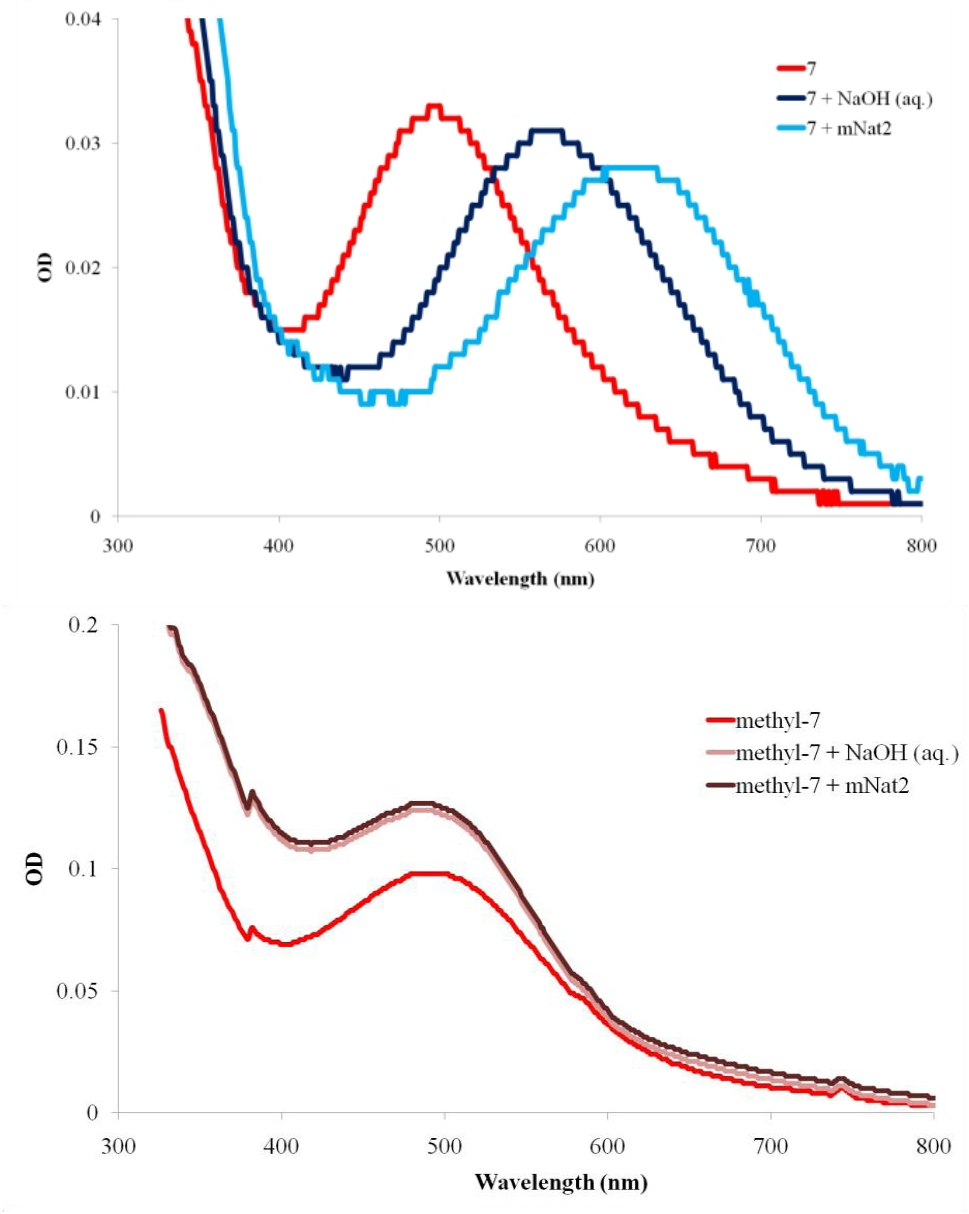


Figure IV.12: Optical properties of 7 and *N*-methyl-7.

(top) Wavelength scans of **7** (10µM) in buffer (20mM Tris.HCl, pH 8, 5% DMSO (v/v)) (red line), **7** (10µM) in alkaline solution (80mM NaOH, 5% DMSO (v/v)) (dark blue line), **7** (10µM) with pure recombinant mNat2 (20µM) in buffer (as above) (light blue line). All values of optical density were measured against an appropriate blank. **(bottom)** Wavelength scans of *N*-methyl-**7** (15µM) in buffer (20mM Tris.HCl, pH 8, 5% DMSO (v/v)) (red line), **7** (15µM) in alkaline solution (80mM NaOH, 5% DMSO (v/v)) (dark brown line), **7** (15µM) with pure recombinant mNat2 (30µM) in buffer (as above) (light brown line). All values of optical density were measured against an appropriate blank.

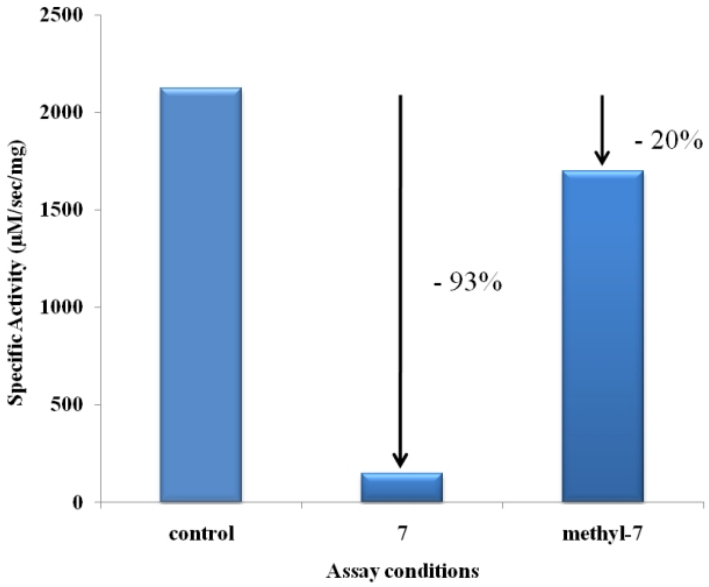


Figure IV.13: Effect of compounds 7 and *N*-methyl-7 on mNat2 activity.

The activities were determined by the AcCoA hydrolysis assay with a total reaction volume of 100µl. Compounds **7** and *N*-methyl-**7** were added to a final concentration of 30µM with 5% DMSO (v/v), and 5% DMSO (v/v) was added in the control assay. The substrate pABA was added to a final concentration of 500µM. 50ng mNat2 was used. The reaction was initiated with AcCoA at a final concentration of 400µM. Results were expressed as mean ± standard deviation of triplicate values.

Besides this, the larger steric size of the *N*-methyl group than that of a single hydrogen atom might affect the binding of *N*-methyl-**7** to mNat2, for the lack of a putative charge-charge interaction or at least H-bond between the sulfonamide-N*H* and the enzyme.

Finally, it was postulated that sulfonamide-N*H* of compounds **1** and **7** were undergoing a deprotonation within the active site of hNAT1 or mNat2 upon isoenzyme-selective binding, thereby generating a visible colour change of the ligand from red to blue.

IV.2.2 Colour change event of compound 7 upon binding to mNat2, as a model for hNAT1

Having established that compound **7** changed colour from red to blue upon deprotonation of the sulfonamide-N*H*, attention turned to investigating which was the alkaline

moiety within the active site of mNat2 able to accept the weak acid proton from **7**. Since compound **7** is a competitive inhibitor of mNat2, alkaline residues or defined alkaline peptidic complexes within the active site pocket were first explored.

From the crystal structure of hNAT1 (Wu et al, 2007) and the consensus catalytic mechanism of transacetylation by NAT enzymes (Wang et al, 2005a; Westwood et al, 2006) (**Figure IV.14**), two residues were taken into account as possible candidates to deprotonate **7** with pK_a values higher than or similar to 9.16:

- Cys68, whose side chain thiolate has a pK_a=9.1 for the corresponding conjugate acid and is highly reactive (Wang et al, 2005a),
- Arg127, which possesses a side chain guanidine group with a pK_a=12.5 for the corresponding conjugate acid (**Table IV.2**).

On the other side, it has been well established that the chemical properties of some residues inside an enzyme can be slightly different, in particular for those residues involed in catalytic reactions (Harris & Turner, 2002).

Indeed, it has previously been established that the pK_a of the thiolate imidazolium ion-pair in shNat2 is 5.2 (Wang et al, 2004b), which enhances the nucleophilicity of the thiolate, allowing the acetylation step of Cys68 (Wang et al, 2004b). A similar assumption has subsequently been extended to all other NATs (Sandy et al, 2005b; Westwood et al, 2006).

In this study, it was considered to investigate initially the colourimetric properties of **7** using single amino acids with consideration of the appropriate limitations, as a first approach to the problem, prior to developing more complex biochemical tools.

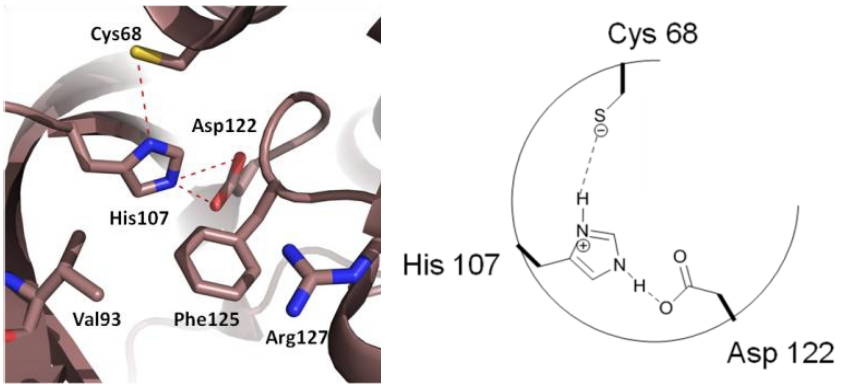
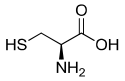
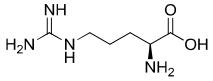


Figure IV.14: Active site of hNAT1.

(left) Insight view of hNAT1 active site (pdb: 2PQT) (Wu et al, 2007) with side chains of key residues drawn in stick representation and labelled with carbon atoms in grey, nitrogen in blue, oxygen in red, and sulfur in orange. **(right)** Recurrent catalytic triad in NAT enzymes.

Table IV.2: pK_a values of non-proteogenic amino acids.

The references for pK_a values are: (Garrett & Grisham, 2005; Harris & Turner, 2002; Rawn, 1989).

Amino acids	Formula	pK_{aCOOH}	pK_{aNH3+}	$pK_{aside\ chain}$	pI
Glycine		2.35	9.78	---	6.07
Cysteine		1.92	10.78	9.10	9.94
Arginine		1.82	8.99	12.48	10.74

A preliminary screening of different amino acids in the presence of compound **7** was performed in 20mM Tris.HCl buffer (pH 8) in order to find out whether any of these amino acids was able to deprotonate **7**.

Visible spectra of compound **7** in the presence of arginine (100mM), cysteine (1mM) and glycine (100mM) were recorded (**Figure IV.15**). 1mM was the highest possible concentration of cysteine in order to avoid precipitation of the amino acid in the buffer. Glycine was chosen as a negative control to evaluate the effect of the zwitterion species of an amino acid at pH 8 towards **7**. Compound **7** did not change colour in the presence of glycine.Whilst cysteine did not support the colour change of **7**, arginine allowed a ba-

thochromic shift in the visible spectrum similar to that occurring upon basification of the compound. Considering that a great concentration of arginine was used in the assay (100mM), it was postulated that the effect was mainly due to a change of the pH in the bulk buffer. Indeed, a pH indicator estimated that the pH in the spectrophotometric assay was around 11.

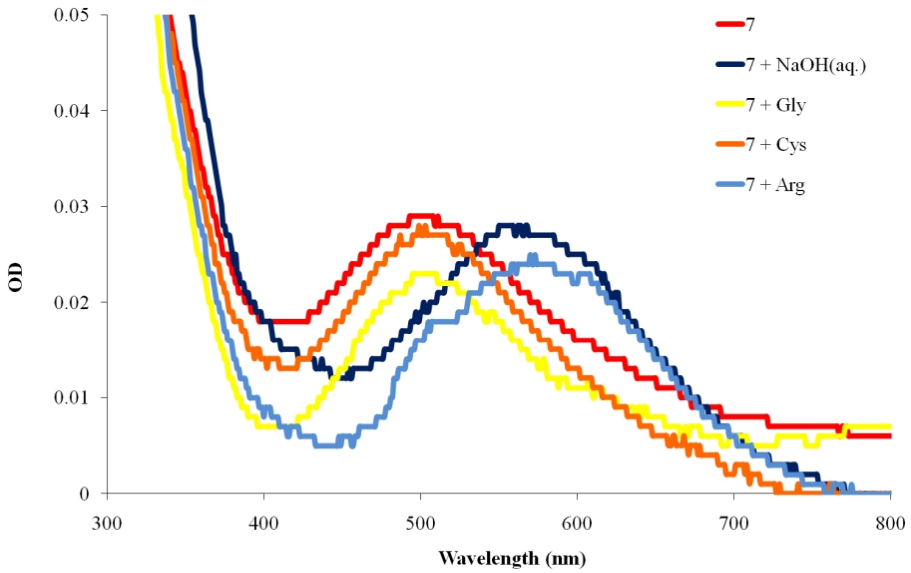


Figure IV.15: Optical properties of 7 in the presence of different amino acids.

Wavelength scans of **7** (10µM) in buffer (20mM Tris.HCl, pH 8, 5% DMSO (v/v)) (red line), **7** (10µM) in alkaline solution (80mM NaOH) (dark blue line), **7** (10µM) in the presence of Glycine (100mM) in buffer (as above) (yellow line), **7** (10µM) in the presence of Cysteine (1mM) in buffer (as above) (orange line), **7** (10µM) in the presence of Arginine (100mM) in buffer (as above) (light blue line). All values of optical density were measured against an appropriate blank.

However, despite the selectivity of the colour change of compound **7** with arginine, further investigations would be needed in order to depict the basic functional group of the amino acid responsible for the proton uptake, either guanidine or amine groups, in relation to the isoelectric point (pI) of the amino acid (pI=10.74) (**Table IV.2**).

Nevertheless, within the active site of both hNAT1 and mNat2, Arg127 remained a highly probable candidate as the residue being responsible for the colour change event of compound **7** upon binding to one of these enzymes.

IV.2.2.1 Investigating the possible role of Cys68 in the colour change event

In order to mimic the chemical reactivity of Cys68, a sulfur-based nucleophile, sodium ethanthiolate (NaSEt), was added to a solution of **7** and the colourimetric properties of **7** were investigated. Visible spectra showed that when NaSEt (100 mM) was incubated with **7**, a bathochromic shift in λ_{max} was observed similar to that in an aqueous NaOH solution (**Figure IV.16**).

This could be due to the higher pK_a value of the corresponding conjugate acid of NaSEt (11.6) than **7** (9.16), which would originate a proton acid-base exchange between the two counterparts. This would also suggest that a thiolate, like in Cys68, could act as possible proton acceptor in interaction with the sulfonamide-N*H* of compound **7**. However, like in the spectrophotometric assay run with arginine (100mM) and compound **7**, the resulting deprotonation of the sulfonamide-N*H* of compound **7** by NaSEt seemed to be due to an overall change of buffer pH from pH 8 to pH 11.

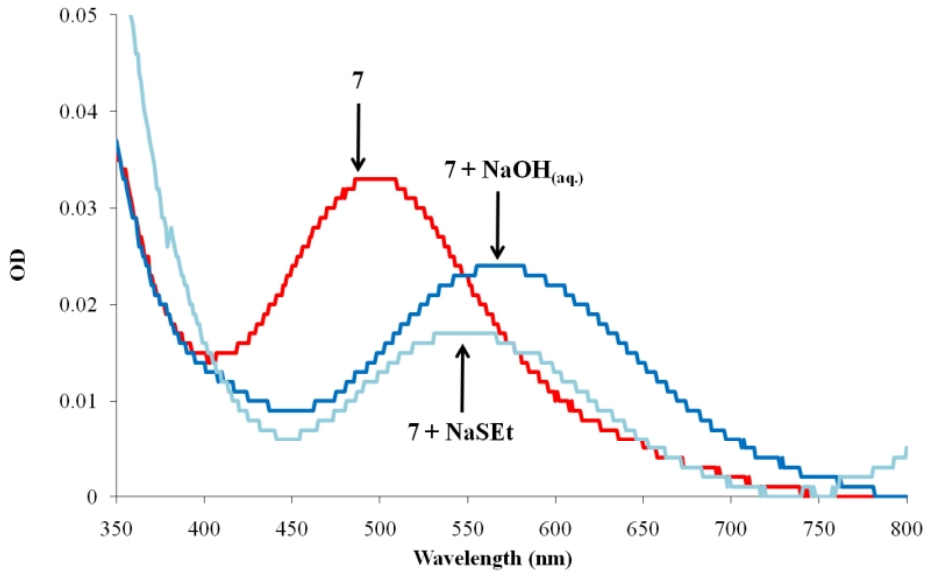


Figure IV.16: Colourimetric properties of 7 in the presence of NaSEt.

Wavelength scans of **7** (15µM) in buffer (20mM Tris.HCl, pH 8, 5% DMSO (v/v)) (red line), **7** (15µM) in alkaline solution (80mM NaOH, 5% DMSO (v/v)) (dark blue line), **7** (15µM) with 100mM sodium ethanethiolate in buffer (20mM Tris.HCl, pH 8, 5% DMSO (v/v)) (light blue line).

The role of catalytic reactive cysteines has largely been investigated using reactive thiol specific modifier, like iodoacetamide, or bromoacetamide showing that the reactive sulfhydryl group is sufficiently nucleophilic to react rapidly in solution (Wang et al, 2004a; Wang et al, 2004b; Westwood et al, 2006).

It was not possible to carry out site-directed mutagenesis studies on Cys68 since the formation of an inactive recombinant enzyme would be inadequate for kinetic studies.

On the other hand, previous studies demonstrated that when shNat2, which possesses 92% identity in the primary sequence compared to that of mNat2, was preincubated with iodoacetamide, the enzyme was not active and the inactivation followed a 1:1 stochiometric relationship (Wang et al, 2004b). MALDI-TOF studies unambiguously identified the active site Cys68 as the only alkylated Cys residue (Wang et al, 2004b). Moreover, Wu et al. reported the exclusive alkylation of Cys68 in hNAT1 by halogenated electrophiles, such as 2-iodoacetamide and 2-bromoacetanilide (Wu et al, 2007).

Following a similar protocol to that described by Wang et al. (Wang et al, 2004b), 1mM iodoacetamide was incubated with pure recombinant mNat2 in order to alkylate Cys68 in order to evaluate the possible role of Cys68 of mNat2 in relation to **7**.

The electrophile-treated enzyme was found to be completely inactive with arylamine pABA and AcCoA, consistent with alkylation of the catalytic Cys68 residue (**Figure IV.17-left**). Afterwards, a visible wavelength scan of **7** was recorded in the presence of catalytically inactive mNat2 and compared with untreated mNat2. A bathochromic shift was observed in the presence of treated mNat2 similar to that recorded with untreated mNat2 (**Figure IV.17-right**), thereby supporting that another residue, and not Cys68, within the active site of mNat2 was responsible for the colour change event of compound **7**.

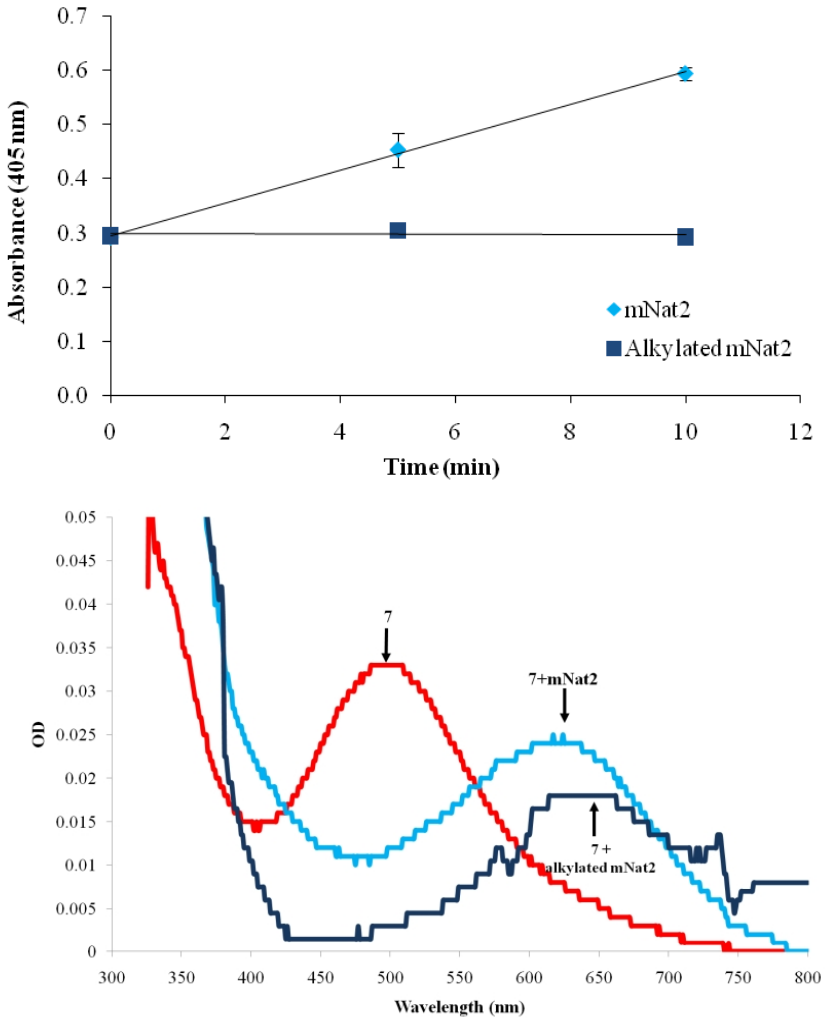


Figure IV.17: Optical properties of compound 7 with inactive mNat2 after treatment with iodoacetamide.

(top) Following a 5 h incubation of 25µl of pure recombinant mNat2 (150µM) with 2-iodoacetamide (1mM) at 4°C, an AcCoA-hydrolysis assay of treated and untreated mNat2 (100ng and 500ng respectively) was carried out with AcCoA (400µM) and pABA (500µM) as arylamine substrate: ♦, untreated enzyme; ■, 2-iodoacetamide-treated enzyme. Results are given as an average with error bars ± standard deviation of triplicate assays. **(bottom)** Wavelength scans of **7** (15µM) in buffer (20mM Tris.HCl, pH 8, 5% DMSO (v/v)) (red line), **7** (15µM) with pure recombinant mNat2 (30µM) in buffer (as above) (light blue line), **7** (15µM) with Cys^{68}-alkylated mNat2 (30µM) in buffer (as above) (dark blue line). The background noise in the spectrum of **7** with alkylated mNat2, which influences the quality of the spectrum, is partly due to free 2-iodoacetamide present in the solution.

IV.2.2.2 Investigating the possible role of Arg127 in the colour change event

The arginine side chain ends with a guanidine functional group and the pK_a value of its conjugate acid is ~12.5 (Rawn, 1989). Since pK_a of compound **1** is ~9.5 (Crawford, 2007) and that of compound **7** is ~9.16, the guanidine group of Arg127 could act as base towards both naphthoquinones. Moreover, this residue is uniquely present in the primary sequence of the active site of both hNAT1 and mNat2 in relation to other NAT isoforms (**Figure IV.1**).

In order to understand the possible role of Arg127 in the colour change of **7** from red to blue upon binding to mNat2, site-directed mutagenesis studies were carried out to alter Arg127 into a residue with dissimilar side chain properties.

The DNA codon for Arg127 in *mNat2* is **cgt** and a single-site mutagenesis was performed using the primers presented in **Table IV.3**, in order to substitute **cgt** with either **ggt** or **ctt**. The former would result in a Gly residue in lieu of the Arg at position 127 (R127G), whereas the latter would result in a Leu residue (R127L).

Table IV.3: Primers used for site-directed mutagenesis PCR reaction.

The imbedded mutations for each generation of each mutant of mNat2 are shown in bold.

Primer name	Sequence (5'→ 3')
wt forward	gctgggtttgga**cgt**tcctaccagatgtgggagcc
wt reverse	ggctcccacatctggtagga**acg**tccaaacccagc
R127G forward	gctgggtttgga**ggt**tcctaccagatgtgggagcc
R127G reverse	ggctcccacatctggtagga**acc**tccaaacccagc
R127L forward	gctgggtttgga**ctt**tcctaccagatgtgggagcc
R127L reverse	ggctcccacatctggtagga**aag**tccaaacccagc

The pET28b(+) vector containing the *mNat2* gene insert was used as template and sin-

gle base pair mutations for R127G or R127L change were introduced following 16 cycled-PCR (**Figure IV.18**). The *E. coli* colonies containing the DNA insert were checked by T7-primed PCR analysis, followed by T7-primed sequencing analysis (**Figure IV.18**). These results confirmed that the correct single point mutation had been introduced without other unwanted changes, insertions or deletions.



Figure IV.18: Multiple sequence alignment of wild-type *mNat2* gene and mutated *mNat2* genes.

The alignment was conducted by ClustalW (Thompson et al, 1994). Mutated nucleotides are highlighted in colour. The single site-directed mutagenesis were designed in order to obtain mNat2 mutants at residue R127. The mutated sequences encode R127G (orange) and R127L (green) mutants. * indicates nucleotide identity among all three genetic sequences. No additional mutations were generated during the site direct mutagenesis.

The pET28b(+) plasmids containing the desired mNat2 mutants were transformed into *E. coli* strain JM109 and further transformed into Rosetta(DE3)pLysS (Novagen) after confirming the correct insert sequence (DNA Sequencing Facility, Biochemistry, University of Oxford). The positive transformants were grown in LB to midlog phase at 37°C with shaking (180 rpm) and stored at -80°C with 10% glycerol (v/v).

mNat2_WT and R127G and R127L mNat2 proteins (referred to as R127G and R127L

subsequently), were expressed in RosettaBlue (DE3)pLysS *E. coli* with an *N*-terminal His-tag from plasmid pET28b(+) as previously described with minor modifications (Kawamura et al, 2008). The expression and the purification of the two mutants were performed in collaboration with Varney A., excellent Part II Biochemistry student, University of Oxford.

Expression was induced by adding IPTG to a final concentration of 0.1mM once the OD value at 600 nm reached 0.6, followed by incubation for 18 h at 27°C with shaking (180 rpm) (**Figure IV.19**). The growth rate of *E. coli* was followed at 600nm, and retardation in rate was observed in IPTG-induced cultures relative to uninduced controls. This observation was consistent with previous observations highlighting that recombinant protein expression is metabolically stressful to the *E. coli* cell (Soriano et al, 2002).

It was also noted that the growth rate of *E. coli* expressing the R127L mutant construct was marginally lower than each of the other induced cultures, which could be due to the concentration of cells in the initial inoculate.

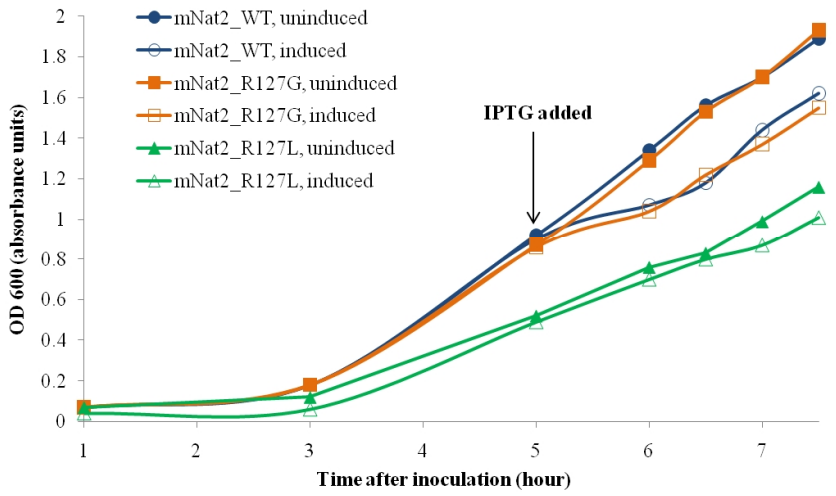


Figure IV.19: Growth curves of *E. coli* cultures expressing mNat2 variants.

Growth of Rosetta(DE3)pLysS *E. coli* transfected with the plasmid pET28b(+) containing the appropriate *mNat2* construct was followed by measuring absorbance at 600nm. When OD_{600} readings exceeded the threshold of 0.6, cells were induced with IPTG (open markers) to express the relevant *mNat2*: WT(○), R127G (□) and R127L (Δ). Control cultures (solid markers) were not induced with IPTG, but sterile water was added in place: WT (●), R127G (■) and R127L (▲)

All three mNat2 mutant recombinant proteins were purified in a very good yield using around 5ml Ni-NTA column (**Figure IV.20**). The major quantities of the three mNat2 mutants were eluted into the 250mM imidazole washes, but these fractions also contained contaminating bands. SDS-page gels highlighted that last 250mM and all 500mM imidazole washes eluted only pure His-tagged mNat2 proteins (**Figure IV.20**).

The pure fractions were used for all subsequent enzymatic assays. The first 250mM imidazole washes containing abundant recombinant mNat2 were then purified *via* size-exclusion chromatography for crystallisation purposes (**Section IV.2.3.1**).

The purification process gave good yields in 250mM imidazole eluates for mNat2_WT (69%) and R127L (68%), although the protein contained small amounts of impurities (**Table IV.4**). R127G gave a lower yield (30%) in 250mM imidazole eluates, but a greater yield in the 500mM imidazole eluates (**Table IV.4**).

Although a proportion of each recombinant protein was lost during the wash steps, typically at least 40 mg of pure recombinant protein per litre of *E. coli* culture was achieved (**Table IV.4**).

The yield was consistent with previous studies on wild-type mNat2 and highlighted the optimal combination of the pET28b(+) vector with *mNat2* constructs and the *E.coli* strain RosettaBlue (DE3)pLysS (Kawamura et al, 2008).

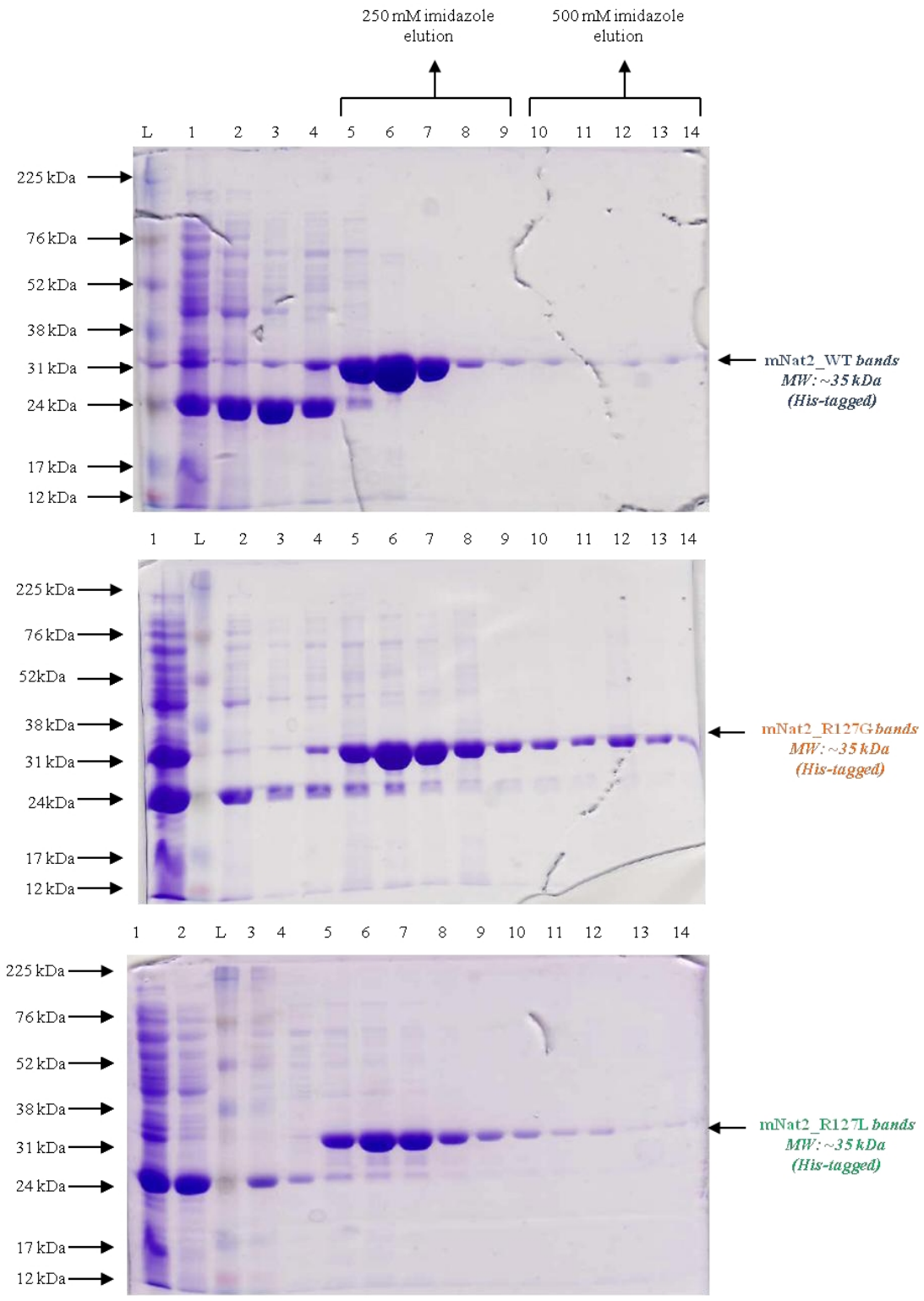


Figure IV.20: SDS-PAGE gels following purification of mNat2 variants *via* Ni-NTA affinity chromatog-raphy.

Figure IV.20: SDS-PAGE gels following purification of mNat2 variants *via* Ni-NTA affinity chromatography.

Coomassie Blue-stained 12% SDS-PAGE of each fraction from the Ni-NTA affinity purification process of recombinant mNat2_WT **(top)**, mNat2_R127G **(middle)**, and mNat2_R127L **(bottom)**. The soluble fraction obtained after sonication of grown Rosetta(DE3)pLysS *E.coli* cells was loaded onto the Ni-NTA column and washed with buffered Tris.HCl solutions containing increasing concentrations of imidazole. Each well was loaded with 5µl sample in 15µl reduced gel loading buffer, except **L** (Ladder) where 6µl high range molecular weight Rainbow markers (GE Healthcare) were loaded. **Lanes: 1** Unbound fraction, **2** 0mM imidazole wash, **3** 10mM imidazole wash, **4** 25mM imidazole wash, **5-9** 250mM imidazole washes, **10-14** 500mM imidazole washes.

Table IV.4: Purification of mNat2 variants using Ni-NTA affinity chromatography.

The soluble fractions obtained following cell sonication were loaded onto the Ni-NTA affinity column and washed with increasing concentrations of imidazole as outlined in Materials and Methods, and volumes of column eluates were measured. Yield and purification fold of mNat2_WT, mNat2_R127G and mNat2_R127L were calculated.

[a] - Protein concentrations were measured using the Bradford assay in triplicate (given to the nearestmg)

[b] - Activity was measured using the AcCoA-hydrolysis assay in triplicate samples as outlined in Materials and Methods (given to the nearest $\mu M.min^{-1}$). The linearity of the activity over time was checked.

Table IV.4: Purification of mNat2 variants using Ni-NTA affinity chromatography.

mNat2_WT

Fraction	Volume (ml)	Total Protein[a] (mg)	Total Activity[b] (µM.min^{-1})	Specific Activity (µM.min^{-1}.mg^{-1})	Purification Fold	Yield (%)
Soluble Cell Lysate	20	1097	5936	5.41	1.00	100
Unbound Lysate	20	653	374	0.57	0.11	6
0mM imidazole wash	10	163	18	0.11	0.02	0
10mM imidazole wash	10	85	58	0.68	0.13	1
25mM imidazole wash	10	120	480	4.00	0.74	8
250mM imidazole wash	18.4	51	4096	79.78	14.75	**69**
500mM imidazole wash	20.5	3	39	14.50	2.68	1

mNat2_R127G

Fraction	Volume (ml)	Total Protein[a] (mg)	Total Activity[b] (µM.min^{-1})	Specific Activity (µM.min^{-1}.mg^{-1})	Purification Fold	Yield (%)
Soluble Cell Lysate	18.5	934	1465	1.57	1.00	100
Unbound Lysate	18	632	433	0.69	0.44	30
0mM imidazole wash	10	104	15	0.15	0.09	1
10mM imidazole wash	10.25	22	25	1.17	0.75	2
25mM imidazole wash	10.25	21	43	2.04	1.30	3
250mM imidazole wash	20.25	95	438	4.60	2.93	**30**
500mM imidazole wash	20.25	28	197	7.07	4.51	13

mNat2_R127L

Fraction	Volume (ml)	Total Protein[a] (mg)	Total Activity[b] (µM.min^{-1})	Specific Activity (µM.min^{-1}.mg^{-1})	Purification Fold	Yield (%)
Soluble Cell Lysate	18	1282	44	0.03	1.00	100
Unbound Lysate	17.5	865	6	0.01	0.19	13
0mM imidazole wash	11	198	1	0.00	0.10	2
10mM imidazole wash	10	60	0	0.00	0.00	0
25mM imidazole wash	10.25	11	0	0.00	0.00	0
250mM imidazole wash	19.25	48	29	0.61	18.05	**68**
500mM imidazole wash	19	2	3	2.10	61.74	8

All fractions containing mNat2 proteins eluted with similar concentrations of imidazole were pooled, dialysed and treated with thrombin to remove the *N*-terminal hexa-His tags (**Figure IV.21**). No additional bands were observed in the gels, thereby suggesting no further thrombin-dependent degradation of mNat2 proteins. Recombinants proteins were concentrated in 20mM Tris.HCl buffer (pH 8.0) and 5% glycerol (v/v) added as a cryoprotectant, following which they were aliquoted and stored at -80°C.

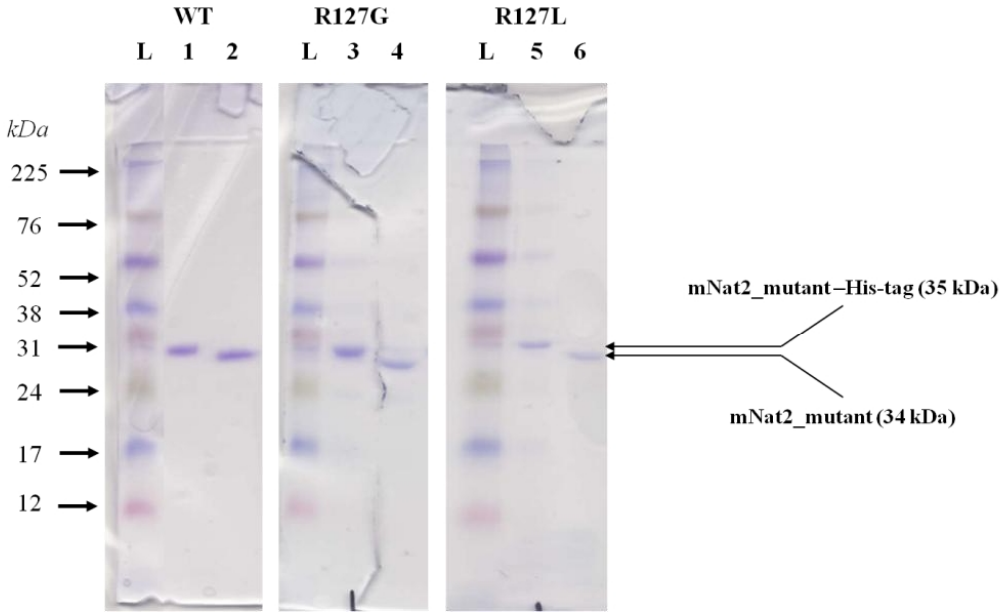


Figure IV.21: Thrombin cleavage of His-tag from recombinant mNat2 variants.

Coomassie Blue-stained 12% SDS-PAGE of fractions prior to and after the thrombin cleavage process of recombinant mNat2_WT, mNat2_R127G, and mNat2_R127L. Purified and concentrated His-tagged mNat2 variants were incubated with thrombin (5U.mg$^{-1}_{protein}$) at 4ºC for 16 h for complete His-tag cleavage. Each well was loaded with 5µl sample in 15µl reduced gel loading buffer **Lanes: L:** ladder (6µl high range molecular weight Rainbow markers - GE Healthcare), **1, 3, 5:** His-tagged mNat2 mutants; **2, 4, 6:** Thrombin-treated mNat2 mutants.

All three enzymes were found to be active, and both AcCoA-hydrolysis and arylamine-acetylation assays were carried out and optimised for each mNat2 variant. All subsequent assays were performed over the appropriate period of time to obtain a linear initial velocity (**Figure IV.22**). The linearity of the enzymatic activity of all three mNat2 mu-

tants suggested the correct folding of the three proteins. 5% DMSO (v/v) was also shown not to affect NAT activity levels, allowing subsequent measurement of activity with inhibitors which were DMSO-soluble.

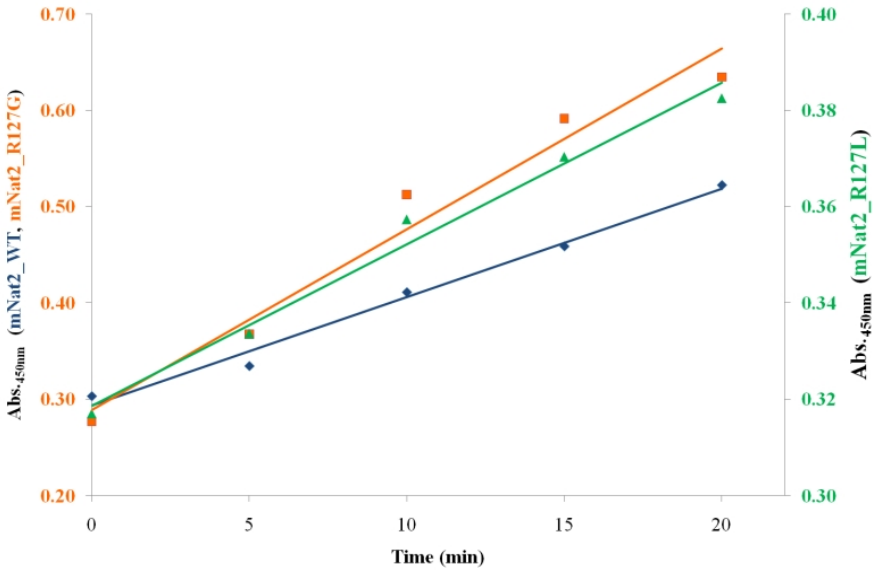


Figure IV.22: End-point NAT activity assays conducted with three mNat2 mutants over time.

AcCoA-hydrolysis assays of mNat2_WT, mNat2_R127G, and mNat2_R127L were carried out over a period of 20 minutes using AcCoA (400µM) and pABA (500µM) as arylamine substrate: ♦, mNat2_WT (1µl); ■, mNat2_R127G (2µl); ▲, mNat2_R127L (4µl). The orange y-axis refers to activity values for mNat2_WT and mNat2_R127G, whereas the green y-axis refers to activity values for mNat2_R127L.

The activity of each mNat2 mutant enzyme was tested in the presence of different concentrations of compound **7**, the percentages of specific activities obtained were then plotted against concentrations of **7**, and IC_{50} curves were fitted (**Figure IV.23**).

A concentration-dependent inhibition was observed with all three enzymes: the IC_{50} value of **7** *versus* mNat2_WT was 1.34µM, which is of the same order of magnitude as the previously reported value (0.99µM) (Laurieri, 2008), whereas the IC_{50} value with R127G and R127L were 51.7 and 102.5 µM respectively. This suggested that **7** also bound to both mutated mNat2 enzymes, assuming that its binding mode was conserved in all three mNat2 mutants despite the single residue difference at position 127.

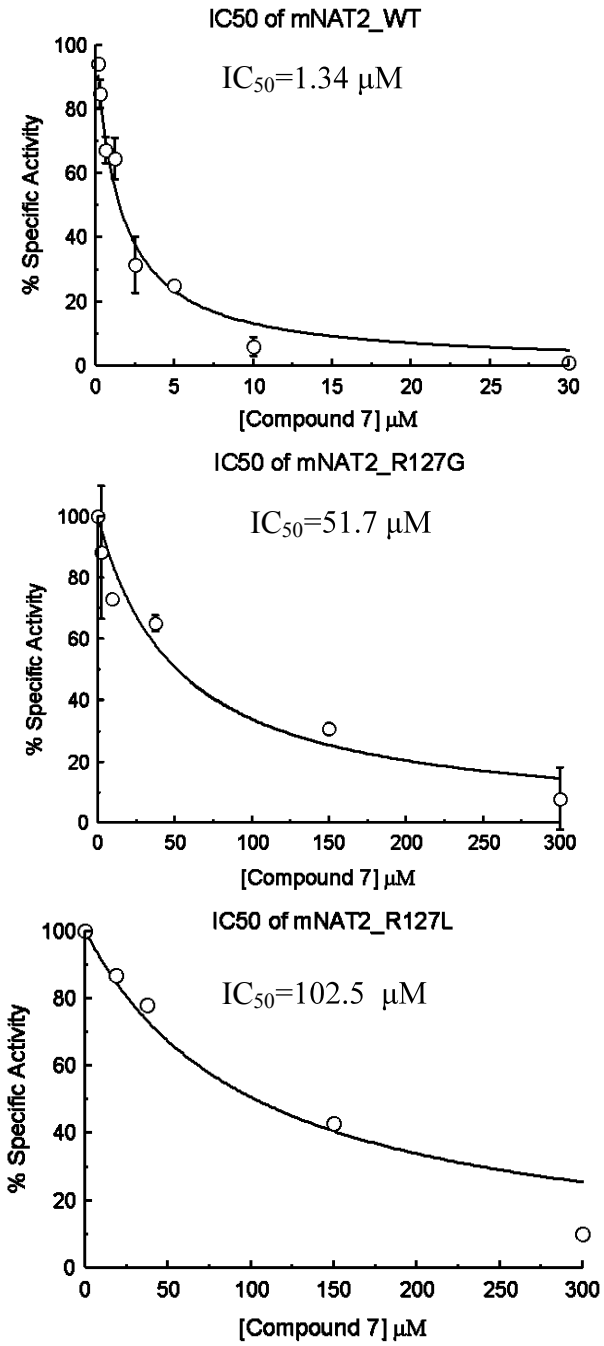


Figure IV.23: IC_{50} curves of compound 7 as inhibitor of different mNat2 variants.

AcCoA-hydrolysis assays were performed using pABA (500µM) as arylamine substrate, AcCoA (400µM), and serial dilutions of compound **7** *versus* mNat2_WT (1.4µg) **(top)** 100% = 94.07µM.sec^{-1}.mg^{-1}, mNat2_R127G (0.8µg) 100% = 344.11µM.sec^{-1}.mg^{-1} **(middle)**, and mNat2_R127L (5.5µg), 100% = 4.09µM.sec^{-1}.mg^{-1} **(bottom)**. Results were blank corrected to eliminate interference by the inherent colourimetric properties of compound **7**. Data points are given as averages with error bars ± standard deviation of triplicate assays. Curves were fitted using KyPlot® software and given with p-values ≤ 0.01, considered significant.

Spectrophotometry studies with these mutants were then carried out with reasonable confidence that any colourimetric effects would be as a result of inhibitor binding.

Full visible wavelength scans were obtained with compound **7** in the presence of the three mNat2 variants at pH 8.0 (**Figure IV.24**). A bathochromic shift was observed with mNat2, but no colour change from red to blue was observed with either R127G or R127L (**Figure IV.24**). This strongly suggests that Arg 127 is required for deprotonation of compound **7** and subsequent colour change of the inhibitor.

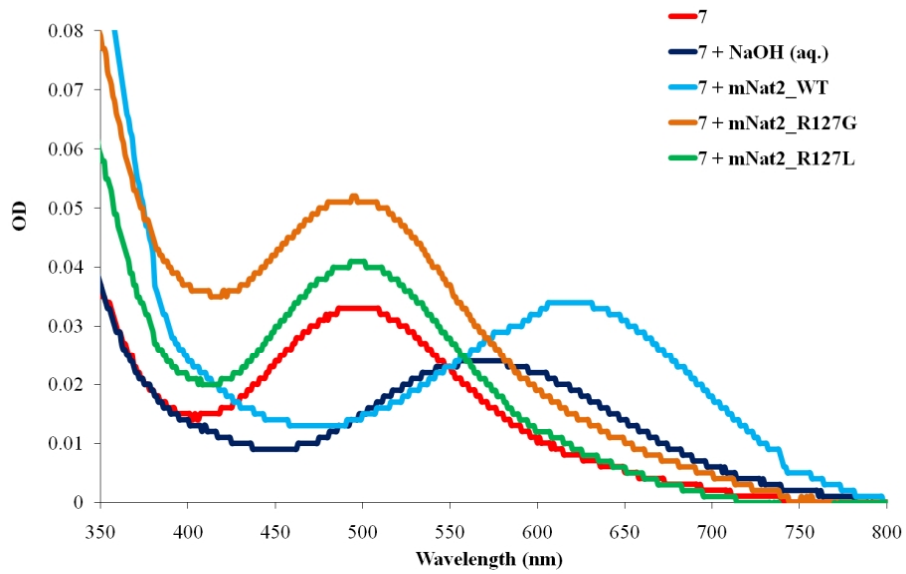


Figure IV.24: Visible spectra of compound 7 in the presence of different mNat2 variants.

15 µM compound **7** was prepared at different conditions: 20mM Tris.HCl at pH 8.0 (red line), 80mM NaOH at pH 13.0 (dark bleu line), with. mNat2 variants (30µM) at pH 8.0 (mNat2 (light blue line), R127G (orange line), R127L (green line)). Wavelength scans from 800 to 350 nm were recorded against the appropriate blank (20mM Tris-HCl, pH 8.0, 5% DMSO (v/v)).

IV.2.2.3 The importance of Phe125 and Tyr129 in inhibitor selectivity

Previous studies highlighted the importance of two other residues in the active site of hNAT1 for substrate specificity: Phe125 and Tyr129 (Goodfellow et al, 2000; Wu et al, 2007). Since compound **7** was found to be a competitive inhibitor of mNat2, and by

analogy hNAT1, the possible role of these other two residues in relation to inhibitor binding was considered.

Dr Isaac Westwood, using mNat2 as a model for hNAT1, previously produced another mNat2 mutant, wherein the residue Phe125 was mutated into Ser, which is the residue at position 125 in hNAT2. The mutation F125S in mNat2 was performed following the analogous hNAT1_ F125S mutant generated in other studies (Wu et al, 2007), in order to explore the key role of the residue Phe125 in both hNAT1 and mNat2 substrate specificities. This mNat2 mutant is subsequently referred to as F125S in this thesis.

Pure recombinant F125S was previously expressed in RosettaBlue (DE3)pLysS *E. coli* with an *N*-terminal His-tag from plasmid pET28b(+) and subsequently purified using Ni-NTA chromatography (Dr I. Westwood, unpublished work), following previously described protocols with minor modifications (Kawamura et al, 2008). F125S was used to test possible inhibition of this mutant by compound **7**. In particular, it was questioned whether a colour change of the inhibitor occurred upon treatment with the enzyme, since Arg127 was not modified in the active site of F125S.

An IC_{50} curve was obtained after pABA-acetylation activity of F125S was tested in the presence of increasing concentrations of **7**, and gave an IC_{50} value of 68.7 μM (**Figure IV.26**). This suggested that compound **7** bound to F125S.

Therefore, spectrometric properties of **7** were then explored in its interaction with this mNat2 mutant. No bathochromic shift of **7** was observed in the presence of the F125S mutant of mNat2, despite the presence of Arg127 in the active site (**Figure IV.27**).

This could be due to reduced affinity, modified orientation or altered binding mode of compound **7** within the active site of mNat2_F125 relative to mNat2. Possibly, the residue Phe125 could help stabilise and favour a suitable orientation of **7** within the active site of mNat2 and hNAT1 in order to allow the colour change event from red to blue.

Furthermore in order to probe the possible role of Tyr129 to form compound **7**-mNat2

complex, a different study was conducted on Syrian hamster NAT 2 (shNat2). These enzymes share 93% identical primary sequence, and shNat2 has 81% sequence identity to hNAT1 (**Figure IV.25**).

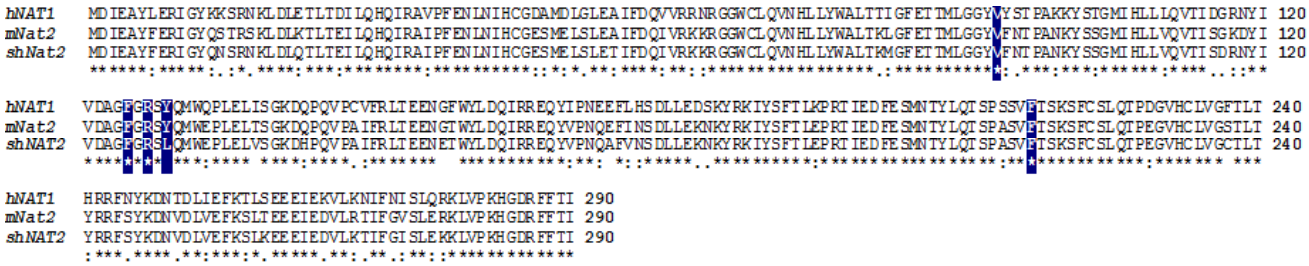


Figure IV.25: Multiple sequence alignment of hNAT1, mNat2 and shNAT2 proteins.

The alignment was conducted by ClustalW (Thompson et al, 1994). Key residues of hNAT1 and mNat2 active site are highlighted in colour. * indicates identical residues, : conserved residues, and . semi-conserved residues among all three primary sequences.

shNat2 and mNat2 have identical key-residues in their active site, except that shNat2 possesses a leucine at position 129, instead of a tyrosine as in mNat2.

Testing shNat2 acetylation activity with different concentrations of **7** revealed that compound **7** is a weaker inhibitor of shNat2 compared to mNat2, with a corresponding IC_{50} value of 89.04 μM with shNat2 *versus* 0.99 μM with mNat2 (**Figure IV.26**).

Assuming that compound **7** also bound to shNat2 active site similar to mNat2, a visible wavelength scan of **7** in the presence of shNat2 was performed in an enzyme:inhibitor ratio of 2:1. A moderate bathochromic shift was observed, suggesting that **7** was partially deprotonated, and the colour observed is given by a mixture of both the red and blue species of **7** (**Figure IV.27**).

Increasing the ratio of enzyme:inhibitor up to 8:1 in the assay gave a more distinctive bathochromic shift very similar to that in mNat2, although the background noise generated by the highly concentrated protein did not allow a clear peak to be observed (**Figure IV.27**). Nevertheless, a clear pale blue colour was observed in the cuvette. This was

consistent with the fact that compound **7** is a less potent inhibitor of shNat2 compared to mNat2, and supported a significant role for Tyr129 in forming the complex mNat2-**7**.

In order to investigate around the possible key residues involved in the formation of mNat2-**7** complex, another murine NAT enzyme was studied: mNat1. This enzyme shares 81% sequence identity with mNat2, and two single residues are different into their respective actives sites: whilst residue 127 is an Arg in mNat2, but a Gly in mNat1, residue 125 is a Phe in mNat2, but a Tyr in mNat1. In this case, it was assumed that the overall folding of mNat1 was similar to that of human NATs (Wu et al, 2007).

The acetylation of 5AS by mNat1 was measured in the presence of varying concentrations of **7**, and an IC_{50} curve was obtained, giving an IC_{50} value of 129.7 μM (**Figure IV.26**).

A wavelength scan of **7** in the presence of mNat1 was performed for a second time, confirming that the colour change event did not occur (**Figure IV.27**).

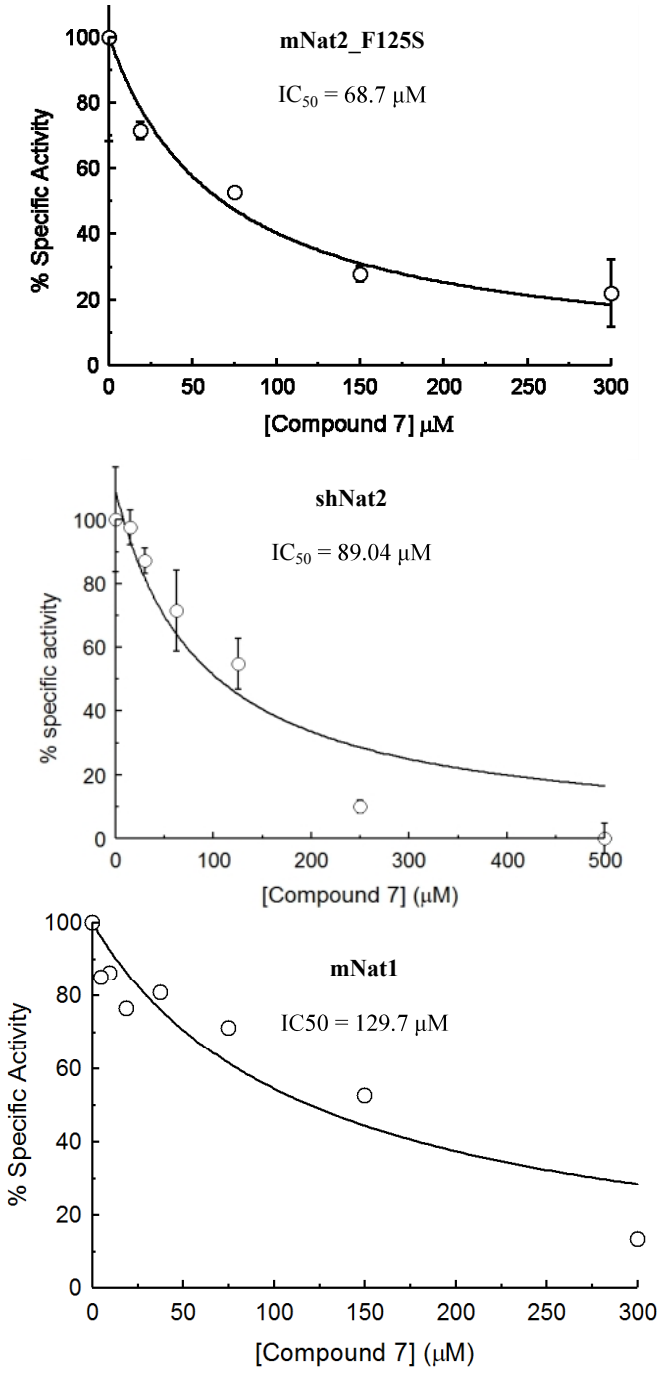


Figure IV.26: IC_{50} curves of compound 7 as inhibitor of different mammalian NATs.

AcCoA-hydrolysis assays were performed using appropriate arylamine substrate (500µM, pABA for mNat2_F125S and shNat2, and 5AS for mNat1), AcCoA (400µM), and serial dilutions of compound **7** *versus* **(top)** mNat2_F125S (0.65µg), 100% = 440.88µM.sec^{-1}.mg^{-1}, **(middle)** shNat2 (0.1µg) 100% = 1098. 03µM.sec^{-1}.mg^{-1}, and **(bottom)** mNat1 (1.5µg), 100% = 170.81µM.sec^{-1}.mg^{-1}. Results were blank corrected to eliminate interference by the inherent colourimetric properties of compound **7**. Data points are given as averages with error bars ± standard deviation of triplicate assays. Curves were fitted using KyPlot® software and given with p-values ≤ 0.01, considered significant.

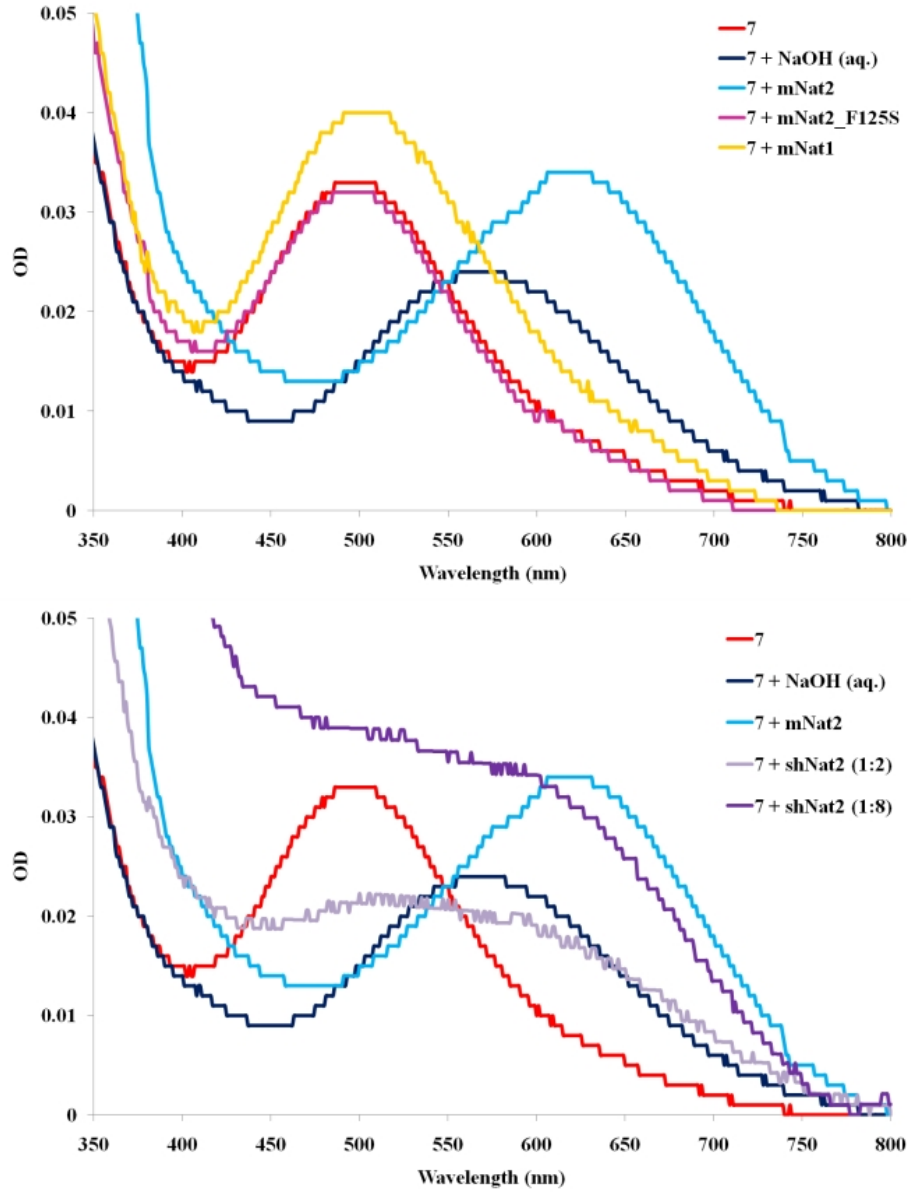


Figure IV.27: Visible spectra of compound 7 in the presence of different mammalian Nat variants. **(top)** 15 µM compound **7** was incubated at different conditions: 20mM Tris.HCl at pH 8.0 (red line), 80mM NaOH at pH 13.0 (dark bleu line), with NAT variants (30µM) at pH 8.0 (mNat2_WT (light blue line), mNat2_F125S (mauve line), mNat1 (yellow line)). Wavelength scans from 800 to 350 nm were recorded against the appropriate blank (20mM Tris-HCl, pH 8.0, 5% DMSO (v/v)). **(bottom)** 15 µM compound **7** was incubated at different conditions: 20mM Tris.HCl at pH 8.0 (red line), 80mM NaOH at pH 13.0 (dark bleu line), with shNat2 (30µM) at pH 8.0 (light violet line), and with shNat2 (120µM) at pH 8.0 (dark violet line).

IV.2.2.4 Screening mammalian NATs with inhibitor 7

Finally, compound **7** was also tested at 30 µM against hNAT2, kindly provided by Dr J. Dairou from the University of Paris VII, and compared to the other NATs tested in this study.

While more than 90% inhibition was exclusively observed with hNAT1 and mNat2, the inhibition of the NAT activity for hNAT2 was less than 20% (**Figure IV.28**). A partial cross reactivity of inhibitor **7** was observed for mNat1 and mNat2_R127G.

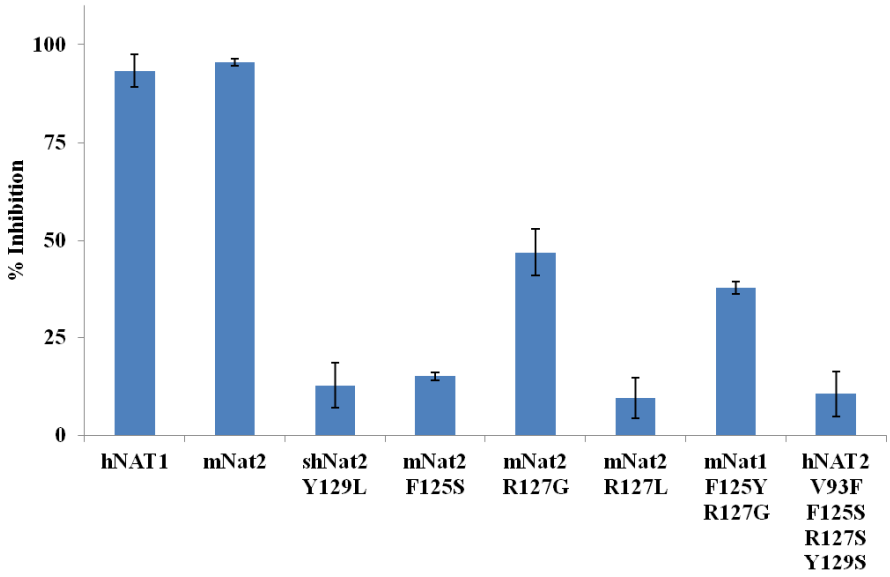


Figure IV.28: Screening of different wt mammalian NATs and mNat2 mutants with compound 7.

The NAT activity was measure following the AcCoA (400µM) hydrolysis rate in the presence of the appropriate arylamine substrate (500µM, pABA for hNAT1, mNat2, shNat2; 5AS for mNat mutants and mNat1; 2AF for hNAT2) and compound **7** at 30µM.

IV.2.3 structural studies

IV.2.3.1 Crystal trials

In order to achieve crystallography-grade protein, 250mM imidazole eluates containing pure recombinant mNat2 from Ni-NTA purification column, were subjected to further purification using size exclusion chromatography. Optimal conditions were identified, giving reproducible results.

Following gel filtration, single bands corresponding to mNat2 were observed on SDS-PAGE gels indicating that contaminating protein had been removed and the molecular weight of the purified protein is slightly higher than 31 kDa (**Figure IV.29**), consistent with a molecular weight of 34kDa for mNat2.

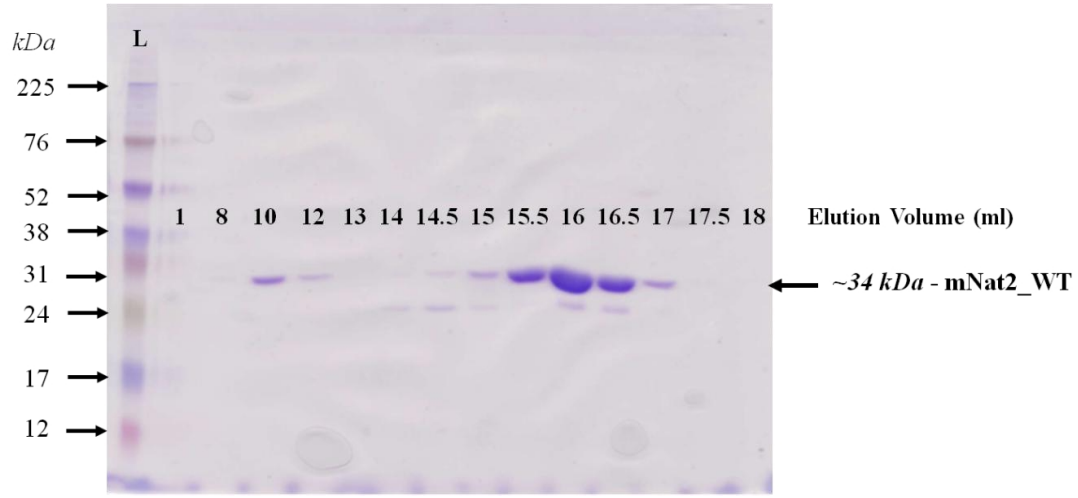


Figure IV.29: SDS-PAGE gel of fractions obtained after purification of mNat2 *via* size-exclusion chromatography.

Coomassie Blue-stained 12% SDS-PAGE of different fractions from the purification process of impure recombinant mNat2_WT *via* size-exclusion chromatography on Superdex200 column. Each well was loaded with 5µl sample in 15µl reduced gel loading buffer, except **L** (Ladder) where 6µl high range molecular weight Rainbow markers (GE Healthcare) were loaded. Each lane has been labeled with the corresponding elution volume.

Moreover, pABA-acetylation activity was measured for most of the fractions containing protein traces. Only the fractions with elution samples between volume 14.5 and 17.0 ml, showed NAT activity, consistent with the presence of pure recombinant mNat2 as reported (**Figure IV.30**).

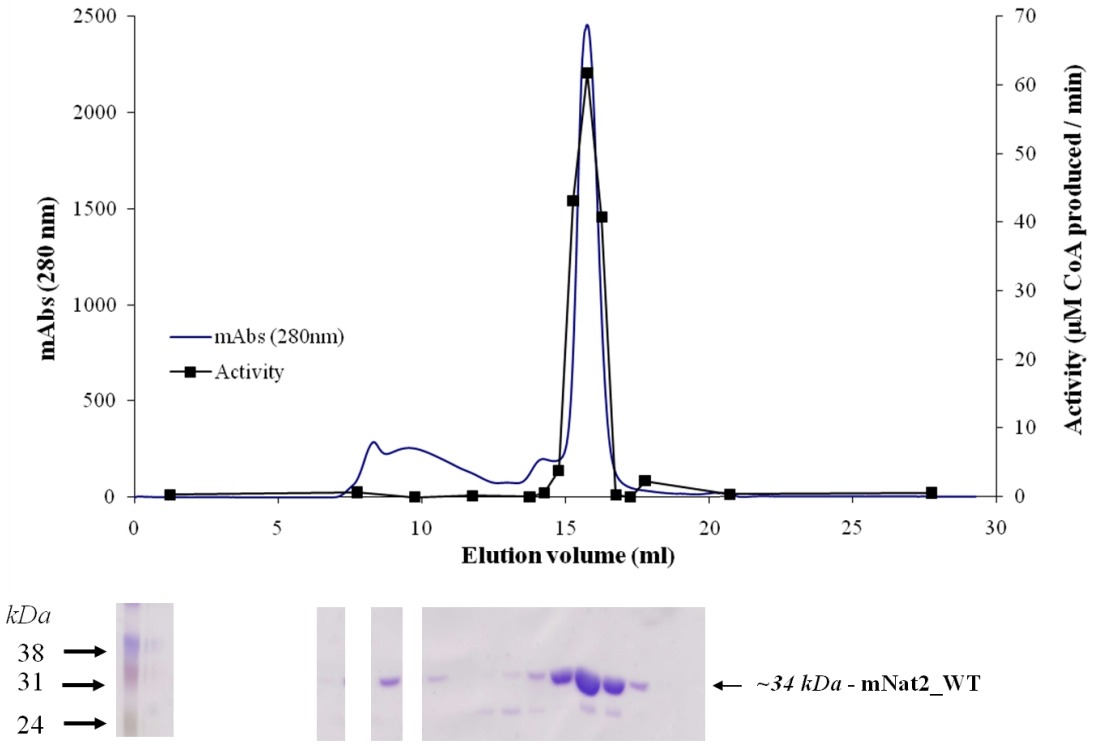


Figure IV.30: Purification of recombinant mNat2 *via* size-exclusion chromatography.

(top) A concentrated impure fraction of mNat2 (~0.5 ml) from the 250mM imidazole fraction was loaded on a Superdex200 column. The graph shows absorbance at 280 nm of the sample plotted against column elution volume (blue line). NAT activity of 1µl from suitable column eluates (■) was tested using pABA (500µM) and AcCoA (400µM) following the AcCoA hydrolysis method. The activities were determined from the linear initial rates of reaction. **(bottom)** SDS-PAGE gel (**Figure IV.29**) of several fractions after purification of mNat2_WT *via* size-exclusion chromatography on Superdex200 has been split. Each lane is located under the appropriate volume value. **L** = Ladder.

Moreover, protein standards, ovalbu min (45 kDa) and Soybean Trypsin Inhibitor (SBTI) (21.5 kDa), were run in order to assess the molecular weight of the purified pro-

tein (**Figure IV.31**). The peak corresponding to mNat2 is between the two peaks of the two standards, suggesting that the molecular weight of the purified mNat2 is consistent with the predicted value of 34 kDa. Therefore, it could be also concluded that mNat2 is expressed and active as a monomer.

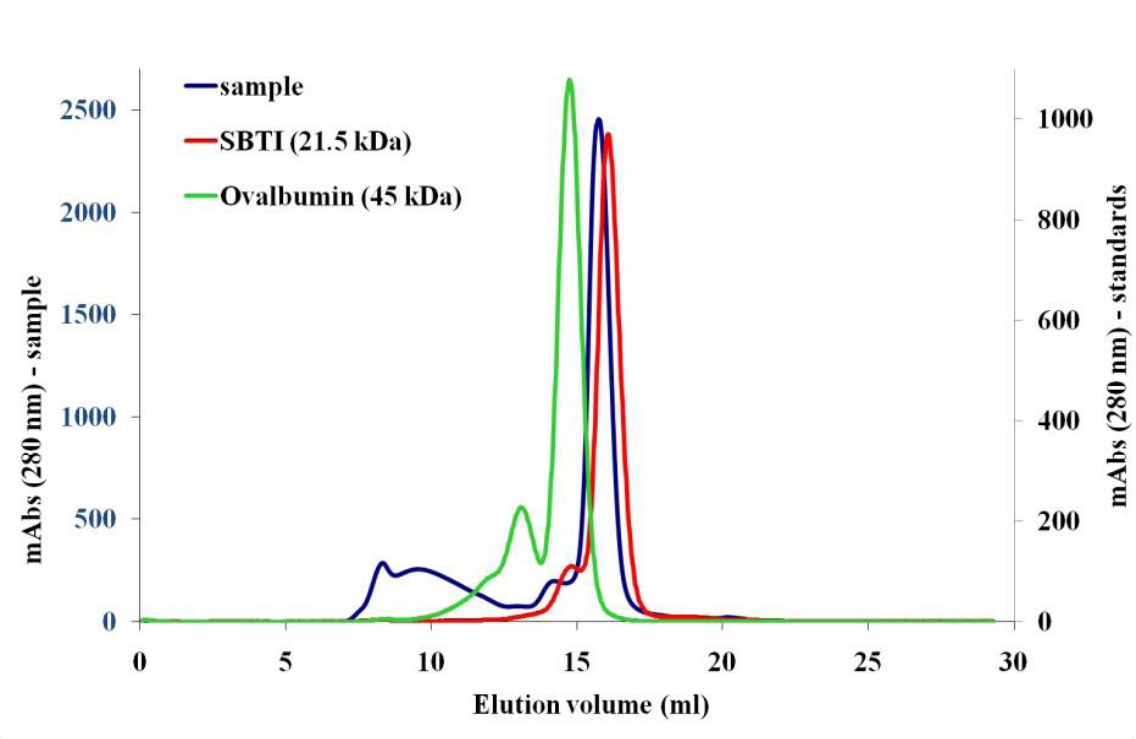


Figure IV.31: Size-exclusion chromatograms of impure recombinant mNat2 and two protein standards.

A concentrated impure fraction of mNat2 (~1mg) from the 250mM imidazole fraction was loaded on a Superdex200 column. The graph shows absorbance at 280 nm of the sample plotted against column elution volume (blue line), and was shown to be reproducible, since six repeats gave overlaying graphs (not shown). ~1 mg of ovalbu min (45kDa) and ~1 mg of SBTI (21.5kDa) were separately loaded on the same column, as standards for molecular weights.

Crystal trials were set using mNat2 and R127G complexed with **1**/**7**/CoA/folate as shown in **Table IV.5**. No harvestable crystals were obtained. In some cases this might have been due to the low concentrations of protein used. **Table IV.5** lists the conditions for which interesting observations were made (**Figure IV.32**).

In particular, attempts of crystallizing mNat2 with and without inhibitor **1** were also carried out using a JCSG-plus kit with 96 different conditions. Tiny crystals of pure recombinant mNat2 were observed in a solution containing 0.2 M zinc acetate, 0.1 sodium acetate, PEG 3000 10% w/v and 5mg.ml^{-1} mNat2, but they did not diffract.

Attempt to improve these conditions with higher protein concentrations did not afford any mNat2 crystals.

Table IV.5: Conditions screened in crystallisation trials.

The list of the reservoirs (well or tube) corresponding to the conditions at which interesting observations were made, is added in **Appendix 1**.

Protein (mg.ml^{-1})	Ligand	Screen	Temperature	Well (CAP.-nb.) or Tube (nb.)	Observations
mNat2 (20)	**1** (500µM)	JCSG*plus*™	4°C	1.31	small crystal-like entities
			25°C	-	
mNat2 (4.1)	**7** (500µM)	Morpheus™	4°C	G2, G3, G6	needles
			25°C	B6, D1, H1	small crystal-like entities
		Wizard™I/II	4°C	1.6, 1.7, 1.22, 2.31	needles
			25°C	1.33	small crystal-like entities
mNat2 (6.3)	CoA (2mM)	Morpheus™	4°C	-	
			25°C	-	
		JCSG*plus*™	4°C	-	
			25°C	-	
mNat2 R127G (10)	CoA (2mM)	Morpheus™	4°C	-	
			25°C	A11, C1	needles (A11), small crystal-like entities (C1)
		JCSG*plus*™	4°C	1.26, 1.39, 1.44, 2.6, 2.15, 2.19, 2.32	needles
			25°C	-	
		Index™	4°C	-	
			25°C	9	needles
		PACT™	25°C	-	
mNat2 R127G (10)	folate (2mM)	Morpheus™	4°C	-	
			25°C	C7, F10	needles
		PEG/Ion™ 1/2	4°C	-	
			25°C	1.12, 1.24, 2.48	needles
		Index™	25°C	-	
mNat2 (10)	**7** (500µM)	Structure™	4°C	B1, B2, C6, D2, D7, E7, F3, F8, G5	red crystal of compound **7** (D2, F3), and needles
			25°C	C%, D9, D10, E4, G10	needles
		Morpheus™	4°C	B6, B7, B11	needles
			25°C	-	
		Wizard™I/II	25°C	1.37	needles

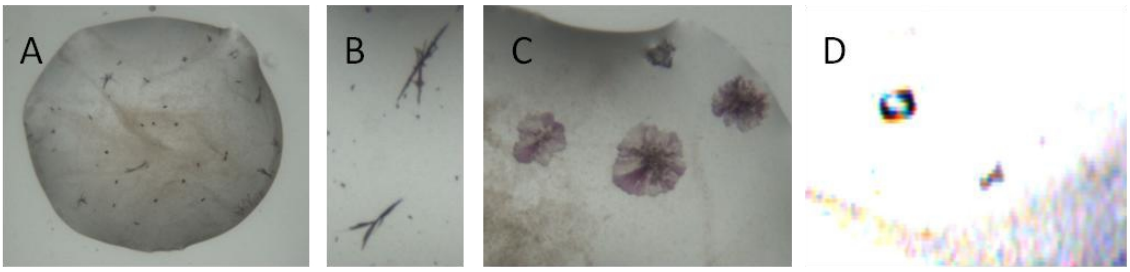


Figure IV.32: Illustrative pictures of interesting crystallization trials.

(A) Example of needles as observed for a number of wells. Microscope picture of well B6 from Morpheus™ screen with mNat2 (10mg.ml^{-1}) and **7** (500µM), at 4°C. **(B)** Microscope picture of well B7 from the same screen. **(C)** Example of flower-like crystals of **7**. Microscope picture of well D2 from Structure screen ™ with mNat2 (10mg/ml^{-1}) and **7** (500µM), at 4°C. **(D)** Example of a small crystalline-like entity. Microscope picture of well C1 from Morpheus™ screen with R127G (10mg.ml^{-1}) and CoA (2mM), at 25°C.

IV.2.3.1 *In silico* docking of compound 7 within the active site of hNAT1 and mNat2

Crystal structures of hNAT1 and hNAT2 were obtained by Plotnikow and co-workers, from the Structural Genomics Consortium, University of Toronto (Wu et al, 2007). Halogenated electrophiles were used to covalently modify the reactive Cys68 within the active site of hNAT1 and thus possibly facilitate the crystallisation of the protein, whereas hNAT2 was co-crystallised with exogenous CoA.

hNAT1 structure (pdb:2PQT) was used to build a structural model for mNat2 in order to help rationalise the selective interaction between compound **7** and hNAT1 or mNat2.

Swiss-Model software (Arnold et al, 2006; Guex & Peitsch, 1997; Schwede et al, 2003) was used for this purpose, and the "automated mode" was usually suited for cases where the target-template similarity was sufficiently high to allow fully automated modelling. Generally, automated sequence alignments seemed to be sufficiently reliable when target and template share more than 50% of sequence identity.

The high sequence identity between mNat2 and hNAT1 (82%) provided significant null E-values, which confirmed the reliability of the template, and good Qmean-Score4 and Z-score values, which validated the high quality of the model obtained (**Table IV.6**).

Swiss-model® software also allows the estimation of the per-residue accuracy for the model and then its visualisation through hNAT1 structure coloured using an appropriate gradient according to the potential reliability of each peptidic region (**Figure IV.33**).

In the mNat2 model, many regions were estimated to be reliable, but only few regions were not, in particular regions around residues Trp15, Met47 and Trp96, which were the regions with lowest similarity compared to hNAT1 template (**Table IV.7**).

Table IV.6: Parameters estimating the general quality of mNat2 model.

E-value describes the random background noise which exists for matches between sequences; the closer the E-value is to 0, the higher is the significance of the match. Qmean offers a composite scoring function for the estimation of the global quality of the entire model (Benkert et al, 2008). Qmean-Score4 is a reliability score for the whole model which can be used in order to compare and rank alternative models of the same target. Qmean Z-score represents a measure of the absolute quality of a model by providing an estimate of the 'degree of nativeness' of the structural features observed in a model and by describing the likelihood that a given model is of comparable quality to experimental structures (Benkert et al, 2011).

Value	Range	Best value	Meaning	mNat2 over hNAT1
% identity	0-100	> 50	identity of residue sequences	82
E-value	0-1	0	significance of the match	6.79E(-145)
Qmean-Score4	0-1	1	quality of the model	0.8
Z-score	$\Re$	> ~ -1	absolute quality of the model	-0.4

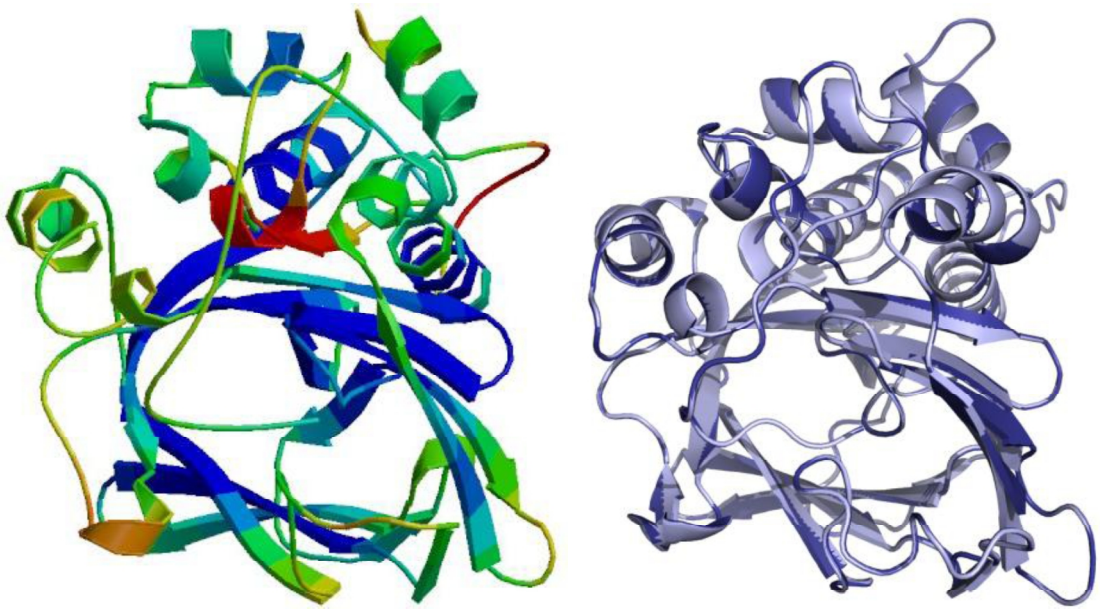


Figure IV.33: Overlay of hNAT1 template structure and corresponding structural mNat2 model. **(left)** Estimated per-residue accuracy visualised using hNAT1 template (pdb: 2PQT) with a colour gradient from blue (more reliable regions) to red (potentially unreliable regions). **(right)** Ribbon diagram showing the overlaid structures of hNAT1 (dark blue) and mNat2 (light blue) modelled on hNAT1 using the software SwissModel®.

Table IV.7: Residues from unreliable regions in murine NAT models.

Enzyme	central residue of unreliable region	Residue differences against template (model *versus* template)
mNat2	Trp15	Q13K, S14K, S17N
	Met47	E45D, S46A, E49D
	Trp96	F94Y, N95S

Compound **7** was docked separately into the active site of both hNAT1 structure and mNat2 model. Before docking analysis, the molecular editor Avogadro was used to predict the ground state conformation of **7**. The covalent modification to Cys68 by 2-bromoacetanilide from the crystal structure of hNAT1 was removed before performing docking studies using the software GOLD®.

After defining a docking site as a region of 10 Å around a key residue of the active site (Arg127), **7** was successfully docked. The scoring function (GOLD Score Fitness function) ranked the generated binding modes, and the best 10 conformations from that

ranking were analysed. The information obtained from these experiments was used as a guide to rationalise the mode of interaction of **7** (**Figure IV.34**).

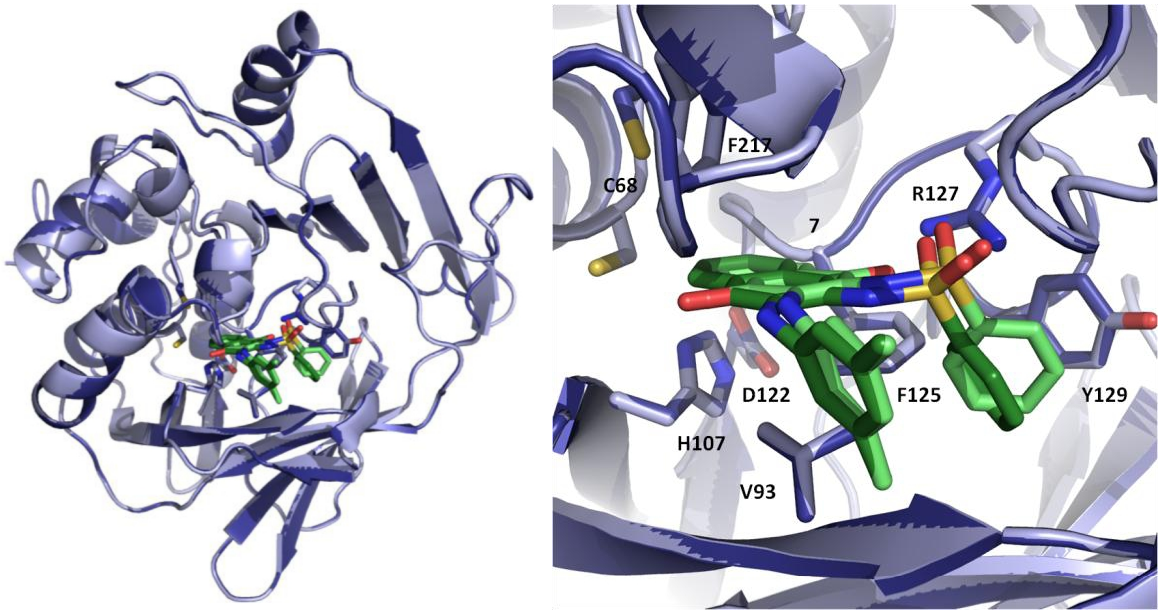


Figure IV.34: Overall structures of hNAT1 and mNat2 with compound 7 docked.

(left). Ribbon diagram showing the overlaid structures of hNAT1 (dark blue - pdb: 2PQT) and mNat2 (light blue) modelled on hNAT1. The structures were aligned using the program PyMOL (W. L. DeLano (2002) PyMOL, DeLano Scientific, San Carlos, CA). Compound **7** was docked separately into the active site of the enzymes using the program GOLD (Verdonk et al, 2003) and best scored solution is drawn (dark green for **7** into hNAT1, and light green for **7** into mNat2). Side chains of the key residues of both the active sites are drawn in sticks. **(right)** Maximised view of the active sites of both hNAT1 and mNat2 with compound **7** docked. Side chains of key residues within the active site are drawn in stick representation and labelled.

Four distinctive interactions between **7** and hNAT1 or mNat2 were observed in this docking study.The most important interaction appeared to be the close contact (≤ 3Å) between the sulfonamide functionality of **7** and Arg127 guanidine.

In particular, one of the two sulfonamide oxygen atoms seemed to interact with one guanidine nitrogen of Arg127, whereas the other oxygen with the back bone amide ketone of Phe 287.

Moreover, the C1 ketone from the naphthoquinone core seemed to be close to the other nitrogen atom of Arg127 guanidine (**Figure IV.35**).

This interaction looked highly consistent with the hypothesis of an acid-base proton exchange between **7** sulfonamide and Arg127 guanidine, which was responsible for colour change from red to blue of the ligand (**Figure IV.35**).

Two other distinctive interactions between compound **7** and hNAT1 or mNat2 were:

- the hydrophobic Van-der-Waals interactions between the naphthoquinone core of **7** and the hydrophobic plane defined by the side chain arene of Phe125 and the isopropyl side chain of Val93 (3 to 4 Å),
- the parallel-displaced π-π stacking between the C_2 sulfonamide arene of ligand **7** and the side chain arene of Tyr129 (~4 Å) (**Figure IV.35**).

No steric clashes (<2.5Å) were found in any docking result.The first interaction seemed consistent with the hypothesised role of Phe125 in stabilising the aromatic core of arylamine substrates within the active site of hNAT1 (Wu et al, 2007).

The general panel of chemical interactions of hNAT1 or mNat2 with the competitive inhibitor **7** was consistent with earlier biochemical hypotheses about the colour change event.

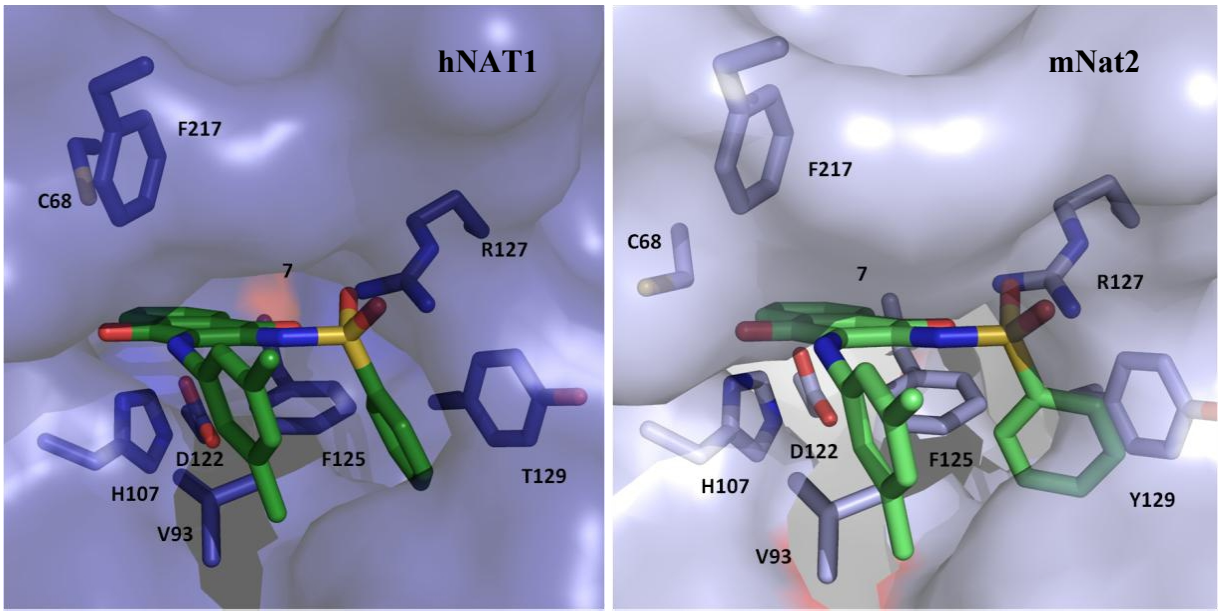


Figure IV.35: Substrate binding pockets of hNAT1 and mNat2 with compound 7 docked.

(left) The active site of hNAT1 with docked compound **7** is shown in surface and stick representation respectively. The residues involved in compound **7** binding and substrate specificity are shown in stick representation and labelled with carbon atoms in dark blue, nitrogen in blue, oxygen in red, and sulfur in orange. Compound **7** is labelled with carbon atoms in dark green, nitrogen in blue, oxygen in red, and sulfur in orange. **(right)** The active site of mNat2 with docked compound **7** is shown in surface and stick representation respectively. The residues involved in compound **7** binding and substrate specificity are shown in stick representation and labelled with carbon atoms in light blue, nitrogen in blue, oxygen in red, and sulfur in orange. Compound **7** is labelled with carbon atoms in light green, nitrogen in blue, oxygen in red, and sulfur in orange. The figures were generated with the program PyMOL.

Moreover, in order to investigate around the role of Tyr129 in hydrophobic interactions between compound **7** and both hNAT1 and mNat2, a model of shNat2 was built using SwissModel®, based on hNAT1 and subsequently compared to mNat2, considering the 93% sequence identity of shNat2 compared to mNat2. The accuracy of the model generated is presented in **Table IV.8**.

Table IV.8: Parameters estimating general quality of shNat2 model

Value	Range	Best value	Meaning	shNat2 over hNAT1
% identity	0-100	> 50	identity of residue sequences	81
E-value	0-1	0	significance to the match	4.15E(-143) = ~0
Qmean-Score4	0-1	1	quality of the model	0.73
Z-score	ℜ	> ~ -1	absolute quality of the model	-0.82

The active site of shNat2 model was almost superimposable to that of mNat2, except the residue 129 which is a leucine in shNat2 instead of a tyrosine as in mNat2 (**Figure IV.36**). The fact that **7** was found to be a poorer inhibitor of shNat2 than mNat2 suggested that π-π stacking interactions between the sulfonamide arene of compound **7** and the side chain arene of Tyr129 were important factors in the recognition of mNat2 by **7**.

A model of shNat2 was previously deposited in the protein data bank and was generated from NMR analyses (Zhang et al, 2006). The overall folding of that model was similar to the model generated in this study except the position of the inter-domain loop characteristic to the eukaryotic NAT (**Figure IV.37**). This could be due to the fact that the NMR-based shNat2 model helped predict only the secondary structure of the protein, whilst the inter-domain loop had not been found to be constituted by either α-helices or β-sheets (**Figure IV.37**). The loop in the shNat2 model presented in this study conversely relied on the crystal structure of hNAT1, wherein both secondary and tertiary structures were well-characterised.

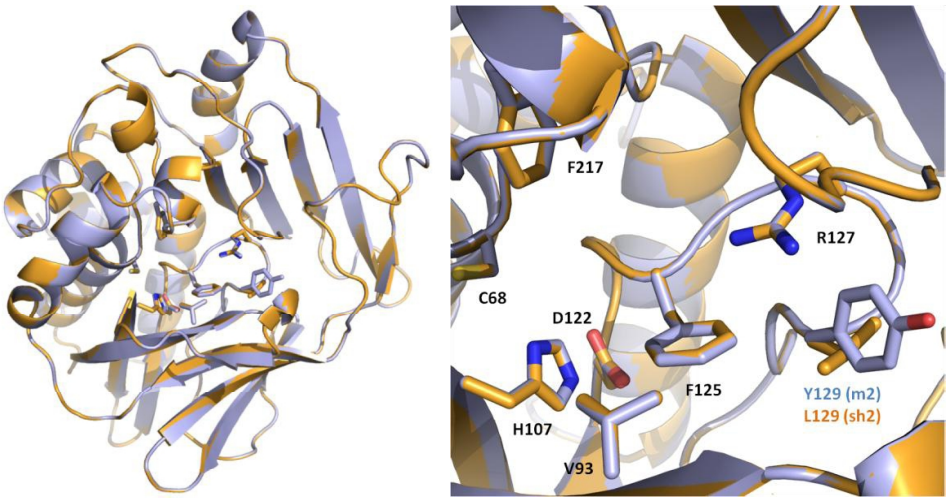


Figure IV.36: Overall structures of mNat2 and shNat2 models overlaid.

(left). Cartoon diagram showing the overlaid structural models of mNat2 (light blue) and shNat2 (gold) modelled on hNAT1 using the software SwissModel® (Arnold et al, 2006; Kiefer et al, 2009; Peitsch, 1995b). The structures aligned using the program PyMOL. Side chains of the key residues of both the active sites are drawn in sticks. **(right)** Maximised view of the active sites of both hNAT2 and mNat1. Side chains of key residues within the active site are drawn in stick representation and labelled. Dissimilar residues are labelled in colour, m1=mNat1, m2=mNat2.

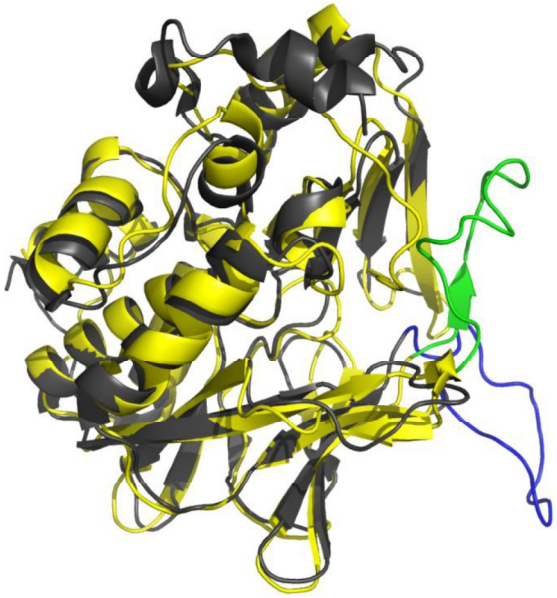


Figure IV.37: Overall structures of two different models of shNat2.

Cartoon diagram showing the two different structural models of shNat2 overlaid: NMR-based shNat2 model (pdb:2GWV, grey) (Zhang et al, 2006) and shNat2 modelled on hNAT1 using the software SwissModel® (yellow) (Arnold et al, 2006; Kiefer et al, 2009; Peitsch, 1995b). The structures were generated and aligned using the program PyMOL. The inter-domain loop characteristic to eukaryotic NATs is shown in blue for the first model and in green for the second model.

IV.3 Discussion

The selective colourimetric detection of pure recombinant proteins hNAT1 and mNat2 using naphthoquinone **7** *via* non-covalent binding was found to possess great potential in order to develop a detection method for native hNAT1 in breast cancer cell lysates.

The work presented in this chapter describes different physico-chemical and biochemical experiments which together support the hypothesis that when compound **7** binds to pure recombinant mNat2 within its active site, the sulfonamide-N*H* of **7** is deprotonated by the Arg127 side chain guanidine of the enzyme, thereby causing the colour change of the ligand from red to blue. Based on the functional homology and sequence identity between hNAT1 and mNat2 (Kawamura et al, 2008), similar assumptions were made for hNAT1.

In particular, the pK_a of compound **7** was estimated to be 9.16 through a pH titration experiment, which is similar to the pK_a value of compound **1** (9.50, (Crawford, 2007)). In the presence of strong bases, such as NaOH, DBU, or NaSEt, the deprotonation of the sulfonamide-N*H* of **7** also occurred, with a spectrophotometric shift from 498 nm (red colour) towards higher wavelengths (550-650nm) in the visible spectrum (blue colour) (**Figure IV.38**).

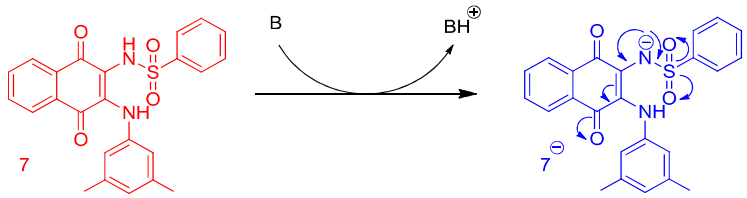


Figure IV.38: Acid-base proton exchange between compound 7 and a base (B) at the origin of the colour change event.

This was also confirmed by NMR tests conducted on a ^{15}N-labelled derivative of compound **7** and recorded in two differently buffered deuterated solutions at pH 8 and pH

13 respectively. Spectrophotometric studies performed on a derivative of compound **7** with an *N*-methylated sulfonamide (*N*-methyl-**7**) lacking the acidic sulfonamide acidic proton as in **7** showed no colour change upon basification or binding to mNat2.

Moreover, as regards the chemical properties of compound 7, the use of a reducing agent such as DTT at 34 μM was not followed by a colour conversion from red to blue, but at higher concentrations of the DTT or dithionite (100mM) the molecule became colourless. This confirms that the presence of small amounts (≤ 34μM) of reducing agents in all spectrometric experiments carried out with samples of pure recombinant enzymes throughout this study was not the cause of the bathochromic shift of **7**.

Moreover, the disappearance of the red colour of compound **7** with very high amounts of DTT or dithionite would anticipate that the main chromophoric group of **7** is the quinone moiety.

On the other hand, mutating Arg127 of mNat2 into a Gly or a Leu helped support hypotheses regarding the interaction of **7** with hNAT1.

The production of pure recombinant mNat2 mutant proteins mNat2_R125G and mNat2_R125L, was successfully achieved with a high level of purity. The two mNat2 variants were properly folded and active as supported by enzymatic studies, and did not give rise to a colour change upon treatment with compound **7**, unlike mNat2, although compound **7** was found to inhibit both mutants to a lesser extent than the wild-type enzyme.

This observation supported the importance of Arg127 residue in the recognition between mNat2 and **7**, and suggested that the guanidine from Arg127 was able to deprotonate the sulfonamide-N*H* within **7**, causing the colour change of the ligand from red to blue (**Figure IV.39**).

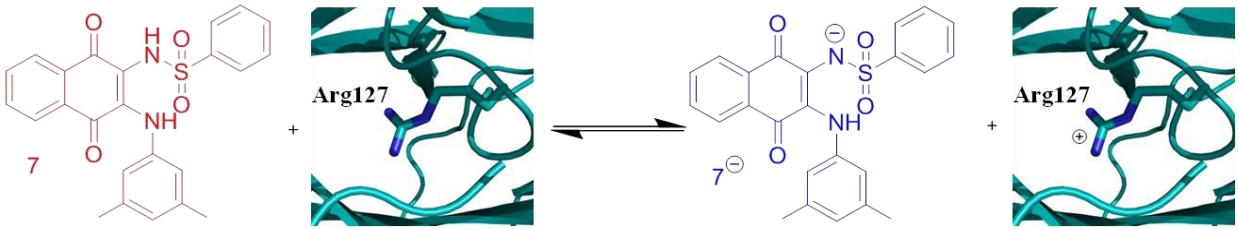


Figure IV.39: Possible acid-base proton exchange between compound 7 and Arg127 of mNat2, generating the colour change.

mNat2 model is based on hNAT1 structure (Wu et al, 2007).

Similar molecular interactions were hypothesised to explain the formation of the blue complex hNAT1-**7** for both high sequence identity and functional homology between mNat2 and hNAT1 (Kawamura et al, 2008) (**Figure IV.40**).

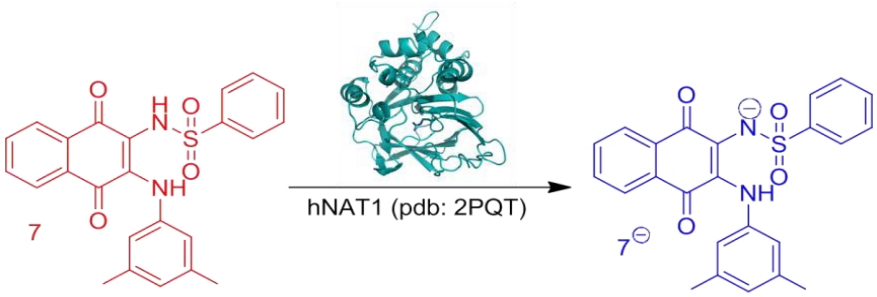


Figure IV.40: Possible acid-base proton exchange between compound 7 and hNAT1, generating the colour change event.

The crystal structure of hNAT1 was drawn with the software ChemBio3D Ultra 12.0, using the pdb file 2PQT (Wu et al, 2007).

Other alternative possibilities to explain the colour change event of **7** in the presence of both hNAT1 and mNat2 were investigated and were found to be negative.

For instance, the side chain thiolate of catalytic Cys68 was also considered as possible nucleophilic base able to either attack the naphthoquinone moiety or deprotonate sulfonamide-N*H*.

The first hypothesis was excluded as compound **7** was shown to be a reversible inhibitor of mNat2, which would be inconsistent with the previous hypothesis of a covalent nucleophilic addition.

As regards the second hypothesis, the deprotonation of **7** and the subsequent colour change still occurred when the ligand was mixed with a solution of mNat2 which was previously treated with an alkylating electrophile and whose Cys68 thiolate would be incapable of acting as base after possible alkylation.

Furthermore, kinetic analyses conducted with similar mammalian NAT isoenzymes underlined that even a single mutation of one of the three residues at positions 125, 127, 129 could diminish the affinity of the inhibitor towards the enzyme, as shown by the higher IC_{50} values obtained with compound **7** for all enzymes compared to hNAT1/mNat2 (**Table IV.9**).

Moreover, spectrophotometric studies have shown that Arg127 is necessary, but not sufficient, to provoke the colour change of **7** from red to blue upon binding: indeed, mNat2_F125S still had Arg127, but no colour change of **7** was observed with this enzyme. This might suggest the vital importance of Phe125 in forming the ligand-protein complex between hNAT1/mNat2 and **7**, or aligning the ligand in the correct orientation within the active site to alow interaction between Arg127 and the sulfonamide-N*H* of compound **7** (**Table IV.9**).

Conversely, compound **7** still changed colour upon binding to shNat2, but its affinity for shNat2 was lower, consistent with the requirement of increasing amount of shNat2 enzyme in the assay to observe a complete conversion of **7** from protonated (red) to deprotonated (blue) species (**Table IV.9**). This was consistent with the higher IC_{50} of **7** with shNat2 than hNAT1 or mNat2 which could be due to the difference of the residue at position 129 between hNAT1 (Tyr) and shNat2 (Leu).

Therefore, the presence of all the three residues (Phe125, Arg127, Tyr129) seems to constitute a crucial requirement for selective recognition of hNAT1 and mNat2 by naphthoquinone **7**, generating a proton transfer from the sulfonamide-N*H* of **7** and Arg127 guanidine.

Table IV.9: Summary of the effects of 7 on different mammalian NATs.

Enzyme	hNAT1	mNat2	R127G	R127L	F125S	shNat2	mNat1
Primary sequence identity (%) *versus* hNAT1	100	82	82	82	82	81	74
Mutations *versus* hNAT1 active site residues	-	-	R127G	R127L	F125S	Y129L	F125Y R127G
IC_{50} with 7 (µM)	5.3	1.86	51.7	102.5	68.7	89.04	129.7
λ_{max} of 7 (nm) (ratio [enzyme]:[7])	**585** 2:1	**625** 2:1	**498** 2:1	**498** 2:1	**498** 2:1	**525** 2:1 **590** 8:1	**498** 2:1

Despite many attempts, no suitably diffracting crystals of the ligand-protein complex (compound **7** with hNAT1 or mNat2) were afforded. The inhibitor **7** was therefore docked within the active site of both enzymes, hNAT1 (pdb: 2PQT, (Wu et al, 2007)) and mNat2 (model), in order to confirm initial hypotheses about the critical importance of the residues Arg127, together with Phe125 and Tyr129, in forming the ligand-enzyme complex (**Figure IV.41**). This helped elucidate the molecular interactions between the two counterparts of the complex, and determine a likely orientation of the ligand inside the active site pocket.

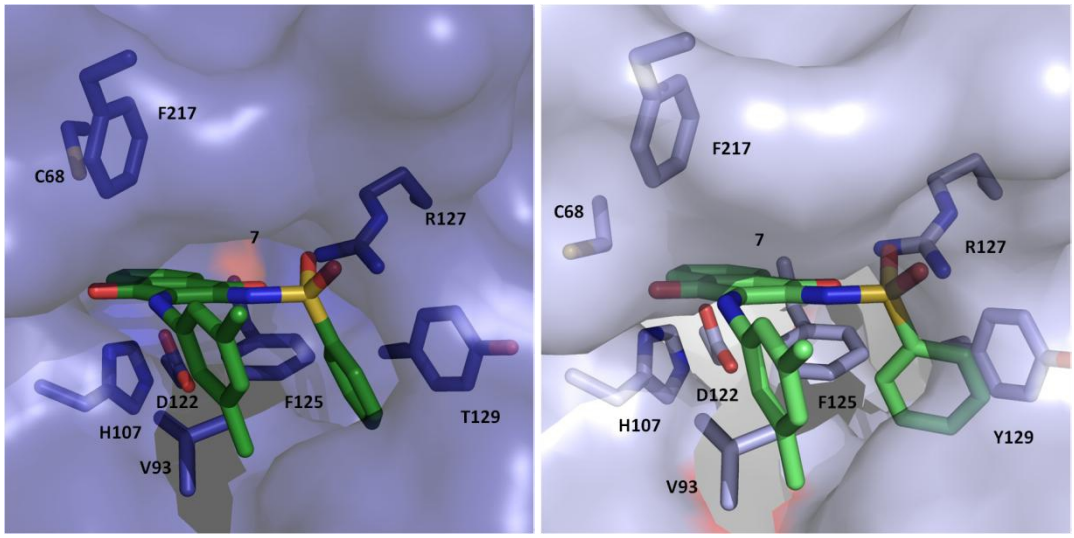


Figure IV.41: Substrate binding pockets of hNAT1 and mNat2 with compound 7 docked.

(left) The active site of hNAT1 crystal structure with docked compound **7** is shown in surface and stick representation respectively. The residues involved in compound **7** binding and substrate specificity are shown in stick representation and labelled with carbon atoms in dark blue, nitrogen in blue, oxygen in red, and sulfur in orange. Compound **7** is labelled with carbon atoms in dark green, nitrogen in blue, oxygen in red, and sulfur in orange. **(right)** The active site of mNat2 structural model with docked compound **7** is shown in surface and stick representation respectively.

The best docking results obtained for hNAT1/mNat2 enzymes showed common patterns of interaction between compound **7** and the residues of their corresponding active sites (**Figure IV.42**):

- a close interaction, possibly ionic, between the side chain guanidine of Arg127 and an oxygen of the sulfonamide of compound **7** (2.5-2.9 Å);
- a hydrogen bond between the same guanidine and the quinone oxygen at position C_1 (2.5-3.0 Å);
- a polar interaction between the main chain ketone of Phe287 and the other oxygen of the sulfonamide (2.5 Å);
- a π-π stacking between the hydrophobic plane created by Val94 and Phe125 side chains and the naphthoquinone core of the inhibitor **7** (3.5-4 Å);
- Van-der-Waals hydrophobic interaction between Tyr129 side chain and the phenyl of the moiety at position C_3 of the ligand (4.2-4.8 Å).

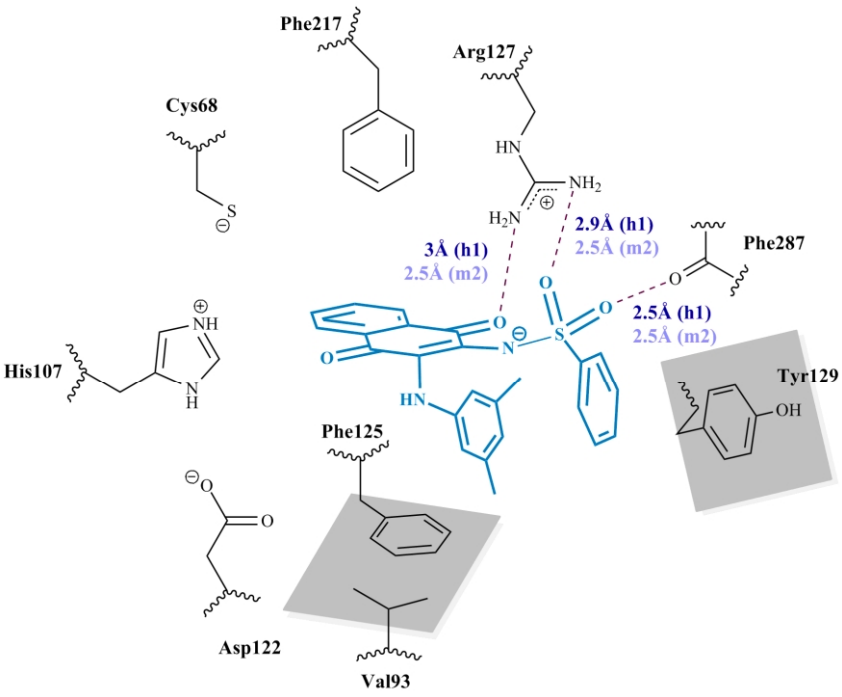


Figure IV.42: Schematic representation of compound 7 modelled in hNAT1 and mNat2 active sites.

In schematic diagrams, **7** is coloured in blue. The residues involved in inhibitor binding and specificity are labelled. Hydrogen bonds are drawn as dashed lines. The Van der Waals surfaces in the enzyme's pocket are shown as grey planes.

Although all docking results need to be considered with appropriate caution, these observations were consistent with previous studies on the arylamine binding site of hNAT1 *versus* hNAT2 (Wu et al, 2007) and the role of Phe125, Arg127, and Tyr129 in substrate selectivity (Goodfellow et al, 2000).

Finally, comparing the residues within the active site of the mammalian NATs screened with compound **7** highlighted that only the concomitant presence of Phe125, Arg127 and Tyr 129 correctly folded could ensure a suitable fitting of the naphthoquinone **7** within the active site to highly inhibit the catalytic activity of the NAT enzyme (**Figure IV.43**).

This greatly supports the idea of continuing improving the efficiency of naphthoquinone **7** as selective inhibitor and colourimetric biosensor to target native hNAT1 in breast cancer cell lysate.

	NAT enzymes							
Residue	hNAT1	mNat2	shNat2	mNat2 F125S	mNat2 R127G	mNat2 R127L	mNat1	hNAT2
125	F	F	F	S	F	F	Y	S
127	R	R	R	R	G	L	G	S
129	Y	Y	L	Y	Y	Y	Y	S

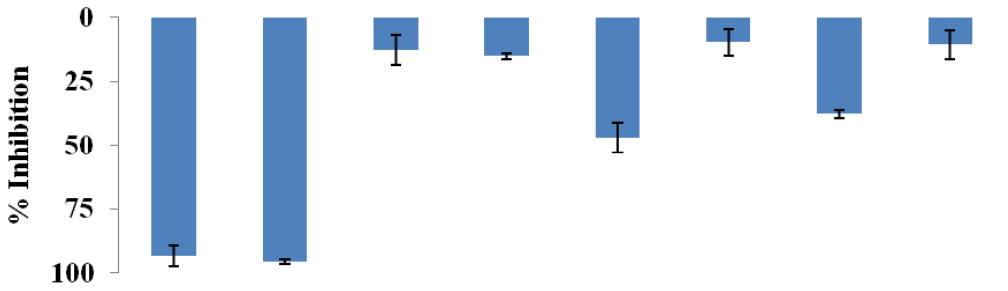


Figure IV.43: Relationship between NAT key residues in substrate specificity and NAT inhibition by 7.

Residues which differ from the corresponding residues in hNAT1 are labelled in red. % of inhibition of NAT activity was calculated using 30 µM compound **7** as reported in **Section IV.2.2.4**.

Chapter V:

Substrate specificity of mammalian NAT isoenzymes



BATHSHEBA AT HER BATH (1654), BY REMBRANDT HARMENSZOON VAN RIJN (1606-1669).

The left breast of the model shows a skin discolouration, distortion of symmetry with axillary lymph nodes and also a skin reddening. These features were considered to depict clinical signs of breast cancer (Braithwaite & Shugg, 1983). (Musée du Louvre, Paris).

V.1 Introduction

Previous studies compared the arylamine substrate profiles of both hNAT1 and hNAT2 to shNat2 (Kawamura et al, 2005) and mNat2 (Kawamura et al, 2008), and underlined a functional homology of both shNat2 and mNat2 towards hNAT1.

In particular, the appropriate probe substrate for each enzyme was identified for subsequent investigations: the arylamine folate catabolite pABAglu for hNAT1, mNat2 and shNat2, and the arylhydrazine isoniazid (INH) for hNAT2 (Kawamura et al, 2005) (Kawamura et al, 2008). The antitubercolar drug INH was also found to be a probe substrate for the other functional murine isoenzyme: mNat1 (Martell et al, 1992).

The recent crystal structures of hNAT1 and hNAT2 (Wu et al, 2007) highlighted some elements of the structural basis of substrate-binding in human NAT enzymes, confirming previous hypotheses about the region of key residues in substrate selectivity: residues 125-129 (Goodfellow et al, 2000). Nevertheless, the exact role of the residues within this region has not been elucidated yet.

Moreover, comprehensive substrate specificity profiles of other two murine recombinant NATs, mNat1 and mNat2_F125S, were previously obtained by Dr A. Kawamura (unpublished work) and Dr I. Westwood (unpublished work) respectively, but not evaluated in relation to other NAT substrate profiles available.

As regards mNat2_F125S, this mutant was conceived and generated in response to the similar mutated protein of hNAT1 (hNAT1_F125S) presented by Wu et al. (Wu et al, 2007), in order to investigate the role of Phe125 on substrate selectivity.

The production of the two mNat2 mutants R127G and R127L, as presented in **Chapter IV** could give further insight into the substrate selectivity of mammalian NATs.

As regards the other substrate of the NAT reaction, AcCoAs, the use of DTNB was previously extended to detect other types of NAT-catalysed hydrolyses of thioester com-

pounds using diverse AcylCoA substrates (Kawamura & Sim, 2005).

In fact, the hydrolysis of some AcylCoA was initially observed with pure recombinant shNat2, hNAT1, and hNAT2 in the presence of the appropriate arylamine substrate (Kawamura & Sim, 2005), assuming that during these reactions the acyl group was transferred to the aromatic amine, consistent with the initial findings on AcCoA (Brooke et al, 2003b).

Moreover, the hydrolysis of the AcylCoA thioesters by NATs decreased with the acyl chain length increasing by up to six carbon atoms. This preliminary study highlighted the ability of all these three mammalian NATs to use *n*-propionylCoA as substrate in their catalytic reaction.

While the consequence of using *n*-propionylCoA as NAT substrate remains still unclear in mammalian systems, the cellular importance of this was conversely assessed in some species from the prokaryotic kingdom.

The hydrolysis of the thioester group from a panel of different AcylCoAs was also detected with TBNAT and *n*-propionylCoA was the most reactive substrate after AcCoA (Lack et al, 2009). This catalytic reaction was hypothesised to be critical in the cholesterol degradation pathway. Indeed, *TBNAT* (Rv3566) was found to be encoded in the same operon as other genes (*hsaA* (Rv3570c), *hsaB* (Rv3567c), *hsaC* (Rv3568c), and *hsaD* (Rv3569c), the last encoding for 2-hydroxy-6-oxo-6-phenylhexa-2,4-dienoic acid hydrolase (Anderton et al, 2006)), whose products are involved in the oxidation and the meta-cleavage of the four-ring cholesterol skeleton (**Figure V.1**).

Moreover, the degradation of the remaining C17 acyl chain from cholesterol could produce one molecule of AcCoA and two molecules of *n*-propionylCoA per cholesterol molecule, and TBNAT could consume both species, possibly for accelerating the cholesterol catabolism and promoting their homeostasis for cell wall synthesis (Lack et al, 2009).

Considering the importance of cholesterol for the intracellular survival of *Mycobacterium tuberculosis* (Brzostek et al, 2007; Pandey & Sassetti, 2008), this study provided evidence of a first potential endogenous role of a NAT enzyme in prokaryotics.

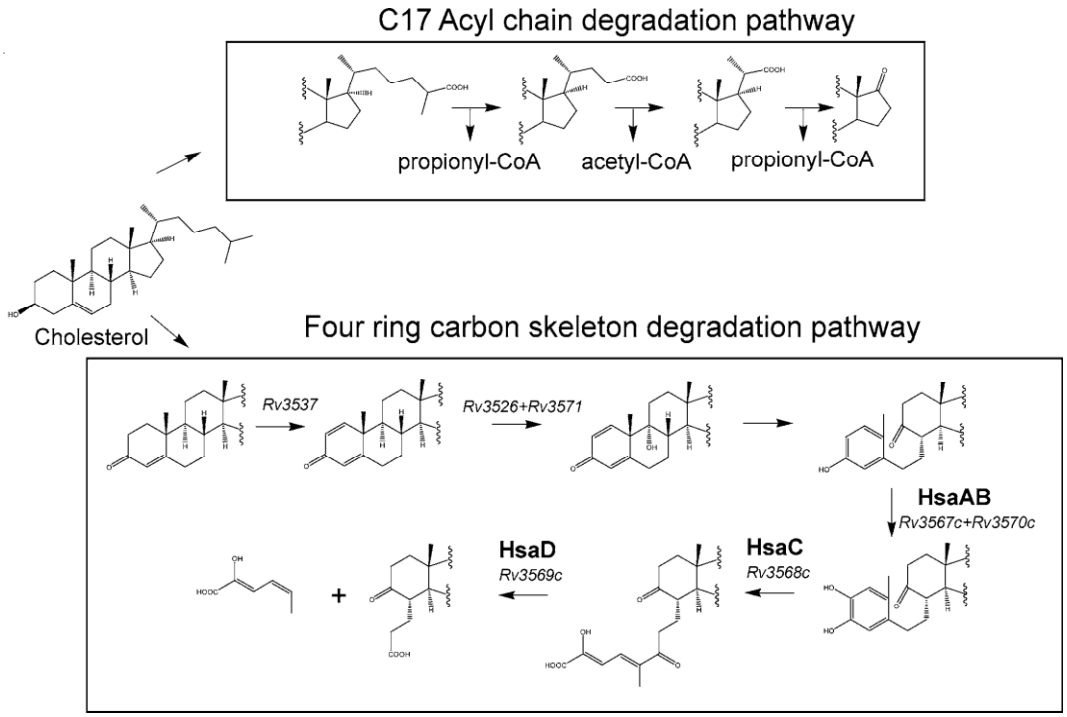


Figure V.1: Proposed pathway of cholesterol metabolism.

Pathway of cholesterol catabolism as proposed by Sih et al. (Sih et al, 1966), Horinouchi et al. (Horinouchi et al, 2005) and Van der Geize et al. (Van der Geize et al, 2007). The figure was adapted from the paper Lack et al. 2009 (Lack et al, 2009).

In order to advance the study concerning the AcylCoA substrates of NAT enzymes, several AcylCoA species would need to be similarly screened with murine NATs and other prokaryotic NATs.

AIMS

In this chapter, further studies on the biochemical characterisation of substrate selectivity of a panel of different eukaryotic and prokaryotic NATs will be presented, including the following:

- determination of the arylamine substrate profiles of the two mNat2 mutants R127G and R127L;
- comparison of the arylamine substrate profiles of different mammalian NATs (hNAT1, hNAT2, mNat2, mNat1, shNat2, mNat2_F125S, mNat2_R127G, mNat2_R127L);
- modelling mNat1 based on the available human NAT structures;
- enzymatic characterisation of murine and prokaryotic NATs with different AcylCoA entities.

V.2 Results

V.2.1 Arylamine substrate profiles of mNat2 mutants R127G and R127L

In order to better elucidate the role of the residue Arg127 in the arylamine substrate preference of mNat2, as a model for hNAT1, the two mNat2 mutants, R127G and R127L, introduced in **Chapter IV**, were biochemically characterised and compared to wild-type mNat2. In particular, an exhaustive panel of typical arylamine NAT substrates, mainly arylamines and arylhydrazines were tested with all three mNat2 enzymes (**Figure V.2**).

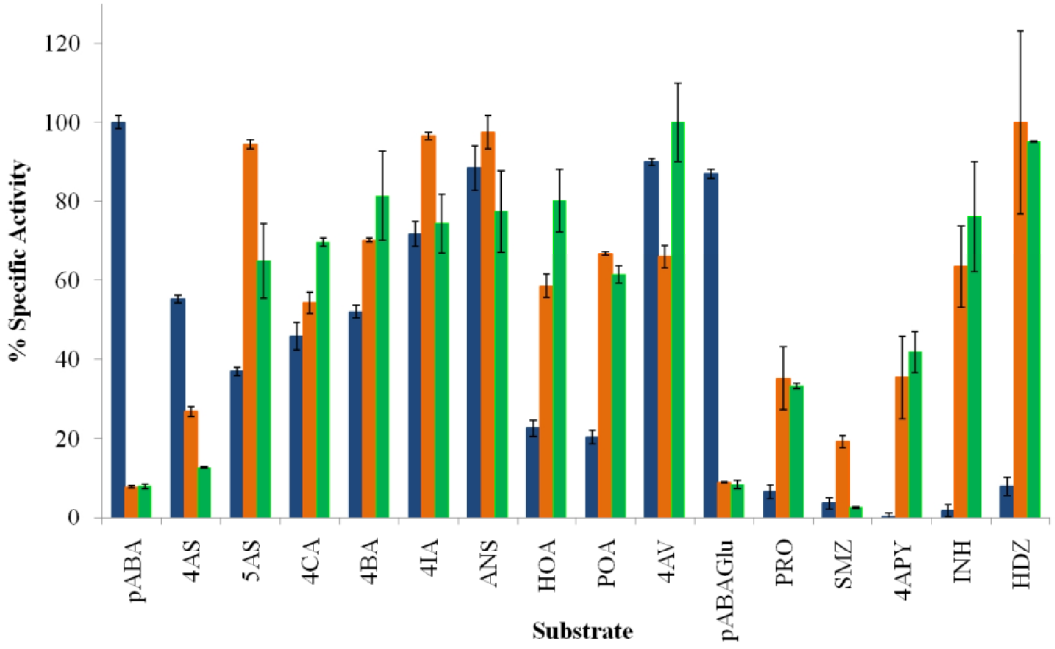


Figure V.2: Comparison of arylamine substrate specificities of mNat2, R127G, and R127L.

The substrate specific activity profiles for mNat2 (blue bars), mNat2_R127G (orange bars) and mNat2_R127L (green bars) are shown. The activity of mNat2 mutants was determined by measuring the rate of AcCoA hydrolysis. All measurements are expressed as mean ± standard deviation relative to the most rapidly acetylated substrate, in particular 100% specific activity values are: 196µM.sec^{-1}.mg^{-1} for mNat2 with pABA, 1385µM.sec^{-1}.mg^{-1} for mNat2_R127G with HDZ, and 82.5µM.sec^{-1}.mg^{-1} for mNat2_R127L with 4AV. Abbreviations of the names of the chemicals used as substrates for NAT in this study are detailed in **Section II.2.5.2.1**.

The activity of R127G and R127L with pABA and pABAglu, probe substrates for wild-type mNat2, was very low. Moreover, a notable arylhydrazine acetylation activity was observed with both R127G and R127L, whilst mNat2_WT was known to be unable to efficiently acetylate those substrates.

V.2.2 Modelling mNat1 based on the structure of hNAT2

After modelling mNat2 structure based on hNAT1 crystal structure (Wu et al, 2007) (**Chapter IV**), a structural model of mNat1 was also needed in order to rationalise the substrate selectivity of all mammalian NATs investigated in this study.

Considering the similarities of the probe substrate of hNat2 and mNat1, in particular the antitubercolar drug isoniazid (INH), and their high percentage of identity (72%), hNAT2 structure (pdb:2PFR, (Wu et al, 2007)) was used to build a model for mNat1 using the software Swiss-Model® (Arnold et al, 2006; Guex & Peitsch, 1997; Schwede et al, 2003).

The parameters estimating the overall quality of mNat1 structural model created based on hNAT2 structure, suggested that the initial choice of the template was accurate and the final virtual result was highly probable (**Table V.1**).

Table V.1: Parameters estimating general quality of mNat1 model.

Value	Range	Best value	Meaning	mNat1 over hNAT2
% identity	0-100	> 50	identity of residue sequences	72
E-value	0-1	0	significance to the match	9.47E(-118) = ~0
Qmean-Score4	0-1	1	quality of the model	0.7
Z-score	ℜ	> ~ -1	absolute quality of the model	-0.6

Moreover, in the model of mNat1 generated, the structural folding for many peptidic regions were estimated to be reliable, but only few regions were not, in particular those around residue Trp15 and Trp96, as in the model for mNat2 shown in **Chapter IV**

(**Figure V.3**).

This could be due to differences in residue sequence between mNat1 and hNAT2 (**Table V.2**).

Table V.2: Residues of the unreliable regions in murine NAT models.

Enzyme	central residue of unreliable region	Residue differences against template (model *versus* template)
mNat1	Trp15	V16R
	Trp96	V93F, T96P, S99N

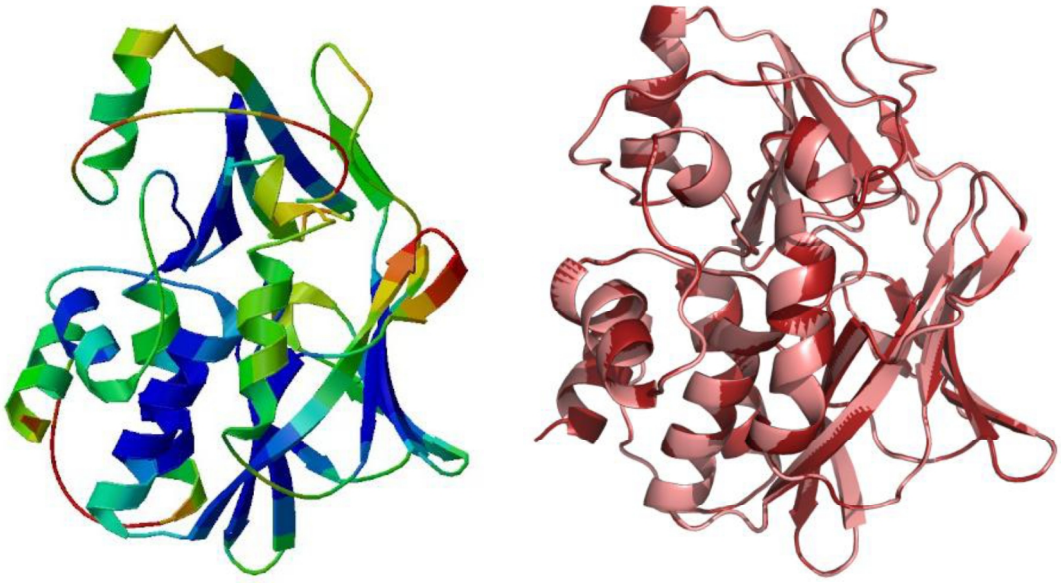


Figure V.3: Overlay of hNAT2 template structure and corresponding structural mNat1 models.
(left) Estimated per-residue accuracy visualised using hNAT2 template (pdb: 2PFR) with a colour gradient from blue (more reliable regions) to red (potentially unreliable regions). **(right)** Ribbon diagram showing the overlaid structures of hNAT2 (purple) and mNat1 (pink) modelled on hNAT2 using the software SwissModel® (Arnold et al, 2006; Kiefer et al, 2009; Peitsch, 1995b).

An overlaid overview of hNAT2 structure and mNat1 model and a zoomed view of their respective active sites are shown in **Figure V.4**.

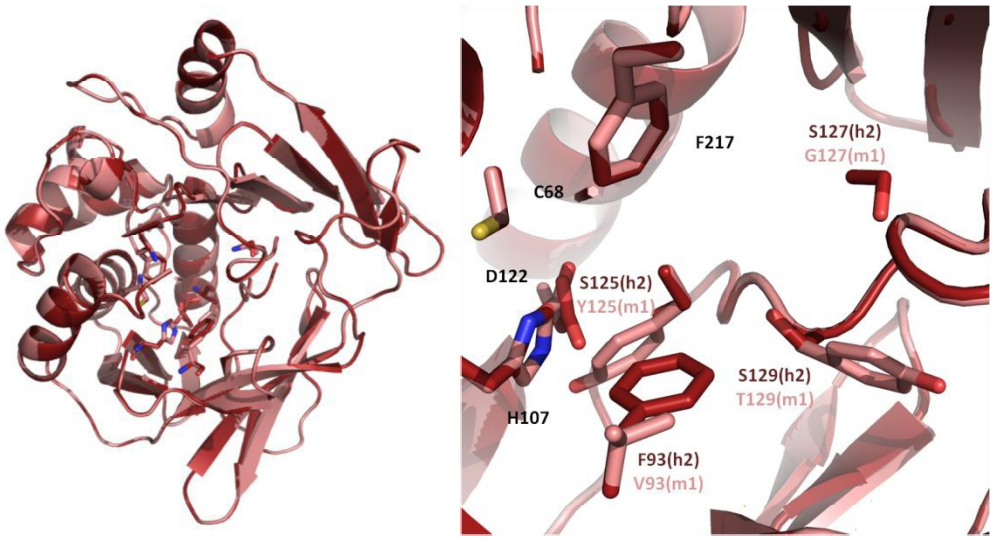


Figure V.4: Overlay of hNAT2 structure and mNat1 model.

(left). Ribbon diagram showing the overlaid structures of hNAT2 (red) and mNat1 (pink) modelled on hNAT2 using the software SwissModel®. The structures were aligned using the program PyMOL. Side chains of the key residues of both the active sites are drawn in sticks. **(right)** Maximised view of the active sites of both hNAT2 and mNat1. Side chains of key residues within the active site are drawn in stick representation and labelled. Dissimilar residues are labelled in colour, h2=hNAT2, m1=mNat1.

V.2.3 AcylCoA substrate profiles of murine NATs

Two different methods have largely been used to detect NAT activity in the assays, as previously mentioned: the acetylation state of the arylamine substrate by DMAB reacting with non-acetylated substrate (Andres et al, 1985) and the hydrolysis rate of the AcCoA by DTNB detecting the CoA formed throughout the enzymatic reaction (Brooke et al, 2003b).

As previously shown (Kawamura & Sim, 2005; Lack et al, 2009), some NAT enzymes were able to hydrolyse different AcylCoAs, assuming that the transfer of the acyl group to the arylamine substrate concomitantly occurred.

In this study, pure recombinant murine NATs were tested with different AcylCoA substrates, and both AcylCoA hydrolysis and arylamine acylation were monitored in order to verify the complete transfer of the acyl group to the aromatic amine of the arylamine

(**Figure V.5**).Both methods similarly reveraled the ability of mNat2 and mNat1 to transfer the acyl group from AcCoA or *n*-propionylCoA to the arylamine.

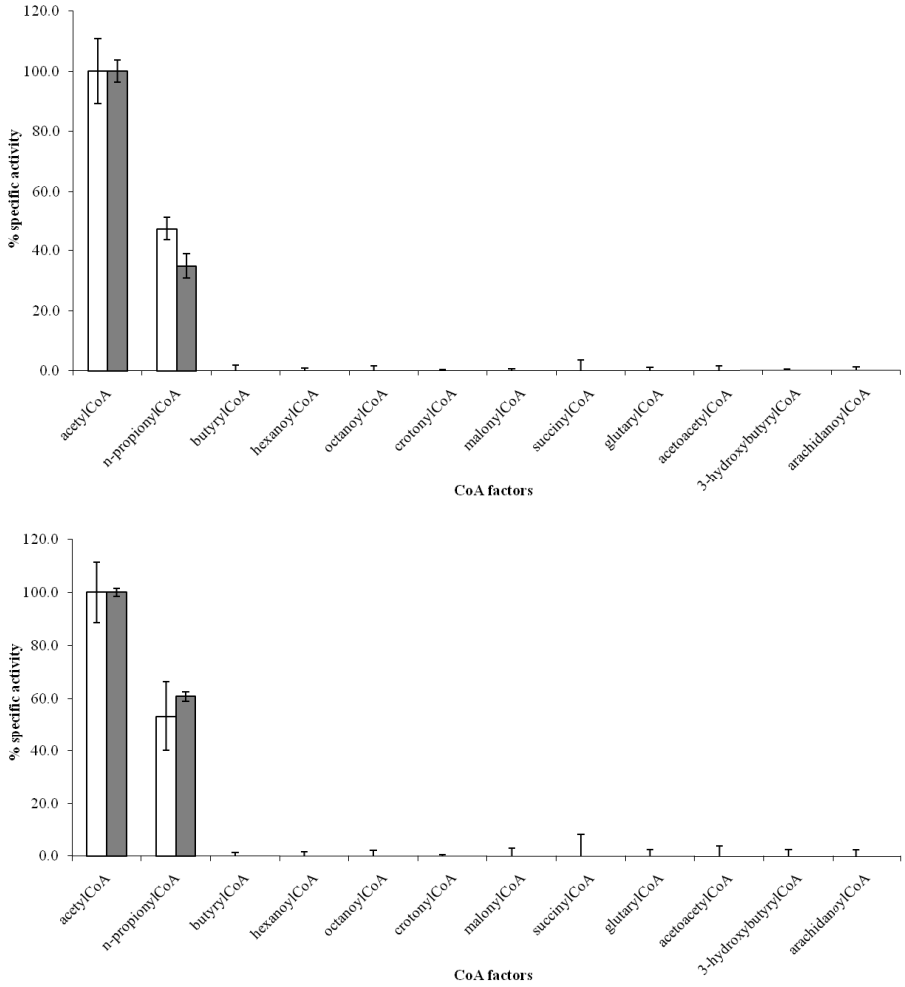


Figure V.5: AcylCoA substrate profile of murine NATs.

NAT activity was determined by measuring both the AcylCoA hydrolysis rate and the arylamine acetylation rate. **(top)** mNat2, **(bottom)** mNat1. **AcylCoA hydrolysis assay** - The appropriate arylamine substrate (500µM), pABA for mNat2 or 5AS for mNat1, was incubated with the NAT enzyme (50ng for mNat2, 100ng for mNat1), at 37˚C for 5 min in a 96-well plate (Corning). Pre-warmed AcylCoA (400µM) was added to start the reaction (final volume 100µL). 100% corresponds to 3476.3µM.sec^{-1}.mg^{-1} for mNat2 and 89.8µM.sec^{-1}.mg^{-1} for mNat1). **Arylamine acetylation assay** (Ac, *n*-propionyl, succinyl, acetoactyl CoA) - samples of enzyme (10ng for mNat2, 40ng for mNat1) and the arylamine substrate (150µM), pABA for mNat2 or 5AS for mNat1, were pre-incubated at 37°C in assay buffer (20mM Tris.HCl, pH 8.0, 1mM DTT) for 5 min in a 96-well plate (Corning). Pre-warmed AcylCoA (400 µM final concentration, 37°C) in assay buffer was added to start the reaction (final volume of 45µl), which was allowed to proceed at 37°C. 100% corresponds to 9523.2µM.sec^{-1}.mg^{-1} for mNat2 and 242.4µM.sec^{-1}.mg^{-1} for mNat1.

The hydrolysis of other AcylCoAs, such as succinyl and acetoacetyl CoA, was also observed in the assays with DTNB with both enzymes. However, arylamine acetylation assays conducted using these AcylCoAs and the appropriate arylamine substrates did not show the corresponding acylation of the aromatic amine. Parallel controls without enzymes showed that both succinylCoA and acetocetylCoA reacted with DTNB after 20 minutes. This suggested that the reactivity of both species with DTNB was due to their instability in enzymatic assays, but not to the catalytic activity of the NAT enzyme.

On the other hand, the importance of using *n*-propionylCoA by TBNAT and its possible involvement in the cholesterol catabolism and cellular survival (Lack et al, 2009) strongly suggested investigating similar experiences with other prokaryotic NATs, in order to have a more comprehensive overview of the phenomenon.

STNAT, MMNAT, MSNAT, and PANAT, were also able to catalyse the transfer of the *n*-propionyl chain from the corresponding CoA derivative to the primary amine of 5AS to diverse extents (**Figure V.6**). TBNAT was also tested as positive control (Lack et al, 2009). The appropriate controls without enzyme in the assays were also performed.

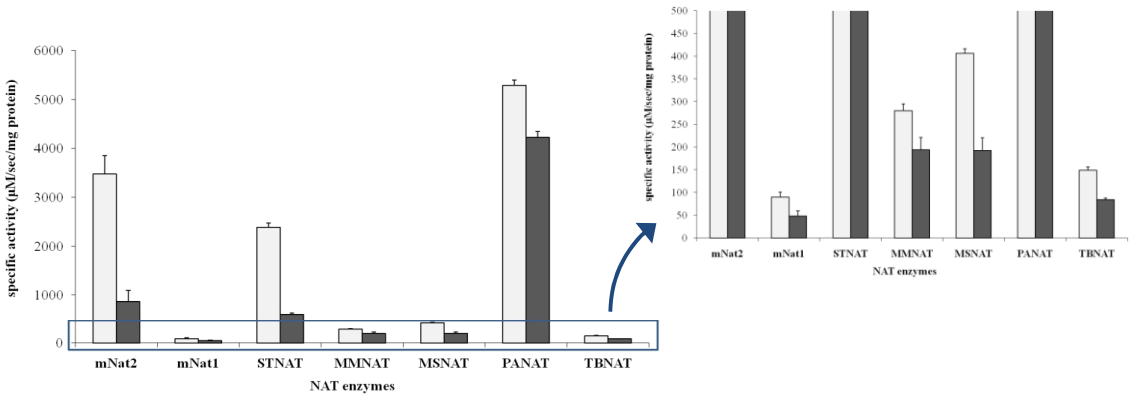


Figure V.6: Specific activity of different NATs with two different AcylCoA as substrates.

Specific activity ($\mu M.sec^{-1}.mg^{-1}$) of NAT enzymes was determined as hydrolysis of the AcylCoA (AcCoA (grey columns), *n*-propionylCoA (black columns)) in the presence of 5AS as arylamine substrate. 5AS (500µM) was incubated with the appropriate NAT enzyme (50ng for mNat2, 100ng for mNat1, MMNAT and MSNAT, 1µg for TBNAT, and 200ng for the other NATs), at 37°C for 5 min in a 96-well plate (Corning). Pre-warmed AcylCoA (400µM) was added to start the reaction (final volume 100µl).

V.3 Discussion

V.3.1 Arylamine substrate specificity of NAT isoenzymes

Docking **7** within the active site of hNAT1, as presented in **Chapter IV**, identified that the elements constituting the rationale behind the NAT isoenzyme selectivity for the inhibitor were in the region from residues 125 to 129: Phe125, Arg127, Tyr129 (**Figure V.7**). As reported in previous papers (Goodfellow et al, 2000; Wu et al, 2007), the region 125-129 was also likely to underpin the substrate specificity (**Figure V.7**). In particular, Val93, Phe125, Arg127, Tyr129, and Phe217 in hNAT1 and Phe93, Ser125, Phe217, and Ser287 in hNAT2 were found to be critical to describe their substrate specificities (Wu et al, 2007).

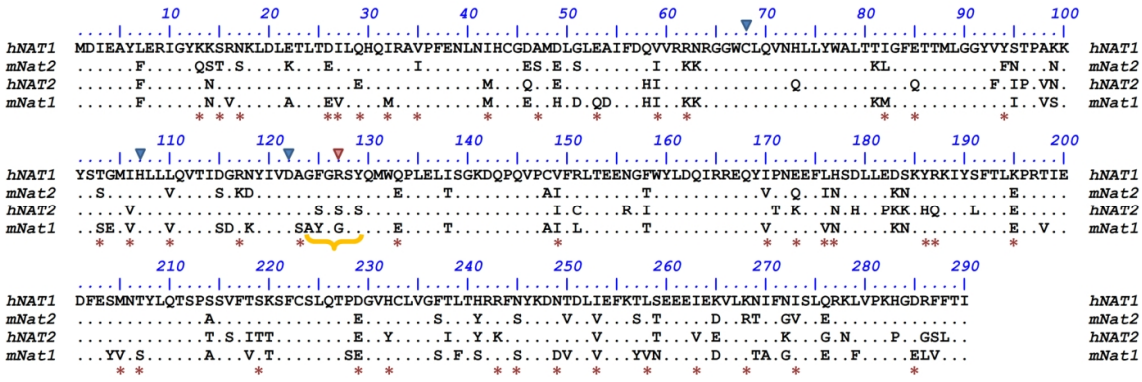


Figure V.7: Multiple sequence alignment of human and murine NAT proteins.

Human and murine NAT proteins are aligned. Residues which are identical in comparison to hNAT1 sequence are replaced by a black spot. Key residues of the catalytic triad Cys68-His106-Asp122 are pointed with a blue triangle, the residue Arg127 involved in inhibitor selectivity is identified by a green triangle, and key residues in substrate specificity are highlighted with a yellow bracket. Alignment was generated using Clustal W (Thompson et al, 1994). Figure was prepared using BioEdit (Hall, 1999).

Therefore, the comparison of the substrate profile of different NATs in relation to the crystal structures or models of their respective active sites helped highlight some bio-

chemical features for each enzyme.

The substrate specificity profile of mNat2 described in this thesis was found to be equivalent to the data represented by Kawamura et al. 2008 (Kawamura et al, 2008). A combined substrate profile was then drawn for mNat2 and compared to the substrate profiles of hNAT1 and hNAT2 previously published (Kawamura et al, 2005), and to that of mNat1 (unpublished work by Dr Kawamura) (**Figure V.8**).

The high selectivity of hNAT1 and mNat2 to both pABA and pABAglu was consistent with previous observations (Kawamura et al, 2008), as was the specificity of hNAT2 and mNat1 for SMZ and the arylhydrazine substrates tested (INH, HDZ, and PHZ) (**Figure V.8**).

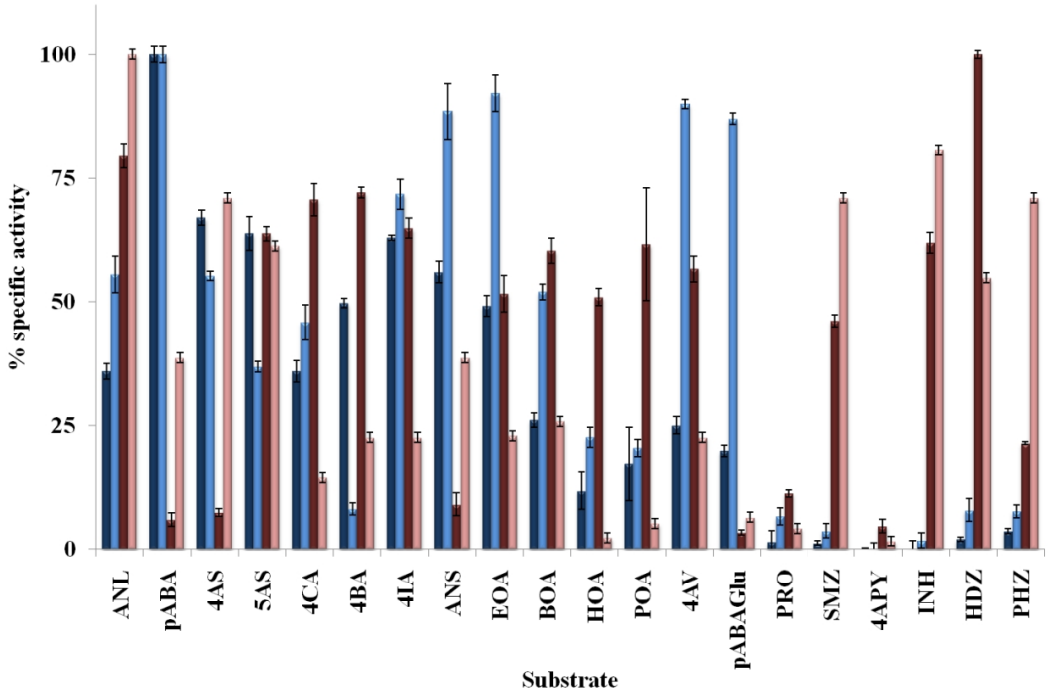


Figure V.8: Comparison of the substrate specific activity profiles of hNAT1, mNat2, hNAT2, and mNat1.

The substrate specific activity profiles of hNAT1 ( ), mNat2 ( ), hNAT2 ( ), and mNat1 ( ) are shown. % specific activity data for hNAT1 and hNAT2 were adapted from published work (Kawamura et al, 2005), and as regards mNat1, the data were obtained by Dr. Kawamura (unpublished work). Abbreviations of the names of the chemicals used as substrates for NAT in this study are detailed in **Section II.2.5.2.1**.

The recent crystal structure of hNAT1 with 4AS docked within its active site underlined that the negative charge of the carboxylate substituent would mainly interact with Arg127 guanidine (Wu et al, 2007). This non-catalytic residue with its ionisable guanidine moiety constitutes the unique example of a highly polarisable residue within the hydrophobic active pocket of both hNAT1 and mNat2, which could explain their preference for arylamine substrates with charged *para* substituents at physiological pH or at enzymatic assay pH (pH 8.0), such as pABA, pABAglu and 4AS.

However, a partial cross reactivity of mNat1 was also observed with some hNAT1-specific arylamine substrates, such as pABA, 4AS, ANS (**Figure V.8**). Although mNat1 possesses an apolar glycine residue at position 127, this partial cross reactivity could be linked to a different structural conformation of the active site of mNat1 relative to hNAT1 or mNat2 (**Figure V.9**).

Possibly, the presence of a smaller residue, like glycine, could help accommodate larger substrates and allow them to interact with the side chain of other moderately polar residues in the active site, such as Tyr125 and Tyr129 (**Figure V.9**). Possibly, the π-π stacking interactions between the aromatic core of an arylamine substrate and Phe125 in hNAT1 could be similarly ensured by the side chain arene of Tyr125 in mNat1.The model of mNat1 created on the basis of hNAT2 does not shown a suitable folding of the Tyr125 residue side chain compared to that in both hNAT1 structure and mNat2 model (**Figure V.10**). This apparent discrepancy was circumvented when the structural model of mNat1 was built on the crystal structure of hNAT1. Thus, the side chain of Tyr125 in mNat1 was superimposable to that of Phe125 in hNAT1 or mNat2.

This could also provides a possible explanation why compound **7** was observed to be partially reactive towards mNat1, through possible π-π stacking interactions between Tyr125 and the naphthoquinone core of **7**.

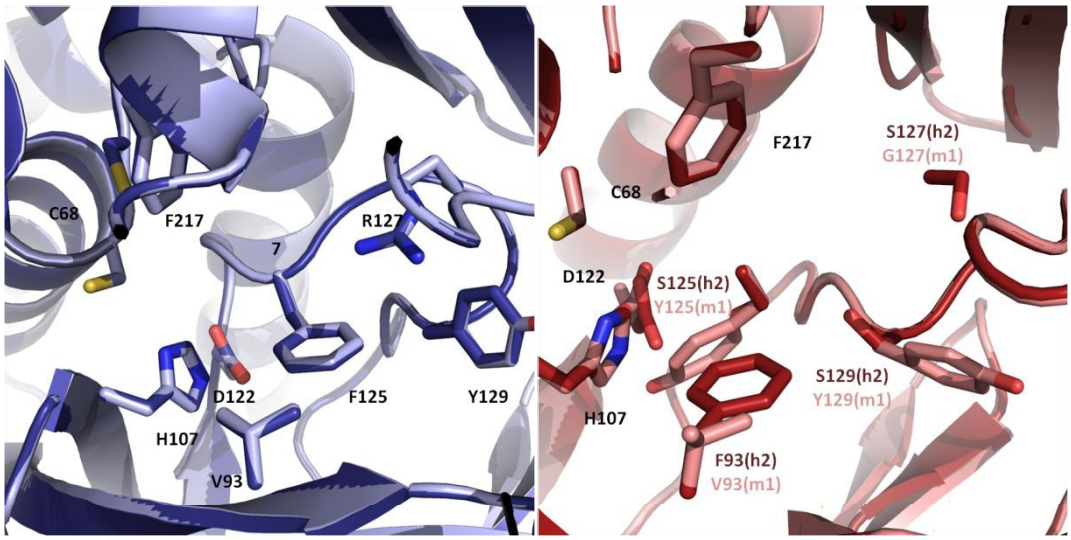


Figure V.9: Zoomed view of the active sites of human NAT structures and murine NAT models.

(left). Maximised view of the active sites of both hNAT1 (bark blue) and mNat2 (light blue). Side chains of key residues within the active site are drawn in stick representation and labelled. **(right)** Maximised view of the active sites of both hNAT2 (purple) and mNat1 (salmon). Side chains of key residues within the active site are drawn in stick representation and labelled. Dissimilar residues are labelled in colour, h2=hNAT2 and m1=mNat1.

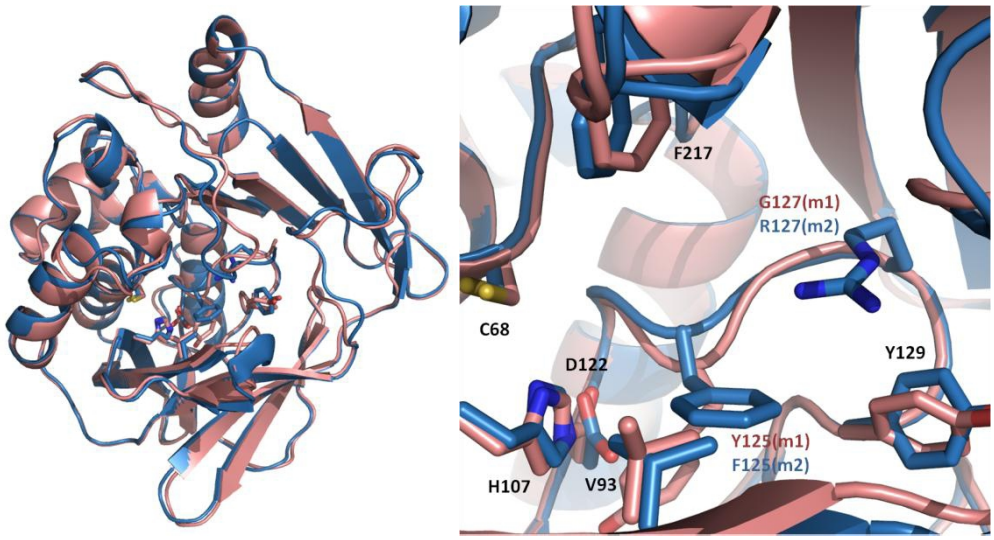


Figure V.10: Overlay of mNat2 and mNat1 structural models.

(left). Ribbon diagram showing the overlaid structural models of mNat2 (blue) and mNat1 (pink). The structures were generated and aligned using the program PyMOL (W. L. DeLano (2002) PyMOL, DeLano Scientific, San Carlos, CA). Side chains of the key residues of both the active sites are drawn in sticks. **(right)** Maximised view of the active sites of both hNAT2 and mNat1. Side chains of key residues within the active site are drawn in stick representation and labelled. Dissimilar residues are labelled in colour, m1=mNat1, m2=mNat2.

In general, modelling protein structures on the basis of existing crystals of analogous proteins with >70% sequence identity is a useful tool in virtual studies and the choice of the template structure seems to be crucial. Even though SwissModel® software offers a preliminary insight into the possible three-dimensional structure of a protein, discussions around subtle residue discrepancies using virtual models needs to be developed with appropriate precautions.

Previous research conducted by Martell et al. on mouse NATs highlighted a similarity in substrate preference between mNat1 and hNAT2, as both being uniquely able to acetylate INH in comparison to other human and murine isoenzymes (Martell et al, 1992).

Besides this, the substrate profile of mNat1 presented in this study contradicted the prior finding that SMZ was not a substrate for either murine NAT (Martell et al, 1992), but showed that SMZ could act as probe substrate for mNat1, as opposed to mNat2. These studies may help explain previous data about the absence of SMZ metabolism in *mNat1/2* knock-out clones compared to wild-type mice (Sugamori et al, 2003).

On the other hand, mNat1 is functionally different from hNAT2 as regards some other arylamine substrates with a *para*-substituent, such as 4CA, HOA and POA.

Despite the homology in arylhydrazine specificity for both hNAT2 and mNat1, this seemed not sufficent to state a functional homology between these two enzymes to the same extent as for the couple hNAT1 and mNat2. Indeed, few studies have generally been conducted on *mNat1* gene and mNat1 protein (Martell et al, 1992; Sugamori et al, 2003) and Nebert et al. previously pointed out that assigning the status of orthology to a couple of genes exclusively according to the substrate specificities of their corresponding proteins appeared inaccurate, since the isoenzymes may have differing catalytic activities (Nebert et al, 1991).

The substrate specific profiles of the recombinant mammalian mNat2 mutant enzymes involved in this study were compared to those of mNat2 and mNat1: mNat2_R127G,

mNat2_R127L, and mNat2_F125S (unpublished work of Dr Westwood).

As regards the role of Arg127 in substrate specificity of mNat2, the two Arg127 mutants of mNat2 generated in this study were successfully screened against a panel of different substrates (**Figure V.11**). Assuming that the general folding of both mutants was highly similar to that of the wild-type mNat2 for the single mutation, the loss of an Arg at position 127 drammatically was shown to decrease the acetylation of pABA and pABAglu, probe substrates for both hNAT1 and mNat2 (**Figure V.11**). This mutation conversely increases the acetylation of the arylhydrazines (INH, HDZ), which were earlier shown to be probe substrates of hNAT2 and mNat1 (**Figure V.11**).

This would imply an important role for Arg127 in discriminating between arylamines and arylhydrazines as substrates for hNAT1 and mNat2. This considerable shift in substrate specificity supports the importance of Arg127 in substrate binding, consistent with previous hypotheses (Goodfellow et al, 2000; Wu et al, 2007).

Moreover, although R127G significantly prefers HDZ (1,385μM.sec^{-1}.mg^{-1}), its rate of reaction with poor arylamine substrates, such as pABA (108μM.sec^{-1}.mg^{-1}), was found to be of the same order of magnitude to that of mNat2 for pABA as its probe-substrate (196μM.sec^{-1}.mg^{-1}). This seemed consistent with the fact that the general turnover of R127G mutant was higher than that of mNat2 (**Figure V.11**).

This could be related to the R127G mutation, in particular for the significant difference in residue side chain between an Arg and a Gly. Indeed, substituting Arg127 by a Gly was proposed to increase the three-dimensional size of the active site pocket, thereby affecting the overall catalytic rate of an enzyme.

As regards the other mutant, R127L, comparing the specific activity values of both mNat2 and R127L for their best substrates, pABA (196μM.sec^{-1}.mg^{-1}) and 4AV (82.5μM.sec^{-1}.mg^{-1}) respectively, suggested that the general turnover of R127L enzyme is lower than that of mNat2 (**Figure V.11**).

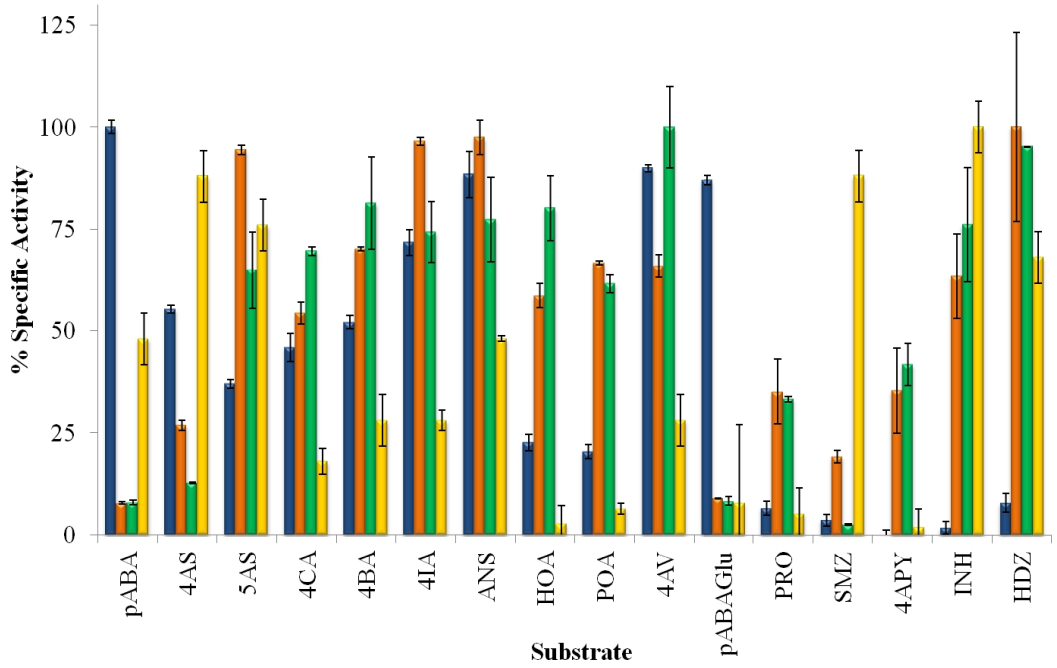


Figure V.11: Comparison of the substrate profiles of mNat2, R127G, R127L and mNat1.

The substrate specific activity profiles of mNat2 (), mNat2_R127G (), mNat2_R127L () and mNat1 () are shown. % specific activity data for mNat1 were adapted from unpublished work by Dr. Kawamura. 100% specific activity values are: 196µM.sec^{-1}.mg^{-1} for mNat2 with pABA, 1385µM.sec^{-1}.mg^{-1} for mNat2_R127G with HDZ, and 82.5µM.sec^{-1}.mg^{-1} for mNat2_R127L with 4AV. Abbreviations of the names of the chemicals used as substrates for NAT in this study are detailed in **Section II.2.5.2.1**.

F125S mutation in mNat2 partially reduces mNat2 preferences for pABA and pABAglu and augments arylhydrazine acetylation activity, without shift in activity preference from 4AS to SMZ (**Figure V.12**).

Actually, in accordance with earlier hypotheses (Goodfellow et al, 2000), the substitution F125S in hNAT1 seemed to modify the substrate preference of hNAT1 from the hNAT1-probe substrate 4-aminosalycilic acid (4AS) to another hNAT2-probe substrate, sulfamethazine (SMZ) (Wu et al, 2007). Thus, the substrate specificity of hNAT1_F125S was thought to resemble to that of hNAT2 (Wu et al, 2007).

In general, although the percentages of specific activity showed no other significant differences between the wild-type and the mutated enzyme, maximum activity rates of

mNat2_F125S were around 7.5 times lower than those of wild-type mNat2: the greatest activity of mNat2 with pABA (100%) was 196µM.sec^{-1}.mg^{-1}, whereas the maximum catalytic activity of the mutated enzyme with EOA (100%) was 26µM.sec^{-1}.mg^{-1}.

In general, F125S mutation does not significantly change mNat2 substrate preferences to mNat1 specificities, except for an higher arylhydrazine acetylation by F125S compared to mNat2 (**Figure V.12**).

This could be related to the fact that the *N*-*N* bond of arylhydrazine might be off the plane defined by the remaining aromatic atoms, as highlighted in the crystal structure of phenylhydrazine (Srinivasan & Swaminathan, 1968). Therefore, the F125S mutation might shift the catalytic preference of mNat2 for bent substrates, such as arylhydrazines, as opposed to planar arylamines.

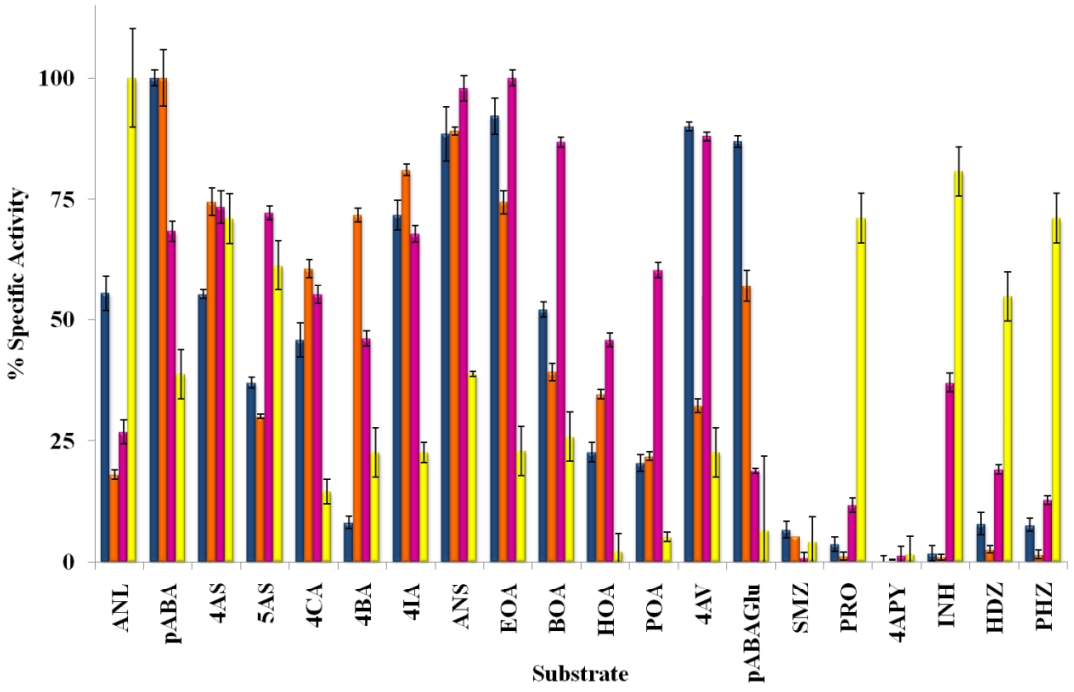


Figure V.12: Comparison of the substrate profiles of mNat2, shNat2, mNat2_F125S and mNat1.

The substrate specific activity profiles of mNat2 (■), shNat2 (■), mNat2_F125S (■) and mNat1 (■) are shown. % specific activity data for shNat2 were adapted from published work (Kawamura et al, 2005), and as regards mNat2 _F125S and mNat1, the data were obtained by Dr. Westwood and Dr. Kawamura respectively (unpublished work). Abbreviations of the names of the chemicals used as substrates for NAT in this study are detailed in **Section II.2.5.2.1**.

Finally, the substrate specificity profiles of mNat2 and shNat2 (Kawamura et al, 2005) emerged as very similar (**Figure V.12**). Moreover, The structural model of shNat2 generated on the basis of hNAT1 (Wu et al, 2007) showed an evident resemblance to the model of mNat2, which could be due to the high percentage of identity between mNat2 and shNat2 (91%), but also to the bias of using the same template (hNAT1) (**Figure V.13**). Residue Arg129 seemed to play an important role in defining both the steric configuration and the polarity of the active pocket of shNat2, as previously suggested for both hNAT1 and mNat2.

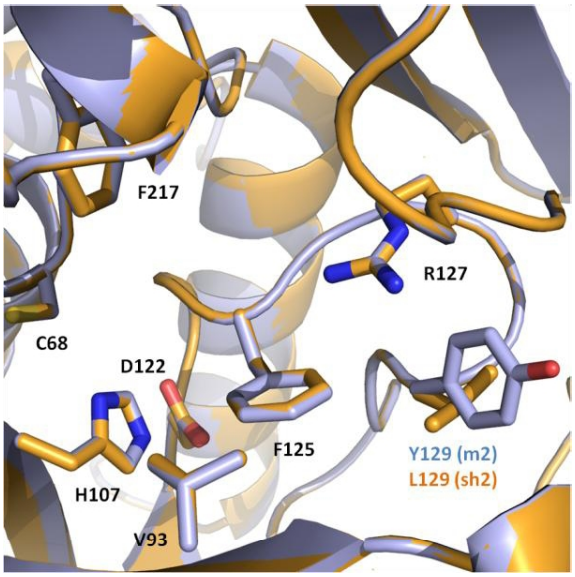


Figure V.13: Zoomed view of the active sites of mammalian NAT models: mNat2 and shNat2.

Maximised view of the active sites of both mNat2 (blue) and shNat2 (yellow). Side chains of key residues within the active site are drawn in stick representation and labelled. Dissimilar residues are labelled in colour, m2=mNat2 and sh2=shNat2.

Overall, the size of the cavity of the active site could also importantly influence the substrate specificity in addition to the steric size and the polarity of the substituents around the arene of the arylamine. Indeed, the dissimilarities amongst the key residues of the active sites of the NATs investigated would considerably modify the dimensions of the active pockets, therefore affecting the substrate specificity.

In order to present a general overview of substrate selectivity of mammalian NATs, a comprehensive three-dimensional view of all the substrate specificity profiles was realised using the software MatLab® (**Appendix 4**). The view of the xy-plane is also presented in **Figure V.14**. The view of the yz-plane is presented in **Appendix 4** in order to show accurately the height of the 100% specific acitivity columns. A separate view of each NAT substrate profile presented in this study is shown in **Appendix 2**.

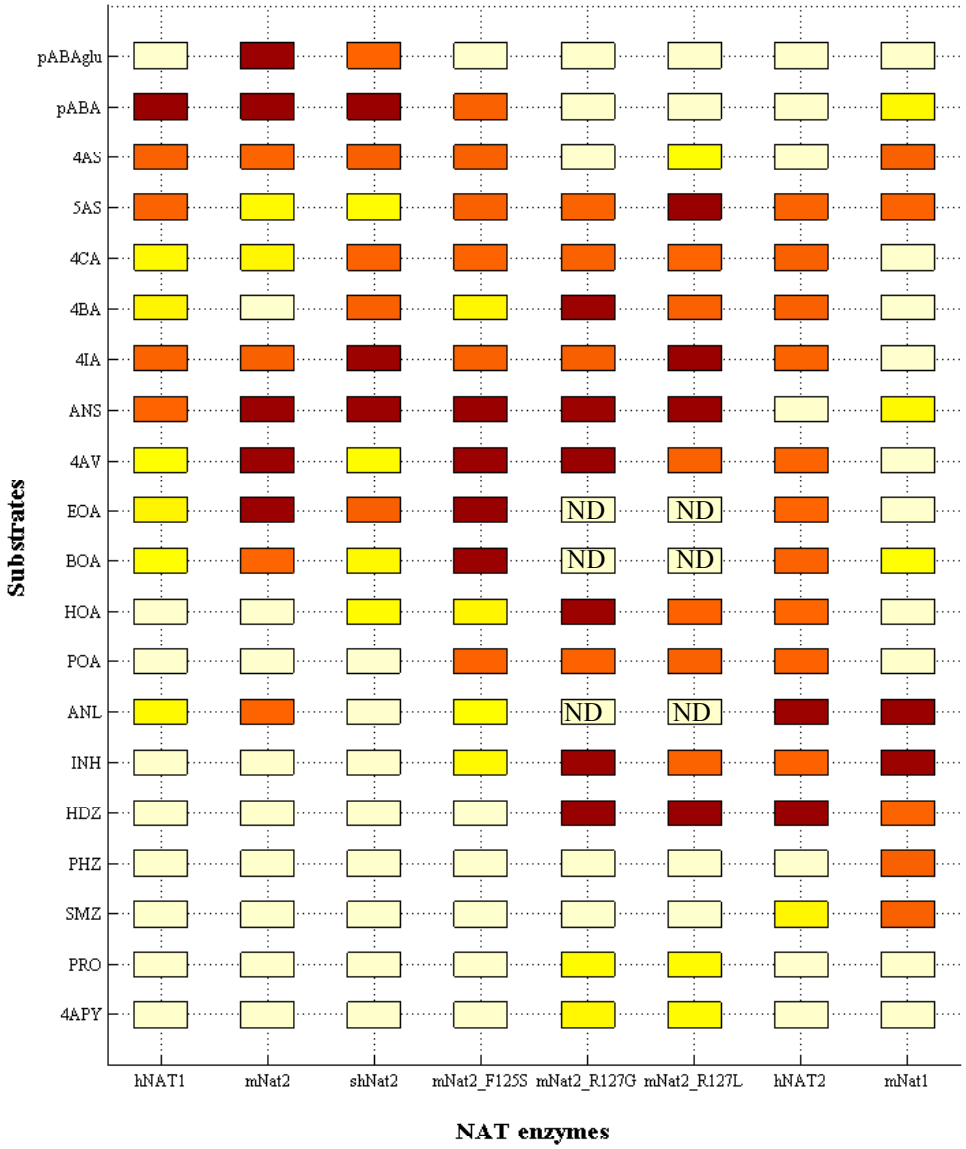


Figure V.14: Comparison of specific activity profiles of NATs investigated in this study.

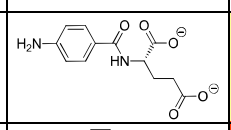
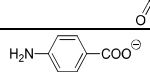
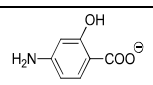
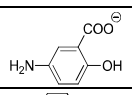
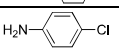
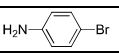
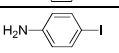
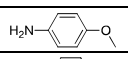
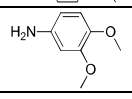
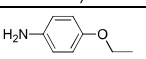
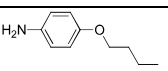
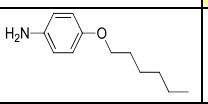
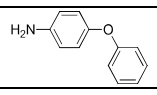
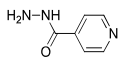
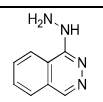
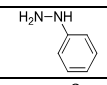
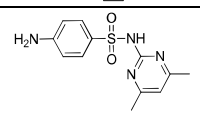
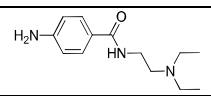
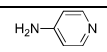
The two-dimensional view of the x-y plane is shown. ■ for 75-100%, ■ for 50-74.9%, ■ for 25-49.9%, and ■ for 0-24.9%. ND=not determined. Abbreviations of the names of the chemicals used as substrates for NAT in this study are detailed in **Section II.2.5.2.1**.

Moreover, a table relating the specific activity percentages of NAT enzymes to the chemical structures of the arylamine substrates used in this study, has been drawn with the ionic charges at the pH of enzymatic assays (pH 8.0) and the partition coefficient values (AlogP) estimated using Virtual Computational Chemistry Laboratory (Tetko et al, 2005) (**Table V.3**).

NAT enzymes were arranged starting from hNAT1 protein from *hNAT1*4* gene and aligned according to the number of residue mutations within the active site *versus* hNAT1 protein. Arylamine and arylhydrazine substrates were regrouped by their functional sub-groups and ordered according to the number of negative charges at pH 8, the electron-richness and then the size of their substituents. Then, the colour of the table cells was assigned according to the corresponding percentage of specific activity value with the appropriate NAT.

At first sight, the substrate preference, which is mainly characterised by the red cells in the table, appeared to follow a diagonal trend. In particular, the more polar the substituent(s) of the arylamine substrate, the more probable is its acetylation by hNAT1 and its homologues, mNat2 and shNat2. Conversely, less polar substituent or no substituents around the aromatic core would be associated to the preference for hNAT2, mNat1, and Arg127-mutated mNat2 enzymes.

Table V.3: Comparison of arylamine substrate profiles of different mammalian NATs in relation to the physicochemical properties of the substrates tested. Different symbols and gradual cell colours are used to show four ranges of percentage of specific activity per each substrate and enzyme: ++ for 75-100%, + for 50-74.9%, - for 25-49.9%, and -- for 0-24.9%. NAT enzymes are ordered starting from hNAT1 followed by enzymes with increasing residue substitutions within their active sites in relation to hNAT1. hNAT1 sequence corresponds to the protein generated from *hNAT1*4* gene, and hNAT2 from *hNAT2*4* gene. Ionic charges of substrates at pH 8 are shown according to pK_a values of their substituents. *References:* (Dismer et al, 2008; Szakacs & Noszal, 2006), website A: http://www.drugbank.ca/drugs/DB00233, (H.C. Brown et al, 1955; Nobilis et al, 2006), website B: http://www.chemicalbook.com/, website C: http://www.zirchrom.com/organic.htm, website D: http://web.squ.edu.om/, (Doamaral et al, 1966; Machado et al, 2002). [a]AlogP values were determined using Virtual Computational Chemistry Laboratory (Tetko et al, 2005). Abbreviations of the names of the chemicals used as substrates for NAT in this study are detailed in **Section II.2.5.2.1**.

Physico-chemical group	Group	NAT Substrate	Chemical structure	NAT enzymes (active site differences *vs.* hNAT1)								Annotations/References	
				hNAT1	mNat2	shNat2	mNat2 F125S	mNat2 R127G	mNat2 R127L	mNat1	hNAT2	pKa	AlogP[a]
				-	-	Y129L	F125S	R127G	R127L	F125Y R127G	V93F F125S R127S Y129S		
arylamine substrates with negatively charged substituents at pH 8.	folate catabolites	pABAglu		-	++	+	-	--	--	--	--	2.7 (NH_3^+), 3.6 (α-COOH), 4.7 (γ-COOH). (Zoltán Szakács and Béla Noszál, 2006)	0.110
		pABA		++	++	++	+	--	--	-	--	2.4 (NH_3^+), 1.9 (COOH) (Lukfics M. et al. 2008)	0.780
	salicylic acids	4AS		+	+	+	+	-	--	+	--	2.3 (NH_3^+), 6.0 (COOH), 13.2 (OH) (website A)	0.620
		5AS		+	-	-	+	++	+	+	-	3.0 (NH_3^+), 6.0 (COOH), 13.9 (OH) (Nobilis M. Et al., 2006)	0.750
arylamine substrates with neutral electron-rich functional substituents	halogenated anilines	4CA		-	-	+	+	+	+	--	+	3.8 (NH_3^+) (Brown H.C. et al. 1955)	1.950
		4BA		-	--	+	-	+	++	--	+	3.4 (NH_3^+) (Brown H.C. et al. 1955)	2.100
		4IA		+	+	++	+	++	++	--	+	3.8 (NH_3^+) (website B)	2.580
	alkyl- and aryl-oxyanilines	ANS		+	++	++	++	++	++	-	--	5.2 (NH_3^+) (Brown H.C. et al. 1955)	1.010
		4AV		-	++	-	++	+	++	--	+	4.7 (NH_3^+) (website B)	1.080
		EOA		-	++	+	++	ND	ND	--	+	5.2 (NH_3^+) (website C)	1.640
		BOA		-	+	-	++	ND	ND	-	+	-	1.980
		HOA		--	--	-	-	+	++	--	+	-	3.000
		POA		--	--	--	+	+	+	--	+	-	2.540
arylamine and arylhydrazine substrates without substituent	aniline	ANL		-	+	--	-	ND	ND	++	++	4.6 (NH_3^+) (Brown H.C. et al. 1955)	0.890
	arylhydrazines	INH		--	--	--	-	+	++	++	+	2.0 (NH_2^+-NH_3^+) 3.9 (NH-NH_3^+), 10.8 (pyridine) (website D)	0.170
		HDZ		--	--	--	--	++	++	+	++	7.3 (NH-NH_3+) (Machado J.D. et al., 2002)	0.660
		PHZ		--	--	--	--	ND	ND	+	--	5.25 (NH-NH_3+) (Do Amalar L. et al., 1966)	0.950
other aniline drugs		SMZ		--	--	--	--	--	-	+	-	2.4 (NH_3^+) 7.4 (sulfonamide) (website D)	0.430
		PRO		--	--	--	--	-	-	--	--	9.2 (NR_3H^+) (website D)	1.420
		4APY		--	--	--	--	-	--	--	--	5.0 (NH_3^+) (website D)	0.080

Moreover, when specific activity percentages obtained with arylamine substrates exclusively were plotted for each NAT enzyme against the AlogP values of the substrates, a varying distribution of the data points was observed on the graph. The general tendency of the spots throughout each plot was estimated by linear regression despite the relatively low R values obtained (<70%). In general, positive values of the slope of the trendline corresponded to a catalytic preference for lipophilic arylamine substrates.

The plots obtained with hNAT1 and hNAT2 are shown in **Figure V.15** as representative examples of the relationship between slope positivity and substrate lipophilicity.

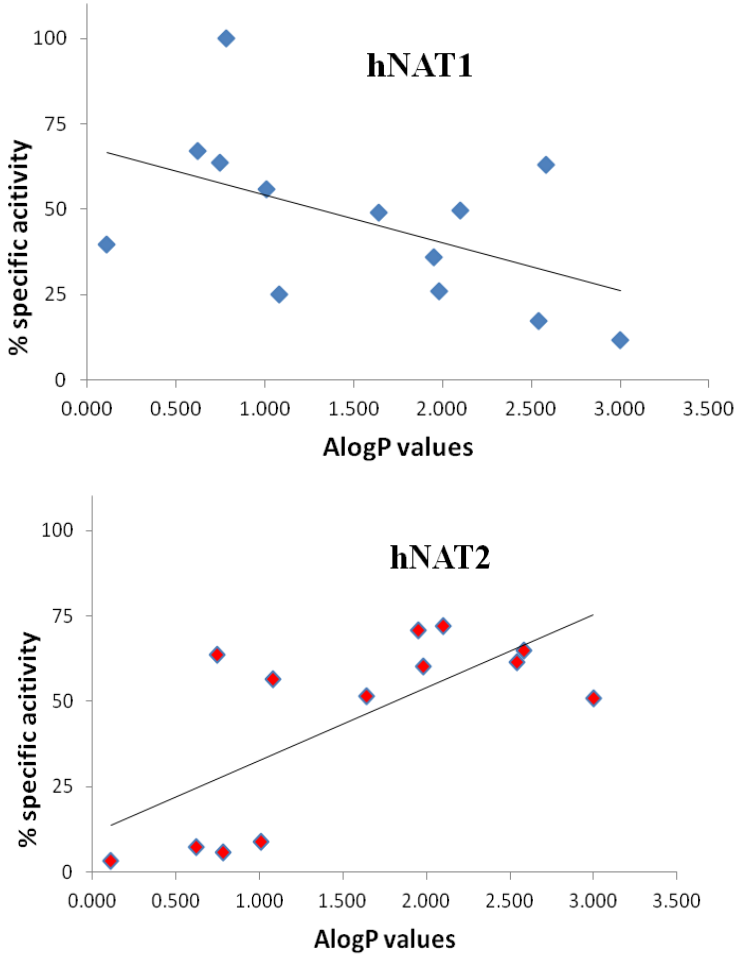


Figure V.15: Plots of percentage of specific NAT activities against the calculated AlogP value of all the substrates tested.

The percentages of specific activity are selected from previous work (Kawamura et al, 2005). AlogP values were estimated using using Virtual Computational Chemistry Laboratory (Tetko et al, 2005). R=0.37 for hNAT1, R=0.49 for hNAT2.

In the end, ordering the slope values obtained helped visualise the intricate correspondence among mammalian NAT enzymes, substrate selectivity and substrate lipophilicity (**Figure V.16**): on one hand, the homologous hNAT1, mNat2, and shNat2 prefer less hydrophobic substrates; on the other hand, hNAT2 and mNat2 mutants tend to catalyse the acetylation of more hydrophobic substrates (**Figure V.16**).

This result combined with **Table V.3** would propose that changing the main key residues of the hNAT1 active site, Arg127, significantly modifies the polar architecture of the active pocket towards a more hydrophobic conformation. Therefore, the more lipophilic the substrate, the easier it would fit within the active site of a mammalian NAT enzyme without an Arg at position 127.

As highlighted in previous paragraphs, mNat1 possesses a considerable catalytic activity towards a panel of different arylamine with less hydrophobic substituents, despite F125Y and R127G differences in mNat1 active site compared to hNAT1. This would confer a negative value to the slope of mNat1.

Moreover, the data about the substrate selectivity of the mammalian NATs tested in this study were consistent with the inhibitor selectivity of each enzyme (**Section IV.3**). In general, whilst mNat2 represents a very good model for hNAT1, mNat1 constitutes a hybrid in terms of its substrate specificity and also inhibitor properties.

This parallelism between substrate selectivity and inhibitor selectivity constitutes an important observation supporting further medicinal chemistry studies addressed to improve the selective efficiency of naphthoquinone **7** towards native hNAT1 in breast cancer cell lysates.

	NAT enzymes							
Residue	hNAT1	mNat2	shNat2	mNat2 F125S	mNat2 R127G	mNat2 R127L	mNat1	hNAT2
125	F	F	F	S	F	F	Y	S
127	R	R	R	R	G	L	G	S
129	Y	Y	L	Y	Y	Y	Y	S

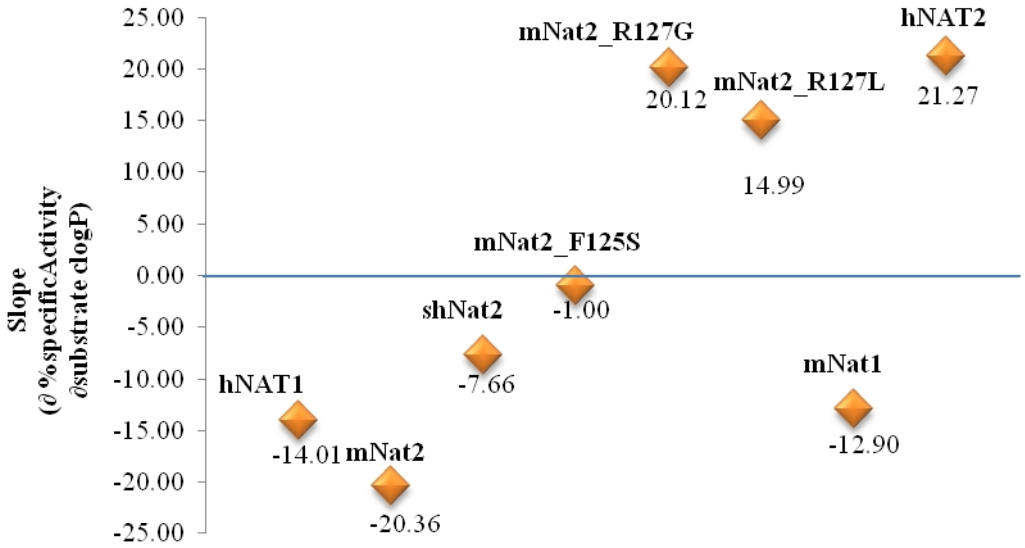


Figure V.16: Variation of NAT activity against arylamine substrate AlogP.

For each enzyme, percentages of specific activities were selected from earlier substrate profiles and were plotted against the AlogP values of the substrates tested. A linear regression was fitted in each plot, giving an estimation of the variation of the NAT activity against substrate AlogP (value under each diamond).

V.3.2 The use of different AcylCoAs by NATs

As regards the use of different Acyl donors as NAT substrates, a panel of AcylCoAs with increasing length of the acyl chains were tested with murine mNat2 and mNat1, detecting both the AcylCoA hydrolysis and the arylamine acetylation in the enzymatic assays.

Both murine enzymes were only able to transfer an acyl chain of maximum 3 carbon units from the acyl donor to the aromatic amine. Conversely, human NATs could hydrolyse AcylCoA co-factors with more than 3 carbon atoms up to 6, but this was not proved to correspond to a concomitant acylation of the arylamine substrate (Kawamura

& Sim, 2005).

Moreover, all prokaryotic NATs tested could also hydrolyse the thioester group of *n*-propionylCoA and presumably transfer the acyl chain to the aromatic amine of 5AS.

Moreover, whilst all bacterial NATs preferred AcCoA, some of them possessed a catalytic activity with *n*-propionylCoA higher than 40% relative to the AcCoA activity.

In particular, PANAT could hydrolyse *n*-propionylCoA at a very high rate in comparison to the AcCoA hydrolysis rate (80%) (**Table V.4**). The high activity of this prokaryotic NAT compared to the other bacterial NATs tested could be due to differences in size, shape and recognition properties of their respective active sites.

Table V.4: Comparison of acetyl transfer and *n*-propionyl transfer activities by NATs.

NAT enzyme	mNat2	mNat1	STNAT	MMNAT	MSNAT	PANAT	TBNAT
Activity ratio (*n*-propionylCoA/AcCoA)	0.25	0.53	0.26	0.69	0.47	0.80	0.57

Amongst the resolved structures of prokaryotic NATs, only one structure, MMNAT, was obtained in complex with CoA within the active site cleft (Fullam et al, 2008), while STNAT (Sinclair et al, 2000), MSNAT (Sandy et al, 2002), and PANAT (Westwood et al, 2005) were purely crystallised as apoenzymes (**Figure V.18**).

Comparing the zoomed view of the catalytic pocket of all four bacterial NATs tested, the size of the active site entrance of PANAT is slightly larger (**Figure V.18**). This could help accommodate a longer acyl chain, like in *n*-propionylCoA, and increase the catalytic AcylCoA turnover, in comparison with other NATs.

The evidence that all NAT enzymes were also able to use *n*-propionylCoA as a substrate could either be due to the ability of all bacterial NAT enzymes to provide the adequate space into their active site pocket for an additional carbon in the acyl chain, or suggest a new potential role for NAT enzymes in relation to propionate metabolism.

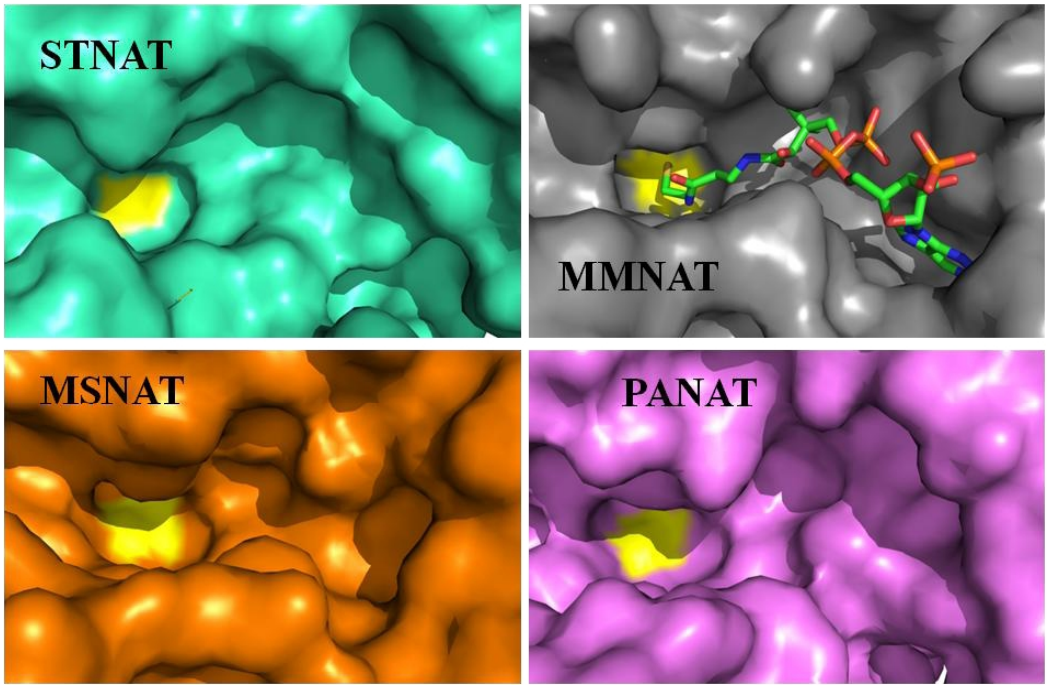


Figure V.17: Zoomed view of the active site pocket of four bacterial NAT structures.

The active sites of four bacterial Nat enzymes are shown in surface representation. The catalytic Cys is labelled in yellow. The pdb codes for the structures used are as follows: 1E2T (STNAT) (Sinclair et al, 2000), 2VFC (MMNAT) (Fullam et al, 2008), 1GX3 (MSNAT) (Sandy et al, 2002), 1W4T (PANAT) (Westwood et al, 2005). The figures were generated with the program PyMOL.

From *in vitro* studies, TBNAT was previously found to possess higher affinity for *n*-propionylCoA than for AcCoA and was hypothesised to increment the cholesterol catabolism by increasing *n*-propionylCoA hydrolysis turnover: this would help maintain a regular homeostasis of *n*-propionylCoA (Lack et al, 2009) in the context of the cell wall synthesis.

This could be extended to other mycobacterial NATs, like MSNAT, which were earlier found to play a role in endogenous metabolism leading to cell wall synthesis (Bhakta et al, 2004).

A similar hypothetical role could also be assigned to the other two prokaryotic NATs tested, whose function in xenobiotic metabolism was strongly supported by their catalytic reaction with arylamines, but whose physiological role has not been defined yet.

n-propionylCoA could be mostly originated from the degradation of odd-chain fatty acids, highly present in bacteria (Rezanka & Sigler, 2009), and following three enzymatic reactions could be converted into succinylCoA which could then enter into the citric acid cycle (Berg et al, 2007). *n*-propionylCoA might constituted the link between these two processes, the odd-chain fatty acid degradation and Krebs cycle. NAT could then make the connection between the two physiological chain of reactions, by regulating the homeostasis of *n*-propionylCoA.

In respect of mammalian species, *n*-propionylCoA mainly constitutes the end product of the metabolism of odd-chain and methyl-branched fatty acids together with AcCoA. It is also a metabolite of the aminoacids valine, isoleucine, and methionine (Berg et al, 2007). The conversion of *n*-propionylCoA into succinylCoA occurs following three catalytic reactions, as in bacteria, and the final product could enter the Krebs cycle to generate energy for cells. Also in this case, the regulation of the amount of *n*-propionylCoA could help maintain the suitable balance between the fatty acid degradation and the aerobic production of energy in cells.

The fact that all mammalian NATs tested in this study, as well as in previous investigation, are also able to hydrolyse *n*-propionylCoA could support new significant perspectives about their physiological role, in particular for those enzymes whose endogenous role had only been hypothesised, but not defined, for instance hNAT1.

Chapter VI:

Applying compound 7 for detection and targeting of hNAT1 in breast cancer cells



DIANA AND HER NYMPHS SURPRISED BY SATYRS (1638-1640), BY SIR PETER PAUL RUBENS (1577-1640).

The woman lying on her back at the first level of representation presents a breast with a skin dimpling and an inward retraction of the entire breast, which has been interpreted as a breast tumour (Grau et al, 2001b) (Palacio del Buen Retiro, Madrid, Spain).

VI.1 Introduction

The work presented in chapters 3 and 4 underlined the selectivity of compound **7** for hNAT1 and mNat2 compared to a panel of prokaryotic and eukaryotic NAT isoenzymes, and also explained the molecular mechanism of the interaction between the chemical ligand and hNAT1 and mNat2 pure proteins.

However, native proteins are found in complex mixtures and hNAT1 is a cytosolic enzyme. Its overexpression in ER+ve BC cells was underlined by Adam et al. (Adam et al, 2003) and its detection using naphthoquinone colourimetric probes could be a useful tool for BC diagnosis and prognosis.

The questions addressed in the work presented in this chapter are:

- Would compound **7** inhibit hNAT1 in tumour cell lysates despite the rich diversity and abundance of other proteins and biomacromolecules within a cellular environment?
- Would compound **7** be sensitive enough to undergo a visible colour change upon binding to hNAT1 in BC cell lysates?

Subsequently, further questions will arise *vis-à-vis* the possible effect that compound **7** could have towards intact BC cells:

- Would compound **7** permeate intact cells to recognise selectively hNAT1?
- Would compound **7** be able to affect cell viability and BC cell growth in cellular cultures?

Previous studies on the hit-compounds identified from the secondary HTP screening, namely naphthoquinone **1** and rhodanine **5** (Russell et al, 2009), found that compound **1** was not cytotoxic up to $10\mu g.ml^{-1}$(Crawford, 2007), whilst compound **5** showed significant cytotoxicity at $10\mu g.ml^{-1}$(Russell et al, 2009) towards mouse macrophage cells.

Therefore, it was considered necessary to undertake enzymatic inhibitory assays with

the lead compound **7** using hNAT1 in a BC cell lysate, along with cellular studies, including cell viability and cell proliferation tests.

AIMS

The aim of the work presented in this chapter was to investigate the inhibitory effect of compound **7** towards breast tumour cells, through the following series of approaches:

- immuno-chemical estimation of hNAT1 content in the BC cell line, ZR-75-1, to establish the quantity of the protein in cell lysates;
- inhibitory characterisation of compounds **1** and **7** towards native hNAT1 expressed in the same BC cell line;
- effect of compound **7** on the growth of different cell cultures.

VI.2 Results

VI.2.1 Estimation of hNAT1 in ZR-75-1 cell line

Previous studies highlighted that ER+ve BC cell line ZR-75-1 over-expressed hNAT1 compared with other BC cell lines including ER-ve BC cell lines (Wakefield et al, 2008b). It was therefore important to quantify the amount of hNAT1 per cell in order to better estimate the potential of compound **7**, as a colourimetric probe of hNAT1 in lysates, and to ascertain the level of optimisation required.

A polyclonal antipeptide antiserum (serum 195) was previously raised against the C-terminal decapeptide of hNAT1 (Loehle et al, 2006), and was found to be isoenzyme specific in relation to the other human isoform, hNAT2 (Stanley et al, 1996; Wakefield et al, 2008a). Therefore, the antibody was used for detecting hNAT1 in ZR-75-1 lysates. The antibody was found to detect also mNat2 which has an identical C-terminal decapeptide compared to hNAT1 (Stanley et al, 1998).

Firstly, in order to verify whether the binding of the antibody from antiserum 195 to pure recombinant mNat2 was also specific for native hNAT1, a western blot was performed with both pure recombinant mNat2 and ZR-75-1 tumour cell lysates. A single band at ~34kDa was observed for all the samples loaded on the gel, assuming that he recognition of both mNat2 and hNAT1 by the antibody was concentration-dependent and the affinity for both target proteins was similar.

Considering the isoenzyme selectivity of the antibody for both recombinant and native mNat2 and hNAT1 (Stanley et al, 1998; Stanley et al, 1996) and assuming equivalent molecule recognition of the two proteins by the antibody, the distinct band visualised at ~34kDa in the BC cell lysate would suggested that there was no significant non-specific cross-reactivity of other proteins in the cell lysate with the antibody.

Moreover, previous studies have shown that the antibody 195 does not recognise hNAT2 and ZR-75-1 cell line does not express significant amounts of hNAT2 (~34kDa) (Stanley et al, 1996; Wakefield et al, 2008a). Moreover, in normal breast tissue hNAT2 is very low expressed (Williams et al, 2001). Therefore, the band at 34kDa can be considered to be hNAT1 and a rough calculation of the amount of hNAT1 in the cell lysate was performed.

In preparing lysate, approximately $5x10^7$ cells were lysed in one ml of lysis buffer. Assuming a linear relationship between the intensity of the bands and the levels of antibody binding in western blot, samples with similar intensity were compared. Comparing the band intensities in Lanes 3 and 6 suggested that less than 60ng.µl^{-1} of hNAT1 was present in ZR-75-1 cell lysates. (**Figure VI.1-left**).

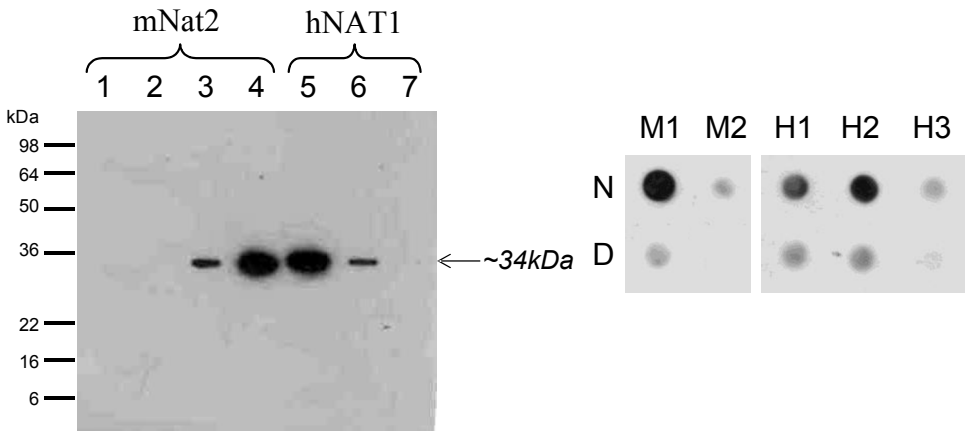


Figure VI.1: Detection and quantification of hNAT1 in ZR-75-1 cell lysate.

(left) Detection of purified recombinant mNat2 and hNAT1 in cell lysate by Western Blotting. Molecular weights and positions of the protein bands in the SeeBlue® Plus2 Pre-Stained Standard used are shown on the left. **Lanes: 1-4**, 0.1, 1, 5 and 10ng mNat2; **5-7**, 10, 100 and 1000 fold diluted cell lysate. **(right)** Detection of mNat2 and hNAT1 in cell lysate by dot blotting as native and denatured proteins. Native protein samples (**N**) were dissolved in an equal volume of buffer (200mM Tris (pH 8.0)), while denatured proteins (**D**) were prepared in an equal volume of buffer with 2% SDS and boiling at 95 ºC for 5min, then the temperature was restored at 37 ºC. **Lanes: M1**, 0.031ng.µl^{-1} mNat2; **M2**, 0.0078ng.µl^{-1} mNat2; **H1**, 100 fold diluted cell lysate; **H2**, 500 fold diluted cell lysate; **H3**, 2500 fold diluted cell lysate.

Subsequently, since the recognition was highly specific, dot-blotting studies as opposed to SDS-PAGE were carried out, varying the amounts of pure recombinant mNat2 and ZR-75-1 cell lysates, in both native and denatured conditions (**Figure VI.1-right**).

The results of comparing native and denatured protein samples indicated that the anti-body had a higher affinity for native hNAT1 rather than denatured hNAT1, which was consistent with previous studies (Johnson & Sim, 2001).

In comparing samples with apparent similar intensity, more than 20ng of hNAT1 per µl of lysate was found in the ZR-75-1 cell lysate (**Figure VI.1-right**). Thus, a range of 0.42-1.26µg of hNAT1 would be estimated per million cells, meaning roughly 1pg of NAT per cell. In terms of concentration values, a range of 0.59-1.17 µM of hNAT1 in the lysate preparation was able to be used for subsequent biochemical studies (**Table VI.1**).

The total protein concentration in cell lysates was estimated by Bradford assay as 11.5µg.µl^{-1}. Hence, the concentration of hNAT1 was estimated to be about 0.17-0.52% of total protein in the cell lysate (**Table VI.1**).

Table VI.1: Different estimations of the amount of hNAT1 in ZR-75-1 cell lysates.

Unit of measurement	Value
ng of hNAT1 perµl of cell lysate	20-60
µM of hNAT1 in cell lysate preparation	0.59-1.17
µg of hNAT1 per million cells	0.42-1.26
pg of hNAT1 per cell	~1
million molecules per cell	~17.7
percentage of hNAT1 in the cell proteome	0.17-0.52%

In order to move forward in studying the effect of the lead compounds **1** and **7** towards hNAT1, standard enzymatic assays with pABA, as arylamine hNAT1-probe substrate, and AcCoA were performed in the presence of a pre-determined amount of ZR-75-1 cell lysate, as a source of hNAT1, as established through optimisation of the assay.

Two techniques were used: the detection of AcCoA hydrolysis with DTNB in the presence of an arylamine substrate and the detection of the amount of non-acetylated arylamine with DMAB. Both techniques gave equivalent results, contradicting a concern that other possible reduced molecules in the lysate might react with DTNB.

Our studies confirmed that the very small amount of lysate introduced in the assay, 10µl of a 50-fold diluted lysate in 100µl of reaction mixture, allowed an accurate detection of the initial rate of AcCoA hydrolysis by hNAT1. The initial velocity followed a linear trend for the period of time that the enzyme was tested (**Figure VI.2-top**).

Using Lineweaver-Burk plots, the apparent kinetic constants for hNAT1 in ZR-75-1 cell lysates, with pABA as substrate, were determined, consistent with the Michaelis-Menten behaviour of the enzyme (**Figure VI.2- middle & bottom**). Apparent V_{max} for hNAT1 was 24.2µM.min^{-1}, and K_m value was calculated as 126.8µM.

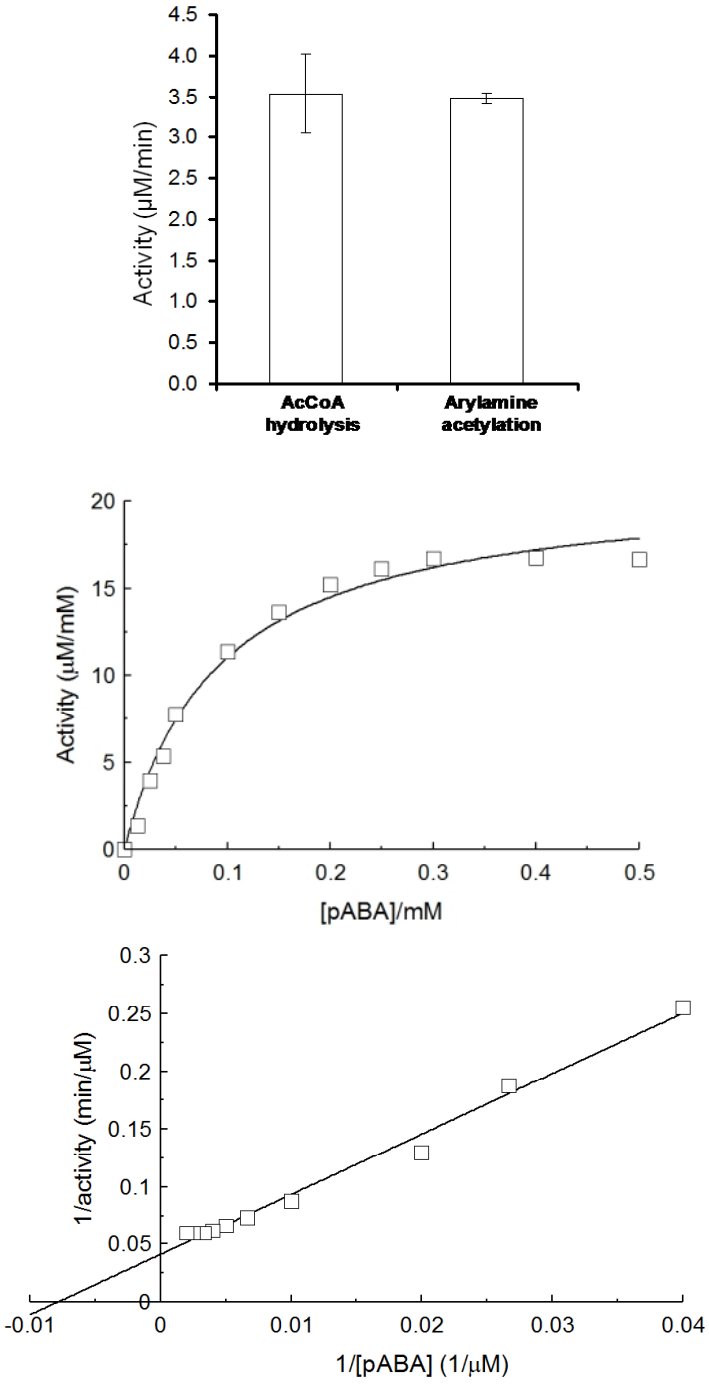


Figure VI.2: Enzymological characterisation of native hNAT1 from BC cell lysate.

(top) Comparison of AcCoA hydrolysis and arylamine acetylation methods in determination of NAT activity. Results were expressed as mean ± standard deviation from triplicates. 10µl of a 50-fold diluted lysate and 150 µM pABA were mixed in the assay and subsequently incubated for 5 min at 37°C. 400 µM AcCoA was added in order to start the reaction. **(middle)** Michaelis-Menten curve drawn after measuring initial velocities of assays containing hNAT1, 400 µM AcCoA, and different concentrations of pABA (0, 12.5, 25, 37.5, 50, 100, 150, 200, 250, 300, 400 and 500µM) in 20mM Tris.HCl buffer (pH 8.0). **(bottom)** Lineweaver-Burk plot drawn using values from Michaelis-Menten curve.

Since quantification experiments estimated, on average, 40ng of hNAT1 per µl of ZR-75-1 cell lysate and 10µl of a 50 fold diluted lysate were used in 100µl of reaction mixture, the apparent V_{max} became 3025µM.min^{-1}.µg^{-1} of hNAT1.

VI.2.2 Inhibitor study on ZR-75-1 breast cancer cell line

After estimating the approximate amount of hNAT1 in ZR-75-1 cell lysates and validating that native hNAT1 is active in cell lysates, both lead compounds, **1** and **7**, were tested in order to check their inhibitory activity against hNAT1 in cell lysates.

Since inhibitors **1** and **7** were soluble in DMSO and 5% DMSO was present in all inhibitory assays, preliminary enzymatic assays were initially performed to check whether DMSO could affect the stability and the measurement of hNAT1 activity in cell lysates by the AcCoA hydrolysis method. DMSO at 5% affected the activity of hNAT1 present in the ZR-75-1 cell lysate by ~30% (**Figure VI.3-left**). As DMSO was needed to dissolve the inhibitors, 5% DMSO was then used with a compromise of a slight drop in hNAT1 activity.

1 and **7** were tested in order to determine whether they would be able to exert inhibition towards native hNAT1 within a complex cellular environment, such as ZR-75-1 cell lysate. Both compounds had an inhibitory effect on hNAT1 activity, with **7** being a slightly better inhibitor than **1**. At 5µM, **7** inhibited hNAT1 by 94%, while **1** inhibited the enzyme by 74% (**Figure VI.3-right**).

This confirmed the inhibitory potency of this family of naphthoquinones as selective inhibitors of hNAT1 also in BC cell lysates, in contrast with other hNAT1 selective inhibitors which worked exclusively with pure recombinant proteins but not in cellular mixtures (Russell et al, 2009).

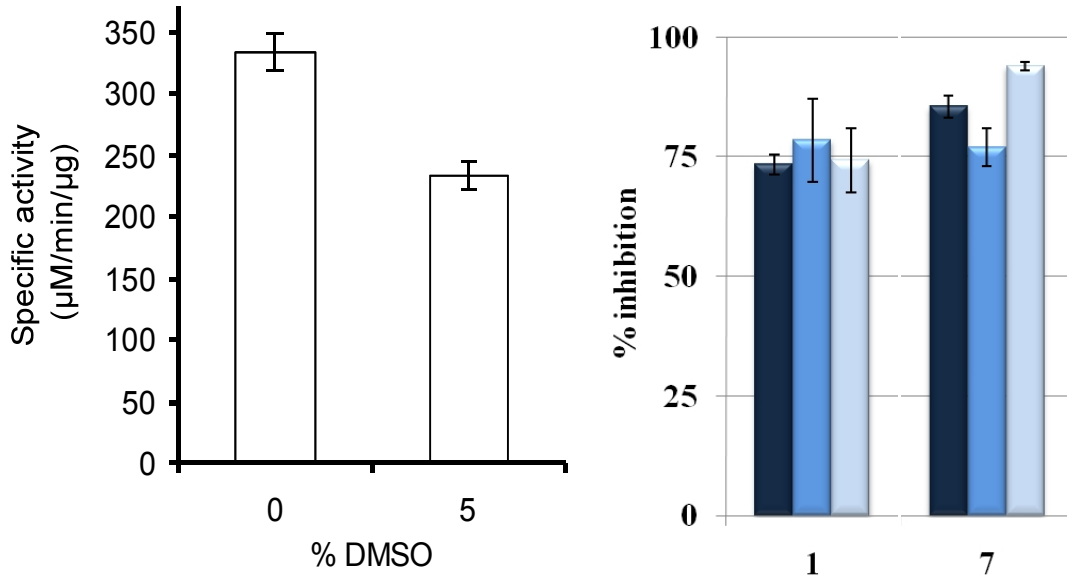


Figure VI.3: Enzymatic assays with hNAT1 in the presence of naphthoquinones 1 and 7.

(left) Effect of DMSO on hNAT1 in ZR-75-1 cell lysate. The activities were determined by the AcCoA hydrolysis assay. The substrate pABA was added to a final concentration of 500µM. The reaction was initiated with AcCoA at a final concentration of 400µM. Results were expressed as mean ± standard deviation from triplicates. **(right)** Screening of **1** and **7** (5µM) against pure mNat2 (9ng, dark blue columns), hNAT1 in *E. coli* cell lysate (300 fold diluted *E. coli* lysate blue columns), and hNAT1 in BC cell lysate (2000 fold diluted ZR-75-1 BC cell lysate, light blue columns). NAT activity was determined as acetylation of pABA, 500µM, in the presence of AcCoA, 400µM. Results were expressed as mean ± standard deviation from triplicates.

After estimating the amount of hNAT1 in ZR-75-1 BC cell lines and validating the significant effect of compound **7** on hNAT1 activity within a complex cellular microenvironment, several trials of obtaining spectra of cell lysates in the presence of compound **7** were carried out.

In previous studies, **7** was incubated with a two-fold excess of pure recombinant hNAT1, under which conditions compound **7** turned from red to blue. The concentration of native hNAT1 in the ZR-75-1 lysate was estimated on average as 1.18µM. Hence, to retain the same ratio (1:2), compound **7** was used at a final concentration of 0.5 µM in 400µl of ZR-75-1 cell lysate.

The visible spectrum was, however, overwhelmingly dominated by the tail of the protein peak at 280 nm from the high overall protein content of the sample, such that it obscured detection of 0.5 μM of **7** (**Figure VI.4**). When corrected for the baseline, the spectrum looked like a noisy flat line and no useful information could be obtained.

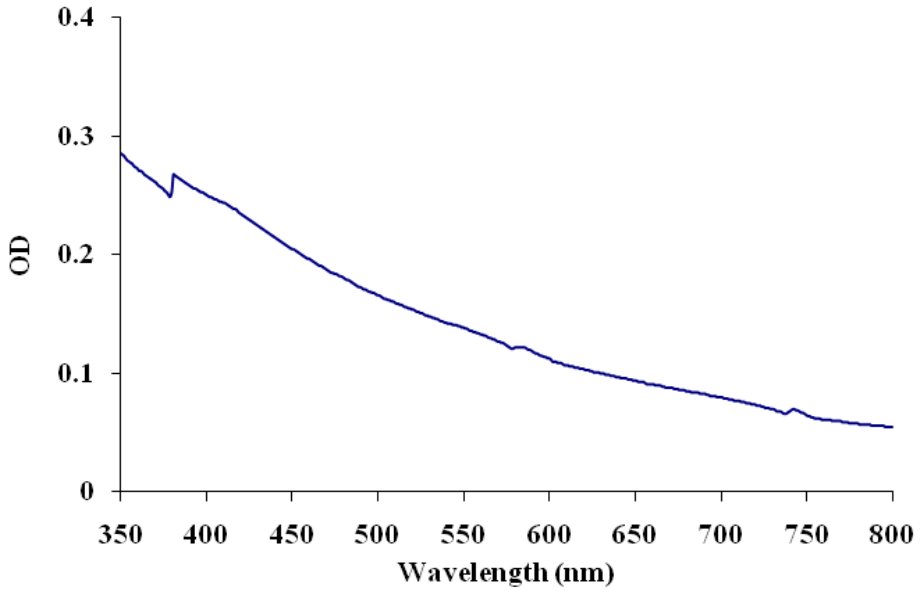


Figure VI.4: Spectrophotometric study of compound 7 in ZR-75-1 cell lysates.

Visible wavelength scan from 800 to 350 nm of **7** (0.5 μM final concentration) incubated with 399.5μl of ZR-75-1 cell lysate.

Thus, assuming that an acid-base proton exchange and a concomitant colour shift from red to blue occurred when **7** bound to hNAT1 active site according to the mechanism described in **Chapter IV**, the colour intensity of **7** and the concentration of hNAT1 in the lysate did not allow a successful observation of the colour change of **7** within this complex mixture.

In order to identify the scale of the problem to detect hNAT1 by eye using naphthoquinone inhibitors, different theoretical scenarios were established.

This study was based on three elements: the equation underlying the dissociation reaction of the complex hNAT1-**7** (P:**7**) (**Equations VI.1 & VI.2**), the range of hNAT1

concentrations in ZR-75-1 cell lysate (0.59 - 1.77μM), and the molar extinction coefficients (MECs) of compound **7**, 14,336 $M^{-1}.cm^{-1}$ at 514 as unbound ligand (red species) and 14,215 $M^{-1}.cm^{-1}$ at 625 nm as ligand complexed to mNat2 (blue species), as estimated following studies presented in **Chapter III**.

$$\text{hNAT1-7 (P:7)} \overset{K_d}{\rightleftharpoons} \text{hNAT1 (P)} + \mathbf{7}$$

Equation VI.1: Dissociation reaction of the complex hNAT1-7.

$$K_d = \frac{[P]\cdot[7]}{[P:7]}$$

Equation VI.2: Definition of K_d constant.

Three different scenarios are illustrated in **Table VI.2**, wherein a range of K_d and MEC values of the ligand were considered.

Initially (scenario A, **Table VI.2**), supposing that the dissociation constant value between hNAT1 and **7** could be estimated from an average K_d value determined for the complex mNat2-**7** in **Chapter III** (7.95μM), the concentrations of both protonated and deprotonated species of **7** were calculated when 1 μM of **7** was ideally incubated in 400μl of ZR-75-1 cell lysate. The OD of the red species would be predominant, even though the ligand bound to the enzyme could turn to blue.

In order to improve the detection of hNAT1 by the colourimetric probe **7**, two properties of the ligand **7** needed to be addressed: the affinity of **7** for the enzyme, as would be determined by the K_d value, and its colour intensity, as determined by the MEC values of **7** as both unbound and complexed forms.

In scenario B (**Table VI.2**), the dissociation constant was diminished several folds up to 1 nM and this would allow in theory to bias the equilibrium in favour of the blue species, thus a lower concentration of the probe would be required in order to give detectable colour change. Indeed, a decrease in K_d value to the nM range would result in a

preponderance of the blue species rather than the red species in the assay. However, with compound **7** the absorbance values would remain too low to be accurately detectable either by eye or by a spectrometer. Indeed, the MECs of the red and blue species of compound **7** would result in OD values lower than 0.1 for the blue species at the levels of hNAT1 in the cell lysate. Improvements in detection would be observed when the MECs of both species of analogue of **7** were increased by a factor of 10 at least, provided that K_d is in a nM scale (scenario C, **Table VI.2**).

Table VI.2: Prediction for optimal affinity and colour intensity of the ligand.

Concentrations values of hNAT1in ZR-75-1 cell lysate were previously estimated using western and dot blots (**Section VI.2.1**). Following the formation of the complex hNAT1-ligand according to the equilibrium $\text{hNAT1-ligand} \overset{K_d}{\rightleftharpoons} \text{hNAT1} + \textbf{ligand}$, concentrations of both bound and unbound species of the ligand were estimated. The corresponding OD for each species in the assay was estimated using molar extinction coefficient values of compound **7** measured from standard curves: 14,336 $M^{-1}cm^{-1}$ at 514 nm for red species and 14,215 $M^{-1}cm^{-1}$ at 625 nm for the blue complex mNat2-**7**. The predominant OD value in each case is highlighted in bold.

hNAT1 ($ng.\mu l^{-1}$)	[hNAT1] (µM)	K_d (µM)	7 (µM)	$OD_{th.}$ Protonated Ligand (red species)	$OD_{th.}$ Deprotonated Ligand (blue species)
Scenario A:	**Actual characteristics of 7 and cell lysate of ZR-75-1 cells**				
20	0.59	7.95	1	**0.0134**	0.0025
40	1.18	7.95	1	**0.0126**	0.0028
60	1.77	7.95	1	**0.0119**	0.0038
Scenario B:	**Effect of improved affinity (K_d) using compound 7 ***				
40	1.18	0.1	1	0.0030	**0.0111**
40	1.18	0.01	1	0.0006	**0.0134**
40	1.18	0.001	1	0.0001	**0.0139**
Scenario C:	**Effect of improved molar extinction coefficient of the ligand ****				
40	1.18	0.1	1	0.0295	**0.1112**
40	1.18	0.01	1	0.0062	**0.1340**
40	1.18	0.001	1	0.0008	**0.1392**

* modelled using spectrophotometric characteristics of **7** as both unbound and mNat2-complexed species

** modelled using tenfold MEC values of **7** as both unbound and mNat2-complexed species.

Achieving these improvements in the colourimetric and biochemical characteristics of an analogue of **7** would considerably facilitate the spectrophotometric recognition of the colour change event generated following formation of the complex hNAT1-ligand, thereby enabling eye visible detection of the biomarker.

Hence, the required characteristics of an analogue of compound **7** were defined as follows to allow colour change to be detected by eye in its interaction with hNAT1 in BC cell lysate:

- compound should change colour upon binding to hNAT1;
- compound should have a K_d for hNAT1 in a nM range;
- compound should have a molar extinction coefficient of at least 150,000$M^{-1}cm^{-1}$ in both protonated and deprotonated states.

A preliminary optimisation of compound **7** in accordance with these criteria will be described in the following chapter.

VI.2.3 Effect of compound 7 on growing cell cultures

VI.2.3.1 Cellular intake of compound 7

hNAT1 is found in the cytosol of the cells (Weber & Hein, 1985), and if compound **7** is to inhibit hNAT1 in tumour cells, it needs to be able to penetrate the cell prior to binding to the enzyme.

Conventional techniques for cell uptake experiments with drugs have used radiolabelled compounds or HPLC/LC-MS detection techniques in order to assess the amount of compound in both intracellular and extracellular environments. Since compound **7** was detectable and quantifiable with a spectrometer, the colourimetric estimation of **7** was considered as a helpful characteristic in determining whether **7** would penetrate cells.

In order to establish whether **7** would be able to penetrate eukaryotic cells, lymphoblastoid Raji cells derived from Burkitt lymphoma cells were chosen for this experiment as models for eukaryotic cells. The general, low levels of hNAT1 expression in lymphocyte cell lines (Coroneos & Sim, 1993; Cribb et al, 1995; Kelly & Sim, 1991) supported the choice of the lymphoblastoid Raji cell line, in order to avoid any bias due to compound **7** changing colour upon binding to native hNAT1 in the cytosol.

Cultures of Raji cells were grown and then incubated with compound **7** for 15 min at 37°C. The short period of time was estimated to be adequate to allow compound **7** to permeate cell membranes without possible cytotoxic effects. Checking cell cultures under an inverted microscope (x40) showed no difference in cell shape, and measuring cell viability by trypan blue exclusion verified that cell numbers did not change. Cell viability was higher than 95%, even though 0.5% DMSO was present in the mixture.

Two different protocols were defined in order to separate the extracellular medium from cells (**Section II.2.8.3.1**). In a first trial, a final red cell pellet and a colourless supernatant were obtained after spinning the cells (14,000×g for 5min), which suggested that the compound was able to bind tightly to cells (**Figure VI.5**).



Figure VI.5: Cell pellet and colourless supernatant observed after centrifugation of Raji cells incubated with 7.

In order to find out whether **7** could be dissociated from the extracellular fluid, a second attempt was performed with cells and medium centrifuged through an equivalent vol-

ume of mineral oil (100µl) (**Figure VI.6**): this technique has been used in order to separate intact cells from the bathing medium (Sim & Sim, 1981; Stahl et al, 1980). However, compound **7** was soluble in mineral oil, the organic phase was red, and the cellular pellet under the oil was also red, suggesting a strong interaction between **7** and cells.

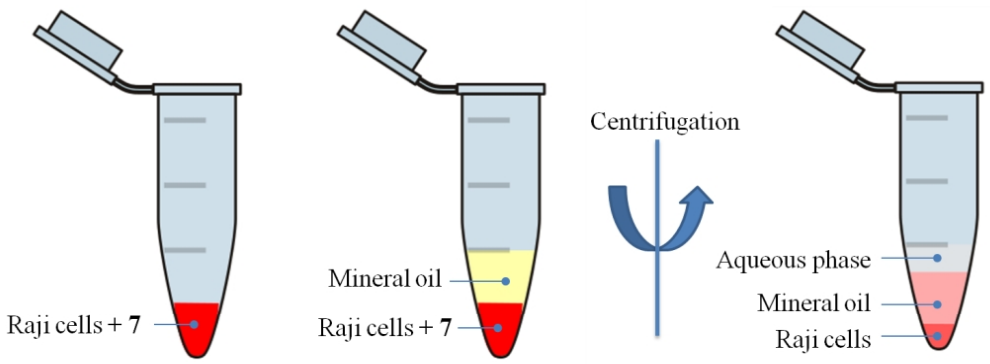


Figure VI.6: Schematic representation of the technique used to extract extracellular compound 7.

A suspension containing Raji cells (150µl) was incubated for 15 min at 37°C with 4µl of 20mM compound **7** (~2.5% DMSO (v/v)). Incubated cells were layered on 150µl mineral oil and centrifuged at 14,000 *g* for 1 min. The aqueous supernatant and the oil layer were separated.

In order to estimate the amount of **7** in the cytosolic fraction by spectrophotometry, the separation of the soluble fraction from the unsoluble fraction in cells was required.

The cell pellets obtained from these two trials were separately lysed by resuspending cells in PBS buffer with 5% DMSO (v/v). Following centrifugation, the cell debris pellet was still visibly red in both trials (**Figure VI.7**) and the soluble fraction appeared almost colourless. This soluble fraction was scanned from 800 to 326 nm with the aim of estimating the amount of naphthoquinone **7** in cytosol (**Figure VI.7**). However, no peak was observed in the visible spectrum, except a high baseline noise due to the complex mixture of cellular components (**Figure VI.7**). Finally, in order to extract the compound **7** bound to cell debris, the cell pellet was then resuspended in pure DMSO and centrifuged. The liquid phase became red and the solid pellet was clear, consistent with

compound **7** binding to hydrophobic components of the cells, possibly to the cell membrane (**Figure VI.7**).

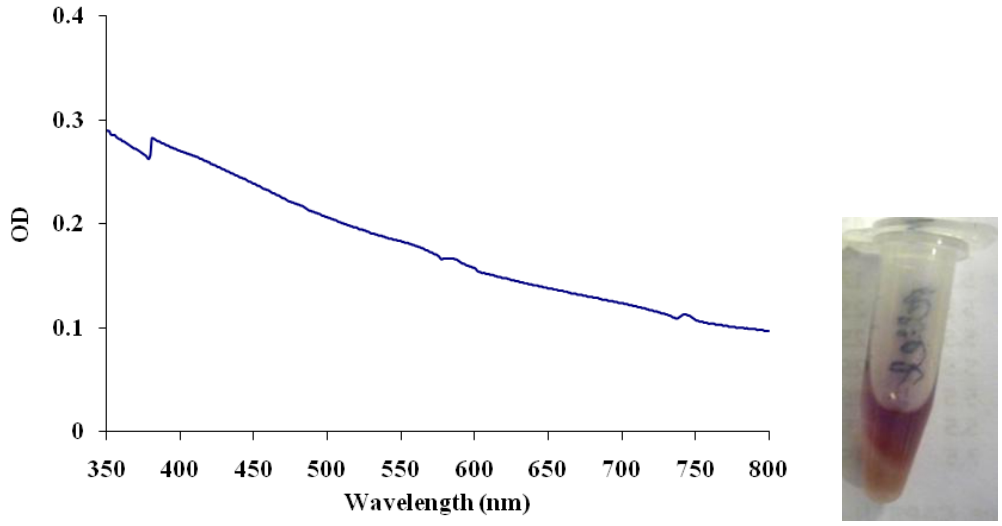


Figure VI.7: Experimental results on cellular intake of compound 7.

(left) Spectrophotometric scan of cellular soluble fraction of Raji cells incubated with **7**. **(right)** Cellular debris of Raji cells incubated with **7**, after treatment with pure DMSO.

VI.2.3.2 Effects of compound 7 on cell cultures

The possible effect of compound **7** on cell growth was next investigated with the BC cell line ZR-75-1.

This human tumour cell line, which has a high level of hNAT1 (Wakefield et al, 2008b), was grown in the presence of increasing concentrations of compound **7**. Whilst at different amounts of compound **7** the percentage of viable cells was higher than 80%, and even 95% at 5μg.ml^{-1}, the cell number was drastically reduced as well as the cell size at higher concentrations (50 and 100μg.ml^{-1}) (**Figure VI.8**).

This would suggest that compound **7** is cytotoxic at the higher concentrations used and the cell growth was partially inhibited. Despite the small number of concentrations tested, the overall effect seemed to be concentration-dependent.

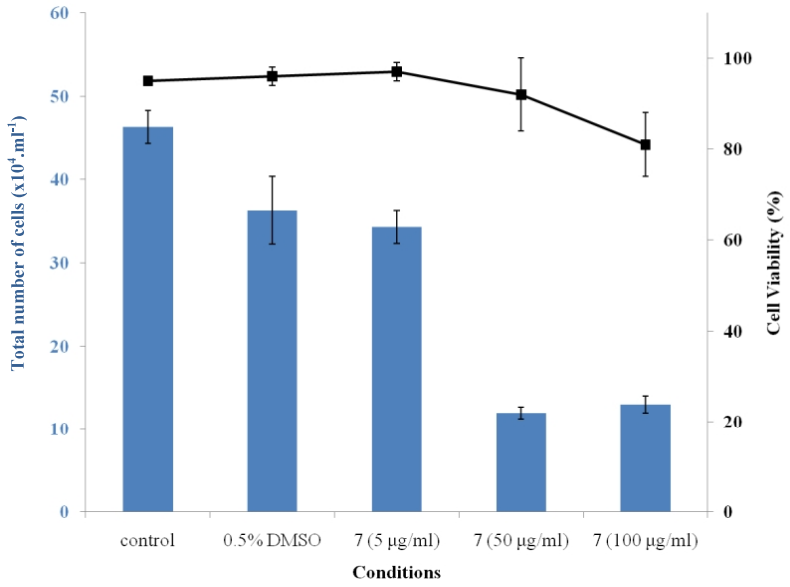


Figure VI.8: Effect of compound 7 on the breast cancer cell line ZR-75-11.

ZR-75-1 cells were grown in RPMI media at final conditions 0.5% DMSO (v/v) and varying concentrations of compound **7**. Cells were counted using a haemocytometer and cell viability was expressed as a percentage of live cells over total cells. All results are given as average ± standard deviation from duplicate experiments. Blue primary y-axis and blue columns refer to the total number of cells ($x10^4$ per ml of lysate), whereas black secondary y axis and black line refer to percentage of cell viability.

From this preliminary experiment it was not possible to determine whether these effects were due to the inhibition of hNAT1, since they would require **7** to transverse the cell membrane and this had not been proven so far.

It was necessary, then to find out whether **7** could affect the cell viability and growth of other types of cell, or whether it would be specific towards a cell line overexpressing hNAT1, such as ZR-75-1.

As a preliminary study, other types of mammalian cell lines and prokaryotic cells were grown and incubated with compound **7** ($100\mu g.ml^{-1}$): the lymphoblastoid Raji derived from a Burkitt lymphoma, the mouse leukaemic monocyte macrophage Raw 264.7 and the *E. Coli* strain JM 109.

hNAT1 activity in monocyte and lymphocyte cell lines was previously found to be low

compared with BC cell lines (Coroneos & Sim, 1993; Cribb et al, 1995; Kelly & Sim, 1991; Wakefield et al, 2008b): these cells lines were therefore chosen to determine whether the effect on ZR-75-1 cells was as a result of **7** interacting with hNAT1.

Cell cultures were performed using 0.5% DMSO as control and 100µg.ml^{-1} of compound **7** significantly diminished the cell number as well as the cell viability, as shown in **Figure VI.9**. This would primarily suggest that naphthoquinone **7** did not influence exclusively the cell viability and growth of the BC cell line ZR-75-1, but also affected those of other types of mammalian cells at high concentrations. However, the dose of **7** used for this study was highly cytotoxic.

Further investigations on a broader range of cells are needed to confirm these hypotheses with intermediary and lower concentrations of compound **7**.

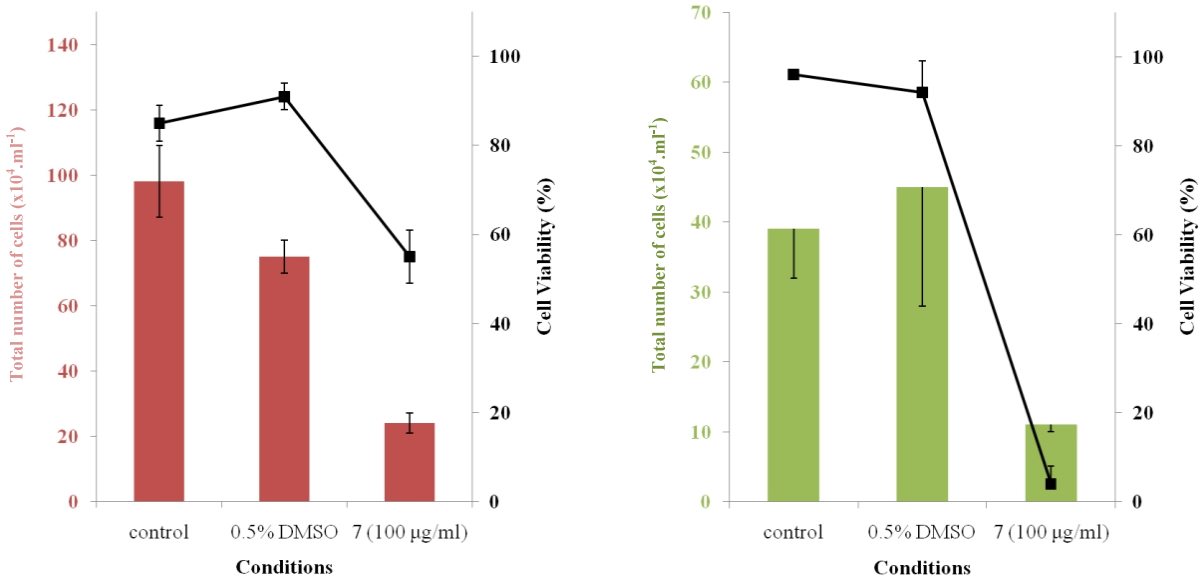


Figure VI.9: Effect of compound 7 on other mammalian cell lines.

Cells from lymphoblastoid Raji (red columns) and mouse macrophage Raw 264.7 (green columns) were grown at final conditions 0.5% DMSO (v/v) and 100µg.ml^{-1} of compound **7**. Cells were counted using a haemocytometer and cell viability was expressed as a percentage of live cells over total cells. All results are given as average ± standard deviation from triplicate experiments. Coloured primary y axis and coloured columns refer to the total number of cells (x10^4 per ml of lysate), whereas black secondary y axis and black line refer to percentage of cell viability.

Overall, although these studies are preliminary in exploring the effect of these inhibitors towards the eukaryotic cells, **7** seemed to affect appreciably the growth and the viability of some mammalian cells (**Figure VI.10**), but still needs to be further investigated with a more comprehensive study on cells.

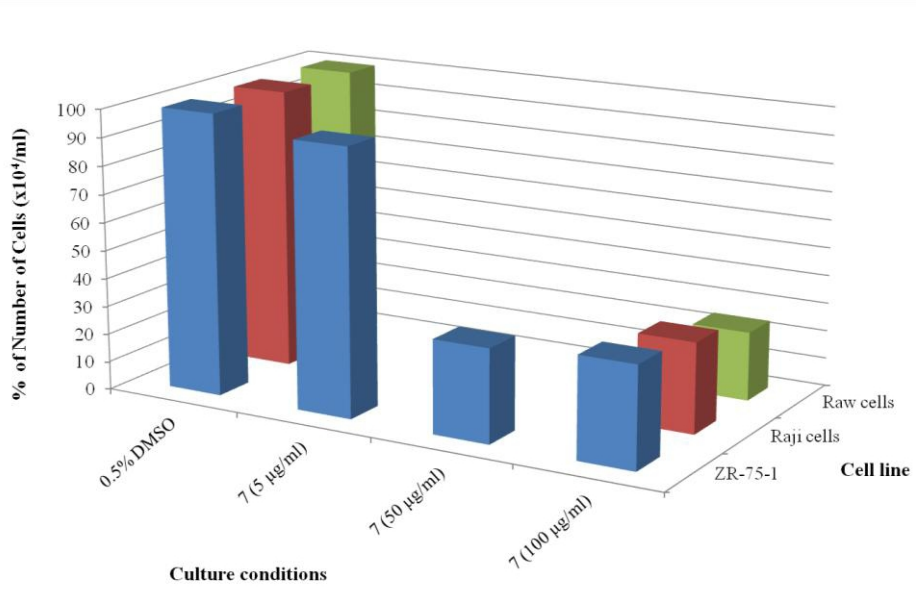


Figure VI.10: Overview of the results obtained from cell proliferation studies conducted with inhibitor 7.

Alongside the study on eukaryotic cells, an additional experiment was carried out with prokaryotic cells. In order to check whether compound **7** could also affect prokaryotic cell growth and viability, *E.coli* JM 109 cells were spotted and grown on an agar-based LB medium in the presence of different concentrations of compound **7** from 10 to 100µg.ml^{-1}, with the appropriate controls (**Figure VI.11**).

After 24 h, a spot colony was observed in each well, proposing that compound **7** did not inhibit prokaryotic cell growth.

However, a discolouration of the gel was observed around the colony in the well containing high amount of compound **7** (50 and 100µg.ml^{-1}) (**Figure VI.11**). Following ex-

periments on oxidoreduction of compound **7** described in **Chapter IV**, the decolourisation seemed likely to be due to a reduction of compound **7** by the bacteria. These studies suggest that compound **7** does not affect prokaryotic cells but the metabolism of compound **7** by these cells may differ from any effects on eukaryotic cells.

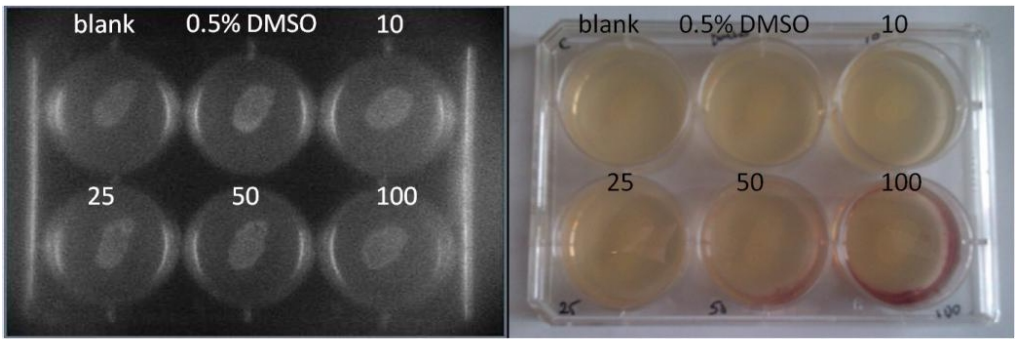


Figure VI.11: Effect of compound 7 on the growth of *E. coli* JM109.

Increasing concentrations of compound **7** (0 - 100µg.ml^{-1}) were mixed with LB Agar. The solid media was then spotted with competent cells *E. coli* JM 109 and incubated for 24 h at 37°C. The concentration of DMSO was consistent (0.5 %) for all wells apart from control. The plate was visualized using a Gel Doc 2000 UV/Visible illuminator (BioRad, Hemel Hempstead, UK).

VI.3 Discussion

The status of hNAT1 as a biomarker would be greatly enhanced by establishing the endogenous role of hNAT1 (Wakefield et al, 2007), as well as by exploiting the considerable overexpression of *hNAT1* observed in ER+ve BC (Tozlu et al, 2006).

Since the cell line ZR-75-1 was shown to be of particular interest for its extensive overexpression of *hNAT1* (Wakefield et al, 2008b), western blotting and dot blotting were used to estimate the amount of hNAT1 in the ER+ve BC cell line ZR-75-1: $10\text{-}20\times10^6$ hNAT1 molecules per cell were immunochemically estimated using a hNAT1 specific antibody. The hNAT1 level corresponded to approximately 1 pg per cell. This result was used as a reference to be compared with the estimation of hNAT1 by the colourimetric naphthoquinone probes.

Overall, it would be suitable to quantify the amount of hNAT1 in different types of cancers to study its possible differential expression for comparison, and possibly elucidate the endogenous role of hNAT1 relative to cancer progression.

When native hNAT1 enzyme present in the ZR-75-1 cell lysate was enzymatically detected using pABA and AcCoA, as substrates, NAT activity was equally detectable by both enzymatic methods: the arylamine acetylation method and the AcCoA hydrolysis method. This highlighted the equivalent validity of both enzymatic recognition techniques not only with pure recombinant proteins (Brooke et al, 2003b), but also hNAT1 in cells. Moreover, as different concentrations of pABA were used as substrate with hNAT1, the enzyme was shown to behave as a Michaelis-Menten enzyme.

This experiment supported the exploitation of ZR-75-1 cell lysates as an excellent source of native hNAT1 for the inhibitory studies conducted with **1** and **7**. These compounds were found to be potent inhibitors of the hNAT1 expressed in the BC cell line ZR-75-1, similarly to the pure recombinant enzymes hNAT1 and mNat2: in all cases, **7**

was shown to be a more potent inhibitor than **1**.

The molecular inhibition of hNAT1 by **7** in the BC cell lysate, suggested that an acid-base proton exchange between the **7** sulfonamide-N*H* and Arg127 guanidine from the hNAT1 would occur concomitantly within the cell lysate. Nevertheless, the amount of hNAT1 in ZR-75-1 cell line and the affinity of **7** for hNAT1, estimated based on the affinity of **7** for mNat2, revealed that it was currently not possible to detect either spectrophotometrically or by eye the biomarker hNAT1 using the naphthoquinone probe **7**.

For these purposes, theoretical studies highlighted the necessity to improve the affinity of the ligand for the protein target by at least 500 fold, with a simultaneous enhancement of the molar extinction coefficient of no less than tenfold.

With regard to using naphthoquinone compounds as inhibitors of hNAT1 *in vivo*, two major issues needed to be addressed: the cell permeability and the cellular effects of the molecules. In fact, previous studies highlighted both a proliferative effect of the overexpression of hNAT1 in breast cells (Adam et al, 2003) and an anti-tumour potential of inhibiting hNAT1 in BC cells (Tiang et al, 2010).

This study made preliminary investigations into cell-penetrating ability of compound **7** using Raji cells. The techniques employed relied on detecting compound **7** in the extra and intracellular fractions using spectrophotometry. However, equivocal results were obtained, mainly due to the separation of the extracellular medium from cell pellet. The apolarity of compound **7** appeared to result in hydrophobic binding of **7** to cells, which interfered with the oil-based technique used in this study. The non-specific binding of compound **7** to other cellular components needs to be further investigated and methodological refinements would be required. Moreover, additional sensitivity of compound **7** towards hNAT1 needs to be addressed in further studies.

Despite the technical difficulties faced in determining the real cellular uptake of compound **7**, cellular cultures of ZR-75-1 were set up in the presence of the inhibitor **7** to

find out the impact of the molecule on cell viability and cell proliferation.

This pilot experiment indicated that **7** negatively influenced the growth of the ZR-75-1 cell line, without affecting the cell viability at lower concentrations. However, this work did not determine whether the observed effect on cell growth was due to inhibition of hNAT1.

However, the decrease in cell viability observed for ZR-75-1 cells at higher concentrations of **7** suggested a possible cytotoxic effect. When **7** was tested with other cell lines, such as Raji and Raw cells, a cytotoxic effect was noticed at a high concentration of $100\mu g.ml^{-1}$. Differential effects of compound **7** on different cell lines need to be investigated and correlated with their respective cellular hNAT1 levels.

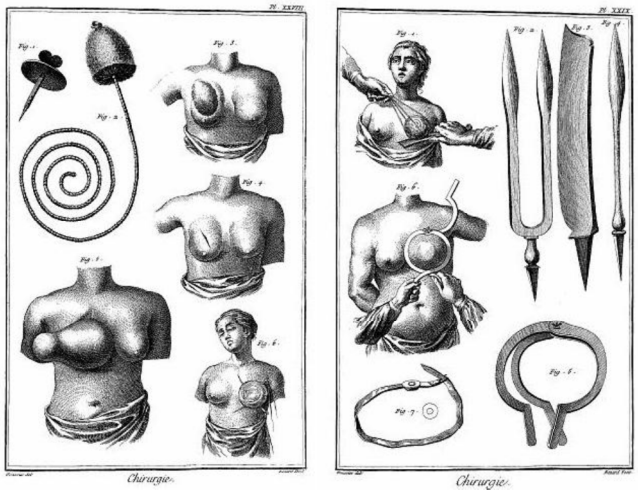
This cytotoxic effect could be due to a possible redox cycle inside cells of compound **7** since it is a quinone (Gutierrez, 2000). This may induce cell death through the production of reactive oxygen species, likewise a number of other clinical anticancer agents, such as Epirubicin (Salvatorelli et al, 2006). Redox cycling should be monitored in any further development of the compound, considering the presence of human quinone reductase enzymes in both physiological and pathological conditions.

When *E. coli* colonies were grown in the presence of compound **7**, the agar-based medium was red and afterwards became colourless around the bacterial colonies. This seemed consistent with the hypothesis of the reduction of compound **7** by some quinone reductase enzymes from the bacterial strains, such as quinone reductases or azoreductases (Hayashi et al, 1996; Nakanishi et al, 2001; Patridge & Ferry, 2006).

Finally, this chapter has highlighted the need of developing a set of novel higher-affinity biomarkers of hNAT1 with improved colour intensity (**Chapter VII**), and throwing light on the cellular endogenous role of the same enzyme in both normal and cancerous cells (**Chapter VIII**).

Chapter VII:

Colour chemistry and structure-activity relationship of hNAT1 inhibitors



BREAST SURGERY AT THE 18TH CENTURY (1775), BY DENIS DIDEROT (1713-1784) & JEAN BAPTISTE LE ROND D'ALEMBERT (1717-1783).

Instruments for breast surgery, Goussier Louis-Jacques, Livourne, Italy (National Library of Medicine. Instruments for breast surgery, www.nlm.nih.gov/).

VII.1 Introduction

VII.1.1 Glossary

The following brief glossary has been drawn in order to elucidate the meaning of some technical terms of photochemistry used throughout this chapter, based on the IUPAC Gold Book (McNaught et al, 1997)

- **bathochromic shift (or effect) :** Shift of a spectral band to lower frequencies (longer wavelengths) owing to the influence of substitution or a change in environment. It is informally referred to as red shift. A colour is more bathochromic than another if it corresponds to a higher spectrophotometric wavelength.
- **hypsochromic shift (or effect) :** Shift of a spectral band to higher frequency or shorter wavelength upon substitution or change in medium. It is informally referred to as blue shift.
- **colour brightness :** This term is reserved for non-quantitative reference to physiological perception of light. It is also related to the sharpness of spectrophotometric band: the sharper the spectral band, the brighter the colour (Christie & Royal Society of Chemistry (Great Britain). 2001).

VII.1.2 Colour chemistry

The original colour change of **1** observable by eye in the presence of both hNAT1 and mNat2 at physiological pH suggested a potential opportunity to develop compound **1** as a colourimetric biosensor for the detection and quantisation of hNAT1 in ER+ve breast tumour lysates.

Two values estimated in previous chapters could be used to evaluate the possibility of

using compound **1** and its analogues as biosensors of hNAT1 in BC cells:

- the amount of hNAT1 in an ER+ve breast tumour cell line, ZR-75, (1 pg per cell, *i.e.* 7.95 μM of hNAT1 cell lysates);
- the dissociation constant (K_d) of **7** towards mNat2 (4.45-11.45μM) as a possible approximation for the K_d of the complex hNAT1-**7**.

These two measurements were taken into account in order to approximately calculate the optimal K_d value of the complexe hNAT1-**7** and the enhancement in MEC which would be required for visible detection of hNAT1 at the μM levels previously determined.

Improving the colour intensity of these prospective biosensors together with increasing their affinity for the enzyme hNAT1 was therefore essential to develop a valuable method of recognition of hNAT1 in breast tumour cells.

The physicochemical causes of the colour and the structure-colour relationship in dyes were investigated for this purpose.

The literature specifies five physical and chemical mechanisms, as causes of colour (Christie & Royal Society of Chemistry (Great Britain). 2001; EncyclopædiaBritannicaOnline, 2011):

- Simple excitations, by gas (*e.g.* vapour lamps, neon lamps) or vibrations and rotations (*e.g.* ice, halogens);
- Ligand field effects (*e.g.* transition metal compounds);
- Molecular orbitals (*e.g.* organic compounds and charge transfer);
- Electronic band structures (*e.g.* metals and semiconductors);
- Phenomena of geometrical and physical optics (*e.g.* dispersion, interference, and diffraction).

From the time when first synthetic dye was discovered in 1856 by William Henry Perkin (Perkin & Meldola, 1907), chemists have always been fascinated by the associa-

tion of the colour of a dye and its molecular structure.

In 1867, two German chemists, Graebe and Liebermann, synthesised alizarin for the first time, a synthetic substitute for a vegetable dye derived from the madder, and also observed that treating dyes with reducing agents was able to destroy their colour (Graebe & Liebermann, 1868).

Subsequently, in 1876, Otto N. Witt suggested that two types of functional groups were responsible for the colour of dyes (Witt, 1876; Witt, 1886): one was referred as chromophore, as the group conveying the colour, and the other named auxochrome or anchoric group, as the group providing an enhancement of the colour intensity by salt formation(Armstrong, 1888) .

Afterwards, Hewitt and Mitchell proposed in 1907 that resonance conjugation was essential to give colourimetric properties to a molecule (Hewitt & Mitchell, 1907), and in 1928 Dilthey and Witzinger improved Witt's theory (Dilthey & Wizinger, 1928), recognising that chromophores were electron-withdrawing groups and many auxochromes were electron-releasing groups. They also introduced the concept that a donor-acceptor system generating the colour, called chromogen, would be suitable in a relatively extended conjugated system.

Finally, this "Chromophore-Auxochrome Theory" (Christie & Royal Society of Chemistry (Great Britain). 2001) postulated that important chromophores were azo, nitro, carbonyl, thiocarbonyl groups, and their corresponding conjugated systems, such as dicarbonyl, ethylenic, quinonic and conjugated groups (**Figure VII.1**).

The presence of a chromophore was not considered to be sufficient to develop a colour. Auxochromic groups, while not producing colour themselves, were postulated to generate the colour of a dye when they were present along with a chromophore in an organic substance. The most representative auxochromes were either acidic or alkaline groups: hydroxyl, carboxylic, sulfonic, amino, alkylamino, dialyliamino groups (**Figure VII.1**).

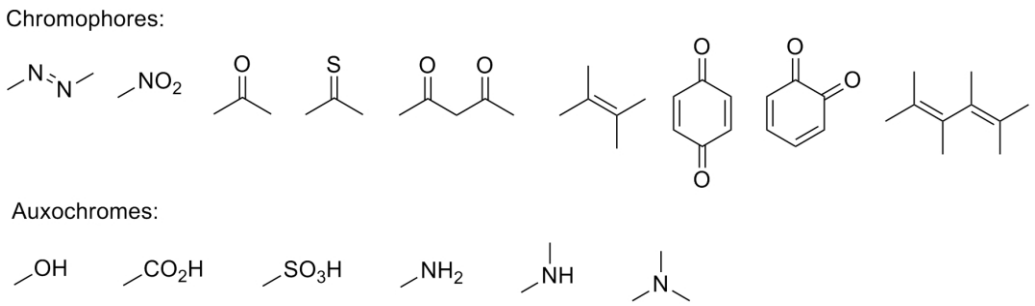


Figure VII.1: chemical structures of some common chromophores and auxochromes.

Modern theories of chemical bonding, based on either the valence-bond or the molecular orbital approaches, were able to provide a more comprehensive account of the relationships between colour and chemical constitution.

The valence-bond approach, also called resonance theory (Campaigne, 1959; Ingold, 1934; Lucas & Jameson, 1924), was developed in the first half of the twentieth century, and attempted to explain the colourimetric properties of aromatic compounds, based on the canonical or resonance forms of the dye.

In particular, the more resonance structures that were drawn for a particular dye, the higher the λ_{max} of the dye in the visible range, corresponding to a bathochromic effect in the absorption spectrum of the dye (Christie & Royal Society of Chemistry (Great Britain). 2001).

This theory postulated that many dye molecules could be represented as resonance hybrids of a number of resonance forms, and the most stable resonance forms most closely resembled the ground electronic state of the coloured molecule, whilst the less stable form corresponded to the first excited state of the dye.

As a consequence of Planck's equation ($\Delta E = hc/\lambda$), the difference in energy between the ground state and the first excited state was strongly related to the bathochromicity of the dye, in particular being inversely proportional to the wavelength at which the dye absorbed.

The bathochromicity would be most pronounced when the donor and acceptor groups were conjugated with one another, allowing a full mesomeric interaction between the two groups. Therefore, the absorption of a dye could be shifted to much longer wavelengths by incorporating a number of electron-withdrawing and -donating groups on the same resonance system.

However, this theoretical approach failed to be used to account for the colour intensity and quantitative measurements. Quantitative treatments of the light absorption properties of a dye were then made possible by developing a new theory: the molecular orbital theory (Fukui, 1971; Fukui, 1975).

In the molecular orbital theory, electrons were considered according to their wave nature rather than their particulate nature. Quantum theory stated that electrons could only exist in a fixed series of discrete energy states and were contained in regions of high probability, called orbitals, as formulated by Schrödinger in 1925.

Molecular orbitals were thought to be generated by the overlap of atomic orbitals. The overlap could be direct, giving rise to bonding σ-orbitals, occupied by two electrons in the ground state of a molecule, or antibonding σ^*-orbitals, unoccupied. On the other hand, the overlap could be also indirect, creating π-molecular orbitals.

In particular, extended conjugation systems with a skeleton of σ-bonds associated with a π-system were found in many examples of coloured organic molecules. The absorption of these dyes in either the UV or visible regions of the spectrum was originated by π-π^* transitions, rather than σ-σ^* transitions, which were characterised by much high energy, and therefore less energetically favourable (Fleming, 2010).

In 1930, Hückel proposed that the molecular orbitals could be expressed as a lineal combination of the atomic orbitals in the molecular structure: this method was named the Hückel molecular orbital (HMO) theory (Hückel, 1931; Hückel, 1932; Hückel, 1937; Lennard-Jones, 1929). Only π-electrons were considered to be involved in all

electronic transitions in conjugated systems.

Whilst the complexity of the mathematical equations in the HMO theory allowed the prediction of energy levels only for certain simple molecules, like ethene, benzene and butadiene, the HMO method was extensively applied to the calculation of the colourimetric properties of a dye *via* the use of complex computational approaches (Williams et al, 2009).

The HMO theory also suggested that the thermodynamically most stable form of a dye was the species possessing the greatest energy gap between the highest occupied molecular orbital (HOMO) and lowest unoccupied molecular orbital (LUMO), and this energy was inversely proportional to the λ_{max} at which the dye absorbed, as a consequence of Planck's equation.

In this study, earlier observations suggested that chromogen of **7** could be identified in the naphthoquinone moiety. Indeed, at the different stages of synthesis the only coloured species, 2,3-dichloronaphthalene-1,4-dione was subjected to bathochromicity from yellow to red, when both benzene sulfonamide and 3,5-methylaniline, colourless reagents, were added at positions C_2 and C_3 respectively (**Figure VII.2**).

In accordance with the chromophore-auxochrome theory, sulfonamide and aniline substituents at C_2 and C_3 positions might play a role in enhancing the bathochromicity of the dye. Also, the frontier molecular orbital theory suggests that the addition of these two substitutions would reduce the HOMO-LUMO energy gap (**Figure VII.2**).

Furthermore, as highlighted in **Chapter IV**, the reduction of naphthoquinone **7** into the corresponding naphthoquinol was shown to be responsible for the complete decolourisation of the molecule.

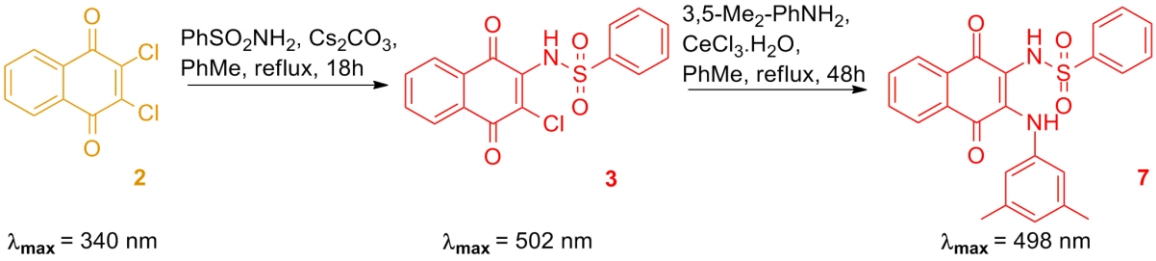


Figure VII.2: chemical synthesis of compound 7 as inhibitor of hNAT1 and mNat2.

The chemical structure of each compound is highlighted with the appropriate colour of the powdery species. All reagents labelled in black were colourless. λ_{max} values were obtained after visible wavelength scanning of a sample containing the appropriate chemical (70µl at 600µM).

Moreover, the lead compound **7** was found to be red at pH 8 and to turn blue at pH 13. This was attributable to a charge transfer along the quinone resonance system, as rationalised by the molecular orbital theory.

Indeed, in accordance with the HMO theory, the deprotonation event of **7** might generate a smaller HOMO-LUMO energy gap in the deprotonated species, which would be responsible for colour conversion of **7** from red to blue (**Figure VII.3**).

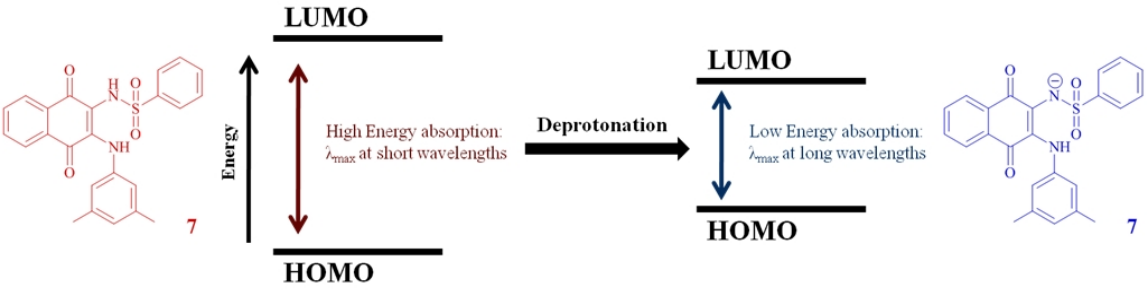


Figure VII.3: Explanation of the colour change event of 7 according to the molecular orbitals theory.

Upon deprotonation, the Energy Absorption of the dye **7** is lower, thereby shifting the λ_{max} towards longer wavelength.

The chromophore-auxochrome theory was firstly taken into account in order to con-

ceive a medicinal chemistry approach to synthesise a set of new analogues of compound **7**, introducing auxochromic groups as substituents of either the main naphthoquinone core or the aromatic branches at C_2 and C_3 positions. This constituted the first method used to try enhancing the colour intensity of the dye.

Furthermore, along the lines of the resonance theory, the possible integration of electron-withdrawing and -donating functional groups on the chemical structure of compound **7** could further develop the mesomeric system, allowing a more bathochromic colour of the dye.

VII.1.1 Solvatochromism of naphthoquinone 7

When compound **7** was incubated with deprotonating chemical or biological reagents, the λ_{max} of the deprotonated species differed in each sample as a possible result of the diverse environment in the assay (Williams & Fleming, 1989).

This could be related to a phenomenon called solvatochromism, whereby a dye might change colour when dissolved in different solvents, consistent with a concomitant shift of the spectral bands in the absorption spectrum of the molecule. This was linked to the effect of the solvent on the stabilisation of energy gap between the ground state and the excited state of the dye (Suppan et al, 1997).

A bathochromic shift of the spectral band with increasing solvent polarity is usually related to a positive solvatochromism, whereas a hypsochromic shift is referred to a negative solvatochromism (Suppan et al, 1997) (**Figure VII.4**).

Solvatochromic shifts are commonly used as simple univocal indices to classify the environment, but also reflect complex dynamic phenomena involving many different intermolecular forces (Reichardt & Welton, 2011; Suppan et al, 1997).

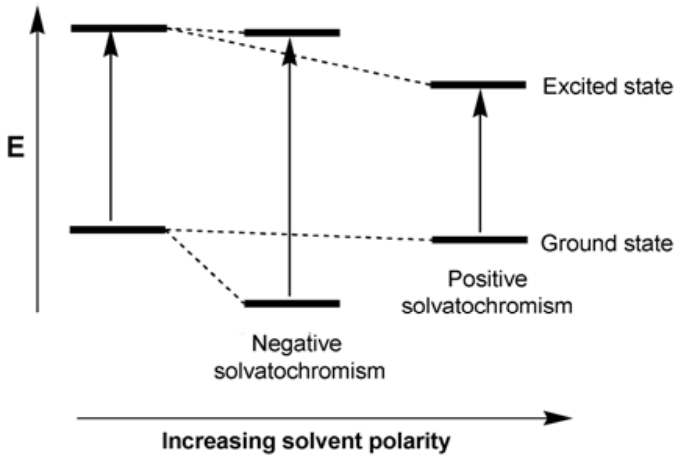


Figure VII.4: Positive and negative solvatochromisms of a dye.

The figure is adapted from (Bae et al, 2008).

In this study, the presence of biological reagents, such as NAT enzymes, in the assays resulted in a bigger bathochromic shift of the λ_{max} of compound **7** upon deprotonation compared to other chemical reagents, except DBU in DMSO (**Figure VII.5**). This exception could be explained by the fact that DBU, used in an organic solvent like DMSO, created a more hydrophobic environment than the other aqueous chemicals used (NaOH, NaSEt, Arg).

This seemed to be linked to the hydrophobicity of the environment or the microenvironment around compound **7** within the assay.

In particular, the λ_{max} of the deprotonated form of compound **7** was found to increase with the polarity of either the general environment of the assay or the particular microenvironment within the enzyme binding site (**Figure VII.5**), consistent with the hydrophobicity of NAT active sites, as previously highlighted (Abuhammad et al, 2010; Wu et al, 2007).

In particular, the solvatochromism effect observed was consistent with a negative solvatochromism.

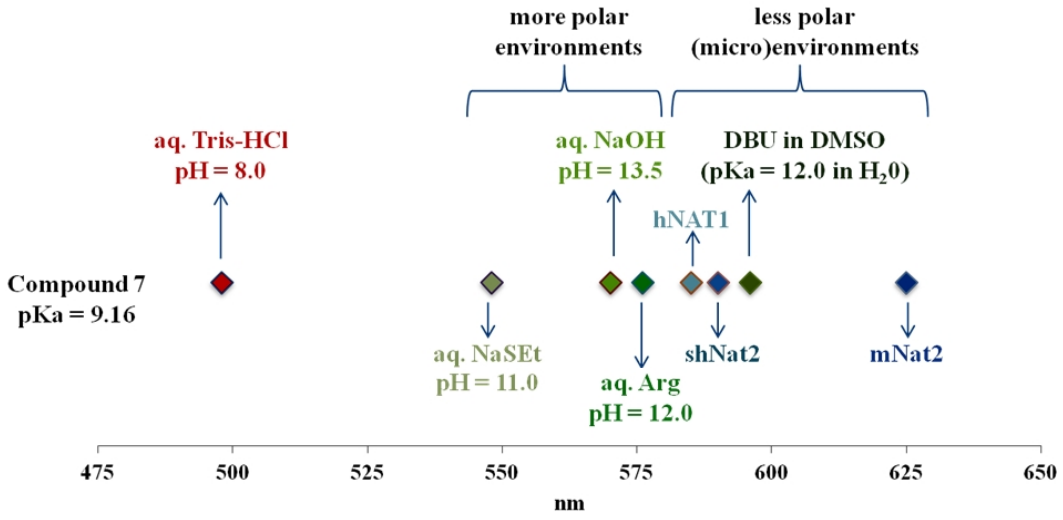


Figure VII.5: λ_{max} of compound 7 in the presence of organic, inorganic or biological reagents.

λ_{max} of compound **7** (15µM) in the presence of Tris-HCl (20mM), NaSEt (100mM), NaOH (80mM), Arg (100mM), hNAT1 (30µM), shNat2 (120µM), DBU (100mM) or mNat2 (30µM). All organic and inorganic compounds either can create an alkaline pH (NaOH, NaSEt, Arg) or possess a pK_a value (DBU) higher than the pK_a of **7** (9.16): this is consistent with the assumption that deprotonating **7** by a base is the cause of the colour conversion from red to blue. Reference for the pK_a value of DBU: (Granitza et al, 1995).

VII.1.2 Ideal characteristics of selective hNAT1 biosensors

At this stage, the physicochemical and biochemical characteristics of the ideal analogue inhibitor based on the characteristic the hit-compound of **7** could be defined:

- A weak acidic group at position C_2 resonating with quinone moiety, which would be responsible for the colour change event;
- A pK_a value in the range from 8.5 to 12, so that deprotonation of sulfonamide-N*H* would not occur at physiological pH 8, but only upon interaction with the Arg127 guanidine group of hNAT1/mNat2 , whose pK_a value is pK_a 12.5 for the free amino acid;
- A single sharp spectral bandin the visible spectra of both protonated and depro-

tonated species with a width of at most 100nm;

- A spectrophotometric bathochromic or hypsochromic shift of at least 70 nm when deprotonating the inhibitor, possibly giving rise to a visible colour change (suitably from a colour to its corresponding complementary colour);
- A molar extinction coefficient (MEC) higher than that of **7** (14,336 $M^{-1}.cm^{-1}$ at 514nm), ideally 50,000 $M^{-1}.cm^{-1}$ or higher;
- A pharmacological affinity towards hNAT1/mNat2, estimated by enzymatic IC_{50} or kinetic K_I values, both preferably in a nM range (<100nM);
- A biochemical affinity towards hNAT1/mNat2, estimated by a K_d value within a nM range (<100nM).

VII.1.3 Parallel chemical syntheses

During initial studies, a series of analogues was prepared to probe the extent of the coloured recognition event between **1** and hNAT1/mNat2 to confirm the original isoenzyme selectivity of this family of compounds (Laurieri, 2008).

From this small library of derivatives with varying aniline substituents, **7** was identified as a new lead compound with improved potency and absorbance in the visible spectrum, which allowed an extensive study on understanding the colour change event. The observations around the colour change of the ligand **7** bound to hNAT1 and mNat2, suggested that it would be an extremely helpful starting point for improving the inhibitor as a coloured titrating agent of hNAT1 in BC cells *via* its colourimetric properties.

In collaborative studies conducted with two outstanding successive Part II Students in Chemistry, Cyrille Thinnes and James Egleton, under the supervision of Dr Angela Russell, the library of naphthoquinone **7** analogues was extended with around 75 novel compounds with varying R^1, R^2 and R^3 groups, where R^1 = sulfonamide, amide; R^2 =

aryl, arylamine, phenol, aliphatic amine; $R^3 = NO_2$, NH_2 (**Figure VII.6**) (Egleton, 2011; Thinnes, 2010).

The compounds synthesised were then subjected to pharmacological tests in order to estimate their inhibitory potency against both hNAT1 and mNat2, with subsequent colourimetric analyses of their potential as biosensors. R^1 and R^2 were investigated primarily with the intention of determining structure-activity relations, and alterations at R^3 were undertaken in order to both improve colour intensity and inhibitory potency.

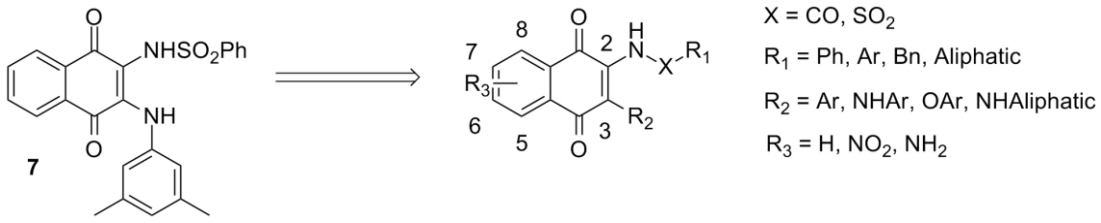


Figure VII.6: Hit compound 7 and substitution pattern of variation.

For a detailed chemical syntheses of these compounds, see (Egleton, 2011; Thinnes, 2010).

The majority of **7** analogues displayed inhibitory activity against both hNAT1 and mNat2, with varying extents, and the structural variations of **7** produced a range of diverse colourimetric properties. The pH range at which the colour change occurred, varied over a broad range. As a result, some compounds were found to display improved colourimetric properties as well as inhibitory activity against mNat2 relative to hit compound **7** (**Figure VII.7**). In particular, compounds with aromatic functional groups at C_2 were potent inhibitors of both enzymes, *e.g.* **i**, whilst alkyl sulfonamides or alkyl amines at positions C_2 and C_3 respectivelly diminished the potency of the naphthoquinone inhibitors, *e.g.***ii** and **iii** (**Figure VII.7**).

Moreover, analogues of **7** with amide substituents at C_2 were synthesised in an attempt to improve inhibitor binding to Arg127 by planar ionic interaction, and to allow investigation of the flexibility around the sulfonamide group of **7**. Analogues with phenyl am-

ides at C_2, such as **iv**, were poor mNat2 inhibitors, although **iv** was able to change colour upon binding to mNat2 (**Figure VII.7**). This suggested that whilst these analogues had a strong ionic interaction with Arg127 guanidine, they would interact poorly with Tyr129 as a consequence of the planar conformation of the amide group. Therefore, benzyl amides were synthesised in order to maintain interaction with Arg127, and simoultaneously allow sufficient flexibility to simultaneously interact with Tyr129.

v showed much improved mNat2 inhibition compared to **iv**, thereby highlighting the importance of π-π binding interactions of benzyl ring with Tyr129 side chain arene (**Figure VII.7**). Although the deprotonation of **v** upon basification gave rise to a clear colour change event, unfortunately the inhibitor did not change colour in the presence of mNat2 (**Figure VII.7**). This also helped to explain the reason why derivatives with aliphatic sulfonamides at C_2 position, *e.g.* **iii**, were unable to interact to Tyr129 and thus weakly bind to mNat2.

Derivatives of **7** with phenolic substituents at C_3 were also synthesised, such as **vi** (**Figure VII.7**). Overall, they possessed similar inhibitory potencies compared to **7**, but they had lower pK_a values which caused their deprotonation at physiological pH, with subsequent colour change (**Figure VII.7**).

A library of analogues of **7** with nitro and amino substituents at C_5-C_8 was also generated and, as predicted by Witt's theory, they displayed, at a first sight, much higher colour intensity than **7**. it was therefore decided to perform further chemical and biochemical investigations on these derivatives.

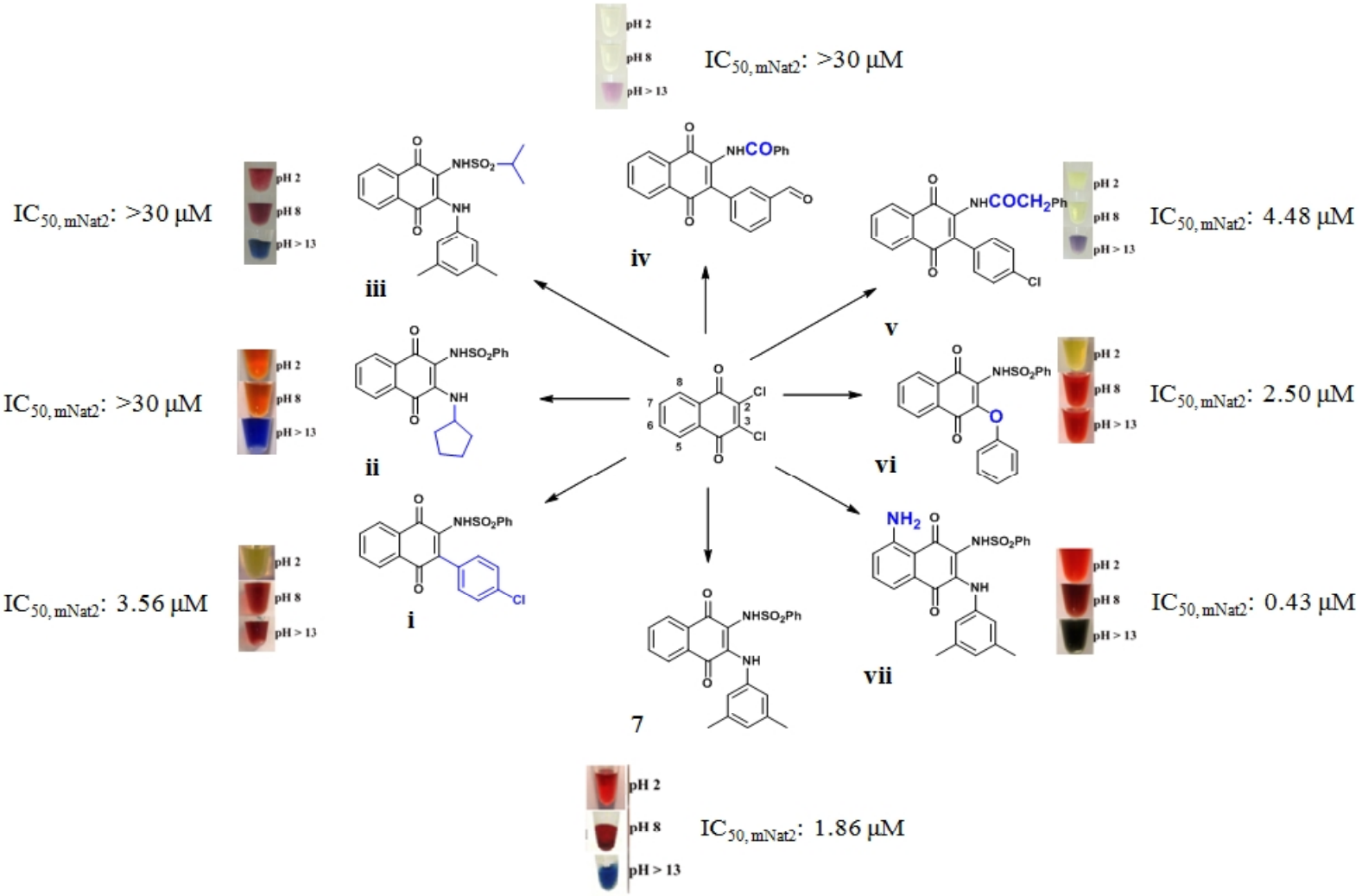


Figure VII.7: Representative examples of naphthoquinone analogue series.

Inhibitory potency of illustrative analogues of **7** was tested by AcCoA hydrolysis assays with mNat2, and IC_{50} values were obtained. These derivatives were dissolved in different buffers: 20mM Gly.HCl at pH2, 20mM Tris.HCl at pH 8, and 80mM NaOH aq. pH > 13.

AIMS

The aim of the work presented in this chapter is to advance understanding of the structure-activity relationship (SAR) of the naphthoquinone family of inhibitors, through the following series of approaches:

- physicochemical and biochemical characterisation of analogous inhibitors possessing visually brighter colour than **7** at both physiological and alkaline pHs;
- physicochemical and biochemical characterisation of derivatives of compound **7**, with nitro and amino substituents around the naphthoquinone core at positions C_5-C_8;
- docking inhibitors with best colourimetric and pharmacological properties into the active site of hNAT1.

VII.2 Results

VII.2.1 Characterisation of analogues of 7

Following a parallel collaborative chemical synthesis conducted by C. Thinnes in the Department of Chemistry, Oxford, some compounds (**10-12**) seemed to fulfil some requirements for a biosensor potential, displaying both inhibitory potency and evident colour change from pH 8 to 13, with high colour intensity (**Figure VII.8, Table VII.1**).

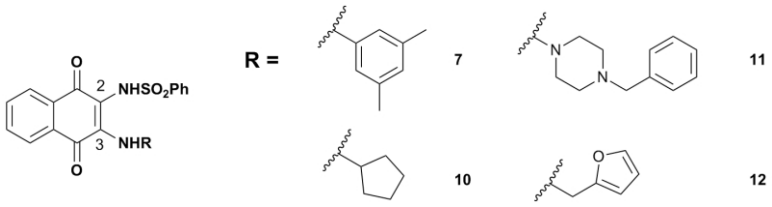


Figure VII.8: Molecular structure of compounds 7, 10-12.

These inhibitors possessed a different substituent at the C_3 position and were tested against pure recombinant mNat2, as previously expressed, and both human NAT isoenzymes, in collaboration with Dr Julien Dairou, University of Paris VII, Paris, who provided both pure recombinant proteins.

Table VII.1: Colourimetric characterisation of compounds 7, 10-12.

λ_{max}, pK_a and ε values determined according to methods outlined in Section.

R	Compound	λ_{max} (nm) (pH 8)	$\Delta\lambda_{max}$ (nm) (pH >13)	pK_a	ε_N ($M^{-1}cm^{-1}$)	$\varepsilon_N/\varepsilon_N(9)$	ε_{CB} ($M^{-1}cm^{-1}$)	$\varepsilon_{CB}/\varepsilon_{CB}(9)$
3,5-Me-Phenyl	**7**	498	+ 79	9.17 ± 0.11	13781	1	10021	1
Cyclopentyl	**10**	471	+ 141	10.12 ± 0.13	10076	0.73	4474	0.45
1-Benzylpiperazinyl	**11**	506	+ 84	9.05 ± 0.51	9377	0.68	5001	0.50
Furfuryl	**12**	461	+ 129	9.61 ± 0.09	11478	0.83	6045	0.60

All compounds were found to be highly selective towards both hNAT1 and mNat2 in comparison with hNAT2, but none of them displayed better inhibitory potency than compound **7** at 30 µM (**Figure VII.9**).

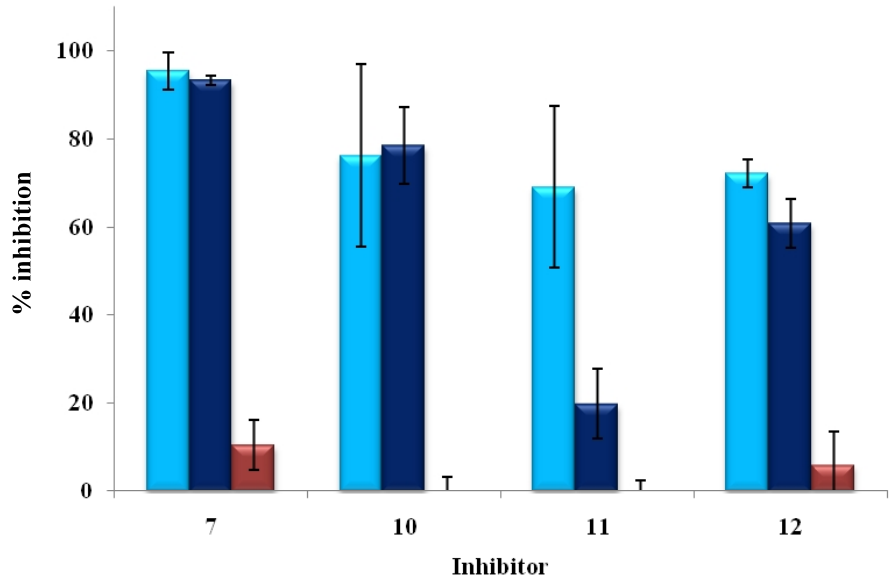


Figure VII.9: effect of compounds 7, 10-12 on mNat2, hNAT1 and hNAT2 activity.

The activities were determined by the AcCoA hydrolysis assay with a total reaction volume of 100µl. All the inhibitors were added to a final concentration of 30µM with DMSO at 5% v/v, and DMSO was added as 5% v/v in the control assay. The arylamine substrate pABA was added for both mNat2 (100ng -) and hNAT1 (100ng -), and 2AF for hNAT2 (5µg -) to a final concentration of 500µM. The reaction was initiated with AcCoA at a final concentration of 400µM. Results were expressed as mean ± standard deviation from triplicates.

Moreover, despite their brighter colours at both pH 8 and 13 and suitable pK_a values, none of them had higher MEC than **7** or bound to mNat2 with sufficiently high affinity upon binding to the enzyme. In fact, partial, but minimal bathochromic shift is observed for compounds **10** and **12** in the presence of mNat2 (**Figure VII.10**).

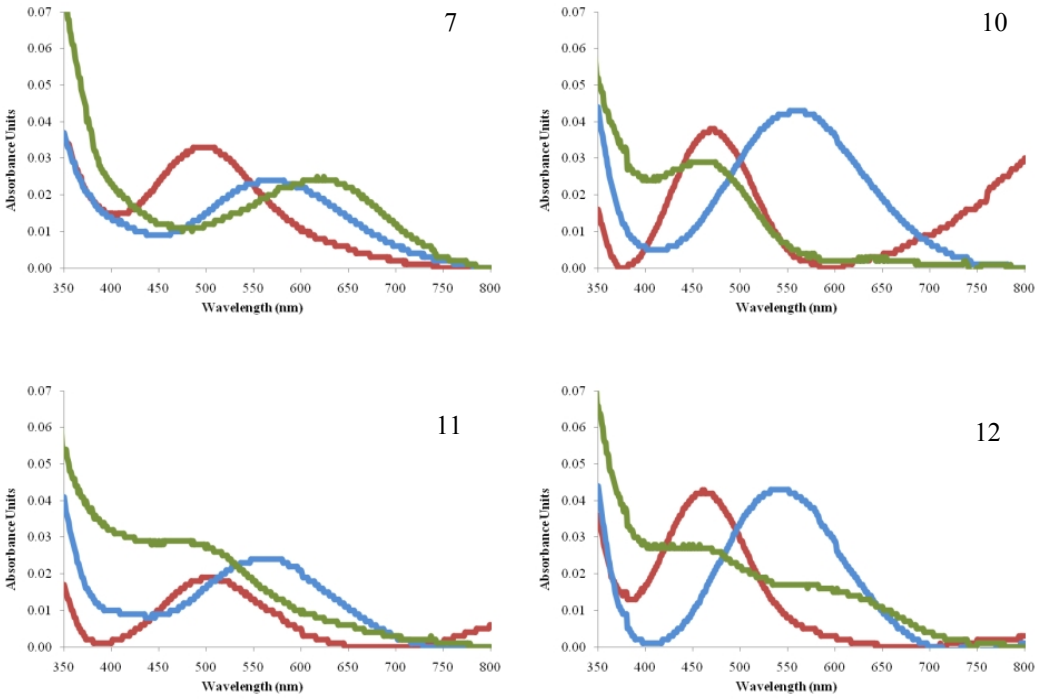


Figure VII.10: Optical properties of 7, 10-12.

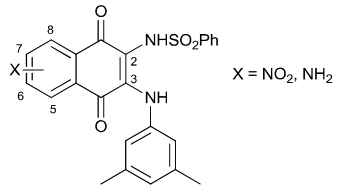
Wavelength scans of the appropriate compound (15µM) in buffer (20mM Tris.HCl, pH 8, 5% DMSO (v/v)) (red line), in alkaline solution (80mM NaOH, 5% DMSO (v/v)) (blue line), and with pure recombinant mNat2 (30µM) in buffer (pH 8 as defined above) (green line). All values of optical density were measured against the appropriate blank.

In order to study the SAR of this family of inhibitors in relation to hNAT1 and mNat2 enzymes, analogues of compound **7** with nitro or amino substituent around the naphthoquinone core at positions 5-8 were synthesised in the same parallel study in collaboration with both C. Thinnes and J. Egleton in the Department of Chemistry, Oxford (Egleton, 2011; Thinnes, 2010) (**Table VII.2**).

The relevant interest of these compounds was twofold:

- the introduction of substituents around the naphthoquinone would generate new potential inhibitors of both hNAT1 and mNat2 and give an insight into the SAR around the main core;
- these substitutions were suggested by the chromophore-auxochrome theory and should help improve the colour intensity by the MEC.

Table VII.2: Structural substitution around the naphthoquinone core.



Substituent	Position	Compound
-	-	**7**
NO_2	**5**	**13**
	6	**14**
	7	**15**
	8	**16**
NH_2	**5**	**17**
	6	**18**
	7	**19**
	8	**20**

All these compounds were firstly tested with pure recombinant mNat2 and shown to be good inhibitors of mNat2 to varying extent, with a remarkable improvement for compound **20** possessing an amine at position C_8. In fact the IC_{50} value of **20** was decreased by a factor of three relative to **7** (**Table VII.3**).

Table VII.3: IC_{50} values for 7, 13-20 against mNat2 and hNAT1.

[a] = hNAT1 enzyme was not available for testing.

Substituent	Position	Compound	IC_{50} (mNat2) (µM)	IC_{50} (hNAT1) (µM)
-	-	**7**	1.34 ± 0.61	5.29 ± 1.46
NO_2	**5**	**13**	2.68 ± 0.77	6.62 ± 2.73
	6	**14**	> 30	[a]
	7	**15**	> 30	[a]
	8	**16**	> 30	> 25
NH_2	**5**	**17**	25.53 ± 9.31	4.20 ± 1.25
	6	**18**	> 30	[a]
	7	**19**	2.50 ± 0.87	[a]
	8	**20**	0.43 ± 0.06	0.54 ± 0.13

Next, in collaboration with Dr Julien Dairou, University of Paris VII, Paris, selected analogues were tested with pure recombinant hNAT1 and hNAT2 at 30µM.

Most of the inhibitors tested, in particular **7, 13, 17,** and **20,** were found to be highly po-

tent against hNAT1 and mNat2 compared to hNAT2, whose activity was very poorly affected by these naphthoquinones, thereby confirming the selectivity of this family of compounds towards hNAT1/mNat2. (**Figure VII.11**)

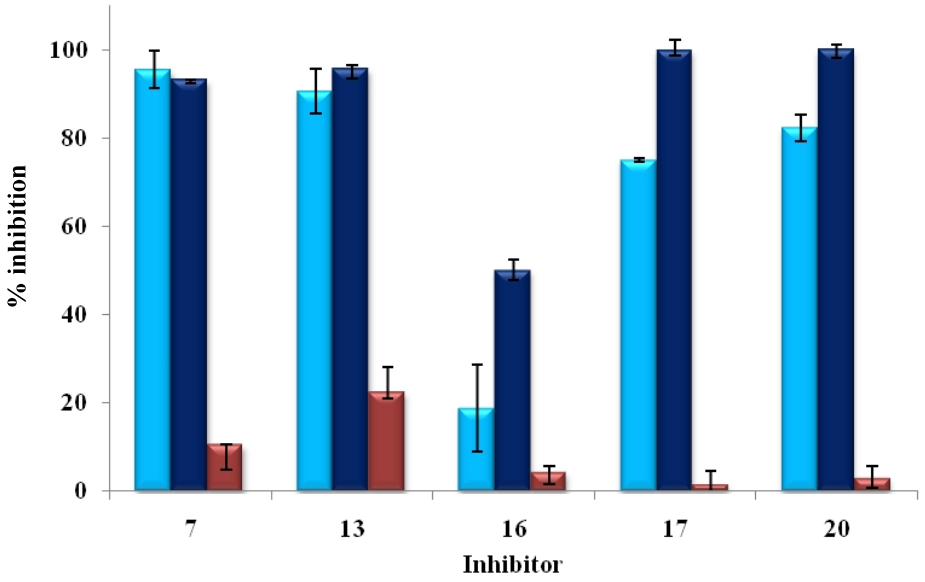


Figure VII.11: effect of compounds 7, 13, 16, 17 and 20 on mNat2, hNAT1 and hNAT2 activity.

The activities were determined by the AcCoA hydrolysis assay with a total reaction volume of 100µl. All the inhibitors were added to a final concentration of 30µM with DMSO in 5% v/v, and DMSO was added as 5% v/v in the control assay. The arylamine substrate pABA was added for both mNat2 (100ng -) and hNAT1 (100ng -), and 2AF for hNAT2 (5µg -) to a final concentration of 500µM. The reaction was initiated with AcCoA at a final concentration of 400µM. Results were expressed as mean ± standard deviation from triplicates.

Moreover, the IC_{50} values obtained for these five inhibitors with hNAT1 confirmed their specific inhibitory trend found with mNat2, consistent with previous data supporting the use of mNat2 as an excellent model for hNAT1.

More interestingly, an amine present at position C_8 improved about tenfold the inhibitory potency of the inhibitor against hNAT1, when comparing the IC_{50} values of **7** and **20** (**Table VII.3**). Thus, this amino group should play a key role in **20** in binding more tightly within the active site of the enzyme.

In the light of these results, the colourimetric properties of these novel inhibitors upon

binding to mNat2 were subsequently investigated.

Firstly, spectroscopic characteristics were determined for most compounds. In particular, the λ_{max} at both pH 8 and 13 were useful to estimate their pK_a values and MECs were calculated as an index for the colour intensity of both protonated and deprotonated species (**Table VII.4**).

All nitro-substituted species showed only one λ_{max} at both pH 8 and 13; their spectral bands were not sharp enough, but extended over a range of wavelengths from ~450 to ~650 nm (**Table VII.4**). All protonated species were more bathochromic than **7**, but this did not allow a distinguishable eye-visible colour change when treated with sodium hydroxide, similar to that obtained with compound **7** (**Table VII.4**). Moreover, none of these compounds, as both protonated and deprotonated species, had a higher MEC than **7** (**Table VII.4**).

Whilst the amino-substituted naphthoquinones **18** and **20** had similar characteristics to the nitro-substituted compounds, the inhibitors **17** and **19** displayed at first sight an evident colour change from pH 8 to 13 (**Table VII.4**). Indeed, spectroscopic data indicated that only these two compounds had a λ_{max} under 500 nm at pH 8, which resulted in an orange colour (**Table VII.4**). However, their λ_{max} did not shift considerably towards higher wavelengths under alkaline conditions, but additional peaks were observed in their spectra, which extended over the entire visible range. This produced a colour change which was difficult to define and characterise by eye.

Therefore, the method used to estimate pK_a values was not sufficiently accurate enough for compounds **17-19**. However, it gave accurate pK_a values for all the other inhibitors and allowed an assessment of which compounds had suitable pK_a values for further investigation with mNat2: compounds **13, 16,** and **20**.

Table VII.4: Colourimetric data for compounds 7, 13-20.

λ_{max}, pK_a and ε values were determined according to methods outlined in Section. Where more than one definite λ_{max} is quoted, the corresponding ε values are given on the same line. [a] Not possible to determine by this method.

Group	Position	Compound	λ_{max} (nm) (pH 8)		$\Delta\lambda_{max}$ (nm) (pH >13)		pK_a	ε_N ($M^{-1}cm^{-1}$)	$\varepsilon_N/\varepsilon_N(7)$	ε_{CB} ($M^{-1}cm^{-1}$)	$\varepsilon_{CB}/\varepsilon_{CB}(7)$
-	-	**7**	498		+ 79		9.17 ± 0.11	13781	1	10021	1
NO_2	**5**	**13**	555		+ 23		8.20 ± 0.27	7698	0.56	4517	0.45
	6	**14**	527		+ 73		7.49 ± 0.02	4503	0.33	2241	0.22
	7	**15**	529		+ 87		7.98 ± 0.37	7721	0.56	3879	0.39
	8	**16**	515		+ 58		8.55 ± 0.25	5503	0.40	2737	0.27
NH_2	**5**	**17**	474		+ 16 + 114		[a]	22418	1.63	15796 10888	1.58 1.09
	6	**18**	398 552		- 9 + 42		[a]	9833 4612	0.71 0.33	12542 3068	1.25 0.31
	7	**19**	410		+ 10 + 185		[a]	37310	2.71	21892 4644	2.18 0.46
	8	**20**	542		- 63 + 46[a]		8.37 ± 0.24	15092	1.10	12384	1.24

Compounds **13** and **20** were good selective inhibitors of both hNAT1 and mNat2 and therefore were tested with mNa2. Compound **16** was shown to be a poor inhibitor with both enzymes, and thus its colourimetric interaction with mNat2 was not explored (**Figure VII.12**). Taking into account that compounds **17** and **19** exhibited higher MECs (thus higher colour intensity) than **7** and a clear orange colour at pH 8, they were tested with mNat2. In the presence of pure recombinant mNat2, only **13** underwent a distinctive bathochromic shift similar to **7** (**Figure VII.12**).

All the other compounds tested with mNat2 showed a spectrum over a broad range of wavelengths, which was similar to that of their corresponding deprotonated species in alkaline solution. This supported the theory of deprotonation of these compounds by the protein. However, their absorbance across a wide range of wavelengths was deemed unsuitable for the purposes of this study.

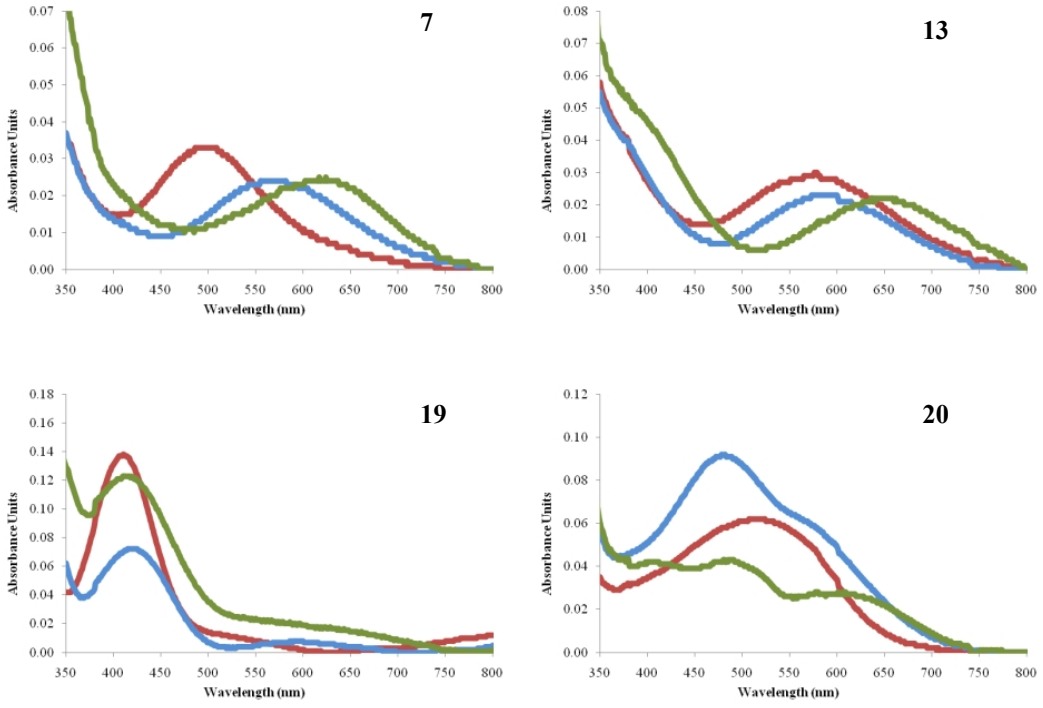


Figure VII.12: Optical properties of 7, 13, 19, and 20.

Wavelength scans of the appropriate compound (15µM) in buffer (20mM Tris.HCl, pH 8, 5% DMSO (v/v)) (red line), in alkaline solution (80mM NaOH, 5% DMSO (v/v)) (blue line), and with pure recombinant mNat2 (30µM) in buffer (as above) (green blue line). All OD values were measured against the appropriate blank.

VII.2.2 Docking studies of compound 20 with hNAT1

From previous screenings, only one modification to the molecular structure of the hit-compound **7** seemed to significantly improve its inhibitory potency: an amino group at position C_8.

In order to better understand the reason why the amino substitution positively affected the inhibitory strength of the hit compound, compound **20** was docked within the active site of hNAT1 (Wu et al, 2007), using Arg127 as a reference.

With the conventional precautions taken in all docking studies, two docked results were chosen as possessing the highest score in the GOLD SCORE solutions (>70.0 %).

As shown by **Figure VII.13**, inhibitor **20** was predicted to bind further into hNAT1 binding pocket, allowing shorter distances (from 2.9 to 2.3 Å) and thus stronger ionic interactions between one sulfonamide oxygen and one Arg127 guanidine nitrogen.

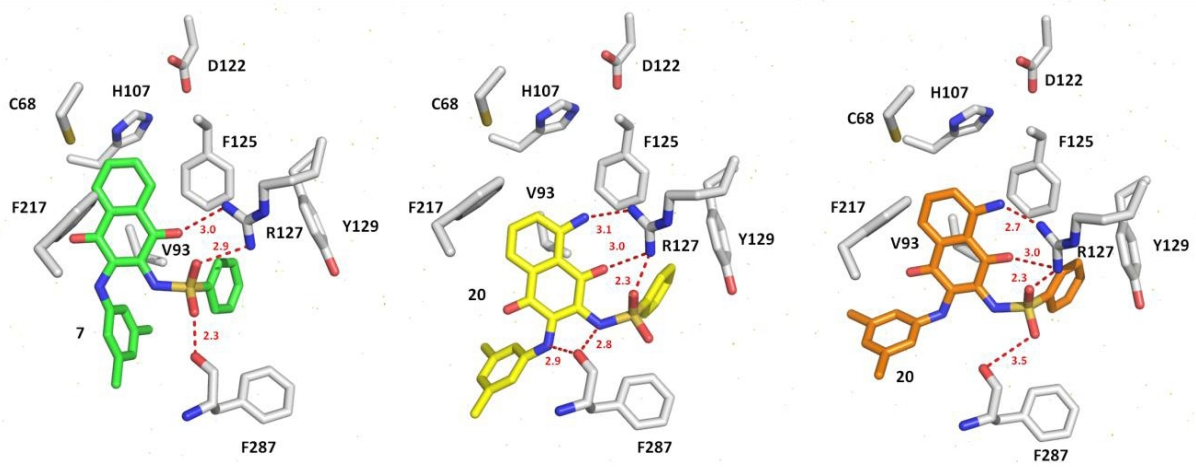


Figure VII.13: Substrate binding pockets of hNAT1 with compounds 7 and 20 docked.

Key residues of hNAT1 (Wu et al, 2007) active site with docked compounds **7 (left)** and **20 (middle and right)** are shown in stick representation and labelled, with carbon atoms in grey blue, nitrogen in blue, oxygen in red, and sulfur in orange. Compounds **7** and **20** are labelled, with carbon atoms in green or yellow or orange respectively, nitrogen in blue, oxygen in red, and sulfur in orange. The intramolecular interactions, both ionic forces or hydrogen bonds, are highlighted in red and the corresponding distance is labelled in red. The **middle** and **right** figures display the best first and second solutions from docking results, respectively.

An additional hydrogen bond was hypothesised between the primary amine of compound **20** and the other Arg127 guanidine nitrogen, in both virtual models (**Figure VII.13**): this might help explain the more intense binding of **20** to hNAT1 active site than **7**, as suggested by their respective IC_{50} values with this enzyme (**Table VII.3**).

Another residue implicated in all these virtual docking solutions was Phe287 which appeared to have a significant role in adjusting the fitting of **20** into the active site in various ways, *via* interactions either with the secondary amines or the second sulfonamide oxygen of **20** (**Figure VII.13**).

Moreover, hydrophobic interactions were also hypothesised in both docking results with compound **20** similar to docking studies with compound **7**:

- π-π stacking between the naphthoquinone moiety of the ligand and the non-polar planar region delimited by Phe125 and Val93 side chains,
- hydrophobic interactions between Tyr129 side chain and sulfonamide arene at C_2 position (**Figure VII.13**).

This reinforced the importance of both Phe125 and Tyr129 in rationalizing the selectivity of this family of inhibitors, as earlier suggested in **Chapter IV**.

VII.3 Discussion

The purpose of this chapter was to investigate the pharmacological and colourimetric properties of some analogues of **7** in relation to their chemical structures and their interaction with hNAT1 and mNat2 enzymes, in order to throw light on the SAR of this family of ligands.

Indeed, as regards the derivatives with aniline and phenol substituents at C_3 position, their pK_a values seemed to be affected by the direction of the equilibrium between the inductive effect induced by the electronegative atom at C_3 (N or O, respectively) and the mesomeric effect of the lone pair of the same atom at C_3 (**Figure VII.14**).

Most of the derivatives with a C_3-substituent linking to the main core *via* a secondary amine group showed a pK_a value higher than pH 8 and presented a clear bathochromic shift from pH 8 to pH 13. This could be explained by the fact that the mesomeric effect of the negative charge in the conjugate base might be prevalent compared to the inductive effect generated by the secondary amine nitrogen (**Figure VII.14**).

Conversely, the pK_a values of all C_3-phenolic derivatives were lower than that of **7** (9.16), and this might be related to the predominance of the electron-withdrawing inductive effect of the oxygen over the electron-donating mesomeric effect of the lone pair, thereby stabilising the negative charge of the conjugate base (**Figure VII.14**).

All C-C bonded analogues at position C_3 showed lower pK_a values than **7** (9.16), and this could be due to the stabilisation of the negative charge generated after the deprotonation of these compounds by delocalisation onto the arene at C_3 position (**Figure VII.14**).

As could be suggested by the colour of the different analogues of **7** so far synthesised (**Figure VII.7**), only the compounds possessing a C_3 substituent linking to the main core *via* a nitrogen presented a clear and visible bathochromic shift from pH 8 to 13.

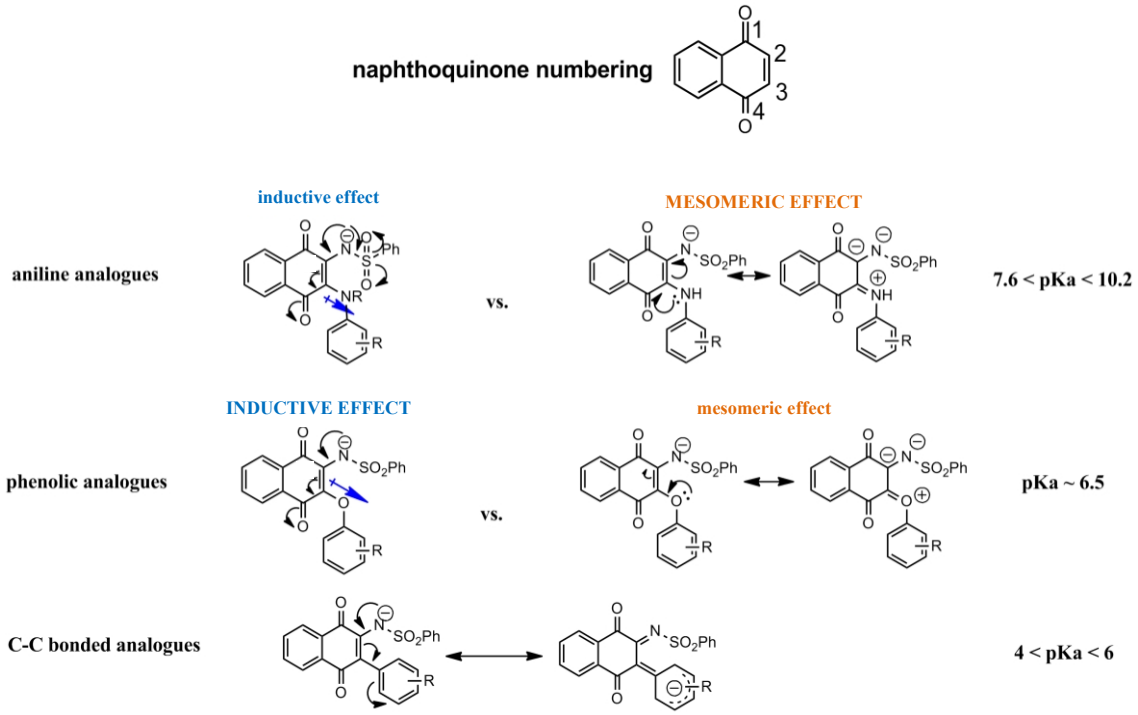


Figure VII.14: Inductive and mesomeric effects at the basis of the different weak acidity of some analogues of compound 7.

The predominant effect in pK_a determination for the family of analogues is labelled in capitals.

Considering structural modifications at position C_2, analogues with an amide group instead of a sulfonamide at C_2 position were still weak acids with pK_a values from 10 up to 14. These values were higher than those of the corresponding sulfonamide species. However, increasing the pK_a value of a naphthoquinone ligand may prevent the acid-base proton exchange between the biosensor and Arg127 guanidine (pK_a=12.5 of the conjugated acid).

The increased pK_a values of amide analogues *versus* sulfonamide derivatives seemed consistent with the hypothesis that the negative charge generated upon deprotonation of the amide is less stabilised (**Figure VII.15**).



sulphonamide analogues amide analogues

Figure VII.15: Delocalisation of the negative charge generated after deprotonating sulfonamide and amide analogues.

The number of the possible canonical forms generated by delocalising the negative charge in the conjugate base was found to decrease when the amide replaced the sulfonamide.

Compounds **10-12** were chosen to be investigated for the visual brightness of their colours compared to compound **7**. The sharpness of the bands in their visible spectra at both pH 8 and pH 13 was consistent with their visual brightness. Moreover, the bathochromic shift observed at pH changing from 8 to pH 13 was greater than 70nm, as desired. Nevertheless, the remarkable colourimetric properties of these compounds were not supported by a suitable affinity with either mNat2 or hNAT1 in order to reproduce the colour change event upon binding to these enzymes. Moreover, the MECs of **10-12** were not improved compared to **7**.

In order to better understand the SAR of this family of naphthoquinone inhibitors, another set of derivatives of the lead-compound **7** was synthesised (compounds **13-20**) with nitro and amino functionalities being added onto the naphthoquinone core at positions 5-8.

Whilst most of these compounds were still highly selective towards hNAT1 and mNat2 *versus* hNAT2, many of them did not show improved pharmacological properties compared to **7**. Considerable improvements of the inhibitory activity were only observed when an amino group was substituted at position C_8: the IC_{50} values of compound **20** with both hNAT1 and mNat2 were approximately ten and three times lower respectively, compared with the IC_{50} values obtained with **7**.

Whilst the high lipophilicity of NAT active site residues (Abuhammad et al, 2010; Wu et al, 2007) would not facilitate the accommodation of highly polar substituents onto the main core of the inhibitor, a polar functional group within the active site seemed essential to explain the improved inhibitory potency of compound **20** towards hNAT1/mNat2 for its C_8 amino group.

Virtual modelling programs docked **20** into the active site of hNAT1 and the two best solutions confirmed the importance of Arg127 as the polar key residue for this inhibitor to bind to the enzyme. In accordance with the proposed mechanism of interaction between hNAT1 and **7**, the Arg127 guanidine seemed to be firstly protonated after a proton exchange with the sulfonamide moiety of **20**, as indicated by spectrophotometric studies. Then, according to docking studies, Arg127 could also constitute the only polar residue able to interact with the polar C_8 amine of **20** in an otherwise broadly hydrophobic environment, such as that of the active site: this could allow hydrogen bonding between the guanidinium group and the primary amine at position C_8 in compound **20**.

Furthermore, as shown in **Figure VII.13**, a planar sliding of the naphthoquinone moiety of **20** over the hydrophobic flat surface generated by Phe125 and Val93 side chains, appeared to constitute an important interaction, as also illustrated for compound **7** docked into hNAT1 active site.

Whilst the inhibitory activity of the initial hit compound **7** was improved tenfold in inhibitor **20**, only a few naphthoquinone-modified compounds fulfilled some of the ideal spectrophotometric requirements to be a biosensor for the biomarker hNAT1.

All the inhibitors were weak acids for their functional sulfonamide group, as indicated by their respective pK_a values, but compounds **14** and **15** possessed pK_a values of slightly lower than 8, which would not be suitable for using it with the NAT enzyme in a Tris.HCL buffer at pH 8.

All nitro-substituted analogues possessed a single sharp spectral band in both protonated

and deprotonated species, but their bathochromic shift did not give rise to a visible colour change and was generally not greater than 70nm, except for **15** (**Table VII.5**).

On the other hand, many of the amino-substituted derivatives gave a undesired photometric spectrum with multiple bands at both pH 8 and pH 13, and the bathochromic shift between the two major spectral bands was unfortunately less than 70 nm (**Table VII.5**). Moreover, a few amino-substituted compounds (**17, 19, 20**) possessed higher MEC values than compound **7**.

In general, whilst a nitro group did not significantly increase the colour intensity of the inhibitors compared to **7**, an amino groups did increase the molar extinction coefficient of the compounds, but their optical absorbance was broader over the visible region with unsuited multiple peaks in the spectrum.

After recording spectra of compounds **13, 17, 19** and **20** with twice the concentrations of mNat2, the spectra appeared similar to those of the deprotonated species, confirming the deprotonation of sulfonamide-N*H* of the ligand within mNat2 active site (**Table VII.5**).

Table VII.5: Colourimetric data for compounds 7, 13-20, interacting with mNat2.

Where more than one definite λ_{max} is quoted, the corresponding ε values are given on the same line of the table. [a]Emerging shoulder. NT = not tested,

substituent	-	**NO_2**				**NH_2**			
position	-	**5**	**6**	**7**	**8**	**5**	**6**	**7**	**8**
compound	**7**	**13**	**14**	**15**	**16**	**17**	**18**	**19**	**20**
λ_{max} (nm) (pH 8)	498	555	527	529	515	474	552	410	542
$\Delta\lambda_{max}$ (nm) (pH >13)	+ 79	+ 23	+ 73	+ 87	+ 58	+ 16 + 114[a]	- 9 + 42	+ 10 +185[a]	- 63 +46[a]
$\Delta\lambda_{max}$ (nm) with mNat2 (pH 8)	+ 112	+ 95	NT	NT	NT	+ 16 + 114[a]	NT	0 + 210[a]	- 62 + 58
$IC_{50,\ mNat2}$ (μM)	1.34 ± 0.61	2.68 ± 0.77	> 30	> 30	> 30	25.53 ± 9.31	> 30	2.50 ± 0.87	0.43 ± 0.06

Finally, as predicted by the valence-bond theory, the presence of a nitro substituent onto the naphthoquinone core shifted λ_{max} of the protonated **7** by 20-50 nm towards longer wavelengths. This significantly altered the visible colour of the deprotonated form com-

pared to the original red colour of compound **7**. Moreover, the modification of the colour after alkaline treatment was not clearly appreciable by eye.

In contrast, an amino group at positions C_5-C_8 modified the quinonic chromogen creating additional peaks over the spectrum. While compounds **17** and **19** presented an eye-appreciable colour change with pH increasing, their spectrophotometric and pharmacological data would not support their use as colourimetric biosensors.

Wwhilst the pharmacological activity of the best inhibitor of both hNAT1 and mNat2 (compound **20**), was improved in relation to **7**, its spectrophotometric properties would not be sufficient for use in visible detection of hNAT1 in cancer cell lysates.

In addition to using hNAT1 in biomarker detection, targeting hNAT1 for anticancer treatment has also been proposed (Wakefield et al, 2008b). This study highlighted the importance of an amine at position C_8 and a nitro group at C_5 to improve the pharmacological inhibitory potency of the hit-naphthoquinone **7** towards hNAT1. However, nitro or amino functions would raise concerns over the potential use of these compounds as drug-like molecules since these functionalities have been associated with carcinogenic effects (Ford & Griffin, 1992; Ford & Herman, 1992; Goeptar et al, 1995; Kerdar et al, 1993; Miller & Miller, 1960; Testa & Krämer, 2008), and alternative bioisosteres without these side effects should next be explored.

Considering the hydrophobicity of the active site pocket residues and the virtual position of **20** within the binding site, the addition of small hydrophobic substituents, like methyl groups, at positions C_5-C_7 might permit a better fitting of the inhibitor.

Finally, as regards the general colourimetric properties of these compounds, the chromogen was identified to be constituted by the naphthoquinone moiety conjugated with the sulfonamide at C_2. The chromophore-auxochrome theory may suggest that the introduction of electron-withdrawing or realising groups along the naphthoquinone resonance system could improve the colour intensity of the ligand.

Chapter VIII:

Investigating around the endogenous role of hNAT1



MRS PRINCE, AFTER SURGICAL REMOVAL OF A BREAST (1841), BY NICOLAS HENRI JACOB (1782-1871).

One of the six portraits forming a group of works entitled "Gentlefolk of Leeds Afflicted with Disease" (from www.cerebral-coffins.com/spk/medical-illustrations.html).

VIII.1 Introduction

Having established the selectivity of compound **7** as inhibitor of both hNAT1 and mNat2, from a chemical genetics perspective, the same ligand could be used to determine the function of the protein hNAT1 in both physiological and pathological conditions by selective modulation.

Following previous hypotheses about the endogenous role of both enzymes in folate catabolism (Minchin, 1995; Minchin et al, 2007; Ward et al, 1995), mNat2 needed to be further investigated as murine homologue of hNAT1 in order to give further insight into the possible endogenous role of hNAT1 in cell and/or disease.

As regards the homology between hNAT1 and mNat2, knock-out studies on mNat2 were previously conducted on mice and helped corroborate the hypothesis that both hNAT1 and mNat2 played a role in folate catabolism (Payton et al, 1999b; Stanley et al, 1998). Moreover, the overexpression of hNAT1 in mice provoked neural tube defects usually associated with folate deficiency (Cao et al, 2005; Sim et al, 2003; Sim et al, 2007).

The strong association between hNAT1 and folate has also been supported by genetic and clinical studies conducted on orofacial cleftings. The chromosomal region marked by *hNAT1* and *hNAT2* loci was found to influence the incidence of sporadic and teratogen-induced orofacial clefting; in particular enhanced expression of hNAT1 seemed to have detrimental effects, thereby increasing the incidence and the gravity of the orificail clefting (Erickson, 2010).

Moreover, folate-containing supplementation during pregnancy seems to reduce the incidence of oral clefts in newborns (Czeizel et al, 1999). The loss of function induced by particular polymorphisms in *hNAT1* also seemed to protect against spina bifida (Jensen et al, 2006).

Moreover, the expression of mNat2 seemed to be subject to epigenetic regulation: specifically, CpG methylation in its promoter region was found to be tissue-specific and increased after functional deletion of the same gene or following dietary folate supplements (Wakefield et al, 2010) (**Figure VIII.1**). This was found to be strongly linked to the folate-dependent methylation cycle in cells and seemed consistent with evidence associating aberrant expression of *hNAT1/mNat2* genes in certain developmental defects and cancers (Wakefield et al, 2010) (**Figure VIII.1**).

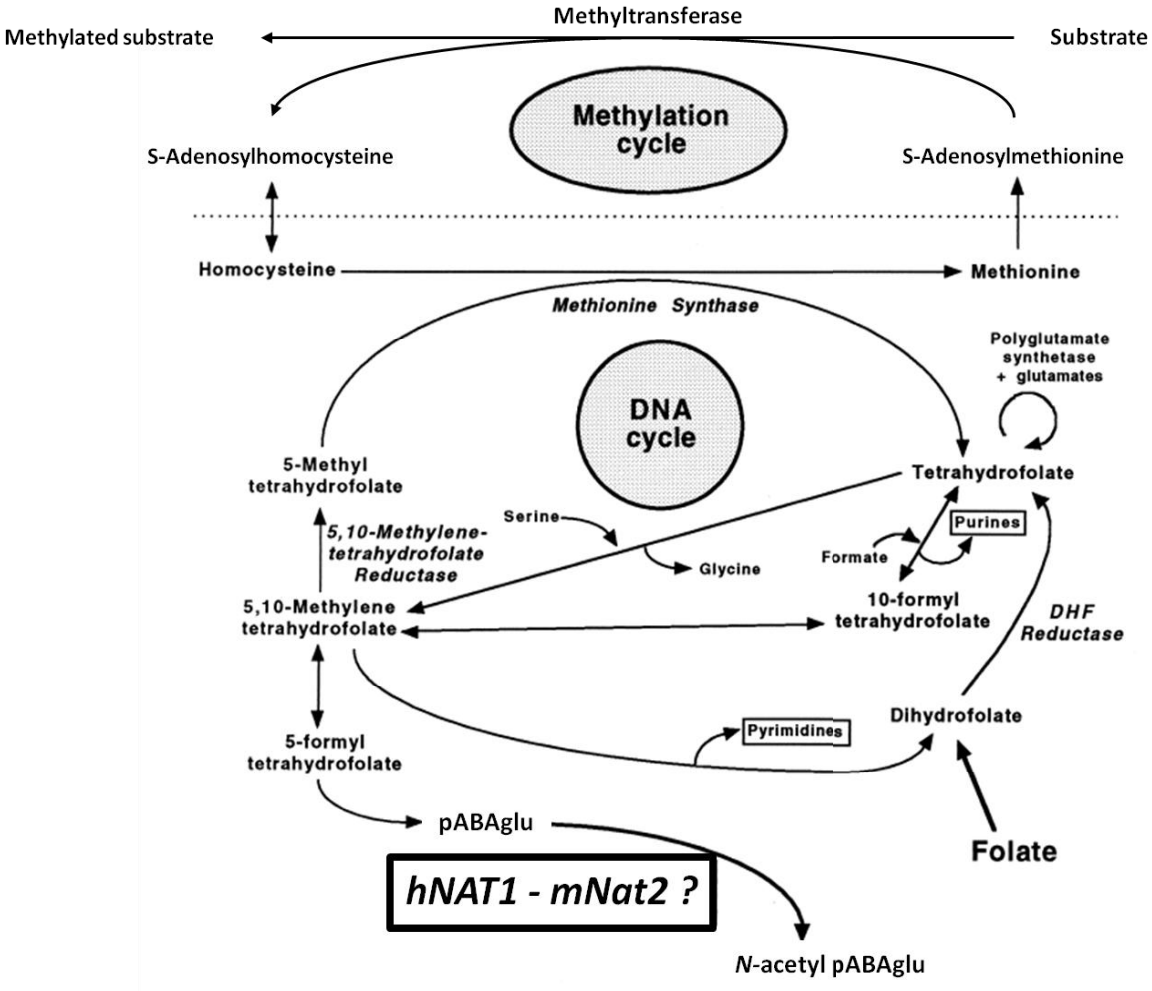


Figure VIII.1: Scheme of the methylation cycle of folate and homocysteine metabolism proposing an endogenous role for hNAT1 and mNat2.

The figure is modified from (Payton et al, 1999b) based on (Stanley et al, 1998).

Other connections between hNAT1 and folic acid were also evident during earlier in-

vestigations into human NATs: folate and its analogues were identified as inhibitors of the arylamine NAT activity, measured with several sources of enzymes, from cell lysates (erythrocytes (Ward et al, 1992), pigeon liver (Andres et al, 1983b)) to pure recombinant proteins (hNAT1 (Ward et al, 1995)).

Another interesting discovery was recently made by Dr Julien Dairou, University of Paris VII: pure recombinant hNAT1 could act as AcCoA hydrolase in the presence of folate alone in the enzymatic assay (**Figure VIII.2**), with an apparent $K_{m,app}^{folate}$=75 µM and an apparent $V_{max,app}$=3500nmol.min^{-1}.mg^{-1}.

This behaviour belonged uniquely to hNAT1 as opposed to hNAT2, and could be also observed in the presence of other folate analogues or moieties, such as methotrexate, pterin, and pteroic acid, but with less efficiency.

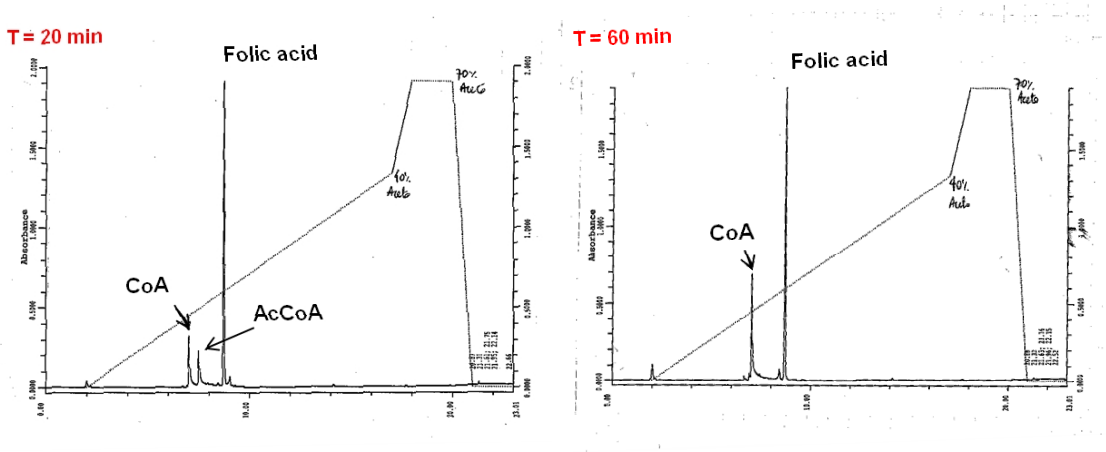


Figure VIII.2: AcCoA hydrolysis activity of hNAT1 in the presence of folic acid in the assay.

Activity of pure recombinant hNAT1 protein was measured using reverse-phase HPLC as previously described (Grant et al, 1991). Samples of enzyme were first incubated with folate (500µM, final 5% DMSO (v/v)) in assay buffer (25mM Tris-HCl, pH 7.5) at 37°C for 5min. AcCoA (400 µM final) was added to start the reaction, and the samples (100µl final volume) were incubated at 37°C for various periods of time (up to 60 min). The reaction was quenched by adding 100µl of ice-cold aqueous perchlorate (15% w/v), and proteins were recovered by centrifugation for 5 min at 12,000×g. 20µl of the supernatant was injected into the C_{18} reverse-phase HPLC column.

Therefore, given the homology of hNAT1 and mNat2, further similar investigations seemed essential with mNat2, in order to determine the possible parallelism between the two isoenzymes also in a folate-rich environment, and to throw further light on the endogenous role of hNAT1, in particular the connection between hNAT1 and folate.

AIMS

The aim of the work presented in this chapter was to advance understanding the endogenous role of hNAT1 and mNat2 in relation to folate trough the following series of approaches:

- development of appropriate single-time point hydrolytic assays to test mNat2 as AcCoA hydrolyse in the presence of folate alone;
- determination of isoenzyme selectivity of the folate-dependent AcCoA hydrolytic activity using a panel of different murine and prokaryotic NATs;
- characterisation of the folate-dependent AcCoA hydrolytic activity of appropriate NAT enzymes using ^{1}H-NMR real-time assays.

VIII.2 Results

VIII.2.1 Single-time point activity assays

Following the discovery of the unique trend of hNAT1 to hydrolyse AcCoA in the presence of folate, it was therefore questioned whether mNat2, the murine homologue of hNAT1, could also act as folate-dependent AcCoA hydrolase in comparison with other mammalian and prokaryotic NAT isoforms.

Prior to performing similar enzymatic reaction with mNat2, it was needed to ensure that the right molecular reaction was followed during end-point assays.

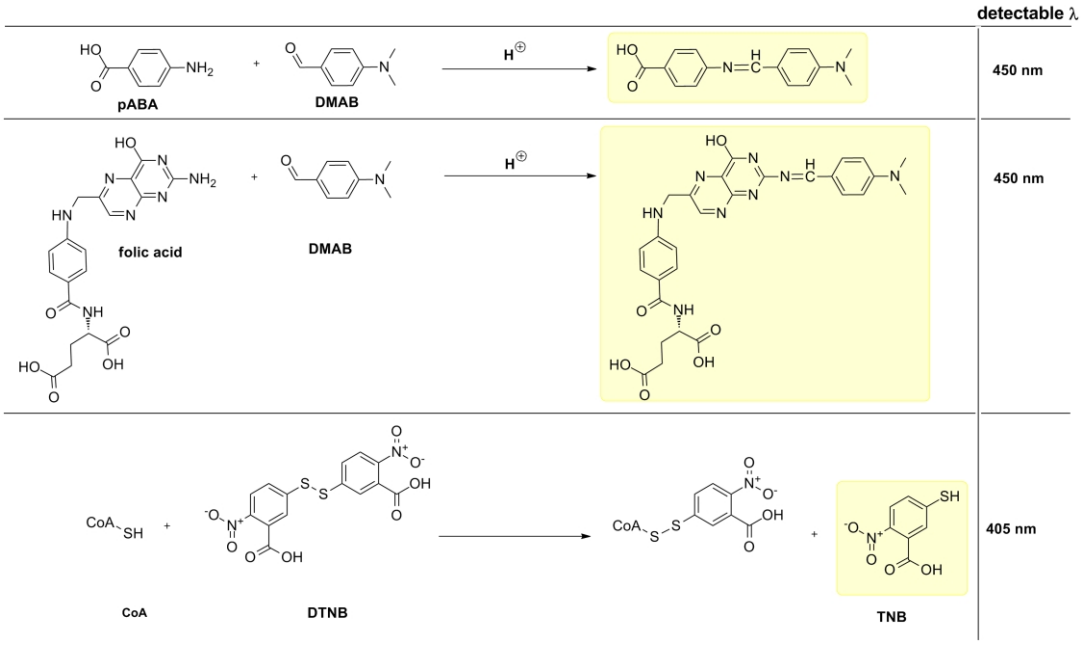
Therefore, standard curves of all chemical reagents present in the enzymatic assay were separately performed using the appropriate chemical in order to verify a precise and selective detection of each reagent during the catalytic reaction (**Table VIII.1, Figure VIII.3**).

pABA was measurable using DMAB. As folate possesses a primary amino group on the pteridine moiety which could potentially act as an acetyl acceptor, this primary amine was found to react with DMAB forming a possible Schiff's base detectable at 450 nm (**Table VIII.1**). Conversely, the formation of the product CoA could be estimated using DTNB, as in previous assays (**Table VIII.1**).

The reactivity of folic acid with DMAB was lower than that of pABA; nevertheless an appreciable concentration-dependent linearity of the absorbance was observed at 450 nm allowing the use of DMAB to detect free folate (and consequently possible folate acetylation) (**Figure VIII.3**).

Table VIII.1: Detection of reagents involved in NAT assays.

DMAB can form Schiff's base with aromatic primary amines in pABA and folic acid, detectable at 450nm. DTNB can react with free CoA thiols and give TNB detectable at 405nm. Detectable reagents are highlighted in yellow boxes.



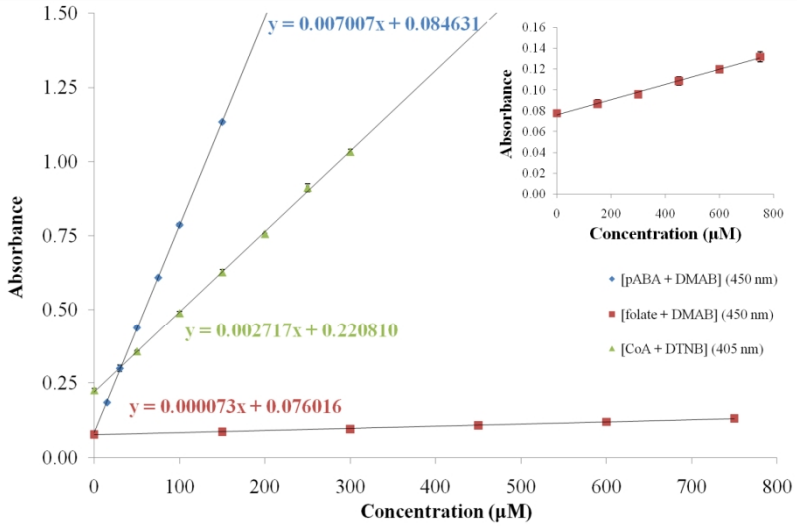


Figure VIII.3: Standard curves of detectable reagents in assays with NATs.

Increasing concentrations of different reagents detectable in NAT assay were incubated with the appropriate chemical, either DMAB or DTNB, in a 96-well place using a plate reader. In particular pABA and folic acid (45µl) were incubated with 45µl of 20% (w/v) aqueous TCA solution at 0°C, then 150µl of DMAB (5%(w/v) in 90% aqueous CH_3CN solution) was added, and finally the absorbance at 450 nm was measured. Concerning free CoA (100µl), it was incubated with 25µl of DTNB solution (5mM DTNB in 100mM Tris.HCl, 6.4M guanidine.HCl, pH 7.3), then the absorbance at 405 nm was read.

Initially, in order to assess whether the enzyme mNat2 could also work as AcCoA hydrolase in the presence of folate, three diverse enzymatic assays were carried out: the first containing only pABA and AcCoA as substrates (a), the second including pABA and folate (in equimolar concentrations) with AcCoA (b), and the last one with folate and AcCoA (c) (**Figure VIII.4**).

The first assay (a) confirmed the conventional NAT role of mNat2 with AcCoA and arylamine pABA (**Figure VIII.4**).

The second assay (b) highlighted that the presence of 150 μM folic acid in the standard assay did not alter pABA acetylation by mNat2, despite the possible cross reactivity of DMAB with both pABA and folate in the assay (**Figure VIII.4**). Nevertheless, the spectroscopic sensitivity of the Shiff's base formed by pABA with DMAB was ~100 times higher than that formed by folate and this supported the reliability of the assay (b).

Finally, in the last assay (c), DTNB could detect a time-dependent depletion of AcCoA through hydrolysis by mNat2 in the presence of folate, whereas enzymatic assays with DMAB supported the fact that the pteridine amine of folate was not acetylated at the moment of detection (**Figure VIII.4**).

As a negative control, when folate and AcCoA were mixed in a simulated enzymatic assay without pure recombinant mNat2, the spectrometer did not reveal any AcCoA hydrolysis. This underlined the essential role of mNat2 to hydrolyse the thioester functionality of AcCoA in the presence of folate.

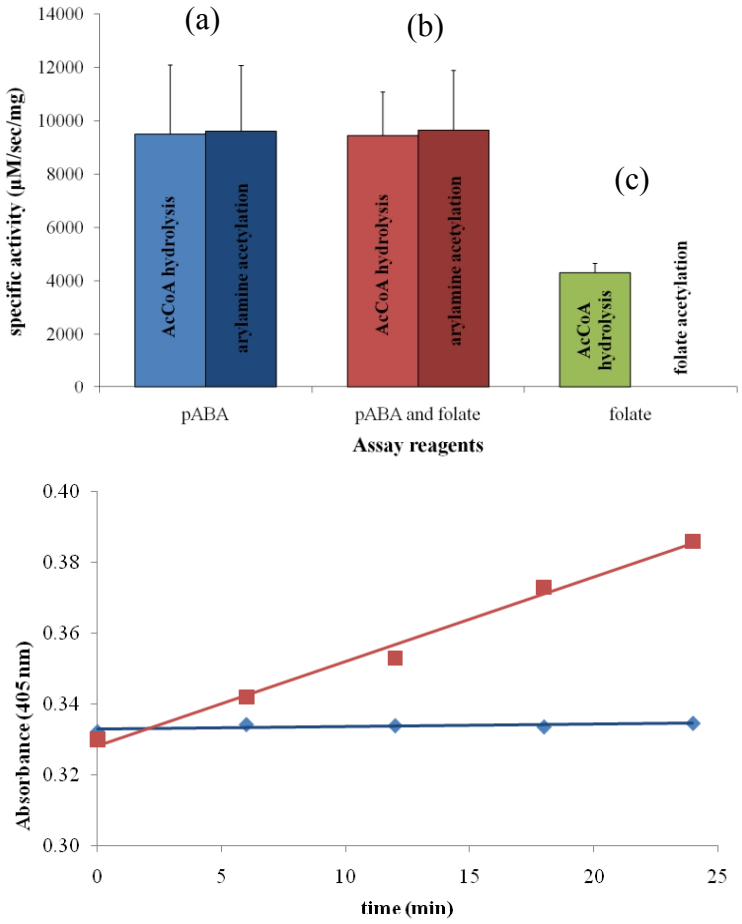


Figure VIII.4: AcCoA hydrolysis by mNat2 in the presence of folic acid alone in the assay.

(top) Specific pABA (150µM) acetylation activity by mNat2 (5ng) with (red columns) and without (purple columns) an equimolar concentration of folate in the assay; AcCoA was present at 400 µM concentrations in all assays. Specific AcCoA (400µM) hydrolysis activity by mNat2 (5ng) was detected in the presence of folate (150µM) in a AcCoA hydrolysis assay without the arylamine substrate (green column). No acetylation of folate was detected in a corresponding arylamine acetylation assay. **(bottom)** Negative control (blue diamonds): enzymatic assay containing AcCoA (400µM) and folate (150µM) only, without mNat2, positive control (red squares): enzymatic assay containing AcCoA (400µM) and folate (150µM), with 5ng mNat2.

Similar enzymatic assays were performed with other murine and prokaryotic NATs available, in order to verify the specificity of mNat2 to act as AcCoA hydrolase in the presence of folic acid (**Figure VIII.5**).

While no inhibition of 5AS acetylation activity was observed for any NAT isoform in the presence of folate, mNat2 was found to be the only NAT isoenzyme capable of hydrolysing AcCoA in the presence of folate alone without an acceptor arylamine sub-

strate being added to the reaction mixture (360µM.sec^{-1}.mg^{-1}) (**Figure VIII.5**).

Similarly, *n*-proprionylCoA, another acyl donor substrate of mNat2, was hydrolysed by the enzyme at a slightly lower activity (290µM.sec^{-1}.mg^{-1}) compared to AcCoA (**Figure VIII.5**).

This would emphasise the role of folate as possible cofactor of both hNAT1 and mNat2, since no acetylation of its primary amine by NAT was observed using DMAB.

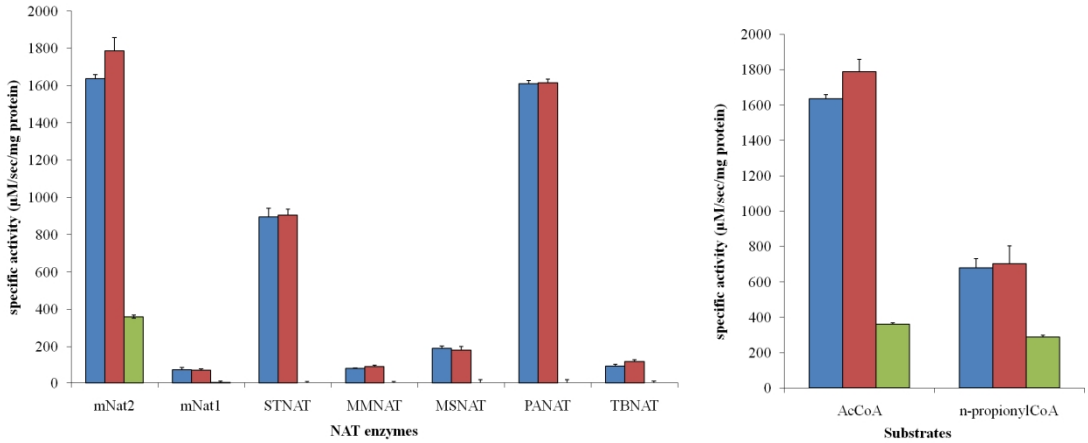


Figure VIII.5: Screen of mammalian and bacterial NATs as AcCoA hydrolases in the presence of folate.

(left) Different NAT enzymes were tested in three diverse AcCoA (400µM) hydrolysis assays in the presence of: 5AS as arylamine substrate (150 µM - blue columns), both 5AS and folate (each at 150 µM - red columns), and folate alone (150 µM - green columns). **(right)** mNat2 could act as AcylCoA hydrolase with both AcCoA and *n*-propionylCoA. mNat2 was tested in three diverse hydrolysis assays with the appropriate acylCoA (400µM) and in the presence of: 5AS as arylamine substrate (150 µM - blue columns), both 5AS and folate (each at 150 µM - red columns), and folate alone (150 µM - green columns).

In order to estimate the affinity of folate for mNat2, increasing concentrations of folate were tested with mNat2 for hydrolysis of AcCoA (400µM) (**Figure VIII.6**).

The maximum mNat2 hydrolytic activity was observed with 150µM folate, and above this concentration, folate seemed to act as inhibitor of the enzymatic activity. Plotting the values of specific activity of AcCoA hydrolysis by mNat2 gave a curve similar to that obtained for enzymatic studies showing enzyme inhibition by high substrate con-

centrations (Yon-Kahn et al, 2010) (**Figure VIII.6**).

The first four values of mNat2 hydrolytic activity were used to estimate an apparent Michaelis-Menten K_m value around 71.0µM, which was similar to the K_m value for hNAT1 (75.0µM) calculated by Dr J. Dairou, University of Paris VII.

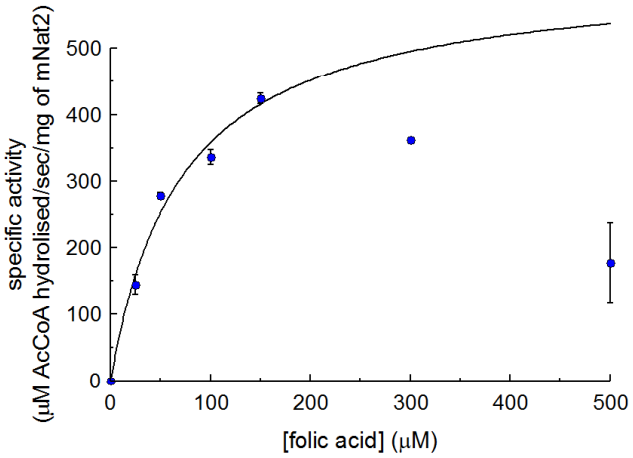


Figure VIII.6: Initial linear activities of mNat2, as AcCoA hydrolase in the presence of varying concentrations of folate.

AcCoA hydrolysis assays were performed in triplicate with mNat2 (250ng), AcCoA (400µM) and folate (varying concentrations). A Michaelis-Menten curve was fitted using the first four values: $y = \frac{V_{max} \times [folate]}{K_m + [folate]}$

with V_{max}=612.6µM.sec^{-1}.mg^{-1} and K_m = 71.0µM.

VIII.2.2 NMR real-time activity assay

An important question arose about the AcCoA hydrolysis mechanism (**Figure VIII.7**): would the acetyl group be catalytically cleaved and transferred to the bulk solvent as acetate (a)? Or would an amine function of folate be firstly acetylated, thereby forming an *N*-acetylfolate intermediate, but then immediately deacetylated due to its instability (b)?

In preliminary studies conducted by our colleagues from University of Paris VII, HPLC analyses did not identify any *N*-acetylated species of folate after AcCoA hydrolysis by

hNAT1 nor was acetate detectable for the sensitivity of the analytical technique, except the initial folate and the final CoA product formed (**Figure VIII.2**).

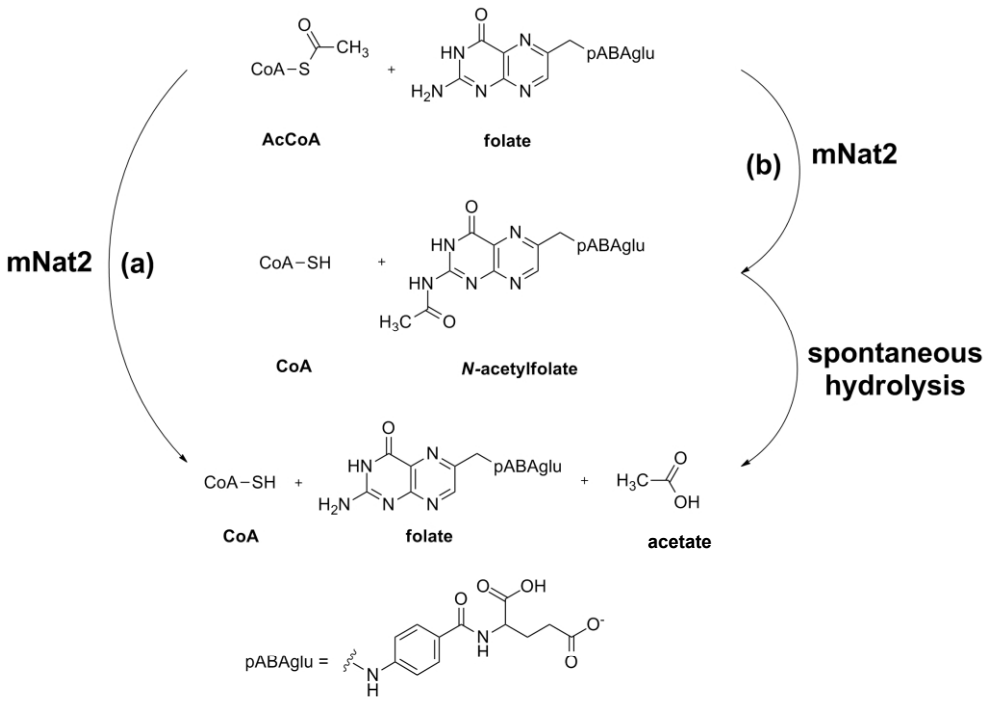


Figure VIII.7: Two hypotheses for the catalytic AcCoA hydrolysis reaction by mNat2 in the presence of folate.

pABA=para-aminobenzoylglutamate.

The biochemical techniques used to follow AcCoA hydrolysis by mNat2 so far, were mainly single-time point assays: they could selectively detect either an initial substrate or a final product in the mixture, without giving information about all the intermediary steps of the catalytic mechanism.

^{1}H-NMR real-time analyses of an appropriate enzymatic assay were therefore undertaken in order to attempt giving real-time information about structural modifications of all chemicals during the catalytic reaction in the assay.

Prior to performing a real-time assay with mNat2, folate and AcCoA, a number of preliminary controls needed to be performed in order to ensure the feasibility of the experiment.

Firstly, the same concentrations as those used in single-time point assays (400μM for AcCoA and CoA, 150μM for folate) were chosen for all reagents in NMR experiments as suitable conditions.

The high resolution of NMR spectrometers available at the Chemistry Research Laboratories, University of Oxford, would easily help detect such small amounts of chemicals. The following experiment was performed in collaboration with Dr Tim Claridge, Chemistry Research Laboratory, University of Oxford.

Initially, ^{1}H-NMR spectra were recorded for each possible reagent and product of the assay at the following concentrations: AcCoA (400μM), folate (150μM), CoA (400μM), and acetate (400μM) (**Figure VIII.8**). Each peak was then assigned to the corresponding proton consistent with previous full assignments (Patel & Walt, 1987; Rossi et al, 1993a; Wu et al, 1998) (**Figure VIII.8**).

Whilst most of the chemical shifts of AcCoA and CoA protons were similar, protons 6" and 9" possessed different chemical shifts in each of these two compounds and were chosen as markers of these two molecules in a real-time NMR assay (**Figure VIII.8**).

The concentrations of folate used in the assay (150μM) still allowed adequate and punctual recognition of all spectral bands (**Figure VIII.8**).

In a parallel experiment, the possible acetate product was clearly identifiable from a singlet at 1.97 ppm (**Figure VIII.9**).

Finally, the characteristic spectral bands of all reagents and products were found to be suitably distinguishable in the assay mixture at the concentrations stated, as shown in (**Figure VIII.9**), and the range from 3.2 to 1.6 ppm was chosen as the most adequate region to follow the enzymatic AcCoA hydrolysis by mNat2 in the presence of folate.

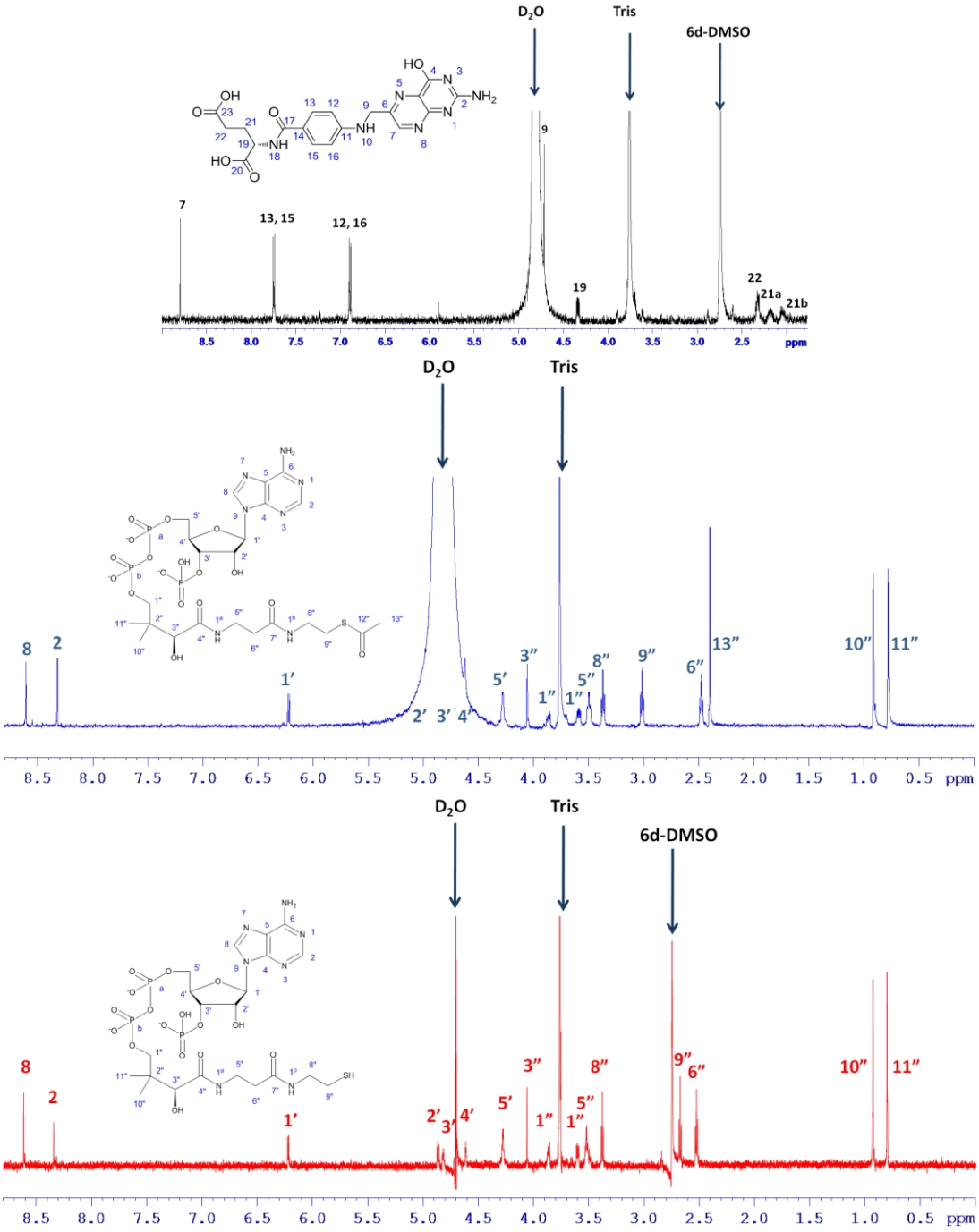


Figure VIII.8: Structures and proton NMR spectra of AcCoA and CoA.

(top) 500MHz spectrum of 400 µM AcCoA in D_2O, pD 7.4, 25°C (room temperature). Fully resolved spectral assignment was made on the basis of previous studies (Lam & Kotowycz, 1972; Rossi et al, 1993b). **(middle)** 500MHz spectrum of 400 µM AcCoA in D_2O, pD 7.4, 25°C (room temperature). Fully resolved spectral assignment was made on the basis of previous studies (Patel & Walt, 1987; Wu et al, 1998), therefore spectral bands of proton 2', 3' and 4' were supposed to be under D_2O signal. Traces of Tris.HCl buffer from AcCoA stock solutions were observed. **(bottom)**700MHz spectrum of 400 µM Ac-CoA in D_2O, pD 7.4, 25°C (room temperature). Fully resolved spectral assignment was made on the basis of previous studies (Patel & Walt, 1987; Rossi et al, 1993a; Wu et al, 1998).

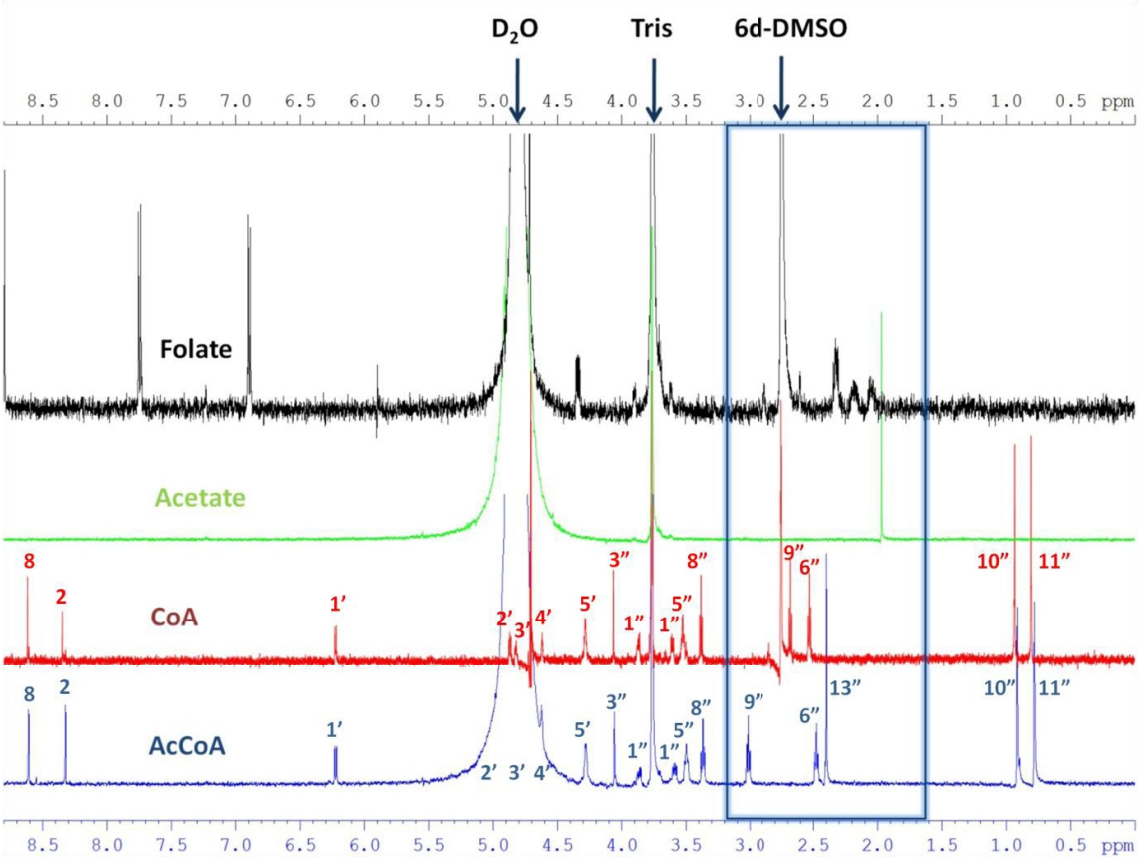


Figure VIII.9: NMR spectra of reagents and possible products present in an AcCoA hydrolysis assay with mNat2.

NMR spectra were recorded with Bruker AVC500 (folate, acetate, AcCoA) at 500MHz or AV700 (CoA) at 700MHz at the optimal concentrations used in the AcCoA enzymatic assay: 400 µM for acetate, CoA, AcCoA, and 150 µM for folate. The blue square highlights the range of chemical shifts chosen to follow the enzymatic assay over time. Full assignment of chemical shifts of CoA and AcCoA refers to **Figure VIII.8**.

As a last preliminary check, a standard NAT assay was prepared in an NMR tube using mNat2, AcCoA and pABA as arylamine substrate, and tested at 37°C (**Figure VIII.10**). The pABA acetylation catalytic reaction occurred and could be followed by ^{1}H-NMR.

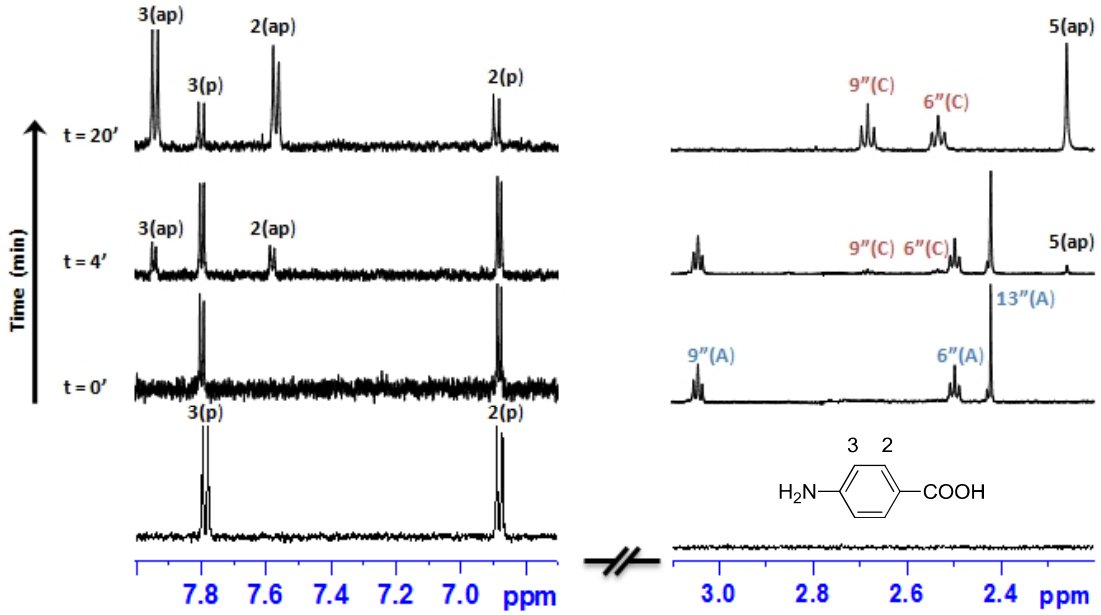


Figure VIII.10: Real-time ^{1}H-NMR analysis of mNat2 activity with pABA **as arylamine substrate in PBS-D_2O.**

Selected regions of the spectra (8.0 to 6.8, and 3.1 to 2.3 ppm) are shown. The signals are labelled as follows: pABA **(p)**, p-(carboxyamino) benzoic acid **(ap)**, AcCoA **(A)**, CoA **(C).** Purified recombinant mNat2 (10µg) was mixed with pABA **(p)** (500µM) in the presence of AcCoA **(A)** (400µM) in buffer PBS-D_2O (pD 7.4). The enzyme activity during real time NMR was carried out at 37°C.nmR data were collected before (bottom spectra) and after adding AcCoA (t = 0min).

Finally, considering that the completion of the NAT reaction occurred within 20 min using 10µg of mNat2 and the efficiency of mNat2 as folate-dependent AcCoA hydrolase is lower than as NAT, a higher amount of pure recombinant enzyme seemed to be required in a ^{1}H- NMR AcCoA hydrolysis assay.

Several amounts of mNat2 were tested (from 15µg up to 25µg) in order to find out suitable conditions to obtain the complete disappearance of the CH_3 peak from the acetyl group of AcCoA on the spectrum in a reasonable period of time (1 hour maximum) and achieve a stable final situation for five minutes afterwards.

25µg of mNat2 were mixed with 400 µM AcCoA and 150 µM folate in the assay and gave complete AcCoA hydrolysis in ~40 min (**Figure VIII.11**).

Spectroscopic data revealed that the acetyl CH_3 from AcCoA (2.41 ppm) disappeared in

conjunction with the appearance of a CH_3 peak at 1.97 ppm consistent with that of acetate (**Figure VIII.11**). This seemed consistent with the hypothesis that AcCoA was entirely hydrolysed by mNat2 into CoA in the presence of folate, and the acetyl group of AcCoA was transferred to the bulk solvent as acetate.

The chemical shifts of folate protons did not seem to change over the enzymatic reaction, suggesting that the chemical structure of folate was not modified during the reaction and thus an *N*-acetylated intermediate of folate was not hypothesised to be formed.

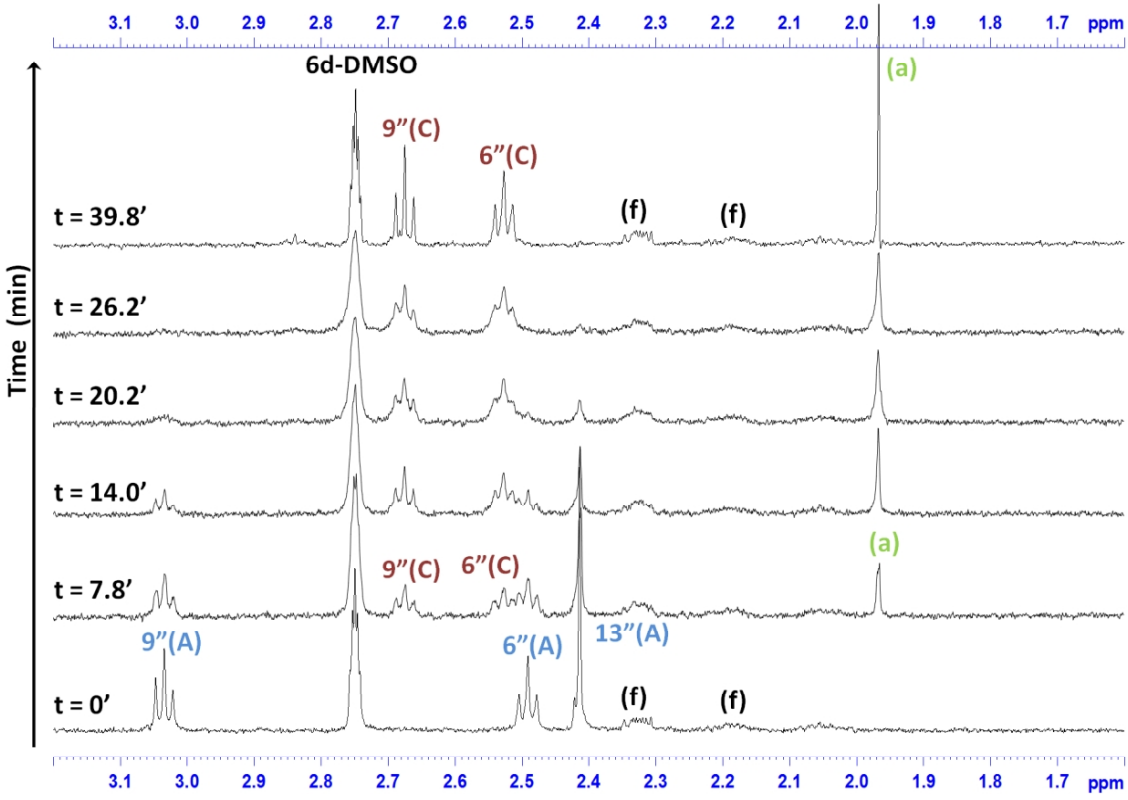


Figure VIII.11: Real-time ^{1}H-NMR analysis of mNat2 activity as folate-dependent AcCoA hydrolase performed in PBS-D_2O.

Purified recombinant mNat2 (25µg) was mixed with folate **(f)** (150µM), and AcCoA **(A)** (400µM) in buffer PBS-D_2O (pD 7.4). The enzyme activity during real time NMR was carried out at 37°C. NMR data were collected before adding the enzyme (t = 0 min), and subsequently 5 min after enzyme addition and NMR shimming. Selected region of the spectra (3.2 to 1.6 ppm) is shown. The signals are labelled as follows: folate (**f**), AcCoA **(A)**, CoA **(C)**, acetate **(a)**.

Nevertheless, in the case that an *N*-acetylfolate intermediate was developed, the acetyl group of this intermediate may not be subtly detected for its possible fast hydrolysis in the assay and NMR analyses could not be enough rapid and sensitive for this purpose. This would depend on the enzymatic velocity of mNat2 in AcCoA hydrolysis combined with the laps of time necessary to run an NMR spectrum.

In order to visualise the kinetics of the folate-dependent AcCoA hydrolysis by mNat2, enzymatic reaction progress curves were drawn using the integration values of some characteristic spectral bands of the reagent, AcCoA, and the products, CoA and acetate, over time, in relation to DMSO (5% (v/v) as internal standard (**Figure VIII.12**). The spectral bands corresponding to the acetyl CH_3 groups from both AcCoA and acetate, and the spectral bands of the methylene (-CH_2-) groups at α position to the sulfur in both AcCoA and CoA, were also taken in account (**Figure VIII.12**).

The curves obtained showed a non-linear progression of the loss of the starting reagent and the formation of the resulting molecules, which was characteristic for Michaelis-Menten kinetics (**Figure VIII.12**).

According to these progress curves, the disappearance of the initial AcCoA appeared to be complete after ~23 min and the formation of both products reached a maximum value after the same period of time approximately (**Figure VIII.11**). This correspondence indicated the completion of mNat2 activity in the assay at around 25min. Moreover, the plateaux observed during the last period of recording indicated the stability of all the chemical components in the assay.

However, the integration values of final acetate CH_3 were found to be lower than the values of AcCoA acetyl CH_3 resonances in the progress curves (**Figure VIII.12**). This difference could be attributed to the relaxation properties of the acetate CH_3 protons. Indeed, methyl groups could be slow to recover to equilibrium and thus could easily saturate do to have reduced integrals. Since the saturation effect should be the same for all

spectra and all the integration values were referenced to an internal standard (DMSO 5% (v/v)), the integration values could be monitored and corrected by an appropriate factor.

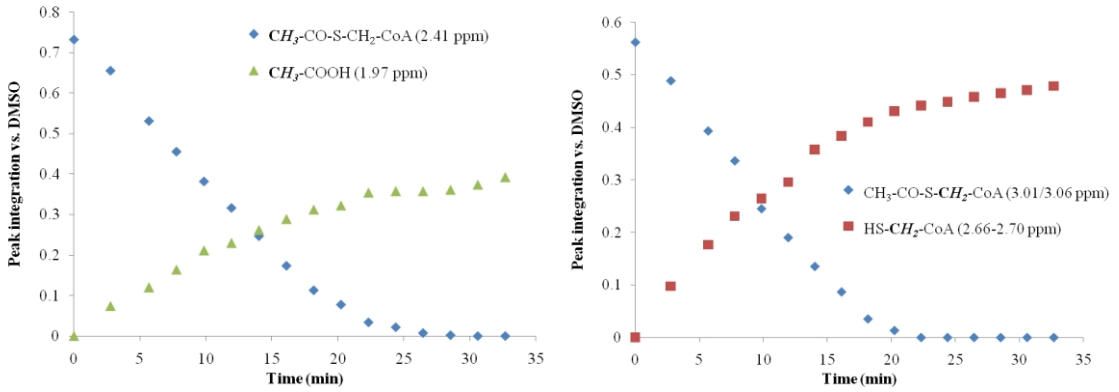


Figure VIII.12: Enzymatic reaction progress curves of folate-dependent AcCoA hydrolytic activity by mNat2.

Folate-dependent AcCoA hydrolysis by mNat2 was monitored by following characteristic peaks of both reagent and products *versus* 6*d*-DMSO, as internal standard. Consistent enzymatic activity plateaux were observed for loss of substrate. **(left)** The activity was followed by measuring integration of peaks at: 2.41 ppm for **C*H*$_3$**-CO-S-CH$_2$-CoA and 1.97 ppm for **C*H*$_3$**-COOH for acetate. **(right)** The activity was followed by measuring integration of peaks at: 3.06-3.01 ppm for CH$_3$-CO-S-**C*H*$_2$**-CoA and 2.70-2.66 ppm for SH-**C*H*$_2$**-CoA for CoA.

When spectra of both AcCoA and acetate at 400 µM were separately recorded, a difference was observed in the integration of the spectral bands corresponding to the two acetyl C*H*$_3$ groups and the ratio was estimated to be at 1.72 (AcCoA/acetate) (**Figure VIII.13-top**).

In the same way, spectra of both AcCoA and CoA (400µM) were recorded and the ratio of the integrations of the α-sulfur methylene groups was calculated at 1.17 (AcCoA/CoA) (**Figure VIII.13-bottom**). These factors were then used to scale the integration values of both acetate and CoA in relation to AcCoA.

Finally, all the integrations were converted into concentration values and plotted against

time (**Figure VIII.14**), giving four equivalent estimates of the initial enzymatic velocity, on average 21.62±2.08µM.min^{-1} (**Table VIII.2**).

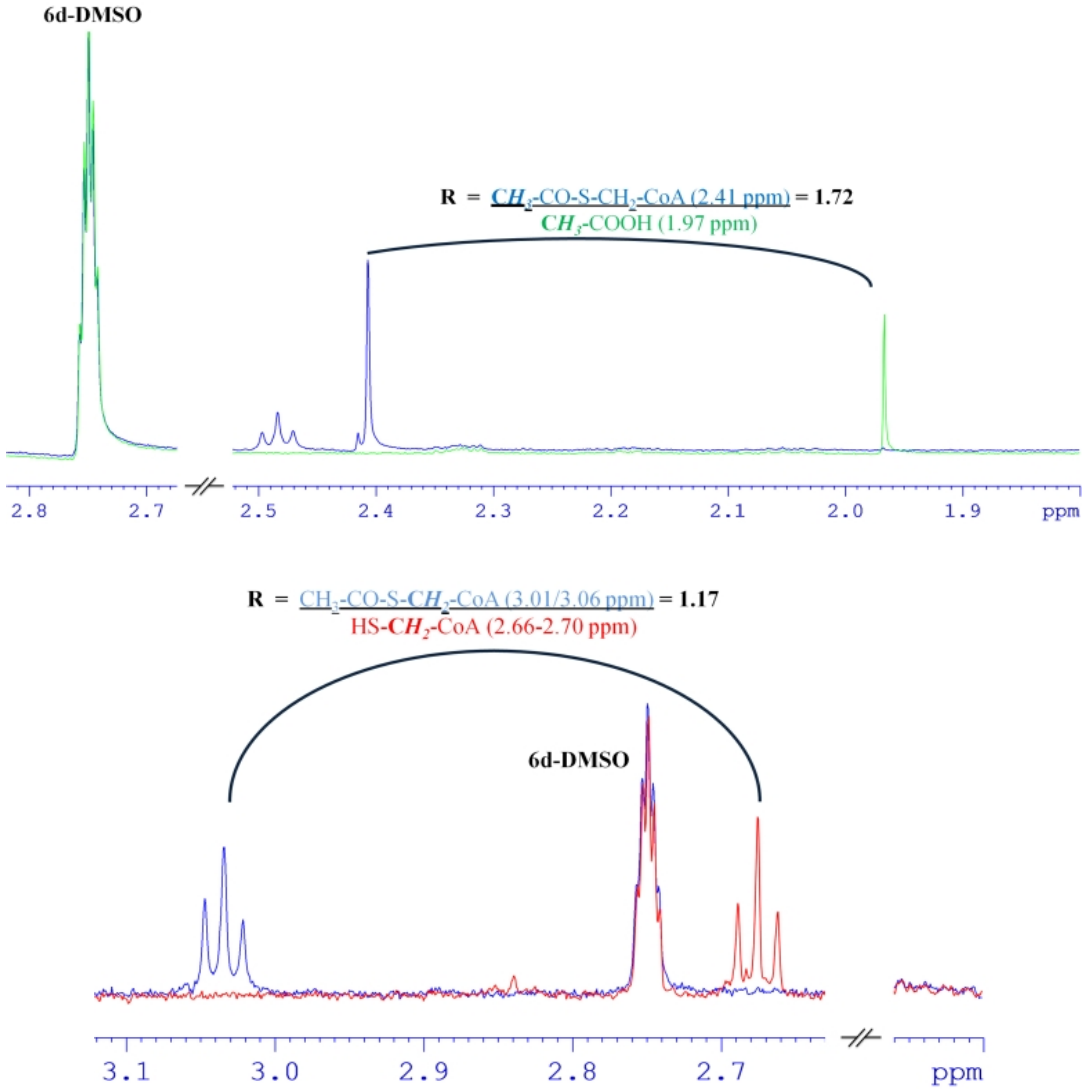


Figure VIII.13: Comparison of the integration of characteristic peaks of both substrate and products *versus* 6*d*-DMSO, as internal standard.

Ratio of integrations of AcCoA peak over appropriate product peak was measured. All reagents were used at 400 µM with 5% DMSO (v/v) in the assay. **(top)** Methyl peak integration was measured at 2.41 ppm for **C*H*$_3$**-CO-S-CH$_2$-CoA and 1.97 ppm for **C*H*$_2$**-COOH for acetate. NMR spectra were recorded with Bruker AVC500 (AcCoA, acetate) at 500MHz **(bottom)** CH$_2$ peak integration was measured at 3.06-3.01 ppm for CH$_3$-CO-S-**C*H*$_2$**-CoA and 2.70-2.66 ppm for SH-**C*H*$_2$**-CoA for CoA. NMR spectra were recorded with Bruker AV700 700MHz.

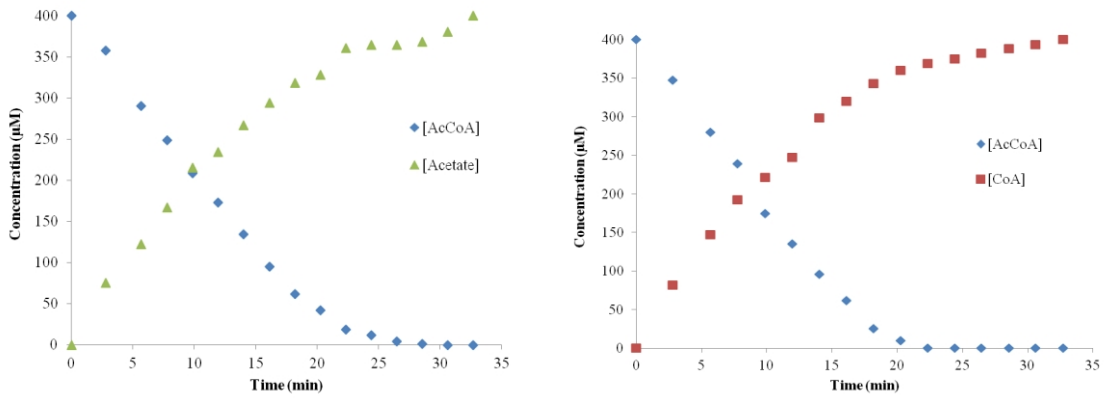


Figure VIII.14: Reaction progress curves of mNat2 activity as AcCoA hydrolase in the presence of folate, estimated using ^{1}H-NMR after correction.

Table VIII.2: Estimates of folate-dependet AcCoA hydrolysis by mNat2.

Proton bands at different chemical shifts were considered on the real-time ^{1}H-NMR assay.

	Acetyl C*H*$_3$		**Sulfur-C*H*$_2$**	
Monitored protons (chemical shift)	**C*H*$_3$**-CO-S-CH$_2$-CoA (2.41 ppm)	**C*H*$_3$**-COOH (1.97 ppm)	CH$_3$-CO-S-**C*H*$_2$**-CoA (3.01-3.06 ppm)	HS-**C*H*$_2$**-CoA (2.66-2.70 ppm)
mNat2 activity (µM.min^{-1})	19.87	20.99	24.64	20.95

Considering that the time for running a ^{1}H-NMR spectrum was around 4 sec, the average initial rate of AcCoA hydrolysis by mNat2 (21.62µM.min^{-1}) could give an estimate of the possible *N*-acetylfolate intermediate formed during the reaction: this would amount to 1.44 µM in the assay, which was 0.96% of the initial amount of folate (150µM).

In the initial ^{1}H-NMR spectra recorded at the beginning of the enzymatic assay, no appreciable differences were observed in the range of chemical shifts corresponding to the aromatic protons of the folate (ppm 6.5-9.0).

Finally, ^{1}H-NMR analyses depicted the formation of acetate by mNat2 using AcCoA in the presence of folate.

VIII.2.3 Inhibitor study of mNat2 as folate-dependent AcCoA hydrolase

Previous studies helped develop new enzymatic assays to test mNat2 as AcCoA hydrolase in the presence of folate. They also drew attention to the first catalytic step of the NAT reaction and suggested a new possible function of the enzyme.

Compounds **1** and **7**, being competitive inhibitors of mNat2, were therefore tested in these new folate-dependent enzymatic assays in order to establish their effective role as mNat2 inhibitors. The compounds were investigated in three diverse assays which were set up to follow as many reactions: the standard arylamine *N*-acetyltransferase reaction, the arylamine *N*-acetyltransferase reaction in the presence of folate, and the folate-dependent AcCoA hydrolysis reaction (**Figure VIII.15**).

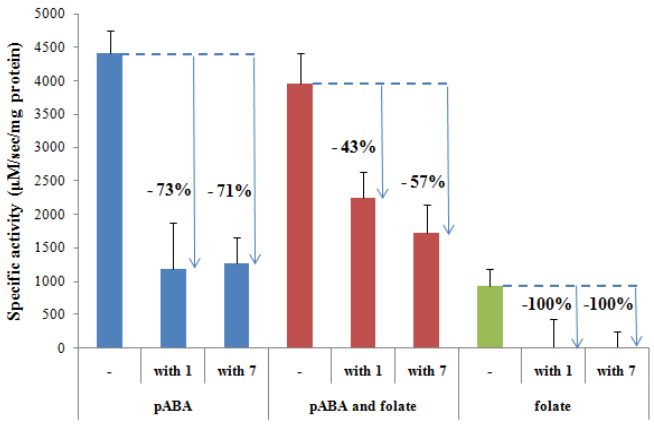


Figure VIII.15: Screening of different enzymatic assays with mNat2 in the presence of inhibitors 1 and 7.

Different AcCoA hydrolysis assays were carried out in order to monitor the inhibitory potency of naphthoquinones **1** and **7** at 10µM. Specific pABA (150µM) acetylation activities by mNat2 (5ng) with (red columns) and without (purple columns) an equimolar concentration of folate in the assay were perfomed. Specific AcCoA (400µM) hydrolysis activity by mNat2 (5ng) was detected in the presence of folate (150µM) in a DTNB assay without arylamine, as substrate (green columns). AcCoA was present at 400 µM concentrations in all assays. Percentage of reduction of mNat2 specific activity are measured against a control containing only 5% DMSO (v/v) in the assay.

As previously showed, both molecules were confirmed to be good inhibitors of mNat2 in the arylamine NAT reaction (**Figure VIII.15**); however, the inhibition was diminished by at least 20% when folate was added in the NAT assay (**Figure VIII.15**).

In contrast, the folate-dependent AcCoA hydrolytic activity of mNat2 was totally inhibited by both compounds **1** and **7** (**Figure VIII.15**).

In order to determine whether the inhibition of the lead compound **7** was not an artefact of the enzymatic assay, decreasing concentrations of the compound (from 10 to 0µM) were screened with mNat2 in folate-dependent AcCoA hydrolysis assays (**Figure VIII.16**).

An IC_{50} curve was drawn from the specific activity values obtained and 50% inhibition was estimated to occur at around 0.102 µM inhibitor in the assay. This IC_{50} value was roughly tenfold lower than the IC_{50} value of **7** calculated in a standard NAT assay with mNat2 (0.99µM).

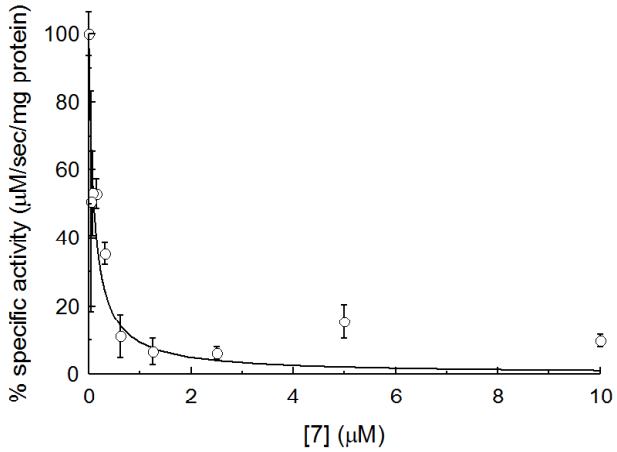


Figure VIII.16: IC_{50} curve of compound 7 as inhibitor of folate-dependent AcCoA hydrolytic activity by mNat2.

AcCoA-hydrolysis assays were performed using mNat2 (510ng), AcCoA (400µM), folate (150µM) as cofactor, and serial dilutions of compound **7**, 100% = 198.23µM.sec^{-1}.mg^{-1}. Data points are given as averages with error bars ± standard deviation of triplicate assays. Curve was fitted using KyPlot® software and given with p-values ≤ 0.01, considered significant.

VIII.3 Discussion

VIII.3.1 Selectivity of hNAT1 and mNat2 as AcCoA hydrolases in the presence of folate

The major question addressed in the experiments described in this chapter was the ability of some NAT enzymes to catalytically hydrolyse AcCoA in the presence of folate without the need of an arylamine substrate.

Dr J. Dairou, University of Paris VII, found that hNAT1 could produce CoA from AcCoA in the presence of folate alone, according to HPLC analyses. The interests of this preliminary catalytic reaction were twofold: firstly, AcCoA hydrolysis was not followed by an acetyl transfer, since the folate peak remained unchanged in the HPLC chromatogram; secondly, only hNAT1 was able to perform this catalysis, but not the other human isoenzyme, hNAT2.

In the same way, mNat2 distinctively acts as AcCoA hydrolase in the presence of folate alone in comparison to a panel of other mammalian and prokaryotic NATs, using different single-time assays. The exclusivity to both hNAT1 and mNat2 could be related to their high homology in primary sequence identity, substrate specificity and tissue functionality (Kawamura et al, 2008).

Moreover, ^{1}H-NMR real-time assay provided support for the acetyl group from AcCoA being cleaved and transferred as acetate to the buffer.

Amongst the initial suppositions about the folate-dependent mechanism of AcCoA hydrolysis by mNat2 and hNAT1, it was questioned whether the primary amine of folate would be firstly acetylated forming a possible *N*-acetylfolate intermediate, and subsequently hydrolysed.

Since the primary amine of folic acid (pK_a=8.4) (Jastrebova et al, 2006; Martin & Soniat, 2009; Noszai & Szakacs, 2006; Poe, 1973) would be protonated at the pH of en-

zymatic assays (pH 8), this amine would not constitute a good nucleophile to hydrolyse acetyl-Cys68 contrary to aniline, whose pK_a (pK_a=4.6) allows the substrate to act as a good nucleophile towards acetylated enzyme (pH 8) (**Figure VIII.15**).

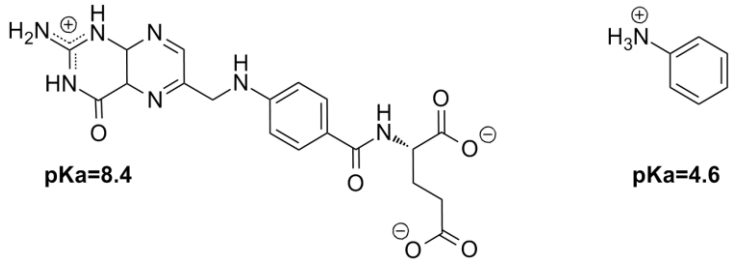


Figure VIII.17: Comparison of pK_a values of folate and aniline.

pK_a of folate (Poe, 1973), pK_a of aniline (H.C. Brown et al, 1955).

The more likely hypothesis relates with a new role of mNat2 as AcCoA hydrolase in the presence of folate, without forming an *N*-acetylated folate intermediate. More accurate analytical techniques would be needed to depict possible intermediate steps of the Ac-CoA hydrolysis reaction by mNat2 in the presence of folate in the assay.

Interestingly, another common acetyl donor used in other enzymatic assays with NATs, para-nitro phenyl acetate (Wang et al, 2005a; Wang et al, 2004b), was also found to be hydrolysed by hNAT1 in the presence of folate in the assay. This could support that whatever the acetyl donor, the intermediate acetylated form of hNAT1 or mNat2 becomes unstable in the presence of folate so that acetyl-Cys68 is hydrolysed.

The folate-dependent AcCoA hydrolysis corresponds to the first step of the bi-bi ping-pong reaction of NAT catalysis in the presence of an arylamine substrate. Whilst in a conventional NAT reaction the aromatic primary amine is considered to attack the thiolester function of the transitional acetyl-Cys68 to achieve the *N*-acetyl transfer to the arylamine (Wang et al, 2005a), in an AcCoA hydrolysis reaction by mNat2 in the presence of folate, the acetyl-Cys68 was hypothesised to be deacetylated by a molecule of water to form acetate.

Different questions arise from these experiments.

1) Firstly, how in a standard NAT reaction is acetyl-Cys68 protected from attack by water to deacetylate the catalytic residue such that an exogenous aromatic amine can act as acetyl acceptor?

As highlighted in a number of recent prokaryotic and eukaryotic NAT structures, an hydrophobic environment is required in the NAT active site pouch for substrate binding (Abuhammad et al, 2010; Wu et al, 2007). Following the acetylation of the catalytic cysteine, the hydrophobicity of the catalytic pocket would allow the enzyme to accept only highly hydrophobic molecules to be acetylated, such as arylamines and arylhydrazines (Westwood et al, 2006). Thus, molecules of water from the bulk solvent would be excluded from the active site for their polarity.

Indeed, control reactions of enzymatic NAT assays without arylamine do not show any appreciable AcCoA hydrolysis in the presence of mNat2: this would confirm that the possible acetylated form of the enzyme is enough stable in those conditions (Brooke et al, 2003b).

Conversely, in the presence of folate, the acetyl-Cys68 is directly hydrolysed, despite the hydrophobicity of the active site pocket, and this phenomenon follows a Michaelis-Menten trend.

This seems consistent with the hypothesis that folic acid somehow modifies the hydrophobicity of the catalytic site upon binding to the enzyme, thereby allowing water to enter the active site pocket and cleave acetyl-Cys68. A change in mNat2 folding is therefore hypothesised as induced by folate binding to the enzyme.

2) Secondly, how in a folate-rich enzymatic assay could folate act as either a cofactor or an inhibitor?

The folate-dependent AcCoA hydrolysis reaction was found to be related to folate concentrations in the assay: in the range 0-150 μM the hydrolysis of AcCoA increased as the folic acid concentrations increased, whereas over 150 μM the same enzymatic reaction seemed to be inhibited.

Comparing apparent affinity constants of both pABA and folate towards mNat2 as estimated in this study, the arylamine probe substrate has higher affinity than folate for the enzyme mNat2 (**Table VIII.3**). On the contrary, kinetic data obtained for hNAT1 from two different experiments seemed to be contradictory to previous observations with mNat2. This could be due to using different sources of hNAT1 enzymes: ZR-75-1 cell lysates for pABA and pure recombinant protein for folate. The same source of hNAT1 enzyme and the same experimenter would next be suited for a more accurate comparative study.

Table VIII.3: Apparent kinetic constants determined for mNat2 and hNAT1.

The apparent kinetic constants estimated for pure recombinant mNat2 using pABA or folate together with those measured for native hNAT1 in ZR-75-1 cell lysate using pABA were obtained throughout this study, whereas the data regarding hNAT1 with folate are provided by Dr J. Dairou, University of Paris VII [a].

Kinetic constants	mNat2		hNAT1	
V_{max}	449 ($\mu M.min^{-1}.\mu g^{-1}$)	613 ($\mu M.sec^{-1}.mg^{-1}$)	53 ($\mu M.min^{-1}.\mu g^{-1}$)	583 ($\mu M.sec^{-1}.mg^{-1}$)[a]
K_m^{app} (μM)	51 (pABA)	71 (folate)	127 (pABA)	75 (folate)[a]

Analogous with earlier observations by Dr. Dairou, folate at equimolar concentrations to the arylamine substrate (150μM) did not play an inhibitory role in any NAT assay presented in this study.

However, past studies showed that eukaryotic NATs are inhibited by folic acid or methotrexate either competitively or non-competitively to varying extents (**Table VIII.5**).

Although this seemed slightly contradictory with the results presented in this thesis, this discrepancy could be related to the method used to estimate NAT activity, in particular to the arylamine acetylation method rather than AcCoA hydrolysis method.

Indeed, the fact that folate could destabilise the intermediate acetylated form of NAT could bring up the accuracy of some enzymological techniques used to follow NAT activity, for instance the use of DMAB in the presence of folate.

In particular, in certain previous folate inhibitor studies with hNATs (Ward et al, 1992) measuring only the acetylation of the arylamine in a NAT assay might not have taken in account the possible additional catalytic hydrolysis of AcCoA to acetate in the bulk solvent. Nevertheless, in this study the arylamine acetylation method did not give inconsistent results compared to a DTNB-based approach at low concentrations of folate (150µM) (**Figure VIII.4**).

In general, for concentrations of folate higher than 150µM, inhibition of hNAT1 and mNat2 catalytic efficiency could be considered as without bias, whereas for concentrations lower than that threshold, kinetic inhibition values by folate would need to be optimised to accurately estimate both inhibition and possible AcCoA hydrolysis.

A few molecular details about the binding mode of folate in NAT were previously underlined, such as that the amethopterin inhibition of acetyl transfer depends to some extent on the presence of a methyl group at position R_2 (Jacobson, 1960) (**Figure VIII.18**). A crystal structure of one NAT enzyme with folic acid bound would help to define its real binding site, since kinetic studies could be sometimes biased by the accuracy of the detection method for catalytic activity, data processing and experimental context.

Compound	R_1	R_2
folate	OH	H
amethopterin	NH_2	CH_3

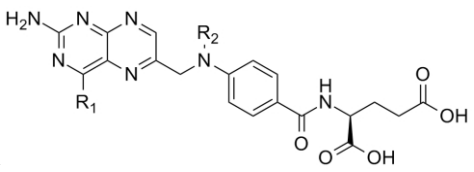


Figure VIII.18: Structures of folic acid and amethopterin

Table VIII.4: Summary of inhibition studies conducted on NATs with folate analogues.

[a]AcCoA was used as acetyl donor

Enzyme (source)	inhibitor (maximum concentrations tested)	Detection of NAT activity	inhibited substrate	mode of inhibition	K_I (µM)	Reference
NAT (Pigeon liver)	amethopterin (12µM)	p-nitroaniline formation	p-nitroacetanilide aniline	competitive non-competitive	32.5 ~ 9	(Jacobson, 1960)
NAT (Pigeon liver)	amethopterin (5µM)	p-nitroaniline disappearance	AcCoA p-nitroaniline	non-competitive non-competitive	3 3	(Andres et al, 1983b)
mNat C57BL/6J	folate (5mM) amethopterin (5mM)	arylamine acetylation (DMAB)	2AF[a] 2AF[a]	non-competitive non-competitive	1.1 0.9	(Hultin & Weber, 1985)
mNat A/J	folate (5mM) amethopterin (5mM)	arylamine acetylation (DMAB)	2AF[a] 2AF[a]	non-competitive non-competitive	2.8 2.4	(Hultin & Weber, 1985)
hNAT1	folate (100µM) amethopterin (100µM)	HPLC	pABA[a] pABA[a]	competitive competitive	13.3 9.5	(Ward et al, 1995)
hNAT1 (erythrocyte)	folate (2mM) amethopterin (2mM)	DMAB	-	-	~200 (IC_{50}) ~200 (IC_{50})	(Ward et al, 1992)

3) Finally, how could only hNAT1 and mNat2 selectively act as AcCoA hydrolase in the presence of folate, but none of the other NAT isoenzymes tested?

Since no harvestable crystals of mNat2 with folate as ligand were obtained, comparing existing human NAT structures was thought to help discriminate against the behaviour of each NAT towards AcCoA and folate.

As regards the overall folding of NAT enzymes from both prokaryotic and eukaryotic kingdoms, the major difference between prokaryotic and eukaryotic NATs consisted in the existence of a loop between domains two and three (Payton et al, 2001b; Sandy et al, 2005b), and this loop was found to be important in CoA binding specificity (Fullam et al, 2008; Wu et al, 2007) (**Figure VIII.19**).

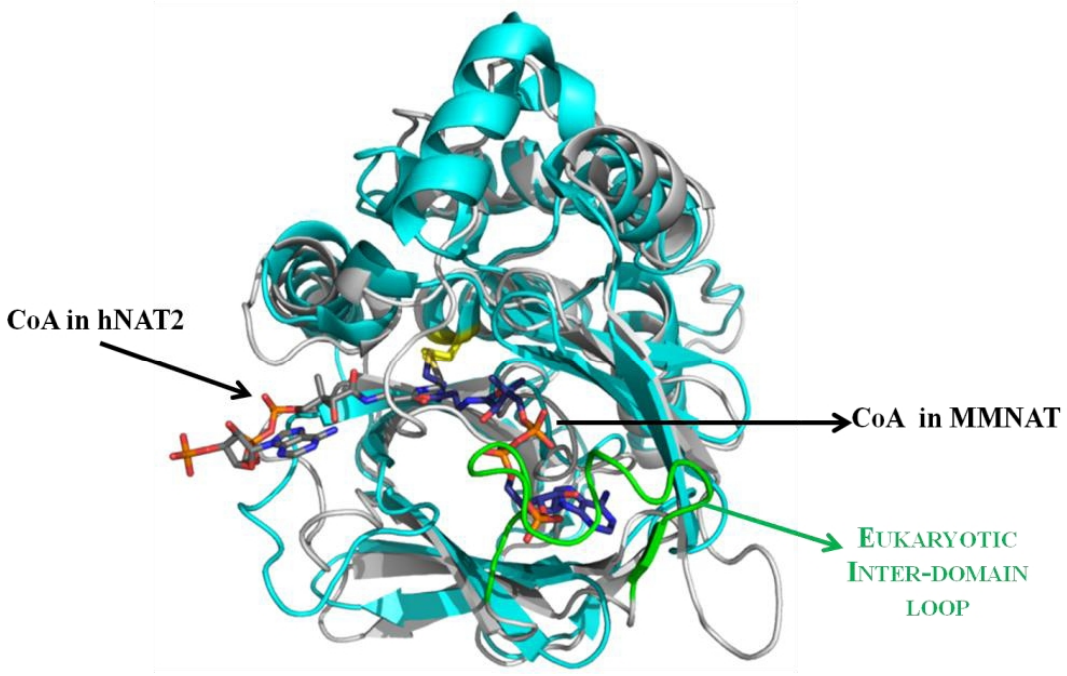


Figure VIII.19: Overall structure of hNAT2 and MMNAT, both with CoA bound.

Ribbon diagram showing the overlaid structures of hNAT2 (grey - pdb: 2PFR) (Wu et al, 2007) and MMNAT (blue - pdb: 2VFC) (Fullam et al, 2008). The CoA co-crystallised with the appropriate enzyme, is shown in sticks and labelled with carbon atoms in accoding to the enzyme colour, nitrogen in blue, oxygen in red, and sulfur in orange. The characteristic eukaryotic loop is coloured in green.

Moreover, shortening the third domain of STNAT, either completely or partially (Mushtaq et al, 2002), resulted in an increased hydrolysis of AcCoA and an inability of

the enzyme to transfer an acetyl group to an aromatic amine following formation of the acetyl-enzyme intermediate (Mushtaq et al, 2002).

Besides this, Wang et al. formerly discovered that acetyl-NAT could be also hydrolysed in the absence of arylamine substrate or in the presence of non-strong nucleophilic arylamine (Wang et al, 2005a). Also, a truncated version of hNAT1 with only the first 204 residues was found to hydrolyse AcCoA without concomitant acetylation of the arylamine substrate (Sinclair & Sim, 1997).

These discoveries could be linked to the folate-dependent AcCoA hydrolysis by hNAT1 and mNat2. They might suggest that folate could bind to these enzymes as a cofactor, thereby modifying their folding, and probably their third domain, involved in AcCoA turn over. This would consequently increase enzymatic efficiency in AcCoA hydrolysis, by further opening the hydrophobic active site to the bulk solvent.

After comparing the overall three-dimensional folding of human NATs (Wu et al, 2007), and in particular their corresponding third domain, no evident binding pocket appeared to be suitable for docking folate in order to explain somewhat its preference for hNAT1 and in parallel for mNat2 (**Figure VIII.20**).

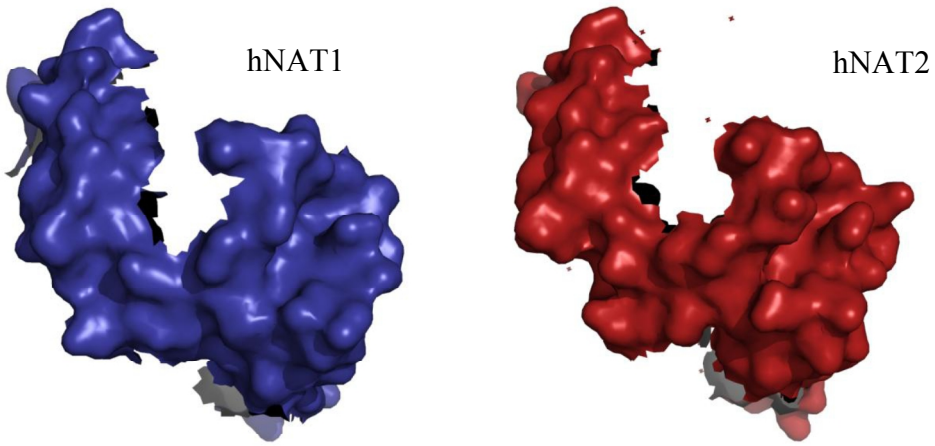


Figure VIII.20: Third domain of two human NAT enzymes.

The third domain of two NATs is shown in surface representation respectively. Pdb codes: 2PQT (hNAT1), and 2PFR (hNAT2).

Moreover, the exclusivity of both hNAT1 and mNat2 to act as AcCoA hydrolases in the presence of folate, appeared relatively close to the exclusivity of the same enzymes to use pABAglu as arylamine probe substrate. However, the fact that the inhibition mode of folate towards hNAT1 and mNat2 was differently defined in previous studies, as either competitive or non-competitive, did not help hypothesise a possible region wherein folate could bind (**Table VIII.5**). Structural modelling and enzymatic experiments have not been conclusive in determining the selective mode of binding between hNAT1 and folate.

VIII.3.2 Possible physiological significance of the AcCoA depletion by hNAT1

Since AcCoA is known to convey a 2-carbon unit through the acetyl group into the citric acid cycle for energy production, the cleavage of the acetyl group from AcCoA to acetate could look at first sight as a futile reaction for the waste of energy for cells (**Figure VIII.21**).

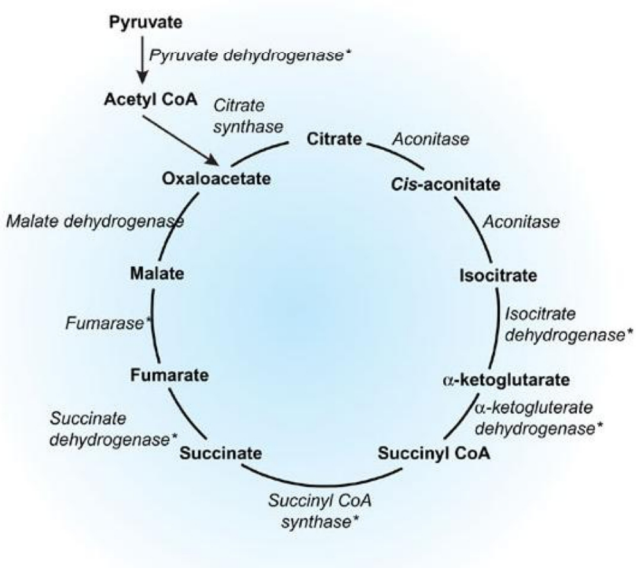


Figure VIII.21: The Krebs cycle.

Enzymes are in italics; asterisks indicate known enzymopathies. The figure is adapted from (Munnich, 2008).

There are two major sources of AcCoA in cells: pyruvate and fatty acids. The former is part of glucose metabolism, the latter is linked to fat degradation.

In general, oxidative cellular stress induces acceleration of fat catabolism, thereby producing greater amount of AcCoA to go through the citric acid cycle (Randle et al, 1963). The increase of the AcCoA/CoA ratio generated from fatty acid catabolism would obstruct AcCoA production from pyruvate by inhibiting the pyruvate dehydrogenase enzyme (Garland & Randle, 1964). Therefore, AcCoA concentrations in a cell could play a possible role in shifting cellular metabolism from glucose to fat.

Following the discovery of both hNAT1 and mNat2 enzymes acting as AcCoA hydrolases in the presence of an appropriate amount of folic acid, this reaction could be hypothesised to help enhance the catabolic turnover of fat, by augmenting the AcCoA hydrolysis rate. Since folic acid has generally been reported to also have an antioxidant power against reactive oxygen species (Matte et al, 2009; Moat et al, 2000), it is interesting to make a theoretical link between hNAT1 and folate regarding their combined role in fatty acid catabolism in conditions of oxidative stress: folate could help hNAT1 hydrolyse disproportionate AcCoA generated from fat catabolism to regulate AcCoA/CoA homeostasis in cells.

Compounds **1** and **7**, being selective inhibitors of hNAT1 and its homologue mNat2 also as folate-dependent AcCoA hydrolase, could be useful to modulate native enzymes and follow metabolic patterns thereafter.

VIII.3.3 Potential association between hNAT1 and folate in treating cancer

Considering pathological scenarios such as BC, the overexpression of *hNAT1* seems to have a functional significance for its strong relationship to the ER positivity in some

ER+ve breast tumours (Sim et al, 2008b; Wakefield et al, 2008b). Moreover, when the overexpression of hNAT1 has been induced in non-cancerous human breast cell lines, a cellular proliferation was observed (Adam et al, 2003).

The use of potent selective drug-like inhibitors against hNAT1 could possibly reduce tumour growth, as suggested throughout this thesis (**Chapter VI**) and in other previous studies (Tiang et al, 2010), and would make hNAT1 a new drug target for BC therapy.

Furthermore, amongst current chemotherapies, the folate analogue methotrexate had been largely used as anti-metabolite of DHFR with modest success (Bonadonna et al, 1995), to inhibit purine synthesis and stop cancer cell proliferation.

The studies presented in this chapter show a possible dynamic interaction between hNAT1, folate breakdown and AcCoA depletion.

On one side, a possible endogenous role of hNAT1 interacting with folate is hypothesised in fat catabolism *via* AcCoA hydrolysis. This could be related to cellular fat metabolism in normal or unhealthy BC cells, whose fat levels seemed to be influenced by diet and could affect the genesis and the development of the tumour (Alexander et al, 2010; Welsch, 1987).

The overexpression of hNAT1 in some ER+ve BCs might therefore enhance the hydrolytic depletion of AcCoA generated from fat catabolism. The functional significance of this hypothesis will still need further investigation, possibly using selective naphthoquinone inhibitors of hNAT1.

On the other side, since hNAT1 seems to be involved in folate catabolism through acetylation of pABAglu (Stanley et al, 1998), the degradation of methotrexate, as folate analogue, could give raise to pABAglu formation and thus be linked to hNAT1 for their homology in chemical structure.

Although the clinical relevance of using hNAT1 inhibitors to avoid promotion of BC still needs to be established, these compounds may also help decelerate methotrexate ca-

tabolism *via* inhibition of pABAglu acetylation by hNAT1. This might enhance the chemotherapeutic effects of methotrexate, as anti-metabolite drug. The combination of both methotrexate and hNAT1 inhibitors could be proposed to better treat BC.

Chapter IX:

Conclusions and further work



GIRL IN A CHEMISE (1905), BY PABLO PICASSO (1881-1973).

Picasso has only depicted one breast clearly, whereas the other breast is merely hinted *via* shading and high-lighting on her dress. It has also been hypothesised that the right breast has been removed (Tate collection, UK).

IX.1 Final conclusions

The extent to which the aims described in **Section 1.4** have been met in this thesis are discussed below:

- **To characterise the inhibition of the new hit compound 7 towards pure recombinant hNAT1 and its murine homologue, mNat2, *versus* other NAT isoenzymes (Chapter III).**

Naphthoquinone **7** was found to inhibit selectively hNAT1 and mNat2 to a much greater extent than other pure recombinant prokaryotic and eukaryotic NATs and to undergo a colour change from red to blue upon binding exclusively to these two NAT homologues. Ligand **7** was likely to reversibly bind to mNat2 and was also found to change colour only upon binding to properly folded protein.

The affinity constant, K_d, between **7** and mNat2 was estimated by spectrophotometry to be around 7.95 μM with one single binding site. Kinetic investigation suggested that inhibitor **7** was competitive towards mNat2 (K_I=420nM), therefore proposing that the compound could bind to mNat2 within its active site. In view of the homology between mNat2 and hNAT1, it is proposed that inhibition of hNAT1 by compound **7** is also competitive.

- **To elucidate the molecular mechanism of interaction between compound 7 and mNat2, as a model for hNAT1 (Chapter IV).**

In the complex formed by naphthoquinone **7** and mNat2, the deprotonation of sulfonamide-N*H* of **7** by the guanidine group of Arg127 within the active site of the enzyme was strongly supported by a range of physicochemical, biochemical and computational studies, which also elucidated the colour change mechanism of the ligand from red to

blue. It is proposed that Arg127 is also involved in the colour change of naphthoquinone **7** in the complex hNAT1-**7**.

Moreover, docking studies with hNAT1/mNat2 and compound **7** and biochemical investigation around other NAT isoforms highlighted the importance of other two residues in support of the selectivity of compound **7** towards hNAT1 and mNat2: Phe125 and Tyr129. The residue Phe125 is hypothesised to orientate naphthoquinone **7** within the active site of hNAT1/mNat2 in order to allow the acid base proton exchange between **7** and Arg127; the residue Tyr129 is likely to enhance the affinity between the ligand and the target enzyme *via* hydrophobic π-π stacking interactions.

The trio of Phe125, Arg127, and Tyr129 is unique in both hNAT1 and mNat2 amongst other NATs including hNAT2, supporting the development of these selective hNAT1/mNat2 inhibitors for further investigation.

- **To study substrate specificity of human and murine native proteins *versus* mutant NAT enzymes (Chapter V).**

Mutating Arg127 into either Gly or Leu in mNat2 helped support the key role of Arg127 into preferring arylamine substrates with negatively charged *para*-substituents at pH 8.

The mutation F125S of mNat2 allowed increase of arylhydrazine acetylation, consistent with an alteration of the structural conformation of the active site.

A more comprehensive comparison of the substrate specificities of eight different mammalian NATs (hNAT1, hNAT2, mNat2, mNat1, shNat2, mNat2_F125S, mNat2_R127G, mNat2_R127L) reinforced the theory that the residues at positions 125, 127, and 129 in this set of mammalian NATs plays a crucial role in substrate selectivity.

The combined role of Arg127, Phe 125, and Tyr 129 in both inhibitor and substrate selectivity of hNAT1/mNat2 underpins also the use of compound **7** as a colourimetric

probe to detect selectively hNAT1 in breast cancer cell lysate.

- **To apply the lead compound 7 for detection of hNAT1 in the BC cell line ZR-75-1 and to investigate its effect on cells (Chapter VI).**

Lysates of the ER+ve cell line ZR-75-1 were found to be a good source of active native hNAT1 and were used to determine the inhibitory potency of both compounds **1** and **7** towards hNAT1 in a cellular environment. Western blotting and dot blotting were used to estimate the amount of hNAT1 in ZR-75-1 cell lysates: ~17.7 million molecules of hNAT1 per cell. Nevertheless, it was not possible to detect either spectrophotometrically or by eye the biomarker hNAT1 in ZR-75-1 cell lysates using the colourimetric properties of biosensor **7**. The extent, to which improvement of the properties of compound **7** was required, was estimated: an affinity (K_d) of the ligand for the protein target in a nM range and a tenfold enhancement of the molar extinction coefficient of the probe compared to that of compound **7**.

Preliminary investigations around the effect of naphthoquinone **7** on cell viability and cell proliferation highlighted that compound **7** negatively influenced the growth of the ZR-75-1 cell line, without affecting the cell viability for concentrations <5µg.ml^{-1}. With other cell lines, such as RAJI and RAW cells, a drastic cytotoxic effect was noticed at high concentration (100µg.ml^{-1}). No cytotoxic effects were observed when *E. coli* colonies were grown in the presence of compound **7** at 100µg.ml^{-1}, although the metabolism of compound **7** by these cells was proposed to be linked to the decolourisation of the dye in the extracellular medium.

- **To optimise the affinity of compound 7 towards hNAT1 and mNat2 (Chapter VII).**

After determining the ideal characteristics of a biosensor to detect native hNAT1 in ZR-

75-1 breast cancer cell lysates (**Section VII.1.3**), structure-activity relationship (SAR) studies were carried out on a sub-library of compound **7** analogues using pure recombinant hNAT1, mNat2 and hNAT2, as negative control.

As regards the SAR of this family of ligands, the substituents at position C_2 (sulfonamide, amine) and C_3 (aniline, phenol, arene) on the naphthoquinone core were found to have a major influence on the pK_a of the ligands, without particularly enhancing their inhibitory potency compared to naphthoquinone **7**. Considerable improvements of inhibitory activity were observed only when an amino group was substituted at position C_8 on the naphthquinone core.

Virtual docking studies on hNAT1 highlighted possible hydrogen bonding between the guanidinium group of Arg127 and the primary amine at C_8. However, the spectrophotometric properties of the ligand with an amino group at C_8 were not adequate for use in visible detection of hNAT1 in cancer cell lysates.

The introduction of auxochromic groups (nitro or amine groups) on the naphthoquinone moiety of the lead compound **7** resulted undesirable additional peaks into the spectrum of the dyes. Modifying the conjugation system of the hit compound **7** was suggested to be further developed in order to increase the bathochromicity and the brightness of the chromogen of the lead ligand in accordance with resonance theory.

- **To investigate the endogenous role of hNAT1 and mNat2 as folate-dependent-AcCoA hydrolases (Chapter VIII).**

Similar to hNAT1, mNat2 was found to be distinctively able to act as AcCoA hydrolase in the presence of folate without the need for an arylamine substrate, in comparison to a panel of other mammalian and prokaryotic NATs, using different single-time assays. ^{1}H-NMR real-time assays provided support that the acetyl group from AcCoA was cleaved by mNat2 and transferred to the bulk solvent as acetate.

The exclusivity to both hNAT1 and mNat2 was hypothesised to be related to the high homology of both enzymes in primary sequence identity, tissue distribution and endogenous functionality in early development. The overall protein folding and the hydrophobicity of both hNAT1 and mNat2 within the catalytic active site were proposed to be modified by folate binding as cofactor, thereby allowing water to enter the active side pocket and cleave the intermediate acetyl-Cys68.

These studies add information to understanding of the endogenous role of hNAT1 in health and disease. The AcCoA hydrolytic reaction by this enzyme was proposed to act as a link between folate and AcCoA at the heart of the catabolic turnover of fat in both physiological and pathological conditions.

Compounds **1** and **7** were found to act as selective inhibitors of mNat2 when tested as folate-dependent AcCoA hydrolases. These naphthoquinones were therefore proposed to help further define the precise endogenous role of hNAT1 in metabolism.

The inhibitory effects of these compounds on both folate-dependent AcCoA hydrolysis and pABAglu acetylation may warrant further investigations of chemotherapeutic strategies targeting folate metabolism.

IX.2 Further work

IX.2.1 Biosensor development

The work presented in this thesis has advanced the understanding of the molecular interactions of the colour change event involving the colourimetric probe **7** and hNAT1, through studies conducted on its murine homologue, mNat2 (**Chapters IV**). Nevertheless, a co-crystal structure of compound **7** (or a more potent derivative) and hNAT1, or mNat2, is desired to further validate the hypothesised binding mode of **7** towards mNat2

as a model for hNAT1.

Therefore, a set of novel inhibitors with higher affinity for the enzyme and improved solubility in water may circumvent these issues.

Moreover, there is still the need to improve these selective naphthoquinones as biosensors for hNAT1 in breast cancer. In particular, investigations conducted on the cell permeability, the cytotoxicity (**Chapter VI**) and the SAR of this family of naphthoquinones (**Chapter VII**) has highlighted several requirements:

- to enhance the affinity of the ligand for the protein target by at least 500 times;
- to improve the colour intensity of the probe by augmentating the molar extinction coefficient by no less than tenfold.

In order to generate brighter naphthoquinone dyes as biosensors of hNAT1, avoiding introducing additional peaks into their visible spectra, the valence-bond theory could be taken in account: the more conjugated the resonance system generating the colour, the more bathochromic the colour of the dye. Modification of the conjugation system of compound **7** should be considered by increasing the number of possible dislocations of the negative charge in the conjugate base.

Therefore, at position C_3, instead of an aniline moiety, a further double bond should be added, such as C=C or an azo group, continuing with an aromatic group preferably ending with a strong electron-withdrawing group (**Figure IX.1**).

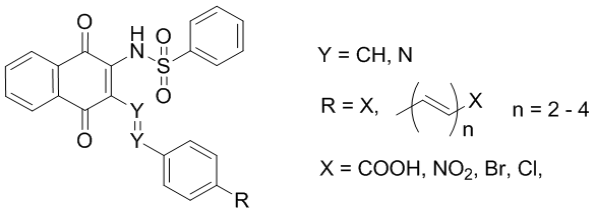
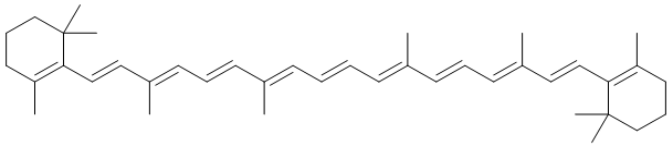


Figure IX.1: Possible compounds to be synthesised in order to improve colour intensity.

If the pharmacological and spectrophotometric properties of these new dyes were consistent with the parameters selected in this study (**Section VII.1.3**), further conjugation

should be added to the same system, as inspired by the β-carotene structure (**Figure IX.2**), which possesses one of the highest molar extinction coefficients recorded to date (139,500 $M^{-1}.cm^{-1}$ at 451 nm (Zechmeister, 1962)).



***β*-carotene**

Figure IX.2: Chemical structure of *β*-carotene.

Moreover, over the course of this study, this family of naphthoquinones have been observed to possess poor aqueous solubility, which needs to be addressed in downstream development.

Ideally, amine and nitro groups, introduced on the naphthoquinone core to enhance the ligand affinity for hNAT1, could be substituted with hydroxyl and carboxylate respectively in order to maintain the physicochemical properties of the original substituents.

This might both improve the solubility of the compound in aqueous solutions, thereby facilitating the performance of all biological assays and crystallisation trials, and also reducing their possible carcinogenic effects in cells.

IX.2.2 Drug development

Moreover, besides improving solubility in aqueous solutions and cell permeability of naphthoquinones by introducing polar substituents, it is necessary to develop more comprehensive studies on cell specificity, toxicity, permeability and viability of this family of naphthoquinones in relation to the amount of hNAT1 in each cell line tested, estimated using western blot and dot blot analyses.

In particular, the comparison of the effect of these hNAT1 inhibitors on ER+ve *versus*

ER-ve cell lines, PR+ve *versus* PR-ve cell lines, could help support the development of these compounds as drugs targeting cell strains overexpressing hNAT1.

IX.2.3 Investigation about hNAT1 endogenous role

There is also a need for further investigation on the endogenous role of hNAT1, particularly in relation to its possible involvement in cellular metabolism *via* AcCoA and *n*-propionylCoA depletion in the presence of folate.

As regards the molecular mechanism of this catalysis, more sensitive spectroscopic techniques, such as infrared spectroscopy, could be used to assess the possible formation of an *N*-acetylfolate in the folate-dependent AcCoA-hydrolysis assay with mNat2 or hNAT1. Stereoselective chemical acetylation of the primary amine could also help give further insight on the additional catalytic role of hNAT1 or mNat2 as AcCoA hydrolases.

In the absence of a co-crystal structure of either hNAT1 or mNat2 with folate, NMR spectroscopy of proteins might help define the binding site of folate within both enzymes, for instance using NOESY-based methods with ^{15}N-labelled enzymes (Kawamura et al, 2008).

Besides this, similar kinetic studies may also be conducted with hNAT1/mNat2 using folate derivatives, such as methotrexate, pterin, pteroate, or polyglutamate folate, in order to better define the important moiety within folate necessary to allow hNAT1/mNat2 to deplete AcCoA.

Finally, hNAT1/mNat2 inhibitors with higher affinity would be required for more comprehensive cell studies, such as gene expression profiling and metabolism profiling, after selective inhibition of hNAT1/mNat2 in both physiological and pathological conditions, including breast cancer.

References

Abuhammad A, Lack N, Schweichler J, Staunton D, Sim RB, Sim E (2011) Improvement of the expression and purification of Mycobacterium tuberculosis arylamine N-acetyltransferase (TBNAT) a potential target for novel anti-tubercular agents. *Protein Expr Purif*

Abuhammad AM, Lowe ED, Fullam E, Noble M, Garman EF, Sim E (2010) Probing the architecture of the Mycobacterium marinum arylamine N-acetyltransferase active site. *Protein Cell* **1:** 384-392

Adam PJ, Berry J, Loader JA, Tyson KL, Craggs G, Smith P, De Belin J, Steers G, Pezzella F, Sachsenmeir KF, Stamps AC, Herath A, Sim E, O'Hare MJ, Harris AL, Terrett JA (2003) Arylamine N-acetyltransferase-1 is highly expressed in breast cancers and conveys enhanced growth and resistance to etoposide in vitro. *Mol Cancer Res* **1:** 826-835

Airley R (2009) *Cancer chemotherapy*, Chichester, UK ; Hoboken, NJ: Wiley-Blackwell.

Alexander DD, Morimoto LM, Mink PJ, Lowe KA (2010) Summary and meta-analysis of prospective studies of animal fat intake and breast cancer. *Nutr Res Rev* **23:** 169-179

Allred DC, Mohsin SK, Fuqua SA (2001) Histological and biological evolution of human premalignant breast disease. *Endocr Relat Cancer* **8:** 47-61

Ambrosone CB, Kropp S, Yang J, Yao S, Shields PG, Chang-Claude J (2008) Cigarette smoking, N-acetyltransferase 2 genotypes, and breast cancer risk: pooled analysis and meta-analysis. *Cancer Epidemiol Biomarkers Prev* **17:** 15-26

Anderson E (2002) The role of oestrogen and progesterone receptors in human mammary development and tumorigenesis. *Breast Cancer Res* **4:** 197-201

Anderton MC, Bhakta S, Besra GS, Jeavons P, Eltis LD, Sim E (2006) Characterization of the putative operon containing arylamine N-acetyltransferase (nat) in Mycobacterium bovis BCG. *Mol Microbiol* **59:** 181-192

Andres HH, Klem AJ, Schopfer LM, Harrison JK, Weber WW (1988) On the active site of liver acetyl-CoA. Arylamine N-acetyltransferase from rapid acetylator rabbits (III/J). *J Biol Chem* **263:** 7521-7527

Andres HH, Klem AJ, Szabo SM, Weber WW (1985) New spectrophotometric and radiochemical assays for acetyl-CoA: arylamine N-acetyltransferase applicable to a variety of arylamines. *Anal Biochem* **145:** 367-375

Andres HH, Kolb HJ, Schreiber RJ, Weiss L (1983a) Characterization of the active site, substrate specificity and kinetic properties of acetyl-CoA:arylamine N-acetyltransferase from pigeon liver. *Biochim Biophys Acta* **746:** 193-201

Andres HH, Kolb HJ, Weiss L (1983b) Purification and physical-chemical properties of acetyl-CoA:arylamine N-acetyltransferase from pigeon liver. *Biochim Biophys Acta* **746:** 182-192

Anslyn EV (2010) Supramolecular and chemical cascade approaches to molecular sensing. *J Am Chem Soc* **132:** 15833-15835

Antoniou (2003) Average risks of breast and ovarian cancer associated with BRCA1 or BRCA2 mutations detected in case series unselected for family history: A combined analysis of 22 studies (vol 72, pg 1117, 2003). *American Journal of Human Genetics* **73:** 709-709

Antoniou AC, Easton DF (2006) Risk prediction models for familial breast cancer. *Future Oncol* **2:** 257-274

Armstrong HE (1888) Abstracts of the Proceedings of the Chemical Society, Vol. 4, No. 49. *Proceedings of the Chemical Society, London* **4:** 27-34

Arnold K, Bordoli L, Kopp J, Schwede T (2006) The SWISS-MODEL workspace: a web-based environment for protein structure homology modelling. *Bioinformatics* **22:** 195-201

Ashburn TT, Thor KB (2004) Drug repositioning: identifying and developing new uses for existing drugs. *Nat Rev Drug Discov* **3:** 673-683

Assersohn L, Gangi L, Zhao YD, Dowsett M, Simon R, Powles TJ, Liu ET (2002) The feasibility of using fine needle aspiration from primary breast cancers for cDNA microarray analyses. *Clin Cancer Res* **8:** 794-801

Atkins GL, Nimmo IA (1975) A comparison of seven methods for fitting the Michaelis-Menten equation. *Biochem J* **149:** 775-777

Atkins PW (1998) *Physical chemistry*, 6th edn. Oxford: Oxford University Press.

Baan R, Straif K, Grosse Y, Secretan B, El Ghissassi F, Bouvard V, Altieri A, Cogliano V, Monograph WIARC (2007) Carcinogenicity of alcoholic beverages. *Lancet Oncol* **8:** 292-293

Bae JS, Son YA, Kim SH (2008) Solvatochromism of Indonaphthol Dye. *Fiber Polym* **9:** 659-660

Ballester PJ, Richards WG (2007) Ultrafast shape recognition to search compound databases for similar molecular shapes. *J Comput Chem* **28:** 1711-1723

Ballester PJ, Westwood I, Laurieri N, Sim E, Richards WG (2010) Prospective virtual screening with Ultrafast Shape Recognition: the identification of novel inhibitors of arylamine N-acetyltransferases. *J R Soc Interface* **7:** 335-342

Barker DF, Husain A, Neale JR, Martini BD, Zhang X, Doll MA, States JC, Hein DW (2006) Functional properties of an alternative, tissue-specific promoter for human arylamine N-acetyltransferase 1. *Pharmacogenet Genomics* **16:** 515-525

Beers MH, Merck Research Laboratories. (2006) *The Merck manual of diagnosis and therapy*, 18th edn. Whitehouse Station, N.J.: Merck Research Laboratories.

Beland FA, Kadlubar FF (1985) Formation and persistence of arylamine DNA adducts in vivo. *Environ Health Perspect* **62:** 19-30

Belletti B, Vaidya JS, D'Andrea S, Entschladen F, Roncadin M, Lovat F, Berton S, Perin T, Candiani E, Reccanello S, Veronesi A, Canzonieri V, Trovo MG, Zaenker KS,

Colombatti A, Baldassarre G, Massarut S (2008) Targeted intraoperative radiotherapy impairs the stimulation of breast cancer cell proliferation and invasion caused by surgical wounding. *Clin Cancer Res* **14:** 1325-1332

Benkert P, Biasini M, Schwede T (2011) Toward the estimation of the absolute quality of individual protein structure models. *Bioinformatics* **27:** 343-350

Benkert P, Tosatto SC, Schomburg D (2008) QMEAN: A comprehensive scoring function for model quality assessment. *Proteins* **71:** 261-277

Beral V, al. (1997) Breast cancer and hormone replacement therapy: collaborative reanalysis of data from 51 epidemiological studies of 52,705 women with breast cancer and 108,411 women without breast cancer. *Lancet* **350:** 1047-1059

Beral V, Bull D, Doll R, Peto R, Reeves G, Cancer CGoHFiB (2001) Familial breast cancer: collaborative reanalysis of individual data from 52 epidemiological studies including 58 209 women with breast cancer and 101 986 women without the disease. *Lancet* **358:** 1389-1399

Beral V, Bull D, Doll R, Peto R, Reeves G, La Vecchia C, Magnusson C, Miller T, Peterson B, Pike M, Thomas D, van Leeuwen F, Cancer CGoHFiB (2002) Breast cancer and breastfeeding: collaborative reanalysis of individual data from 47 epidemiological studies in 30 countries, including 50 302 women with breast cancer and 96 973 women without the disease. *Lancet* **360:** 187-195

Berg JM, Tymoczko JL, Stryer L (2007) *Biochemistry*, 6th edn. New York: W. H. Freeman.

Bernstein J, Lott WA, Steinberg BA, Yale HL (1952) Chemotherapy of experimental tuberculosis. V. Isonicotinic acid hydrazide (nydrazid) and related compounds. *Am Rev Tuberc* **65:** 357-364

Berrino F, De Angelis R, Sant M, Rosso S, Bielska-Lasota M, Coebergh JW, Santaquilani M (2007) Survival for eight major cancers and all cancers combined for European adults diagnosed in 1995-99: results of the EUROCARE-4 study. *Lancet Oncol* **8:** 773-783

Berstein LM, Santen RJ (2008) *Innovative endocrinology of cancer*, New York ; London: Springer.

Bhakta S, Besra GS, Upton AM, Parish T, Sholto-Douglas-Vernon C, Gibson KJ, Knutton S, Gordon S, DaSilva RP, Anderton MC, Sim E (2004) Arylamine N-acetyltransferase is required for synthesis of mycolic acids and complex lipids in Mycobacterium bovis BCG and represents a novel drug target. *J Exp Med* **199:** 1191-1199

Bieche I, Girault I, Urbain E, Tozlu S, Lidereau R (2004) Relationship between intratumoral expression of genes coding for xenobiotic-metabolizing enzymes and benefit from adjuvant tamoxifen in estrogen receptor alpha-positive postmenopausal breast carcinoma. *Breast Cancer Res* **6:** R252-263

Bieche I, Lidereau R (2011) Genome-based and transcriptome-based molecular classification of breast cancer. *Curr Opin Oncol* **23:** 93-99

Bingham SA, Luben R, Welch A, Wareham N, Khaw KT, Day N (2003) Are imprecise methods obscuring a relation between fat and breast cancer? *Lancet* **362:** 212-214

Blackburn GL, Wang KA (2007) Dietary fat reduction and breast cancer outcome: results from the Women's Intervention Nutrition Study (WINS). *American Journal of Clinical Nutrition* **86:** 878s-881s

Blum M, Grant DM, Demierre A, Meyer UA (1989) N-acetylation pharmacogenetics: a gene deletion causes absence of arylamine N-acetyltransferase in liver of slow acetylator rabbits. *Proc Natl Acad Sci U S A* **86:** 9554-9557

Blum M, Grant DM, McBride W, Heim M, Meyer UA (1990) Human arylamine N-acetyltransferase genes: isolation, chromosomal localization, and functional expression. *DNA Cell Biol* **9:** 193-203

Bonadonna G, Valagussa P, Moliterni A, Zambetti M, Brambilla C (1995) Adjuvant cyclophosphamide, methotrexate, and fluorouracil in node-positive breast cancer: the results of 20 years of follow-up. *N Engl J Med* **332:** 901-906

Bordwell FG, Algrim D (1976) Nitrogen Acids .1. Carboxamides and Sulfonamides. *J Org Chem* **41:** 2507-2508

Bordwell FG, Algrim DJ (1988) Acidities of Anilines in Dimethyl-Sulfoxide Solution. *Journal of the American Chemical Society* **110:** 2964-2968

Boukouvala S, Fakis G (2005) Arylamine N-acetyltransferases: what we learn from genes and genomes. *Drug Metab Rev* **37:** 511-564

Boukouvala S, Price N, Plant KE, Sim E (2003) Structure and transcriptional regulation of the Nat2 gene encoding for the drug-metabolizing enzyme arylamine N-acetyltransferase type 2 in mice. *Biochem J* **375:** 593-602

Boukouvala S, Price N, Sim E (2002) Identification and functional characterization of novel polymorphisms associated with the genes for arylamine N-acetyltransferases in mice. *Pharmacogenetics* **12:** 385-394

Boyd NF, Stone J, Vogt KN, Connelly BS, Martin LJ, Minkin S (2003) Dietary fat and breast cancer risk revisited: a meta-analysis of the published literature. *Brit J Cancer* **89:** 1672-1685

Braithwaite PA, Shugg D (1983) Rembrandt's Bathsheba: the dark shadow of the left breast. *Ann R Coll Surg Engl* **65:** 337-338

Brooke EW, Davies SG, Mulvaney AW, Okada M, Pompeo F, Sim E, Vickers RJ, Westwood IM (2003a) Synthesis and in vitro evaluation of novel small molecule inhibitors of bacterial arylamine N-acetyltransferases (NATs). *Bioorg Med Chem Lett* **13:** 2527-2530

Brooke EW, Davies SG, Mulvaney AW, Pompeo F, Sim E, Vickers RJ (2003b) An approach to identifying novel substrates of bacterial arylamine N-acetyltransferases. *Bioorg Med Chem* **11:** 1227-1234

Brzostek A, Dziadek B, Rumijowska-Galewicz A, Pawelczyk J, Dziadek J (2007) Cholesterol oxidase is required for virulence of Mycobacterium tuberculosis. *FEMS Microbiol Lett* **275:** 106-112

Brzozowski AM, Pike AC, Dauter Z, Hubbard RE, Bonn T, Engstrom O, Ohman L, Greene GL, Gustafsson JA, Carlquist M (1997) Molecular basis of agonism and antagonism in the oestrogen receptor. *Nature* **389:** 753-758

Burris HA, 3rd (2004) Dual kinase inhibition in the treatment of breast cancer: initial experience with the EGFR/ErbB-2 inhibitor lapatinib. *Oncologist* **9 Suppl 3:** 10-15

Burstein HJ (2005) The distinctive nature of HER2-positive breast cancers. *N Engl J Med* **353:** 1652-1654

Butcher NJ, Arulpragasam A, Pope C, Minchin RF (2003) Identification of a minimal promoter sequence for the human N-acetyltransferase Type I gene that binds AP-1 (activator protein 1) and YY-1 (Yin and Yang 1). *Biochem J* **376:** 441-448

Butcher NJ, Tetlow NL, Cheung C, Broadhurst GM, Minchin RF (2007) Induction of human arylamine N-acetyltransferase type I by androgens in human prostate cancer cells. *Cancer Res* **67:** 85-92

Campaigne E (1959) The contributions of Fritz Arndt to resonance theory. *Journal of Chemical Education* **36:** 336

Cancer-Reserch-UK. (2011) Breast Cancer Types - http://info.cancerresearchuk.org/cancerstats/types/breast/.

CancerResearchUK. (2007) UK Breast Cancer incidence statistics. http://info.cancerresearchuk.org/cancerstats/types/breast/incidence/.

Cao W, Chau B, Hunter R, Strnatka D, McQueen CA, Erickson RP (2005) Only low levels of exogenous N-acetyltransferase can be achieved in transgenic mice. *Pharmacogenomics J* **5:** 255-261

Cartwright RA, Glashan RW, Rogers HJ, Ahmad RA, Barham-Hall D, Higgins E, Kahn MA (1982) Role of N-acetyltransferase phenotypes in bladder carcinogenesis: a pharmacogenetic epidemiological approach to bladder cancer. *Lancet* **2:** 842-845

Chan MF, Dowsett M, Folkerd E, Bingham S, Wareham N, Luben R, Welch A, Khaw KT (2007) Usual physical activity and endogenous sex hormones in postmenopausal women: The European prospective investigation into cancer - Norfolk Population Study. *Cancer Epidemiology Biomarkers & Prevention* **16:** 900-905

Cheon HG, Boteju LW, Hanna PE (1992) Affinity alkylation of hamster hepatic arylamine N-acetyltransferases: isolation of a modified cysteine residue. *Mol Pharmacol* **42:** 82-93

Cheon HG, Hanna PE (1992) Effect of group-selective modification reagents on arylamine N-acetyltransferase activities. *Biochem Pharmacol* **43:** 2255-2268

Christie RM, Royal Society of Chemistry (Great Britain). (2001) *Colour chemistry*, Cambridge: Royal Society of Chemistry.

Ciocca DR, Elledge R (2000) Molecular markers for predicting response to tamoxifen in breast cancer patients. *Endocrine* **13:** 1-10

Cleland WW (1963) The kinetics of enzyme-catalyzed reactions with two or more substrates or products. I. Nomenclature and rate equations. *Biochim Biophys Acta* **67:** 104-137

Collaborative-Group-on-Hormonal-Factors-in-Breast-Cancer (1996) Breast cancer and hormonal contraceptives: collaborative reanalysis of individual data on 53 297 women with breast cancer and 100 239 women without breast cancer from 54 epidemiological studies. *The Lancet* **347:** 1713-1727

Cornish VA, Pinter K, Boukouvala S, Johnson N, Labrousse C, Payton M, Priddle H, Smith AJ, Sim E (2003) Generation and analysis of mice with a targeted disruption of the arylamine N-acetyltransferase type 2 gene. *Pharmacogenomics J* **3:** 169-177

Coroneos E, Sim E (1993) Arylamine N-acetyltransferase activity in human cultured cell lines. *Biochem J* **294 (Pt 2):** 481-486

Cravatt BF, Wright AT, Kozarich JW (2008) Activity-based protein profiling: from enzyme chemistry to proteomic chemistry. *Annu Rev Biochem* **77:** 383-414

Crawford MHJ (2007) Specific Inhibitors of Arylamine N-Acetyltransferase From Eukaryotes, Part II Thesis Dept. of Chemistry, University of Oxford, Oxford

Cribb AE, Tsui B, Isbrucker R, Michael RT, Gillespie CT, Brown-Bonomo J, Barrett P, Levatte T, Renton KW (1995) Assessment of arylamine N-acetyltransferase (NAT1) activity in mononuclear leukocytes of cystic fibrosis patients. *Br J Clin Pharmacol* **39:** 85-89

Curado M. P., Edwards B., Shin H. R., Storm H., Ferlay J., Heanue M., P. B (2008) Cancer incidence in five continents. Volume IX. *IARC Sci Publ***:** 1-837

Curtis RE (2006) *New malignancies among cancer survivors : SEER cancer registries, 1973-2000*, Washington, D.C.: U.S. Dept. of Health and Human Services, National Institutes of Health, National Cancer Institute.

Czeizel AE, Timar L, Sarkozi A (1999) Dose-dependent effect of folic acid on the prevention of orofacial clefts. *Pediatrics* **104:** e66

Dairou J, Atmane N, Dupret JM, Rodrigues-Lima F (2003) Reversible inhibition of the human xenobiotic-metabolizing enzyme arylamine N-acetyltransferase 1 by S-nitrosothiols. *Biochem Biophys Res Commun* **307:** 1059-1065

Dairou J, Atmane N, Rodrigues-Lima F, Dupret JM (2004) Peroxynitrite irreversibly inactivates the human xenobiotic-metabolizing enzyme arylamine N-acetyltransferase 1 (NAT1) in human breast cancer cells: a cellular and mechanistic study. *J Biol Chem* **279:** 7708-7714

Dairou J, Flatters D, Chaffotte AF, Pluvinage B, Sim E, Dupret JM, Rodrigues-Lima F (2006) Insight into the structure of Mesorhizobium loti arylamine N-acetyltransferase 2 (MLNAT2): a biochemical and computational study. *FEBS Lett* **580:** 1780-1788

Deapen D, Liu LH, Perkins C, Bernstein L, Ross RK (2002) Rapidly rising breast cancer incidence rates among Asian-American women. *International Journal of Cancer* **99:** 747-750

Deroo BJ, Korach KS (2006) Estrogen receptors and human disease. *J Clin Invest* **116:** 561-570

Desmedt C, Piette F, Loi S, Wang Y, Lallemand F, Haibe-Kains B, Viale G, Delorenzi M, Zhang Y, d'Assignies MS, Bergh J, Lidereau R, Ellis P, Harris AL, Klijn JG, Foekens JA, Cardoso F, Piccart MJ, Buyse M, Sotiriou C (2007) Strong time dependence of the 76-gene prognostic signature for node-negative breast cancer patients in the TRANSBIG multicenter independent validation series. *Clin Cancer Res* **13:** 3207-3214

Dilthey W, Wizinger R (1928) Über eine Erweiterung der Wittschen Farbtheorie auf koordinationschemischer Grundlage. *Journal für Praktische Chemie* **118:** 321-348

Dismer F, Petzold M, Hubbuch J (2008) Effects of ionic strength and mobile phase pH on the binding orientation of lysozyme on different ion-exchange adsorbents. *J Chromatogr A* **1194:** 11-21

Doamaral L, Sandstro.Wa, Cordes EH (1966) Some Aspects of Mechanism and Catalysis for Carbonyl Addition Reactions. *Journal of the American Chemical Society* **88:** 2225-&

Duke T, Mai M (1999) Meningitis or madness: a delicate balance. *J Paediatr Child Health* **35:** 319-320

Dunmire V, Wu CL, Symmans WF, Zhang W (2002) Increased yield of total RNA from fine-needle aspirates for use in expression microarray analysis. *Biotechniques* **33:** 890-+

Dupret JM, Goodfellow GH, Janezic SA, Grant DM (1994) Structure-function studies of human arylamine N-acetyltransferases NAT1 and NAT2. Functional analysis of recombinant NAT1/NAT2 chimeras expressed in Escherichia coli. *J Biol Chem* **269:** 26830-26835

Egleton JE (2011) Synthesis of Mechanistic Evaluation of Colorimetric Probes for the Specific Detection of Human Arylamine N-Accetyltransferase 1, Part II Thesis. Dept. of Chemistry, University of Oxford, Oxford

Ellard GA, Gammon PT (1976) Pharmacokinetics of isoniazid metabolism in man. *J Pharmacokinet Biopharm* **4:** 83-113

Ellis IO, Bartlett J, Dowsett M, Humphreys S, Jasani B, Miller K, Pinder SE, Rhodes A, Walker R (2004) Best Practice No 176: Updated recommendations for HER2 testing in the UK. *J Clin Pathol* **57:** 233-237

EncyclopædiaBritannicaOnline. (2011) "colour" - Retrieved from: http://www.britannica.com/EBchecked/topic/126658/colour. In Inc. EB (ed.), Vol. 2011.

Engel LW, Young NA, Tralka TS, Lippman ME, O'Brien SJ, Joyce MJ (1978) Establishment and characterization of three new continuous cell lines derived from human breast carcinomas. *Cancer Res* **38:** 3352-3364

Erickson RP (2010) Genes, environment, and orofacial clefting: N-acetyltransferase and folic acid. *J Craniofac Surg* **21:** 1384-1387

Espinel CH (2002) The portrait of breast cancer and Raphael's La Fornarina. *Lancet* **360:** 2061-2063

Evans DA (1989) N-acetyltransferase. *Pharmacol Ther* **42:** 157-234

Evans DA, Manley KA, Mc KV (1960) Genetic control of isoniazid metabolism in man. *Br Med J* **2:** 485-491

Evans DA, White TA (1964) Human Acetylation Polymorphism. *J Lab Clin Med* **63:** 394-403

Ewertz M, Duffy SW, Adami HO, Kvale G, Lund E, Meirik O, Mellemgaard A, Soini I, Tulinius H (1990) Age at 1st Birth, Parity and Risk of Breast-Cancer - a Metaanalysis of 8 Studies from the Nordic Countries. *International Journal of Cancer* **46:** 597-603

Fakis G, Boukouvala S, Buckle V, Payton M, Denning C, Sim E (2000) Chromosome mapping of the genes for murine arylamine N-acetyltransferases (NATs), enzymes involved in the metabolism of carcinogens: identification of a novel upstream noncoding exon for murine Nat2. *Cytogenet Cell Genet* **90:** 134-138

Feig SA, Hendrick RE (1997) Radiation risk from screening mammography of women aged 40-49 years. *J Natl Cancer Inst Monogr***:** 119-124

Ferlay J, Shin HR, Bray F, Forman D, Mathers C, Parkin DM (2010) Estimates of worldwide burden of cancer in 2008: GLOBOCAN 2008. *Int J Cancer*

Flammang TJ, Yamazoe Y, Guengerich FP, Kadlubar FF (1987) The S-acetyl coenzyme A-dependent metabolic activation of the carcinogen N-hydroxy-2-aminofluorene by human liver cytosol and its relationship to the aromatic amine N-acetyltransferase phenotype. *Carcinogenesis* **8:** 1967-1970

Fleming I (2010) *Molecular orbitals and organic chemical reactions*, Reference edn. Chichester: Wiley.

Ford GP, Griffin GR (1992) Relative stabilities of nitrenium ions derived from heterocyclic amine food carcinogens: relationship to mutagenicity. *Chem Biol Interact* **81:** 19-33

Ford GP, Herman PS (1992) Relative stabilities of nitrenium ions derived from polycyclic aromatic amines. Relationship to mutagenicity. *Chem Biol Interact* **81:** 1-18

Franks LM, Teich NM (1997) *Introduction to the cellular and molecular biology of cancer*, 3rd edn. Oxford: Oxford University Press.

Fukui K (1971) Recognition of stereochemical paths by orbital interaction. *Accounts of Chemical Research* **4:** 57-64

Fukui Ki (1975) *Theory of orientation and stereoselection*, Berlin ; New York: Springer-Verlag.

Fukutome K, Watanabe M, Shiraishi T, Murata M, Uemura H, Kubota Y, Kawamura J, Ito H, Yatani R (1999) N-acetyltransferase 1 genetic polymorphism influences the risk of prostate cancer development. *Cancer Lett* **136:** 83-87

Fullam E, Kawamura A, Wilkinson H, Abuhammad A, Westwood I, Sim E (2009) Comparison of the Arylamine N-acetyltransferase from Mycobacterium marinum and Mycobacterium tuberculosis. *Protein J* **28:** 281-293

Fullam E, Westwood IM, Anderton MC, Lowe ED, Sim E, Noble ME (2008) Divergence of cofactor recognition across evolution: coenzyme A binding in a prokaryotic arylamine N-acetyltransferase. *J Mol Biol* **375:** 178-191

Gallagher SS, Sable JE, Sheetz MP, Cornish VW (2009) An In Vivo Covalent TMP-Tag Based on Proximity-Induced Reactivity. *Acs Chemical Biology* **4:** 547-556

Gane PJ, Dean PM (2000) Recent advances in structure-based rational drug design. *Curr Opin Struct Biol* **10:** 401-404

Garcia-Closas M, Brinton LA, Lissowska J, Chatterjee N, Peplonska B, Anderson WF, Szeszenia-Dabrowska N, Bardin-Mikolajczak A, Zatonski W, Blair A, Kalaylioglu Z, Rymkiewicz G, Mazepa-Sikora D, Kordek R, Lukaszek S, Sherman ME (2006) Established breast cancer risk factors by clinically important tumour characteristics. *Br J Cancer* **95:** 123-129

Garland PB, Randle PJ (1964) Control of pyruvate dehydrogenase in the perfused rat heart by the intracellular concentration of acetyl-coenzyme A. *Biochem J* **91:** 6C-7C

Garrett R, Grisham CM (2005) *Biochemistry*, 3rd edn. Belmont, Calif. ; London: Thomson Brooks/Cole.

Gasteiger E, Gattiker A, Hoogland C, Ivanyi I, Appel RD, Bairoch A (2003) ExPASy: The proteomics server for in-depth protein knowledge and analysis. *Nucleic Acids Res* **31:** 3784-3788

Gasteiger E, Hoogland C, Gattiker A, Duvaud A, Wilkins M, Appel RD, Bairoch A (2005) Protein Identification and Analysis Tools on the ExPASy Server. In *The Proteomics Protocols Handbook*, Walker JM (ed), pp 571-607. Totowa: Humana Press

Giepmans BNG, Adams SR, Ellisman MH, Tsien RY (2006) The Fluorescent Toolbox for Assessing Protein Location and Function. *Science* **312:** 217-224

Glass AG, Lacey JV, Jr., Carreon JD, Hoover RN (2007) Breast cancer incidence, 1980-2006: combined roles of menopausal hormone therapy, screening mammography, and estrogen receptor status. *J Natl Cancer Inst* **99:** 1152-1161

Goeptar AR, Scheerens H, Vermeulen NP (1995) Oxygen and xenobiotic reductase activities of cytochrome P450. *Crit Rev Toxicol* **25:** 25-65

Goodfellow GH, Dupret JM, Grant DM (2000) Identification of amino acids imparting acceptor substrate selectivity to human arylamine acetyltransferases NAT1 and NAT2. *Biochem J* **348 Pt 1:** 159-166

Gouet P, Courcelle E, Stuart DI, Metoz F (1999) ESPript: multiple sequence alignments in PostScript. *Bioinformatics* **15:** 305-308

Graebe C, Liebermann C (1868) Ueber Alizarin und Anthracen. *Berichte der deutschen chemischen Gesellschaft* **1:** 49–51

Granitza D, Beyermann M, Wenschuh H, Haber H, Carpino LA, Truran GA, Bienert M (1995) Efficient Acylation of Hydroxy Functions by Means of Fmoc Amino-Acid Fluorides. *J Chem Soc Chem Comm***:** 2223-2224

Grant DM, Blum M, Beer M, Meyer UA (1991) Monomorphic and polymorphic human arylamine N-acetyltransferases: a comparison of liver isozymes and expressed products of two cloned genes. *Mol Pharmacol* **39:** 184-191

Grant DM, Hughes NC, Janezic SA, Goodfellow GH, Chen HJ, Gaedigk A, Yu VL, Grewal R (1997) Human acetyltransferase polymorphisms. *Mutat Res* **376:** 61-70

Grau JJ, Estape J, Diaz-Padron M (2001a) Breast cancer in Rubens paintings. *Breast Cancer Res Treat* **68:** 89-93

Grau JJ, Prats M, Diaz-Padron M (2001b) [Breast cancer in the Rubens and Rembrandt paints]. *Med Clin (Barc)* **116:** 380-384

Guex N, Peitsch MC (1997) SWISS-MODEL and the Swiss-PdbViewer: an environment for comparative protein modeling. *Electrophoresis* **18:** 2714-2723

Guo Z, Wagner CR, Hanna PE (2004) Mass Spectrometric Investigation of the Mechanism of Inactivation of Hamster Arylamine N-Acetyltransferase 1 by N-Hydroxy-2-Acetylaminofluorene. *Chemical Research in Toxicology* **17:** 275-286

Gutierrez PL (2000) The metabolism of quinone-containing alkylating agents: free radical production and measurement. *Front Biosci* **5:** D629-638

H.C. Brown, D.H. McDaniel, Haflinger P (1955) *Determination of Organic Structures by Physical Methods*, New York: Academic Press.

Hall TA (1999) BioEdit: a user-friendly biological sequence alignment editor and analysis program for Windows 95/98/NT. *Nucleic Acids Symposium Series* **41:** 95-98

Halo TL, Appelbaum J, Hobert EM, Balkin DM, Schepartz A (2009) Selective Recognition of Protein Tetraserine Motifs with a Cell-Permeable, Pro-fluorescent Bis-boronic Acid. *Journal of the American Chemical Society* **131:** 438-+

Hanna W, Kahn HJ, Trudeau M (1999) Evaluation of HER-2/neu (erbB-2) status in breast cancer: from bench to bedside. *Mod Pathol* **12:** 827-834

Hannon GJ, Rossi JJ (2004) Unlocking the potential of the human genome with RNA interference. *Nature* **431:** 371-378

Harris TK, Turner GJ (2002) Structural basis of perturbed pKa values of catalytic groups in enzyme active sites. *IUBMB Life* **53:** 85-98

Harvey JM, Clark GM, Osborne CK, Allred DC (1999) Estrogen receptor status by immunohistochemistry is superior to the ligand-binding assay for predicting response to adjuvant endocrine therapy in breast cancer. *J Clin Oncol* **17:** 1474-1481

Hasegawa Y, Honda A, Umezawa K, Niino Y, Oka K, Chiba T, Aiso S, Tanimoto A, Citterio D, Suzuki K (2009) Cell-based in vivo dual imaging probes using genetically expressed tags and chemical contrast agents. *Chemical Communications***:** 4040-4042

Hayashi M, Ohzeki H, Shimada H, Unemoto T (1996) NADPH-specific quinone reductase is induced by 2-methylene-4-butyrolactone in Escherichia coli. *Biochimica Et Biophysica Acta-Bioenergetics* **1273:** 165-170

Hayes DF, Thor AD (2002) c-erbB-2 in breast cancer: development of a clinically useful marker. *Semin Oncol* **29:** 231-245

Hein DW, Boukouvala S, Grant DM, Minchin RF, Sim E (2008) Changes in consensus arylamine N-acetyltransferase gene nomenclature. *Pharmacogenet Genomics* **18:** 367-368

Hein DW, Doll MA, Fretland AJ, Leff MA, Webb SJ, Xiao GH, Devanaboyina US, Nangju NA, Feng Y (2000a) Molecular genetics and epidemiology of the NAT1 and NAT2 acetylation polymorphisms. *Cancer Epidemiol Biomarkers Prev* **9:** 29-42

Hein DW, Grant DM, Sim E (2000b) Update on consensus arylamine N-acetyltransferase gene nomenclature. *Pharmacogenetics* **10:** 291-292

Hery C, Ferlay J, Boniol M, Autier P (2008) Changes in breast cancer incidence and mortality in middle-aged and elderly women in 28 countries with Caucasian majority populations. *Ann Oncol* **19:** 1009-1018

Hess KR, Anderson K, Symmans WF, Valero V, Ibrahim N, Mejia JA, Booser D, Theriault RL, Buzdar AU, Dempsey PJ, Rouzier R, Sneige N, Ross JS, Vidaurre T, Gomez HL, Hortobagyi GN, Pusztai L (2006) Pharmacogenomic predictor of sensitivity to preoperative chemotherapy with paclitaxel and fluorouracil, doxorubicin, and cyclophosphamide in breast cancer. *J Clin Oncol* **24:** 4236-4244

Hewitt JT, Mitchell HV (1907) CXVII.-Colour and constitution of azo-compounds. Part I. *Journal of the Chemical Society, Transactions* **91:** 1251-1266

Hickman D, Palamanda JR, Unadkat JD, Sim E (1995) Enzyme kinetic properties of human recombinant arylamine N-acetyltransferase 2 allotypic variants expressed in Escherichia coli. *Biochem Pharmacol* **50:** 697-703

Hickman D, Pope J, Patil SD, Fakis G, Smelt V, Stanley LA, Payton M, Unadkat JD, Sim E (1998) Expression of arylamine N-acetyltransferase in human intestine. *Gut* **42:** 402-409

Hickman D, Risch A, Buckle V, Spurr NK, Jeremiah SJ, McCarthy A, Sim E (1994) Chromosomal localization of human genes for arylamine N-acetyltransferase. *Biochem J* **297 (Pt 3):** 441-445

Higa GM, Abraham J (2007) Lapatinib in the treatment of breast cancer. *Expert Rev Anticancer Ther* **7:** 1183-1192

Holton SJ, Dairou J, Sandy J, Rodrigues-Lima F, Dupret JM, Noble ME, Sim E (2005) Structure of Mesorhizobium loti arylamine N-acetyltransferase 1. *Acta Crystallogr Sect F Struct Biol Cryst Commun* **61:** 14-16

Hoover JRE, Day AR (1954) Preparation of Some Imidazole Derivatives of 1,4-Naphthoquinone. *J Am Chem Soc* **76:** 4148-4152

Horinouchi M, Hayashi T, Koshino H, Kurita T, Kudo T (2005) Identification of 9,17-dioxo-1,2,3,4,10,19-hexanorandrostan-5-oic acid, 4-hydroxy-2-oxohexanoic acid, and 2-hydroxyhexa-2,4-dienoic acid and related enzymes involved in testosterone degradation in Comamonas testosteroni TA441. *Appl Environ Microbiol* **71:** 5275-5281

Horwitz KB, Koseki Y, McGuire WL (1978) Estrogen control of progesterone receptor in human breast cancer: role of estradiol and antiestrogen. *Endocrinology* **103:** 1742-1751

Howell SJ, Johnston SRD, Howell A (2004) The use of selective estrogen receptor modulators and selective estrogen receptor down-regulators in breast cancer. *Best Pract Res Cl En* **18:** 47-66

Huang E, Cheng SH, Dressman H, Pittman J, Tsou MH, Horng CF, Bild A, Iversen ES, Liao M, Chen CM, West M, Nevins JR, Huang AT (2003) Gene expression predictors of breast cancer outcomes. *Lancet* **361:** 1590-1596

Hückel E (1931) Quantentheoretische Beiträge zum Benzolproblem. *Zeitschrift für Physik A Hadrons and Nuclei* **70:** 204-286

Hückel E (1932) Quantentheoretische Beiträge zum Problem der aromatischen und ungesättigten Verbindungen. III. *Zeitschrift für Physik A Hadrons and Nuclei* **76:** 628-648

Hückel E (1937) Grundzüge der Theorie ungesättigter und aromatischer Verbindungen. *Zeitschrift für Elektrochemie und angewandte physikalische Chemie* **43:** 752-788

Hughes HB (1953) On the metabolic fate of isoniazid. *J Pharmacol Exp Ther* **109:** 444-452

Hughes HB, Biehl JP, Jones AP, Schmidt LH (1954) Metabolism of isoniazid in man as related to the occurrence of peripheral neuritis. *Am Rev Tuberc* **70:** 266-273

Hultin TA, Weber WW (1985) Genetic differences in 2-aminofluorene pharmacokinetics between intact C57BL/6J and A/J mice. *Drug Metab Dispos* **13:** 148-150

Humphreys RC, Lydon JP, O'Malley BW, Rosen JM (1997) Use of PRKO mice to study the role of progesterone in mammary gland development. *J Mammary Gland Biol Neoplasia* **2:** 343-354

Ingold CK (1934) Principles of an Electronic Theory of Organic Reactions. *Chemical Reviews* **15:** 225-274

Ivshina AV, George J, Senko O, Mow B, Putti TC, Smeds J, Lindahl T, Pawitan Y, Hall P, Nordgren H, Wong JE, Liu ET, Bergh J, Kuznetsov VA, Miller LD (2006) Genetic reclassification of histologic grade delineates new clinical subtypes of breast cancer. *Cancer Res* **66:** 10292-10301

Jacobson KB (1960) Inhibition of acetyl transfer by amethopterin. *J Biol Chem* **235:** 2713-2716

Janni W, Hepp P (2010) Adjuvant aromatase inhibitor therapy: outcomes and safety. *Cancer Treat Rev* **36:** 249-261

Jastrebova JA, Patring JDM, Lanina SA (2006) Applicability of alkyl-bonded ultra-pure silica stationary phases for gradient reversed-phase HPLC of folates with conventional and volatile buffers under highly aqueous conditions. *Journal of Separation Science* **29:** 889-904

Jemal A, Bray F, Center MM, Ferlay J, Ward E, Forman D (2011) Global cancer statistics. *CA Cancer J Clin* **61:** 69-90

Jenne JW (1965) Partial purification and properties of the isoniazid transacetylase in human liver. Its relationship to the acetylation of p-aminosalicylic acid. *J Clin Invest* **44:** 1992-2002

Jenne JW, Boyer PD (1962) Kinetic characteristics of the acetylation of isoniazid and p-aminosalicylic acid by a liver-enzyme preparation. *Biochim Biophys Acta* **65:** 121-127

Jensen LE, Hoess K, Mitchell LE, Whitehead AS (2006) Loss of function polymorphisms in NAT1 protect against spina bifida. *Hum Genet* **120:** 52-57

John EM, Phipps AI, Knight JA, Milne RL, Dite GS, Hopper JL, Andrulis IL, Southey M, Giles GG, West DW, Whittemore AS (2007) Medical radiation exposure and breast cancer risk: findings from the Breast Cancer Family Registry. *Int J Cancer* **121:** 386-394

Johnson N, Sim E (2001) The role of human arylamine N-acetyltransferase in development and disease. University of Oxford, 2001.,

Johnston SJ, Cheung KL (2010) Fulvestrant - a novel endocrine therapy for breast cancer. *Curr Med Chem* **17:** 902-914

Jones G, Willett P, Glen RC, Leach AR, Taylor R (1997) Development and validation of a genetic algorithm for flexible docking. *J Mol Biol* **267:** 727-748

Jones RF, Land SJ, King CM (1996) Recombinant rat and hamster N-acetyltransferases-1 and -2: relative rates of N-acetylation of arylamines and N,O-acyltransfer with arylhydroxamic acids. *Carcinogenesis* **17:** 1729-1733

Kamoto M, Umezawa N, Kato N, Higuchi T (2009) Turn-on fluorescent probe with visible light excitation for labeling of hexahistidine tagged protein. *Bioorganic & Medicinal Chemistry Letters* **19:** 2285-2288

Katoh M (2010) Genetic alterations of FGF receptors: an emerging field in clinical cancer diagnostics and therapeutics. *Expert Rev Anticancer Ther* **10:** 1375-1379

Kawamura A, Graham J, Mushtaq A, Tsiftsoglou SA, Vath GM, Hanna PE, Wagner CR, Sim E (2005) Eukaryotic arylamine N-acetyltransferase. Investigation of substrate specificity by high-throughput screening. *Biochem Pharmacol* **69:** 347-359

Kawamura A, Sandy J, Upton A, Noble M, Sim E (2003) Structural investigation of mutant Mycobacterium smegmatis arylamine N-acetyltransferase: a model for a naturally occurring functional polymorphism in Mycobacterium tuberculosis arylamine N-acetyltransferase. *Protein Expr Purif* **27:** 75-84

Kawamura A, Sim E (2005) Structural investigations of arylamine N-acetyltransferases from eukaryotes. University of Oxford, 2005.,

Kawamura A, Westwood I, Wakefield L, Long H, Zhang N, Walters K, Redfield C, Sim E (2008) Mouse N-acetyltransferase type 2, the homologue of human N-acetyltransferase type 1. *Biochem Pharmacol* **75:** 1550-1560

Kelly SL, Sim E (1991) Expression of N-acetyl transferase in a human monocytic cell-line, U937. *Hum Exp Toxicol* **10:** 33-38

Kelly SL, Sim E (1994) Arylamine N-acetyltransferase in Balb/c mice: identification of a novel mouse isoenzyme by cloning and expression in vitro. *Biochem J* **302 (Pt 2):** 347-353

Kerdar RS, Dehner D, Wild D (1993) Reactivity and genotoxicity of arylnitrenium ions in bacterial and mammalian cells. *Toxicol Lett* **67:** 73-85

Key TJ, Pike MC (1988) The role of oestrogens and progestagens in the epidemiology and prevention of breast cancer. *Eur J Cancer Clin Oncol* **24:** 29-43

Kiefer F, Arnold K, Kunzli M, Bordoli L, Schwede T (2009) The SWISS-MODEL Repository and associated resources. *Nucleic Acids Res* **37:** D387-392

King CM (1974) Mechanism of reaction, tissue distribution, and inhibition of arylhydroxamic acid acyltransferase. *Cancer Res* **34:** 1503-1515

King EB, Chew KL, Petrakis NL, Ernster VL (1983) Nipple Aspirate Cytology for the Study of Breast-Cancer Precursors. *J Natl Cancer I* **71:** 1115-1121

Kukongviriyapan V, Phromsopha N, Tassaneeyakul W, Kukongviriyapan U, Sripa B, Hahnvajanawong V, Bhudhisawasdi V (2006) Inhibitory effects of polyphenolic compounds on human arylamine N-acetyltransferase 1 and 2. *Xenobiotica* **36:** 15-28

Lack NA, Kawamura A, Fullam E, Laurieri N, Beard S, Russell AJ, Evangelopoulos D, Westwood I, Sim E (2009) Temperature stability of proteins essential for the intracellular survival of Mycobacterium tuberculosis. *Biochem J* **418:** 369-378

Laemmli UK (1970) Cleavage of structural proteins during the assembly of the head of bacteriophage T4. *Nature* **227:** 680-685

Lake DE, Hudis C (2002) Aromatase inhibitors in breast cancer: an update. *Cancer Control* **9:** 490-498

Lam Y-F, Kotowycz G (1972) Self Association of Folic Acid in Aqueous Solution by Proton Magnetic Resonance. *Canadian Journal of Chemistry* **50:** 2357-2363

Laron Z, Pauli R, Pertzelan A (1989) Clinical evidence on the role of estrogens in the development of the breasts. *Proceedings of the Royal Society of Edinburgh B1* **95:** 13-22

Laurieri N (2008) Human Arylamine N-Acetyltransferase 1 - Inhibitor Studies. Msc Thesis, Dept. de Biochimie et Biotechnologies, INSA de Lyon, Lyon

Laurieri N, Crawford MH, Kawamura A, Westwood IM, Robinson J, Fletcher AM, Davies SG, Sim E, Russell AJ (2010) Small molecule colorimetric probes for specific detection of human arylamine N-acetyltransferase 1, a potential breast cancer biomarker. *J Am Chem Soc* **132:** 3238-3239

Lawson JS, Field AS, Champion S, Tran D, Ishikura H, Trichopoulos D (1999) Low oestrogen receptor alpha expression in normal breast tissue underlies low breast cancer incidence in Japan. *Lancet* **354:** 1787-1788

Lee JH, Chung JG, Lai JM, Levy GN, Weber WW (1997) Kinetics of arylamine N-acetyltransferase in tissues from human breast cancer. *Cancer Lett* **111:** 39-50

Lee JH, Lu HF, Wang DY, Chen DR, Su CC, Chen YS, Yang JH, Chung JG (2004) Effects of tamoxifen on DNA adduct formation and arylamines N-acetyltransferase activity in human breast cancer cells. *Res Commun Mol Pathol Pharmacol* **115-116:** 217-233

Lemieux P, Fuqua S (1996) The role of the estrogen receptor in tumor progression. *J Steroid Biochem Mol Biol* **56:** 87-91

Lennard-Jones JE (1929) The electronic structure of some diatomic molecules. *Transactions of the Faraday Society* **25:** 668-686

Lewis JD, Chagpar AB, Shaughnessy EA, Nurko J, McMasters K, Edwards MJ (2010) Excellent outcomes with adjuvant toremifene or tamoxifen in early stage breast cancer. *Cancer-Am Cancer Soc* **116:** 2307-2315

Lipmann F (1945) ACETYLATION OF SULFANILAMIDE BY LIVER HOMOGENATES AND EXTRACTS. *Journal of Biological Chemistry* **160:** 173-190

Liu L, Wagner CR, Hanna PE (2009) Isoform-selective inactivation of human arylamine N-acetyltransferases by reactive metabolites of carcinogenic arylamines. *Chem Res Toxicol* **22:** 1962-1974

Locker GY (1998) Hormonal therapy of breast cancer. *Cancer Treat Rev* **24:** 221-240

Loehle JA, Cornish V, Wakefield L, Doll MA, Neale JR, Zang Y, Sim E, Hein DW (2006) N-acetyltransferase (Nat) 1 and 2 expression in Nat2 knockout mice. *J Pharmacol Exp Ther* **319:** 724-728

Louisville-University. Consensus Human Arylamine N-Acetyltransferase Gene Nomenclature
http://louisville.edu/medschool/pharmacology/NAT.

Lu KH, Lin KL, Hsia TC, Hung CF, Chou MC, Hsiao YM, Chung JG (2001) Tamoxifen inhibits arylamine N-acetyltransferase activity and DNA-2-aminofluorene adduct in human leukemia HL-60 cells. *Res Commun Mol Pathol Pharmacol* **109:** 319-331

Lucas HJ, Jameson AY (1924) ELECTRON DISPLACEMENT IN CARBON COMPOUNDS I. ELECTRON DISPLACEMENT VERSUS ALTERNATE POLARITY IN ALIPHATIC COMPOUNDS. *Journal of the American Chemical Society* **46:** 2475-2482

Lutgerink JT, Stavenuiter JF, Zomer G, Hamzink M, van Dijk P, Westra JG, Kriek E (1989) Synthesis of heterocyclic N-acetoxyarylamines and their reactivity with DNA. *Carcinogenesis* **10:** 1957-1960

Ma H, Bernstein L, Pike MC, Ursin G (2006) Reproductive factors and breast cancer risk according to joint estrogen and progesterone receptor status: a meta-analysis of epidemiological studies. *Breast Cancer Res* **8:** R43

Machado JD, Gomez JF, Betancor G, Camacho M, Brioso MA, Borges R (2002) Hydralazine reduces the quantal size of secretory events by displacement of catecholamines from adrenomedullary chromaffin secretory vesicles. *Circ Res* **91:** 830-836

Martell KJ, Levy GN, Weber WW (1992) Cloned mouse N-acetyltransferases: enzymatic properties of expressed Nat-1 and Nat-2 gene products. *Mol Pharmacol* **42:** 265-272

Martell KJ, Vatsis KP, Weber WW (1991) Molecular genetic basis of rapid and slow acetylation in mice. *Mol Pharmacol* **40:** 218-227

Martin CB, Soniat M (2009) Theoretical Study on the Relative Energies of Anionic Pterin Tautomers. *Pteridines* **20:** 124-128

Masood S, Bui MM (2002) Prognostic and predictive value of HER2/neu oncogene in breast cancer. *Microsc Res Tech* **59:** 102-108

Matte C, Mackedanz V, Stefanello FM, Scherer EB, Andreazza AC, Zanotto C, Moro AM, Garcia SC, Goncalves CA, Erdtmann B, Salvador M, Wyse AT (2009) Chronic hyperhomocysteinemia alters antioxidant defenses and increases DNA damage in brain and blood of rats: protective effect of folic acid. *Neurochem Int* **54:** 7-13

Mayhew SG (1978) The redox potential of dithionite and SO-2 from equilibrium reactions with flavodoxins, methyl viologen and hydrogen plus hydrogenase. *European Journal of Biochemistry* **85:** 535-547

McNaught AD, Wilkinson A, International Union of Pure and Applied Chemistry. (1997) *Compendium of chemical terminology : IUPAC recommendations*, 2nd edn. Oxford: Blackwell Science.

Megdal SP, Kroenke CH, Laden F, Pukkala E, Schernhammer ES (2005) Night work and breast cancer risk: a systematic review and meta-analysis. *Eur J Cancer* **41:** 2023-2032

Michell M (2010) *Breast cancer*, Cambridge: Cambridge University Press.

Miki Y, Swensen J, Shattuck-Eidens D, Futreal PA, Harshman K, Tavtigian S, Liu Q, Cochran C, Bennett LM, Ding W, et al. (1994) A strong candidate for the breast and ovarian cancer susceptibility gene BRCA1. *Science* **266:** 66-71

Miller EC, Miller JA (1960) A mechanism of orthol-hydroxylation of aromatic amines in vivo. *Biochim Biophys Acta* **40:** 380-382

Miller LD, Smeds J, George J, Vega VB, Vergara L, Ploner A, Pawitan Y, Hall P, Klaar S, Liu ET, Bergh J (2005) An expression signature for p53 status in human breast cancer predicts mutation status, transcriptional effects, and patient survival. *Proc Natl Acad Sci U S A* **102:** 13550-13555

Million-Women-Study-Collaborators (2003) Breast cancer and hormone-replacement therapy in the Million Women Study. *The Lancet* **362:** 419-427

Minchin RF (1995) Acetylation of p-aminobenzoylglutamate, a folic acid catabolite, by recombinant human arylamine N-acetyltransferase and U937 cells. *Biochem J* **307 (Pt 1):** 1-3

Minchin RF, Hanna PE, Dupret JM, Wagner CR, Rodrigues-Lima F, Butcher NJ (2007) Arylamine N-acetyltransferase I. *Int J Biochem Cell Biol* **39:** 1999-2005

Minchin RF, Kadlubar FF, Ilett KF (1993) Role of acetylation in colorectal cancer. *Mutat Res* **290:** 35-42.

Mitchell MK, Futscher BW, McQueen CA (1999) Developmental expression of N-acetyltransferases in C57BI/6 mice. *Drug Metab Dispos* **27:** 261-264

Mitchell RS, Bell JC (1957) Clinical implications of isoniazid, PAS and streptomycin blood levels in pulmonary tuberculosis. *Trans Am Clin Climatol Assoc* **69:** 98-102; discussion 103-105

Moat SJ, Bonham JR, Cragg RA, Powers HJ (2000) Elevated plasma homocysteine elicits an increase in antioxidant enzyme activity. *Free Radic Res* **32:** 171-179

Monninkhof EM, Elias SG, Vlems FA, van der Tweel I, Schuit AJ, Voskuil DW, van Leeuwen FE (2007) Physical activity and breast cancer - A systematic review. *Epidemiology* **18:** 137-157

Moreno A, Lloveras B, Figueras A, Escobedo A, Ramon JM, Sierra A, Fabra A (1997) Ductal carcinoma in situ of the breast: correlation between histologic classifications and biologic markers. *Mod Pathol* **10:** 1088-1092

Mote PA, Bartow S, Tran N, Clarke CL (2002) Loss of co-ordinate expression of progesterone receptors A and B is an early event in breast carcinogenesis. *Breast Cancer Res Treat* **72:** 163-172

Munnich A (2008) Casting an eye on the Krebs cycle. *Nat Genet* **40:** 1148-1149

Mushtaq A, Payton M, Sim E (2002) The COOH terminus of arylamine N-acetyltransferase from Salmonella typhimurium controls enzymic activity. *J Biol Chem* **277:** 12175-12181

Mylonas I, Jeschke U, Shabani N, Kuhn C, Kriegel S, Kupka MS, Friese K (2005) Normal and malignant human endometrium express immunohistochemically estrogen receptor alpha (ER-alpha), estrogen receptor beta (ER-beta) and progesterone receptor (PR). *Anticancer Res* **25:** 1679-1686

Nakanishi M, Yatome C, Ishida N, Kitade Y (2001) Putative ACP phosphodiesterase gene (acpD) encodes an azoreductase. *Journal of Biological Chemistry* **276:** 46394-46399

Nakura H, Itoh S, Kusano H, Ishizone H, Deguchi T, Kamataki T (1995) Evidence for the lack of hepatic N-acetyltransferase in suncus (Suncus murinus). *Biochem Pharmacol* **50:** 1165-1170

Nauser T, Dockheer S, Kissner R, Koppenol WH (2006) Catalysis of electron transfer by selenocysteine. *Biochemistry* **45:** 6038-6043

Nebert DW, Nelson DR, Coon MJ, Estabrook RW, Feyereisen R, Fujii-Kuriyama Y, Gonzalez FJ, Guengerich FP, Gunsalus IC, Johnson EF, et al. (1991) The P450 superfamily: update on new sequences, gene mapping, and recommended nomenclature. *DNA Cell Biol* **10:** 1-14

Niesen FH, Berglund H, Vedadi M (2007) The use of differential scanning fluorimetry to detect ligand interactions that promote protein stability. *Nat Protoc* **2:** 2212-2221

Nilsson S, Makela S, Treuter E, Tujague M, Thomsen J, Andersson G, Enmark E, Pettersson K, Warner M, Gustafsson JA (2001) Mechanisms of estrogen action. *Physiol Rev* **81:** 1535-1565

Nobilis M, Vybiralova Z, Sladkova K, Lisa M, Holcapek M, Kvetina J (2006) High-performance liquid-chromatographic determination of 5-aminosalicylic acid and its metabolites in blood plasma. *J Chromatogr A* **1119:** 299-308

Noble ME, Endicott JA, Johnson LN (2004) Protein kinase inhibitors: insights into drug design from structure. *Science* **303:** 1800-1805

Noszai B, Szakacs Z (2006) Determination of dissociation constants of folic acid, methotrexate, and other photolabile pteridines by pressure-assisted capillary electrophoresis. *Electrophoresis* **27:** 3399-3409

Ohsako S, Deguchi T (1990) Cloning and expression of cDNAs for polymorphic and monomorphic arylamine N-acetyltransferases from human liver. *J Biol Chem* **265:** 4630-4634

Ohsako S, Ohtomi M, Sakamoto Y, Uyemura K, Deguchi T (1988) Arylamine N-acetyltransferase from chicken liver II. Cloning of cDNA and expression in Chinese hamster ovary cells. *J Biol Chem* **263:** 7534-7538

Onodera K, Satou K, Hirota H (2007) Evaluations of molecular docking programs for virtual screening. *J Chem Inf Model* **47:** 1609-1618

Osborne CK (1998) Steroid hormone receptors in breast cancer management. *Breast Cancer Res Treat* **51:** 227-238

Paik S, Bryant J, Tan-Chiu E, Romond E, Hiller W, Park K, Brown A, Yothers G, Anderson S, Smith R, Wickerham DL, Wolmark N (2002) Real-world performance of HER2 testing--National Surgical Adjuvant Breast and Bowel Project experience. *J Natl Cancer Inst* **94:** 852-854

Pandey AK, Sassetti CM (2008) Mycobacterial persistence requires the utilization of host cholesterol. *Proc Natl Acad Sci U S A* **105:** 4376-4380

Patel SS, Walt DR (1987) Substrate specificity of acetyl coenzyme A synthetase. *J Biol Chem* **262:** 7132-7134

Patridge EV, Ferry JG (2006) WrbA from Escherichia coli and Archaeoglobus fulgidus is an NAD(P)H : Quinone oxidoreductase. *Journal of Bacteriology* **188:** 3498-3506

Payne SJ, Bowen RL, Jones JL, Wells CA (2008) Predictive markers in breast cancer--the present. *Histopathology* **52:** 82-90

Payton M, Auty R, Delgoda R, Everett M, Sim E (1999a) Cloning and characterization of arylamine N-acetyltransferase genes from Mycobacterium smegmatis and Mycobacterium tuberculosis: increased expression results in isoniazid resistance. *Journal of Bacteriology* **181:** 1343-1347

Payton M, Gifford C, Schartau P, Hagemeier C, Mushtaq A, Lucas S, Pinter K, Sim E (2001a) Evidence towards the role of arylamine N-acetyltransferase in Mycobacterium smegmatis and development of a specific antiserum against the homologous enzyme of Mycobacterium tuberculosis. *Microbiology* **147:** 3295-3302

Payton M, Mushtaq A, Yu TW, Wu LJ, Sinclair J, Sim E (2001b) Eubacterial arylamine N-acetyltransferases - identification and comparison of 18 members of the protein family with conserved active site cysteine, histidine and aspartate residues. *Microbiology* **147:** 1137-1147

Payton M, Smelt V, Upton A, Sim E (1999b) A method for genotyping murine arylamine N-acetyltransferase type 2 (NAT2): a gene expressed in preimplantation embryonic stem cells encoding an enzyme acetylating the folate catabolite p-aminobenzoylglutamate. *Biochem Pharmacol* **58:** 779-785

Payton MA, Sim E (1998) Genotyping human arylamine N-acetyltransferase type 1 (NAT1): the identification of two novel allelic variants. *Biochem Pharmacol* **55:** 361-366

Pedersen JA (1973) Electron-Spin Resonance Studies of Oxidative Process of Quinones and Hydroquinones in Alkaline Solution - Formation of Primary and Secondary Semiquinone Radicals. *Journal of the Chemical Society-Perkin Transactions 2***:** 424-431

Peitsch MC (1995a) Protein Modeling by E-Mail. *Bio-Technology* **13:** 658-660

Peitsch MC (1995b) Protein Modeling by E-Mail (Vol 13, Pg 658, 1995). *Bio-Technology* **13:** 723-723

Perkin WH, Meldola R (1907) *Jubilee of the discovery of mauve and of the foundation of the coal-tar colour industry by sir W.H. Perkin, ed. by R. Meldola, A.G. Green, J.C. Cain*, Lond.

Pharoah PDP, Day NE, Duffy S, Easton DF, Ponder BAJ (1997) Family history and the risk of breast cancer: A systematic review and meta-analysis. *International Journal of Cancer* **71:** 800-809

Pluvinage B, Dairou J, Possot OM, Martins M, Fouet A, Dupret JM, Rodrigues-Lima F (2007a) Cloning and molecular characterization of three arylamine N-acetyltransferase genes from Bacillus anthracis: identification of unusual enzymatic properties and their contribution to sulfamethoxazole resistance. *Biochemistry* **46:** 7069-7078

Pluvinage B, Li de la Sierra-Gallay I, Martins M, Ragunathan N, Dupret JM, Rodrigues-Lima F (2007b) Crystallization and preliminary X-ray characterization of arylamine N-acetyltransferase C (BanatC) from Bacillus anthracis. *Acta Crystallogr Sect F Struct Biol Cryst Commun* **63:** 862-864

Pluvinage B, Sierra-Gallay IL, Kubiak X, Xu X, Dairou J, Dupret JM, Rodrigues-Lima F (2011) The Bacillus anthracis arylamine N-acetyltransferase ((BACAN)NAT1) that

inactivates sulfamethoxazole, reveals unusual structural features compared with the other NAT isoenzymes. *FEBS Lett* **585:** 3947-3952

Poe M (1973) Proton magnetic resonance studies of folate, dihydrofolate, and methotrexate. Evidence from pH and concentration studies for dimerization. *J Biol Chem* **248:** 7025-7032

Rachet B, Maringe C, Nur U, Quaresma M, Shah A, Woods LM, Ellis L, Walters S, Forman D, Steward J, Coleman MP (2009) Population-based cancer survival trends in England and Wales up to 2007: an assessment of the NHS cancer plan for England. *Lancet Oncol* **10:** 351-369

Ragunathan N, Dairou J, Pluvinage B, Martins M, Dupret J-M, Rodrigues-Lima F (2009) Human arylamine N-acetyltransferase 1 (NAT1) as a target of chemotherapeutic drugs in breast cancer: Cisplatin as a model *Mol Cell- Pharm* **1:** 7-10

Randle PJ, Garland PB, Hales CN, Newsholme EA (1963) The glucose fatty-acid cycle. Its role in insulin sensitivity and the metabolic disturbances of diabetes mellitus. *Lancet* **1:** 785-789

Rawn JD (1989) *Biochemistry*, Burlington, N.C: Neil Patterson.

Reeves GK, Pirie K, Beral V, Green J, Spencer E, Bull D (2007) Cancer incidence and mortality in relation to body mass index in the Million Women Study: cohort study. *British Medical Journal* **335:** 1134-1139

Reichardt C, Welton T (2011) *Solvents and solvent effects in organic chemistry*, 4th, updated and enlarged edn. Weinheim: Wiley-VCH.

Rey E, Pons G, Cremier O, Vauzelle-Kervroedan F, Pariente-Khayat A, d'Athis P, Badoual J, Olive G, Gendrel D (1998) Isoniazid dose adjustment in a pediatric population. *Ther Drug Monit* **20:** 50-55

Rezanka T, Sigler K (2009) Odd-numbered very-long-chain fatty acids from the microbial, animal and plant kingdoms. *Prog Lipid Res* **48:** 206-238

Rhodes DR, Yu J, Shanker K, Deshpande N, Varambally R, Ghosh D, Barrette T, Pandey A, Chinnaiyan AM (2004) ONCOMINE: a cancer microarray database and integrated data-mining platform. *Neoplasia* **6:** 1-6

Richard JA, Jean L, Schenkels C, Massonneau M, Romieu A, Renard PY (2009) Self-cleavable chemiluminescent probes suitable for protease sensing. *Organic & Biomolecular Chemistry* **7:** 2941-2957

Richards MA (2008) Trends and inequalities in survival for 20 cancers in England and Wales 1986-2001: population-based analyses and clinical commentaries. Foreword. *Br J Cancer* **99 Suppl 1:** S1

Riddle B, Jencks WP (1971) Acetyl-coenzyme A: arylamine N-acetyltransferase. Role of the acetyl-enzyme intermediate and the effects of substituents on the rate. *J Biol Chem* **246:** 3250-3258

Riddles PW, Blakeley RL, Zerner B (1983) Reassessment of Ellman's reagent. *Methods Enzymol* **91:** 49-60

Riggs BL, Hartmann LC (2003) Selective estrogen-receptor modulators -- mechanisms of action and application to clinical practice. *N Engl J Med* **348:** 618-629

Rinaldi S, Peeters PHM, Bezemer ID, Dossus L, Biessy C, Sacerdote C, Berrino F, Panico S, Palli D, Tumino R, Khaw KT, Bingham S, Allen NE, Key T, Jensen MK, Overvad K, Olsen A, Tjonneland A, Amiano P, Ardanaz E, Agudo A, Martinez-Garcia C, Quiros JR, Tormo MJ, Nagel G, Linseisen J, Boeing H, Schulz M, Grobbee DE, Bueno-de-Mesquita HB, Koliva M, Kyriazi G, Thrichopoulou A, Boutron-Ruault MC, Clavel-Chapelon F, Ferrari P, Slimani N, Saracci R, Riboli E, Kaaks R (2006) Relationship of alcohol intake and sex steroid concentrations in blood in pre- and post-menopausal women: the European Prospective Investigation into Cancer and Nutrition. *Cancer Causes & Control* **17:** 1033-1043

Risch A, Wallace DM, Bathers S, Sim E (1995) Slow N-acetylation genotype is a susceptibility factor in occupational and smoking related bladder cancer. *Hum Mol Genet* **4:** 231-236

Robinson J (2007) Arylamine N-acetyltransferase in Breast Cancer. Msc Thesis, Pharmacology, University of Oxford, Oxford

Rodrigues-Lima F, Dairou J, Diaz CL, Rubio MC, Sim E, Spaink HP, Dupret JM (2006) Cloning, functional expression and characterization of Mesorhizobium loti arylamine N-acetyltransferases: rhizobial symbiosis supplies leguminous plants with the xenobiotic N-acetylation pathway. *Mol Microbiol* **60:** 505-512

Ross JS, Fletcher JA (1999) HER-2/neu (c-erb-B2) gene and protein in breast cancer. *Am J Clin Pathol* **112:** S53-67

Ross JS, Linette GP, Stec J, Clark E, Ayers M, Leschly N, Symmans WF, Hortobagyi GN, Pusztai L (2003) Breast cancer biomarkers and molecular medicine. *Expert Rev Mol Diagn* **3:** 573-585

Ross JS, Linette GP, Stec J, Clark E, Ayers M, Leschly N, Symmans WF, Hortobagyi GN, Pusztai L (2004) Breast cancer biomarkers and molecular medicine: part II. *Expert Rev Mol Diagn* **4:** 169-188

Rossi C, Donati A, Sansoni MR (1993a) Folic-Acid - Solution Structure and Nmr Strategy for Conformational-Analysis. *Spectroscopy Letters* **26:** 1603-1611

Rossi C, Donati A, Sansoni MR (1993b) Folic Acid: Solution Structure and NMR Strategy for Conformational Analysis. *Spectroscopy Letters* **26:** 1603-1611

Rothman N, Garcia-Closas M, Hein DW (2007) Commentary: Reflections on G. M. Lower and colleagues' 1979 study associating slow acetylator phenotype with urinary bladder cancer: meta-analysis, historical refinements of the hypothesis, and lessons learned. *Int J Epidemiol* **36:** 23-28

Russell AJ, Westwood IM, Crawford MH, Robinson J, Kawamura A, Redfield C, Laurieri N, Lowe ED, Davies SG, Sim E (2009) Selective small molecule inhibitors of the potential breast cancer marker, human arylamine N-acetyltransferase 1, and its murine homologue, mouse arylamine N-acetyltransferase 2. *Bioorg Med Chem* **17:** 905-918

Salvatorelli E, Guarnieri S, Menna P, Liberi G, Calafiore AM, Mariggio MA, Mordente A, Gianni L, Minotti G (2006) Defective one- or two-electron reduction of the anticancer anthracycline epirubicin in human heart. Relative importance of vesicular sequestration and impaired efficiency of electron addition. *J Biol Chem* **281:** 10990-11001

Sambrook J, Fritsch EF, Maniatis T (1989) *Molecular Cloning. A Laboratory Manual*, Cold Spring Harbor, NY.: Cold Spring Harbor Laboratory Press.

Sandy J, Holton S, Fullam E, Sim E, Noble M (2005a) Binding of the anti-tubercular drug isoniazid to the arylamine N-acetyltransferase protein from Mycobacterium smegmatis. *Protein Sci* **14:** 775-782

Sandy J, Mushtaq A, Holton SJ, Schartau P, Noble ME, Sim E (2005b) Investigation of the catalytic triad of arylamine N-acetyltransferases: essential residues required for acetyl transfer to arylamines. *Biochem J* **390:** 115-123

Sandy J, Mushtaq A, Kawamura A, Sinclair J, Sim E, Noble M (2002) The structure of arylamine N-acetyltransferase from Mycobacterium smegmatis--an enzyme which inactivates the anti-tubercular drug, isoniazid. *J Mol Biol* **318:** 1071-1083

Sasaki Y, Ohsako S, Deguchi T (1991) Molecular and genetic analyses of arylamine N-acetyltransferase polymorphism of rabbit liver. *J Biol Chem* **266:** 13243-13250

Sasieni PD, Shelton J, Ormiston-Smith N, Thomson CS, Silcocks PB (2011) What is the lifetime risk of developing cancer?: the effect of adjusting for multiple primaries. *Br J Cancer* **105:** 460-465

Schernhammer ES, Hankinson SE (2005) Urinary melatonin levels and breast cancer risk. *J Natl Cancer Inst* **97:** 1084-1087

Schneider G (2010) Virtual screening: an endless staircase? *Nat Rev Drug Discov* **9:** 273-276

Schnitt SJ, Jacobs TW (2001) Current status of HER2 testing: caught between a rock and a hard place. *Am J Clin Pathol* **116:** 806-810

Schrödinger L. The PyMOL Molecular Graphics System, Version 1.3.

Schwede T, Kopp J, Guex N, Peitsch MC (2003) SWISS-MODEL: an automated protein homology-modeling server. *Nucleic Acids Res* **31:** 3381-3385

Shiau AK, Barstad D, Loria PM, Cheng L, Kushner PJ, Agard DA, Greene GL (1998) The structural basis of estrogen receptor/coactivator recognition and the antagonism of this interaction by tamoxifen. *Cell* **95:** 927-937

Sih CJ, Lee SS, Tsong YY, Wang KC (1966) Mechanisms of steroid oxidation by microorganisms. 8. 3,4-Dihydroxy-9,10-secoandrosta-1,3,5(10)-triene-9,17-dione, an intermediate in the microbiological degradation of ring A of androst-4-ene-3,17-dione. *J Biol Chem* **241:** 540-550

Sikora AL, Frankel BA, Blanchard JS (2008) Kinetic and chemical mechanism of arylamine N-acetyltransferase from Mycobacterium tuberculosis. *Biochemistry* **47:** 10781-10789

Sim E, Gill EW, Sim RB (1984a) Drugs That Induce Systemic Lupus-Erythematosus Inhibit Complement Component-C4. *Lancet* **2:** 422-424

Sim E, Gill EW, Sim RB (1984b) Drugs that induce systemic lupus erythematosus inhibit complement component C4. *Lancet* **2:** 422-424

Sim E, Lack N, Wang CJ, Long H, Westwood I, Fullam E, Kawamura A (2008a) Arylamine N-acetyltransferases: structural and functional implications of polymorphisms. *Toxicology* **254:** 170-183

Sim E, Pinter K, Mushtaq A, Upton A, Sandy J, Bhakta S, Noble M (2003) Arylamine N-acetyltransferases: a pharmacogenomic approach to drug metabolism and endogenous function. *Biochem Soc Trans* **31:** 615-619

Sim E, Sim RB (1981) Binding of fluid-phase complement components C3 and C3b to human lymphocytes. *Biochem J* **198:** 509-518

Sim E, Walters K, Boukouvala S (2008b) Arylamine N-acetyltransferases: from structure to function. *Drug Metab Rev* **40:** 479-510

Sim E, Westwood I, Fullam E (2007) Arylamine N-acetyltransferases. *Expert Opin Drug Metab Toxicol* **3:** 169-184

Simon R, Nocito A, Hubscher T, Bucher C, Torhorst J, Schraml P, Bubendorf L, Mihatsch MM, Moch H, Wilber K, Schotzau A, Kononen J, Sauter G (2001) Patterns of her-2/neu amplification and overexpression in primary and metastatic breast cancer. *J Natl Cancer Inst* **93:** 1141-1146

Simpson ER (2003) Sources of estrogen and their importance. *J Steroid Biochem* **86:** 225-230

Sinclair J, Sim E (1997) A fragment consisting of the first 204 amino-terminal amino acids of human arylamine N-acetyltransferase one (NAT1) and the first transacetylation step of catalysis. *Biochem Pharmacol* **53:** 11-16

Sinclair JC, Sandy J, Delgoda R, Sim E, Noble ME (2000) Structure of arylamine N-acetyltransferase reveals a catalytic triad. *Nat Struct Biol* **7:** 560-564

Skynner MJ, Sim JA, Herbison AE (1999) Detection of estrogen receptor alpha and beta messenger ribonucleic acids in adult gonadotropin-releasing hormone neurons. *Endocrinology* **140:** 5195-5201

Skynner MJ, Sim JA, Herbison AE (2001) Detection of estrogen receptor alpha and beta messenger ribonucleic acids in adult gonadotropin-releasing hormone neurons (vol 140, pg 5195, 1999). *Endocrinology* **142:** 492-492

Slamon DJ, Clark GM, Wong SG, Levin WJ, Ullrich A, McGuire WL (1987) Human breast cancer: correlation of relapse and survival with amplification of the HER-2/neu oncogene. *Science* **235:** 177-182

Smelt VA, Upton A, Adjaye J, Payton MA, Boukouvala S, Johnson N, Mardon HJ, Sim E (2000) Expression of arylamine N-acetyltransferases in pre-term placentas and in human pre-implantation embryos. *Hum Mol Genet* **9:** 1101-1107

Soh N (2008) Selective chemical labeling of proteins with small fluorescent molecules based on metal-chelation methodology. *Sensors* **8:** 1004-1024

Soriano E, Borth N, Katinger H, Mattanovich D (2002) Optimization of recombinant protein expression level in Escherichia coli by flow cytometry and cell sorting. *Biotechnol Bioeng* **80:** 93-99

Sorlie T, Perou CM, Tibshirani R, Aas T, Geisler S, Johnsen H, Hastie T, Eisen MB, van de Rijn M, Jeffrey SS, Thorsen T, Quist H, Matese JC, Brown PO, Botstein D, Eystein Lonning P, Borresen-Dale AL (2001) Gene expression patterns of breast carcinomas distinguish tumor subclasses with clinical implications. *Proc Natl Acad Sci U S A* **98:** 10869-10874

Sotiriou C, Neo SY, McShane LM, Korn EL, Long PM, Jazaeri A, Martiat P, Fox SB, Harris AL, Liu ET (2003) Breast cancer classification and prognosis based on gene

expression profiles from a population-based study. *Proc Natl Acad Sci U S A* **100:** 10393-10398

Sotiriou C, Wirapati P, Loi S, Harris A, Fox S, Smeds J, Nordgren H, Farmer P, Praz V, Haibe-Kains B, Desmedt C, Larsimont D, Cardoso F, Peterse H, Nuyten D, Buyse M, Van de Vijver MJ, Bergh J, Piccart M, Delorenzi M (2006) Gene expression profiling in breast cancer: understanding the molecular basis of histologic grade to improve prognosis. *J Natl Cancer Inst* **98:** 262-272

Srinivasan S, Swaminathan S (1968) The crystal structure of phenyl hydrazine, C6H5 · NH · NH2. *Zeitschrift für Kristallographie* **127:** 442-449

Stahl P, Schlesinger PH, Sigardson E, Rodman JS, Lee YC (1980) Receptor-mediated pinocytosis of mannose glycoconjugates by macrophages: characterization and evidence for receptor recycling. *Cell* **19:** 207-215

Stanley LA, Copp AJ, Pope J, Rolls S, Smelt V, Perry VH, Sim E (1998) Immunochemical detection of arylamine N-acetyltransferase during mouse embryonic development and in adult mouse brain. *Teratology* **58:** 174-182

Stanley LA, Coroneos E, Cuff R, Hickman D, Ward A, Sim E (1996) Immunochemical detection of arylamine N-acetyltransferase in normal and neoplastic bladder. *J Histochem Cytochem* **44:** 1059-1067

Stanley LA, Mills IG, Sim E (1997) Localization of polymorphic *N*-acetyltransferase (NAT2) in tissues of inbred mice. *Pharmacogenetics* **7(2):** 121-130

Stark A, Hulka BS, Joens S, Novotny D, Thor AD, Wold LE, Schell MJ, Melton LJ, 3rd, Liu ET, Conway K (2000) HER-2/neu amplification in benign breast disease and the risk of subsequent breast cancer. *J Clin Oncol* **18:** 267-274

Stark JJ, Nelson JK (2000) The breasts of "Night": Michelangelo as oncologist. *N Engl J Med* **343:** 1577-1578

Sticha KR, Bergstrom CP, Wagner CR, Hanna PE (1998) Characterization of hamster recombinant monomorphic and polymorphic arylamine N-acetyltransferases: bioactivation and mechanism-based inactivation studies with N-hydroxy-2-acetylaminofluorene. *Biochem Pharmacol* **56:** 47-59

Stockwell BR (2004) Exploring biology with small organic molecules. *Nature* **432:** 846-854

Sugamori KS, Wong S, Gaedigk A, Yu V, Abramovici H, Rozmahel R, Grant DM (2003) Generation and functional characterization of arylamine N-acetyltransferase Nat1/Nat2 double-knockout mice. *Mol Pharmacol* **64:** 170-179

Suppan P, Ghoneim N, Royal Society of Chemistry (Great Britain). Information Services. (1997) *Solvatochromism*, Cambridge: Royal Society of Chemistry Information Services.

Suzuki H, Ohnishi Y, Horinouchi S (2007) Arylamine N-acetyltransferase responsible for acetylation of 2-aminophenols in Streptomyces griseus. *Journal of Bacteriology* **189:** 2155-2159

Szakacs Z, Noszal B (2006) Determination of dissociation constants of folic acid, methotrexate, and other photolabile pteridines by pressure-assisted capillary electrophoresis. *Electrophoresis* **27:** 3399-3409

Takeshita A, Koibuchi N, Oka J, Taguchi M, Shishiba Y, Ozawa Y (2001) Bisphenol-A, an environmental estrogen, activates the human orphan nuclear receptor, steroid and xenobiotic receptor-mediated transcription. *Eur J Endocrinol* **145:** 513-517

Teschendorff AE, Caldas C (2009) The breast cancer somatic 'muta-ome': tackling the complexity. *Breast Cancer Res* **11:** 301

Testa B, Krämer SD (2008) *The biochemistry of drug metabolism : principles, redox reactions, hydrolyses*, Weinheim ; Chichester: Wiley-VCH.

Tetko IV, Gasteiger J, Todeschini R, Mauri A, Livingstone D, Ertl P, Palyulin VA, Radchenko EV, Zefirov NS, Makarenko AS, Tanchuk VY, Prokopenko VV (2005) Virtual computational chemistry laboratory--design and description. *J Comput Aided Mol Des* **19:** 453-463

Thinnes C (2010) Synthesis of Biosensors as Breast Cancer Diagnostics, Part II Thesis. Msc Thesis, Dept. of Chemistry, , University of Oxford, Oxford

Thompson JD, Higgins DG, Gibson TJ (1994) CLUSTAL W: improving the sensitivity of progressive multiple sequence alignment through sequence weighting, position-specific gap penalties and weight matrix choice. *Nucleic Acids Res* **22:** 4673-4680

Tiang JM, Butcher NJ, Minchin RF (2010) Small molecule inhibition of arylamine N-acetyltransferase Type I inhibits proliferation and invasiveness of MDA-MB-231 breast cancer cells. *Biochem Biophys Res Commun* **393:** 95-100

Tozlu S, Girault I, Vacher S, Vendrell J, Andrieu C, Spyratos F, Cohen P, Lidereau R, Bieche I (2006) Identification of novel genes that co-cluster with estrogen receptor alpha in breast tumor biopsy specimens, using a large-scale real-time reverse transcription-PCR approach. *Endocr Relat Cancer* **13:** 1109-1120

Trepanier LA, Cribb AE, Spielberg SP, Ray K (1998) Deficiency of cytosolic arylamine N-acetylation in the domestic cat and wild felids caused by the presence of a single NAT1-like gene. *Pharmacogenetics* **8:** 169-179

Trepanier LA, Ray K, Winand NJ, Spielberg SP, Cribb AE (1997) Cytosolic arylamine N-acetyltransferase (NAT) deficiency in the dog and other canids due to an absence of NAT genes. *Biochem Pharmacol* **54:** 73-80

Tsukiji S, Wang HX, Miyagawa M, Tamura T, Takaoka Y, Hamachi I (2009) Quenched Ligand-Directed Tosylate Reagents for One-Step Construction of Turn-On Fluorescent Biosensors. *Journal of the American Chemical Society* **131:** 9046-9054

Turesky RJ, Lang NP, Butler MA, Teitel CH, Kadlubar FF (1991) Metabolic activation of carcinogenic heterocyclic aromatic amines by human liver and colon. *Carcinogenesis* **12:** 1839-1845

Turken S, Siris E, Seldin D, Flaster E, Hyman G, Lindsay R (1989) Effects of tamoxifen on spinal bone density in women with breast cancer. *J Natl Cancer Inst* **81:** 1086-1088

Upton A, Smelt V, Mushtaq A, Aplin R, Johnson N, Mardon H, Sim E (2000) Placental arylamine N-acetyltransferase type 1: potential contributory source of urinary folate catabolite p-acetamidobenzoylglutamate during pregnancy. *Biochim Biophys Acta* **1524:** 143-148

Upton AM, Mushtaq A, Victor TC, Sampson SL, Sandy J, Smith DM, van Helden PV, Sim E (2001) Arylamine N-acetyltransferase of Mycobacterium tuberculosis is a polymorphic enzyme and a site of isoniazid metabolism. *Mol Microbiol* **42:** 309-317

Vaidya JS, Baum M, Tobias JS, Massarut S, Wenz F, Murphy O, Hilaris B, Houghton J, Saunders C, Corica T, Roncadin M, Kraus-Tiefenbacher U, Melchaert F, Keshtgar M, Sainsbury R, Douek M, Harrison E, Thompson A, Joseph D (2006) Targeted intraoperative radiotherapy (TARGIT) yields very low recurrence rates when given as a boost. *Int J Radiat Oncol Biol Phys* **66:** 1335-1338

Vaklavas C, Forero-Torres A (2011) How do I treat "triple-negative" disease. *Curr Treat Options Oncol* **12:** 369-388

van 't Veer LJ, Dai H, van de Vijver MJ, He YD, Hart AA, Mao M, Peterse HL, van der Kooy K, Marton MJ, Witteveen AT, Schreiber GJ, Kerkhoven RM, Roberts C, Linsley PS, Bernards R, Friend SH (2002) Gene expression profiling predicts clinical outcome of breast cancer. *Nature* **415:** 530-536

van de Vijver MJ, He YD, van't Veer LJ, Dai H, Hart AA, Voskuil DW, Schreiber GJ, Peterse JL, Roberts C, Marton MJ, Parrish M, Atsma D, Witteveen A, Glas A, Delahaye L, van der Velde T, Bartelink H, Rodenhuis S, Rutgers ET, Friend SH, Bernards R (2002) A gene-expression signature as a predictor of survival in breast cancer. *N Engl J Med* **347:** 1999-2009

Van der Geize R, Yam K, Heuser T, Wilbrink MH, Hara H, Anderton MC, Sim E, Dijkhuizen L, Davies JE, Mohn WW, Eltis LD (2007) A gene cluster encoding cholesterol catabolism in a soil actinomycete provides insight into Mycobacterium tuberculosis survival in macrophages. *Proc Natl Acad Sci U S A* **104:** 1947-1952

Vatsis KP, Weber WW (1993) Structural heterogeneity of Caucasian N-acetyltransferase at the NAT1 gene locus. *Archives of Biochemistry and Biophysics* **301:** 71-76

Vatsis KP, Weber WW, Bell DA, Dupret JM, Evans DA, Grant DM, Hein DW, Lin HJ, Meyer UA, Relling MV, et al. (1995) Nomenclature for N-acetyltransferases. *Pharmacogenetics* **5:** 1-17

Velentzis LS, Cantwell MM, Cardwell C, Keshtgar MR, Leathem AJ, Woodside JV (2009) Lignans and breast cancer risk in pre- and post-menopausal women: meta-analyses of observational studies. *Brit J Cancer* **100:** 1492-1498

Verdoes M, Florea BI, van der Marel GA, Overkleeft HS (2009) Chemical Tools To Study the Proteasome. *European Journal of Organic Chemistry***:** 3301-3313

Verdonk ML, Cole JC, Hartshorn MJ, Murray CW, Taylor RD (2003) Improved protein-ligand docking using GOLD. *Proteins-Structure Function and Genetics* **52:** 609-623

Vogel VG, Costantino JP, Wickerham DL, Cronin WM, Cecchini RS, Atkins JN, Bevers TB, Fehrenbacher L, Pajon ER, Jr., Wade JL, 3rd, Robidoux A, Margolese RG, James J, Lippman SM, Runowicz CD, Ganz PA, Reis SE, McCaskill-Stevens W, Ford LG, Jordan VC, Wolmark N (2006) Effects of tamoxifen vs raloxifene on the risk of developing invasive breast cancer and other disease outcomes: the NSABP Study of Tamoxifen and Raloxifene (STAR) P-2 trial. *JAMA* **295:** 2727-2741

Voice RA, Manis M, Weber WW (1993) Inhibition of human red blood cell N-acetyltransferase. *Drug Metab Dispos* **21:** 181-183

Wakefield L, Boukouvala S, Sim E (2010) Characterisation of CpG methylation in the upstream control region of mouse Nat2: evidence for a gene-environment interaction in a polymorphic gene implicated in folate metabolism. *Gene* **452:** 16-21

Wakefield L, Cornish V, Long H, Griffiths WJ, Sim E (2007) Deletion of a xenobiotic metabolizing gene in mice affects folate metabolism. *Biochem Biophys Res Commun* **364:** 556-560

Wakefield L, Cornish V, Long H, Kawamura A, Zhang X, Hein DW, Sim E (2008a) Mouse arylamine N-acetyltransferase 2 (Nat2) expression during embryogenesis: a potential marker for the developing neuroendocrine system. *Biomarkers* **13:** 106-118

Wakefield L, Robinson J, Long H, Ibbitt JC, Cooke S, Hurst HC, Sim E (2008b) Arylamine N-acetyltransferase 1 expression in breast cancer cell lines: a potential marker in estrogen receptor-positive tumors. *Genes Chromosomes Cancer* **47:** 118-126

Wakefield L, Robinson J, Long H, Ibbitt JC, Cooke S, Hurst HC, Sim E (2008c) Arylamine N-acetyltransferase 1 expression in breast cancer cell lines: A potential marker in estrogen receptor-positive tumors. *Genes, Chromosomes and Cancer* **47:** 118-126

Walraven JM, Doll MA, Hein DW (2006) Identification and characterization of functional rat arylamine N-acetyltransferase 3: comparisons with rat arylamine N-acetyltransferases 1 and 2. *J Pharmacol Exp Ther* **319:** 369-375

Wang H, Guo Z, Vath GM, Wagner CR, Hanna PE (2004a) Chemical modification of hamster arylamine N-acetyltransferase 2 with isozyme-selective and nonselective N-arylbromoacetamido reagents. *Protein J* **23:** 153-166

Wang H, Liu L, Hanna PE, Wagner CR (2005a) Catalytic mechanism of hamster arylamine N-acetyltransferase 2. *Biochemistry* **44:** 11295-11306

Wang H, Vath GM, Gleason KJ, Hanna PE, Wagner CR (2004b) Probing the mechanism of hamster arylamine N-acetyltransferase 2 acetylation by active site modification, site-directed mutagenesis, and pre-steady state and steady state kinetic studies. *Biochemistry* **43:** 8234-8246

Wang H, Vath GM, Kawamura A, Bates CA, Sim E, Hanna PE, Wagner CR (2005b) Over-expression, purification, and characterization of recombinant human arylamine N-acetyltransferase 1. *Protein J* **24:** 65-77

Ward A, Hickman D, Gordon JW, Sim E (1992) Arylamine N-acetyltransferase in human red blood cells. *Biochem Pharmacol* **44:** 1099-1104

Ward A, Summers MJ, Sim E (1995) Purification of recombinant human N-acetyltransferase type 1 (NAT1) expressed in E. coli and characterization of its potential role in folate metabolism. *Biochem Pharmacol* **49:** 1759-1767

Watanabe M, Sofuni T, Nohmi T (1992) Involvement of Cys69 residue in the catalytic mechanism of N-hydroxyarylamine O-acetyltransferase of Salmonella typhimurium. Sequence similarity at the amino acid level suggests a common catalytic mechanism of acetyltransferase for S. typhimurium and higher organisms. *J Biol Chem* **267:** 8429-8436

Weber WW, Hein DW (1985) N-acetylation pharmacogenetics. *Pharmacol Rev* **37:** 25-79

Welsch CW (1987) Enhancement of mammary tumorigenesis by dietary fat: review of potential mechanisms. *Am J Clin Nutr* **45:** 192-202

West M, Blanchette C, Dressman H, Huang E, Ishida S, Spang R, Zuzan H, Olson JA, Jr., Marks JR, Nevins JR (2001) Predicting the clinical status of human breast cancer by using gene expression profiles. *Proc Natl Acad Sci U S A* **98:** 11462-11467

Westwood IM, Holton SJ, Rodrigues-Lima F, Dupret JM, Bhakta S, Noble ME, Sim E (2005) Expression, purification, characterization and structure of Pseudomonas aeruginosa arylamine N-acetyltransferase. *Biochem J* **385:** 605-612

Westwood IM, Kawamura A, Fullam E, Russell AJ, Davies SG, Sim E (2006) Structure and mechanism of arylamine N-acetyltransferases. *Curr Top Med Chem* **6:** 1641-1654

Westwood IM, Kawamura A, Russell AJ, Sandy J, Davies SG, Sim E (2011) Novel small-molecule inhibitors of arylamine N-acetyltransferases: drug discovery by high-throughput screening. *Comb Chem High Throughput Screen* **14:** 117-124

Westwood NJ (2004) Chemical genetics: how does it function? *Philos Transact R Soc Lond A* **362(1825):** 2761-2774

Williams DH, Fleming I (1989) *Spectroscopic Methods in Organic Chemistry*: McGraw-Hill Book Company Ltd. UK.

Williams DL, Flaherty TJ, Alnasleh BK (2009) Beyond λmax Part 2: Predicting Molecular Color. *Journal of Chemical Education* **86:** 333

Williams JA, Stone EM, Fakis G, Johnson N, Cordell JA, Meinl W, Glatt H, Sim E, Phillips DH (2001) N-acetyltransferases, sulfotransferases and heterocyclic amine activation in the breast. *Pharmacogenetics* **11:** 373-388

Windmill KF, Gaedigk A, Hall PM, Samaratunga H, Grant DM, McManus ME (2000) Localization of N-acetyltransferases NAT1 and NAT2 in human tissues. *Toxicol Sci* **54:** 19-29

WisconsinUniversity-Madison. (2001) Bordwell pKa Table (in DMSO). http://www.chem.wisc.edu/areas/reich/pkatable/.

Wishart DS, Knox C, Guo AC, Cheng D, Shrivastava S, Tzur D, Gautam B, Hassanali M (2008) DrugBank: a knowledgebase for drugs, drug actions and drug targets. *Nucleic Acids Res* **36:** D901-D906

Witt ON (1876) Zur Kenntniss des Baues und der Bildung färbender Kohlenstoffverbindungen. *Berichte der deutschen chemischen Gesellschaft* **9:** 522–527

Witt ON (1886) XL.-The eurhodines, a new class of colouring matters. *Journal of the Chemical Society, Transactions* **49:** 391-405

Wolff AC, Hammond ME, Schwartz JN, Hagerty KL, Allred DC, Cote RJ, Dowsett M, Fitzgibbons PL, Hanna WM, Langer A, McShane LM, Paik S, Pegram MD, Perez EA, Press MF, Rhodes A, Sturgeon C, Taube SE, Tubbs R, Vance GH, van de Vijver M, Wheeler TM, Hayes DF (2007) American Society of Clinical Oncology/College of American Pathologists guideline recommendations for human epidermal growth factor receptor 2 testing in breast cancer. *Arch Pathol Lab Med* **131:** 18-43

Wood ER, Truesdale AT, McDonald OB, Yuan D, Hassell A, Dickerson SH, Ellis B, Pennisi C, Horne E, Lackey K, Alligood KJ, Rusnak DW, Gilmer TM, Shewchuk L (2004) A unique structure for epidermal growth factor receptor bound to GW572016 (Lapatinib): relationships among protein conformation, inhibitor off-rate, and receptor activity in tumor cells. *Cancer Res* **64:** 6652-6659

Woods LM, Rachet B, Coleman MP (2006) Origins of socio-economic inequalities in cancer survival: a review. *Ann Oncol* **17:** 5-19

Woosley JT, Muldoon TG (1977) Comparison of the accuracy of the Scatchard, Lineweaver-Burk and direct linear plots for the analysis of steroid-protein interactions. *J Steroid Biochem* **8:** 625-629

Wooster R, Bignell G, Lancaster J, Swift S, Seal S, Mangion J, Collins N, Gregory S, Gumbs C, Micklem G (1995) Identification of the breast cancer susceptibility gene BRCA2. *Nature* **378:** 789-792

Wright AT, Song JD, Cravatt BF (2009) A Suite of Activity-Based Probes for Human Cytochrome P450 Enzymes. *Journal of the American Chemical Society* **131:** 10692-10700

Wu H, Dombrovsky L, Tempel W, Martin F, Loppnau P, Goodfellow GH, Grant DM, Plotnikov AN (2007) Structural basis of substrate-binding specificity of human arylamine N-acetyltransferases. *J Biol Chem* **282:** 30189-30197

Wu SP, Huang RY, Du KJ (2009) Colorimetric sensing of Cu(II) by 2-methyl-3-[(pyridin-2-ylmethyl)-amino]-1,4-naphthoquinone: Cu(II) induced deprotonation of NH responsible for color changes. *Dalton Transactions***:** 4735-4740

Wu WJ, Tonge PJ, Raleigh DP (1998) Stereospecific H-1 and C-13 NMR assignments of crotonyl CoA and hexadienoyl CoA: Conformational analysis and comparison with protein-CoA complexes. *Journal of the American Chemical Society* **120:** 9988-9994

Xue F, Willett WC, Rosner BA, Hankinson SE, Michels KB (2011) Cigarette smoking and the incidence of breast cancer. *Arch Intern Med* **171:** 125-133

Yager JD, Davidson NE (2006) Estrogen carcinogenesis in breast cancer. *N Engl J Med* **354:** 270-282

Yamamoto M, Sobue G, Mukoyama M, Matsuoka Y, Mitsuma T (1996) Demonstration of slow acetylator genotype of N-acetyltransferase in isoniazid neuropathy using an archival hematoxylin and eosin section of a sural nerve biopsy specimen. *Journal of the Neurological Sciences* **135:** 51-54

Yamauchi H, Stearns V, Hayes DF (2001) When Is a Tumor Marker Ready for Prime Time? A Case Study of c-erbB-2 as a Predictive Factor in Breast Cancer. *J Clin Oncol* **19:** 2334-2356

Yon-Kahn J, Hervé G, SpringerLink (Online service). (2010) Molecular and cellular enzymology. Springer, Heidelberg ; New York.

Yoshida K, Miki Y (2004) The role of BRCA1 and BRCA2 as regulators of DNA repair, transcription, and cell cycle in response to DNA damage. *Cancer Science* **95:** 866-871

Zechmeister L (1962) *Cis-trans isomeric carotenoids, vitamins A, and arylpolyenes*, Wien: Springer-Verlag.

Zhang N, Liu L, Liu F, Wagner CR, Hanna PE, Walters KJ (2006) NMR-based model reveals the structural determinants of mammalian arylamine N-acetyltransferase substrate specificity. *J Mol Biol* **363:** 188-200

Zou YK, Yin J (2009) Phosphopantetheinyl Transferase Catalyzed Site-Specific Protein Labeling with ADP Conjugated Chemical Probes. *Journal of the American Chemical Society* **131:** 7548-+

Appendices

Appendix 1

List of the reservoirs (well or tube) corresponding to the conditions at which interesting observations were made (**Table IV.5**)

Index™

Hampton Research (www.hamptonresearch.com)

Tube Number	Salt	Buffer	Precipitant
9	None	0.1 M BIS-TRIS pH 5.5	3.0 M Sodium chloride

JCSG-*plus*™

JCSG-plus HT-96 - Molecular Dimensions (www.moleculardimensions.com)

Tube	Salt	Buffer	pH	Precipitant
1.26	1.0 Lithium chloride	0.1 M Na citrate	4	20% w/v PEG 6000
1.39	0.2 M Sodium chloride	0.1 M Na/K phosphate	6.2	50% v/v PEG 200
1.44	None	0.1 M Tris	8	40% v/v MPD

Tube	Salt	Buffer	pH	Precipitant
2.6	0.2 M zinc acetate	0.1 M imidazole	8	20% w/v PEG 3000
2.15	None	01. M Tris	8	20% v/v MPD
2.19	None	None	7	0.8 M succinic acid
2.32	0.15 M DL - malic acid	None	7	20% w/v PEG 3350

Morpheus™

Morpheus™ MD1-46/MD1-47 - Molecular Dimensions (www.moleculardimensions.com)

Well	Tube	Ligand stock	Conc.	Buffer System	Conc.	pH@ (20° C)	Precipitant stock	Conc.
A11	1-11	Divalents	0.06M	3	0.1M	8.5	GOL_P4K	30.00%
B6	1-18	Halogens	0.06M	2	0.1M	7.5	EDO_P8K	30.00%
B7	1-19	Halogens	0.06M	2	0.1M	7.5	GOL_P4K	30.00%
B11	1-23	Halogens	0.06M	3	0.1M	8.5	GOL_P4K	30.00%
C1	1-25	NPS	0.06M	1	0.1M	6.5	P550MME_P20K	30.00%
C7	1-31	NPS	0.06M	2	0.1M	7.5	GOL_P4K	30.00%
D1	1-37	Alcohols	0.06M	1	0.1M	6.5	P550MME_P20K	30.00%
F10	2-22	Monosaccharides	0.06M	3	0.1M	8.5	EDO_P8K	30.00%
G2	2-26	Carboxylic acids	0.06M	1	0.1M	6.5	EDO_P8K	30.00%
G3	2-27	Carboxylic acids	0.06M	1	0.1M	6.5	GOL_P4K	30.00%
G6	2-30	Carboxylic acids	0.06M	2	0.1M	7.5	EDO_P8K	30.00%
H1	2-37	Amino acids	0.06M	1	0.1M	6.5	P550MME_P20K	30.00%

PEG/Ion™

Hampton Research (www.hamptonresearch.com)

Tube	Salt	Polymer	pH
12	0.2 M Ammonium iodide	20% w/v Polyethylene glycol 3,350	6.2
24	0.2 M Lithium acetate dihydrate	20% w/v Polyethylene glycol 3,350	7.9

PEG/Ion 2™

Hampton Research (www.hamptonresearch.com)

Tube	Salt	Buffer	Polymer
48	1% w/v Tryptone	0.05 M HEPES sodium pH 7.0	20% w/v Polyethylene glycol 3,350

Structure™

Structure™ Screen 1&2 HT-96 - Molecular Dimensions (www.moleculardimensions.com)

Well	Salt	Buffer	pH	Precipitant
B1	0.2 M sodium citrate	0.1 M Na cacodylate	6.5	30 % v/v 2-propanol
B4	0.2 M magnesium acetate	0.1 M Na cacodylate	6.5	30 % v/v MPD
C5	None	0.1 M Na HEPES	7.5	1.4 M tri-sodium citrate
C6	None	0.1 M Na HEPES	7.5	2 % v/v PEG 400, 2.0 M ammonium sulfate
D2	None	0.1 M Tris	8.5	8 % w/v PEG 8000
D7	0.2 M ammonium sulfate	None	None	30 % w/v PEG 4000
D9	None	None	None	4.0 M sodium formate
D10	0.05 M potassium dihydrogen phosphate	None	None	20 % w/v PEG 8000
E4	0.2 M magnesium chloride	None	8.5	3.4 M 1,6-hexanediol
E7	1.5 M ammonium sulfate	0.1 M Tris	8.5	12 % v/v glycerol
F3	None	0.1 M Na HEPES	7.5	2.0 M ammonium formate
F8	None	0.1M MES	6.5	1.6M magnesium sulfate
G5	0.2 M K/Na Tartrate	0.1 M Na citrate	5.6	2.0 M ammonium sulfate
G10	0.01 M manganese chloride	0.1 M Na citrate	5.6	2.5 M 1,6-hexanediol

Wizard™ I

Wizard I random sparse matrix crystallization screen – Emerald BioSystems

(www.emeraldbiosystems.com)

Tube	Crystallant	Buffer (0.1M)	Salt (0.2M)
6	20% (w/v) PEG-3000	Citrate pH 5.5	none
7	10% (w/v) PEG-8000	MES pH 6.0	$Zn(OAc)_2$
33	2.0 M $(NH_4)_2SO_4$	CAPS pH 10.5	Li_2SO_4
37	2.5 M NaCl	Imidazole pH 8.0	none

Wizard™ II

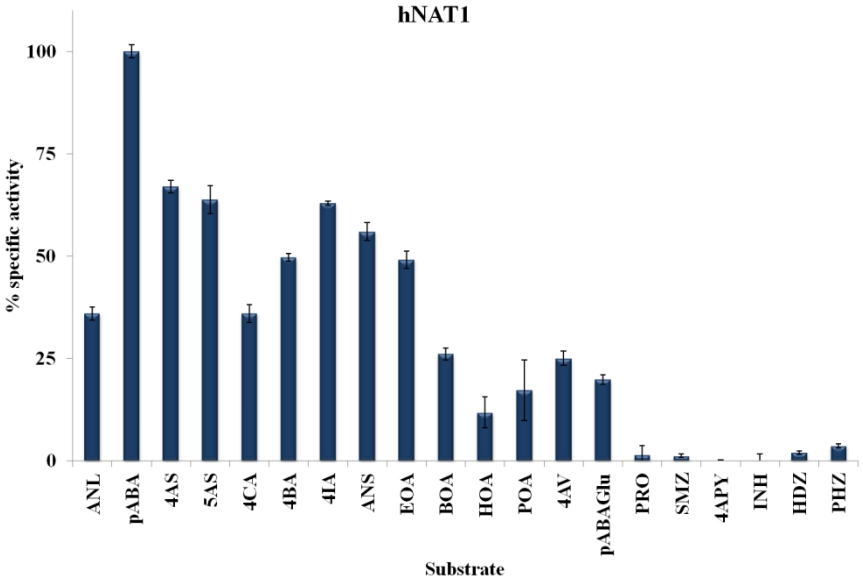
Wizard II random sparse matrix crystallization screen – Emerald BioSystems

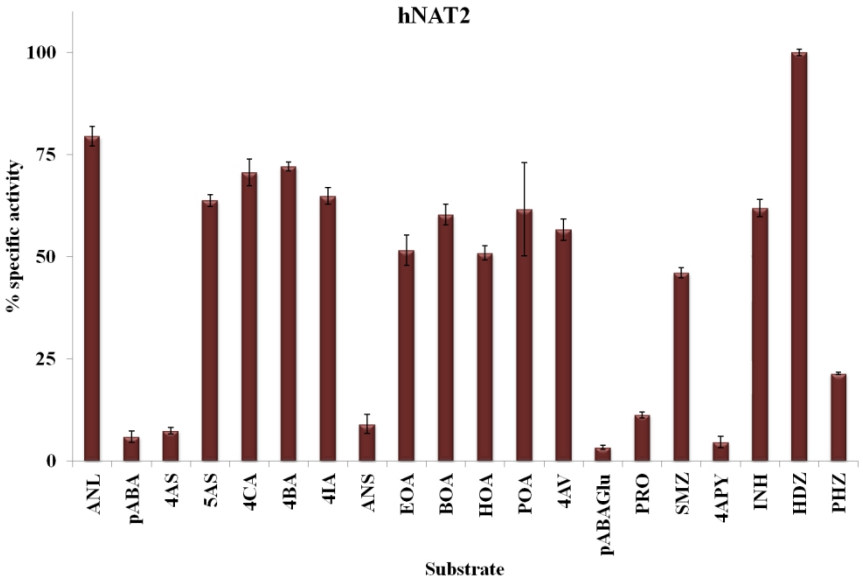
(www.emeraldbiosystems.com)

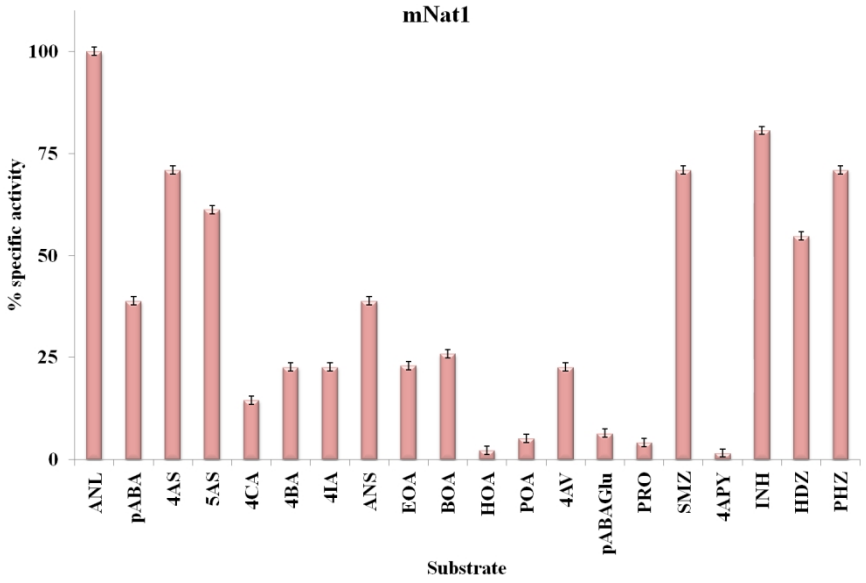
Tube	Crystallant	Buffer (0.1M)	Salt (0.2M)
31	1.0 M sodium citrate	Tris pH 7.0	NaCl

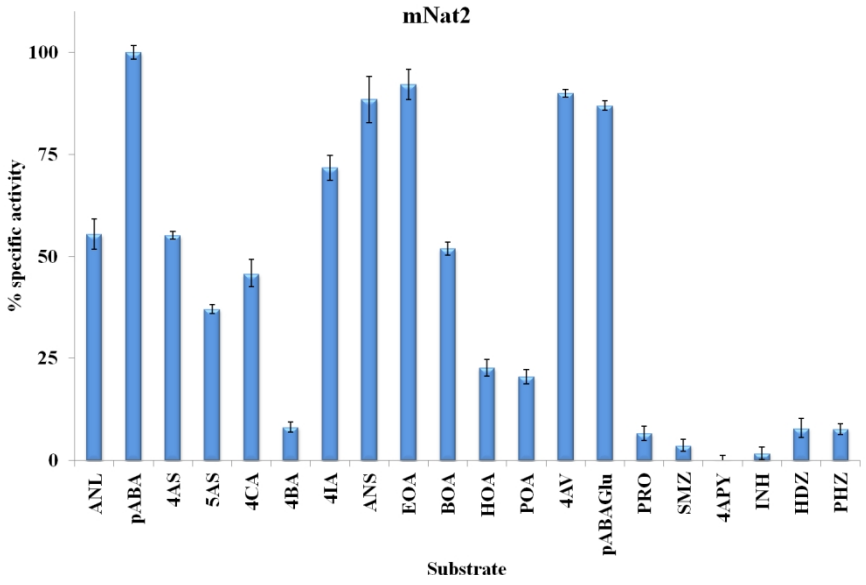
Appendix 2

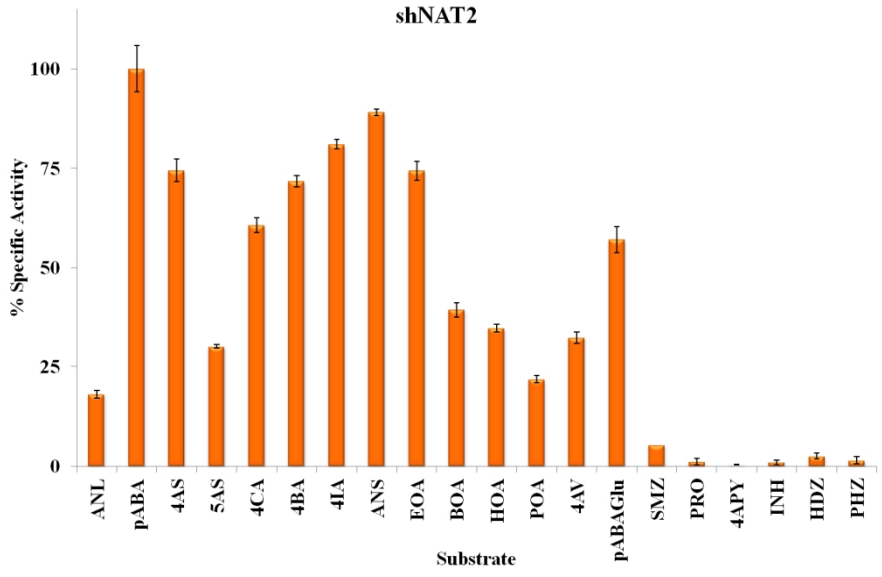
Separate view of NAT substrate profiles presented in this study.

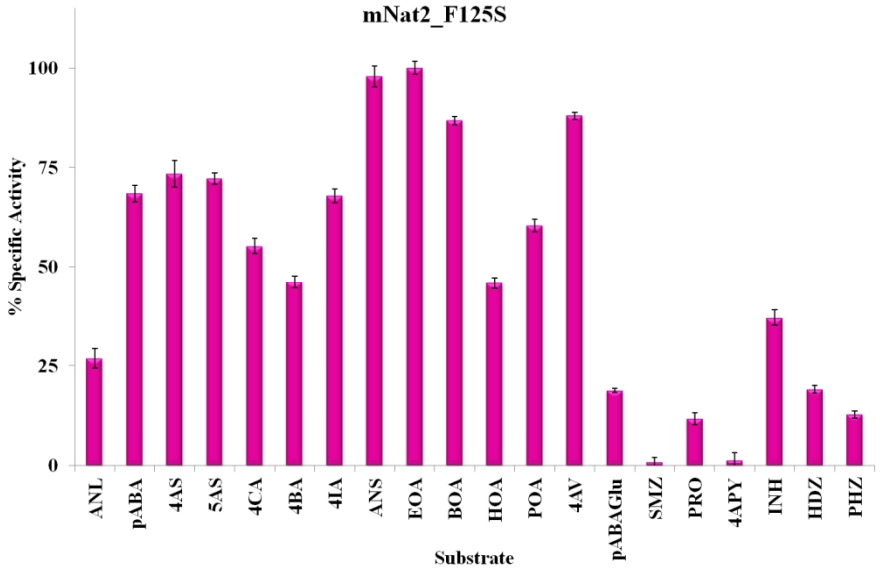


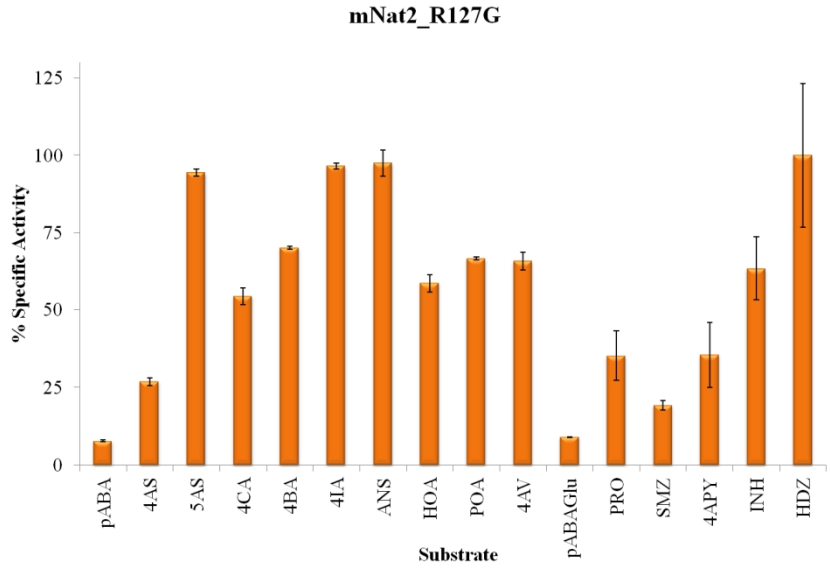


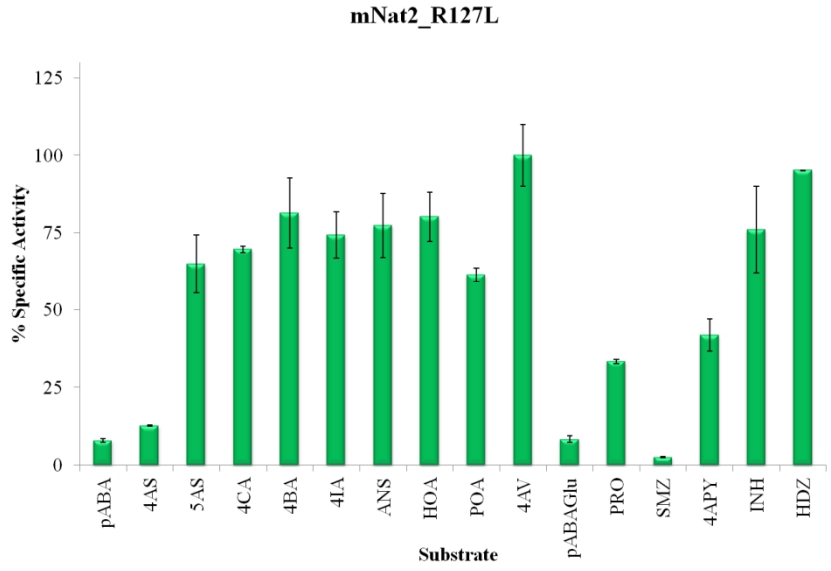

mNat1
% specific activity
100
75
50
25
0
ANL
pABA
4AS
5AS
4CA
4BA
4IA
ANS
EOA
BOA
HOA
POA
4AV
pABAGlu
PRO
SMZ
4APY
INH
HDZ
PHZ
Substrate


mNat2
% specific activity
100
75
50
25
0
ANL
pABA
4AS
5AS
4CA
4BA
4IA
ANS
EOA
BOA
HOA
POA
4AV
pABAGlu
PRO
SMZ
4APY
INH
HDZ
PHZ
Substrate


shNAT2
% Specific Activity
100
75
50
25
0
ANL
pABA
4AS
5AS
4CA
4BA
4IA
ANS
EOA
BOA
HOA
POA
4AV
pABAGlu
SMZ
PRO
4APY
INH
HDZ
PHZ
Substrate

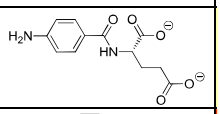
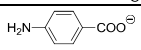
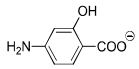
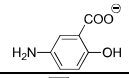
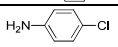
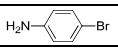
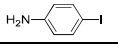
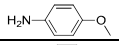
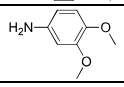
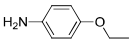
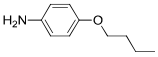
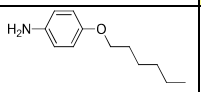
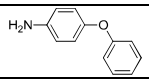
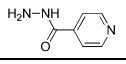
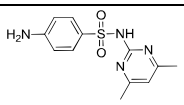
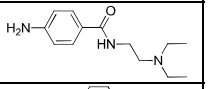

mNat2_F125S
% Specific Activity
100
75
50
25
0
ANL
pABA
4AS
5AS
4CA
4BA
4IA
ANS
EOA
BOA
HOA
POA
4AV
pABAGlu
SMZ
PRO
4APY
INH
HDZ
PHZ
Substrate

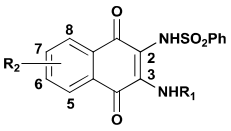

mNat2_R127G
% Specific Activity
125
100
75
50
25
0
pABA
4AS
5AS
4CA
4BA
4IA
ANS
HOA
POA
4AV
pABAGlu
PRO
SMZ
4APY
INH
HDZ
Substrate

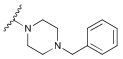

mNat2_R127L
% Specific Activity
125
100
75
50
25
0
pABA
4AS
5AS
4CA
4BA
4IA
ANS
HOA
POA
4AV
pABAGlu
PRO
SMZ
4APY
INH
HDZ
Substrate

Appendix 3

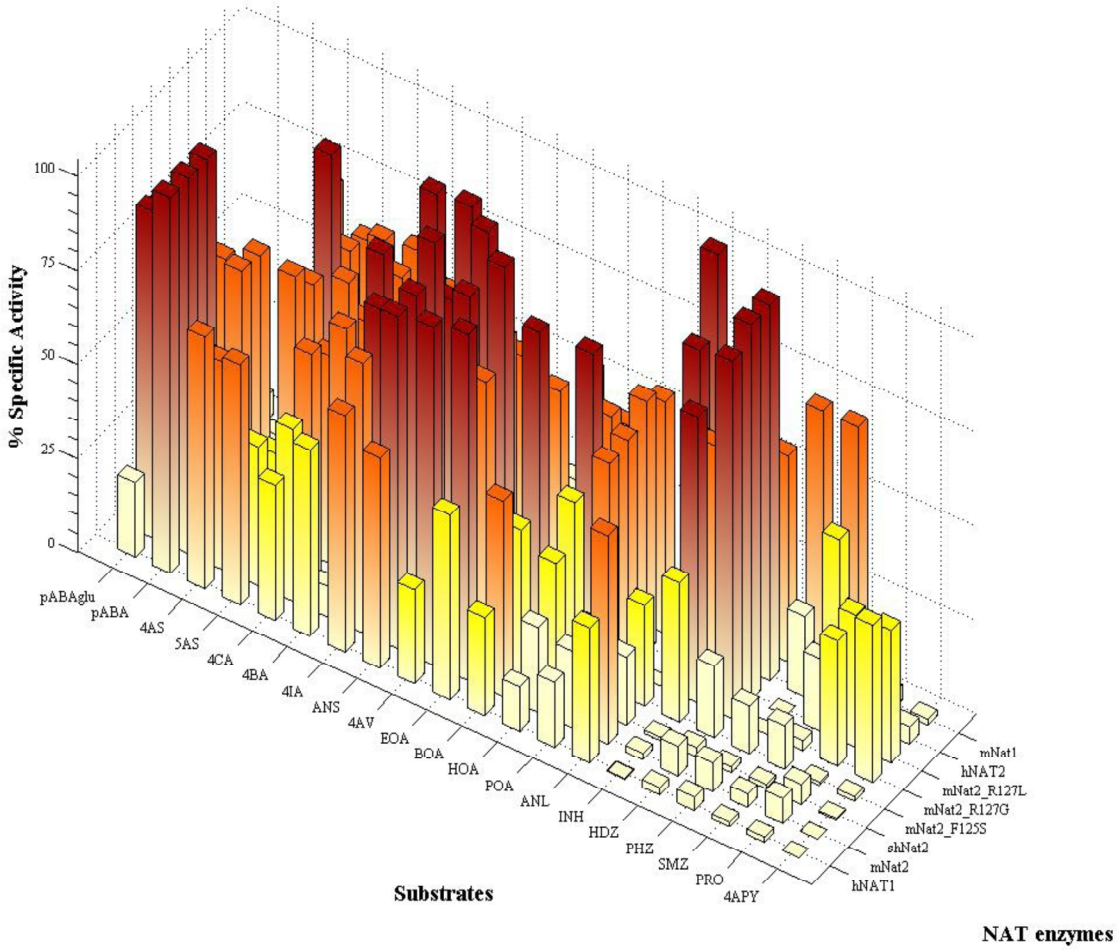
Crib sheet of NAT substrates and inhibitors used in this study.

NAT Substrate	Chemical structure
pABAglu	
pABA	
4AS	
5AS	
4CA	
4BA	
4IA	
ANS	
4AV	
EOA	
BOA	
HOA	
POA	
ANL	
INH	
HDZ	
PHZ	
SMZ	
PRO	
4APY	

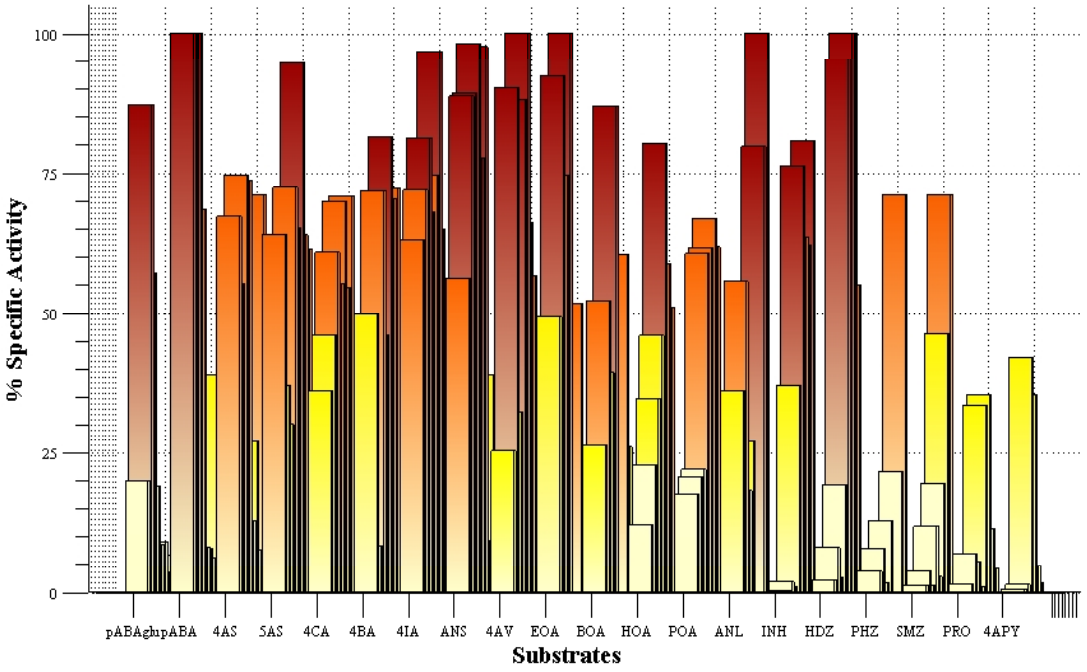


Compound	R_1	R_2 (position)	
1		H	
7		H	
10		H	
11		H	
12		H	
13		NO_2	**5**
14			**6**
15			**7**
16			**8**
17		NH_2	**5**
18			**6**
19			**7**
20			**8**

Appendix 4



Three-dimensional plot of the substrate specificity profiles of all NATs studied in this thesis. ■ for 75-100%, ■ for 50-74.9%, ■ for 25-49.9%, and ■ for 0-24.9%.



Two-dimensional view of the yz-plane is shown. ■ for 75-100%, ■ for 50-74.9%, ■ for 25-49.9%, and □ for 0-24.9%.